



# Geological Fieldwork 2016

A Summary of Field Activities and Current Research



Ministry of  
Energy and Mines



Ministry of Energy and Mines, British Columbia Geological Survey  
Paper 2017-1



British Columbia Geological Survey  
Ministry of Energy and Mines  
[www.em.gov.bc.ca/geology](http://www.em.gov.bc.ca/geology)





Ministry of  
Energy and Mines



# Geological Fieldwork 2016

A Summary of Field Activities and Current Research

Ministry of Energy and Mines  
British Columbia Geological Survey

Paper 2017-1

# Ministry of Energy and Mines Mines and Mineral Resources Division British Columbia Geological Survey

Recommended citation format for individual papers:

Nelson, J., 2017. Composite pericratonic basement of west-central Stikinia and its influence on Jurassic magma conduits: Examples from the Terrace-Ecstall and Anyox areas. In: Geological Fieldwork 2016, British Columbia Ministry of Energy and Mines, British Columbia Geological Survey Paper 2017-1, pp. 61-82.

**Front Cover:** Lower Cretaceous volcanosedimentary strata with low-grade gold mineralization and felsic dikes at Middle ridge, northwestern British Columbia. Peak on right is about 4 km southwest of the Llewellyn fault, a major Jurassic-Eocene structure considered to have controlled regional precious and base-metal mineralization. The photograph was taken at the south end of Tutshi Lake; view to the west.

See: Ootes, L., Elliott, J.M., and Rowins, S.M., 2016. Testing the relationship between the Llewellyn fault, gold mineralization, and Eocene volcanism in northwest British Columbia: A preliminary report, this volume. **Photo by Luke Ootes.**

**Back Cover:** Sampling a gabbro dike that cuts a hornblende-biotite granite (part of the Coast Plutonic Complex) exposed in the foreground and mountainous background. The mafic magmatism recorded by the dikes may be Eocene (~50 Ma), possibly coincident with the timing of low-sulphidation epithermal gold mineralization at Engineer Mine and Mount Skukum. The outcrop is 3 km south of Tutshi Lake, northwest British Columbia; view to the west.

See: Ootes, L., Elliott, J.M., and Rowins, S.M., 2016. Testing the relationship between the Llewellyn fault, gold mineralization, and Eocene volcanism in northwest British Columbia: A preliminary report, this volume. **Photo by Luke Ootes.**

This publication is available, free of charge, from the British Columbia Geological Survey website:  
<http://www.em.gov.bc.ca/Mining/Geoscience/PublicationsCatalogue/Fieldwork>

## British Columbia Cataloguing in Publication Data

Main entry under title:

Geological Fieldwork: - 1974 -

Annual.

Issuing body varies

Vols. for 1978-1996 issued in series: Paper / British Columbia. Ministry of Energy, Mines and Petroleum Resources; vols. for 1997 - 1998, Paper / British Columbia. Ministry of Employment and Investment; vols. for 1999-2004, Paper / British Columbia. Ministry of Energy and Mines; vols. for 2005-2009, Paper / British Columbia. Ministry of Energy, Mines and Petroleum Resources; vols. for 2010, Paper / British Columbia. Ministry of Forests, Mines and Lands; vols. for 2011, Paper / British Columbia. Ministry of Energy and Mines; vols. for 2012- , Paper / British Columbia. Ministry of Energy, Mines and Natural Gas; vols. for 2014- , Paper / British Columbia. Ministry of Energy and Mines.

Includes Bibliographical references.

ISSN 0381-243X=Geological Fieldwork

1. Geology - British Columbia - Periodicals. 2. Mines and mineral resources - British Columbia - Periodicals. 3. Geology - Fieldwork - Periodicals. 4. Geology, Economic - British Columbia - Periodicals. 5. British Columbia. Geological Survey Branch - Periodicals. I. British Columbia. Geological Division. II. British Columbia. Geological Survey Branch. III. British Columbia. Geological Survey Branch. IV. British Columbia. Dept. of Mines and Petroleum Resources. V. British Columbia. Ministry of Energy, Mines and Petroleum Resources. VI. British Columbia. Ministry of Employment and Investment. VII. British Columbia Ministry of Energy and Mines. VIII. Series: Paper (British Columbia. Ministry of Energy, Mines and Petroleum Resources). IX. Series: Paper (British Columbia. Ministry of Employment and Investment). X. Series: Paper (British Columbia Ministry of Energy and Mines). XI. Series: Paper (British Columbia Ministry of Energy, Mines and Petroleum Resources). XII. Series: Paper (British Columbia Ministry of Forests, Mines and Lands). XIII. Series: Paper (British Columbia Ministry of Energy and Mines). XIV. Series: Paper (British Columbia Ministry of Energy, Mines and Natural Gas). XV. Series: Paper (British Columbia Ministry of Energy and Mines).

QE187.46 622.1'09711 C76-083084-3 (Rev.)

Victoria  
British Columbia  
Canada

January 2017

# Preface

## Geological Fieldwork 2016

The 42<sup>nd</sup> edition of Geological Fieldwork is a volume of peer-reviewed papers that present the results of geological research conducted by the British Columbia Geological Survey (BCGS) and its partners in 2016. The volume is a key publication of the BCGS because it provides objective and up-to-date geoscience information at no cost to the public. Many geoscience projects in 2016 were collaborative efforts with partners including the Geological Survey of Canada (GSC), the University of Victoria, the Geological Survey of Japan, Geoscience BC and the Mineral Deposit Research Unit (MDRU) at the University of British Columbia.

Papers in the volume address various aspects of British Columbia's geology, with an emphasis on regional geological studies and associated mineral systems. Papers also include site-specific investigations of mineral deposits and their local geological features. Collaboration between the BCGS and the GSC focused on the second iteration of the five-year Geo-mapping for Energy and Minerals program (GEM 2) and the fifth iteration of the Targeted Geoscience Initiative (TGI-5) program. The GEM 2 program saw Survey geologists investigating the bedrock geology and crustal architecture of northern BC in order to better understand the genesis and distribution of Jurassic and Triassic porphyry copper-gold-molybdenum deposits. The TGI-5 projects ramped up in 2016 and included an investigation of the relationship between gold deposits, magmatism and the Llewellyn fault in northwest BC, specialty metals at the Rock Canyon Creek deposit in southeast BC, and Ni-Cu-PGE-Cr deposits associated with Alaskan-type ultramafic-mafic intrusions.

The Survey delivered a workshop, field trip, and special session on using indicator minerals in Cordilleran exploration, in partnership with the Yukon Geological Survey and the GSC, at the 2016 Geological Association of Canada-Mineralogical Association of Canada (GAC-MAC) annual meeting in Whitehorse. A collection of papers from the workshop will be released as a joint GAC-MAC publication at the 2017 GAC-MAC meeting in Kingston, Ontario. The volume will be the inaugural publication in the new "Topics in Minerals Science" series by the MAC.

January 2016 marked the second year of the 'BC Pavilion' at the Vancouver Convention Centre, the home of the Mineral Exploration Roundup. The Pavilion affords the Survey and its sister government agencies the opportunity to present program highlights and new geoscience information in addition to assisting delegates with permitting and tenure issues. In 2017, the Pavilion will be part of the new 'Passport to Explore' floor, a themed space hosting Canadian provincial and territorial geological surveys and several US state geoscience agencies. The BCGS led designing the floor and developing its technical program, which includes oral sessions that highlight new public geoscience.

MapPlace 2 was launched in November at the annual BCGS Open House in Victoria. MapPlace 2 replaces the original MapPlace, which was developed in 1995 as a web service to help clients browse, visualize, and analyze geoscience and mineral resources data. MapPlace 2 is easier to use, has much improved functionality and performance, can be used on either a Mac or a PC, does not require plug-ins, and works in most web browsers. The power of MapPlace 2 derives from databases that 'talk' to each other, enabling users to conduct queries and generate custom results by connecting many data sources.

The Survey was strengthened in 2016 by the addition of Gabe Fortin and Dejan Milidragovic. Gabe joins us as a Geomatics Geologist focused on advancing MapPlace 2 and Dejan is a Senior Project Geologist specializing in Ni-Cu-PGE metallogeny and ultramafic-mafic rocks. Congratulations also go out to JoAnne Nelson, a 30-year veteran of the BCGS and recipient of a Special Tribute by the Association for Mineral Exploration in recognition of her distinguished career in geoscience work focused on Cordilleran tectonics and metallogeny.

Finally, 2016 ended on a sad note with the passing of Dr. Atholl Sutherland Brown. Atholl served as British Columbia's 8<sup>th</sup> Chief Geologist (1975-1984) and was instrumental in advancing Canadian geoscience and building the BCGS that exists today.



Stephen M. Rowins  
Chief Geologist & Executive Director  
British Columbia Geological Survey

# Table of Contents

---

<b>Hickin, A.S., Jones, L.D., and Clarke, G.:</b> British Columbia Geological Survey annual program review 2016-2017 .....	1	<b>Mihalynuk, M.G., Zagorevski, A., Devine, F.A.M., and Humphrey, E.:</b> A new lode gold discovery at Otter Creek: Another source for the Atlin placers ....	179
<b>Schiarizza, P.:</b> Ongoing stratigraphic studies in the Nicola Group: Stump Lake – Salmon River area, south-central British Columbia .....	17	<b>Green, C., Simandl, G.J., Paradis, S., Katay, F., Hoshino, M., Kon, Y., Kodama, S., and Graf, C.:</b> Geological setting of the Rock Canyon Creek REE-fluorite deposit, British Columbia, Canada.....	195
<b>Angen, J.J., Nelson, J.L., Rahimi, M., and Hart, C.J.R.:</b> Mapping in the Tatsi and Zymo ridge areas of west-central British Columbia: Implications for the origin and history of the Skeena arch.....	35	<b>Hoshino, M., Kon, Y., Kodama, S., Simandl, G.J., Paradis, S., Green, C., Namatame, C., Matsunaga, I., and Takagi, T.:</b> Mineralogy of the Rock Canyon Creek REE-fluorite deposit, British Columbia, Canada.....	205
<b>Ootes, L., Elliott, J.M., and Rowins, S.M.:</b> Testing the relationship between the Llewellyn fault, gold mineralization, and Eocene volcanism in northwest British Columbia: A preliminary report .....	49	<b>Arnold, H., and Hickin, A.S.:</b> Using derived-stereo imagery to map macroscale ice-flow features.....	215
<b>Nelson, J.:</b> Composite pericratonic basement of west-central Stikinia and its influence on Jurassic magma conduits: Examples from the Terrace-Ecstall and Anyox areas .....	61	<b>Appendix:</b> British Columbia Geological Survey publications and peer-reviewed journal papers authored by BCGS staff and released in 2016.....	231
<b>van Straaten, B.I., and Gibson, R.:</b> Late Early to Middle Jurassic Hazelton Group volcanism and mineral occurrences in the McBride-Tanzilla area, northwest British Columbia .....	83		
<b>Milidragovic, D., Zagorevski, A., and Chapman, J.B.:</b> The Mount Hickman ultramafic complex: An Fe-rich Alaskan-type ultramafic intrusion .....	117		
<b>Zagorevski, A., Mihalynuk, M.G., Joyce, N., and Anderson, R.G.:</b> Late Cretaceous magmatism in the Atlin-Tagish area, northern British Columbia (104M, 104N) .....	133		
<b>Mihalynuk, M.G., Zagorevski, A., English, J.M., Orchard, M.J., Bidgood, A.K., Joyce, N., and Friedman, R.M.:</b> Geology of the Sinwa Creek area, northwest BC (104K/14) .....	153		

# British Columbia Geological Survey annual program review 2016-2017



Adrian S. Hickin<sup>1, a</sup>, Larry D. Jones<sup>1</sup>, and Gordon Clarke<sup>2</sup>

<sup>1</sup> British Columbia Geological Survey, Ministry of Energy and Mines, Victoria, BC, V8W 9N3

<sup>2</sup> British Columbia Geological Survey, Ministry of Energy and Mines, Vancouver, BC, V6Z 2G3

<sup>a</sup> corresponding author: Adrian.Hickin@gov.bc.ca

Recommended citation: Hickin, A.S., Jones, L.D., and Clarke, G., 2017. British Columbia Geological Survey annual program review 2016- 2017. In: Geological Fieldwork 2016, British Columbia Ministry of Energy and Mines, British Columbia Geological Survey Paper 2017-1, pp. 1-16.

## 1. Introduction

The British Columbia Geological Survey (BCGS), established in 1895, links government, the minerals industry, and British Columbians to the Province's geology and mineral resources. The BCGS produces geoscience data and knowledge that stimulate exploration activity and attract investment. The Survey strives to be a leader in public government geoscience, providing information to all stakeholders and communities through traditional reports, maps, and databases (Fig. 1), which can be freely accessed online. Headquartered in Victoria, the BCGS is part of the Mines and Mineral Resources Division of the Ministry of Energy and Mines. The Survey has a permanent staff of 29 people (Fig. 2) operating in three sections: 1) Cordilleran Geoscience; 2) Resource Information; and 3) the Mineral Development Office (MDO). The Cordilleran Geoscience Section is responsible for generating new geoscience knowledge, largely through field-based studies and surveys. The Resource Information Section is responsible for maintaining and developing the provincial geoscience databases and disseminating geoscience data online through MapPlace. This section is responsible for evaluating, approving, and archiving mineral and coal exploration assessment reports filed by the exploration and mining industry. The MDO links the province's mineral and coal resources to the investment community, distributes and promotes BCGS technical data, and coordinates the technical outputs of the Regional Geologists Program.

The BCGS is a collaborative agency and partners with federal, provincial, and territorial governments, other national and international organizations, and the mineral exploration industry to develop and deliver geoscience projects. Partnerships maximize effectiveness by optimizing resources and expertise. The Geological Survey of Canada (GSC) and the BCGS continue to benefit from strong partnerships delivering on two main programs, the Cordilleran Project in the second iteration of the Geo-mapping for Energy and Minerals (GEM 2) Program, and the fifth iteration of the Targeted Geoscience Initiative (TGI-5). The Survey has also entered in to a partnership agreement with the Geological Survey of Japan to advance studies on critical and strategic material. Several

projects are being delivered through collaborations with the Department of Earth, Ocean, and Atmospheric Science at the University of British Columbia from TGI-5 grants from the GSC. Formal BCGS partnerships are also in place with the Mineral Deposits Research Unit at the University of British Columbia and Geoscience BC. Since 2003, the Ministry of Energy and Mines as maintained a formal partnership with the University of Victoria (MEM-UVic Partnership). This partnership supports joint research projects and student training that benefits School of Earth and Ocean Science, the Ministry of Energy and Mines, and mineral exploration sector.

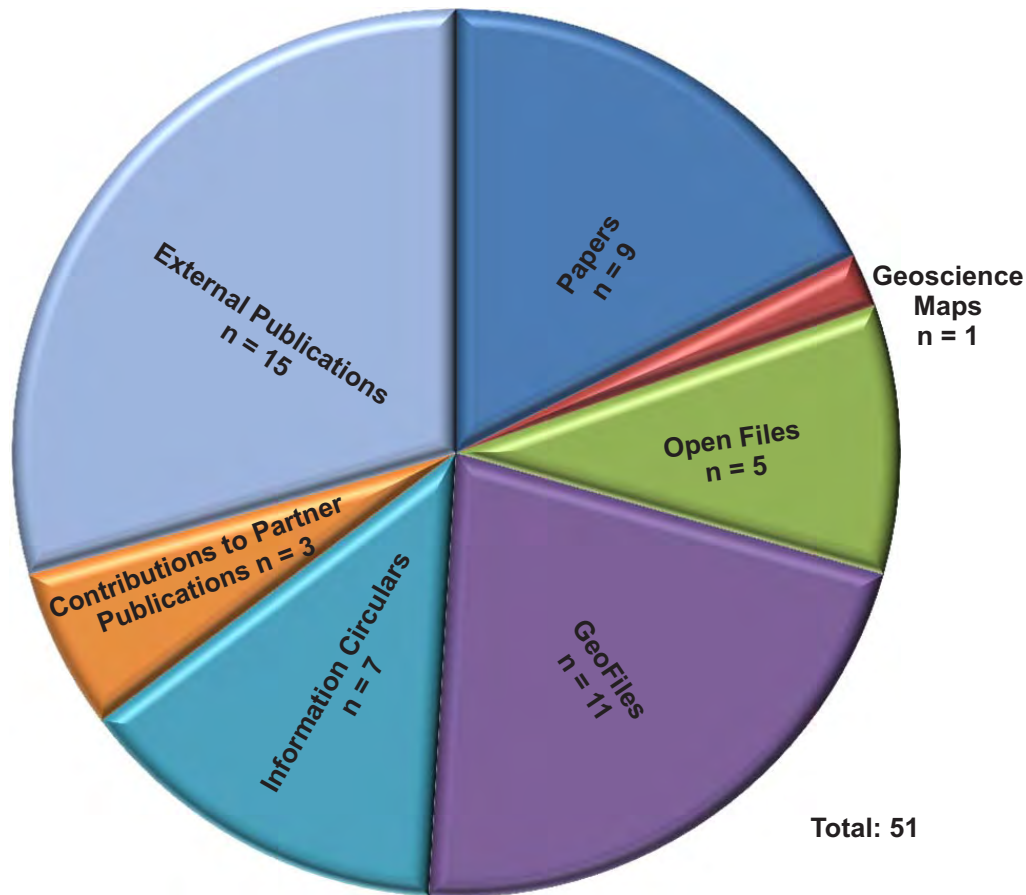
## 2. Cordilleran Geoscience Section

Geologists in the Cordilleran Geoscience Section have expertise in regional bedrock mapping, tectonics, mineral deposits, Quaternary and surficial geology, geochemistry, petrology, mineral exploration methods, metallogeny, and geoscience data management. British Columbia Geological Survey projects are based on short-term objectives and long-term goals. Many current projects are continuations of multi-year efforts, whereas others are new. Projects in 2016 focused on mapping, regional synthesis and map compilation; deposit studies; and exploration methods development (Fig. 3).

### 2.1. Mapping, regional synthesis and map compilations

#### 2.1.1. Stikinia basement – northwest British Columbia

Major porphyry deposits in the Stikine terrane of northwest British Columbia, such as Red Chris and KSM (Clarke et al., 2017), are spatially associated with major, long-lived faults that probably originated as high-strain zones in pre-Devonian basement. Like transcrustal structures in other porphyry districts, they played a vital role in mineralization, serving as conduits for magmas and fluids. Although exposures are limited, this project targets the nature and structural history of deep basement to Stikinia in two ready accessible areas: along a transect from the Terrace area of western Stikinia into the Ecstall belt of the Coast Mountains; and west of the Anyox deposit, where Devonian to Middle Jurassic rocks are exposed (Nelson, 2017, this volume).



### Types of Publications by the British Columbia Geological Survey

**Papers\*:** This series is reserved for reviews and final thematic or regional works. Geological Fieldwork, our annual review of field activities and current research, is released as the first Paper of each year.

**Geoscience Maps:** This series is the BCGS vehicle for publishing final maps

**Open Files:** These maps and reports present the interim results of ongoing research, particularly mapping projects.

**GeoFiles:** These publications enable rapid release of extensive data tables from ongoing geochemical, geochronologic, and geophysical work. As such, they serve the same function as data repositories provided by many journals, providing immediate access to raw data from specific projects.

**Information Circulars:** These publications provide accessible geoscience information to a broad audience in government, industry, and the general public. Included in the Information Circular series are the annual Provincial Overview of Mining and Exploration, \*\*Exploration and Mining in British Columbia, and the Coal Industry Overview.

**Contributions to partner publications:** This category includes reports, maps, and other products published by another agency such as the Geological Survey of Canada or Geoscience BC, but have received contributions from British Columbia Geological Survey staff.

**External publications:** These are contributions to the peer reviewed literature and published in a recognized national or international scientific journal.

\*The count refers to the total number of articles authored by BCGS personnel in a volume.

\*\*Although five articles are included in Exploration and Mining in British Columbia, it is counted as a single volume.

**Fig. 1.** British Columbia Geological Survey publications in 2016.



Fig. 2. Members of the British Columbia Geological Survey on Mount Finlayson, British Columbia.

### 2.1.2. Porphyry environment transitions – northwest British Columbia

The prolific belt of British Columbia's Intermontane porphyry deposits is difficult to track in the Stikine terrane of northwest British Columbia. The Porphyry Environment Transitions project, a collaboration with the GSC through the GEM 2 program, blends topical studies and focused mapping to address the continuity of this prospective Triassic-Jurassic magmatic belt and assess porphyry potential. In 2015, activities focused in the Sinwa Creek area (Mihalynuk et al., 2017a, this volume). In 2016, mapping was completed in the Turtle Lake map area, a region assumed to have been part of the Stuhini forearc (Late Triassic). Topical studies are also being directed at rationalizing the lithostratigraphic framework of prospective Upper Cretaceous rocks using new geochronologic and geochemical data (Zagorevski et al., 2017, this volume), documenting Middle to Late Triassic Alaskan-type ultramafic intrusions with Ni-Cu-PGE potential in northern Stikinia (Milidragovic et al., 2017, this volume), and establishing the boundary between Intermontane arc terranes and the Cache Creek terrane. Mihalynuk et al. (2017b, this volume) report on quartz-gold veins that cut calcareous black phyllite bedrock beneath placer deposits along Otter Creek in the Atlin camp. These veins indicate that lode gold may be genetically related to Late Cretaceous granitic intrusions such as the Surprise Lake batholith rather than to ultramafic rocks, significantly expanding targets for lode gold exploration.

### 2.1.3. Geological mapping, Skeena arch, west-central British Columbia

This project partners the Mineral Development Research Unit at The University of British Columbia, Geoscience BC, and the BCGS. Economically significant porphyry and related mineralization is genetically associated with the Bulkley (Late Cretaceous) and Babine and Nanika intrusive suites (Eocene) in central British Columbia. These intrusions and mineral occurrences are largely restricted to the Skeena arch, a northeast-trending structure that extends transverse to the general trend of Stikine terrane. Nonetheless, the structural history of the Skeena arch and, in particular, the significance of its arc-transverse orientation, has not been well established. Building on mapping in the Terrace area (Nelson et al., 2007, 2008a, 2008b) and aided by new high-resolution aeromagnetic data collected as part of Geoscience BC's SeArch project (Precision GeoSurveys Inc., 2016), 1:2,000-scale mapping documents arch-parallel stratigraphic relationships, structural features, and intrusive-mineralization trends of differing ages, collectively suggesting a long-lived underlying control (Angen et al., 2017, this volume).

### 2.1.4. Geological framework and metallogeny of the Tanzilla-McBride area – northwest British Columbia

This mapping project builds on recent studies in the Dease Lake area of northwestern British Columbia including BCGS mapping west of the study area (Logan et al., 2012) and reconnaissance studies in the Hotailuh batholith to the south

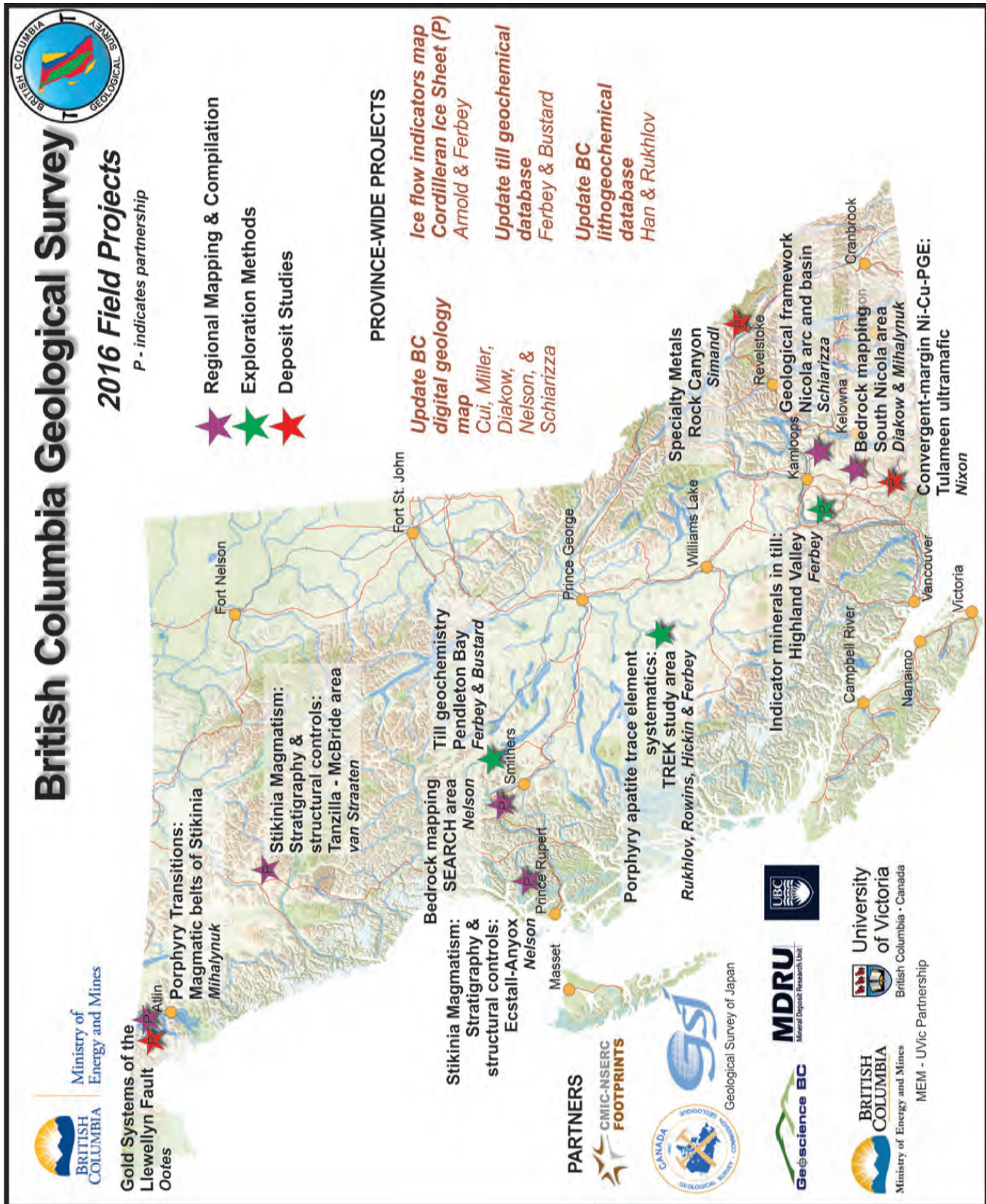


Fig. 3. British Columbia Geological Survey field projects in 2016.

(van Straaten et al., 2012). Volcano-sedimentary rocks north of the Hotailuh batholith previously mapped as Stuhini Group (Late Triassic) were reinterpreted as Hazelton Group (Jurassic) based on detrital zircon geochronology carried out as part of the BCGS program (Iverson et al., 2012). Detailed mapping of volcano-sedimentary units north of the Hotailuh batholith found them to be late Early to Middle Jurassic, essentially coeval with accretion of the Cache Creek and Stikine terranes (van Straaten and Nelson, 2016). Their study included an investigation of the Tanzilla prospect, an advanced argillic lithocap overlying a porphyry system at depth. The 2016 project provides a regional update of the geology east of Dease Lake and north of the Hotailuh batholith (van Straaten and Gibson, 2017, this volume). The project investigates late Early to early Late Jurassic alkaline and subalkaline magmatism and its relationship to porphyry copper potential. This late Early to early Late Jurassic alkaline to subalkaline magmatic episode may represent a new metallogenic epoch in the Canadian Cordillera.

### **2.1.5. Groundhog coalfield compilation – north-central British Columbia**

The Groundhog coalfield compilation (British Columbia Geological Survey, 2016) is the latest in a series of posters that provide overviews of coalfield geology, coal products, annual and historic production, reserves and resource estimates, and past and current projects. Other regions in this series are the East Kootenay coalfields in southeast British Columbia (British Columbia Geological Survey, 2015a) and the Northern Rocky Mountain coalfields in northeast British Columbia (British Columbia Geological Survey, 2015b).

### **2.1.6. Nicola stratigraphy and geological framework – south-central British Columbia**

The Nicola Group records a Mesozoic arc complex that includes Triassic to Jurassic volcanic and sedimentary rocks and related calcalkaline and alkaline intrusions. Originally named for exposures of volcanic rock and limestone on the south side of Nicola Lake (Dawson, 1879), the Nicola Group and coeval to slightly younger intrusions are the defining elements of the Quesnel arc terrane, an important Cu-Au-Mo metallogenic province that contains many porphyry and skarn deposits. Numerous informal subdivisions have been applied to the Nicola Group, but its regional stratigraphic architecture is not well understood. In 2015, BCGS started a multi-year field-based program to synthesize Nicola Group lithostratigraphy and establish a regional stratigraphic framework. This framework, combined with space-time-composition patterns of spatially associated plutons, will contribute to a better understanding of the evolution of the arc, and help establish the settings and controls of mineral occurrences. In 2016, work continued in the eastern part of the Nicola belt south of Kamloops in the Stump Lake – Salmon River area, (Schiarizza, 2017, this volume) tracking units identified about 150 km to the north in the Bridge Lake – Quesnel River area (Schiarizza, 2016).

### **2.1.7. Mapping ice-flow indicators for the Cordillera ice sheet through derived-stereo imagery**

Understanding the extent, flow paths, and history of the most recent Cordilleran Ice Sheet (Late Wisconsinan; ~22-10 ka) comes from interpreting landforms, some of which were created by subglacial processes. Landforms, such as crag-and-tails, drumlins, drumlinoids, and flutes are streamlined along ice-flow directions. As part of a GEM 2 collaboration with the GSC, the first part of this project (Arnold et al., 2016) resulted in a compilation map and an accompanying database of ice-flow controlled landforms that integrated independent databases from British Columbia (Ferbey et al., 2013) and the Yukon (Lipovsky and Bond, 2014). Given the cost of fieldwork in remote regions, data deficiencies remain. The second part of this project was directed at evaluating methods for using inexpensive derived-stereo imagery to remotely map landform features (Arnold and Hickin, 2017, this volume).

## **2.2. Deposit studies**

### **2.2.1. Gold mineralization and the Llewellyn fault in northwest British Columbia**

The Llewellyn fault is a north-northwest striking structure near the British Columbia-Yukon border, ~50 km west of the town of Atlin, British Columbia. A number of disparate gold prospects and past-producing mines (e.g., Engineer, Venus, Mt Skukum) occur near the fault. These deposits have a variety of geological characteristics ranging from shallow epithermal to deeper mesothermal orogenic systems. Some are spatially associated with felsic plutons and others have skarn-like features suggesting the presence of proximal intrusions. This project is aimed at assessing the genetic relationships, if any, between these deposits, the Llewellyn fault and spatially associated magmatism. Large transcrustal strike-slip faults, similar to the Llewellyn fault, host orogenic gold deposits in many Archean greenstone belts. These include the ‘Golden Mile’ (Kalgoorlie) in the Norseman-Wiluna belt of Western Australia, the Kirkland Lake-Larder Lake and Destor-Porcupine ‘Breaks’ in the Abitibi belt of Ontario, and the Con-Giant gold systems in the Yellowknife greenstone belt of the Northwest Territories. To characterize the various gold deposits along the Llewellyn fault, a reconnaissance study was undertaken in partnership with the GSC’s TGI-5 Gold project. Preliminary structural and lithological data were collected from gold deposits in order to determine whether gold mineralization events could be attributed to long-lived deformation occurring along the entire length of the Llewellyn fault. Preliminary conclusions suggest a genetic relationship exists between gold mineralization, Eocene magmatism, and structures associated with the Llewellyn fault (Ootes et al., 2017, this volume).

### **2.2.2. Specialty metals**

Specialty metals are part of the family of critical and strategic materials needed for technologically advanced devices and industrial processes. Also referred to as ‘high technology metals’ or ‘rare metals’, specialty metals include lithium (Li), zirconium

(Zr), yttrium (Y), beryllium (Be), scandium (Sc), tantalum (Ta), niobium (Nb), germanium (Ge), gallium (Ga), and the rare earth elements (REE). The GSC and BCGS are collaborating on a new four-year TGI-5 - Specialty Metals project, which builds on results from TGI-4. As part of this project, the BCGS is also partnering with the Geological Survey of Japan and the University of Victoria. The overarching objective of this project is to investigate the geological conditions responsible for generating mineralizing fluids and for depositing specialty metal ore. The project initially will target carbonatite-related Nb and REE deposits in British Columbia, but is expected to include Ge-, In-, and Ga-bearing deposits. Although much research will be focused in British Columbia, the project will be national in scope. In 2016, the project started at the Rock Canyon Creek REE-fluorite deposit in south central British Columbia. This work focused on better characterizing the deposit, especially its mineralogy (Hoshino et al., 2017, this volume), in order to address questions about the origin of ore-forming fluids and the temporal, structural, and stratigraphic relationship to Mississippi Valley-type and sparry magnesite deposits along the eastern flank of the Canadian Cordillera (Green et al., 2017, this volume).

### 2.2.3. Convergent-margin nickel-copper-platinum group element-chromium (Ni-Cu-PGE-Cr) deposits

This project is a collaboration between the University of British Columbia, the BCGS, and the GSC. It is a TGI-5 contribution that builds upon previous TGI-4 investigations of an emerging class of magmatic Ni-Cu-PGE sulphide deposits hosted by ultramafic-mafic intrusions in supra-subduction or convergent-margin tectonic settings. The principal objective is to determine the fundamental physicochemical controls of magmatic Ni-Cu-PGE-Cr mineralization associated with Alaskan-type ultramafic-mafic intrusions in the Canadian Cordillera. Field investigations and high-precision U-Pb CA-TIMS and  $^{40}\text{Ar}/^{39}\text{Ar}$  geochronology will target two Alaskan-type intrusions in a Late Triassic-Early Jurassic Cordilleran magmatic arc of British Columbia: (1) the Turnagain ultramafic intrusion with its unusual endowment of world-class, low-grade Ni-Cu-PGE sulphides, and (2) the Tulameen ultramafic-mafic intrusion with its dunite-hosted chromitite-PGE alloy association that is more typical of Alaskan-type intrusions globally. The study also will address poorly known occurrences of magmatic Cu-rich sulphides (chalcopyrite, bornite) in late-stage ultramafic and mafic rocks of the Tulameen intrusion that appear to indicate delayed sulphide saturation in fractionated Ni-poor magma(s).

## 2.3. Exploration methods

### 2.3.1. Trace element systematics in apatite

Apatite ( $\text{Ca}_5[\text{PO}_4]_3(\text{F},\text{OH},\text{Cl})$ ), a widespread accessory phosphate mineral in many rocks, is the most abundant phosphate mineral in the world. The crystal structure and chemistry of apatite allow it to accommodate variable concentrations of many trace elements including Na, Mg, Si,

S, V, Mn, Fe, As, Sr, Ba, rare earth elements (REE), Pb, Th and U. The trace-element composition of apatite is very sensitive to its environment of formation and it commonly crystallizes as an early-stage liquidus phase through to fluid saturation of the magma and associated metallic mineralization. Importantly, apatite resists chemical and physical weathering in glacial environments. These criteria make apatite a very good candidate for use as an indicator mineral. Over the last three years, BCGS, in collaboration with researchers from the School of Earth and Ocean Sciences at the University of Victoria have developed techniques that use the trace element chemistry in apatite for a variety of geological application, some of which are highlighted below.

#### 2.3.1.1. Apatite trace-element compositions: A robust new tool for mineral exploration

The use of apatite as an exploration tool continues to be developed. Mao et al. (2016) demonstrated that differences in trace-element compositions between apatites from carbonatites, barren igneous rocks, and mineral deposits (e.g., orogenic Au, porphyry Cu-Au-Mo, IOCG) permit their discrimination using optimized discrimination diagrams. These diagrams were constructed using Discriminant Projection Analysis (DPA), a powerful multivariate statistical technique that uses an a priori knowledge of group members to calculate a set of linear discriminant functions or projections of variables (element concentrations) that maximize the differences between the predefined group. This allows samples to be plotted in the discriminant space so that group separation can be visualized and investigated. To test the discrimination technique, an orientation study using detrital apatite grains from till samples collected at four porphyry Cu±Au±Mo deposits in central BC (Gibraltar, Mt. Polley, Woodjam, and Highland Valley) was undertaken. Results were positive and the discrimination diagrams successfully identified apatites originating from the different types of porphyry deposits up ice-flow direction (Rukhlov et al., 2016). The next step in developing apatite as an indicator mineral using the Mao et al. (2016) discrimination technique is currently underway. Apatite grains recovered from regional till samples collected via Geoscience BC's Targeting Resources through Exploration and Knowledge (TREK) projects on the glaciated Nechako Plateau of central BC (Jackaman and Sacco, 2014; Jackaman et al., 2015) will be used to test areas containing both known and unknown mineral occurrences. This 'blind' test will effectively assess the apatite discrimination technique for grassroots exploration.

#### 2.3.1.2. Redox conditions of porphyry Cu-Au-Mo deposits

Porphyry Cu-Mo-Au deposits form from magmatic-hydrothermal fluids that display a wide range of oxidation states. Most porphyry systems, especially the giant ones, form from fluids and magmas with high oxidation states, although a number form from intrinsically reduced fluids and magmas indicating that the role of oxygen fugacity in porphyry formation is complex. Previous studies have shown that concentrations of

multivalent elements S, V, Cr, Mn, Fe, Ga, As, Ce, and Eu in apatite can be used as redox sensors in magmas and fluids. This project, in collaboration with researchers from the University of Victoria, is assessing the usefulness of apatite trace-element composition as a redox proxy using both new and published electron microprobe and laser-ablation inductively coupled plasma mass spectrometry data from 20 porphyry Cu-Mo-Au deposits exhibiting a wide range of oxidation states.

### **2.3.1.3. Apatite for discriminating tectonic settings**

Using the apatite trace-element dataset of Mao et al. (2016), the DPA multivariate statistical technique has been applied to igneous apatites from different known tectonic settings. Results show that tectonic discrimination diagrams can be constructed in terms of six linear discriminant functions or projections using a variety of trace elements. It may be concluded that the trace-element chemistry of igneous apatite fingerprints tectonic environments, thus extending the utility of apatite as a petrogenetic tool.

### **2.3.2. Porphyry indicator minerals in tills of the Highland Valley Mine area, south-central British Columbia**

Rocks of Quesnel terrane in the Intermontane Belt of south-central British Columbia host many large porphyry deposits, yet vast areas remain underexplored because much of the bedrock in the region is covered by glacial sediments. Nonetheless, geochemical and mineralogical data, particularly from locally derived tills, can help detect deposits buried under Quaternary sediments. The Highland Valley project, a joint investigation between the Canadian Mining Innovation Council (CMIC), the GSC, and BCGS, is a continuation of the collaborative TGI- 4 porphyry indicator mineral project (2011-2015) between the GSC and BCGS. The goal of this project is to develop a new surficial sediment exploration method for porphyry Cu-Mo-Au mineralization in drift-covered areas of British Columbia.

Till samples collected near the Highland Valley Copper mine were analyzed for geochemical, indicator mineral, and grain size determinations to test the utility of the method at a site where the configuration and tenor of ore-grade porphyry Cu mineralization are known. Furthermore, Quaternary geology mapping (Plouffe and Ferbey, 2015) indicates a relatively simple regional Late Wisconsinan ice-flow history. Sediment transport is generally southward, making provenance determinations on subglacial tills relatively straightforward. Results from this project were most recently published in Ferbey et al. (2016).

### **2.3.3. Indicator minerals in till and stream sediments of the Canadian Cordillera – A Geological Association of Canada (GAC) – Mineralogical Association of Canada (MAC) workshop, fieldtrip, and special volume**

In the last five years, significant applied research efforts have been focused on using indicator minerals for exploration in the Canadian Cordillera. At the annual 2016 GAC-MAC meeting in Whitehorse, the BCGS partnered with the GSC

and Yukon Geological Survey to deliver a workshop, a fieldtrip, and a special session dedicated to indicator mineral research. The geology, physiography, and glacial history of the Canadian Cordillera are intertwined and distinct from other less mountainous regions of Canada. Therefore, Cordilleran-specific mineral exploration techniques have evolved and interpretations need to consider the complexities of Cordilleran geology and physiography. The one-day workshop focused on characteristics unique to the Cordillera. In addition to a hands-on exploration exercise using real data from British Columbia, the workshop presented a number of successful indicator mineral case studies from British Columbia that exemplified recent advances. The workshop was followed by a fieldtrip that examined till and other glaciogenic sediments, highlighting features that distinguish subglacial basal tills from other diamicts (Fig. 4). The BCGS and GSC also convened a special session on indicator mineral research at the meeting. A collection of papers, edited by the BCGS and GSC, and devoted to recent developments in indicator mineral research and focused on the Cordillera will be released at the 2017 GAC-MAC meeting in Kingston, Ontario. The volume will be the inaugural publication in the new “Topics in Minerals Science” series by the MAC and the first joint publication of the GAC and MAC.

### **2.3.4. Till Geochemistry of the Pendleton Bay map area (93K/12), central British Columbia**

Regional-scale-till geochemical surveys conducted by the BCGS, GSC, and other organizations have been effective at identifying covered mineralized bedrock sources, including both known and new mineral occurrences (Bustard and Ferbey, 2016). Data sets from these till geochemical surveys typically present determinations on silt-plus-clay size fraction for major, minor, and trace elements. The Pendleton Bay map area (93K/12) is relatively underexplored compared to other areas of the Interior Plateau with high potential for mineralization. Although samples were collected and analyzed in 1998 as part of the NATMAP Nechako Project, results from the Pendleton Bay map area were never released publicly and will be released in 2017.

### **2.3.5. New basal till potential maps for TREK Project study area**

Drift prospecting exploration maps were first produced in British Columbia by the BCGS in 1994 (Giles and Levson, 1994). The purpose of these maps was to represent the value of different surficial sediments for designing geochemical, lithological, and heavy mineral exploration programs. Building on the success of these maps, a new generation of the drift prospecting exploration maps (now called basal till potential maps) has been developed. The new basal till potential maps applies a potential rating to a material type and retains the individual unit’s material classification to provide more information. In collaboration with Geoscience BC, six



**Fig. 4.** Overlooking the Yukon River, participants of the indicator mineral field trip at the GAC-MAC annual meeting held in Whitehorse, hear about the Late Wisconsinan glaciation in the region.

1:50,000-scale basal till potential maps were completed for the TREK project area of the Interior Plateau and will be released in early 2017.

### 2.3.6. Coking Chemistry

Coke strength after reaction (CSR) is a globally accepted measure of how well a coking coal will perform in the blast furnace of a steel mill. The ash chemistry of a coking coal can have an effect on its CSR, which is more pronounced in coalfields that form in freshwater and brackish environments such as the Canadian Rocky Mountain coalfields of the Kootenays and the Peace River. In the past, major oxide analyses of coal ash were routinely done to predict the slagging and fouling properties of the coal. Since the early 1980s, when the importance of ash chemistry to coking coal quality was recognized, comprehensive analyses became more common and detailed. The ash chemistry data in COALFILE and other public sources are being compiled into a database for incorporation into the greater BCGS coal geochemical database. The data, mainly from non-confidential reports, will serve to evaluate the ash chemistry characteristics of the Mist Mountain, Gates and Gething formations.

## 3. Resource Information Section

The British Columbia Geological Survey creates, delivers, and archives geoscience data to help the mineral industry, resource planners, public safety agencies, communities,

First Nations, government, research organizations, and the general public make decisions related to the Earth sciences. In particular, the data and derived products increase exploration effectiveness by enabling users to efficiently gather regional information for property-scale evaluation, and help explorers advance projects without duplicating previous work.

### 3.1. MapPlace

Since 1995, MapPlace has provided web map services to help clients browse, visualize, and analyze geoscience and mineral resource data, such as geology, mineral occurrences, regional geochemical survey, assessment reports, surficial geology, geophysical survey, and mineral tenures. Building on its predecessor, MapPlace 2 beta is now available on the BCGS website. Relative to the original version, MapPlace 2 can be used on either a Mac or a PC, requires no plug-ins and works in most web browsers, has a simpler, more intuitive interface that is easy to use, accesses third-party base maps and imagery from sources such as Google, Bing Maps and OpenStreetMap, and displays province-level data at exceptional speeds. In contrast to other Canadian web map services, MapPlace 2 goes beyond simply displaying information. Databases are continuously updated and talk to each other, enabling users to conduct queries and generate custom results by connecting to current data from many sources. MapPlace 2 is designed for anyone who wants to reduce the costs of accessing and analyzing geoscience data in British Columbia, including the mineral industry, resource

planners, public safety agencies, communities, First Nations groups, government, research organizations, and the general public. Based on Cui et al. (2017), BCGS will offer workshops on how to use MapPlace 2 throughout 2017 (Fig. 5). BCGS will continue to improve MapPlace 2 with advanced applications and access to more databases.

### 3.2. Databases

ARIS is the searchable database of over 35,400 assessment reports submitted to the Ministry of Energy and Mines, in compliance with Mineral Tenure Act (MTA) Regulations. These reports summarize results from exploration programs on mineral claims. After a one-year confidentiality period, the reports become an open resource for planning mineral exploration, investment, research, land use, and resource management. Between 1967 and 2014, ARIS stored work representing expenditures of about \$2.8 billion (Fig. 6a). Digital data are available for download from 450 assessment reports through the ARIS search application and monthly tables.

COALFILE is a library of 990 Coal Assessment Reports submitted by exploration companies since 1900 (Fig. 6b). It includes data from about 15,400 boreholes, 550 bulk samples, 1000 maps, and 3600 trenches. MINFILE is an inventory documenting metallic mineral, industrial mineral, and coal

occurrences in the province. With more than 14,600 entries (Fig. 6c), the database is being updated continuously. Users can query MINFILE by location, identification number, mineralogy, commodity, host rock, deposit type, geological setting, age, production, and references. Property File is a collection of more than 59,600 government, university, personal, and industry documents donated to the British Columbia Geological Survey during the last 150 years (Fig. 6d). Previously available only in hard copy, these documents can now be searched for, and downloaded from, the Property File database. Property File contains: unpublished reports; theses; field notes; company prospectuses; correspondence; hand-drawn maps; claim maps; mine plans; photographs; and geological, geochemical, geophysical, and drill data. The BCGS accepts donations to Property File.

The provincial geochemical databases hold field and geochemical data from multi-media surveys by the GSC, the BCGS, and Geoscience BC. The databases are updated regularly and contain results from: 1) the Regional Geochemical Survey program (RGS) including analyses from stream-sediment, lake-sediment, moss, and water samples (Fig. 6e); 2) till surveys; and 3) rock samples. The current version of the RGS database was completely recompiled from original sources in 2015 (Rukhlov and Naziri, 2015) and consists of five MS Access tables with locations, field observations, analytical results and laboratories, and geology underlying sample sites for about 65,000 stream-, lake- and moss-sediment and water samples (Fig. 7). The analytical determinations include up to 63 analytes from sediment samples and up to 78 analytes from water samples (Fig. 8). Han et al. (2016) published an update to the provincial lithochemical database, which includes a new data model and rigorous quality control (Fig. 9). This database includes data from about 2000 papers and reports published by the BCGS, GSC and universities between 1986 and 2015. The data set consists of about 11,000 samples, including a quarter million determinations analyzed by 26 different methods in 21 laboratories.

### 3.3. British Columbia Digital Geology map

The BCGS has developed a 'geospatial frame data' (GFD) model to simplify compiling, updating, editing, and integrating geological maps into a province-wide spatial database for digital geology. Bedrock polygons are not part of the GFD but are generated from the GFD, which consists only of centroids (describing map units) and lines (defining geological boundaries). The GFD applications automate checking-out, anchoring, integrating, and creating bedrock polygons. These applications also streamline data quality checks, content standardization, and product delivery to web services. Integration of new compilations for the south Nicola, Chilcotin and Bonaparte, Atlin, Dease Lake, Iskut, and Bowser basin areas is currently underway (Fig. 10). The bedrock legend at the provincial scale also has a new colour scheme to highlight major geological units. The Digital Geology data download is updated regularly.

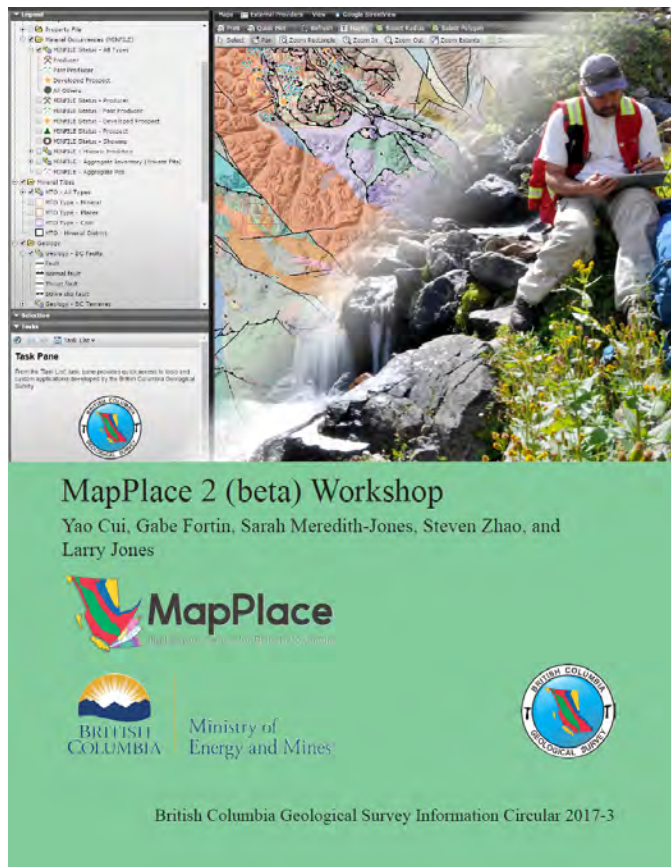


Fig. 5. Workshop notes for MapPlace 2 (Cui et al., 2017) can be downloaded at no charge from <http://www.empr.gov.bc.ca/mining/geoscience/publicationscatalogue/informationcirculares/pages/IC2017-3.aspx>.

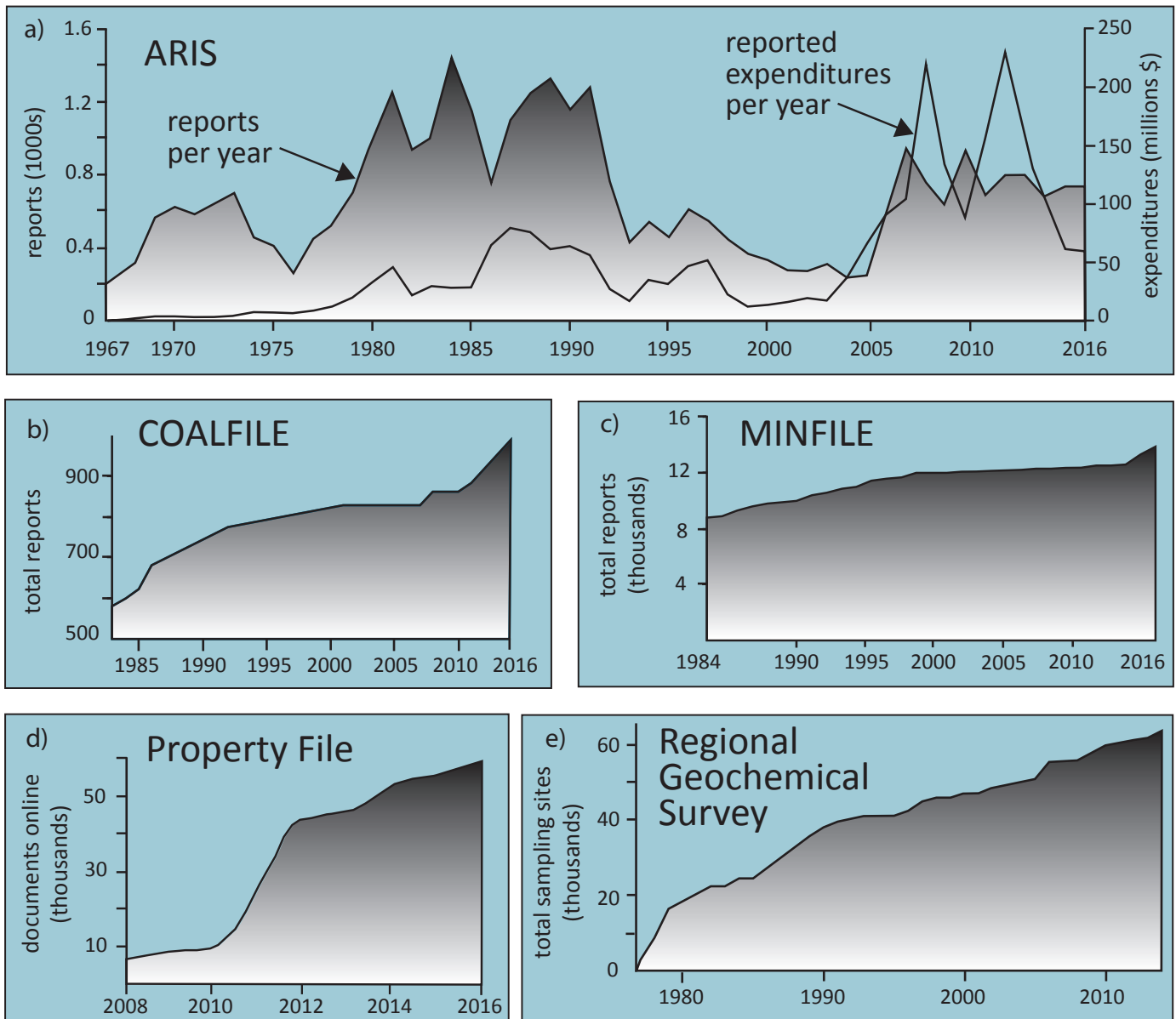


Fig. 6. Growth of key British Columbia Geological Survey databases.

### 3.4. Three-dimension geological modelling

The BCGS conducted a pilot project to test 3D modelling to generate a simple depth-to-bedrock predictive map for the Ootsa Lake porphyry Cu-Mo-Au district using datasets provided by Gold Reach Resources. The completed depth-to-bedrock model predicted overburden thicknesses based on extrapolation between drill holes, surface outcrops, and LiDAR data. When combined with geophysical data and geochemical anomalies identified from Regional Geochemical Survey (RGS) data, the depth-to-bedrock map has proven helpful in ranking exploration targets. Geochemical anomalies in areas of shallow cover ranked higher than similar geochemical anomalies in areas of thicker overburden.

### 4. Mineral Development Office

The British Columbia Mineral Development Office (MDO) in Vancouver provides mineral and coal resource information and is a point of contact on issues affecting the exploration and mining industries. Through formal and informal activities including conferences, business meetings, investment missions, and over the counter contacts, the MDO promotes the province's mineral and coal industries both domestically and abroad.

A primary output is the delivery of a technical marketing campaign that highlights the province's mineral and coal potential, geoscience resources, global expertise, and attractive business climate. This includes developing publications aimed at audiences from large foreign investors through to

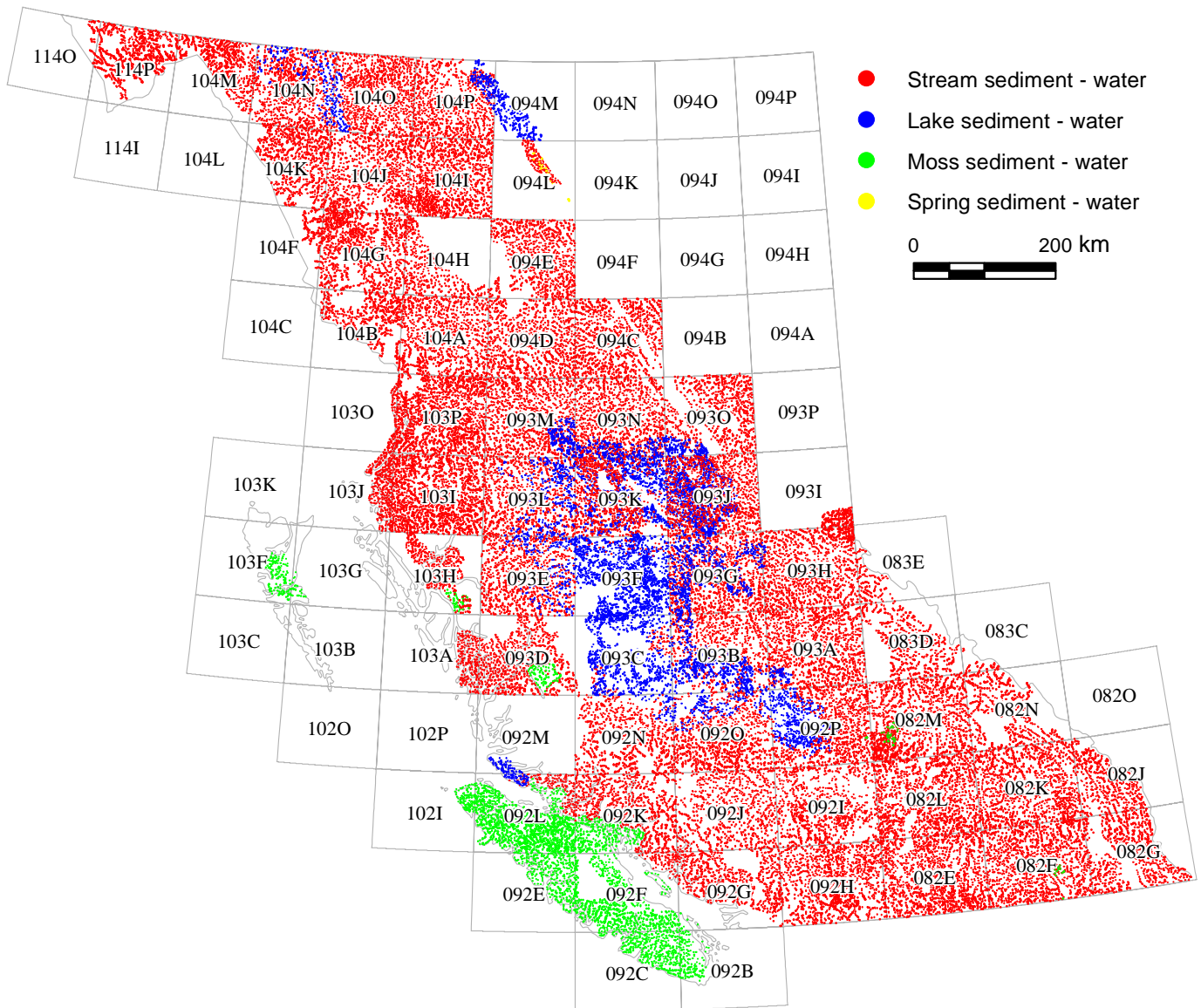


**Fig. 7.** Almost 65,000 regional geochemistry sites cover 80% of the province.

independent domestic entrepreneurs. These publications are distributed widely at conferences, business meetings, over the counter, and online.

In September of 2016, the MDO supported the Ministry of International Trade at a series of events in Asia. The MDO provided materials to raise British Columbia's profile at the China Mining Congress and Expo in Tianjin, the Canada Mineral Investment Forum in Beijing, the Canada Mineral Investment Forum in Seoul, and the Canada Mineral Investment Forum in Tokyo.

In October of 2016, the MDO was part of a British Columbia delegation that met with a visiting Qatari investment group at the Qatar Embassy in Ottawa. The Qatari government was interested in learning about investment opportunities in British

Columbia's non-renewable resource sector. In early 2017, delegates from Qatar along with those from the United Arab Emirates, Saudi Arabia and Kuwait, plan to visit Victoria and Vancouver for further discussions about investment opportunities in British Columbia.

The MDO oversees publication of the "Provincial Overview of Exploration and Mining in British Columbia" a document containing an overview of mineral exploration and mining activities in the different regions of BC written by the Regional Geologists. The most recent annual summaries can be found in Clarke et al. (2017; Provincial overview of exploration and mining in British Columbia, 2016) and BCGS (2017; Coal industry overview, 2016).

Master ID: 092I091691			
SUMMARY			
NTS Map Sheet 092I	Physiography: 3	<b>Lake</b>	<b>Moss Mat</b>
Sample ID: 092I091691	Drainage Pattern: 1	Area (km <sup>2</sup> ): -1	Height (m): -1
UTM Zone: 10	Site Contamination: 8	Perimeter (km): -1	Color: -1
UTM East (NAD27): 643599	Stream Width (m): 1	Depth (m): -1	Health: -1
UTM North (NAD27): 5583407	Stream Depth (cm): 20	Relief: -1	Host: -1
UTM East (NAD83): 643505	Water Color: 0	Water Color: -1	Thickness (m): -1
UTM North (NAD83): 5583614	Bank Precipitation: 0	Sediment Colour: -1	
Latitude: 50.38705	Sediment Composition: 310	Sediment Composition: -1	
Longitude: -120.98128	Sediment Colour: 8	Possible Site Contamination Source: -1	
Elevation (m): 1590	Sediment Precipitation: 0	<b>Waters</b>	
Sample Type: 6	Channel Bed: 3	pH: 7.29	
Replicate Sample Status: 0	Channel Pattern: 1	U: -1	
Stream source: 0		F: 33	
Stream Order: 2		SO4: -1	
Stream type: 1			

AAS Data			ICPMS Data			INAA Data		
Element	Analysis	Unit	Element	Analysis	Unit	Element	Analysis	Unit
Cu	-1	ppm	Al	1.72	%	Au	2	ppb
Pb	-1	ppm	Sb	0.36	ppm	First Duplicate of Au	-1	ppb
Ni	-1	ppm	As	16.2	ppm	Second Duplicate of Au	-1	ppb
Co	-1	ppm	Ba	1060	ppm	Sb	0.6	ppm
Ag	-1	ppm	Bi	0.24	ppm	As	18	ppm
Mn	-1	ppm	Cd	0.6	ppm	Ba	1500	ppm
Fe	-1	%	Ca	1.44	%	Br	48	ppm
Mo	-1	ppm	Cr	13	ppm	Ce	72	ppm
Sn	-1	ppm	Co	16.6	ppm	Cs	-1	ppm
Hg	-1	ppb	Cu	874.1	ppm	Cr	51	ppm
As	-1	ppm	Ga	4.9	ppm	Co	22	ppm
Sb	-1	ppm	Au	2.1	ppb	Eu	-1	ppm
Ba	-1	ppm	Fe	6.21	%	Hf	6	ppm
Cd	-1	ppm	La	44.5	ppm	Fe	7.3	%
V	-1	ppm	Pb	13.47	ppm	La	55	ppm
Bi	-1	ppm	Mg	0.33	%	Lu	0.6	ppm
Cr	-1	ppm	Mn	8355	ppm	Mo	65	ppm
Se	-1	ppm	Hg	210	ppb	Ni	10	ppm
Zn	-1	ppm	Mo	63.51	ppm	Rb	39	ppm
			Ni	12.8	ppm	Sm	10	ppm
			P	0.11	ppm	Sc	13	ppm
			K	0.07	%	Na	1.3	%

Fig. 8. Sample report from MapPlace for a regional geochemical survey data point.

### 5. Regional Geologists

The British Columbia Regional Geologists (Table 1) represent the provincial government on geological matters at a regional level and capture information on industry activity in their jurisdictions. Within their communities, they provide information on exploration trends, possible investment opportunities, land use processes, First Nation capacity building, and public outreach.

Table 1. British Columbia's regional geologists.

Regional Geologist	Office	Region
Vacant	Smithers	Northwest
Paul Jago	Prince George	Northeast and North Central
Jim Britton	Kamloops	South Central
Fiona Katay	Cranbrook	Southeast
Bruce Northcote	Vancouver	Southwest

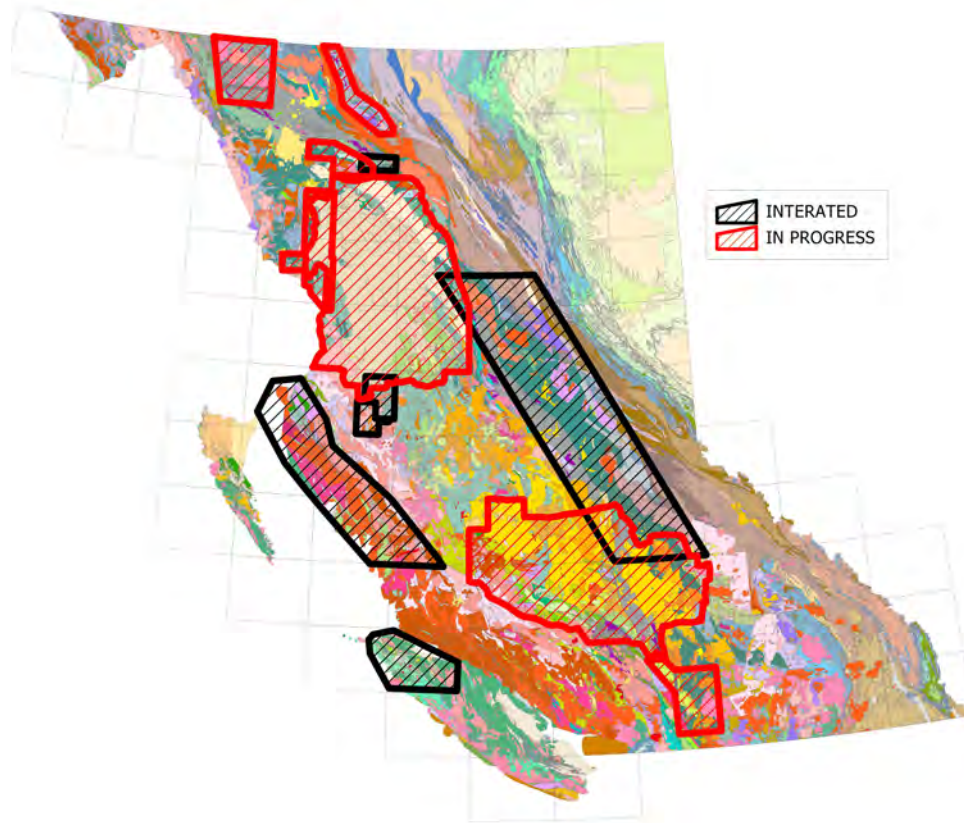


Fig. 9. Areas with recent and ongoing updates to the British Columbia digital geology map.

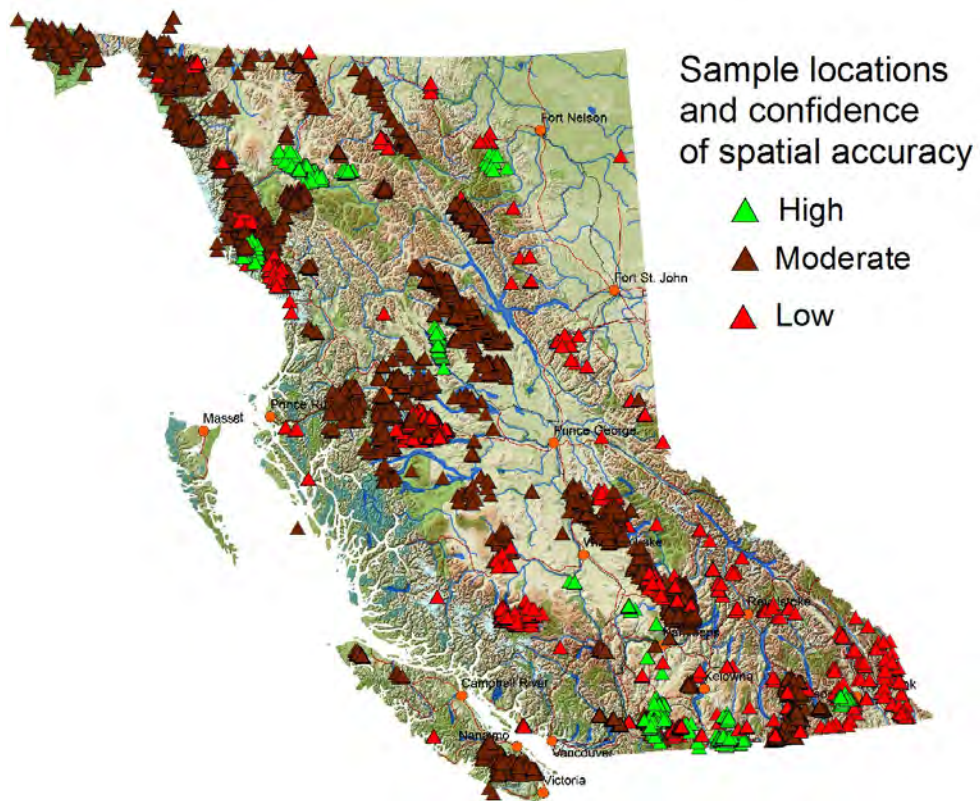


Fig. 10. Lithochemistry data distribution with location confidence.

## 6. Staffing announcements

The Survey was strengthened in 2016 by the addition of Gabe Fortin and Dejan Milidragovic (Fig. 11). Gabe joins us as a Geomatics Geologist focused on advancing MapPlace 2 and Dejan is a Senior Project Geologist specializing in Ni-Cu-PGE metallogeny and ultramafic-mafic rocks. Congratulations also goes out to JoAnne Nelson, a 30-year veteran of the BCGS and recipient of a Special Tribute by the Association for Mineral Exploration in recognition of her distinguished career in geoscience work focused on Cordilleran tectonics and metallogeny.

Laura de Groot, ARIS/MINFILE Database Manager will be retiring after 35 years with the Provincial Government, 31 of which were with the Survey. Laura played an important role in computerizing the MINFILE and ARIS and continues to work on enhancements to both systems and linking them to other datasets. We wish Laura a happy retirement.



**Fig. 11.** New staff at the British Columbia Geological Survey Victoria office. **a)** Dr. Dejan Milidragovic, Senior Minerals Geologist – Nickel metallogeny and igneous geology and **b)** Gabe Fortin Geomatics Geologist.

## Acknowledgment

We thank George Owsiacki of Total Earth Science Services (Victoria) for desktop publishing of this volume.

## References cited

- Angen, J.J., Nelson, J.L., Rahimi, M., and Hart, C.J.R., 2017. Mapping in the Tatsi and Zymo ridge areas of west-central British Columbia: Implications for the origin and history of the Skeena Arch. In: Geological Fieldwork 2016, British Columbia Ministry of Energy and Mines, British Columbia Geological Survey Paper 2017-1, this volume.
- Arnold, H., and Hickin, A.S., 2017. Using derived-stereo imagery to map macroscale ice-flow features. In: Geological Fieldwork 2016, British Columbia Ministry of Energy and Mines, British Columbia Geological Survey Paper 2017-1, this volume.
- Arnold, H., Ferbey, T., and Hickin, A.S., 2016. Ice-flow indicator compilation, British Columbia and Yukon. British Columbia Ministry of Energy and Mines, British Columbia Geological Survey, Open File 2016-04; Geological Survey of Canada, Open File 8083, 1:1,750,000 scale.
- British Columbia Geological Survey, 2017. British Columbia Coal Industry Overview 2016. Ministry of Energy and Mines, British Columbia Geological Survey Information Circular 2017-2, 14p.
- British Columbia Geological Survey, 2016. The Groundhog coalfields. British Columbia Ministry of Energy and Mines, British Columbia Geological Survey Information Circular 2016-5 (poster).
- British Columbia Geological Survey, 2015a. The East Kootenay coalfields. British Columbia Ministry of Energy and Mines, British Columbia Geological Survey Information Circular 2015-10 (poster).
- British Columbia Geological Survey, 2015b. The Peace River coalfields. British Columbia Ministry of Energy and Mines, British Columbia Geological Survey Information Circular 2015-11 (poster).
- Bustard, A.L., and Ferbey, T., 2016. An index of base and precious metal regional- to property-scale subglacial till geochemical and mineralogical surveys in British Columbia. British Columbia Ministry of Energy and Mines, British Columbia Geological Survey Open File 2016-2, 1:2,250,000 scale.
- Clarke, G., Britton, J., Jago, P., Katay, F., and Northcote, B., 2017. Provincial overview of exploration and mining in British Columbia, 2016. British Columbia Ministry of Energy and Mines, British Columbia Geological Survey Information Circular 2017-1, in press.
- Cui, Y., Fortin, G., Meredith-Jones, S., Zhao, S., and Jones, L., 2017. MapPlace 2 (beta) workshop. British Columbia Ministry of Energy and Mines, British Columbia Geological Survey Information Circular 2017-3, 89p.
- Dawson, G.M., 1879. Preliminary report on the physical and geological features of the southern portion of the interior of British Columbia, 1877; Geological Survey of Canada, Progress Report, 1877–1878, pp. 96B–101B.
- Ferbey, T., Arnold, H., and Hickin, A.S., 2013. Ice-flow indicator compilation, British Columbia. British Columbia Ministry of Energy and Mines, British Columbia Geological Survey Open File 2013-06, 1:1,650,000 scale.
- Ferbey, T., Plouffe, A., and Bustard, A., 2016. Geochemical, mineralogical, and textural data from tills in the Highland Valley Copper mine area, south-central British Columbia. British Columbia Ministry of Energy and Mines, British Columbia Geological Survey Geofile 2016-11, 15p.
- Giles, T.R., and Levson, V.M., 1994. Drift prospecting potential of the Fawnie Creek area, NTS 93 F/3. Ministry of Energy, Mines and Petroleum Resources, British Columbia Geological Survey Open File 1994-10, 1:50,000 scale.
- Green, C., Simandl, G.J., Paradis, S., Katay, F., Hoshino, M., Kon, Y., Kodama, S., and Graf, C., 2017. Geological setting of the Rock Canyon Creek REE-fluorite deposit, British Columbia, Canada In: Geological Fieldwork 2016, British Columbia Ministry of Energy and Mines, British Columbia Geological Survey Paper 2017-1, this volume.
- Han, T., Rukhlov, A.S., Naziri, M., and Moy, A., 2016. New British Columbia lithochemical database: Development and preliminary data release. British Columbia Ministry of Energy and Mines, British Columbia Geological Survey GeoFile 2016-4, 6p.
- Hoshino, M., Kon, Y., Kodama, S., Simandl, G.J., Paradis, S., Green, C., Namatame, C., Matsunaga, I., and Takagi, T., 2017. Mineralogy of the Rock Canyon Creek REE-fluorite deposit, British Columbia, Canada. In: Geological Fieldwork 2016, British Columbia Ministry of Energy and Mines, British Columbia Geological Survey Paper 2017-1, this volume.
- Iverson, O., Mahoney, J.B., and Logan, J.M., 2012. Dease Lake geoscience project, part IV: Tsaybahe group: Lithological and geochemical characterization of Middle Triassic volcanism in the Stikine arch, north-central British Columbia. In: Geological Fieldwork 2011, British Columbia Ministry of Energy and Mines, British Columbia Geological Survey Paper 2012-1, pp. 17–22.
- Jackaman, W., and Sacco, D.A., 2014. Regional Geochemical and Mineralogical Data, TREK Project, Interior Plateau, British Columbia. Geoscience BC Report 2014-10, 13p.
- Jackaman, W., Sacco, D.A., and Lett, R.E., 2015. Regional Geochemical and Mineralogical Data, TREK Project – Year 2,

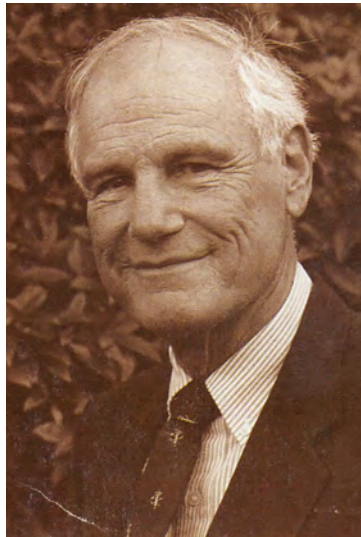
- Interior Plateau, British Columbia. Geoscience BC Report 2015-12, 13p.
- Lipovsky, P.S., and Bond, J.D., 2014. Yukon surficial geology compilation, digital release 1, 08-Apr-2014. Yukon Geological Survey.
- Logan, J.M., Moynihan, D.P., Diakow, L.J., and van Straaten, B.I., 2012. Dease Lake - Little Tuya River geology (NTS 104J/08, 07E). British Columbia Ministry of Energy and Mines, British Columbia Geological Survey Open File 2012-04, scale: 1:50,000.
- Mihalynuk, M.G., Zagorevski, A., Orchard, M.J., English, J.M., Bidgood, A.K., Joyce, N., and Friedman, R.M., 2017a. Geology of the Sinwa Creek area (104K/14). In: Geological Fieldwork 2016, British Columbia Ministry of Energy and Mines, British Columbia Geological Survey Paper 2017-1, this volume.
- Mihalynuk, M.G., Zagorevski, A., Devine, F.A.M., and Humphrey, E., 2017b. A new lode gold discovery at Otter Creek: Another source for the Atlin placers. In: Geological Fieldwork 2016, British Columbia Ministry of Energy and Mines, British Columbia Geological Survey Paper 2017-1, this volume.
- Mildragovic, D., Zagorevski, A., and Chapman, J.B., 2017. The Mount Hickman ultramafic complex: An Fe-rich Alaskan-type ultramafic intrusion. In: Geological Fieldwork 2016, British Columbia Ministry of Energy and Mines, British Columbia Geological Survey Paper 2017-1, this volume.
- Mao, M., Rukhlov, A.S., Rowins, S.M., Spence, J., and Coogan, L.A., 2016. Apatite trace-element compositions: A robust new tool for mineral exploration. *Economic Geology*, 111, pp. 1187-1222.
- Nelson, J., 2017. Composite pericratonic basement of west-central Stikinia and its influence on Jurassic magma conduits: Examples from the Terrace-Ecstall and Anyox areas. In: Geological Fieldwork 2016, British Columbia Ministry of Energy and Mines, British Columbia Geological Survey Paper 2017-1, this volume.
- Nelson, J.L., Kennedy, R., Angen, J., and Newman, S., 2007. Geology of the Terrace Map Area (103I 9,10,15,16), British Columbia; British Columbia Ministry of Energy, Mines and Petroleum Resources, British Columbia Geological Survey Open File 2007-4, 1:70,000.
- Nelson, J.L., Kyba, J., McKeown, M., and Angen, J., 2008a. Terrace Regional Mapping Project, Year 3: Contributions to Stratigraphic, Structural and Exploration Concepts, Zymoetz River to Kitimat River, East-Central British Columbia (NTS 103I/08); In Geological Fieldwork 2007, British Columbia Ministry of Energy, Mines and Petroleum Resources, British Columbia Geological Survey Paper 2008-1, pp.159-173.
- Nelson, J.L., Kyba, J., McKeown, M., and Angen, J., 2008b. Geology of the Chist Creek map area (103I/08); British Columbia Ministry of Energy, Mines and Petroleum Resources, British Columbia Geological Survey Open File 2008-3, 1:50,000 scale.
- Ootes, L., Elliott, J.M., and Rowins, S.M., 2017. Testing the relationship between the Llewellyn fault, gold mineralization, and Eocene volcanism in northwest British Columbia: A preliminary report. In: Geological Fieldwork 2016, British Columbia Ministry of Energy and Mines, British Columbia Geological Survey Paper 2017-1, this volume.
- Plouffe, A., and Ferbey, T., 2015. Surficial geology, Gnawed Mountain area, British Columbia (Parts of NTS 92I/6, 7, 10, 11). Geological Survey of Canada, Geoscience Map 214 (preliminary); British Columbia Ministry of Energy and Mines, British Columbia Geological Survey, Geoscience Map 2015-03, 1:50,000 scale.
- Precision GeoSurveys Inc., 2016. Airborne magnetic survey, SeArch project. Geoscience BC, Report 2016-02, 62 p. <<http://www.geosciencebc.com/s/Report2016-02.asp>> last accessed December, 2016.
- Rukhlov, A.S., and Naziri, M., 2015. New British Columbia's Regional Geochemical Survey (RGS) Database. British Columbia Ministry of Energy and Mines, British Columbia Geological Survey Geofile 2015-03, 4p.
- Rukhlov, A.S., Plouffe, A., Ferbey, T., Mao, M., and Spence, J., 2016. Application of trace-element compositions of detrital apatite to explore for porphyry deposits in central British Columbia. In: Geological Fieldwork 2015, British Columbia Ministry of Energy and Mines, British Columbia Geological Survey Paper 2016-1, pp. 145-179.
- Schiarizza, P., 2016. Toward a regional stratigraphic framework for the Nicola Group: Preliminary results from the Bridge Lake – Quesnel River area. In: Geological Fieldwork 2015, British Columbia Ministry of Energy and Mines, British Columbia Geological Survey Paper 2016-1, pp. 13-30.
- Schiarizza, P., 2017. Ongoing stratigraphic studies in the Nicola Group: Stump Lake – Salmon River area, south-central British Columbia. In: Geological Fieldwork 2016, British Columbia Ministry of Energy and Mines, British Columbia Geological Survey Paper 2017-1, this volume.
- van Straaten, B.I., and Gibson, R., 2017. Late Early to Middle Jurassic Hazelton Group volcanism and mineral occurrences in the McBride-Tanzilla area, northwest British Columbia. In: Geological Fieldwork 2016, British Columbia Ministry of Energy and Mines, British Columbia Geological Survey Paper 2017-1, this volume.
- van Straaten, B.I., and Nelson, J.L., 2016. Syncollisional late Early to early Late Jurassic volcanism, plutonism, and porphyry-style alteration on the northeastern margin of Stikinia. In: Geological Fieldwork 2015, British Columbia Ministry of Energy and Mines, British Columbia Geological Survey Paper 2016-1, pp. 113-143.
- van Straaten, B.I., Logan, J.M., and Diakow, L.J., 2012. Mesozoic magmatism and metallogeny of the Hotailuh Batholith, northwestern British Columbia. British Columbia Ministry of Energy, Mines and Natural Gas, British Columbia Geological Survey Open File 2012-06, 58p.
- Zagorevski, A., Mihalynuk, M.G., Joyce, N., and Anderson, R.G., 2017. Late Cretaceous magmatism in the Atlin-Tagish area, northern British Columbia (104M, 104N). In: Geological Fieldwork 2016, British Columbia Ministry of Energy and Mines, British Columbia Geological Survey Paper 2017-1, this volume.

## In Memoriam

The Survey is saddened to report the passing of former Chief Geologist (1975-1984) Dr. Atholl Sutherland Brown in December, 2016.

Dr. Atholl Sutherland Brown, who served as British Columbia's 8th Chief Geologist from 1975 to 1984, died in Victoria at the age of 93. Atholl was born in Ottawa, but grew up mainly in Victoria. He joined the Royal Canadian Air Force in 1941 and, as a member of the Royal Air Force in Burma, flew 48 missions and was awarded the Distinguished Flying Cross. After the war, Atholl attended the University of British Columbia and subsequently earned a Ph.D. in geology at Princeton. He joined the British Geological Survey in 1951 and was involved in early mapping of the Cariboo and the Queen Charlotte Islands (Haida Gwaii). Atholl was an excellent scientist and wrote numerous papers on the geology and mineral deposits of British Columbia, especially porphyry copper and molybdenum deposits. This expertise led to his editorship of the Canadian Institute of Mining and Metallurgy Special Volume No. 15 on "Porphyry Deposits of the Canadian Cordillera". Atholl also authored several books including two published by the Geological Association of Canada. The first was "British Columbia's Geological Surveys 1895-1995: A Century of Science and Dedication", which was a lively history of the British Geological Survey and its gyrations published in 1998 to mark its 100th year anniversary. His most recent book "Searching for the Origins of Haida Gwaii - Adventures While Mapping the Geology of the Islands 1958-1962" was published in 2013 and is a testament to his incredible energy and fine intellect right to the end of his life. Atholl was a natural leader always looking for ways to give back to the geological community. He served as President of the Geological Association of Canada in 1980 and was a charter member of the Committee of Provincial and Territorial Geologists. The Committee remains instrumental in establishing closer relationships amongst the provincial, territorial and federal geological surveys.

Atholl was an active member of the Victoria geological community and could be counted on to show up at the Survey's alumni golf tournament, Open House, and various social events. He was held in very high regard by the Canadian geological community and will be greatly missed.



# Ongoing stratigraphic studies in the Nicola Group: Stump Lake – Salmon River area, south-central British Columbia



Paul Schiarizza<sup>1, a</sup>

<sup>1</sup> British Columbia Geological Survey, Ministry of Energy and Mines, 300-865 Hornby Street, Vancouver, BC, V6Z 2G3

<sup>a</sup> corresponding author: Paul.Schiarizza@gov.bc.ca

Recommended citation: Schiarizza, P., 2017. Ongoing stratigraphic studies in the Nicola Group: Stump Lake – Salmon River area, south-central British Columbia. In: Geological Fieldwork 2016, British Columbia Ministry of Energy and Mines, British Columbia Geological Survey Paper 2017-1, pp. 17-33.

## Abstract

A regional-scale stratigraphic framework for arc-related volcano-sedimentary rocks of the Nicola Group (Triassic), the defining supracrustal element of the Quesnel arc terrane in southern British Columbia, remains lacking. As part of a multi-year project to address this problem, and building on work started in 2015 in the Bridge Lake – Quesnel River area, mapping in 2016 covered the eastern part of the Nicola belt southeast of Kamloops, between Stump Lake and the Salmon River. Here, the Nicola Group is subdivided into 3 units, which show strong similarities to 3 of the 4 assemblages established in the Bridge Lake – Quesnel River area. Most widespread is the volcanic sandstone unit (assemblage two), consisting of plagioclase-pyroxene sandstone, locally intercalated with volcanic conglomerate and siltstone. The pyroxene basalt unit (assemblage three), overlies the volcanic sandstone unit in the western part of the area, and consists of massive pyroxene-phyric basalt and related breccia. The polymictic conglomerate unit (assemblage 4) comprises conglomerate with a distinctive clast population that includes mafic plutonic rocks. It overlies the volcanic sandstone unit in the eastern part of the area, across a suspected unconformity. Another Triassic unit, the Salmon River succession, includes conglomerate, carbonate-cemented sandstone, and siltstone that occur east of the Nicola Group, where they overlie Paleozoic schist of the Chapperon Group across an angular unconformity. These rocks are correlated with the Slocan Group, and are part of a siliciclastic basin that formed east of, and coeval with, the Nicola arc.

**Keywords:** Nicola Group, Upper Triassic, volcanic sandstone, pyroxene-phyric basalt, conglomerate, Salmon River succession, Slocan Group, Chapperon Group, Quesnel terrane

## 1. Introduction

Quesnel terrane, extending the full length of the Canadian Cordillera (Fig. 1), is an important metallogenic belt that hosts numerous Cu-Au-Mo porphyry and skarn deposits. It is characterized by a Mesozoic arc complex that includes Triassic to Jurassic volcanic and sedimentary rocks and related calcalkaline and alkaline intrusions. In south-central British Columbia the defining supracrustal component is the Nicola Group (Triassic). Although studied for more than a century, with numerous informal subdivisions applied in different areas by authors working at different times and scales, no regional-scale stratigraphy has been established. Therefore, in 2015, the British Columbia Geological Survey initiated a multi-year field-based program to synthesise Nicola Group lithostratigraphy and establish a regional stratigraphic framework. This framework, combined with space-time-composition patterns of spatially associated plutons, will contribute to a better understanding of the architecture of the arc, and help establish the settings and controls of mineral occurrences.

In 2015, initial investigations were carried out in the Bridge Lake – Quesnel River area, where Triassic rocks were separated into Nicola and Slocan groups, and the Nicola rocks subdivided into four broad stratigraphic assemblages (Fig. 2; Schiarizza,

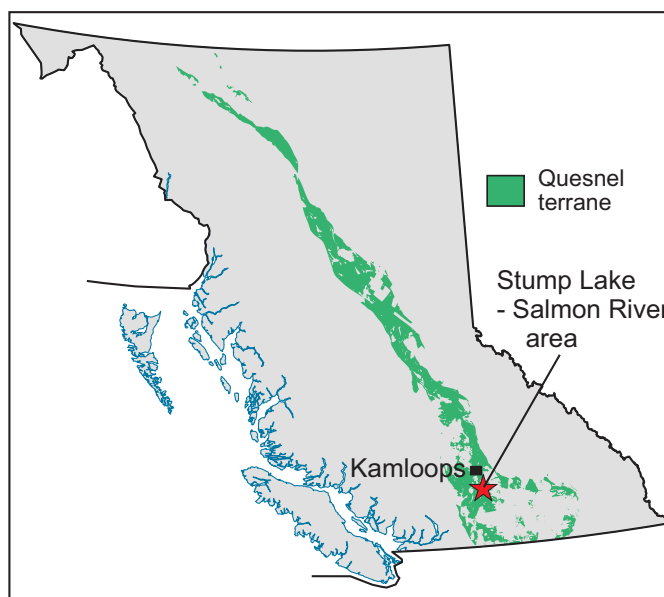


**Fig. 1.** Location of the Stump Lake – Salmon River area and distribution of Quesnel terrane in British Columbia.

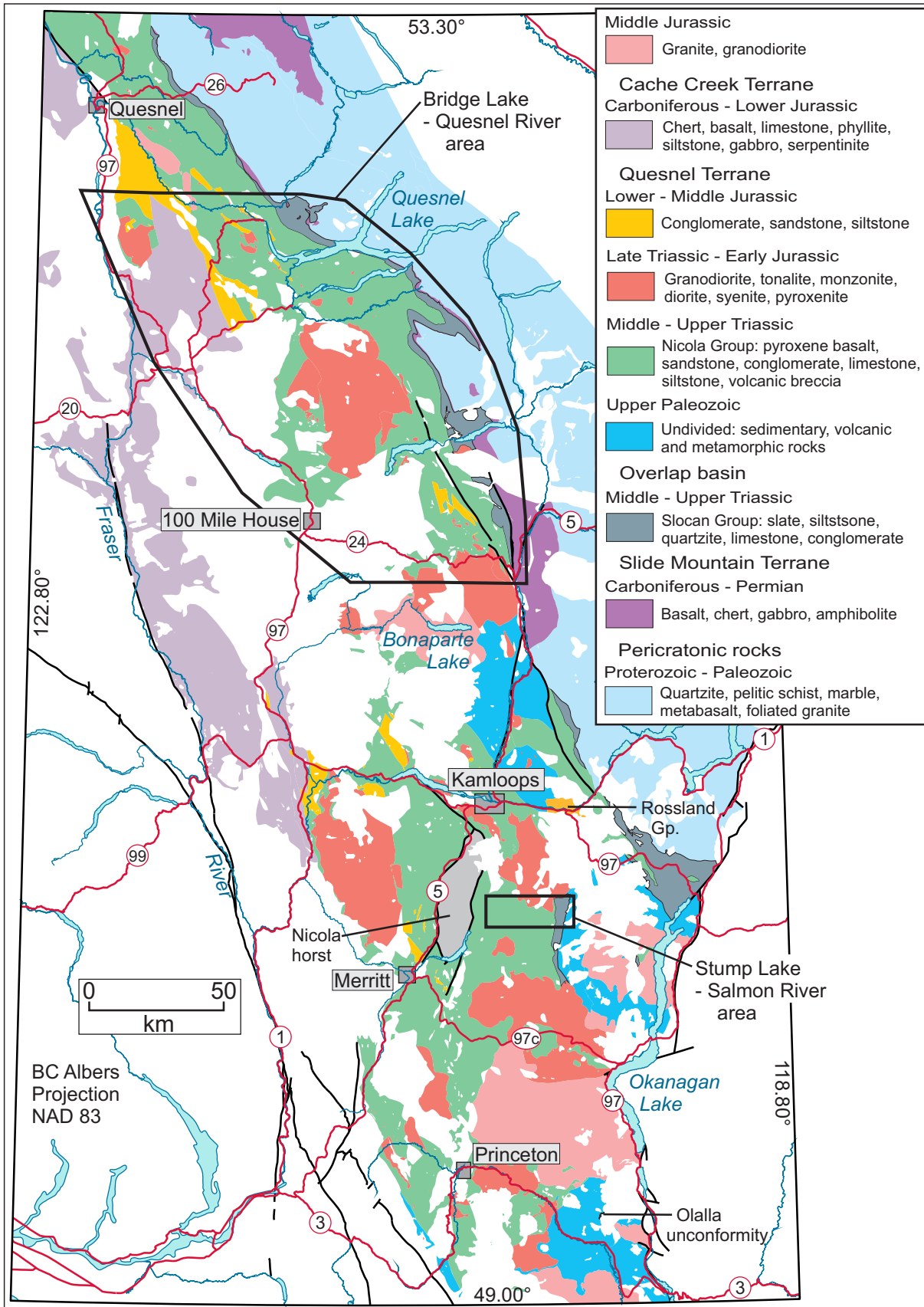


Fig. 2. Geological map of south-central British Columbia showing distribution of Nicola Group, and locations of the Bridge Lake – Quesnel River and Stump Lake – Salmon River study areas. Uncoloured areas mainly Late Jurassic to Recent intrusive, volcanic and sedimentary rocks.

2016). Summarized herein are the results of mapping in a relatively small area in the eastern part of the Nicola belt south of Kamloops, between Stump Lake and the Salmon River (Fig. 2). Nicola Group subdivisions established in this area show some strong similarities to those established to the north, and will compliment recent detailed mapping in the central part of the Nicola belt to the southwest (Mihalynuk et al., 2016).

## 2. Setting

The Stump Lake – Salmon River area is in the central part of the Thompson Plateau physiographic province (Holland, 1976) and encompasses parts of the traditional territories of the Nlaka'pamux, Syilx, and Secwepemc First Nations. Highway 5A, connecting Kamloops and Merritt, is along the west edge of the mapped area, Douglas Lake road crosses the eastern part of the area, and the intervening parts of the map area include numerous Forest Service and logging roads that provide good access. Most of the Stump Lake – Salmon River area is in the Ashcroft (92I) NTS map sheet. The regional geology here was described by Cockfield (1948) and updated by Monger and McMillan (1989), Moore (1989), and Moore et al. (1990). The eastern part of the area is in the Vernon (82L) NTS map sheet, and the geology was described by Jones (1959), with updates and revised interpretations by Preto (1964), Okulitch and Cameron (1976), Read and Okulitch (1977), Okulitch (1979), Daughtry et al. (2000), Daughtry and Thompson (2004), and Thompson et al. (2006).

The Nicola Group (Triassic), the predominant component of the Quesnel arc terrane, forms a continuous belt, 25 to 90 km wide, between the town of Quesnel and the international boundary (Fig. 2). This belt also includes abundant Late Triassic to Early Jurassic calcalkaline and alkaline arc intrusions, and fault-bounded panels of Lower to Middle Jurassic arc-derived siliciclastic sedimentary rocks, which are assigned to the Dragon Mountain succession in the north (Logan and Moynihan, 2009), and the Ashcroft Formation to the south (Monger and McMillan, 1989). Younger rocks in this belt include Middle Jurassic through Eocene granitic intrusions, Cretaceous and Eocene volcanic and sedimentary rocks, and flat-lying Neogene and Quaternary basalt.

The northern and central parts of the Nicola belt are flanked to the west by late Paleozoic to early Mesozoic basalt, chert, and limestone of Cache Creek terrane, which is interpreted as an accretionary complex genetically related to the subduction that generated the Nicola arc. Faulted against the east side of the Nicola belt at this latitude are Triassic sedimentary rocks, mainly black phyllite, slate, and quartz sandstone, of the Slokan Group. These rocks were deposited in a basin that formed above Late Paleozoic oceanic rocks (chert, basalt, gabbro) of Slide Mountain terrane, and Paleozoic pericratonic rocks (quartzite, pelitic schist, limestone), that were juxtaposed by east-directed thrusting in the Late Permian or Early Triassic (Schiarizza, 1989; McMullin, 1990; McMullin et al., 1990).

The southern part of the Nicola belt is flanked to the east by several assemblages of Paleozoic rocks, which have been

included in Quesnel terrane and interpreted as part of the Paleozoic basement on which the Mesozoic arc formed. The Paleozoic rocks north and northeast of Kamloops, and those along and west of northern Okanagan Lake, are included in the Harper Ranch Group (Smith, 1979; Beatty et al., 2006; Thompson et al., 2006), which includes late Paleozoic arc-derived volcanoclastic rocks and Carboniferous and Permian limestone. The exposures west of northern Okanagan Lake also include an inlier of undated schists, the Chapperon Group, which has been correlated with pericratonic rocks to the northeast (Jones, 1959), or inferred to represent a deformed belt of Harper Ranch rocks (Thompson et al., 2006). The southernmost part of the Nicola belt is juxtaposed, southeast of Princeton, with an assemblage of late Paleozoic rocks, including chert, basalt, argillite, limestone, siltstone, quartzite, sandstone and conglomerate, assigned to the Old Tom, Independence, Shoemaker, Bradshaw, Barslow and Blind Creek formations (Bostock, 1940, 1941; Mortensen et al., 2011) and, in part, included in the Apex Mountain Group interpreted by Milford (1984) as a pre-Late Triassic accretionary complex. The easternmost element of this Paleozoic belt comprises undated schists of the Kobau Group, which may correlate with the Chapperon Group to the north (Okulitch, 1973, 1979).

Permo-Triassic deformation, including east-directed thrusting, is documented in Paleozoic rocks of Slide Mountain and Quesnel terranes east of the Nicola belt, and is locally reflected in angular unconformities between these rocks and overlying Triassic sedimentary rocks (Read and Okulitch, 1977; McMullin et al., 1990). Some Triassic rocks above the unconformities have been included in the Nicola Group (Read and Okulitch, 1977), but their relationship to the main belt of Nicola volcanic and volcanoclastic rocks to the west is uncertain. Episodes of Middle Jurassic to Cretaceous contractional deformation are documented in rocks adjacent to, and along the margins of, the Nicola belt (Rees, 1987; Bloodgood, 1990; Phillipone and Ross, 1990; Greig, 1992), and contractional structures occur locally in the main belt of Nicola rocks (Panteleyev et al., 1996; Schiarizza et al., 2002; Mihalynuk et al., 2016), but are poorly understood. The most prominent structures in the Nicola belt are systems of dextral strike slip and extensional faults that formed mainly in the Eocene (Ewing, 1980; Moore et al., 1990; Schiarizza and Israel, 2001). These include normal faults west of Stump Lake that bound the Nicola horst (Fig. 2), an uplifted block of amphibolite-grade metamorphic rocks that includes metavolcanic rocks correlated with the Nicola Group, as well as Late Triassic metadiorite and metatonalite that also may be components of the Mesozoic Quesnel arc (Moore et al., 1990; Erdmer et al., 2002).

## 3. Geologic units

The Stump Lake – Salmon River area (Fig. 3) is underlain mainly by Triassic sedimentary and volcanic rocks of the Nicola Group, which is subdivided into three lithologic units (volcanic sandstone unit; pyroxene basalt unit; polymictic conglomerate unit). Sedimentary rocks in the eastern part

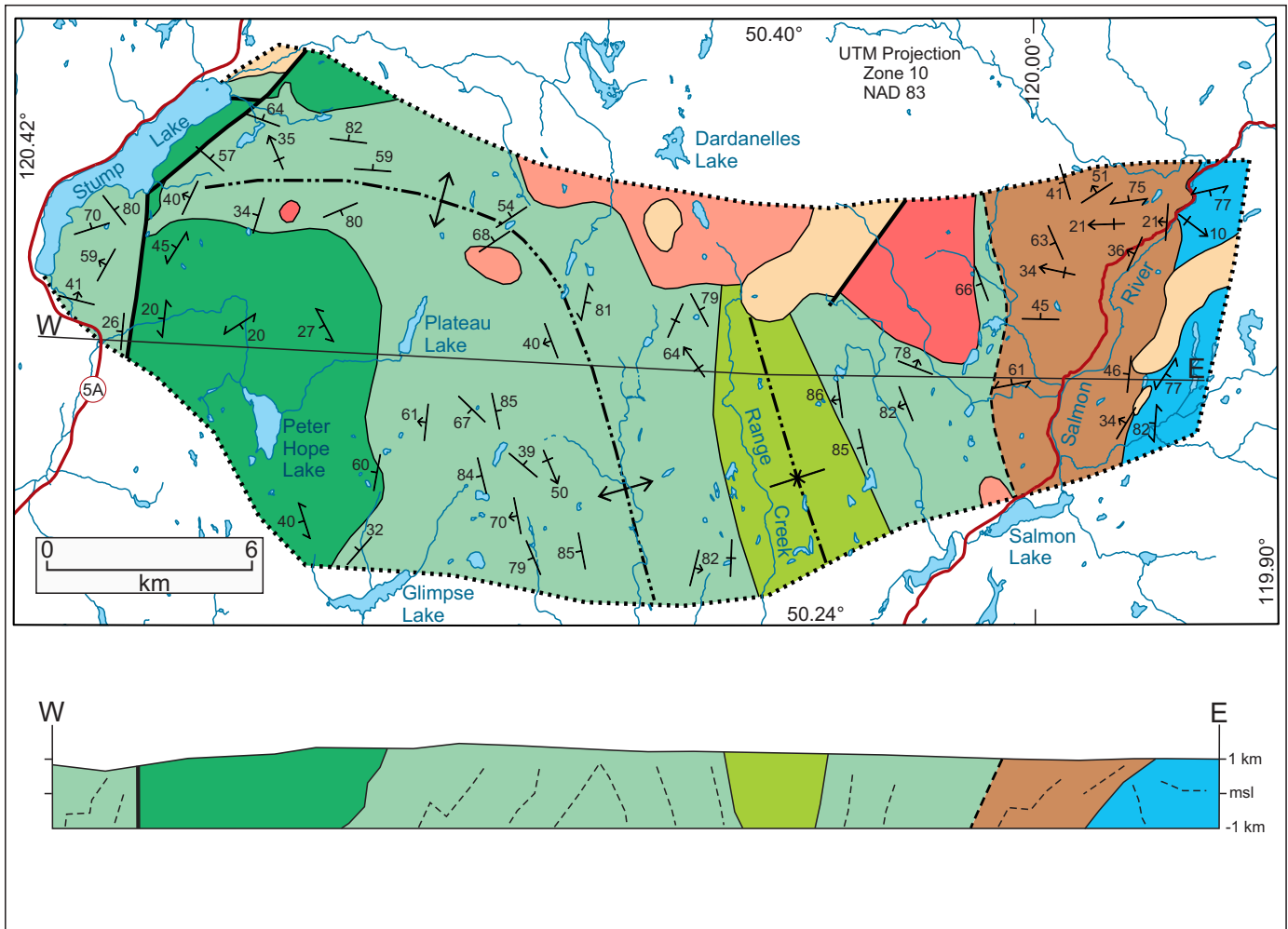


**Fig. 3a.** Geology of the Stump Lake – Salmon River area, with schematic vertical cross-section. Geology based on 2016 fieldwork, with distribution of Jurassic and Eocene rocks taken, in part, from Monger and McMillan (1989) and Daughtry and Thompson (2004).

of the area, also Triassic but of uncertain relationship to the Nicola Group, are assigned to the Salmon River succession. They rest unconformably above the oldest rocks in the map area, Paleozoic schists of the Chapperon Group, which crop out along its eastern edge. Younger rocks include intrusions of granodiorite, tonalite and diorite, Early Jurassic at least in part, and Eocene volcanic rocks of the Kamloops Group.

### 3.1. Chapperon Group

The Chapperon Group comprises greenschist-grade metamorphic rocks that crop out along the eastern edge of the Stump Lake – Salmon River map area, where they are unconformably overlain, to the west, by Triassic rocks of the Salmon River succession (see Jones, 1959; Preto 1964; Read and Okulitch, 1977; and Daughtry et al., 2000).

Much of the Chapperon Group in the current study area comprises fine-grained, medium to dark grey or greenish-grey phyllite and biotite phyllite, locally grading to weakly cleaved argillite or siltstone, and commonly containing many quartz±calcite veins. Massive and thinly bedded chert, and

less common fine-grained quartzite, form local narrow (<1 m) lenses in the phyllite. A section of thinly interbedded chert and quartz phyllite more than 20 m thick forms an isolated outcrop in the southern part of the unit, a short distance east of the unconformity. Dark green calcareous chlorite schist, probably derived from mafic volcanic rocks, is also common in the group, and locally contains lenses of white recrystallized limestone up to several metres thick (Fig. 4). Grey-green, crudely foliated talc-magnesite-serpentine schist, derived from an ultramafic protolith, was observed at two localities, but external contacts were not observed. Jones (1959) referred to these rocks as the Old Dave intrusions, and interpreted them as Paleozoic ultramafic dikes.

The Chapperon Group is undated, but the unconformity at the base of the Salmon River succession shows that the group, and the strong deformation fabrics within it, are pre-Late Triassic. Okulitch (1979) reported that limestone from the group near the Salmon River contains a structure resembling Late Ordovician – Silurian Halysitid corals but, as this structure is of dubious organic origin, this age was considered unreliable.

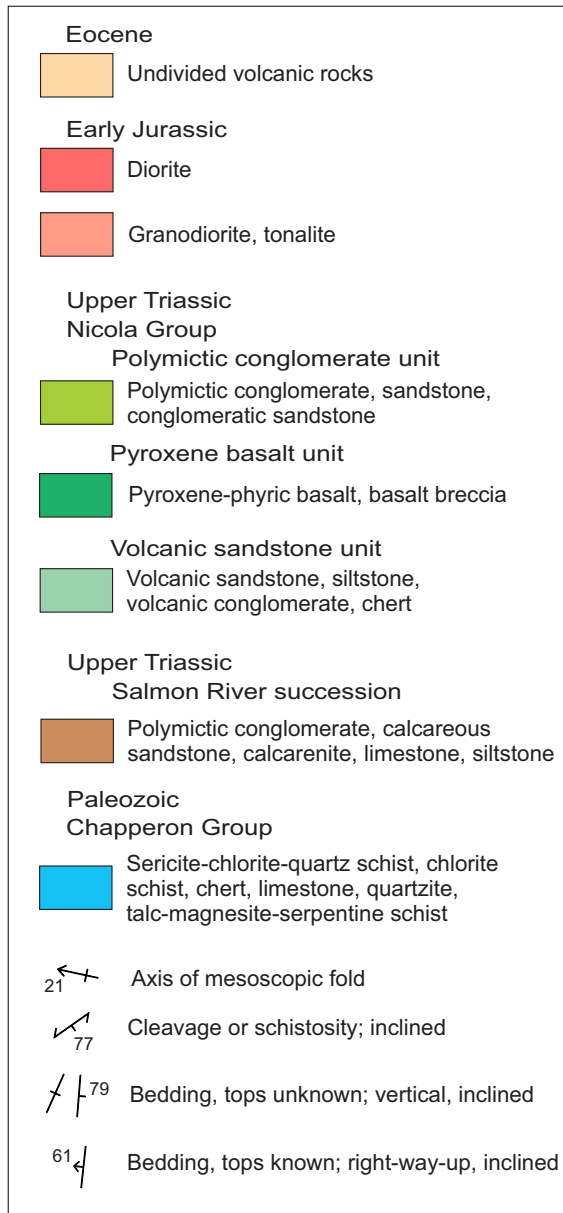


**Fig. 3b.** Legend for Figure 3a.

Stratigraphic relationships south of the current map area indicate that the group is pre-Permian, because it is overlain by, and infolded with, Permian conglomerate (Read and Okulitch, 1977; Okulitch, 1979). Thompson et al. (2006) included these Permian rocks in the Harper Ranch Group, and suggested that the Chapperon Group is a highly deformed belt of Harper Ranch rocks. The Chapperon Group has also been correlated with pericratonic rocks in the Shuswap Lake – Adams Lake area (Jones, 1959; Thompson and Daughtry, 1998), and with the undated, but probably Carboniferous or older, Kobau Group to the south (Okulitch, 1973, 1979).

### 3.2. Salmon River succession

The Salmon River succession forms a belt of Triassic sedimentary rocks, 3.5 to 6 km wide, in the eastern part of



**Fig. 4.** Chlorite schist with limestone boudin (beneath hammer), Chapperon Group, northeast corner of the study area, east of the Salmon River.

the Stump Lake – Salmon River map area. The base of the succession is exposed along the eastern edge of the belt, where it rests unconformably above the Chapperon Group. It is apparently juxtaposed against the Nicola Group (volcanic sandstone unit) to the west, but this contact is in a wide zone of poor exposure, and the nature of the contact is unknown. The rocks of the Salmon River succession were initially included in the Cache Creek Group (Carboniferous-Permian) by Cockfield (1948) and Jones (1959). Late Triassic conodonts were extracted from samples collected near the base of the succession (Campbell and Okulitch, 1973; Okulitch and Cameron, 1976), and the rocks were then assigned to the Nicola Group (Read and Okulitch, 1977; Okulitch, 1979) or Slocan Group (Daughtry and Thompson, 2004).

The predominant rock type in the Salmon River succession is thin to medium-bedded calcareous sandstone. Conglomerate forms a basal unit, from several metres to tens of metres

thick, and is also common elsewhere in the lower part of the succession, where it is intercalated with calcareous sandstone, limestone, calcarenite, and argillite. Siltstone and argillite form relatively thin units that are intercalated with coarser-grained units throughout the succession (above the basal conglomerate), and are apparently the predominant rock types in the poorly exposed westernmost part of the succession.

The basal unit of the Salmon River succession is medium to dark grey-green, poorly stratified polymictic conglomerate, comprising angular to subrounded clasts (mainly <1-5 cm, but locally ~20 cm) in a fine-grained carbonate-cemented sandstone matrix (Fig. 5). The clasts include chert, limestone, fine-grained quartzite, quartz phyllite, green volcanic or volcanoclastic rock, dark grey siliceous argillite, and vein quartz. Many of the clasts resemble rocks in the underlying Chapperon Group, from which they were probably derived.

The basal conglomerate is overlain by a heterogeneous section, estimated to be several hundred metres thick, which includes carbonate-cemented sandstone, conglomerate, limestone, calcarenite, siltstone and argillite. Brown-weathered carbonate-cemented sandstone predominates, and commonly occurs as intervals of thin-bedded, fine- to medium-grained sandstone, punctuated by thin to thick beds of medium- to coarse-grained sandstone. The thin sandstone beds locally display convolute lamination, cross stratification, graded bedding, and load casts, and are typically intercalated with thin beds or laminae of dark grey siltstone (Fig. 6). The medium to thick sandstone beds locally display normal grading, and may have laminated tops. The sandstones contain detrital grains of quartz, feldspar and fine-grained lithic fragments.

Pebble conglomerate is common in the lower part of the Salmon River succession (above the basal conglomerate unit), and typically forms medium to very thick graded beds



**Fig. 5.** Basal conglomerate of the Salmon River succession, northeast corner of the study area, west of the Salmon River.

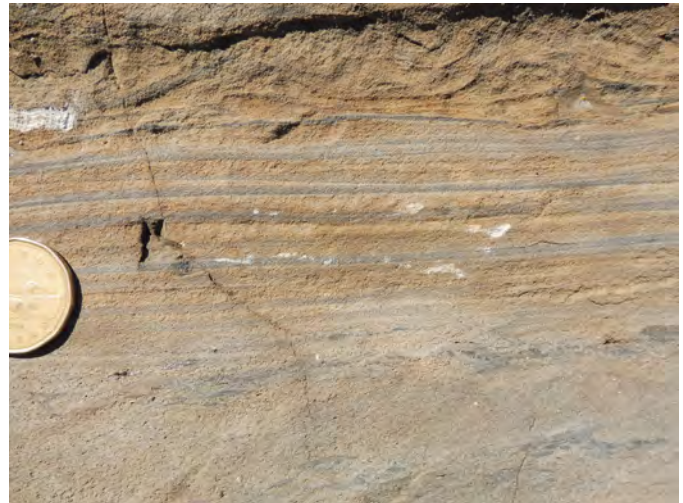


**Fig. 6.** Thin-bedded, medium-grained carbonate-cemented sandstone (brown) and siltstone (grey); grey mudchip intraclasts lower right; likely ripple-drift cross-stratification at top. Lower part of the Salmon River succession, 4 km northeast of Salmon Lake.

in sandstone intervals. Less common is poorly sorted pebble to cobble conglomerate that forms poorly stratified intervals more than 10 m thick. The conglomerate units contain a heterogeneous clast population similar to that of the basal conglomerate.

Limestones, including calcarenites, are relatively minor components in the lower part of the Salmon River succession, forming thin units intercalated with sandstone and siltstone. However, they form local intervals several tens of metres thick, such as a 25 to 30 m thick section exposed on the steep slopes northwest of the Salmon River, 7.5 km north-northeast of Salmon Lake. The lower third of this section consists mainly of platy to flaggy fine-grained limestone and argillaceous limestone; the middle part comprises thin-bedded calcarenite with calcareous shale interbeds, and local interbeds of flaggy limestone and pebbly limestone; and the upper part consists of fissile, gritty to pebbly limestone, containing rare thin interbeds of dark grey fine-grained limestone (Fig. 7). Pebbles within the pebbly limestone units are mainly chert, quartz, and weakly foliated quartz tectonites. Chert, quartz and quartz-rich lithic grains also occur in the calcarenite beds, but are less common than the predominant carbonate grains.

Preto (1964) mapped two narrow mafic igneous units in the lower part of the Salmon River succession, which he interpreted as altered mafic crystal tuffs or flows. Only one of these units was located during the 2016 mapping program. It is a grey plagioclase-hornblende-pyroxene porphyry with scattered xenoliths of hornblendite, which I interpret as a sill, based on its slightly discordant lower and upper contacts with the enclosing thin-bedded sandstone-siltstone sequence.

Higher stratigraphic levels of the Salmon River succession are represented by generally poorly exposed rocks in the western two-thirds of the outcrop belt. Exposures in this part of the belt consist of variable proportions of dark grey siltstone



**Fig. 7.** Pebbly limestone, lower part of the Salmon River succession, northwest side of the Salmon River, 7.5 km north-northeast of Salmon Lake. Resistant weathering pebbles and granules of chert, quartz, and weakly foliated quartz tectonites in a recessive fine-grained limestone matrix.

and fine- to coarse-grained carbonate-cemented sandstone, which occurs as thin to thick beds and contains mainly quartz, feldspar and chert grains (Fig. 8). A single occurrence of pebble conglomerate is exposed at the north end of the belt, 2.4 km east of the inferred contact with the Nicola Group. The conglomerate forms a single bed, about 1.5 m thick, in an interval of carbonate-cemented sandstones. It is predominantly framework supported, and contains small subrounded pebbles of mainly chert and quartz, with some dark grey argillite and beige volcanic(?) lithic grains. Although exposure is poor, it appears that the proportion of siltstone increases westward in the upper part of the Salmon River belt. The westernmost exposures of the succession, in the southern part of the belt, are of dark grey siltstone and argillite without sandstone interbeds.



**Fig. 8.** Brown-weathered carbonate-cemented sandstone beds intercalated with siltstone, central part of the Salmon River succession, near north boundary of the map area.

The Salmon River succession is considered Late Triassic on the basis of late Carnian conodonts extracted from samples of limestone and limy conglomerate from the lower part of the succession east of the Salmon River (Okulitch and Cameron, 1976).

### 3.3. Nicola Group

The Nicola Group underlies most of the Stump Lake – Salmon River map area, where it is subdivided into three components: the volcanic sandstone unit; the pyroxene basalt unit; and the polymictic conglomerate unit. Cockfield (1948) applied a two-fold subdivision to these same rocks, assigning some (the pyroxene basalt unit) to the Nicola Group, but most to the Cache Creek Group (Carboniferous-Permian). Monger and McMillan (1989) mapped Cockfield's Cache Creek rocks (the volcanic sandstone unit of this report) as a sedimentary facies of the Nicola Group, and included both the pyroxene basalt unit and the polymictic conglomerate unit in the eastern volcanic facies of the Nicola Group. Moore et al. (1990) used the same subdivisions as Monger and McMillan, but included the volcanic conglomerate unit in the sedimentary facies of the group, and mapped rocks east of southern Stump Lake, included in the eastern volcanic facies by Monger and McMillan (1989), as part of the sedimentary facies.

#### 3.3.1. Volcanic sandstone unit

The volcanic sandstone unit is the oldest and most widespread component of the Nicola Group in the Stump Lake – Salmon River map area. It consists mainly of volcanogenic sandstone, but also includes volcanic conglomerate, siltstone and, rarely, chert.

Sandstone is grey to green, medium to coarse grained, and commonly gritty (Fig. 9). It is characteristically very feldspathic, but also includes mafic mineral grains (pyroxene



**Fig. 9.** Upper part of thick, gritty, volcanogenic sandstone bed, volcanic sandstone unit of the Nicola Group, east limb of anticline, 8.5 km east of Glimpse Lake. Top of frame is north, beds are right-way-up and dip steeply east.

and less common hornblende), and both feldspathic and mafic volcanic-lithic grains. Much of the sandstone forms massive intervals, metres to tens of metres thick, in which bedding is not apparent, or is defined locally by narrow intervals of vaguely laminated sandstone or thin-bedded siltstone. Elsewhere, sandstone forms thick sections of well-defined thin to very thick beds. Thick to very thick-bedded intervals are fairly common in the central part of the area, on both limbs of the map scale anticline (Fig. 3), and the beds here locally display partial to complete Bouma sequences. Some of the thick-bedded intervals in this part of the area include distinctive dark grey-green gritty sandstone that is very rich in pyroxene grains, and is easily mistaken for gabbro in poor exposures (Fig. 10). Sandstone in the eastern part of the area, east of the polymictic conglomerate unit, commonly forms thin, locally medium or thick, graded beds with laminated tops, in part separated by thin beds of laminated siltstone.

Volcanic conglomerate occurs at several places in the volcanic sandstone panel that crops out adjacent to the south end of Stump Lake, where it forms units from a few metres to ten metres thick, intercalated with volcanic sandstone. The conglomerates are typically matrix supported, comprising angular to subrounded pebbles and small cobbles in a sandy, commonly epidote-altered matrix rich in feldspar and mafic mineral grains. The clasts are mainly pyroxene±plagioclase±hornblende porphyry, but aphyric mafic volcanic rock and fine-grained diorite may also be present, and one conglomerate unit also contains angular sandstone and siltstone fragments probably derived from underlying beds. Volcanic conglomerate also occurs in the main volcanic sandstone belt to the east, where it is represented by exposures 4.5 km east-northeast of Glimpse Lake. Another set of exposures, suspected to be part of the same unit, are 3.7 km east of Plateau Lake (Fig. 11). The conglomerates here are similar to the conglomerate units east of Stump Lake, but are at least several tens of metres thick. Volcanic conglomerate and pebbly sandstone noted elsewhere in the main volcanic



**Fig. 11.** Volcanic conglomerate, volcanic sandstone unit of the Nicola Group, 3.7 km east of Plateau Lake.

sandstone belt comprise the basal parts of thick and very thick sandstone beds.

Siltstone is a common but minor component of many sandstone intervals, where it occurs at the tops of graded sandstone beds, as distinct thin beds, or as laminae separating sandstone beds. Medium to dark grey siltstone, as thin to medium, commonly laminated beds, also occurs as the predominant component of intervals many tens of metres thick, observed mainly in the largest exposure belt of the unit, encompassing both limbs of the major anticline (Fig. 12). These siltstone-predominant intervals typically include some beds of fine- to medium-grained sandstone.

Chert was observed at only one location, near the southern boundary of the map area, 700 m west of the contact with the polymictic conglomerate unit. Here, in an isolated outcrop, medium grey chert occurs as distinct beds, 2-7 cm thick, intercalated with dark grey slaty siltstone (Fig. 13). The exposed



**Fig. 10.** Gritty pyroxene-rich sandstone from a very thick bed, volcanic sandstone unit of the Nicola Group, 4.3 km south of Dardanelles Lake.



**Fig. 12.** Thin-bedded siltstone, volcanic sandstone unit of the Nicola Group, 4 km east of Plateau Lake.



**Fig. 13.** Thin-bedded chert and slaty siltstone, volcanic sandstone unit of the Nicola Group, 8 km west-southwest of Salmon Lake.

section is about 15 m thick, with subequal proportions of chert and siltstone in the west, but with siltstone predominating, in laminated beds up to 30 cm thick, in the east. Nearby outcrops, 300 m to the northeast, consist of dark grey laminated siltstone that is similar to the siltstone units intercalated with chert.

Monger and McMillan (1989) reported probable Norian conodonts from a sample collected 4 km northwest of Plateau Lake, near the contact with overlying volcanic rocks of the pyroxene basalt unit (GSC Loc. No. C-087407; identified by M.J. Orchard). No macrofossils were found during the 2016 field season, and most rocks in the unit are unlikely to contain microfossils, although samples collected from the single chert outcrop will be processed for radiolarians and conodonts.

### 3.3.2. Pyroxene basalt unit

The pyroxene basalt unit comprises pyroxene-phyric basalt flows that overlie the volcanic sandstone unit in the western part of the map area. The main exposures form a large belt encompassing Peter Hope Lake, on the southwest limb of a major anticline with an arcuate axial trace (Fig. 3). The unit is also exposed on the north limb of the anticline, and as a fault panel that forms the eastern shore of northern Stump Lake.

The pyroxene basalt unit is represented mainly by uniform exposures of medium to dark green, brown-weathered pyroxene porphyry (Fig. 14) interpreted as a succession of basalt flows, although contacts between distinct flow units were not identified. The characteristic pyroxene phenocrysts are commonly 1-5 mm long, and form 10-20% of the rock, but in places are considerably larger (to 1.5 cm) and more abundant. These may be accompanied by smaller and less conspicuous plagioclase phenocrysts and, locally, by amygdules containing combinations of calcite, epidote, and quartz. The fine-grained groundmass may include relict plagioclase laths, but is typically overprinted by a predominantly epidote and calcite alteration assemblage. Foliated varieties are calcite-epidote-chlorite schists that contain relict pyroxene phenocrysts, typically



**Fig. 14.** Pyroxene porphyry, pyroxene basalt unit of the Nicola Group, east side of northern Stump Lake.

chlorite-altered and flattened in the foliation plane.

Breccia, consisting of pyroxene porphyry fragments in a matrix of the same material, forms poorly defined units at a number of localities in the main exposure belt of the unit. Some contain angular to amoeboid fragments with sharp to indistinct boundaries enclosed by apparently crystalline pyroxene porphyry, and are interpreted as flow breccias (Fig. 15). Elsewhere, pyroxene porphyry fragments, displaying textural variation, are in an apparently clastic matrix, rich in pyroxene and plagioclase grains, and probably represent local epiclastic accumulations.

Medium to dark green hornblende-pyroxene porphyry is a minor component of the unit. Locally, the hornblende-bearing porphyries are clearly dikes that crosscut adjacent pyroxene-phyric basalt and basalt breccia units but, elsewhere, contact relationships are not displayed, and it is possible that some



**Fig. 15.** Pyroxene porphyry flow(?) breccia, pyroxene basalt unit of the Nicola Group, 3.4 km west-northwest of Plateau Lake.

could be flows. Hornblende-pyroxene±plagioclase porphyry also occurs as dikes in the underlying volcanic sandstone unit, and forms a sill or flow at one locality in the polymictic conglomerate unit.

The pyroxene basalt unit overlies the volcanic sandstone unit across a transition that features a mixture of the rock types found in the two units. The lower part of this transition contains volcanic sandstone cut by dikes of pyroxene porphyry and pyroxene-hornblende porphyry, and the upper part comprises pyroxene-phyric basalt containing screens of volcanic sandstone and siltstone. The pyroxene basalt unit is not directly dated in the Stump Lake – Salmon River map area, but it is suspected to be Norian, because it is a characteristic lithology of Carnian and Norian Nicola rocks, and the upper part of the underlying volcanic sandstone unit yielded conodonts of probable Norian age.

### 3.3.3. Polymictic conglomerate unit

The polymictic conglomerate unit contains conglomerates with a distinctive clast population including medium- to coarse-grained mafic plutonic rocks. These conglomerates are intercalated with minor sandstone to pebbly sandstone, and rare pyroxene-hornblende-plagioclase porphyry. This unit forms a single belt, up to 4 km wide, in the central part of the map area. It is underlain by the volcanic sandstone unit to both the east and west, and is therefore inferred to form the core of a NNW-trending syncline.

The polymictic conglomerate unit commonly forms massive, rounded outcrops that contrast with the more recessive exposures of the adjacent volcanic sandstone unit. The rocks are light to medium green or greenish-grey and weather to lighter shades of brown, brownish-green, or beige. The conglomerates are unstratified, poorly sorted, and matrix-supported, with angular to subrounded clasts that commonly range from several millimetres to 10 cm (locally 20-30 cm; Fig. 16). Common



**Fig. 16.** Matrix-supported conglomerate with angular gabbro and diorite clasts, polymictic conglomerate unit of the Nicola Group, 5.5 km west-northwest of Salmon Lake.

clast types include pyroxene (±plagioclase±hornblende)-phyric volcanic rocks, fine-grained equigranular to weakly porphyritic hypabyssal rocks composed of plagioclase, pyroxene and hornblende, and medium to coarse-grained gabbro/diorite. Small pebbles of hornblende and pyroxenite are also common, whereas clasts of fine-grained quartz diorite, quartz-feldspar porphyry and chert were noted locally, but are rare. The matrix is typically a medium- to coarse-grained feldspathic sandstone that includes sparse to abundant mafic lithic and mineral grains, including hornblende and pyroxene.

Massive, medium to coarse-grained feldspathic sandstone, lithologically similar to the conglomerate matrix, forms a relatively minor proportion of the polymictic conglomerate unit, and locally contains scattered granules and pebbles that display the same range of compositions seen in the conglomerate clasts. In some locations the proportion of sandstone may be overestimated, because conglomerates contain mainly even-textured feldspathic clasts that are difficult to distinguish from the sandy feldspathic matrix.

Pyroxene-hornblende-plagioclase porphyry was observed at one location in the southeastern part of the unit, about 5 km west of Salmon Lake. It comprises 1-5 mm pyroxene phenocrysts (2-5%), sparse hornblende phenocrysts of the same size, and smaller, indistinct, plagioclase phenocrysts, in a fine-grained groundmass. A few metres of coherent porphyry is exposed along the edge of a single outcrop, and passes into conglomeratic sandstone via a zone, several metres wide, of peperite breccia (Fig. 17). This porphyry unit is interpreted as a volcanic rock intercalated with the conglomeratic sandstone, or a sill that cut the host rock before it was completely lithified.

The polymictic conglomerate unit is undated in the Stump Lake – Salmon River area. It is included in the Nicola Group, and suspected to be uppermost Triassic, on the basis of a very strong lithologic similarity with conglomerates in the upper part of the group elsewhere (assemblage four of Schiarizza, 2016).

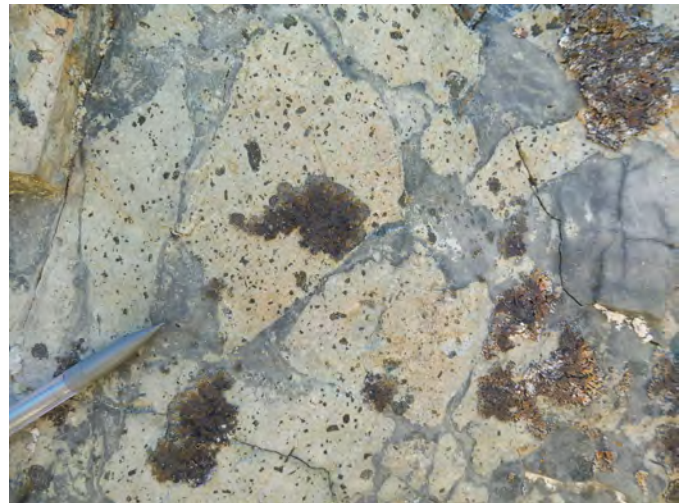


**Fig. 17.** Peperite breccia from contact between coherent pyroxene-hornblende-plagioclase porphyry and pebbly sandstone, polymictic conglomerate unit of the Nicola Group, 5 km west of Salmon Lake.

### 3.4. Jurassic intrusive rocks

Light grey, medium- to coarse-grained, isotropic, equigranular biotite-hornblende granodiorite, which cuts the Nicola volcanic sandstone unit south and southwest of Dardanelles Lake, represents the south margin of the Wildhorse batholith (Monger and McMillan, 1989). A small plug of the same composition cuts the volcanic sandstone unit 2 km southwest of the batholith, and a plug of hornblende-biotite tonalite occurs along the south margin of the study area at Salmon Lake (Fig. 3). A sample collected from the Wildhorse batholith southwest of Dardanelles Lake yielded K/Ar ages of  $161.8 \pm 2.4$  Ma on biotite, and  $169.3 \pm 2.6$  Ma on hornblende (Hunt and Roddick, 1987), whereas a U-Pb zircon crystallization age of  $196 \pm 1$  Ma was obtained from the central part of the batholith, about 20 km farther north (Parrish and Monger, 1992). This batholith is near the centre of a 300-km-long belt of Early Jurassic calcalkaline plutons, including the Thuya and Takomkane batholiths to the north, and the Pennask and Bromley batholiths to the south, which forms a prominent component of Quesnel terrane in southern British Columbia (Schiarizza, 2014).

A diorite unit cuts the Nicola volcanic sandstone unit along the north margin of the study area, about 7 km east-southeast of Dardanelles Lake (Fig. 3; Monger and McMillan, 1989). These rocks are undated, but may form part of a border phase to the Wildhorse batholith. The parts of this unit examined in 2016 comprise grey, medium-grained, equigranular to weakly porphyritic diorite containing 65% plagioclase, 30% hornblende and 5% pyroxene. A different diorite unit forms a small plug 4 km east of Stump Lake, where it cuts the volcanic sandstone unit near its contact with the overlying pyroxene basalt unit. The fine- to medium-grained equigranular diorite of this unit consists of plagioclase, lesser amounts of hornblende and biotite, and traces of quartz.

### 3.5. Kamloops Group

The Kamloops Group, a widespread assemblage of Eocene volcanic and sedimentary rocks (Ewing, 1981), is represented by volcanic rocks that unconformably overlie Mesozoic and Paleozoic rocks at scattered localities in the northern and western parts of the Stump Lake – Salmon River map area. These include fine-grained purple tuff that overlies the Nicola volcanic sandstone unit northeast of Stump Lake, and pale grey plagioclase-quartz-hornblende-biotite-phyric dacite that overlaps the unconformity between the Chapperon Group and Salmon Lake succession near the southeast corner of the map area. The other Eocene outliers were not examined, and are shown on Fig. 3 after Monger and McMillan (1989) and Daughtry and Thompson (2004). The Eocene may also be represented by relatively fresh dikes, including plagioclase porphyry, hornblende-plagioclase porphyry, and hornblende porphyry, that cut the Nicola Group and Salmon River unit at numerous localities within the map area.

## 4. Structural geology

The oldest structures recognized in the Stump Lake – Salmon

River area are a well-developed schistosity (or phyllitic cleavage) and subparallel transposed lithologic contacts in the Chapperon Group. The schistosity is locally re-oriented by younger structures, but typically dips steeply to the south-southeast or north-northwest in the northern part of the area, and steeply to the east or west in the southern part. Folds related to this fabric were not observed, but Read and Okulitch (1977) reported that the schistosity is axial planar to tight mesoscopic folds that plunge gently northeast or southwest. These structures are pre-Late Triassic, because the schistosity and lithologic contacts are truncated by the unconformity at the base of the Salmon River succession (Jones, 1959; Preto, 1964), and variably oriented schistose fragments from the Chapperon Group are in the basal conglomerate of the Salmon River succession (Read and Okulitch, 1977). A Permo-Triassic age is inferred by Read and Okulitch (1977) because similar structures deform Permian rocks that overlie the Chapperon Group to the south, near Dome Mountain.

The lower part of the Salmon River succession, and the unconformity at its base, dip at moderate angles to the west. Higher stratigraphic levels, in the central and western part of the Salmon River belt, are not well exposed, but dips are generally steeper, and dip direction is variable, but typically to the west or north. Mesoscopic folds were observed at scattered localities throughout the Salmon River succession, and have a uniform westward plunge, of 20 to 40° (Fig. 18). The folds typically verge to the south, and the folded rocks locally display a weak axial planar cleavage that dips at moderate to steep angles to the north. North-dipping cleavage is sporadically developed elsewhere in the Salmon River succession, including one exposure in the northeastern part of the belt, one kilometre west of the unconformity, where well-cleaved conglomerate contains moderately flattened clasts with a weak down-dip stretching lineation. Deformation associated with the west-plunging folds is presumed responsible for the variable bedding orientations



**Fig. 18.** Interbedded limestone and calcarenite of the Salmon River succession, deformed by west-plunging mesoscopic fold, northwest side of the Salmon River, 7.4 km north-northeast of Salmon Lake.

in the upper part of the Salmon River succession, and also for local warping of the unconformity at the base of the succession. Southeast-plunging folds that were observed to deform the schistosity within the Chapperon Group, at one locality a short distance beneath the unconformity, may be the same age. Hints of younger deformation are provided by a siltstone exposure in the southeastern part of the Salmon River succession, where the north-dipping slaty cleavage is cut by a weak crenulation cleavage that dips steeply east.

At the outcrop scale, the Nicola Group displays brittle faults and fractures of variable orientations. A weak cleavage is observed locally, but is well developed only in the western part of the pyroxene basalt unit, east of southern Stump Lake, where it dips at gentle to moderate angles to the west. Mesoscopic folds of bedding were observed at only a few scattered localities in the volcanic sandstone unit. These plunge steeply to the northwest or southeast, and do not have an associated axial planar foliation.

At the map scale, the most prominent structure in the Nicola Group is an anticline-syncline pair that is defined by opposing dips and younging directions in the volcanic sandstone unit, and the distribution of the pyroxene basalt and polymictic conglomerate units (Fig. 3). West-dipping and younging rocks of the volcanic sandstone unit, which form the easternmost Nicola exposures, are overlain, to the west, by the polymictic conglomerate unit, which is apparently preserved in the core of a NNW-trending syncline. East-dipping and younging rocks of the volcanic sandstone unit on the west limb of this syncline pass through a poorly-defined anticlinal fold hinge farther west, to form a wide panel of west-dipping and younging rocks that, 7 km west of the anticlinal hinge, is overlain by the pyroxene basalt unit. The anticlinal hinge in the southern part of the map area trends north-northwest, parallel to the adjacent synclinal hinge, but apparently bends to the west to attain an east-west trend in the northwest part of the map area. This east-west trending anticlinal segment is well defined by opposing dip directions in the volcanic sandstone unit, and the distribution of the overlying pyroxene basalt unit on both north and south limbs. It is less certain whether the east-west and north-northwest trending segments are actually parts of a single fold, or are two separate folds, possibly of different ages.

Faults mapped to the east of Stump Lake are relatively young structures, probably related to a complex system of Eocene faults in the region (Ewing, 1980; Moore et al., 1990). One of these, trending north-south, truncates the main exposure belt of the pyroxene-basalt unit, and juxtaposes it against the volcanic sandstone unit to the west. This fault trace is well defined, but the fault itself was not observed. The stratigraphic separation suggests that it has a component of east-side-down displacement. Farther north, a northeast-trending fault truncates the volcanic sandstone unit on the north limb of the map-scale anticline, and juxtaposes it against a panel of pyroxene basalt that forms the eastern shoreline of northern Stump Lake. Where observed, this fault is vertical and marked by several metres of platy ankerite-altered rock, locally cut by veins of magnesite

and quartz.

The contact between the Nicola Group and the Salmon River succession is in an area of very poor exposure. It is broadly constrained to trend north-south, but neither the nature of the contact, nor its orientation, are known. It is suspected to be a fault, because the west-plunging folds and associated north-dipping cleavage in the Salmon River succession were not observed in adjacent Nicola rocks, suggesting juxtaposition of two different structural domains. Working farther south, Moore (1989) suggested that the Nicola Group was thrust eastward over the Chapperon Group, and that to the north (i.e. in the current map area), this thrust zone must cut either above or below the Salmon River unconformity. One possibility, therefore, is that this thrust zone has cut upsection through the footwall and forms the contact between the Nicola Group and the Salmon River succession in the Stump Lake – Salmon River map area.

## 5. Mineral occurrences

Metallic mineral occurrences are known only in the western part of the Stump Lake - Salmon River map area, where they comprise epigenetic polymetallic vein systems of the historic Stump Lake mining camp (Fig. 19). Pyritic alteration zones, unrelated to the Stump Lake vein systems, were noted elsewhere in the western part of the map area, but are not known to host precious or base metal mineralization. The largest alteration zone consists of pyrite-silica-altered siltstones and sandstones of the volcanic sandstone unit, in an area extending from the southwest margin of the Wildhorse batholith to the small satellite stock to the southwest (Fig. 19). Pyritic biotite hornfels was also noted along Fraser Lake (Fig. 19), and may be related to an unidentified intrusion underlying an area of poor outcrop to the east and southeast.

The vein systems of the Stump Lake camp are described by Hedley (1937), Cockfield (1948), and Moore et al. (1990). Mineralization was first reported in the mid-1880s; modest intermittent production extended from 1889 to 1980. The vein systems, suspected to be Eocene, are on both sides of the prominent north-trending fault east of southern Stump Lake. The veins west of the fault are in volcanogenic sandstones of the volcanic sandstone unit; those to the east are in pyroxene-pyritic basalts of the pyroxene basalt unit. Mineralization is in veins, lenses and stringer zones of quartz, which are controlled by fracture zones and shear zones that typically dip at moderate to steep angles to the east (Fig. 20). Metallic minerals are mainly pyrite, galena, sphalerite, tetrahedrite, chalcopyrite, bornite and scheelite, locally with arsenopyrite, pyrrotite and native gold. Alteration adjacent to the veins is mainly Fe-Mg carbonate and pyrite, locally with green mica. Most production from the Stump Lake camp came from the Enterprise vein system, where 71,313 tonnes were mined intermittently from 1926 to 1980 (mainly 1929 to 1941), and produced 7,781,650 g Ag, 254,783 g Au, 1,040,296 kg Pb, 235,148 kg Zn, and 49,562 kg Cu (MINFILE 092ISE028 Production Report).

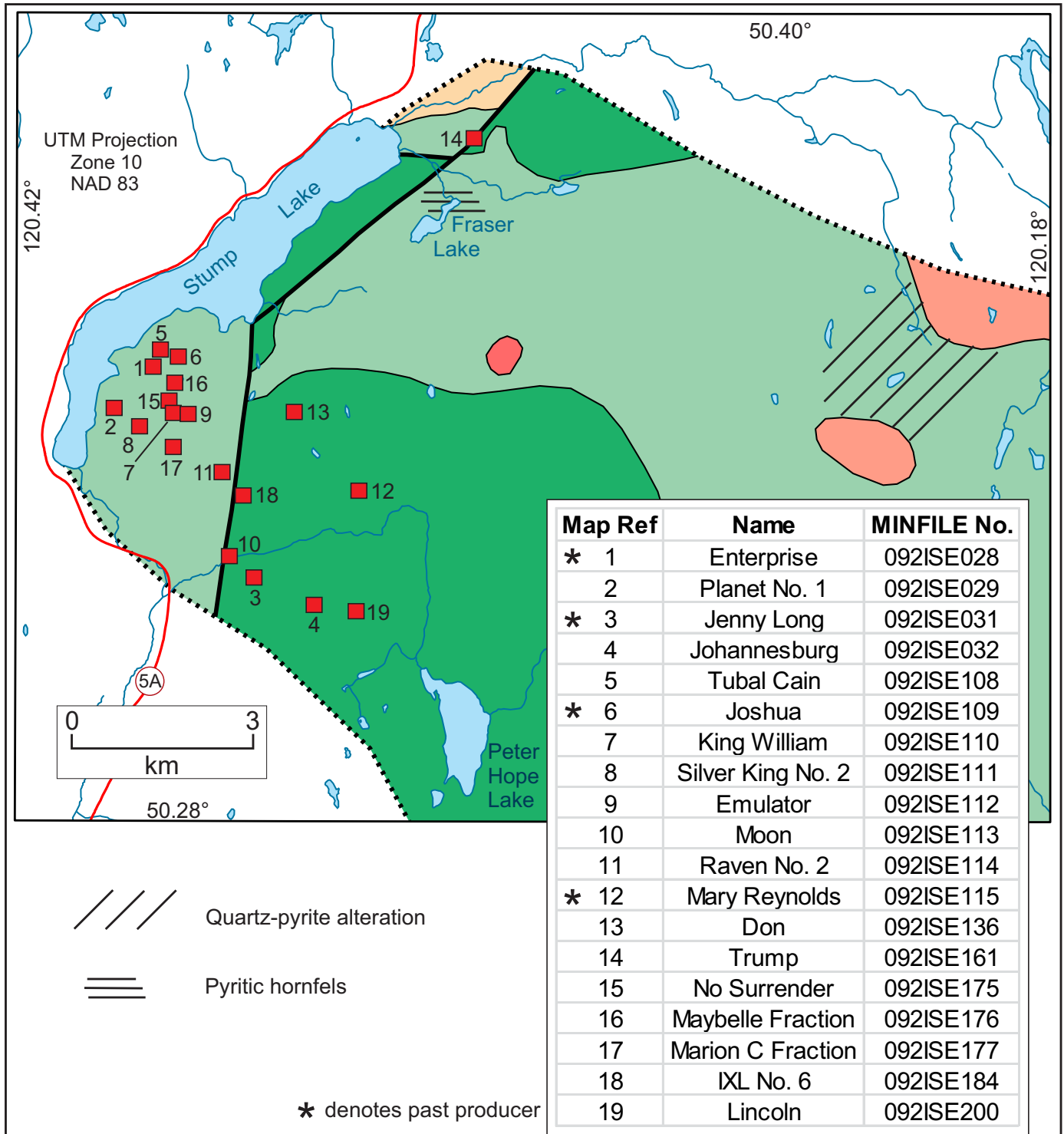


Fig. 19. Mineral occurrences of the Stump Lake mining camp, and pyritic alteration zones in the western part of the Stump Lake – Salmon River map area.



**Fig. 20.** East dipping quartz vein and fracture zone exposed at top of old shaft at the Joshua occurrence. View is south.

**6. Discussion**

**6.1. Comparison of Nicola subunits in the Stump Lake – Salmon River area to those in the Bridge Lake – Quesnel River area**

The Nicola Group in the Stump Lake – Salmon River area consists of three subunits. The volcanic sandstone unit is predominant, and is stratigraphically overlain by the pyroxene basalt unit in the western part of the map area. The polymictic conglomerate unit apparently overlies the volcanic sandstone unit in the central part of the area, where it is inferred to occupy the core of a northerly-trending syncline. The omission of the pyroxene basalt unit in this area, and suspected relationships

of correlative rocks to the north, suggest that the polymictic conglomerate unit was deposited above an unconformity (Fig. 21).

The volcanic sandstone unit consists mainly of plagioclase and pyroxene-rich sandstones that were derived from mafic volcanic rocks. Similar sandstones are the predominant component of assemblage two in the Bridge Lake – Quesnel River area (Schiarizza, 2016). Assemblage two, mainly Carnian and lower Norian, also includes basalt flows and breccias, and may comprise volcanic rocks from numerous local centres, distributed across most of the width of the arc, together with epiclastic deposits derived from them. The lack of coherent volcanic rocks in the volcanic sandstone unit in the Stump Lake – Salmon River area may reflect a position east of most volcanic centres, or a restricted age range for the rocks in this area.

The pyroxene basalt unit is a thick, uniform succession of pyroxene-phyric basalt flows and related breccias that rests stratigraphically above the volcanic sandstone unit. It is identical, in predominant lithology and stratigraphic position, to assemblage three of the Bridge Lake – Quesnel River area, which is inferred to represent a major Norian constructional phase in the Nicola arc (Schiarizza, 2016). Data to establish regional thicknesses, areal extent, and stratigraphic relationships from farther west are required to test this correlation.

The polymictic conglomerate unit contains conglomerates with a distinctive clast population that includes abundant hypabyssal and mafic plutonic rocks. These rocks are identical to conglomerates that predominate in assemblage four of the Bridge Lake – Quesnel River area (Schiarizza, 2016), with which they are correlated. Assemblage four reflects significant

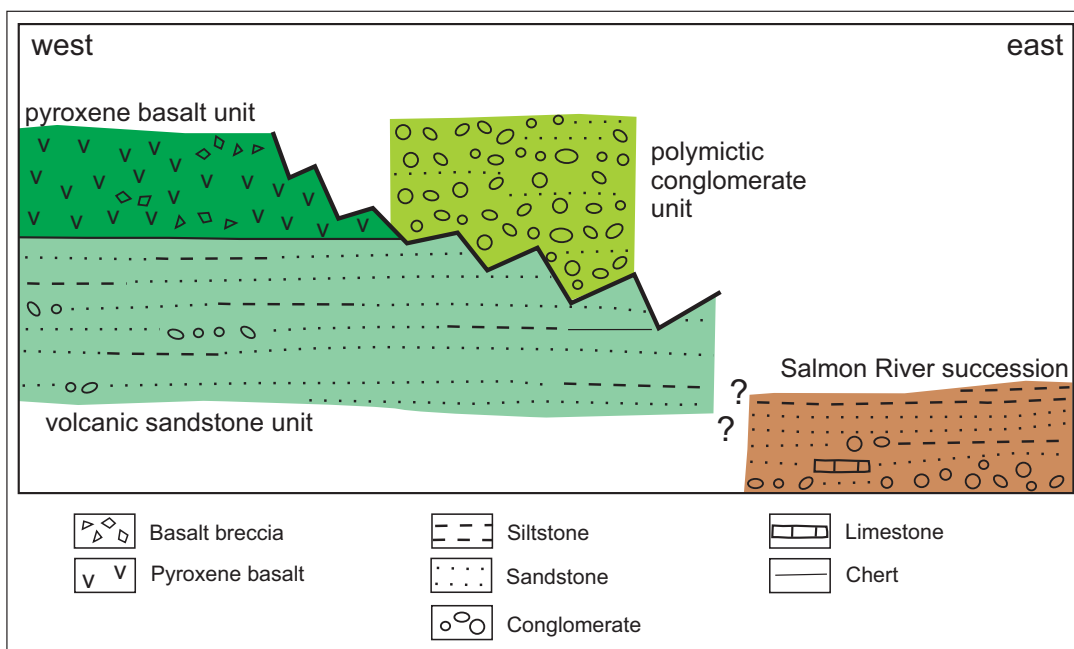


**Fig. 21.** Schematic summary of stratigraphic relations among Triassic rocks of the Nicola Group and Salmon River succession in the Stump Lake – Salmon River map area.

unroofing of the arc, and is suspected to rest above other units of the Nicola Group across an unconformity. An unconformity beneath the polymictic conglomerate unit is likewise invoked to explain stratigraphic relationships in the Stump Lake – Salmon River area (Fig. 21). Schiarizza (2016) questioned if assemblage four might have accumulated in one or more intra-arc rifts. Although mapped as a simple syncline, it is possible that one or both contacts of the polymictic conglomerate unit are faults, consistent with such an interpretation.

## 6.2. Correlation of the Salmon River succession

Upper Triassic sedimentary rocks of the Salmon River succession are excluded from the Nicola Group because they do not include volcanic or volcanoclastic rocks typical of age-equivalent Nicola rocks, and lack stratigraphic ties to rocks of the Nicola Group. They are considered part of the Slocan Group, following Daughtry and Thompson (2004) and Thompson et al. (2006). Upper Triassic sedimentary rocks that unconformably overlie the Old Tom and Shoemaker formations near Olalla, 55 km east-southeast of Princeton (Read and Okulitch, 1977; Fig. 2), are probably correlative and are likewise considered an outlier of the Slocan Group.

The Slocan Group and related rocks represent a Triassic sedimentary basin that formed east of, but coeval with, Nicola Group deposition. Stratigraphic ties between the upper parts of the two groups are suggested by local occurrences of volcanic rock, mapped as Nicola Group, that overlie the Slocan Group east and northeast of Kamloops, and near the north end of Okanagan Lake (Thompson et al., 2006; Fig. 2). However, these volcanic units are undated, and they might actually be Lower Jurassic and part of the Rossland Group (Daughtry and Thompson, 2004; Thompson and Beatty, 2004; Thompson and Unterschutz, 2004). The Rossland Group is a prominent component of Mesozoic Quesnel terrane 150 km east of southern Okanagan Lake, and also unconformably overlies the Harper Ranch Group 20 km east of Kamloops (Beatty et al., 2006; Fig. 2). A better understanding of the mutual relationships between the Nicola, Slocan and Rossland groups in the Kamloops – Okanagan Lake area requires further study.

## 7. Conclusions

The Nicola Group (Triassic) in the Stump Lake – Salmon River area consists of three subdivisions, referred to as the volcanic sandstone unit, the pyroxene basalt unit, and the polymictic conglomerate unit. The volcanic sandstone unit, consisting of pyroxene-feldspar sandstone with intercalations of volcanic conglomerate and siltstone, is predominant. It resembles volcanic-derived sedimentary intervals that are a major component of assemblage two in the Bridge Lake – Quesnel River area (Schiarizza, 2016). The pyroxene basalt unit, a uniform succession of pyroxene-phyric basalt flows and related breccias, overlies the volcanic sandstone unit in the western part of the area. It is similar, in lithology and stratigraphic position, to assemblage three of the Bridge Lake – Quesnel River area. The polymictic conglomerate unit,

comprising conglomerates with a distinctive clast population that includes abundant mafic plutonic rocks, overlies the volcanic sandstone unit in the central part of the map area. It is correlated with assemblage four of the Bridge Lake – Quesnel River area, and is suspected to rest unconformably above older units of the Nicola Group.

The Salmon River succession contains Triassic sedimentary rocks, including calcareous sandstone, conglomerate, limestone, and siltstone, which crop out east of the Nicola Group, across a suspected fault contact. These rocks rest unconformably above Paleozoic metamorphic rocks of the Chapperon Group. They are part of a Triassic basin, represented mainly by the Slocan Group, which formed east of the Nicola Group. Relationships between this basin and the coeval accumulation of volcanic and volcanoclastic rocks represented by the Nicola Group are unknown.

## Acknowledgments

I thank Isato Wada, who assisted with fieldwork for most of the summer, Lori Kennedy, who provided excellent assistance for one week in August, and Jim Britton, who helped with logistics and shared information on regional geology and mineralization. I also thank the Stump Lake Ranch (in particular, Dan Fremlin), and the Douglas Lake Ranch, for granting access to their properties. Lawrence Aspler provided a thorough review that improved the paper.

## References cited

- Beatty, T.W., Orchard, M.J., and Mustard, P.S., 2006. Geology and tectonic history of the Quesnel terrane in the area of Kamloops, British Columbia. In: Colpron, M., and Nelson, J. (Eds.), *Paleozoic evolution and metallogeny of pericratonic terranes at the ancient Pacific margin of North America, Canadian and Alaskan cordillera*, Geological Association of Canada, Special Paper 45, pp. 483-504.
- Bloodgood, M.A., 1990. Geology of the Eureka Peak and Spanish Lake map areas, British Columbia. British Columbia Ministry of Energy, Mines and Petroleum Resources, British Columbia Geological Survey Paper 1990-3, 36p.
- Bostock, H.S., 1940. Geology, Keremeos. Geological Survey of Canada, Map 341A; scale 1:63,360.
- Bostock, H.S., 1941. Geology, Olalla. Geological Survey of Canada, Map 628A; scale 1:63,360.
- Campbell, R.B., and Okulitch, A.V., 1973. Stratigraphy and structure of the Mount Ida Group, Vernon (82L), Adams Lake (82M, W1/2) and Bonaparte (92P) map areas. In: Report of Activities, Part A, April to October 1972, Geological Survey of Canada, Paper 73-1, Part A, pp. 21-23.
- Cockfield, W.E., 1948. Geology and mineral deposits of Nicola map area, British Columbia. Geological Survey of Canada, Memoir 249, 164p.
- Daughtry, K.L., and Thompson, R.I., 2004. Geology, Westwold, British Columbia. Geological Survey of Canada, Open File 4374; scale 1:50,000.
- Daughtry, K.L., Thompson, R.I., and Erdmer, P., 2000. New field studies of the Chapperon Group, Vernon southwest map area, British Columbia. Geological Survey of Canada, Current Research 2000-A19, 4p.
- Erdmer, P., Moore, J.M., Heaman, L., Thompson, R.I., Daughtry, K.L., and Creaser, R.A., 2002. Extending the ancient margin outboard in the Canadian Cordillera: record of Proterozoic crust and Paleocene regional metamorphism in the Nicola horst,

- southern British Columbia. *Canadian Journal of Earth Sciences*, 39, 1605-1623.
- Ewing, T.E., 1980. Paleogene tectonic evolution of the Pacific Northwest. *Journal of Geology*, 88, 619-638.
- Ewing, T.E., 1981. Regional stratigraphy and structural setting of the Kamloops Group, south-central British Columbia. *Canadian Journal of Earth Sciences*, 18, 1464-1477.
- Fillipone, J.A., and Ross, J.V., 1990. Deformation of the western margin of the Omineca Belt near Crooked Lake, east-central British Columbia. *Canadian Journal of Earth Sciences*, 27, 414-425.
- Greig, C.J., 1992. Jurassic and Cretaceous plutonic and structural styles of the Eagle Plutonic Complex, southwestern British Columbia, and their regional significance. *Canadian Journal of Earth Sciences*, 29, 793-811.
- Hedley, M.S., 1937. Part D, southern and central mineral survey districts. In: *Annual Report of the Minister of Mines for 1936*, British Columbia Department of Mines, pp. D14-D23.
- Holland, S.S., 1976. Landforms of British Columbia, a physiographic outline. *British Columbia Department of Mines and Petroleum Resources, British Columbia Geological Survey Bulletin 48*, 138p.
- Hunt, P.A., and Roddick, J.C., 1987. A compilation of K-Ar ages, Report 17. In: *Radiogenic age and isotopic studies: Report 1*, Geological Survey of Canada, Paper 87-2, pp. 143-210.
- Jones, A.G., 1959. Vernon map area, British Columbia. *Geological Survey of Canada, Memoir 296*, 186p.
- Logan, J.M., and Moynihan, D.P., 2009. Geology and mineral occurrences of the Quesnel River map area, central British Columbia (NTS 093B/16). In: *Geological Fieldwork 2008*, British Columbia Ministry of Energy, Mines and Petroleum Resources, *British Columbia Geological Survey Paper 2009-1*, pp. 127-152.
- McMullin, D.W.A., 1990. Thermobarometry of pelitic rocks using equilibria between quartz-garnet-aluminosilicate-muscovite-biotite, with application to rocks of the Quesnel Lake area, British Columbia. Ph.D. thesis, The University of British Columbia, 291p.
- McMullin, D.W.A., Greenwood, H.J., and Ross, J.V., 1990. Pebbles from Barkerville and Slide Mountain terranes in a Quesnel terrane conglomerate: evidence for pre-Jurassic deformation of the Barkerville and Slide Mountain terranes. *Geology*, 18, 962-965.
- Mihalynuk, M.G., Diakow, L.J., Friedman, R.M., and Logan, J.M., 2016. Chronology of southern Nicola arc stratigraphy and deformation. In: *Geological Fieldwork 2015*, British Columbia Ministry of Energy and Mines, *British Columbia Geological Survey Paper 2016-1*, pp. 31-63.
- Milford, J.C., 1984. Geology of the Apex Mountain Group, north and east of the Similkameen River, south-central British Columbia. M.Sc. thesis, The University of British Columbia, 108p.
- Monger, J.W.H., and McMillan, W.J., 1989. Geology, Ashcroft, British Columbia. *Geological Survey of Canada, Map 42-1989*; scale 1:250,000.
- Moore, J.M., 1989. Geology along the lithoprobe transect between the Guichon Creek batholith and Okanagan Lake (92I/1, 2, 7, 8; 82L/3, 4, 5, 6). In: *Geological Fieldwork 1988*, British Columbia Ministry of Energy, Mines and Petroleum Resources, *British Columbia Geological Survey Paper 1989-1*, pp. 93-98.
- Moore, J.M., Pettipas, A., Meyers, R.E., and Hubner, T.B., 1990. Nicola Lake region, geology and mineral deposits. *British Columbia Ministry of Energy, Mines and Petroleum Resources, British Columbia Geological Survey Open File 1990-29*, 30p.
- Mortensen, J.K., Lucas, K., Monger, J.W.H., and Cordey, F., 2011. Geological investigations of the basement of the Quesnel terrane in southern British Columbia (NTS 082E, F, L, 092H, I): Progress Report. In: *Geoscience BC Summary of Activities 2010, Report 2011-1*, pp. 133-141.
- Okulitch, A.V., 1973. Age and correlation of the Kobau Group, Mount Kobau, British Columbia. *Canadian Journal of Earth Sciences*, 10, 1508-1518.
- Okulitch, A.V., 1979. Lithology, stratigraphy, structure and mineral occurrences of the Thompson-Shuswap-Okanagan area, British Columbia. *Geological Survey of Canada, Open File 637*; scale 1:250,000.
- Okulitch, A.V., and Cameron, B.E.B., 1976. Stratigraphic revisions of the Nicola, Cache Creek, and Mount Ida groups, based on conodont collections from the western margin of the Shuswap metamorphic complex, south-central British Columbia. *Canadian Journal of Earth Sciences*, 13, 44-53.
- Panteleyev, A., Bailey, D.G., Bloodgood, M.A., and Hancock, K.D., 1996. Geology and mineral deposits of the Quesnel River - Horsefly map area, central Quesnel Trough, British Columbia. *British Columbia Ministry of Employment and Investment, British Columbia Geological Survey Bulletin 97*, 155p.
- Parrish, R.R., and Monger, J.W.H., 1992. New U-Pb dates from southwestern British Columbia. In: *Radiogenic age and isotopic studies: Report 5*, Geological Survey of Canada, Paper 91-2, pp. 87-108.
- Preto, V.A., 1964. Structural relations between the Shuswap terrane and the Cache Creek Group in southern British Columbia. M.Sc. thesis, The University of British Columbia, 87p.
- Read, P.B., and Okulitch, A.V., 1977. The Triassic unconformity in south-central British Columbia. *Canadian Journal of Earth Sciences*, 14, 606-638.
- Rees, C.J., 1987. The Intermontane - Omineca belt boundary in the Quesnel Lake area, east-central British Columbia: Tectonic implications based on geology, structure and paleomagnetism. Ph.D. thesis, Carleton University, 421p.
- Schiarizza, P., 1989. Structural and stratigraphic relationships between the Fennell Formation and Eagle Bay assemblage, western Omineca Belt, south-central British Columbia: Implications for Paleozoic tectonics along the paleocontinental margin of western North America. M.Sc. thesis, The University of Calgary, 343p.
- Schiarizza, P., 2014. Geological setting of the Granite Mountain batholith, host to the Gibraltar porphyry Cu-Mo deposit, south-central British Columbia. In: *Geological Fieldwork 2013*, British Columbia Ministry of Energy and Mines, *British Columbia Geological Survey Paper 2014-1*, pp. 95-110.
- Schiarizza, P., 2016. Toward a regional stratigraphic framework for the Nicola Group: Preliminary results from the Bridge Lake - Quesnel River area. In: *Geological Fieldwork 2015*, British Columbia Ministry of Energy and Mines, *British Columbia Geological Survey Paper 2016-1*, pp. 13-30.
- Schiarizza, P. and Israel, S., 2001. Geology and mineral occurrences of the Nehalliston Plateau, south-central British Columbia (92P/7, 8, 9, 10). In: *Geological Fieldwork 2000*, British Columbia Ministry of Energy and Mines, *British Columbia Geological Survey Paper 2001-1*, pp. 1-30.
- Schiarizza, P., Heffernan, S., and Zuber, J., 2002. Geology of Quesnel and Slide Mountain terranes west of Clearwater, south-central British Columbia (92P/9, 10, 15, 16). In: *Geological Fieldwork 2001*, British Columbia Ministry of Energy and Mines, *British Columbia Geological Survey Paper 2002-1*, pp. 83-108.
- Smith, R.B., 1979. Geology of the Harper Ranch Group (Carboniferous-Permian) and Nicola Group (Upper Triassic) northeast of Kamloops, British Columbia. M.Sc. thesis, The University of British Columbia, 211p.
- Thompson, R.I., and Daughtry, K.L., 1998. Stratigraphic linkages across Vernon map area, British Columbia. In: *Current Research 1998-A*, Geological Survey of Canada, pp. 181-187.
- Thompson, R.I., and Beatty, T.W., 2004. Geology, Monte Creek, British Columbia. *Geological Survey of Canada, Open File 4381*; scale 1:50,000.
- Thompson, R.I., and Unterschutz, J.L.E., 2004. Geology, Vernon, British Columbia. *Geological Survey of Canada, Open File 4375*; scale 1:50,000.

Thompson, R.I., Glombick, P., Erdmer, P., Heaman, L.M., Lemieux, Y., and Daughtry, K.L., 2006. Evolution of the ancestral Pacific margin, southern Canadian Cordillera: Insights from new geologic maps. In: Colpron, M., and Nelson, J. (Eds.), Paleozoic evolution and metallogeny of pericratonic terranes at the ancient Pacific margin of North America, Canadian and Alaskan cordillera, Geological Association of Canada, Special Paper 45, pp. 433-482.



# Mapping in the Tatsi and Zymo ridge areas of west-central British Columbia: Implications for the origin and history of the Skeena arch



Joel J. Angen<sup>1, a</sup>, JoAnne L. Nelson<sup>2</sup>, Mana Rahimi<sup>1</sup>, and Craig J.R. Hart<sup>1</sup>

<sup>1</sup> Mineral Deposit Research Unit, The University of British Columbia, Vancouver, BC, V6T 1Z4

<sup>2</sup> British Columbia Geological Survey, Ministry of Energy and Mines, Victoria, BC, V8W 9N3

<sup>a</sup> corresponding author: jangen@eoas.ubc.ca

Recommended citation: Angen, J.J., Nelson, J.L., Rahimi, M., and Hart, C.J.R., 2017. Mapping in the Tatsi and Zymo ridge areas of west-central British Columbia: Implications for the origin and history of the Skeena arch. In: Geological Fieldwork 2016, British Columbia Ministry of Energy and Mines, British Columbia Geological Survey Paper 2017-1, pp. 35-48.

## Abstract

Economically significant porphyry and related mineralization is genetically associated with the Bulkley (Late Cretaceous) and Babine and Nanika intrusive suites (Eocene) in central British Columbia. These intrusions and mineral occurrences are largely restricted to the Skeena arch, a northeast-trending paleohigh that extends transverse to the general trend of Stikine terrane. Elongate intrusions and linear trends of intrusions that suggest emplacement was partially localized along the Skeena arch, and strata of the Skeena Group (Lower Cretaceous) are deformed into northeast trending folds. Stratigraphic relationships across the Skeena arch indicate that it became an arc-transverse paleotopographic high between the Middle Jurassic and Early Cretaceous. The northeast-trending folds, along with the northeasterly orientation of plutonic suites and the Skeena arch as a whole, are thought to be manifestations of a fundamental arc-transverse structural anisotropy.

**Keywords:** Skeena arch, Skeena Group, Netazul volcanics, Telkwa Formation, Bulkley suite, Babine suite, Nanika suite, Stikinia, folding, arc transverse, porphyry

## 1. Introduction

Reactivation of pre-existing structures is regarded as a mechanism to localize emplacement of porphyry intrusions and provide conduits for hydrothermal fluids (Heidrick and Titley, 1982; Richards, 2000; Richards et al., 2001; Tosdal and Richards, 2001). In arc terranes, transverse structures are considered preferential hosts for porphyry intrusions and mineralization, particularly where they intersect arc-parallel structures (Schmitt, 1966; Glen and Walshe, 1999; Richards et al., 2001; Hill et al., 2002; Garwin et al., 2005; Gow and Walshe, 2005).

The Skeena arch is an ENE-trending structure that is transverse to the trend of the Stikine arc terrane in central British Columbia (Fig. 1). Lower Jurassic and older rocks exposed along its crest are flanked by Middle Jurassic to Lower Cretaceous units deposited in the Bowser basin to the north and Nechako basin to the south (Fig. 1; Tipper and Richards, 1976a). Most mineral occurrences along the arch are interpreted as being genetically related to the Bulkley (Late Cretaceous) and Babine and Nanika (Eocene) intrusive suites (MacIntyre, 2006). These suites, as well as the Topley and Kleanza suites (Late Triassic to Early Jurassic), align along the northeasterly trend of the Skeena arch (Fig. 1). Despite regional (Tipper and Richards, 1976b) and more detailed (MacIntyre et al., 1989; Desjardins et al., 1990; Nelson et al., 2006, 2008, 2009; Nelson and Kennedy, 2007) mapping, the structural history of the Skeena arch and, in particular, the significance of its arc-

transverse orientation, has not been well established.

To develop a better understanding of structural controls on mineralization in the Skeena arch, herein we present the results of 1:20,000-scale mapping in two areas lacking detailed study: near Zymo ridge northeast of Red Canyon Creek; and near Tatsi in the south Howson Range (Fig. 2). Parallel stratigraphic relationships, structural features, and intrusive-mineralization trends of differing ages suggest a long-lived underlying control.

## 2. Geological setting

Mississippian to Neogene rocks in the Skeena arch (Fig. 2) record island arc magmatism and related sedimentation, followed by continental margin arc magmatism and siliciclastic sedimentation. Mississippian to Permian rocks of the Mt. Attree Formation represent a nascent island arc that terminated with deposition of Ambition Formation limestone (Permian) and then a thin, unnamed Middle Triassic chert-argillite unit (Nelson et al., 2006). Triassic plutonic rocks of the Stuhini arc have been documented in the Skeena arch, although coeval extrusive rocks have not (Deyell et al., 2000).

Upper Triassic to Lower Jurassic arc volcanic rocks of the Telkwa Formation (lower part of Hazelton Group) form most exposures in the Skeena arch. The Telkwa Formation includes rocks that define a transition from subaerial to marine environments from west to east (Tipper and Richards, 1976a). The plutonic equivalents of Telkwa Formation extrusive rocks are the Topley and Kleanza suites, which are distributed in a

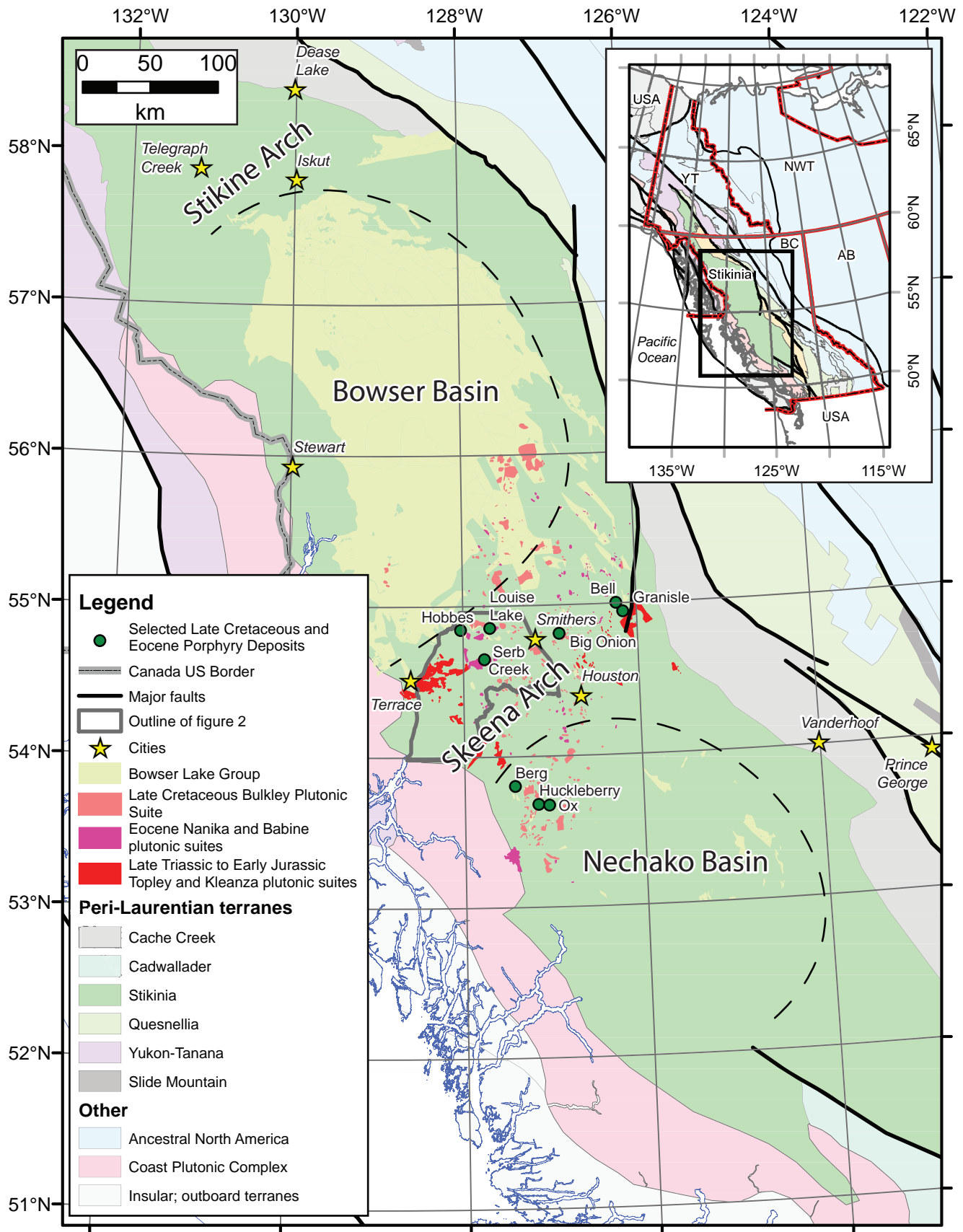


**Fig. 1.** Location of study area in the context of central British Columbia geology. Terranes modified after Colpron and Nelson (2011) and Nelson et al. (2013). Outlines of the Bowser and Nechako basins modified after Tipper and Richards (1976a).

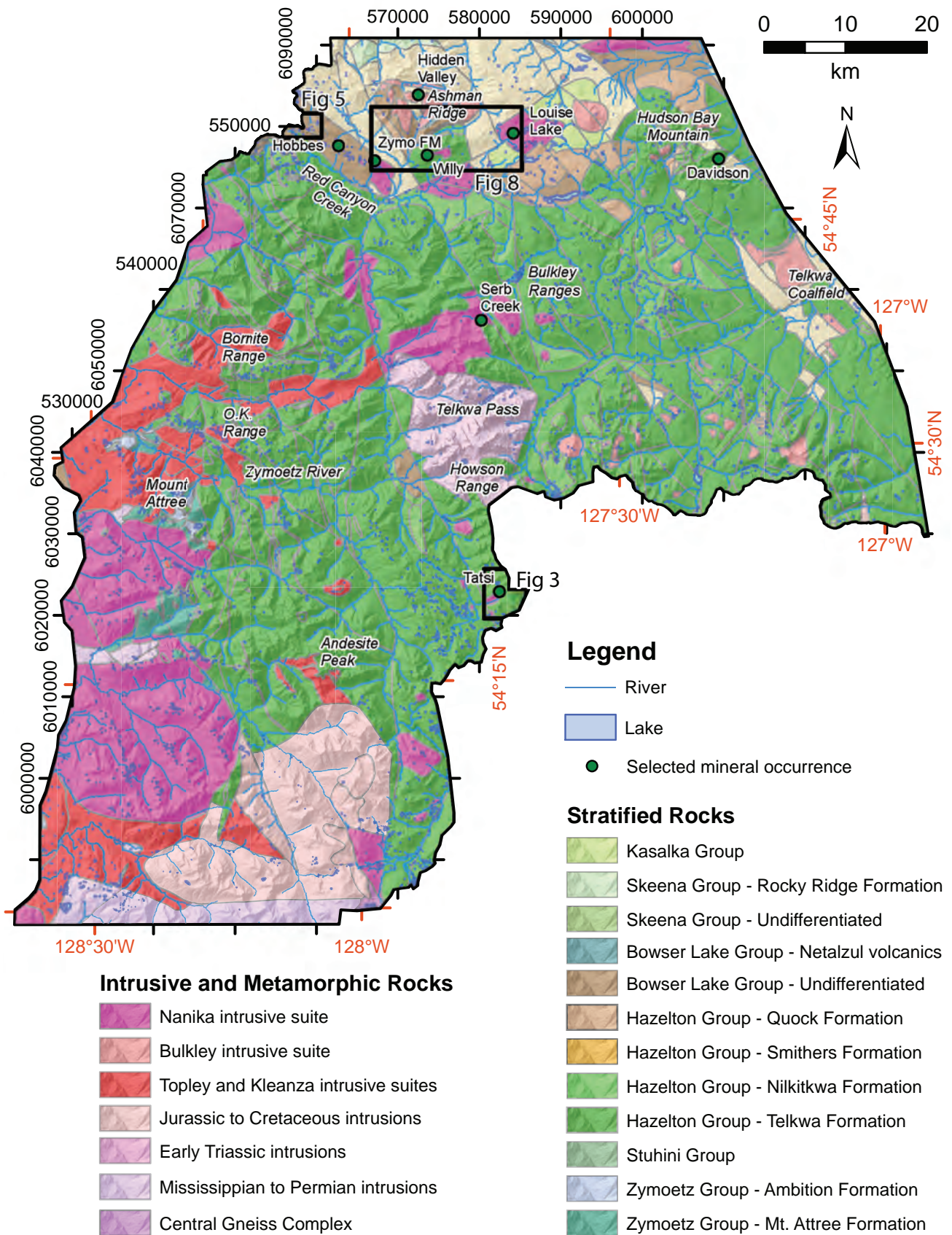


**Fig. 2.** Simplified geology of western Skeena Arch and locations of detailed study areas. Geology modified after British Columbia digital geology compilation (Cui et al., 2015).

northeasterly trend along the axis of the Skeena arch (Nelson, 2017; Figs. 1, 2). Elsewhere in the Stikine terrane, large porphyry and related deposits are genetically associated with Late Triassic and Early Jurassic plutons (Logan and Mihalynuk, 2014). Comparable deposits have not yet been identified in the Skeena arch.

Hazelton arc volcanism waned through the Early and Middle Jurassic, with deposition of mixed volcanic and sedimentary rocks of the Nilkitkwa Formation followed by tuffaceous sedimentary rocks of the Smithers and Quock formations (Gagnon et al., 2012). The Stikine terrane accreted to western North America during the Middle Jurassic, with southwest-vergent fold and thrust deformation documented along the Stikine-Cache Creek terrane boundary (Schiarizza and MacIntyre, 1999; Mihalynuk et al., 2004). At the eastern margin of the Skeena arch, Schiarizza and MacIntyre (1999) documented a southwest-vergent thrust fault crosscut by a 165 ± 2/-1 Ma pluton (U-Pb zircon, Ash et al., 1993).

Accretion was followed by marine sedimentation in the Bowser and Nechako basins (Fig. 1). Middle Jurassic marine deposits are not widespread across the Skeena arch and are limited to isolated localities, such as southwest of Telkwa Pass, where Callovian (Middle Jurassic) fossils have been found in the Bowser Lake Group (Fig. 2; Pálffy et al., 2000). Along the northern margin of the Skeena arch, the Quock Formation is gradationally overlain by Middle Jurassic to Lower Cretaceous marine sedimentary rocks of the Bowser Lake Group (Gagnon et al., 2012). Lower to Upper Cretaceous Skeena Group sedimentary rocks gradationally overlie the Bowser Lake Group within the Bowser basin (Smith and Mustard, 2006), but unconformably overlie the Telkwa Formation in central Skeena arch (Fig. 3; Palsgrove and Bustin, 1991). The Skeena arch was therefore a paleotopographic high by at least the Early Cretaceous. Late Cretaceous to Oligocene rocks obscure older stratigraphic relationships along the southern margin of the Skeena arch.

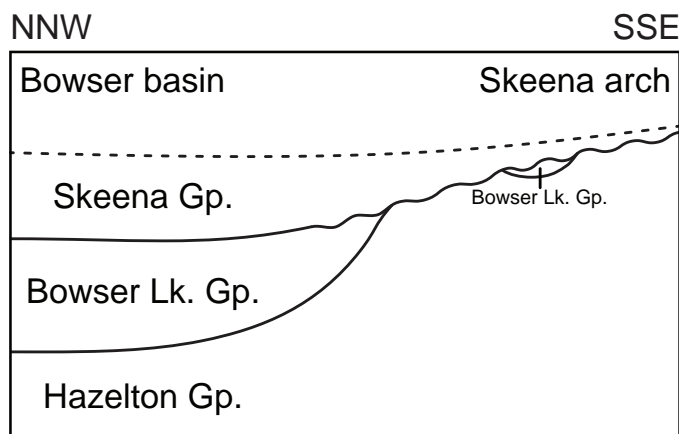


**Fig. 3.** Schematic cross section from the Bowser basin to the Skeena arch during the Early Cretaceous. Straight solid lines reflect conformable contacts, wavy solid lines reflect unconformable contacts, and dashed line is Earth's surface. The Skeena Group conformably overlies the Bowser Lake Group in the Bowser basin but unconformably overlies the Hazelton Group in the Skeena arch.

The Bulkley (Late Cretaceous) and Nanika and Babine (Eocene) plutonic suites, hosts to porphyry mineralization, are widely distributed across the Skeena arch (Fig. 1; MacIntyre, 2006). Although the overall distribution of the Late Cretaceous intrusions follows a broadly north-south trend (Fig. 1), individual intrusions define map traces that trend northeast. For example, at the Huckleberry main zone, a northeasterly shear zone controls the shape of the stock and mineralization (Jackson and Illerbrun, 1995), and the Hidden Valley prospect (MINFILE 093L076) displays a similar trend. The Babine suite intrusions in the eastern Skeena arch are strongly localized along northwest-trending dextral strike-slip faults (Carter et al., 1995; Dirom et al., 1995). The overall extent of Eocene intrusions follows a northeasterly trend, along the axis of the Skeena arch (Fig. 1).

Upper Paleozoic and Upper Triassic strata near Terrace are deformed by northeast-trending, regional-scale folds, and the upper Paleozoic rocks contain a southeast- to east-dipping foliation. These structures are latest Triassic or older because they are crosscut by a ca. 200 Ma phase of the Kleanza pluton (U-Pb zircon, Gareau et al., 1997; Nelson et al., 2008; Angen, 2009). Deformation of Jurassic and younger strata in the Skeena arch west of Smithers and east of the Coast Belt is minimal, predominantly block faulting (MacIntyre et al., 1989; Desjardins et al., 1990). Minor northwest-trending folds are documented in the Telkwa coalfields area (Ryan, 1993).

Relative to the inverted basins that flank it, the Skeena arch region exhibits minimal deformation. Strata of both the Bowser and Nechako basins display folds and thrusts formed during the Cretaceous (Evenchick, 1991; Angen et al., 2016). In the Bowser basin, uncommon northeast-trending folds are interpreted to reflect Early Cretaceous sinistral transpression. These structures developed before northeast-vergent folds considered to record mid- to Late Cretaceous orthogonal shortening (Evenchick, 2001; Waldron et al., 2006). Northeast-trending folds in the southeastern part of the Bowser basin have been attributed to heterogeneities from basement promontories during overall northeast-vergent shortening (Sutherland-Brown, 1960; McMechan, 2007). Folds documented in Nechako basin are consistent with ENE-vergent shortening during the mid-Cretaceous (Hayward and Calvert, 2011; Angen et al., 2016). The western Skeena arch appears to have been unaffected by Cretaceous northeast-vergent deformation. The sole exception is an inferred top-to-the-northeast thrust fault that crosses the Skeena River northeast of Terrace (Nelson et al., 2008). Eocene extensional deformation formed northwest-trending graben across much of the arch (MacIntyre, 1998; Angen, 2009).

### 3. Map unit descriptions

#### 3.1. Stratified rocks

##### 3.1.1. Telkwa Formation (Hazelton Group)

In the Tatsi area (Figs. 2, 4), the Telkwa Formation consists mainly of well-bedded maroon tuffs referred to as the Howson facies, and interpreted as subaerial deposits, by Tipper and

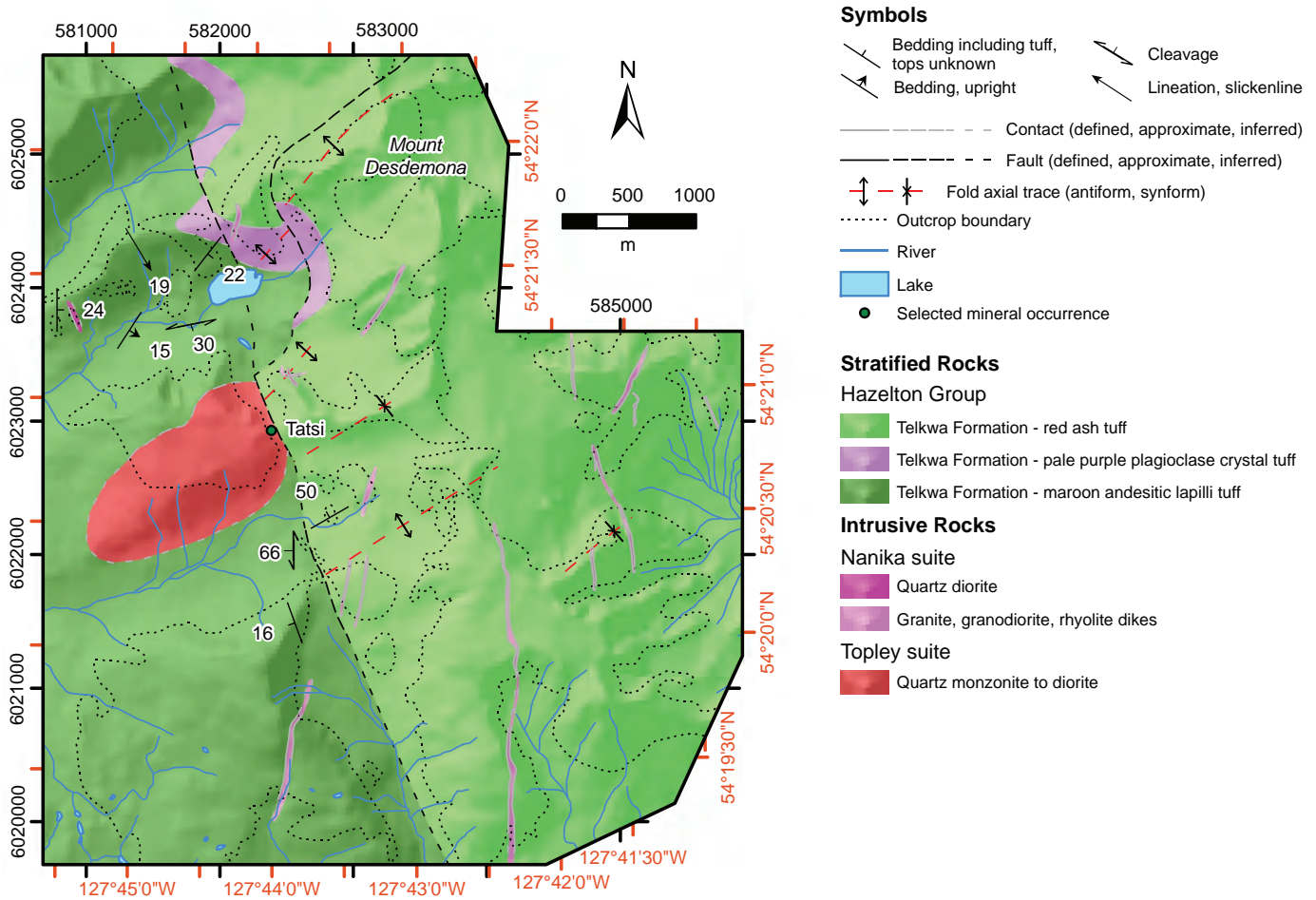


Fig. 4. Bedrock geology of the Tatsi map area, southern Howson Range. See Figure 2 for location.

Richards (1976b). The interpreted base of the Telkwa Formation is exposed north of the Tatsi area. It is marked by a discontinuous cobble conglomerate overlying chlorite- and epidote- altered mafic volcanic rocks that are tentatively considered part of

the Stuhini Group. The conglomerate contains well-rounded cobbles of dark green chlorite and epidote altered mafic volcanic rocks in a maroon to dark purple ash matrix (Fig. 5a). It is overlain by interbedded ash tuff, plagioclase crystal tuff,

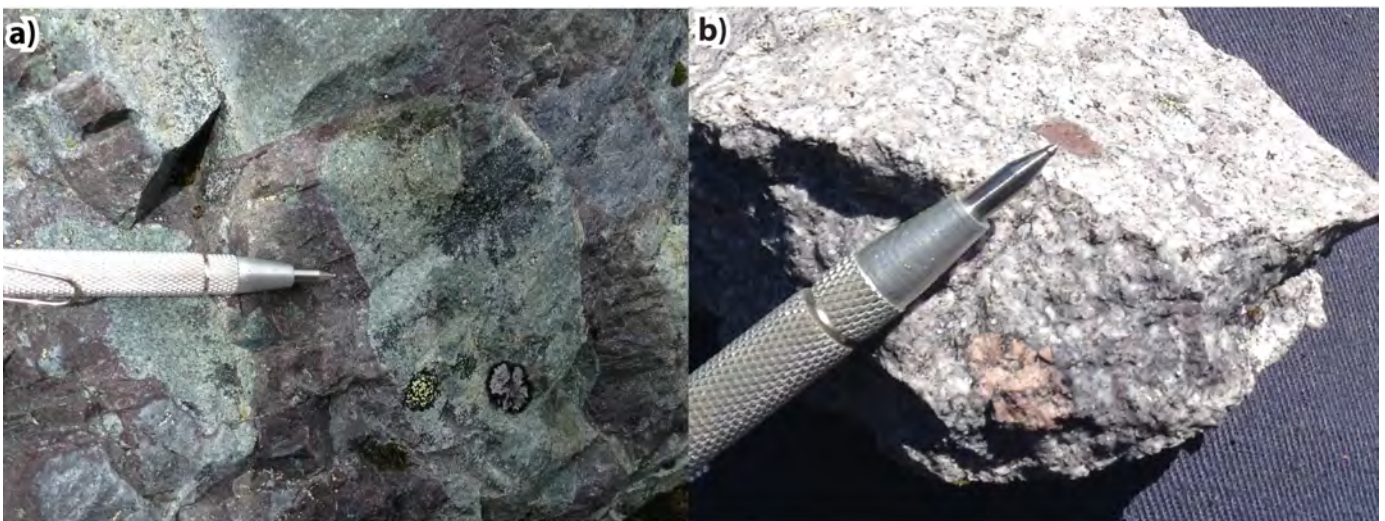


Fig. 5. Features of the Telkwa Formation in the southern Howson Range. a) Conglomerate with subangular to rounded dark green mafic volcanic clasts in a maroon ash matrix. b) Distinctive pale purple crystal tuff marker in the Tatsi area.

lapilli tuff, and dark green amygdaloidal basalt flows. Basalt flows decrease up section, passing into maroon ash to lapilli tuff with ubiquitous plagioclase and local quartz phenocrysts. Minor dark grey siltstone and very fine-grained sandstone are interbedded with tuff.

The stratigraphically lowest rocks in the Tatsi area are thick bedded (up to 30 metres) maroon andesitic lapilli tuffs, about 300 metres thick, that are conformably overlain by a light grey to purple crystal-lithic lapilli tuff marker bed. The marker bed contains up to 35% plagioclase crystals (up to 3 mm) and maroon lapilli similar to the underlying andesitic tuffs, set in a pale grey to purple groundmass (Fig. 5b). It is overlain by at least 200 metres of well-bedded brick red tuffs within which are white sills of biotite hornblende granodiorite. This section of laterally continuous tuff beds differs markedly from highly heterogeneous flow and volcanoclastic stratovolcano deposits in the Telkwa Formation near Terrace (Nelson et al., 2006; 2008; Nelson and Kennedy, 2007; Barresi et al., 2015) and are likely distal equivalents.

### 3.1.2. Bowser Lake Group

The Bowser Lake Group is exposed in the southwest corner of the Zymo ridge area (Fig. 6). It consists of interbedded light grey sandstone, fossiliferous dark grey siltstone, and green to grey andesite flows and lapilli tuffs. The basal contact of the Bowser Lake Group is well documented near Quinlan Mountain immediately west of the Zymo ridge area and at Ashman Ridge to the east (Fig. 2), where siliceous mudstone and tuff of the Quock Formation transition conformably to black and dark grey siltstone, sandstone, and shale (Nelson and Kennedy, 2007; Evenchick et al., 2010; Gagnon et al., 2012).

Sandstone and siltstone beds are 10 cm to 2 m thick. Sandstones are medium to coarse grained and contain granulestone lenses up to 10 cm thick (Fig. 7a). Some bedding planes are marked by fossilized plant debris. Clasts in conglomerate are subangular to subrounded. Most are felsic volcanic rocks with lesser black chert. Exotic chert clasts are ubiquitous in the Bowser Lake Group, but the felsic volcanic clasts are of more local derivation, probably from the Skeena arch (Nelson and Kennedy, 2007). Siltstone beds contain abundant bivalve and belemnite fossils. The combination of bivalve, belemnite, and plant fossils in the same sequence indicate alternating marine and continental sedimentation.

Dark grey, plagioclase-phyric andesite flows have aphanitic chilled margins and peperitic textures along contacts with sandstones. Lenses of hyaloclastite occur within sandstone beds close to andesite flows. Lapilli tuffs contain mostly plagioclase-phyric andesite fragments and lesser white, aphanitic rhyolite fragments. One lapilli breccia contains abundant bivalve and belemnite fossils (Fig. 7b). This breccia is interpreted as a volcanic debris flow that incorporated an unconsolidated fossil bed. Flows with peperitic textures, chilled margins, sandstones with lenses of hyaloclastite, and fossiliferous lapilli breccia indicate coeval volcanism and submarine sedimentation.

We interpret that Bowser Lake Group rocks in the Zymo ridge

area are part of the Netalzul volcanics and Muskaboo Creek assemblage (Tipper and Richards, 1976a; Evenchick et al., 2008; 2010). The Muskaboo Creek assemblage was previously referred to as the the Suskwa facies of the former Trout Creek assemblage (Richards and Jeletzky, 1975; Tipper and Richards, 1976a). Upper Jurassic volcanic rocks of the Netalzul volcanics have been documented along the eastern and southern margins of the Bowser basin (Tipper and Richards, 1976a), and Upper Jurassic to Lower Cretaceous volcanic rocks are a significant component of the Bowser Lake Group in the Nechako Plateau (Diakow et al., 1997; Friedman et al., 2001).

### 3.1.3. Bulkley Canyon and Laventie formations (Skeena Group)

The Skeena Group is well exposed in the Zymo ridge area where it includes nonmarine polymictic conglomerate, sandstone, siltstone, and mudstone (Fig. 6). The lower contact is obscured by vegetation, but bedding is parallel to that in underlying Bowser Lake Group rocks. A clastic dike that cuts the lowermost Skeena Group contains subangular to subrounded fragments of felsic volcanic rocks and chert, similar to the underlying Bowser Lake Group. The Bowser Lake Group was therefore unconsolidated at the onset of Skeena Group deposition. This is consistent with the interpretation (Smith and Mustard, 2006) of a conformable contact between these two groups in southern Bowser basin. In contrast, in the Telkwa coalfield in the central part of Skeena arch, the Skeena Group unconformably overlies the Hazelton Group (Fig. 2; Palsgrove and Bustin, 1991).

#### 3.1.3.1. Bulkley Canyon Formation

At the base of the Skeena Group in the Zymo ridge study area, the Bulkley Canyon Formation (Bassett and Kleinspehn, 1997) is about 200 m thick and consists of cobble conglomerate, sandstone and siltstone. It is light to dark grey on fresh surfaces but weathers bright orange-red. Thick beds of framework-intact polymictic conglomerate (5-30 m) contain subrounded- to well-rounded, locally imbricated clasts of mainly volcanic rock, with lesser plutonic, chert, and sandstone in a matrix of coarse sand. Interpenetration of clasts in conglomerate was observed (Fig. 8b). Arkosic sandstone beds separate conglomerate beds. They are 1 to 5 m thick and exhibit cross stratification. Wood fossils are common, but coal beds are lacking. Some sandstone beds contain brown weathering pods up to 2 m long by 30 cm thick with calcareous cement. Sparse imbricated clasts and cross stratification are consistent with flow towards the northwest and northeast.

#### 3.1.3.2. Laventie Formation

The Bulkley Canyon Formation grades up section to a unit of fine-grained sandstone, siltstone and mudstone, which also weathers orange-red (Fig. 8c), the Laventie Formation of Bassett and Kleinspehn (1997). Sandstone and siltstone form laterally continuous beds 10 to 100 cm thick; black shales form rare beds >4 m thick. Uncommon beds with a carbonate

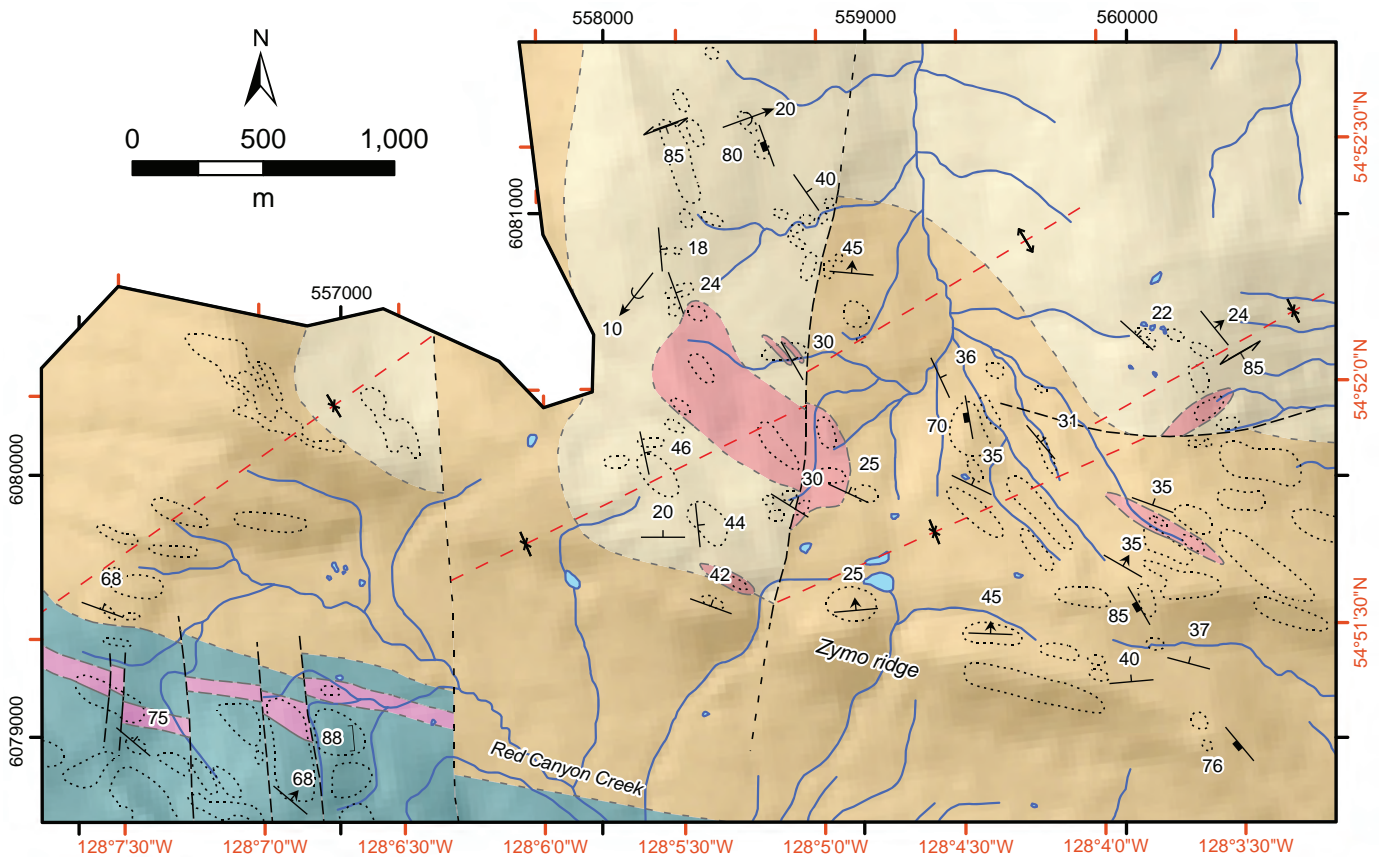


Fig. 6. Bedrock geology of the Zymo ridge area. See Figure 2 for location.

**Symbols**

- Bedding including tuff, tops unknown
- Bedding, upright
- Cleavage
- Lineation, fold hinge line
- Joint

--- Contact (defined, approximate, inferred)

--- Fault (defined, approximate, inferred)

↕ - \* Fold axial trace (antiform, synform)

..... Outcrop boundary

— River

■ Lake

**Stratified Rocks**

**Skeena Group**

■ Laventie Formation - sandstone; siltstone; mudstone

■ Bulkley Canyon Formation - polyolithic conglomerate; sandstone; siltstone

**Bowser Lake Group**

■ Netalzul volcanics and Muskaboo Creek assemblage - sandstone; siltstone; intermediate volcanic rocks

**Intrusive Rocks**

**Nanika suite**

■ Granite, granodiorite, rhyolite dikes

**Bulkley suite**

■ Biotite diorite

cement are rich in bivalve and gastropod fossils. Elsewhere in the southern part of the Bowser basin, the Laventie Formation is gradationally overlain by the Rocky Ridge Formation and the Rocher Debole Formation (Bassett and Kleinspehn, 1997).

**3.2. Plutonic suites**

**3.2.1. Topley suite (latest Triassic to Early Jurassic)**

A coarse-grained equigranular quartz monzonite to diorite stock crosscuts Telkwa andesitic tuffs in the Tatsi area (Fig. 4). Different phases of the stock contain variable plagioclase feldspar (30-55%), pink K-feldspar (up to 25%), quartz (up to 15%) and hornblende and biotite (10-20%). These phases display inconsistent crosscutting relationships. Microdiorite xenoliths are ubiquitous. Mineralized quartz and quartz-carbonate veins and alteration locally crosscut the stock (Tennant and Tompson, 1995).

**3.2.2. Bulkley suite (Late Cretaceous)**

Several small (5 to 10 m wide) diorite dikes and one larger stock (~1 km by 500 m) were observed in the Zymo ridge area (Fig. 6). The dikes trend northwesterly and northeasterly. They are fine grained and composed of dark grey diorite to quartz diorite with up to 5% biotite. Some dikes contain hornblende phenocrysts up to 3 mm long. Similar fine-grained diorite intrusions, interpreted as part of the Bulkley Suite, are spatially associated with Cu-Au mineralization at the Hobbes porphyry prospect (Laird, 2012). A plagioclase phyrlic diorite near the

Fig. 6. Continued.

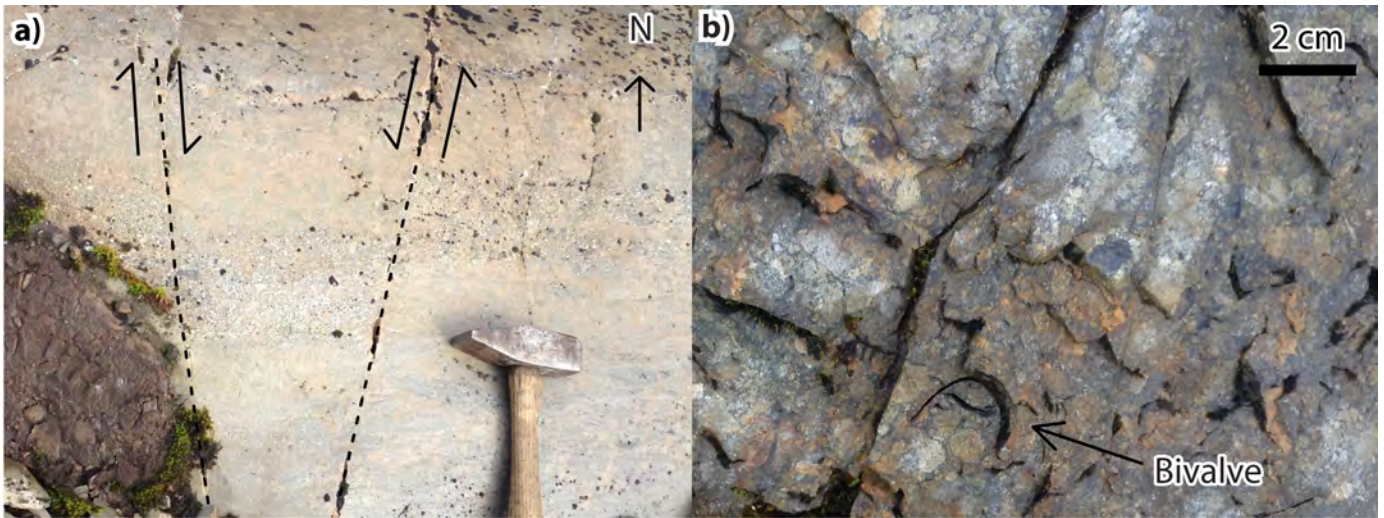


**Fig. 7.** Features of the Bowser Lake Group in the Zymo ridge area. **a)** Granulestone lens in Bowser Lake Group sandstone. Nearly parallel north-striking ( $\pm 10^\circ$ ) minor faults offset the conglomerate lens in opposite directions, reflecting the geometry of offset map units. **b)** Lapilli breccia containing bivalve fossils.

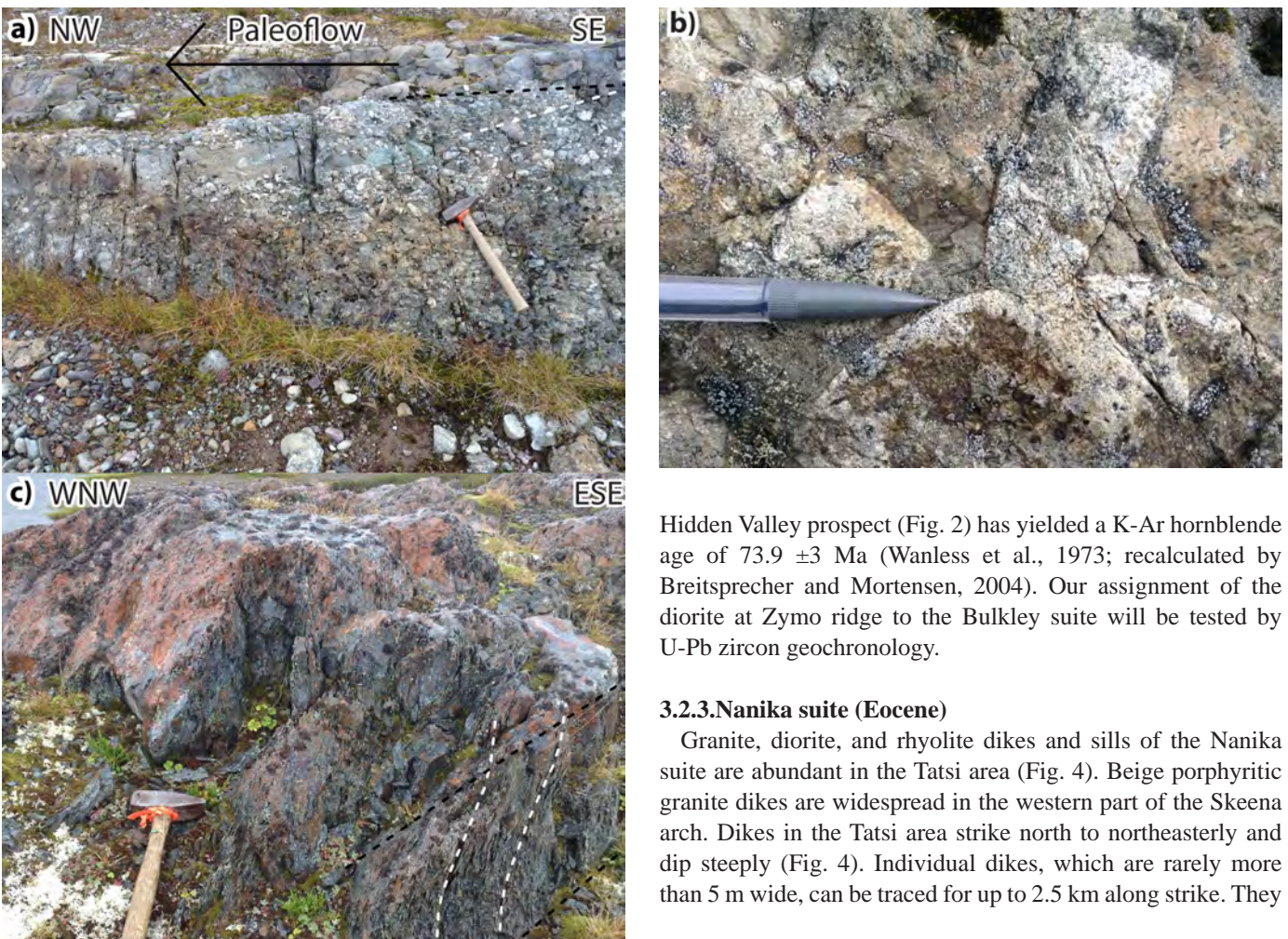


**Fig. 8.** Features of the Skeena Group near Zymo ridge. **a)** Polymictic conglomerate in the Bulkley Canyon Formation. Pebbly layer within sandstone lens marks cross bedding consistent with paleoflow towards the northwest. Dashed black line traces bedding and dashed white line traces cross bedding. **b)** Interpenetration of clasts in conglomerate. **c)** Orange-red weathered siltstone and fine-grained sandstone of the Laventie Formation. Dashed white lines trace spaced cleavage and dashed black lines trace bedding.

Hidden Valley prospect (Fig. 2) has yielded a K-Ar hornblende age of  $73.9 \pm 3$  Ma (Wanless et al., 1973; recalculated by Breitsprecher and Mortensen, 2004). Our assignment of the diorite at Zymo ridge to the Bulkley suite will be tested by U-Pb zircon geochronology.

### 3.2.3. Nanika suite (Eocene)

Granite, diorite, and rhyolite dikes and sills of the Nanika suite are abundant in the Tatsi area (Fig. 4). Beige porphyritic granite dikes are widespread in the western part of the Skeena arch. Dikes in the Tatsi area strike north to northeasterly and dip steeply (Fig. 4). Individual dikes, which are rarely more than 5 m wide, can be traced for up to 2.5 km along strike. They

contain up to 15% plagioclase, 10% hornblende, 5% biotite, and 2% quartz phenocrysts in a fine-grained grey to beige groundmass.

Medium-grained equigranular quartz diorite with locally pegmatitic margins forms a dike that crosscuts folds in the Tatsi map area (Fig. 4). It crosscuts one of the porphyritic sills described above and is therefore interpreted to be a late phase of the Nanika suite. The interior of the dike contains 7% quartz, 30% hornblende, 8% pyroxene, and 55% plagioclase. Along the pegmatitic margins are hornblende crystals, locally >5 cm long.

A beige quartz- feldspar-phyric rhyolite body occurs concordant with bedding within 100 m of the top of the Bowser Lake Group (Fig. 6). It contains 5% plagioclase and 3% quartz phenocrysts (up to 3 mm) in an aphanitic beige groundmass. It remains unclear if the body is a sill or a flow.

A series of aeromagnetic highs form a northeasterly trend immediately south of Ashman Ridge east of the Zymo ridge area (Fig. 9a; Precision GeoSurveys Inc, 2016). This trend is between the Zymo FM Zone porphyry prospect in the west and the Louise Lake porphyry prospect in the east, and includes the Willy polymetallic vein prospect. Each of these prospects is adjacent to or within a previously mapped Nanika suite intrusive body (Fig. 9b). Field mapping in the area confirmed that another aeromagnetic high along this trend corresponds to a plagioclase porphyritic diorite intrusion similar to the one at Louise Lake (Fig. 8b). The strong linear trend of these stocks suggests that a northeasterly structure likely controlled emplacement of Eocene magma locally.

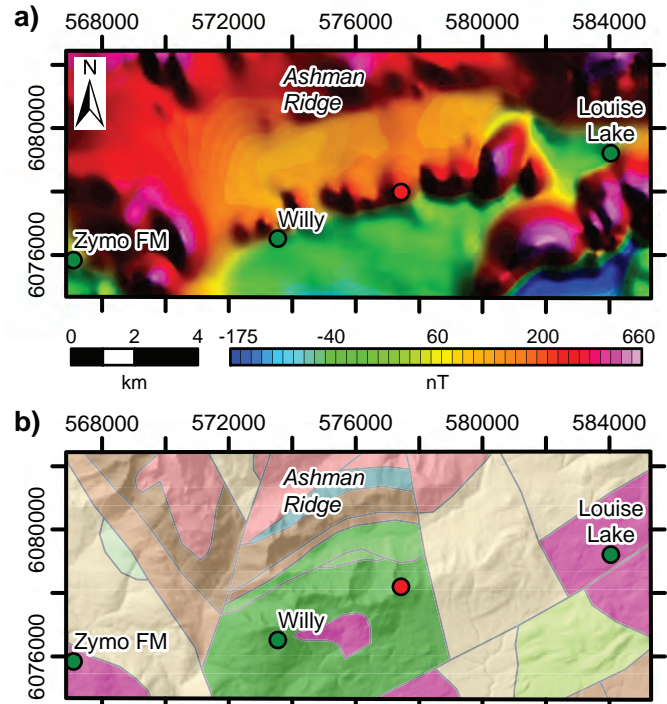
#### 4. Structure

##### 4.1. Zymo ridge

Well-bedded Skeena Group conglomerate, sandstone and mudstone along Zymo ridge are deformed into broad, open, shallowly to moderately northeast-plunging folds with wavelengths of approximately 2 km (Fig. 6). Near the cores of larger folds are similarly oriented outcrop-scale folds with wavelengths of 10 to 20 m (Figs. 9b, 10a).

Fine-grained rocks in the Skeena Group have a steeply northwest, and less commonly southeast, dipping spaced cleavage in which microlithons between cleavage foliae are spaced from 1 to 10 cm (see Powell, 1979; Engelder and Marshak, 1985; Figs. 8b, c). The intersection of this cleavage, likely generated by pressure solution, with bedding-parallel partings results in a pencil cleavage. This cleavage is interpreted as axial planar to the northeast-plunging folds as it is relatively consistent regardless of bedding orientation. Minor refraction of cleavage is present between sandstone and siltstone layers. Pervasive southwest dipping joints are observed throughout the Zymo ridge area (Fig. 10c). These joints correspond to the AC (profile) plane of folds.

Evidence of faults in the Zymo ridge area is scarce. A west-striking fault places conglomerate against black shale; the offset



#### Legend

- Selected mineral occurrence
- 2016 station

#### Stratified Rocks

- Kasalka Group
- Skeena Group - Rocky Ridge Formation
- Skeena Group - Undifferentiated
- Bowser Lake Group - Netalzul volcanics
- Bowser Lake Group - Undifferentiated
- Hazelton Group - Quock Formation
- Hazelton Group - Nilkitkwa Formation
- Hazelton Group - Telkwa Formation

#### Intrusive and Metamorphic Rocks

- Nanika intrusive suite
- Bulkley intrusive suite

**Fig. 9. a)** Reduced to pole aeromagnetic map showing strong linear trend of magnetic highs between the Zymo FM and Louise Lake developed prospects (modified after Precision GeoSurveys Inc., 2016). **b)** Bedrock geology modified after British Columbia digital geology compilation (Cui et al., 2015). See Figure 2 for location.

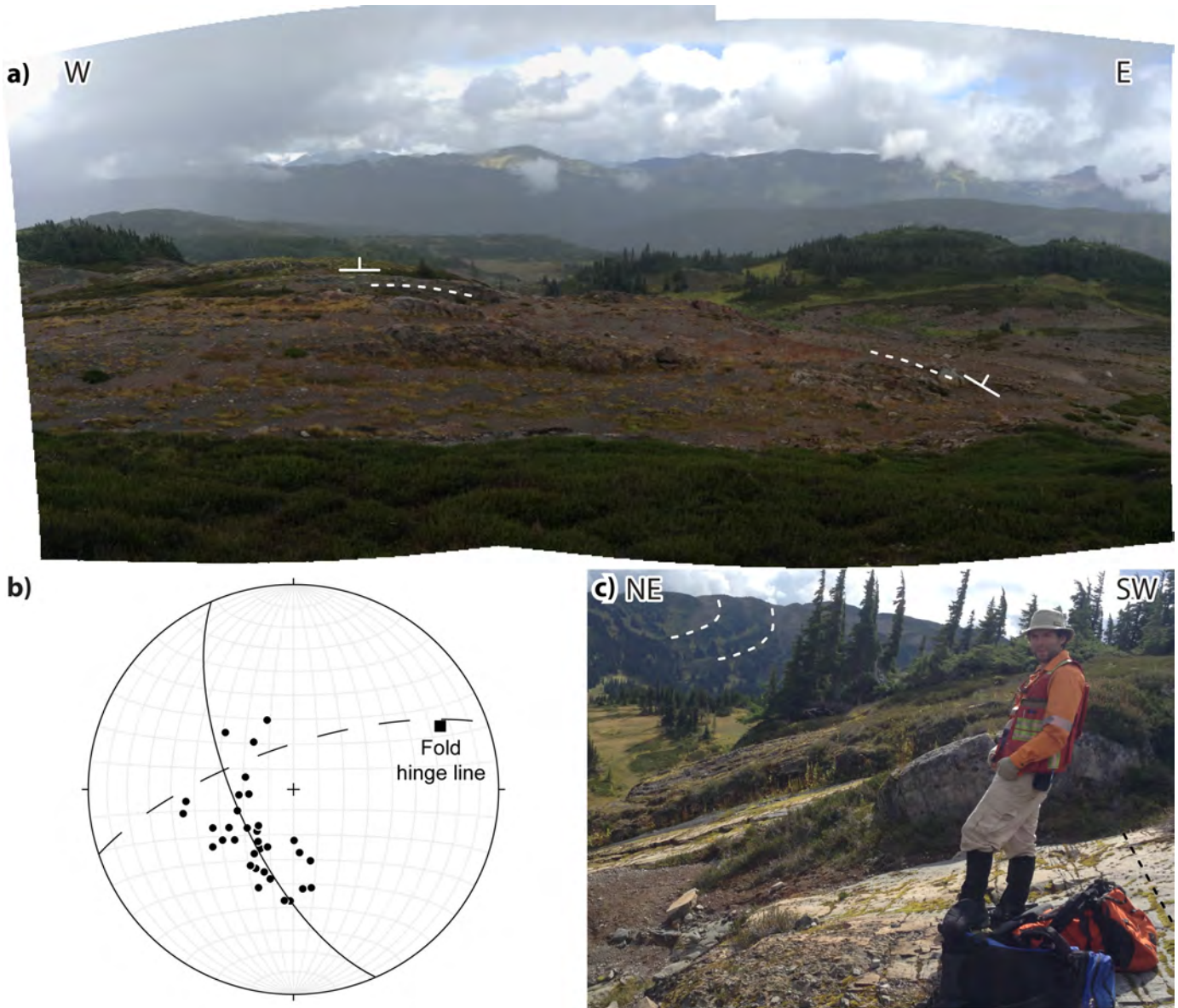


**Fig. 10.** Structures in the Zymo ridge area. **a)** Panorama of parasitic northeast-plunging fold. Dashed white lines trace bedding in two adjacent outcrops that dip to the north and northeast. Photo looking oblique to the hinge line of the fold. **b)** Lower hemisphere, equal area stereonet plot showing the orientation of structures in the Zymo ridge area excluding data from south of Red Canyon Creek. Black circles are poles to bedding. The fold hinge line orientation was calculated using eigenvalues of bedding measurements. Dashed line represents average orientation of cleavage. Solid line represents average orientation of AC joints. **c)** AC joints in Skeena Group sandstone. Dashed black line traces orientation of joints. White dashed lines trace bedding through hinge of a northeast-plunging syncline in the distance.

across the fault indicates either sinistral or north-side-down sense of shear (Fig. 6). A set of south-striking faults separates the Skeena Group into three folded panels with apparent west side down sense of shear. Similarly oriented faults in the Bowser Lake Group are observed to have opposing sense of shear at outcrop (Fig. 7a) and map scale (Fig. 6).

#### 4.2. Tatsi area

The exceptionally well-bedded tuffs in the southern Howson Range are deformed into northeast trending folds. A northwest-vergent fold was observed in the cirque west of Mount

Desdemona (Fig. 11a). In the northern headwall it is accentuated by a pale purple marker tuff that is offset approximately 50 m across the fault. Bedding varies between shallowly southeast and steeply northwest dipping (Fig. 11b). Folds were also identified through air photo interpretation in areas where steep terrane restricted access. Shallowly south- to southeast-dipping quartz veins at the Tatsi prospect host bornite, chalcopyrite, galena, sphalerite, electrum, and native silver (Fig. 4; Tennant and Tompson, 1995). Slickenlines along the margins of one such vein have an azimuth of  $150^\circ$  and a plunge of  $19^\circ$  (Fig. 11b). En-echelon vein sets have enveloping surfaces parallel

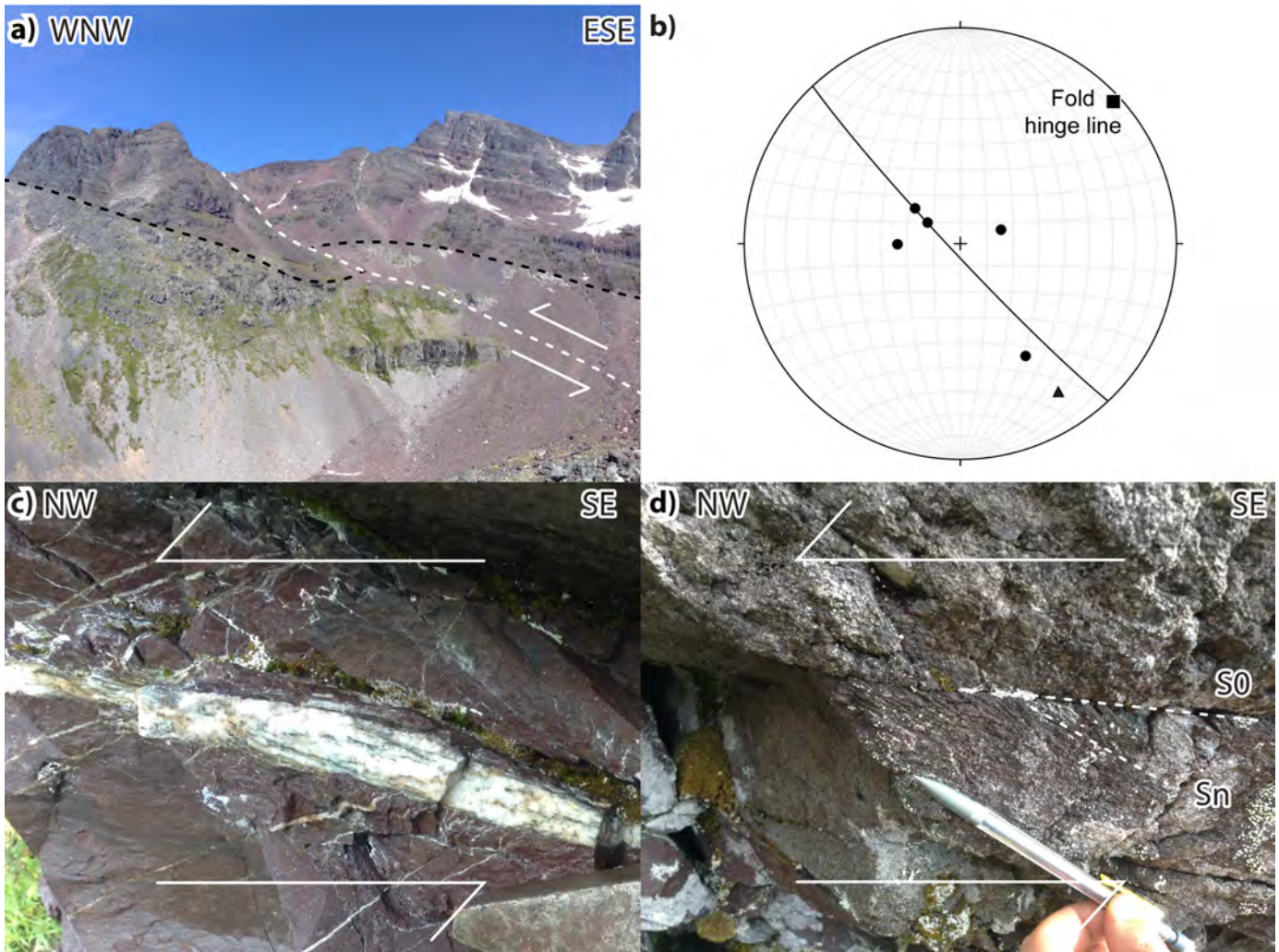


**Fig. 11.** Structural features in the Tatsi map area. **a)** Northwest-vergent thrust fault with minor fold. Dashed white line indicates trace of thrust. Black dashed lines indicate contact between pale purple marker crystal tuff and well bedded red tuffs. **b)** Lower hemisphere, equal area stereonet projection of structural elements in the Tatsi map area. Black circles are poles to bedding. Black Triangle is a slickenline on the surface of the mineralized vein in Figure 10c. The fold hinge line was calculated using eigenvalues of poles to bedding. The solid black line represents best-fit great circle of bedding. **c)** A south-southeast dipping mineralized vein that crosscuts weakly folded north-west dipping veinlets, interpreted sense of shear is top to the north-northwest. **d)** Weak south-southeast dipping foliation developed in fine red tuff indicating north-northwest vergence.

the southeast dipping veins. Individual veins within the sets that dip variably to the northwest; minor folds are consistent with top-to-the-northwest sense of shear (Fig. 11c). Cleavage in one fine ash tuff is oblique to bedding, dipping shallowly to the southeast, consistent with northwest vergence (Fig. 11d).

A northwest-striking, steeply west dipping fault juxtaposes andesite lapilli tuff in the lower part of the lower Telkwa Formation to the west against fine-grained red tuffs in the upper part of the Telkwa Formation to the east (Fig. 4). Near the fault, flattened lapilli in the Telkwa Formation andesitic tuffs define a moderate foliation. A quartz monzonite dike, interpreted to belong to the Topley intrusive suite, crosscuts foliation and is crosscut by several shallowly south dipping veinlets. A locally prominent set of steeply dipping joints follow the same northerly trend as the fault.

## 5. Discussion

The stratigraphic descriptions outlined herein support previous interpretations indicating that the Skeena arch became a northeast-trending topographic highland between Middle Jurassic and Early Cretaceous. Laterally continuous tuff beds in the Telkwa Formation in the Howson Range contrast with the high-standing volcanic edifices farther west (Barresi et al., 2015). The Telkwa Formation in the Howson Range represents the fringes of these stratovolcanoes, transitional to submarine deposition represented by the Babine shelf and Kotsine marine facies farther east (Tipper and Richards, 1976a). Submarine conditions persisted in the Middle Jurassic across most of Stikinia, extending as far south as Telkwa Pass in the Skeena arch region. The transition from the Hazelton Group to the Bowser Lake Group is gradational, marked by

the upwards disappearance of distinctive tuff beds within an otherwise continuous submarine sequence (Evenchick et al., 2010; Gagnon et al., 2012). The Skeena arch underwent uplift from the Middle Jurassic to Early Cretaceous, as recorded by the transition from relatively deep-water sedimentation in the lower part of Bowser Lake Group to predominantly fluvial deposition in the lower part of the Skeena Group at Zymo ridge (Bulkley Canyon Formation). Tipper and Richards (1976a) interpreted that the Skeena arch was a sediment source for parts of the Bowser Lake Group. We interpret that the volcanic and plutonic clasts in polymictic conglomerates of the Bulkley Canyon Formation at Zymo ridge were derived locally, from the uplifted Skeena arch. Why the Skeena arch was uplifted along a northeasterly trend between the Middle Jurassic and Early Cretaceous, in contrast to the northwest trending arc axis indicated by Early Jurassic facies belts, is unknown.

The northeasterly orientation of the Skeena arch is reflected by the trend of folds and plutonic suites in it. Northeast-trending (northwest- and southeast-vergent) fold and thrust deformation is Early Cretaceous or younger because it affected the Skeena Group. Northwest-southeast shortening could have contributed to uplift of the Skeena arch. However, stratigraphic arguments indicate that the arch became a topographic high before the Early Cretaceous. This suggests that uplift of the Skeena arch was a protracted process, with later stages recorded by folds in sedimentary rocks derived from the arch. We speculate that these northeast-trending folds reflect the orientation of a deep crustal structure when considered in conjunction with other parallel features. Structures of this orientation may have been under extension during the Late Triassic to Early Jurassic, contributing to the emplacement of the Topley and Kleanza intrusive suites (Nelson, 2017). It is possible that they were inverted during the Late Jurassic to Early Cretaceous, leading to uplift of the Skeena arch and northeast trending folds in it. This geometry would be compatible with the sinistral transpressional regime interpreted to be responsible for northeast trending folds in the Skeena fold and thrust belt (Evenchick, 2001). The same deep crustal structure (or structures) is interpreted to have remained as a magma conduit into the Late Cretaceous and Eocene, leading to the widespread porphyry and related mineralization across the Skeena arch.

## 6. Conclusion

The Skeena arch is interpreted to reflect a fundamental, long-lived structural anisotropy in Stikine terrane. This anisotropy must have originated during the Triassic or earlier because it accommodated emplacement of Late Triassic to Early Jurassic magma. It was reactivated during inferred Early Cretaceous development of northeast-trending thrusts and folds. We speculate that uplift of the Skeena arch between the Middle Jurassic and Early Cretaceous is an early manifestation of strain that led to fold and thrust deformation. The structural anisotropy also played a role in localizing emplacement of Late Cretaceous and Eocene intrusive suites and mineralization, similar to other examples of arc transverse structures worldwide.

## Acknowledgments

Mapping was carried out as part of the SeArch project, a collaborative effort between the British Columbia Geological Survey, Geoscience BC, and the Mineral Deposit Research Unit of The University of British Columbia. The manuscript benefited from thoughtful reviews of earlier drafts by James Mortensen and Lawrence Aspler. We thank Alexina Boileau, Stephanie Fogg, and Guillaume Lesage for their assistance in the field. Jeff Kyba provided many valuable discussions on tectonics and mineralization in northwestern British Columbia. We appreciate the expert flying of Ryan Hinds and the Silverking Helicopters team and logistical support provided by Stephanie McGuinness in Smithers.

## References cited

- Angen, J.J., 2009. Geospatial structural analysis of the terrace area, west-central British Columbia (NTS 1031/08, 09, 10, 16). In: Geological Fieldwork 2008, British Columbia Ministry of Energy, Mines and Petroleum Resources, British Columbia Geological Survey Paper 2009-1, pp. 21-34.
- Angen, J.J., Hart, C.J.R., Logan, J.M., Kim, R., and Rahimi, M., 2016. TREK mapping project year 2: a structural framework for the northern Interior Plateau. AMEBC Mineral Exploration Roundup (poster), <[www.geosciencebc.com/i/pdf/Roundup2016/2016%20poster\\_Angen.pdf](http://www.geosciencebc.com/i/pdf/Roundup2016/2016%20poster_Angen.pdf)>, last accessed November, 2016.
- Ash, C.H., Macdonald, R.W.J., and Paterson, I.A., 1993. Geology of the Stuart - Pinchi lakes area, central British Columbia parts of (93K/7, 8, 9, 10 and 11). British Columbia Ministry of Energy, Mines and Petroleum Resources Open File 1993-9, 1:100,000 scale.
- Barresi, T., Nelson, J.L., Dostal, J., and Friedman, R.M., 2015. Evolution of the Hazelton arc near Terrace, British Columbia: stratigraphic, geochronological, and geochemical constraints on a Late Triassic - Early Jurassic arc and Cu-Au porphyry belt. *Canadian Journal of Earth Sciences*, 52, 466-494.
- Bassett, K.N., and Kleinspehn, K.L., 1997. Early to middle Cretaceous paleogeography of north-central British Columbia: stratigraphy and basin analysis of the Skeena Group. *Canadian Journal of Earth Sciences*, 34, 1644-1669.
- Breitsprecher, K., and Mortensen, J.K., 2004. BC Age 2004A-1: A database of isotopic age determinations for rock units from British Columbia. British Columbia Ministry of Energy, Mines, and Petroleum Resources, British Columbia Geological Survey Open File 2004-03.
- Carter, N.C., Dirom, G.E., and Ogryzlo, P.L., 1995. Porphyry copper-gold deposits, Babine Lake area, west-central British Columbia. In: Schroeter, T.G., (Ed.), *Porphyry Deposits of the Northwestern Cordillera of North America*. Canadian Institute of Mining, Metallurgy and Petroleum Special Publication 46, pp. 247-255.
- Colpron, M., and Nelson, J.L., 2011. A digital atlas of terranes for the northern Cordillera. Accessed online from Yukon Geological Survey [www.geology.gov.yk.ca](http://www.geology.gov.yk.ca). [November, 2016].
- Cui, Y., Miller, D., Nixon, G., and Nelson, J., 2015. British Columbia digital geology. British Columbia Ministry of Energy and Mines, British Columbia Geological Survey Open File 2015-2.
- Desjardins, P., MacIntyre, D.G., Hunt, J., Lyons, L., and Pattenden, S., 1990. Geology of the Thautil River map area (93L/6). In: Geological Fieldwork 1989, British Columbia Ministry of Energy, Mines and Petroleum Resources, British Columbia Geological Survey Paper 1993-1, pp. 91-99.
- Deyell, C.L., Thompson, J.F.H., Friedman, R.M., and Groat, L.A., 2000. Age and origin of advanced argillic alteration zones and related exotic limonite deposits in the Limonite Creek area, central

- British Columbia. *Canadian Journal of Earth Sciences*, 53, 1093-1107.
- Diakow, L.J., Webster, I.C.L., Richards, T.A., and Tipper, H.W., 1997. Geology of the Fawnie and Nechako ranges, southern Nechako Plateau, central British Columbia (93F/2, 3, 6, 7). In: Diakow, L.J., Newell, J.M., and Metcalfe, P., (Eds.), Interior Plateau geoscience project: summary of geological, geochemical and geophysical studies, British Columbia Ministry of Energy and Mines, British Columbia Geological Survey Open File 1997-2 and Geological Survey of Canada Open File 3448, pp. 7-30.
- Dirom, G.E., Dittrock, M.P., McArthur, D.R., Ogryzlo, P.L., Pardoe, A.J., and Stothart, P.G., 1995. Bell and Granisle porphyry copper-gold mines, Babine region, west-central British Columbia. In: Schroeter, T.G., (Ed.), *Porphyry deposits of the northwestern cordillera of North America*. Canadian Institute of Mining, Metallurgy and Petroleum Special Publication 46, pp. 256-289.
- Engelder, T., and Marshak, S., 1985. Disjunctive cleavage formed at shallow depths in sedimentary rocks. *Journal of Structural Geology*, 7, 327-343.
- Evenchick, C.A., 1991. Geometry, evolution, and tectonic framework of the Skeena Fold Belt, north-central British Columbia. *Tectonics*, 10, 527-546.
- Evenchick, C.A., 2001. Northeast-trending folds in the western Skeena Fold Belt, northern Canadian Cordillera: a record of Early Cretaceous sinistral plate convergence. *Journal of Structural Geology*, 23, 1123-1140.
- Evenchick, C.A., Mustard, P.S., McMechan, M.E., Ritcey, D.H., and Smith, G.T., 2008. Geology, northeast Terrace and northwest Smithers, British Columbia. Geological Survey of Canada Open File 5895, 1:125,000 scale.
- Evenchick, C.A., Poulton, T.P., and McNicoll, V.J., 2010. Nature and significance of the diachronous contact between the Hazelton and Bowser Lake groups (Jurassic), north-central British Columbia. *Bulletin of Canadian Petroleum Geology*, 58, 235-267.
- Friedman, R.M., Diakow, L.J., Lane, R.A., and Mortensen, J.K., 2001. New U-Pb age constraints on latest Cretaceous magmatism and associated mineralization in the Fawnie Range, Nechako Plateau, central British Columbia. *Canadian Journal of Earth Sciences*, 38, 619-637.
- Gagnon, J.F., Barresi, T., Waldron, J.F., Nelson, J.L., Poulton, T.P., and Cordey, F., 2012. Stratigraphy of the Upper Hazelton Group and the Jurassic evolution of the Stikine terrane, British Columbia. *Canadian Journal of Earth Sciences*, 49, 1027-1052.
- Gareau, S.A., Friedman, R.M., Woodsworth, G.J., and Childe, F., 1997. U-Pb ages from the northeastern quadrant of Terrace map area, west-central British Columbia. In: *Current Research, Geological Survey of Canada Paper 1997-A*, pp. 31-40.
- Garwin, S., Hall, R., and Watanabe, Y., 2005. Tectonic setting, geology and gold and copper mineralization in Cenozoic magmatic arcs of Southeast Asia and the west Pacific. In: Hedenquist, J., Goldfarb, R., and Thompson, J., (Eds.), *Economic Geology 100th anniversary volume, Society of Economic Geologists*, pp. 891-930.
- Glen, R.A., and Walshe, J.L., 1999. Cross-structures of the Lachlan orogen: the Lachlan transverse zone example. *Australian Journal of Earth Sciences*, 46, 641-658.
- Gow, P.A., and Walshe, J.L., 2005. The role of pre-existing geologic architecture in the formation of giant porphyry-related Cu+Au deposits: examples from New Guinea and Chile. In: Hedenquist, J., Goldfarb, R., and Thompson, J., (Eds.), *Economic Geology 100th anniversary volume, Society of Economic Geologists*, pp. 819-833.
- Hayward, N., and Calvert, A.J., 2011. Interpretation of structures in the southeastern Nechako Basin, British Columbia, from seismic reflection, well log, and potential field data. *Canadian Journal of Earth Sciences*, 48, 1000-1020.
- Heidrick, T.L., and Titley, S.R., 1982. Fracture and dike patterns in Laramide plutons and their structural and tectonic implications: American southwest. In: Titley, S.R. (Ed.), *Advances in geology of the porphyry copper deposits: southwestern North America*. University of Arizona Press, Tucson, pp. 73-91.
- Hill, K.C., Kendrick, R.D., Crowhurst, P.V., and Gow, P.A., 2002. Copper-gold mineralisation in New Guinea: tectonics, lineaments, thermochronology and structure. *Australian Journal of Earth Sciences*, 49, 737-752.
- Jackson, A., and Illerbrun, K., 1995. Huckleberry porphyry copper deposit, Tahtsa Lake district, west-central British Columbia. In: Schroeter, T.G., (Ed.), *Porphyry Deposits of the Northwestern Cordillera of North America*. Canadian Institute of Mining, Metallurgy and Petroleum Special Publication 46, pp. 313-321.
- Laird, B.L., 2012. 2012 exploration program on the Zymo property, Omineca Mining Division, British Columbia. British Columbia Ministry of Energy, Mines and Natural Gas, Assessment Report 33546, 201p.
- Logan, J.M., and Mihalynuk, M.G., 2014. Tectonic controls on Early Mesozoic paired alkaline porphyry deposit belts (Cu-Au ± Ag-Pt-Pd-Mo) within the Canadian cordillera. *Economic Geology*, 109, 827-858.
- MacIntyre, D.G., 1998. Babine porphyry belt project: bedrock geology of the Nakinilerak Lake map sheet (93M/8), British Columbia. In: *Geological Fieldwork 1997*, British Columbia Ministry of Employment and Investment, British Columbia Geological Survey Paper 1998-1, pp. 2-1 to 2-18.
- MacIntyre, D.G., 2006. Geology and mineral deposits of the Skeena Arch, west-central British Columbia: a Geoscience BC digital data compilation project. In: *Geological Fieldwork 2005*, British Columbia Ministry of Energy, Mines and Petroleum Resources, British Columbia Geological Survey Paper 2006-1, pp. 303-312.
- MacIntyre, D.G., Desjardins, P., and Tercier, P., 1989. Jurassic stratigraphic relationships in the Babine and Telkwa ranges (93L/10, 11, 14, 15). In: *Geological Fieldwork 1989*, B.C. Ministry of Energy, Mines, and Petroleum Resources, British Columbia Geological Survey Paper 1989-1, pp. 195-208.
- McMechan, M., 2007. Nature, origin and tectonic significance of anomalous transverse structures, southeastern Skeena Fold Belt, British Columbia. *Bulletin of Canadian Petroleum Geology*, 55, 262-274.
- Mihalynuk, M.G., Erdmer, P., Ghent, E.D., Cordey, F., Archibald, D.A., Friedman, R.M., and Johannson, G.G., 2004. Coherent French Range blueschist: subduction to exhumation in <2.5 m.y.? *Geological Society of America Bulletin*, 116, 910-922.
- Nelson, J.L., 2009. Terrace project year 4: extension of Paleozoic volcanic belt and indicators of VMS-style mineralization near Kitimat (NTS 103I/02, 07). In: *Geological Fieldwork 2008*, British Columbia Ministry of Energy, Mines and Petroleum Resources, British Columbia Geological Survey Paper 2009-1, pp. 7-20.
- Nelson, J., 2017. Composite pericratonic basement of west-central Stikinia and its influence on Jurassic magma conduits: Examples from the Terrace-Ecstall and Anyox areas. In: *Geological Fieldwork 2016*, British Columbia Ministry of Energy and Mines, British Columbia Geological Survey Paper 2017-1, this volume.
- Nelson, J.L., and Kennedy, R., 2007. Terrace regional mapping project year 2: New geological insights and exploration targets (NTS 103I/16S, 10W), west-central British Columbia. In: *Geological Fieldwork 2006*, British Columbia Ministry of Energy, Mines and Petroleum Resources, British Columbia Geological Survey Paper 2007-1, pp. 149-162.
- Nelson, J.L., Barresi, T., Knight, E., and Boudreau, N., 2006. Geology and mineral potential of the Usk map area (103I/09) near Terrace, British Columbia. In: *Geological Fieldwork 2005*, British Columbia Ministry of Energy, Mines and Petroleum Resources, British Columbia Geological Survey Paper 2006-1, pp. 117-134.
- Nelson, J.L., Kyba, J., McKeown, M., and Angen, J., 2008. Terrace regional mapping project, year 3: contributions to stratigraphic, structural and exploration concepts, Zymoetz River to Kitimat

- River, east-central British Columbia (NTS 103I/08). In: Geological Fieldwork 2007, British Columbia Ministry of Energy, Mines and Petroleum Resources, British Columbia Geological Survey Paper 2008-1, pp. 159-174.
- Nelson, J.L., Colpron, M., and Israel, S., 2013. The Cordillera of British Columbia, Yukon and Alaska: tectonics and metallogeny. In: Colpron, M., Bissig, T., Rusk, B.G. and Thompson, J.F. (Eds.), *Tectonics, Metallogeny and Discovery: The North American Cordillera and Similar Accretionary Settings*. Society of Economic Geologists Special Publication 17, pp. 53-110.
- Pálffy, J., Mortensen, J.K., Smith, P.L., Friedman, R.M., McNicoll, V., and Villeneuve, M., 2000. New U–Pb zircon ages integrated with ammonite biochronology from the Jurassic of the Canadian cordillera. *Canadian Journal of Earth Sciences*, 37, 549-567.
- Palsgrove, R.J., and Bustin, R.M., 1991. Stratigraphy, sedimentology and coal quality of the lower Skeena Group, Telkwa coalfield, central British Columbia (NTS 093L/11). British Columbia Geological Survey Paper 1991-2, 68p.
- Powell, C. McA., 1979. A morphological classification of rock cleavage. *Tectonophysics*, 58, 21-34.
- Precision GeoSurveys Inc., 2016. Airborne magnetic survey, SeArch project. Geoscience BC, Report 2016-02, 62 p. <<http://www.geosciencebc.com/s/Report2016-02.asp>> last accessed December, 2016.
- Richards, J.P., 2000. Lineaments revisited. *Society of Economic Geologists Newsletter*, 42, 1, 14-20.
- Richards, J.P., Boyce, A.J., and Pringle, M.S., 2001. Geological evolution of the Escondida area, northern Chile: A model for spatial and temporal localization of porphyry Cu mineralization. *Economic Geology*, 96, 271-305.
- Richards, T.A., and Jeletzky, O.L., 1975. A preliminary study of the Upper Jurassic Bowser assemblage in the Hazelton, west half, map-area, British Columbia. In: Report of Activities, Geological Survey of Canada Paper 75-1A, pp. 31-36.
- Ryan, B.C., 1993. Geology of the Telkwa coalfield, British Columbia. British Columbia Ministry of Energy, Mines, and Petroleum Resources, British Columbia Geological Survey Open File 1993-21, 1:20,000 scale.
- Schiarizza, P., and MacIntyre, D.G., 1999. Geology of the Babine Lake – Takla Lake area, central British Columbia. In: Geological Fieldwork 1998, British Columbia Ministry of Energy and Mines, British Columbia Geological Survey Paper 1999-1, pp. 33-68.
- Schmitt, H.A., 1966. The porphyry copper deposits in their regional setting. In: Titley, S.R., and Hicks, C.L., (Eds.), *Geology of the porphyry copper deposits, southwestern North America*. University of Arizona Press, Tucson, pp. 17-33.
- Smith G.T., and Mustard, P.S., 2006. Supporting evidence for a conformable southern contact of the Bowser Lake and Skeena groups. In: Geological Fieldwork 2005, British Columbia Ministry of Energy, Mines and Petroleum Resources Paper 2006-1, pp.125-134.
- Sutherland-Brown, A., 1960. Geology of the Rocher Debole Range. British Columbia Department of Mines and Petroleum Resources Bulletin 43, 85p.
- Tennant, S.J., and Tompson, W.D., 1995. 1995 Geological, geophysical and diamond drilling assessment report on the Tatsi gold-silver-copper prospect, Kitnayakwa River area, Omineca Mining Division, British Columbia. British Columbia Ministry of Energy, Mines and Petroleum Resources, Assessment Report 24175, 186p.
- Tipper, H.W., and Richards, T.A., 1976a. Jurassic stratigraphy and history of north-central British Columbia. *Geological Survey of Canada Bulletin* 270, 73p.
- Tipper, H.W., and Richards, T.A., 1976b. Smithers map-area. Geological Survey of Canada Open File 351, 1:253,440 scale.
- Tosdal, R.M., and Richards, J.P., 2001. Magmatic and structural controls on the development of porphyry Cu ± Mo ± Au deposits. *Society of Economic Geologists, Reviews*, 14, 157-181.
- Waldron, J.W.F., Gagnon, J-F., Loogman, W., and Evenchick, C.A., 2006. Initiation and deformation of the Jurassic-Cretaceous Bowser Basin: implications for hydrocarbon exploration. In: Geological Fieldwork 2005, British Columbia Ministry of Energy, Mines and Petroleum Resources Paper 2006-1, pp. 349-360.
- Wanless, R.K., Stevens, R.D., Lachance, G.R., and Delabio, R.N., 1973. Age determinations and geological studies, K-Ar isotopic ages, report 11. Geological Survey of Canada Paper 73-2, 139p.

# Testing the relationship between the Llewellyn fault, gold mineralization, and Eocene volcanism in northwest British Columbia: A preliminary report



Luke Ootes<sup>1, a</sup>, Jessica M. Elliott<sup>2</sup>, and Stephen M. Rowins<sup>1, 2</sup>

<sup>1</sup>British Columbia Geological Survey, Ministry of Energy and Mines, Victoria, BC, V8W 9N3

<sup>2</sup>School of Earth and Ocean Sciences, University of Victoria, Victoria, BC, V8P 5C2

<sup>a</sup>corresponding author: Luke.Ootes@gov.bc.ca

Recommended citation: Ootes, L., Elliott, J.M., and Rowins, S.M., 2017. Testing the relationship between the Llewellyn fault, gold mineralization, and Eocene volcanism in northwest British Columbia: A preliminary report. In: Geological Fieldwork 2016, British Columbia Ministry of Energy and Mines, British Columbia Geological Survey Paper 2017-1, pp. 49-59.

## Abstract

The Llewellyn fault represents a significant geological feature in northwest British Columbia. The fault is at least 100 km long, northwest striking, and steeply dipping. An early ductile history is preserved as foliations, lineations, and local folds in the wallrocks. The fault has a later brittle history, preserved as gouge and multiple fracture sets. Dextral offset related to the brittle deformation overprints earlier ductile fabrics. The quartz-carbonate vein-hosted, past-producing Engineer gold deposit (epithermal, low-sulphidation type) is related to this late brittle deformation. Available geochronological data indicate that the deposit formed in the Eocene (ca. 55-50 Ma). Along the likely extension of the Llewellyn fault to the north in the Yukon (Tally-Ho shear zone) are the Mount Skukum gold deposit and a series of gold deposits at Montana Mountain, also of the low-sulphidation epithermal-type. Both the host volcanic rocks at Mount Skukum (Sloko Group) and gold mineralization are coeval (ca. 55 Ma). Because Mount Skukum gold mineralization is directly related to Eocene volcanism, and Engineer gold mineralization is both spatially and temporally coincident with Eocene magmatism, preliminary comparisons suggest a three-part relationship between large-scale structure, gold mineralization, and Eocene magmatism in northwest British Columbia and southwest Yukon.

**Keywords:** Llewellyn fault, gold mineralization, Eocene magmatism, Mount Skukum Mine, Engineer Mine

## 1. Introduction

More than 100 km long, the Llewellyn fault is a major, steeply dipping, northwest-striking structure in northwest British Columbia (Figs. 1, 2; Mihalynuk et al., 1994; 1999). Spatially related to the fault are quartz-carbonate vein-hosted gold-silver and base-metal prospects, including the past-producing Engineer mine (Fig. 2; Mauthner et al., 1996; Millonig et al., 2015). Also spatially related are Eocene volcano-plutonic centres (Fig. 2; Mihalynuk et al., 1999). The Llewellyn fault appears to continue northwest into Yukon (Tally-Ho shear zone, Fig. 2; Doherty and Hart, 1988; Hart and Pelletier, 1989) as indicated by similarities in vein-hosted precious and base-metal deposits and spatially related Eocene volcanic complexes (Doherty and Hart, 1988; Love, 1989; Love et al., 1998).

The spatial relationship between the Llewellyn fault and vein-hosted mineralization supports a structural link, and geochronological data indicate a temporal link between gold mineralization (Engineer and Mount Skukum mines) and Eocene volcanism (Love et al., 1998; Mihalynuk et al., 1999; Millonig et al., 2015). Many of the gold deposits are epithermal (Nesbitt et al., 1986; Walton, 1986; Love, 1989; Mauthner et al., 1996; Mihalynuk et al., 1999; Love et al., 1998; Millonig et al., 2015), although some, like those at Montana Mountain (Fig. 2) are considered mesothermal (Hart and Pelletier, 1989). The apparent relationship between structure, mineralization,

and magmatism points to the intrusion-related, epizonal, end-member of the orogenic gold deposit model because such deposits are typically related to first-order crustal breaks and synchronous magmatism (e.g., Goldfarb et al., 2005). To gain a better understanding of the spatial and temporal relationships between the Llewellyn fault, gold mineralization, and Eocene magmatism and the possible connections to the orogenic-style of gold mineralization, we conducted three weeks of field reconnaissance along the trace of the northern segment of the fault in British Columbia. This work included inspecting spatially related gold prospects, past-producing deposits and, where possible, Eocene volcanic rocks in British Columbia and Yukon. This report summarizes this reconnaissance and proposes future avenues of research.

## 2. Geologic setting

We examined the Llewellyn fault between Engineer Mine and Bennett Lake near the British Columbia-Yukon border and investigated rock units adjacent to the Klondike Highway between the communities of Carcross and Fraser (Fig. 2). Excursions were also made to the past-producing Mount Skukum and Montana Mountain gold-silver mines in the southern Yukon (Roots, 1981; Hart and Pelletier, 1989; Love, 1989). Foot traverses were set out by truck along maintained roads, ATV's on trails (Bennett Plateau and Mount Skukum),

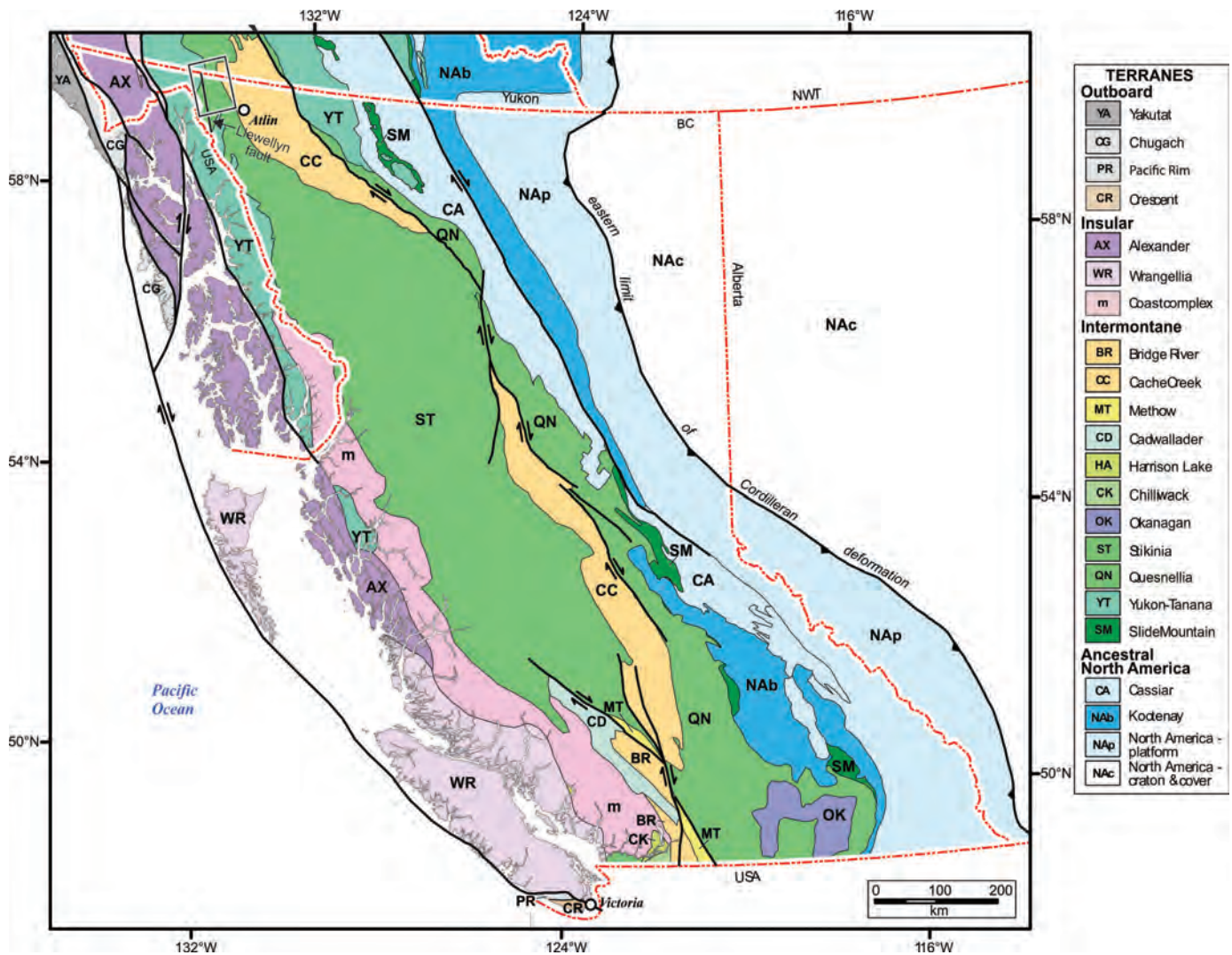


Fig. 1. Geological terrane map of British Columbia and neighbouring jurisdictions. The study area in northwest BC is highlighted by a black outline. Modified after Nelson et al. (2013).

and helicopter in more remote areas.

The part of the study area in British Columbia was previously mapped at 1:50,000 scale and incorporated into a regional geological map at 1:100,000 scale (Mihalynuk et al., 1999). Geological features in the area of Mount Skukum, Yukon, were mapped at 1:50,000 scale by Doherty and Hart (1988); detailed deposit-scale studies were by McDonald (1987), McDonald and Godwin (1986), Pride (1986), and Love (1989; 1990a, b). Roots (1981, 1982) and Hart and Pelletier (1989) described geology of the Montana Mountain area, Yukon, including the past-producing Venus gold-silver and other mines.

The Llewellyn fault is a northwest-striking, steeply-dipping strike-slip deformation zone that displays an early ductile history overprinted by brittle fabrics (Fig. 3). The fault extends from the Tulsequah area in the south (where the fault crosses into Alaska), to Bennett Lake, British Columbia, and likely continues northward into Yukon as the Tally-Ho shear zone (Doherty and Hart, 1988; Hart and Pelletier, 1989; Mihalynuk

et al., 1999; Tizzard et al., 2009). South of Atlin Lake, the Llewellyn fault may merge with the southeast striking King Salmon thrust fault (e.g., Mihalynuk et al., 1999). Between Tagish and Bennett lakes (see figure 2-1 in Mihalynuk et al., 1999) the Llewellyn fault marks the eastern extent of the Wann River gneiss, Florence River Metamorphic suite, and the Boundary Ranges metamorphic suite, rocks all considered to be Triassic or older. East of the Llewellyn fault are Triassic-Jurassic rocks of the Stuhini and Laberge groups. Triassic-Jurassic, Early Cretaceous, and Late Cretaceous-Tertiary plutons and minor volcanic complexes are on both sides of the Llewellyn fault along its strike length; the volcanic rocks have been assigned to the Sloko Group (Fig. 2; Mihalynuk et al., 1999). In the study area, these magmatic centres generally cap older units, forming steep, high-elevation terrain. Examples of these centres include

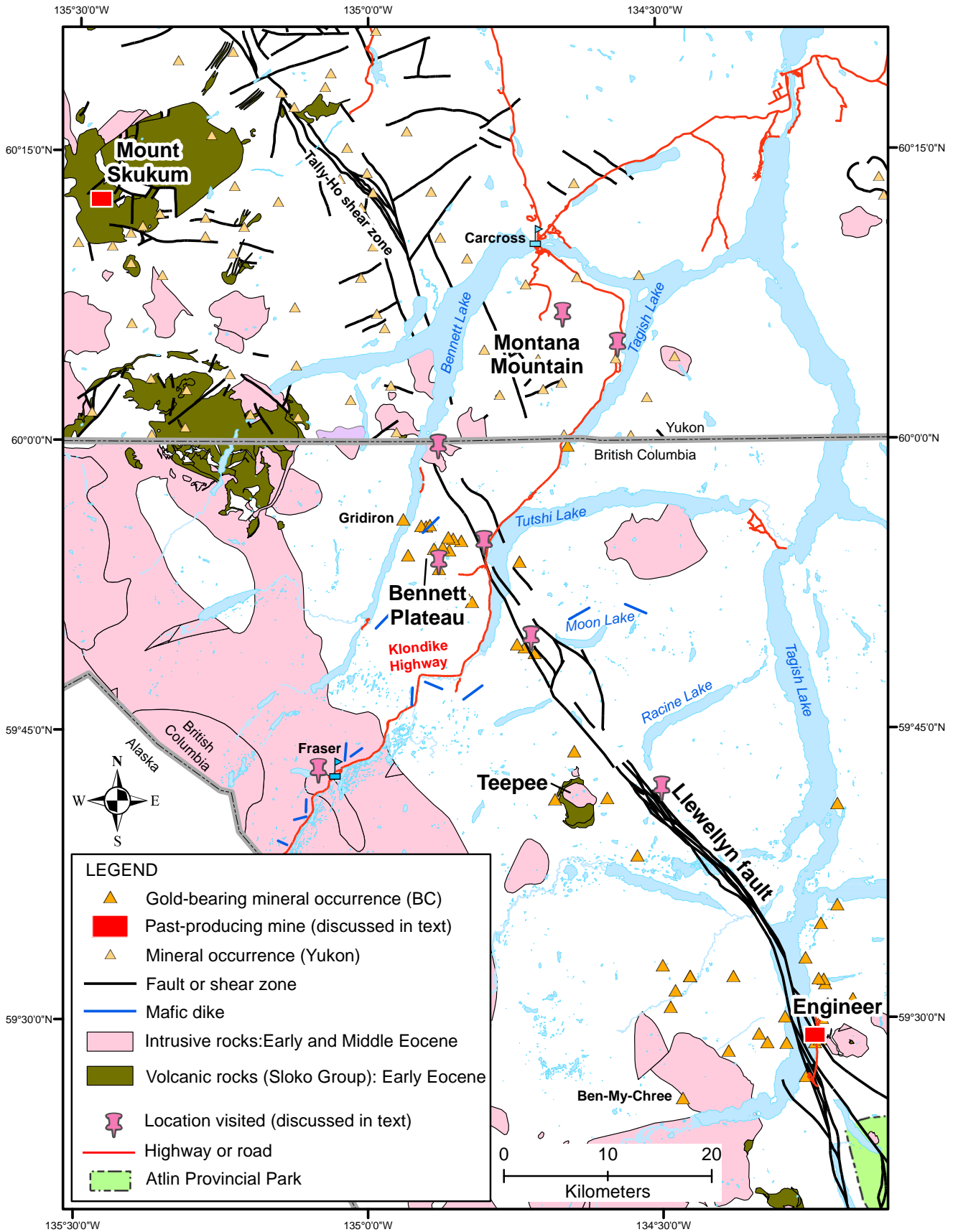


Fig. 2. Simplified geology (Eocene rock units only) near the Llewellyn fault, northwest British Columbia (Doherty and Hart, 1988; Mihalynuk et al., 1999).

**Table 1.** Temporally relevant magmatism and gold mineralization near the Llewellyn fault, northwest BC and southwest Yukon.

Location	Interpretation	Age (Ma)	Mineral	Method	Source
Engineer Mountain	rhyolite - SPS	ca. 54	zircon	U-Pb - age only presented	Mihalynuk et al. 1999
Atlin Mountain west	ignimbrite - SG	ca. 54	zircon	U-Pb - age only presented	Mihalynuk et al. 1999
Mount Switzer	rhyolite - SG	ca. 55	zircon	U-Pb - age only presented	Mihalynuk et al. 1999
	quartz monzonite - SPS	ca. 56	zircon	U-Pb - age only presented	Mihalynuk et al. 1999
	diorite - SPS	ca. 56	zircon	U-Pb - age only presented	Mihalynuk et al. 1999
West of Mount Switzer	granite - CPC	ca. 55	biotite	K-Ar - age only presented	Mihalynuk et al. 1999
Teepee Peak	granodiorite-tonalite - SPS	ca. 55	biotite	K-Ar - age only presented	Mihalynuk et al. 1999
	rhyolite flow - SG	ca. 56	zircon	U-Pb - age only presented	Mihalynuk et al. 1999
				U-Pb (TIMS) lower intercept	
Skelly Lake middle ridge	massive rhyolite - SG	58.5 ±1.5	zircon	intercept	Mihalynuk et al. 1999
	rhyolite	124.9 ±1.5	zircon	U-Pb (TIMS) upper intercept	Mihalynuk et al. 2003
Montana Mountain*	Late Cretaceous?	N/A			Roots 1981
	Mid Cretaceous	ca. 95 to 85			Hart 1995
Mount Skukum*	syn-ore intermediate dike - SG	55.7 ±0.3	zircon	U-Pb (TIMS) Concordia	Love et al. 1998
	pre-ore rhyolite dike - SG	56.3 ±0.4	zircon	U-Pb (TIMS) Concordia	Love et al. 1998
Diorite dykes along Klondike Highway	Eocene - CPC	51 ±1	biotite & whole rock	K-Ar	Symons et al. 2000
<b>Mineralization</b>					
Engineer	mineralization	49 ±0.5	V-bearing muscovite	<sup>40</sup> Ar/ <sup>39</sup> Ar step heating	F. Devine, pers. comm. 2016
Mount Skukum*	ore-related alteration	54.1 ±0.3	adularia	<sup>40</sup> Ar/ <sup>39</sup> Ar step heating	Love et al. 1999
	pre-ore alteration	55.7 ±0.3	alunite	<sup>40</sup> Ar/ <sup>39</sup> Ar step heating	Love et al. 1999
Montana Mountain*	post-Cretaceous	N/A			Hart and Pelletier 1989

\*Yukon  
CPC - Coast Plutonic Complex  
SG - Sloko Group  
SPS - Sloko plutonic suite  
N/A – no radiometric age available. Relative age from field interpretations

Engineer Mountain and Teepee Peak in the study area (Fig. 2; Mihalynuk et al., 1999), and the Bennett Lake and Mount Skukum volcanic complexes in the Yukon (Fig. 2; Doherty and Hart, 1988; Morris and Creaser, 2003).

The Llewellyn fault displays early high-strain fabrics that are overprinted by later brittle features (Mihalynuk et al., 1999; Tizzard et al., 2009). Early ductile deformation is marked by a belt of rocks with a strong northwest striking, steeply dipping penetrative foliation (Fig. 3a), rare lineations, and local minor folds. Similar, possibly correlative fabrics are in the Tally-Ho shear to the north (Doherty and Hart, 1988; Hart and Pelletier, 1989; Mihalynuk et al., 1999; Tizzard et al., 2009). Tizzard et al. (2009) interpreted that ductile movement along the Tally-Ho shear zone took place between ca. 208 and 173 Ma. The timing is based on U-Pb zircon ages of a leucogabbro that transitions into mylonite in the hangingwall of the shear zone, and a post-deformation megacrystic granite that crosscuts the leucogabbro and other mylonites (Tizzard et al., 2009). These ages support timing arguments presented by Mihalynuk et al. (1999). Although the Llewellyn fault and Tally-Ho shear zone are along strike of one another and share early penetrative deformation, they differ. First, the early fabrics in the Llewellyn fault are consistently subvertical (Fig. 3; Mihalynuk et al., 1999), whereas the Tally-Ho shear zone is folded (Tizzard et al., 2009). Second, the Llewellyn fault is a low-grade strike-slip shear zone (Mihalynuk et al., 1999), and the Tally-Ho shear

zone is considered a west-over-east thrust fault with mylonite development (Tizzard et al., 2009).

The Llewellyn fault is mainly defined by a corridor of brittle features (Fig. 2), such as fault gouge and vein-filled fractures that overprint the older ductile deformation fabrics (Fig. 4). The brittle fabrics are thought to coincide with up to 2 km of dextral offset along the fault (Mihalynuk et al., 1999). Brittle overprinting of the early ductile fabrics is also documented along the Tally-Ho shear zone (Tizzard et al., 2009). The precise timing of brittle deformation remains uncertain, but components of it are likely Eocene (Table 1; Mihalynuk et al., 1999; Tizzard et al., 2009).

### 3. Mineralization

More than 50 mineral occurrences spatially related to the Llewellyn fault have been documented in the study area (Fig. 2; for details see Table 14-1 and Figure 14-2 in Mihalynuk et al., 1999). Many of these deposits and prospects have been known for more than 100 years, following discoveries during the Klondike gold rush of the late 1890s. Not surprisingly, these occurrences are in clusters near road and rail routes and water access sites at Bennett and Tutshi lakes in the northwest, and Tagish Lake in the southeast.

Three past-producing vein-hosted precious and base-metal deposits are in the British Columbia part of the study area. The Engineer Mine was the most productive gold deposit;

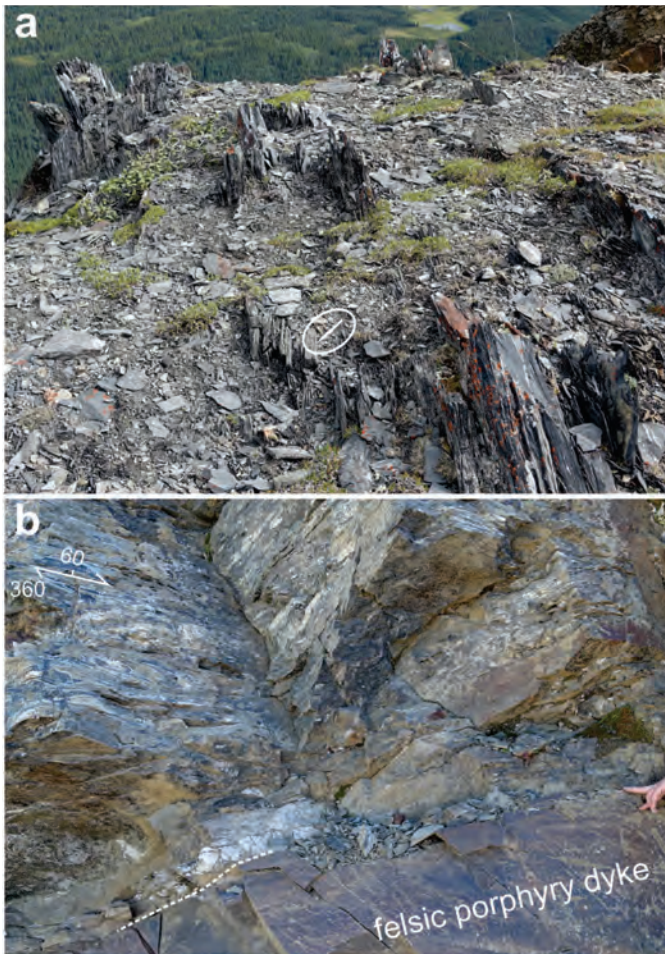


**Fig. 3.** Early ductile features near the Llewellyn fault trace. **a)** Well-developed cleavage in shale of the Stuhini Group (Triassic; Mihalynuk et al., 1999). View is southeast, scribe for scale (circled). **b)** Ductile deformation fabrics in well-foliated amphibolite gneiss of the Stuhini Formation or Laberge Group (Mihalynuk, et al., 1999). Amphibole+quartz veins are flattened, folded and boudinaged. In the foreground is a felsic hornblende-plagioclase porphyry dike that was injected along foliation in the host rocks. We collected a sample for U-Pb geochronology. From the Skarn Zone mineral prospect on Bennett Plateau, east of Bennett Lake; view is to the east.

production at Gridiron and Ben-My-Chree was relatively minor (Fig. 2). Gold has been mined intermittently at the Engineer Mine for more than 90 years. BCGold Corp. reported a NI 43-101-compliant Inferred Mineral Resource of about 41,000 tonnes grading 19.0 g/t of total contained gold (5 g/t cut-off grade; Dominy and Platten, 2011). Surficial and underground maps of the Engineer deposit are presented by Millonig et al. (2015).

The Engineer mine consists of several gold-bearing quartz-carbonate veins. Because of historical mining, very little of the original surface exposures remain (Fig. 5a) and veins and mineralization are generally only visible in sample dumps (underground workings are currently inaccessible). The mine workings have collapsed and these provide the orientation of past ore-hosting veins (Fig. 5a). The structures hosting ore at

the Engineer mine are related to splays of the Llewellyn fault, 10 km south of a 20° bend (Fig. 2; Mihalynuk et al., 1999; Millonig et al., 2015). Ore-related alteration includes a mica that is colloquially referred to as roscoelite, but is a different vanadium-bearing muscovite (L. Millonig et al., 2015; pers. comm. 2016). A sample of this mineral has yielded an  $^{40}\text{Ar}/^{39}\text{Ar}$  step-heating age of ca. 49 Ma (F. Devine, pers. comm. 2016). This age supports a temporal relationship between structure, gold mineralization, and possibly Sloko Group magmatism at Engineer, although Sloko Group volcanic rocks are slightly older (ca. 55 Ma; Table 1).

In addition to the past-producers, many vein-hosted precious and base-metal mineralized prospects and skarn-like precious metal prospects appear spatially related to the Llewellyn fault. Collectively referred to as the Golden Eagle project, many of these prospects are currently held by Troymet Exploration Corp. One example is the the Skarn Zone gold prospect at Bennett Plateau (Fig. 2), that is in a zone of deformed quartz and amphibolite veins and intruded by granitic porphyry dikes (Fig. 3b).

Similar to British Columbia, many mineral occurrences are adjacent to the Llewellyn fault in the Yukon. We visited three past-producing vein-hosted precious and base-metal mines in the Yukon including Mount Skukum (e.g., Love, 1989), and two on Montana Mountain (Venus and Arctic Caribou mines; e.g., Roots, 1981). At Mount Skukum, only minor parts of the mineralized structures are preserved at the surface, but the collapsed underground workings provide a visual aid to the historic location and orientation of the ore-hosting veins (Fig. 5b; Love, 1989, 1990b; Love et al., 1998). The Venus mine is the most significant past-producer at Montana Mountain, but mineralization is rarely exposed on surface and therefore sample dumps provide the best material to study (Fig. 5c). At Arctic Caribou, bedrock is not exposed and only scattered waste-rock is available along a dilapidated rail-track leading from an abandoned mine portal.

#### 4. Ongoing and future work

In addition to regional structural analysis, we are conducting geochronologic studies along the length of the Llewellyn fault. The purpose of the geochronology is to address the timing of fault movement and to assess the significance of mafic dikes (ca. 51 Ma; Symons et al., 2000), some of which may be lamprophyres.

##### 4.1. Structural analysis

Key questions arising from our reconnaissance are: what is the structural and/or genetic relationship between the Llewellyn fault and gold mineralization, and how do the structural relations compare between deposits?

The Engineer and Mount Skukum mines are well mapped (Love, 1989) and, although the apparent timing of gold mineralization is similar (Eocene; Table 1), these deposits have never been directly compared. Love (1990b) used the vein distribution at Mount Skukum to present a kinematic solution

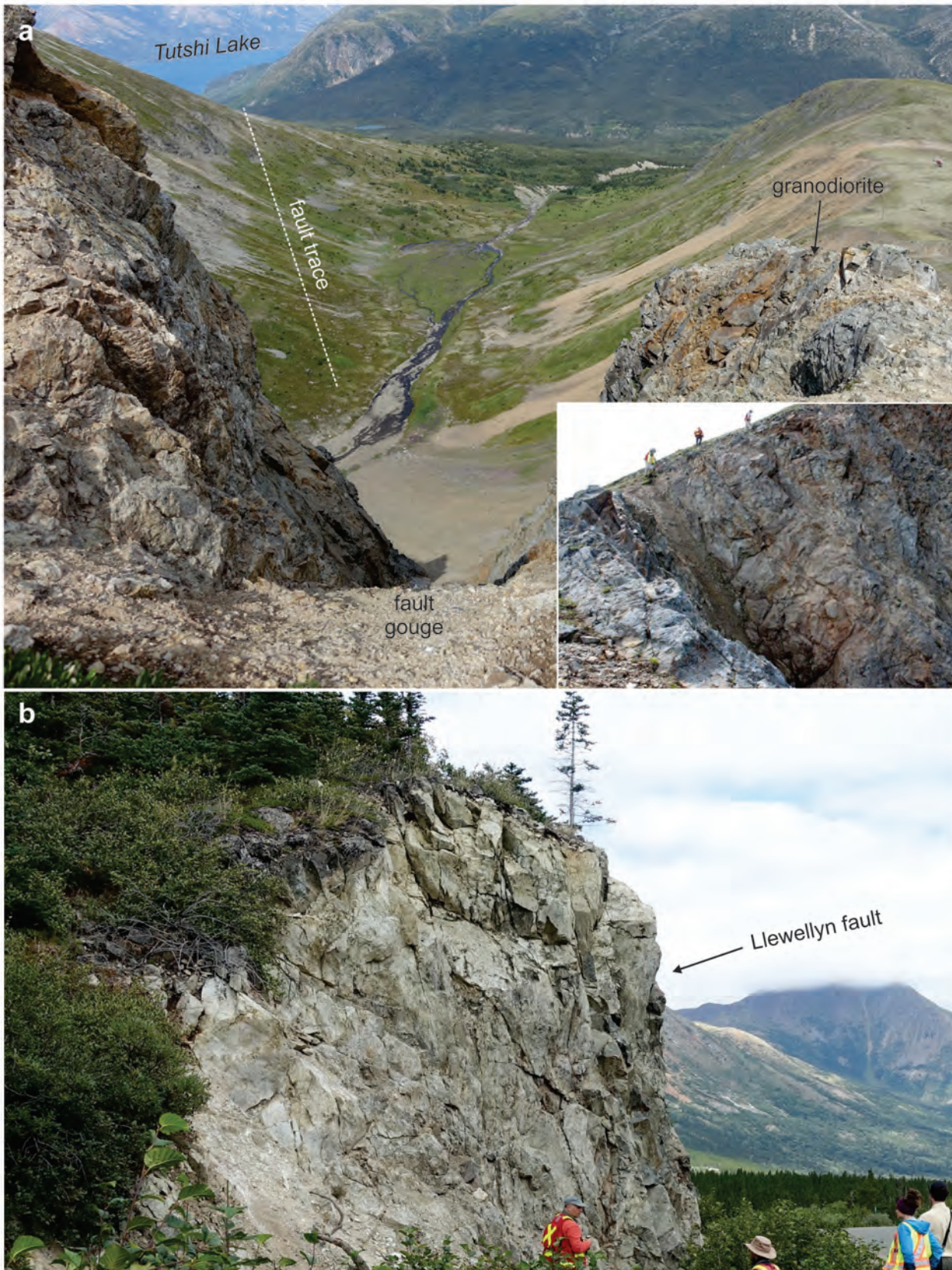


**Fig. 4.** Late brittle features along the Llewellyn fault. **a)** Fault gouge with brittle deformation features (e.g., fractures) preserved in granodiorite wall-rock (Mesozoic?). Location is west of Moon Lake and view is to the northwest. Inset is a view of the wall of the fault. **b)** Road-cut exposure of the Llewellyn fault preserving brittle deformation features, including cracks and quartz vein-filled fractures in granodiorite (Mesozoic?). Outcrop is adjacent to the Klondike Highway west of Tutshi Lake.

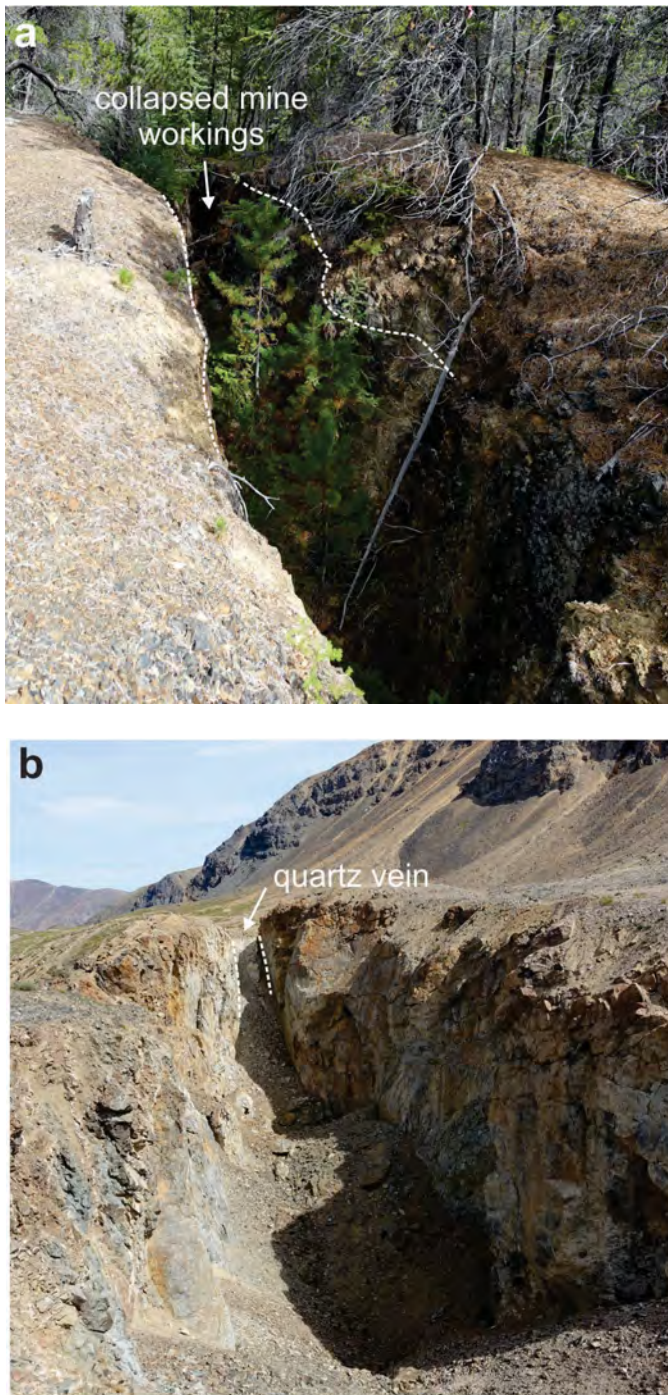


**Fig. 5.** Surface remains of past-producing gold mines. **a)** Collapsed and overgrown mine workings at Engineer Mine. The 1.5 metre-wide, 030°-striking crevasse (collapsed workings, not a trench) represents the width and strike of mined out hydrothermal veins. **b)** Mostly mined out, 3-metre-wide, 040°-striking quartz vein, Cirque Zone, Mount Skukum. The pit in the foreground is above collapsed underground workings. All bedrock exposures hosting the hydrothermal veins are volcanic rocks of the Sloko Group (ca. 55 Ma). **c)** Waste-rock-pile at the past-producing Venus Mine, Yukon, adjacent to the Klondike Highway.



for the deposit (see upper left inset, Fig. 6). Millonig et al., 2015 mapped the vein distribution at Engineer Mine (see lower right inset, Fig. 6). Based on these summaries, the veins at both the Mount Skukum and Engineer mines appear to have formed under north-northeast directed compression with subsequent development of strike-slip faults and related fault structures (Fig. 6). Some veins could have formed along Riedel shears (R and R'); others may be sigmoidal veins formed normal to the least principal stress direction ( $\sigma_3$ ) in the  $\sigma_1$ - $\sigma_2$  plane (Fig. 6). The kinematics depicted in Figure 6 are idealized, but anisotropy created during ductile deformation could have promoted non-idealized geometries during later brittle faulting. Further structural analysis is required to more accurately relate vein formation to the evolution of regional structures.

## 4.2. Geochronology

We collected a systematic suite of samples in an attempt to better document the timing of movement(s) along the Llewellyn fault, magmatism, and mineralization; results are pending.

### 4.2.1. Skarn Zone prospect

We collected a sample of the hornblende-plagioclase porphyry dike that injected parallel to ductile fabrics (Fig. 3b) at the Skarn Zone prospect for U-Pb zircon geochronology. The Skarn Zone contains low-grade gold mineralization in veins of amphibole and quartz that are now strongly deformed. The dike is undeformed and strikes parallel to the main wallrock foliation. The crystallization age of this dike will provide both a minimum age for the ductile deformation in this area and this style of gold mineralization.

### 4.2.2. Granite pluton east of Bennett Lake

A granitic pluton east of Bennett Lake at the British Columbia-Yukon border appears to crosscut the Llewellyn fault (Fig. 6),

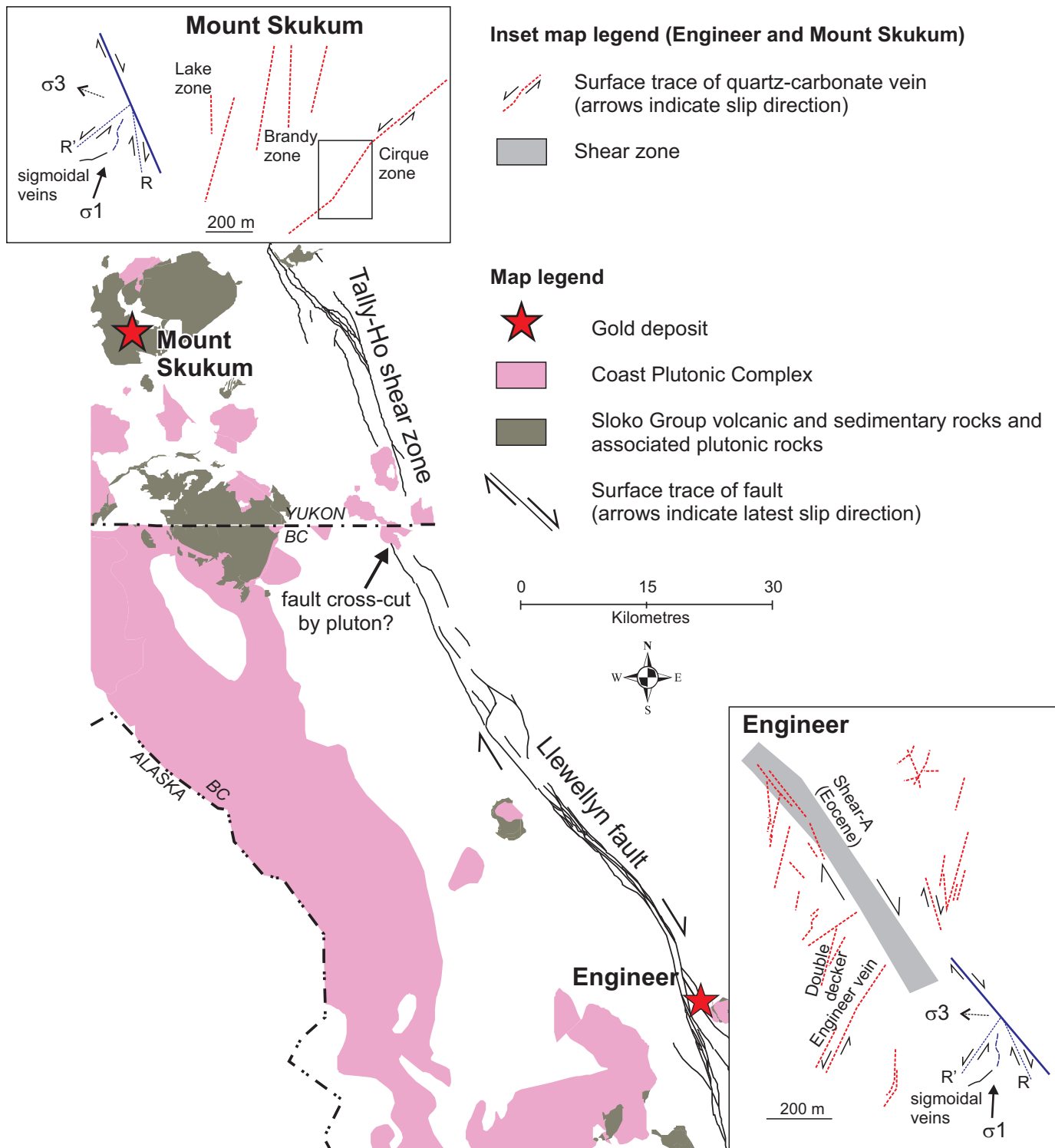


**Fig. 6.** Map of Llewellyn fault - Tally-Ho shear zone, Coast Plutonic Complex and Sloko Group volcano-plutonic complexes (Eocene), and locations of past-producing Mount Skukum and Engineer vein-hosted gold mines. The location where a granitic pluton has been mapped crosscutting the Llewellyn fault is also located. Geology is simplified after Doherty and Hart (1988) and Mihalynuk et al. (1999). Inset maps show surface traces of gold-bearing quartz-carbonate veins at Engineer and Mount Skukum. Principal stress directions are based on major faults and demonstrate veins are likely related to associated fracture sets (R and R' and sigmoidal veins). Engineer is simplified after Millonig et al. (2015) and Mount Skukum is modified after Love (1990b). Both demonstrate veining at each of the deposits is related to north-northeast directed compression.

as mapped by Mihalynuk et al. (1999). The granite post-dates the early ductile deformation but is cut by a fracture set parallel to the strike of the fault indicating it may be older than the late brittle deformation. A U-Pb zircon crystallization age of this granite will help provide a limit to the timing of both ductile and brittle strain.

#### 4.2.3. Engineer Mine

A sample of monzodiorite was collected from drill core at the Engineer Mine. This granodiorite is part of a suite that cuts the early ductile fabrics at Engineer, but is offset by discrete brittle faults and veins. A U-Pb zircon crystallization age for this monzodiorite would yield a minimum age for the ductile deformation and a maximum age for the gold-related hydrothermal system.

#### 4.2.4. Granodiorites near Llewellyn fault, west of Moon Lake

We collected samples of undeformed granodiorite adjacent to the Llewellyn fault and granodiorite that underwent brittle deformation in Llewellyn fault (Fig. 4a). These samples will be used for lower temperature thermochronology including  $^{40}\text{Ar}/^{39}\text{Ar}$  (hornblende, biotite, and muscovite) U-Pb (monazite and titanite) and U/Th-He (zircon and apatite). Results of such analyses will help provide a thermal history of movement along the Llewellyn fault.

#### 4.2.5. Venus and Arctic Caribou mines, Yukon

Specimens collected from sample dumps at the Venus and Arctic Caribou mines at Montana Mountain contain arsenopyrite that may be amenable to Re-Os isochron geochronology (e.g., Morelli et al., 2007). These ages could accurately date the time of mineralization. Previous constraints indicate the timing of mineralization at Montana Mountain is younger than Paleocene (Table 1; Hart and Pelletier, 1989).

### 4.3. Establishing the significance of 51 Ma (?) mafic dikes flanking the Llewellyn fault

A series of mafic (gabbro/diabase) dikes cut Cretaceous and younger plutons of the Coast Plutonic Complex (Figs. 2, 7; Mihalynuk et al., 1999; Symons et al., 2000). At least some of which were emplaced at ca. 51 Ma, as determined by K-Ar whole rock and biotite dating (Table 1; Symons et al., 2000). We recognized similar, but previously undocumented mafic dikes, flanking the Llewellyn fault. Possibly lamprophyres, these dikes might be related to early Eocene gold mineralization along the fault (Table 1). The dikes all have near-vertical dips but have three distinct strikes (Fig. 2), north ( $010^\circ$ ,  $n=3$ ), northeast ( $040^\circ$  to  $055^\circ$ ,  $n=6$ ), and east-southeast ( $110^\circ$ ,  $n=3$ ).

The indirect relationship between mafic magmatism, particularly lamprophyric magmatism, and gold mineralization throughout geologic time has been recognized globally (e.g., Rock and Groves, 1988; Wyman and Kerrich, 1988). Testing this relationship in northwest British Columbia, in conjunction with the relationship between Eocene volcano-plutonism and



**Fig. 7.** Vertically dipping,  $010^\circ$ -striking mafic dike (ca. 51 Ma) that crosscuts Cretaceous-Paleogene granite of the Coast Plutonic Complex (beige). Adjacent the Klondike Highway near Fraser, BC.

the deep structure of the Llewellyn fault, could increase its attractiveness for mineral exploration.

## 5. Discussion

The Llewellyn fault represents a long-lived, structure of significant strike length along which numerous gold occurrences are distributed. Similar structures in other parts of the North American Cordillera (e.g., Bohlke and Kistler, 1986; Nesbitt et al., 1989) are much better mineralized, as are the structural ‘breaks’ in the Archean Abitibi greenstone belt of the Superior Province in central Canada (e.g., Dubé and Gosselin, 2007). The apparent difference in degrees of gold mineralization between superficially similar structures raises the important question of whether the Llewellyn fault is actually well mineralized but underexplored, or whether it has simply failed to produce and preserve large gold deposits; did late motion along the faults lead to exposure and erosion? Dating gold mineralization and associated igneous rocks, further structural analysis of the deposits and their host rocks, and fluid inclusion and isotopic studies of ore fluids will help characterize the physicochemical conditions of ore formation and identify the key parameters controlling the location of gold deposits along the Llewellyn

fault.

Whether or not there are more economic deposits to be discovered remains to be demonstrated. Unfortunately, much of the Llewellyn fault in the study area lacks regional geophysical coverage and remains a blank-spot on Canadian geophysical maps. Historically such geophysical mapping has generated new exploration interest in remote areas of Canada. The area also lacks significant publicly available high-resolution digital imagery. The 50+ mineral prospects and past-producing gold deposits in a relatively infrastructure-poor region indicates potential for future mineral exploration. Geophysical and remote sensing mapping may help attract mineral exploration and investment to the region.

The timing of gold mineralization and the relationship to Eocene magmatism adjacent to the Llewellyn fault is replicated by some gold occurrences in central British Columbia (e.g., Blackdome mine; Bordet et al., 2011; 2014). Further definition of the structural and temporal relationship between the Llewellyn fault, gold mineralization, and Eocene magmatism (Fig. 6) will permit comparison between these districts and will help establish if, collectively, these areas represent an Eocene orogenic gold belt.

#### Acknowledgments

The project is a partnership of the British Columbia Geological Survey with the Geological Survey of Canada's Targeted Geoscience Initiative (TGI) and we benefited from field visits and discussions with P. Mercier-Langevin and Sébastien Castonguay (GSC Quebec), Adrian Hickin (BCGS), and F. Devine (Merlin Geoscience). Helicopter support was provided by Discovery Helicopters, Atlin, BC. The Yukon Geological Survey kindly provided use of an ATV. BCGold Corp., Troymet Exploration Corp., and Eagle Plains Resources shared knowledge and allowed access to their properties. Constructive reviews by S. Castonguay and F. Devine helped improve the manuscript.

#### References cited

- Bolke, J.K., and Kistler, R.W., 1986. Rb-Sr, K-Ar, and stable isotope evidence for the ages and sources of fluid components of gold-bearing quartz veins in the northern Sierra Nevada foothills metamorphic belt, California. *Economic Geology*, 81, 296-322.
- Bordet E., Hart, C.J.R., and McClenaghan, L. 2011. Epithermal-style Au-Ag mineralization in Cretaceous to Eocene felsic volcanic complexes, central British Columbia, western Canada. Extended Abstract, SGA 11th Biennial Meeting, Antofagasta, Chile, September 2011.
- Bordet, E., Mihalynuk, M.G., Hart, C.J.R., Mortensen, J.K., Friedman, R.M., and Gabites, J., 2014. Chronostratigraphy of Eocene volcanism, central British Columbia. *Canadian Journal of Earth Sciences*, 51, 56-103.
- Doherty, R.A. and Hart, C.J.R., 1988. Preliminary geology of Fenwick Creek (105D/3) and Alligator Lake (105D/6) map areas. Yukon Geological Survey, Open File 1988-2, 2 maps, 1:50,000 scale.
- Dominy, S.C. and Platten, I.M., 2011. BCGold Corporation: Engineer Gold Project, BC, Canada. 43-101 Technical Report for BCGold Corporation, April 2011, 96p. <http://www.bcgoldcorp.com>.
- Dubé, B., and Gosselin, P. 2007. Greenstone-hosted quartz-carbonate vein deposits, in Goodfellow, W.D., (Ed.) *Mineral Deposits of Canada: A Synthesis of Major Deposit-Types, District Metallogeny, the Evolution of Geological Provinces, and Exploration Methods*. Geological Association of Canada, Mineral Deposits Division, Special Publication No. 5, pp. 49-73.
- Goldfarb, R.J., Baker, T., Dubé, B., Groves, D.I., Hart, C.J.R., and Gosselin, P., 2005. Distribution, character, and genesis of gold deposits in metamorphic terranes. In: *Economic Geology 100<sup>th</sup> Anniversary Volume*, Hedenquist, J.W., Thompson, J.F.H., Goldfarb, R.J., Richards, J.P., (Eds.), pp. 407-450.
- Hart, C.J.R. and Pelletier, K.S., 1989. Geology of Carcross (105D/2) and Part of Robinson (105D/7) Map Areas. Indian and Northern Affairs Canada, Yukon Geological Survey Open File 1989-1, 84p.
- Love, D.A., 1989. Geology of the epithermal Mount Skukum gold deposit, Yukon Territory. Geological Survey of Canada, Open File 2123, 47p.
- Love, D.A., 1990a. Volcanic stratigraphy and some aspects of the zonation in the western part of the Mount Skukum volcanic complex, southwestern Yukon. Geological Survey of Canada, Paper 90-1E, pp. 297-308.
- Love, D.A., 1990b. Structural controls on veins of the Mount Skukum gold deposit, southwestern Yukon. Geological Survey of Canada, Paper 90-1E, pp. 337-346.
- Love, D.A., Clark, A.H., Hodgson, C.J., Mortensen, J.K., Archibald, D.A., and Farrar, E., 1998. The timing of adularia-sericite-type mineralization and alunite-kaolinite-type alteration, Mount Skukum epithermal gold deposit, Yukon Territory, Canada; <sup>40</sup>Ar-<sup>39</sup>Ar and U-Pb geochronology. *Economic Geology*, 93, 437-462.
- Mauthner, M.H.F., Groat, L.A., and Raudsepp, M., 1996. The Engineer Mine, Tagish Lake, British Columbia. *The Mineralogical Record*, 27, 263-273.
- McDonald, B.W.R., 1987. Geology and genesis of the Mount Skukum tertiary epithermal gold – silver vein deposit, southwestern Yukon Territory. Unpublished M.Sc. Thesis, University of British Columbia, Vancouver, BC, 177p.
- McDonald, B.W.R. and Godwin, C.I., 1986. Geology of Main Zone at Mt. Skukum, Wheaton River area, southern Yukon. In: *Yukon Geology, Vol. 1: Exploration and Geological Services, Yukon, Indian and Northern Affairs Canada*, pp. 6-10.
- Mihalynuk, M.G., Smith, M., Hancock, K.D., Dudka, S.F., and Payne, J., 1994. Geology of the Tulsequah River and Glacier Creek Area (NTS 104K/12, 13). Ministry of Energy, Mines and Petroleum Resources, British Columbia Geological Survey Open File 1994-03, 3 sheets, 1:50,000 scale.
- Mihalynuk, M.G., Mountjoy, K.J., Currie, L.D., Smith, M.T., and Rouse, J.N., 1999. Geology and mineral resources of the Tagish Lake area (NTS 104M/8, 9, 10E, 15 and 104N/12W) northwestern British Columbia. Ministry of Employment and Investment, British Columbia Geological Survey Bulletin 105, 190p.
- Mihalynuk, M.G., Devine, F., and Friedman, R.M., 2003. Marksmen partnership: potential for shallow submarine VMS (Eskay-style) and intrusive-related gold mineralization, Tutshi Lake area. Ministry of Energy and Mines, British Columbia Geological Survey, GeoFile 2003-09, 1 poster.
- Millonig, L.J., Groat, L.A., and Linnen, R., 2015. Geological and mineralogical report: Engineer Mine. Prepared for BCGold Corp., 53p. <http://www.bcgoldcorp.com/>.
- Morelli, R., Creaser, R.A., Seltmann, R., Stuart, F.M., Selby, D., and Graupner, T., 2007. Age and source constraints for the giant Muruntau gold deposit, Uzbekistan, from coupled Re-Os-He isotopes in arsenopyrite. *Geology*, 35, 795-798.
- Morris, G.A. and Creaser, R.A., 2003. Crustal recycling during subduction at the Eocene Cordilleran margin of North America: a petrogenetic study from the southwestern Yukon. *Canadian Journal of Earth Sciences*, 40, 1805-1821.
- Nelson, J.L., Colpron, M., and Israel, S., 2013. The Cordillera of

- British Columbia, Yukon and Alaska: tectonics and metallogeny. In: Colpron, M., Bissig, T., Rusk, B.G. and Thompson, J.F. (Eds.), *Tectonics, Metallogeny and Discovery: The North American Cordillera and Similar Accretionary Settings*. Society of Economic Geologists, Special Publication, Volume 17, pp. 53-110.
- Nesbitt, B.E., Murowchick, J.B., and Muehlenbachs, K., 1986. Dual origins of lode gold deposits in the Canadian Cordillera. *Geology*, 14, 506-509.
- Pride, M.J., 1986. Description of the Mount Skukum volcanic complex, southern Yukon. In: *Yukon Geology Volume 1: Exploration and Geological Services, Yukon, Indian and Northern Affairs Canada*, pp. 148-160.
- Rock, N.M.S. and Groves, D.I., 1988. Can lamprophyres resolve the genetic controversy over mesothermal gold deposits? *Geology*, 16, 538-541.
- Roots, C.F., 1981. Geological setting of gold-silver veins on Montana Mountain. In: *Yukon Geology and Exploration 1979-80*, Exploration and Geological Services Division, Indian and Northern Affairs Canada, pp. 116-122.
- Roots, C.F., 1982. *Geology of the Montana Mountain area, Yukon*. Unpublished M.Sc. thesis, Carleton University, Ottawa, ON, 127p.
- Symons, D.T.A., Harris, M.J., Gabites, J.E., and Hart, C.J.R., 2000. Eocene (51 Ma) end to northward translation of the Coast Plutonic Complex: paleomagnetism and K–Ar dating of the White Pass Dikes. *Tectonophysics*, 326, 93-109.
- Tizzard, A.M., Johnston, S.T., and Heaman, L.M., 2009. Arc imbrication during thick-skinned collision within the northern Cordilleran accretionary orogen, Yukon, Canada. *Geological Society, London, Special Publications*, 318, 309-327.
- Walton, L., 1986. Textural characteristics of the Venus vein and implications for ore shoot distribution. In: *Yukon Geology Volume 1*, Exploration and Geological Services Division, Indian & Northern Affairs Canada, pp. 67-71.
- Wyman, D., Kerrich, R., 1988. Archean shoshonitic lamprophyres associated with Superior Province gold deposits: Distribution, tectonic setting, noble metal abundances and significance for gold mineralization. *Economic Geology Monograph 6 – The Geology of Gold Deposits: The Perspective in 1988*, pp. 651-667.



# Composite pericratonic basement of west-central Stikinia and its influence on Jurassic magma conduits: Examples from the Terrace-Ecstall and Anyox areas



JoAnne Nelson<sup>1, a</sup>

<sup>1</sup> British Columbia Geological Survey, Ministry of Energy and Mines, Victoria, BC, V8W 9N3

<sup>a</sup> corresponding author: JoAnne.Nelson@gov.bc.ca

Recommended citation: Nelson, J., 2017. Composite pericratonic basement of west-central Stikinia and its influence on Jurassic magma conduits: Examples from the Terrace-Ecstall and Anyox areas. In: Geological Fieldwork 2016, British Columbia Ministry of Energy and Mines, British Columbia Geological Survey Paper 2017-1, pp. 61-82.

## Abstract

The nature and affinity of the pre-mid-Paleozoic basement of Stikinia remains poorly known. However, this basement exerted a fundamental control on the location and distribution of intrusions and intrusion-related mineral deposits. A transect from west-central Stikinia near Terrace to the Ecstall belt (considered a possible correlative of the Yukon-Tanana terrane in the central Coast Mountains) indicates commonalities of basement; a comparison of detrital zircons from a Jurassic conglomerate (considered part of the Eskay rift) suggests that basement of central Stikinia differs from the Yukon-Tanana basement in the north.

Near Terrace, stratified upper Paleozoic and Mesozoic rocks of western Stikinia are cut by the Kleanza pluton, an ENE-elongate, multiphase Early Jurassic body. To the west, this section is juxtaposed with highly strained lower crustal rocks of the Central Gneiss Complex and Shames River intrusive complex (Early Jurassic) across the Shames River normal fault. Farther west, the Coast Shear zone marks the eastern boundary of the Ecstall belt, a mid-Paleozoic (in part Middle Devonian) magmatic arc complex cut by a Mississippian 'central diorite suite' and Early Jurassic plutons (Foch and Johnson). Geological continuity across the Terrace-Ecstall transect is demonstrated by similar igneous geochemical signatures of coeval Mississippian and Early Jurassic suites. Volcanic rocks of the Mt. Attree Formation and a small cogenetic pluton in the Terrace area are ca. 323-325 Ma (U-Pb zircon), somewhat younger than, but within error of, a previously published Mississippian age ( $336.8 \pm 17.7$  Ma) from a pluton in the Ecstall belt. Both suites are silica bimodal, showing strong subduction influence in felsic rocks and non-arc immobile element signatures in metabasalts. Early Jurassic intrusive phases from all three areas show a continuum on modified alkali-lime, aluminum saturation and Fe\* vs. silica plots, and generally increasing LREE/HREE and HREE/MREE with silica. Trace and major element chemistry show strong influence of plagioclase and hornblende fractionation. The Early Jurassic intrusions (ca. 200-180 Ma) are interpreted as having evolved in related magma chambers in a structurally controlled permeability corridor corresponding to the Skeena arch, which trends across the terrane at a high angle.

Late Early to Middle Jurassic stratified rocks on Mt. Clashmore, west of the Anyox deposit at the southern end of the Eskay rift, consist of basalt, rhyolite, and sedimentary rocks including monomictic breccias and cherty argillites with tuffaceous laminae. They are correlated with the Iskut River Formation of the Eskay rift in the Iskut region. Evenchick and McNicoll (2002) reported non-northwest Laurentian detrital zircons (1058-517 Ma) from a conglomerate at Mt. Clashmore that may have been derived from a fragment of accreted exotic pericratonic basement that was exposed in a horst or rift shoulder adjacent to the Eskay rift in the mid-Jurassic.

Rocks of the Ecstall belt and the cryptic Precambrian source of detrital zircons at Mt. Clashmore are parts of the composite, pre-late Paleozoic basement of Stikinia. Major long-lived (Late Devonian to Recent) N-S and E-W fault corridors in the terrane cut across different basement components, suggesting that their precursors formed after amalgamation of its basement but before or coeval with the oldest units in the Stikine assemblage.

**Keywords:** Stikinia, Stikine assemblage, Ecstall belt, Anyox, Mt. Clashmore, Eskay, Kleanza pluton, Jurassic

## 1. Introduction

Stikinia (Fig. 1) is a long-lived, multi-episodic, Devonian to Jurassic island arc terrane that extends for about 1000 km along the length of the Canadian Cordilleran orogen. Stikinia, Quesnellia (a similar multi-phase island arc), and other terranes such as Cache Creek make up the Intermontane terrane belt. These terranes developed in the northeastern Pacific peri-Laurentian realm (Nelson et al., 2013) before Middle Jurassic

amalgamation and accretion to the continental margin. Stikinia hosts much of BC's copper, gold, and silver in Late Triassic to Middle Jurassic porphyry, epithermal, and VMS deposits, which formed during the latest episodes of arc activity and subsequent terrane amalgamation. Notable Mesozoic deposits (Fig. 1) include: porphyry Cu-Au at Red Chris mine, KSM, and Galore; porphyry Cu at Schaft Creek; epithermal Au at Brucejack and along the Premier-Stewart trend; and

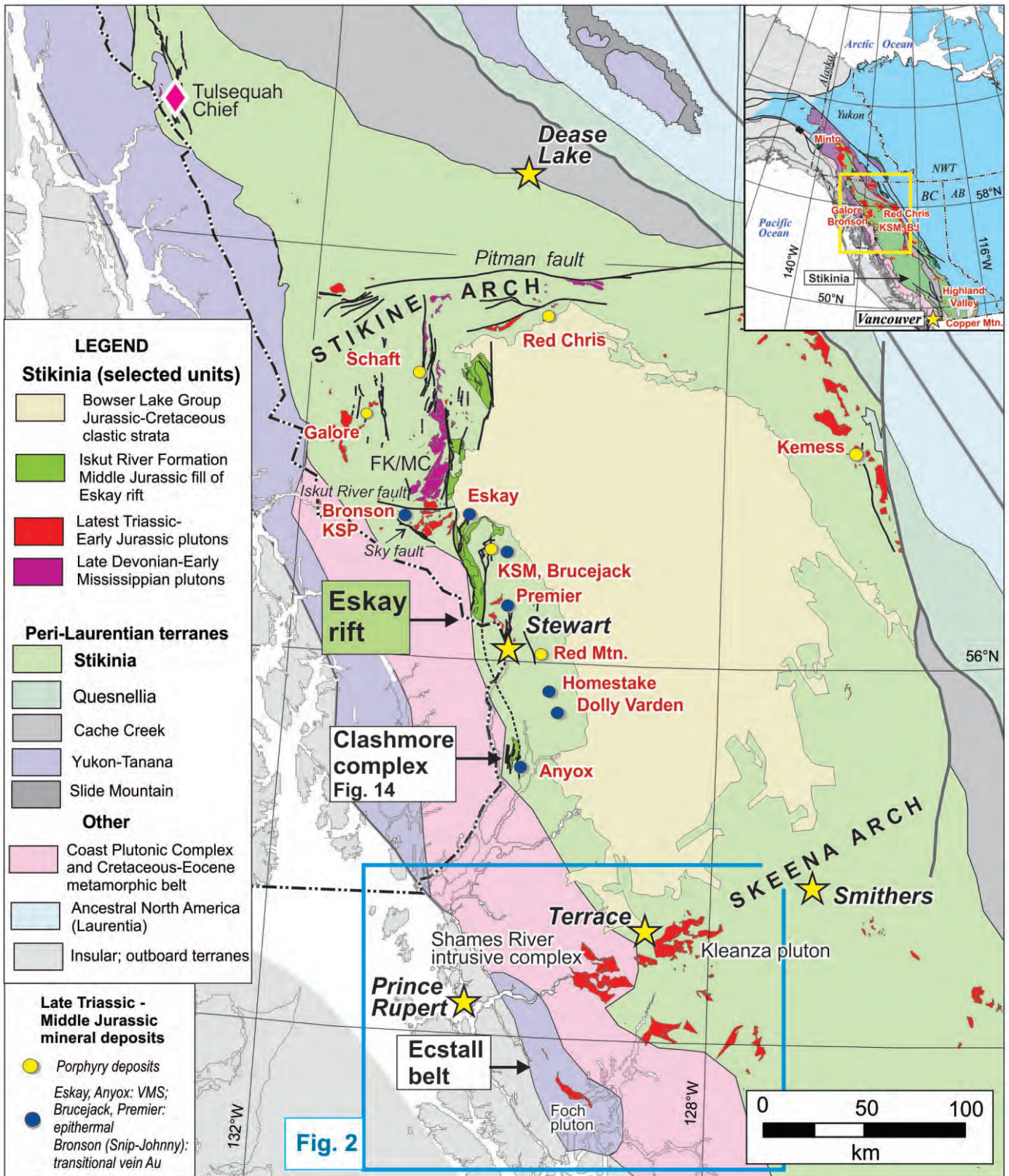


**Fig. 1.** Central and northern Stikinia. Long-lived, multiply reactivated N-S and E-W fault sets from Alldrick (2001). Selected map units from digital map of British Columbia (Cui et al., 2015) include latest Triassic-Early Jurassic intrusions, Devonian-Mississippian intrusive bodies, and the Middle Jurassic Iskut River Formation, which exhibit spatial and causative relationships to the major faults. FK/MC = Forrest Kerr and More Creek plutons.

volcanogenic massive sulphides at the Au-Ag-rich Eskay and Cu-rich Anyox mines (past producers) in the Eskay rift (Middle Jurassic). These and many related occurrences show spatial and, in many cases, genetic associations with major, long-lived and multiply reactivated N-S and E-W structural corridors (Nelson, 2014).

Prominent sets of northerly trending lineaments transect western Stikinia (Fig. 1). The N-S elongate Forrest Kerr-More Creek pluton (Late Devonian; Logan et al., 2000) and the NNW-trending Tulsequah Chief volcanogenic deposit (Late Mississippian) are the oldest features that show control by these faults (Nelson, 2014). The Eskay rift, a north-trending, 300 km-long, complex graben, formed over a brief period (ca. 178-174 Ma) coincident with collision of Stikinia and inboard Cache Creek terrane (Mihalynuk et al., 2004) and probably the outboard Insular terranes (Nelson et al., 2013). East of the rift, the KSM-Brucejack deposits show structural control by Early Jurassic basin-bounding transcurrent faults (Nelson and Kyba, 2014). A major fault in this system was later remobilized as the Sulphurets thrust during mid-Cretaceous sinistral transpression of western Stikinia; it forms the immediate hanging wall of the KSM porphyry deposits (Kirkham and Margolis, 1995; Evenchick, 2001).

Stikinia also contains westerly fault and lineament sets, the Pitman fault system along the Stikine arch, the Iskut River fault and Skeena arch structures (Fig. 1). In the north, the Pitman fault system marks an apparent northern limit to a prominent set of northerly structures of central-western Stikinia (Fig. 1), although cross-cutting relationships are not observed. The Red Stock, the ca. 204 Ma body that hosts the Red Chris porphyry deposit, is along the Boundary fault (Rees et al., 2015), a minor ENE-striking structure that is part of the Pitman array. The Pitman fault array coincides with the Stikine arch, a long-lived paleogeographic high at a high angle to the long axis of Stikinia (Fig. 1). Farther south, the Iskut River fault (Fig. 1) interrupts, and may offset, the faults bounding the Eskay rift (Alldrick, 2000). Early Jurassic Au vein and porphyry deposits of the Bronson-KSP camp developed between the Iskut River fault and the Sky fault (WNW striking), which underwent syn-mineral dextral-normal displacement (Kyba and Nelson, 2015). In the far south, the Skeena arch, a long-lived ENE paleogeographic high in central Stikinia near Smithers and Terrace, marks the southern edge of Bowser basin (Jurassic-Cretaceous), and hosts a swarm of Eocene plutons (Babine intrusions). The Kleanza pluton (Early Jurassic; 200-180 Ma) was emplaced along faults parallel to the axis of the Stikine arch (Figs. 1, 2; Nelson et al., 2008).

The northerly and westerly fault and lineament sets shown on Figure 1 are characteristic of, and are apparently confined to, Stikinia. They appear to have exerted strong spatial and, in many cases, genetic control on mineral deposits, by creating conduits for magmas and hydrothermal fluids. Long reactivation histories suggest that they reflect fundamental discontinuities in the pre-mid-Paleozoic basement of Stikinia, but the nature and affinity of this basement remains poorly known. Increased

knowledge of Stikinia's basement will aid in understanding of the origin of these fundamental lineaments.

The oldest rocks exposed in the terrane, the Stikine assemblage and its correlatives, are Devonian and younger. The oldest known unit is a fossiliferous Emsian limestone west of the Forrest Kerr pluton (Logan et al., 2000). This may point to a subjacent crustal infrastructure thick enough to support shallow-water conditions in the Early Devonian, but the nature and lateral extent of such crust is unknown. Juvenile isotopic signatures from that part of Stikinia are inconsistent with the presence of pericratonic crust (Samson et al., 1989), as is the absence of Precambrian cores in zircons recovered from the Forrest Kerr-More Creek pluton (Late Devonian; Logan et al., 2000), compared to their abundance in coeval plutons of the Yukon-Tanana terrane. In contrast, near Tulsequah Chief in far northern Stikinia (Fig. 1), Devonian-Mississippian strata rest unconformably on, and pass transitionally into, pericratonic rocks of the Boundary Ranges suite (Mihalynuk et al., 1994; Mihalynuk, 1999; Currie and Parrish, 1997). The Boundary Ranges suite is continuous to the north with the Yukon-Tanana terrane of Yukon and eastern Alaska, a large peri-Laurentian terrane that rifted from the western North American margin during Late Devonian back-arc extension (Nelson et al., 2006a). The belt of pericratonic rocks in the Coast Mountains of southeastern Alaska has also been correlated with the Yukon-Tanana terrane (Gehrels et al., Pecha et al., 2016), although contrasting Precambrian detrital signatures and Ordovician-Silurian magmatism in SE Alaska suggest significant differences between the two. The difference between evolved basement character in northern Stikinia and juvenile basement character in central Stikinia could reflect either primary heterogeneity or pre-Late Devonian amalgamation of oceanic and pericratonic terranes.

Direct observation of potential basement components of Stikinia is generally difficult. High-grade metamorphism, intense deformation, and extensive Cretaceous and Eocene plutonism of the Coast Mountains orogen obscure most of the western edge of the terrane, where the deepest exposures occur and possible links to pre-Devonian pericratonic strata might be preserved. Fieldwork in 2016 was designed to evaluate proposed links between Stikinia and terranes to the west, taking advantage of two areas in which evidence for connection between Jurassic rock units of Stikinia and pericratonic fragments to the west have been identified by previous workers.

In this paper I first examine a transect across the Coast Mountains orogen from Terrace to Prince Rupert (Figs. 1, 2). This transect crosses from Stikinia in the east, through the Central Gneiss Complex, which includes metamorphosed Early Jurassic intrusive rocks (Heah, 1991), and through the Ecstall belt, a Yukon-Tanana correlative intruded by Mississippian and Early Jurassic plutons that Gareau (1991) and Gareau and Woodsworth (2001) recognized as common with Stikinia. Our work focused primarily on geochronologic and geochemical sampling of Early Jurassic intrusive bodies and late Paleozoic intrusions and comagmatic volcanic rocks. Some of the

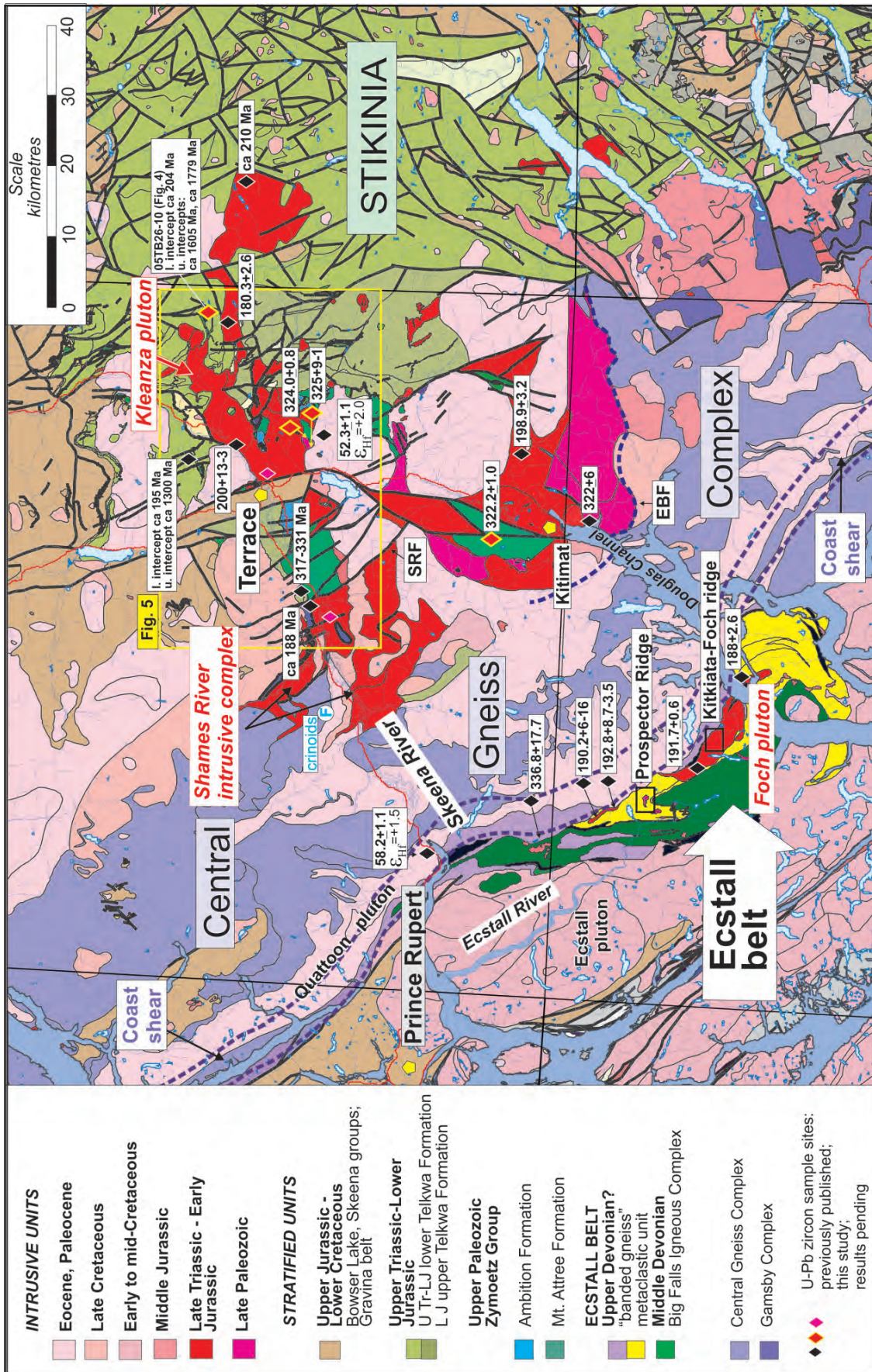


**Fig. 2.** Geology of Stikinia and the adjacent Coast Mountains orogen in the Terrace-Prince Rupert area (Cui et al., 2015). U-Pb ages from Heah (1991), Gareau et al. (1997) Gehrels et al. (2009), and this study. Selected  $\epsilon_{\text{Hf}}$  values from Cecil et al. (2011). EBF = Eastern bounding fault of Central Gneiss Complex (Rusmore et al., 2005), SRF = Shames River fault (Heah, 1991). Crinoid locality from Hill (1985). 2016 traverses in the Ecstall belt covered northern Prospector Ridge and Kitkiata-Foch ridge areas. See Figure 1 for regional context.

geochronologic work is ongoing, but this paper presents four previously unpublished U-Pb ages from the Terrace area.

I then examine a Toarcian-Bajocian volcanosedimentary succession near Mt. Clashmore on the western flank of the southern Eskay rift, near Anyox (Fig. 1). This conglomerate has yielded a limited suite of detrital zircons with non-northwest Laurentian Precambrian ages (Evenchick and McNicoll, 2002), pointing at an unknown pericratonic source that contributed sediment to the rift. Mapping of the Mt. Clashmore area supported recollecting detrital zircon samples from the conglomerate reported by Evenchick and McNicoll (2001).

## 2. Terrace-Ecstall transect

### 2.1. Regional geology

Paleocene and Eocene faults divide the area between Terrace and the Ecstall River into three structural-tectonic domains: western Stikinia, the Central Gneiss Complex, and the Ecstall belt (Figs. 2, 3). Near Terrace on the east, upper Paleozoic through Lower Cretaceous strata of Stikinia and the Kleanza pluton (Early Jurassic) are bound by the Shames River normal fault (Eocene; east-side-down). To the west, in the core of the Coast Mountains orogen, polydeformed amphibolite- to granulite-grade rocks of the Central Gneiss Complex are structurally overlain by the Shames River mylonite zone, which Heah (1991) interpreted as an early Tertiary east-side-down low-angle detachment. It comprises interleaved panels of Early Jurassic granitic rocks (Shames River orthogneiss), paragneiss probably equivalent to that in the main Central Gneiss Complex, and ca. 69 Ma syntectonic plutons. The Coast shear zone forms the boundary between the Central Gneiss Complex and the Ecstall belt farther west (Fig. 2). It is a steep, generally east-side-up dextral-reverse fault (Hollister and Andronicus, 2000) with a strike length over 1200 km (Rusmore et al., 2001). The Quottoon pluton (Paleocene) was emplaced during motion on the fault (Rusmore et al., 2001). The Ecstall belt consists of Middle to Upper Devonian arc-related metavolcanic and metasedimentary strata of arc and pericratonic affinity, intruded by Late Mississippian (ca. 336 Ma) and Early Jurassic (ca. 191-193 Ma) plutons (Gareau and Woodsworth, 2000; Alldrick et al., 2001). It is considered part of the belt of Yukon-Tanana equivalents in the Coast Mountains (Gareau and Woodsworth, 2000; Pecha et al., 2016).

The section of stratified rocks near Terrace is typical of Stikinia overall. Upper Paleozoic volcanic rocks of the Mt. Attree Formation and small cogenetic intrusions are overlain by richly fossiliferous Permian limestones of the Ambition Formation (Nelson et al., 2008). This sequence, the Zymoetz Group, is equivalent to the Stikine assemblage farther north (Nelson et al., 2008). Above the limestone, the Stuhini Group comprises an unusually thin (<50 m) unit of dark grey to black Upper Triassic chert and argillite. Uppermost Triassic-Lower Jurassic volcanic-rich rocks of the Telkwa Formation (Hazelton Group) unconformably overlie the older rocks, and are in turn overlain by upper Hazelton strata, including the Red Tuff Member of the Nilkitkwa Formation and the Smithers

and Quock formations (Barresi et al., 2015). Upper Jurassic to Lower Cretaceous strata of the Bowser Lake Group form the top of the succession. The Kleanza pluton intrudes as high as the upper part of the Telkwa Formation. Igneous ages of ca. 204, ca. 193-195 and ca. 178 Ma from volcanic rocks (Gareau et al., 1997; Barresi et al., 2015) show a roughly similar range to two Kleanza samples at  $200 \pm 13/-3$  Ma and  $180.3 \pm 2.6$  Ma (Gareau et al., 1997; Gehrels et al., 2009). Although complicated by numerous high-angle faults, the Terrace stratigraphic section youngs progressively to the east (Fig. 2), suggesting prevailing eastward dips. As is the case in most of Stikinia, the nature of the basement is not directly known. Precambrian lower crustal domains are hinted at by zircon inheritance in a Telkwa Formation rhyolite near the northeastern end of the Kleanza pluton (Figs. 2, 3, this study; see below). Gareau et al. (1997) reported Mesoproterozoic inheritance (ca. 1300 Ma) from an Early Jurassic unit 25 km to the west (Fig. 2). Zircon from an Eocene intrusion southeast of the Kleanza pluton shows an unusually low  $\epsilon_{\text{Hf}}$  value of +2.0, indicative of old continental crust (Cecil et al., 2011; Fig. 2). Precambrian domains cannot be extensive, because isotopic signatures are mostly juvenile and most igneous zircon populations lack inherited components.

The Central Gneiss Complex remains one of the most enigmatic rock units in the Cordillera. Consisting of Cretaceous orthogneiss and older paragneiss and orthogneiss, it represents the roots of the Coast Mountains arc as it evolved between 90 and 45 Ma (Rusmore et al., 2005). Rocks of the Central Gneiss Complex underwent recumbent folding and kyanite- and sillimanite-grade metamorphism, followed by as much as 28 km (8.5 kb) of early Tertiary exhumation (Rusmore et al., 2005). Low-angle detachment faulting along the Shames River mylonite zone and its southern equivalent near Douglas Channel, the Eastern Boundary detachment fault (Fig. 2), played an important role in this unroofing (Rusmore et al., 2005). The hanging wall of the detachment comprises subgreenschist- and greenschist-grade rocks of Stikinia, which formed part of the upper crustal load during Cretaceous metamorphism. The Shames River 'orthogneiss' is a layered mafic to intermediate meta-intrusive complex that forms extensive panels in the Shames River mylonite zone (Fig. 2). It has yielded a U-Pb zircon multi-grain age of  $188 \pm 8$  Ma (Heah, 1991), which falls within the latest Triassic-Early Jurassic range of ages for the Kleanza pluton and Telkwa Formation. The Shames River intrusive complex is a potential deep-level equivalent of the Kleanza pluton, decapitated by the early Tertiary detachment system (Fig. 3). Cretaceous-Tertiary tectonic burial-exhumation has largely obscured evidence for protoliths and tectonic affinity of the pre-plutonic gneisses. Although detailed isotopic data are lacking, most plutons intruding the complex have juvenile  $\epsilon_{\text{Hf}}(t)$  signatures (+10.2 - +15.1), indicating minimal interaction with old crust (Cecil et al., 2011). A calc-silicate paragneiss north of the Skeena River contains well-preserved large crinoid fragments (Fig. 2; Hill, 1985), similar to those in the Ambition Formation near Terrace. Based on similar juvenile crustal signatures, structural juxtaposition, and lack of a major

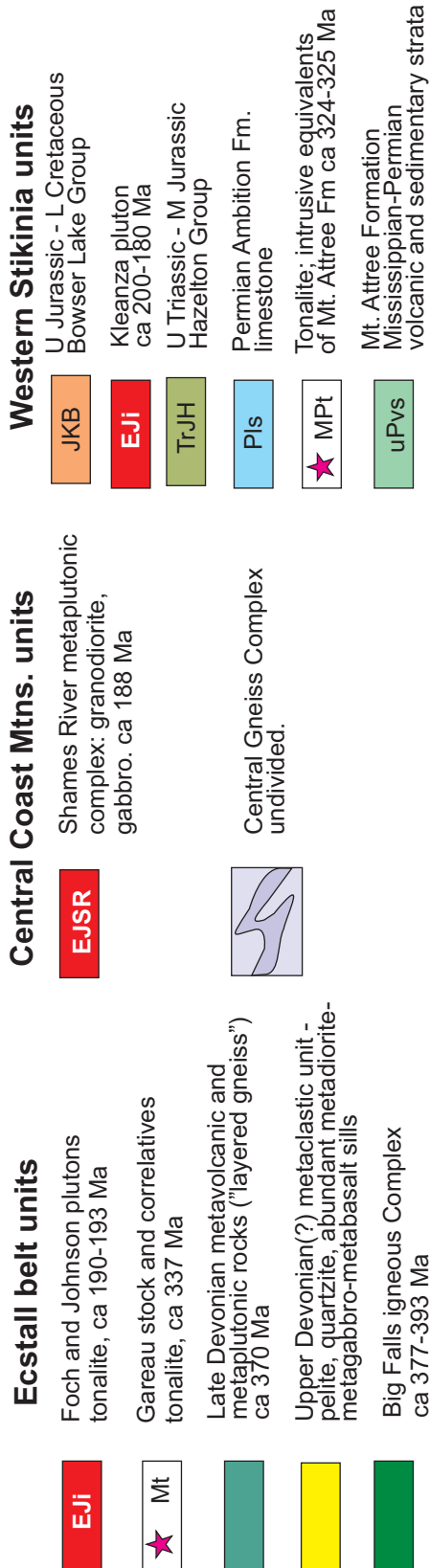
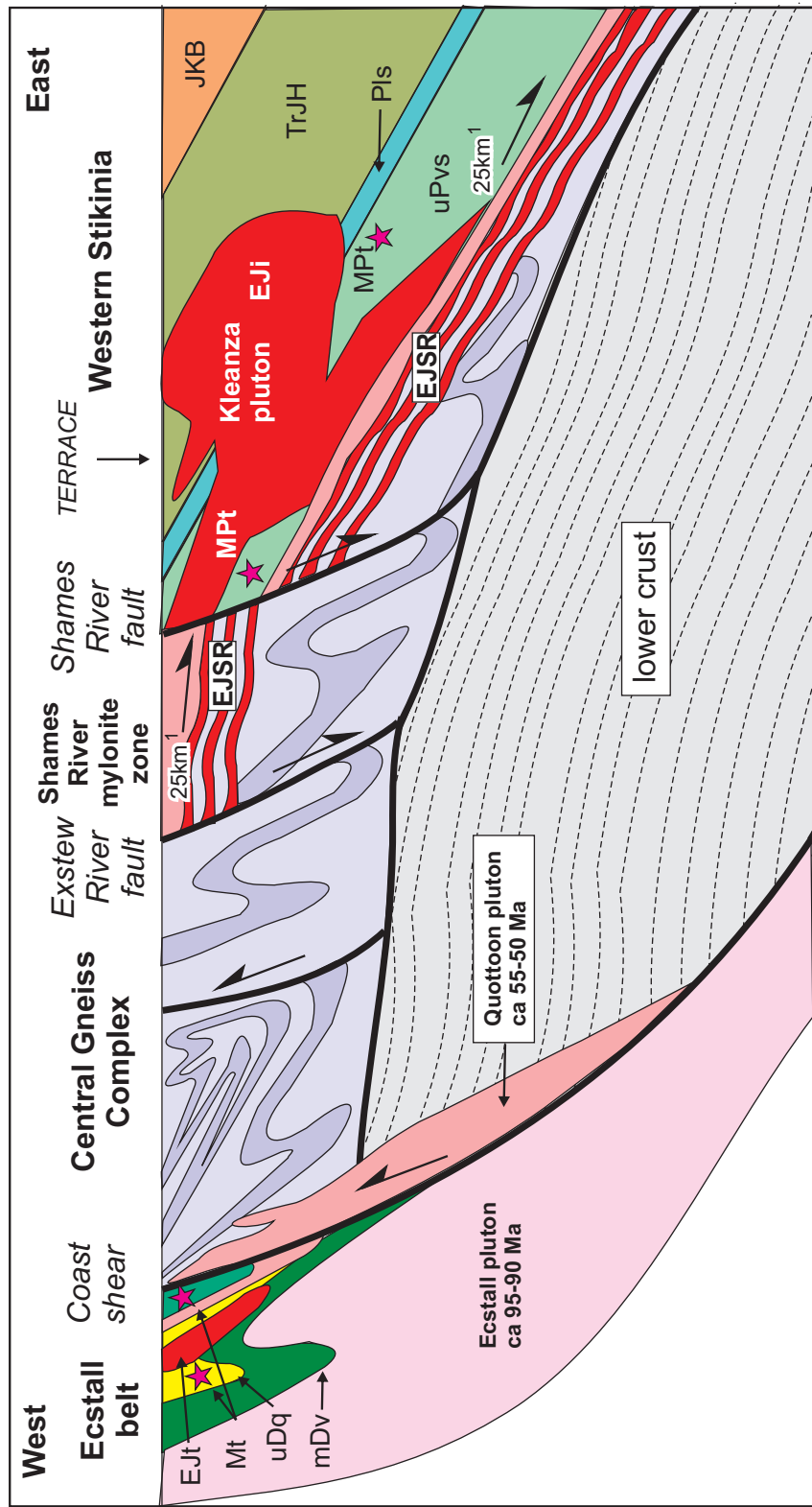


**Fig. 3.** Schematic east-west crustal cross-section of Stikinia and the eastern and central parts of the Coast Mountains orogen, approximately along the Skeena River. General relationships from Heath (1991), Hollister and Andronicos (2000), Angen (2009). \*Estimated displacement on Shames River mylonite zone from Heath (1991).

intervening suture, the Central Gneiss Complex is thought to be basement (infrastructure) to Stikinia (Cecil et al., 2011).

The Ecstall belt (Alldrick 2001; Alldrick et al., 2002), also referred to as the Scotia-Quaal belt (Gareau and Woodsworth, 2000) is a tightly folded, amphibolite facies metavolcanic-metaplutonic-metasedimentary package. Metavolcanic and metaplutonic rocks of the Big Falls igneous complex, the stratigraphically lowest unit in the belt, have 377 to 393 Ma (Middle Devonian) U-Pb zircon ages (Alldrick et al., 2001). It hosts several significant volcanogenic massive sulphide prospects. A regionally extensive unit of quartz-rich metaclastic strata (Figs. 2, 3) overlies the volcanic unit. It consists of a lower dark grey to black meta-siltstone with interlayers of granite clast-bearing conglomerate, and an upper white to light grey quartzite (meta-sandstone) with micaceous partings (Alldrick 2001). The metaclastic unit is overlain by metavolcanic 'layered gneiss', which yielded a Late Devonian, ca. 370 Ma U-Pb zircon age (Alldrick et al., 2001; Gareau and Woodsworth, 2000).

A small, weakly foliated quartz diorite stock that intrudes the layered gneiss is  $336.8 \pm 17.7/-7.1$  (Gareau, 1991). Similar bodies in the belt (Central diorite suite) are correlated with this mid-Mississippian pluton (Fig. 2; Alldrick et al., 2001; Alldrick et al., 2002). Two Early Jurassic plutons, the Johnson Lake equigranular tonalite (ca. 193-190 Ma) and the Foch Lake plagioclase-megacrystic tonalite (ca. 192 Ma), cut units and early foliation of the belt (Gareau and Woodsworth, 2000). These plutons may constitute a link with Stikinia, in which intrusions of this age are common (Gareau and Woodsworth, 2000; Alldrick, 2001). Other features of the Ecstall belt have led to correlations with pericratonic rocks in the Yukon-Tanana terrane (Gareau and Woodsworth, 2000). The Big Falls complex (Middle Devonian) and its volcanogenic deposits have been compared to the Finlayson assemblage of Yukon-Tanana terrane, although their ages differ by 20-30 million years (380-390 Ma vs. 352-360 Ma; Nelson et al., 2006a). Limited  $\epsilon_{Nd}$  data from metaclastic rocks are -1.5 to -4.5 (Gareau and Woodsworth, 2000). An  $\epsilon_{Hf}(t)$  value of -1.5 in ca. 58 Ma zircons from the Quatoon pluton in the Coast Shear Zone near the northern end of the Ecstall belt reflects significant incorporation of old continental crust (Cecil et al., 2011). The abundance of metaclastic quartzites in the Ecstall belt and evolved isotopic signatures suggest that it may have formed as an arc in continental margin setting similar to, but older than, Late Devonian-Early Mississippian (370-345 Ma) arc development in the main Yukon-Tanana terrane of Yukon and east-central Alaska (Nelson et al., 2006b). Early Middle to Late Devonian (393-370 Ma) igneous ages in the Ecstall belt overlap Silurian-Devonian (428-365 Ma) ages in the Endicott Arm assemblage, the middle unit of the Yukon-Tanana terrane in southeast Alaska (Pecha et al., 2016).

## 2.2. New geological, geochronological and geochemical data

Two igneous suites, late Paleozoic and Early Jurassic, may be common to Stikinia near Terrace and the Coast Mountains

orogen. Geochronologic and geochemical data from our study will aid in comparing these suites. Below I present four previously unpublished U-Pb zircon data sets, three from Late Paleozoic units in the Terrace-Kitimat area, and one from a Telkwa rhyolite. Analyses are pending for two geochronologic samples, collected in 2016, from the Kleanza pluton near Terrace and a Shames River complex granodiorite. Geochemical samples of Early Jurassic intrusive bodies are from the Kleanza pluton, its unnamed extension along the Skeena River west of Terrace, the Shames River meta-intrusive complex, and the Foch pluton on Kitkiata-Foch ridge in the Ecstall belt. Late Paleozoic units were sampled for geochemistry on Prospector Ridge, along the Skeena River west of Terrace, and in the Williams Creek valley southeast of Terrace.

### 2.2.1. Late Paleozoic units

Volcanic and metavolcanic rocks of the Mt. Attree Formation form the oldest and most westerly exposures of stratified rocks in the western Stikinia domain (Figs. 2-4; Nelson et al., 2008; Nelson, 2009). Before this study, a single Permian U-Pb zircon age of  $285 \pm 9$  Ma was obtained from these rocks (Gareau et al., 1997). Small tonalitic plutons intrude the sequence in Williams Creek southeast of Terrace (Fig. 4) and on Mt. Clague, northwest of Kitimat (Fig. 2). Except for the single fossiliferous marble (see above), Paleozoic protoliths are not recognized in the Central Gneiss Complex. In the Ecstall belt, a group of small diorite and tonalite intrusions (Central diorite suite) cut older stratified units (Alldrick, 2001; Alldrick et al., 2001). A pluton of this suite yielded a ca. 336 Ma age (Gareau, 1991; Alldrick et al., 2001). Late Paleozoic supracrustal rocks are not exposed in the Ecstall belt, presumably because of deep erosion to Devonian strata.

U-Pb TIMS zircon data from samples collected in 2007 and 2008 document late Paleozoic ages for the pluton in Williams Creek and a dacite tuff in the Mt. Attree Formation near Kitimat (Figs. 2, 4; see Nelson and Friedman, 2017 for full data and analytical techniques). A small tonalite pluton cuts the Mt. Attree Formation on the north side of Williams Creek, 8 km southeast of Terrace. It is quartz-rich, varying from equigranular to quartz- and plagioclase-phyric, and well-foliated (Fig. 5a). Original mafic minerals are recrystallized to smears of biotite and ragged actinolite. Intrusive contacts with surrounding metavolcanic rocks are partly overprinted by foliation. Both the pluton and the Mt. Attree Formation are crosscut by fresh, unfoliated granodiorite of the Kleanza pluton. Of two samples from this body, 07JK17-09 yielded a well-constrained age of  $324.0 \pm 0.8$  Ma from five concordant grains (Fig. 6a). The other, 07JA05-01, shows more complicated systematics and probable lead loss, with an estimated age of  $325 \pm 9/-1$  Ma (Fig. 6b). An inlier of well-foliated, greenschist-grade metavolcanic rocks outcrops in the valley north of Kitimat and on the lower slopes of Mt. Clague (Fig. 2). A sample of pale green dacite with lavender-blue opaline quartz phenocrysts (Fig. 5b), 08JN01-03, gave an age of  $322.2 \pm 1.0$  Ma, based on a weighted average of three concordant grains.

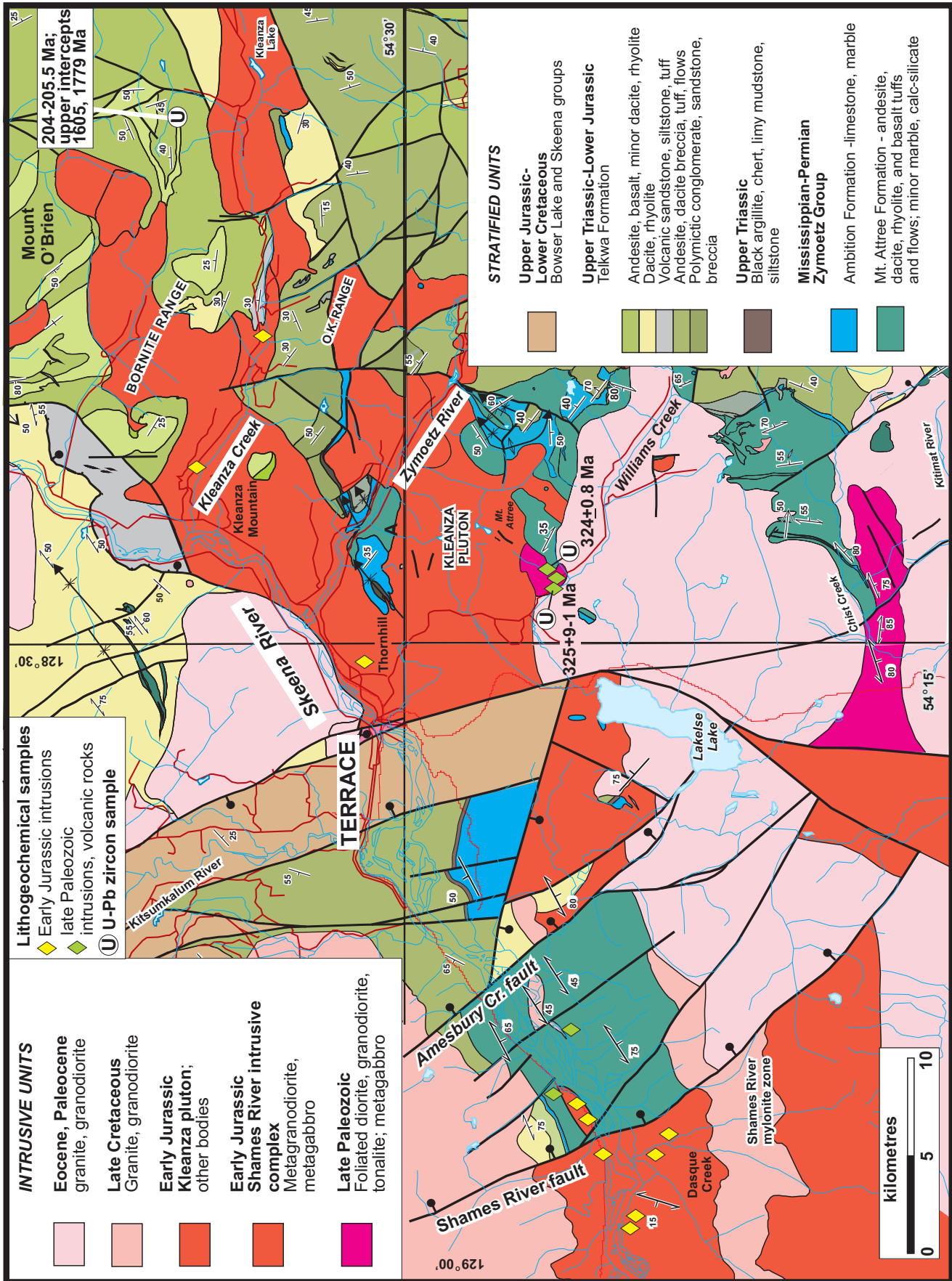
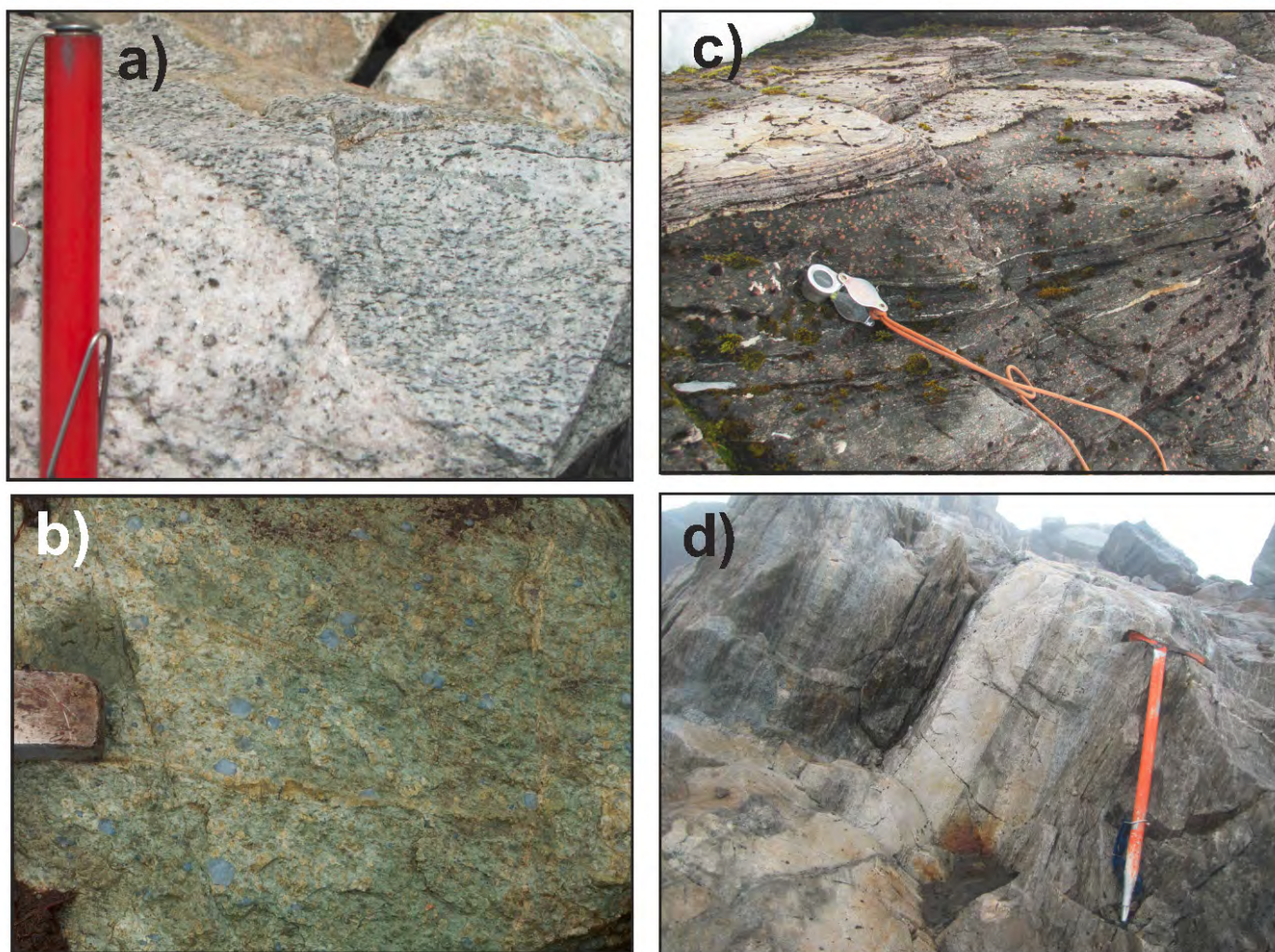


Fig. 4. Geology of western Stikinia and eastern Coast Mountains orogen near Terrace, with locations of U-Pb geochronological and lithochemical samples presented in this paper.



**Fig. 5.** Photos of Paleozoic units. **a)** Well-foliated metatonalite, Williams Creek, at U-Pb sampling site 07JA05-01, cut by fresh, unfoliated Kleanza granodiorite dike, 535436 E, 6031818 N. **b)** Opaline quartz-eye dacite, west of Kitimat, 07JN05-08, 517824 E, 5993220 N. **c)** Garnet amphibolite in contact with layered quartz-rich metaclastic schist, northern Prospector Ridge, 16JN01-04, 470628 E, 5967336 N. **d)** Metatonalite with leucotonalite sill, northern Prospector Ridge, 16JN03-04, 470991 E, 5966833 N.

All three ages coincide within error, indicating a significant ca. 325-322 Ma volcanic-intrusive event close to the Mississippian-Pennsylvanian boundary. They overlap the intrusive ages of 331-317 Ma reported by Heah (1991) along the Skeena River, and  $322 \pm 6$  Ma reported by Rusmore et al. (2005) near Kitimat (Fig. 2). Because of large errors, the  $336.8 \pm 17.7$  Ma age of the Gareau stock in the Ecstall belt also overlaps this cluster.

In 2016, a suite of nine late Paleozoic samples were collected for whole rock and trace element analysis, including two dacites and a metabasalt of the Mt. Attree Formation, three tonalites from the pluton in Williams Creek, two tonalites and a diorite from the 'Central diorite suite' on Prospector Ridge, and two garnet amphibolite dikes or sills that cut the Upper Devonian(?) metaclastic unit, also on Prospector Ridge (Table 1; see Nelson and Friedman, 2017 for full geochemical data and analytical techniques).

On northern Prospector Ridge, sill-like garnet amphibolite bodies form metre- to decimetre-thick layers that alternate

regularly with quartz-rich metaclastic schists (Fig. 5c). Contacts are sharp and, in some cases, the mafic units cross-cut transposed compositional layering in the schists. These bodies are interpreted as sills or completely transposed dikes. Most are uniformly fine grained, and are probably metabasalts. Remnant intrusive textures are present in a few zones, including unfoliated plagioclase-hornblende intergrowths and acicular hornblende-bearing mafic pegmatites. An inhomogeneous felsic body, mainly pale brownish tonalite with leucotonalite sills (Fig. 5d) and mafic enclaves, intrudes both the mafic and surrounding metaclastic rocks.

The Paleozoic suite shows clear bimodality on Harker-type, X vs.  $\text{SiO}_2$  plots, with the basalt and garnet amphibolite samples at  $<50\%$   $\text{SiO}_2$  and the dacites and tonalites at  $65\%$  to  $75\%$   $\text{SiO}_2$  (Figs. 7, 8). The suite plots within the calc-alkalic to calcic field (Fig. 7) on the Modified Alkali-Lime Index vs.  $\text{SiO}_2$  plot of Frost et al. (2001). On a  $\text{Fe}^*$  vs.  $\text{SiO}_2$  plot (Fig. 8), it is entirely magnesian; typical of magmatic arc rather than

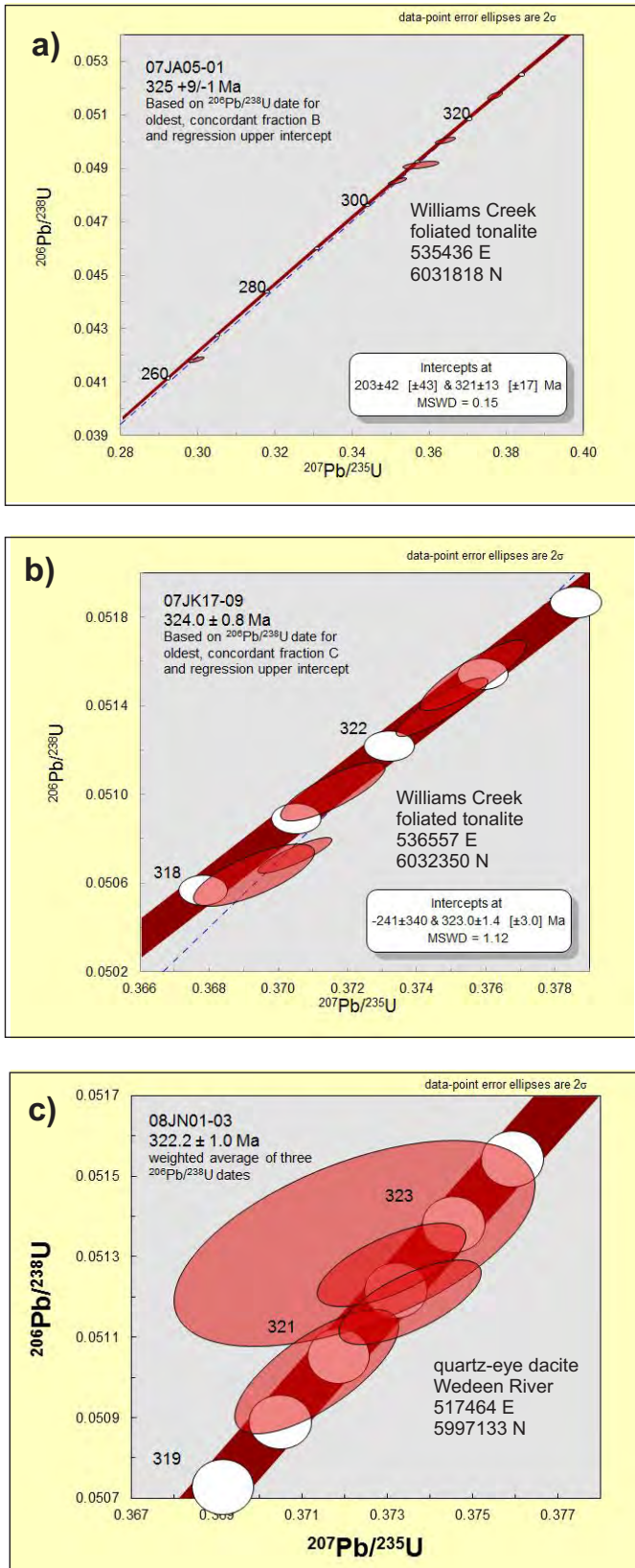


Fig. 6. Concordia plots for Paleozoic units.

A-type affinities (Frost et al., 2001). The mafic rocks show overall enrichment in immobile trace elements normalized with respect to primitive mantle, and smooth, uniform profiles that characterize non-arc igneous rocks (Fig. 9a). The Ecstall garnet amphibolites display slight negative REE slopes and Nb enrichment characteristic of enriched mid-ocean ridge basalts (E-MORB), whereas the Mt. Attree metabasalt has a flat REE profile and slight negative Nb anomaly typical of back-arc basin basalts (BABB; Piercey et al., 2006). In contrast, profiles for all the felsic rocks show relative depletions in Nb, Ti, V, and Sc which typify subduction-related signatures (Figs. 9b-d). All but one sample (16JN14-01, a quartz-eye dacite south of the Skeena River) display negative REE slopes and significant Th enrichment, all features of calc-alkaline suites. Compared to those from the Ecstall belt, the Stikinia tonalite samples show similar to greater Nb and Ti troughs, lower Sm, and higher Al. The Ecstall and Williams Creek (Stikinia) tonalites differ in absolute abundance of HREE, with a somewhat higher level in the Ecstall pluton. This implies a difference in the REE enrichment of the mantle source area.

In summary, U-Pb ages from the late Paleozoic igneous suites in Stikinia and the Ecstall belt overlap, ranging from Middle Mississippian to lowermost Pennsylvanian. Both suites are bimodal, with coexisting non-arc-derived mafic and calc-alkaline felsic magmatism. Mt. Attree Formation mafic rocks are of back-arc basin affinity, whereas those from the Ecstall belt are E-MORB. The Ecstall felsic samples show overall greater enrichment of REE, particularly LREE. The similar ages and geochemistry of these two suites suggest general consanguinity. However, systematic differences suggest separate magma sources and/or processes of magma evolution.

### 2.2.2. Early Jurassic intrusive and extrusive bodies

Early Jurassic intrusions occur throughout the transect, from the Kleanza pluton and its correlatives in western Stikinia, through the Shames River orthogneiss of the central Coast Mountains orogen, to the Foch and Johnson plutons in the Ecstall belt (Fig. 2). They thus represent a potential link between Stikinia and the older assemblages to the west, and more specifically may have crystallized at different crustal depths within a series of interconnected magma chambers. Sampling in 2016 concentrated on the Early Jurassic bodies to test these hypotheses. Five geochemical samples were collected from the Kleanza pluton and correlatives along the Skeena River west of Terrace, five from the Shames River suite, and five from the Foch Lake pluton. Two geochronological samples were collected to address current knowledge gaps and will be reported on elsewhere: a granodiorite of the Thornhill phase of the Kleanza pluton from a roadside outcrop along Highway 37 just south of its intersection with Highway 16 (16JN18-06); and a granodiorite from the Shames River intrusive suite near Dasque Creek south of the Skeena River (16JN14-03; Table 1).

**Table 1.** Descriptions of lithogeochemical samples shown on Figures 8, 9, 10, 12, 13.

Station	UTME	UTM N	Area	Map unit	Age	Rock name	Description
16JN01-01	470295	5967536	Ecstall belt - Prospector Ridge	sill in quartz metaclastic unit	Late Paleozoic	garnet amphibolite	In meta-arenite and meta-pelite.
16JN01-03	470476	5967481	Ecstall belt - Prospector Ridge	sill in quartz metaclastic unit	Late Paleozoic	garnet amphibolite	Concordant with layering in metaclastic unit. Areas of metadioritic texture (sill or transposed dike).
16JN03-04	470991	5966833	Ecstall belt - Prospector Ridge	central diorite complex	Mississippian	metatonalite	Equivalent to Gareau stock. Metatonalite-metadiorite- metaleucotonalite; layered.
16JN03-07	471396	5967033	Ecstall belt - Prospector Ridge	central diorite complex	Mississippian	metadiorite	Salt and pepper medium- to fine-grained metadiorite; same body as sample 16JN03-04.
16JN03-08	471300	5966976	Ecstall belt - Prospector Ridge	central diorite complex	Mississippian	metadiorite/ tonalite	Slabby metadiorite or tonalite, hb-qz-plag with leucotonalite layers. Same unit as 16JN03-04.
16JN18-01	535429	6031827	Williams Creek	unnamed pluton	Mississippian	tonalite/ granodiorite	07JA05-01, ca 323 Ma foliated granitoid, tonalite- granodiorite, 30% plag, 10% Kspar, 15% qz, 20% hb, bi; 25% irresolvable matrix.
16JN18-02	535873	6031778	Williams Creek	unnamed pluton	Mississippian	tonalite	Tonalite, well foliated, fine-med grained, small mafic xenoliths. 45% plag, 35% qz, 20% bi (some secondary after hb). Same body as sample 16JN18-01.
16JN18-03a	536405	6032082	Williams Creek	unnamed pluton	Mississippian	tonalite	Tonalite, same body as sample 16JN18-01
16JN14-01	512716	6030900	Skeena River	Mt. Attwood Formation	Late Paleozoic	dacite	Metadacite, blue quartz eyes, pale green, aphanitic matrix.
16JN16-07	509371	6031627	Skeena River	Mt. Attwood Formation	Late Paleozoic	dacite	Plag-quartz-phyric dacite with some blue quartz eyes. 40% plag, 10% qz, 5% hb, 5% bi, 30% aphanitic matrix. Near Heah's (1991) 317-331 Ma U-Pb sample.
16JN18- 03b	536405	6032082	Williams Creek	Mt. Attwood Formation	Late Paleozoic	metabasalt	Metabasalt in contact with tonalite
16JN05-03	483415	5953006	Ecstall belt	Foch pluton	Early Jurassic	metatonalite	Coarse-grained metatonalite, 50% plagioclase .5-1 cm, 20% quartz, 25% smaller hb, trace tit, ga, ep, msc
16JN05-07	484225	5951404	Ecstall belt	Foch pluton	Early Jurassic	metadiorite	Salt and pepper metadiorite, border phase of Foch pluton
16JN05-10	484307	5951316	Ecstall belt	Foch pluton	Early Jurassic	metadiorite	Salt and pepper metadiorite, border phase of Foch pluton
16JN06-01	483367	5953468	Ecstall belt	Foch pluton	Early Jurassic	metatonalite	Metatonalite, relatively mafic-rich. 42% plagioclase, 25% quartz, 30% hb, 3% biotite, tr tit, ep, ga.
16JN07-04	483123	5956367	Ecstall belt	Foch pluton	Early Jurassic	Plagioclase porphyry	Metatonalite/metagranodiorite, well layered, near pluton margin. Plagioclase phryric.

Table 1. Continued.

Station	UTME	UTM N	Area	Map unit	Age	Rock name	Description
16JN13-02	493493	6032977	Exstew River	Shames River intrusive complex	Early Jurassic	Tonalite(?)	Fine-grained tonalite, well foliated. 35% quartz, 25% plag, 30% hb, 10% bi, tr mt.
16JN13-03	491801	6032777	Exstew River	Shames River intrusive complex	Early Jurassic	gabbro	Hornblende-rich gabbro, spaced well foliated and unfoliated panels.
16JN14-02	507286	6025714	Dasque Creek	Shames River intrusive complex	Early Jurassic	gabbro	Powerhouse outcrop, layered coarse gabbro, black amphibolite, leucotonalite. Gabbro is 60% hb, 25% plag, 5% qz, 10% bi, tr py.
16JN14-03	506759	6026369	Dasque Creek	Shames River intrusive complex	Early Jurassic	granodiorite	Foliated granodiorite, 50% plag, 25% qz, 15% bi, 3% hb, .5% mt., trace titanite.
16JN14-05	502442	6027963	Dasque Creek	Shames River intrusive complex	Early Jurassic	tonalite	Tonalite, medium-grained, equigranular, well foliated and lineated. 40% plag, 39% qz, 23% hb, 5% bi, 2% mt.
16JN14-06	502482	6027731	Dasque Creek	Shames River intrusive complex	Early Jurassic	granodiorite	Granodiorite, strongly foliated, protomylonitic. 35% plag, 25% qz., 15% Kspar, 15% hb., 8% bi, 2% mt.
16JN16-01	506497	6029206	Shames River	Shames River intrusive complex	Early Jurassic	tonalite	Heah's (1991) classic outcrop, ca 188 Ma U-Pb zircon sample site. Interlayered mafic and felsic intrusive rock, protomylonitized. Tonalite 40% plag, 25% qz, 25% bi, 8% hb, 2% mt.
16JN12-01	531934	6042021	Terrace	Kleanza intrusive suite	Early Jurassic	granodiorite	Thornhill phase of Kleanza pluton. Unfoliated, cliff-forming granodiorite, 30% plagioclase, 30% quartz, 20% Kspar, 10% hornblende, 5% biotite.
16JN15-01	540649	6050285	Kleanza Creek	Kleanza intrusive suite	Early Jurassic	granodiorite	Medium-grained granodiorite, 25% quartz, 25% plagioclase, 15% Kspar, 35% hornblende.
16JN15-03	548117	6046651	Kleanza Creek	Kleanza intrusive suite	Early Jurassic	microdiorite	Crowded porphyritic (pl-hb) microdiorite. 40% plag, 7% hb., 3% ep, 3% py, 1% mt, 46% dark microcrystalline matrix.
16JN16-03	508226	6029924	Skeena River	Kleanza intrusive suite	Early Jurassic	granodiorite	Granodiorite, moderately well foliated. 35% plag, 30% qz., 15% hb, 10% bi, 10% Kspar. Good candidate for transition from Shames River to Kleanza.
16JN16-04	508920	6030302	Skeena River	Kleanza intrusive suite	Early Jurassic	hornblende diorite	Hornblende diorite, related to granodiorite of 16-3 but with characteristic texture of felted acticular hb. Weak, sporadic foliation developed in epidote metazones.

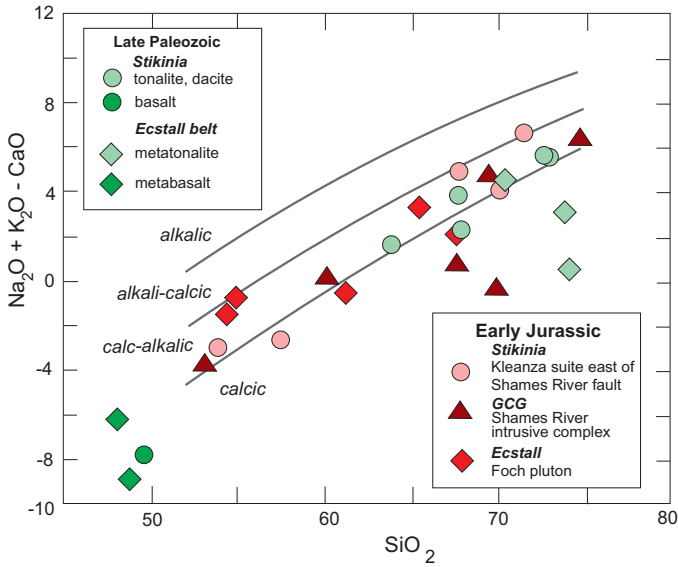


Fig. 7. Paleozoic and Early Jurassic samples on a MALI (modified alkali-lime vs. silica) plot of Frost et al. (2001).

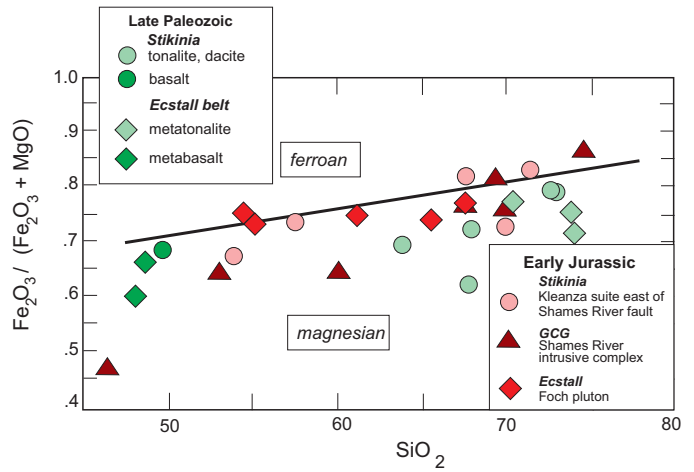


Fig. 8. Paleozoic and Early Jurassic samples on a  $\text{Fe}^*$  vs. silica plot of Frost et al. (2001).

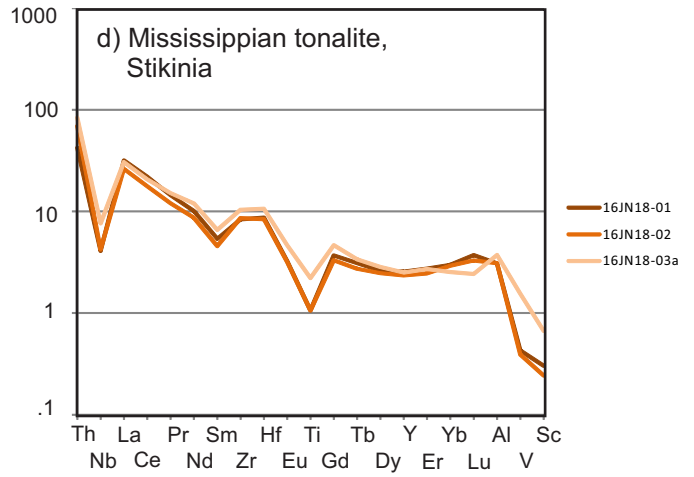
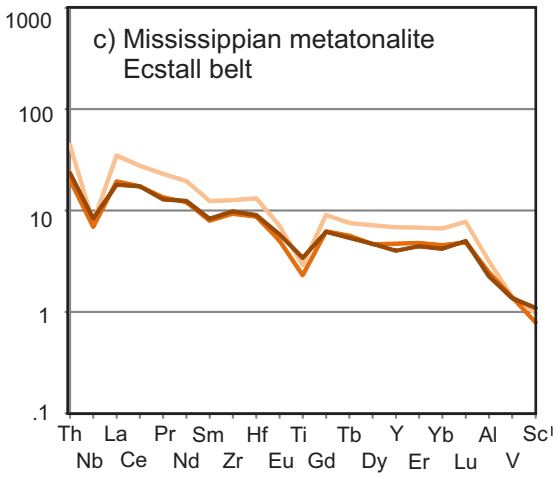
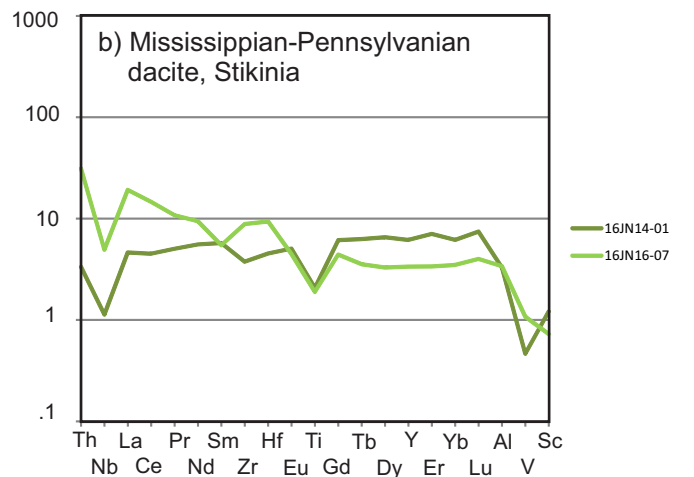
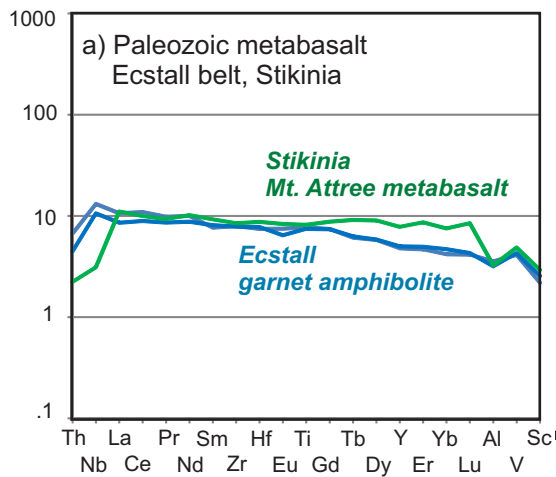


Fig. 9. Spider plots of immobile trace elements for Paleozoic samples, normalized against primitive mantle values of Sun and McDonough (1989). Choice and order of elements from most to least compatible after Piercy et al. (2006).

### 2.2.2.1. Kleanza plutonic suite

Coarse-grained, moderately- to weakly-foliated diorite and granodiorite cut deformed late Paleozoic metavolcanic and metaplutonic rocks along the Skeena River west of Terrace. The main Kleanza pluton extends in three lobes up to 40 kilometres east-northeast from Terrace, including the prominent cliffs north of Thornhill (Fig. 10a). It comprises many phases of differing composition and texture. Coarse-grained, equigranular to K-feldspar-megacrystic granodiorite and granite (Fig. 10b) predominate in its southern and western exposures, from Mt. Thornhill to Kleanza Mountain, cutting the upper part of the Zymoetz Group and lower Telkwa Formation. The ca. 200 Ma U-Pb age (Gareau et al., 1997) is from a highway cut in this phase. North and east, higher-level, porphyritic diorite and monzonite phases are in the Bornite Range; on Mt. O'Brien, subvolcanic andesite passes transitionally to ca. 195 Ma flows of the upper Telkwa Formation (Nelson et al., 2006b; Barresi et al., 2015). This overall pattern is interpreted to signify post-emplacement eastward tilting of the pluton along with its stratified hosts. Coarse-grained, pink quartz-rich granite and monzogranite occur in the Kleanza Creek drainage. Gehrels et al. (2009) reported a ca. 181 Ma U-Pb zircon age from near Kleanza Lake. Minor muscovite occurs in the granite near the U-Pb sample site. Because these granites represent a distinct, significantly younger phase compared to most of the Kleanza pluton, they are not included in the geochemical study.

### 2.2.2.2. Shames River intrusive complex

The Shames River intrusive complex outcrops extensively at low elevations west of the Shames River fault (Fig. 2). Although termed an 'orthogneiss' by Heah (1991), its compositional variations are primary rather than metamorphic; therefore the term 'intrusive complex' is preferred. Phases range in composition from hornblende gabbro to diorite, tonalite and granodiorite. Some bodies are homogeneous over several square kilometres. Rafts of mafic xenoliths occur near the margins of more felsic bodies (Fig. 10c). In some outcrops, well-foliated and sheared tonalite/granodiorite and gabbro bodies are interlayered on a metre to decimetre scale (Fig. 10d). Inter-phase contacts are sharp, and textures in both mafic and felsic components are igneous rather than gneissic. These bodies are interpreted as transposed sill complexes. They may occur in parts of the complex that have undergone higher ductile strain. Shear sense indicators in them show normal-sense (top-to-east) displacement (Heah, 1991; this study).

### 2.2.2.3. Foch pluton

The Foch pluton is a 5 by 25 km, northwest-elongate tonalite body that intrudes stratified metavolcanic and metaclastic rocks of the Ecstall belt. Compared to the strong transposition fabric of its hosts, it is variably foliated. Sparse metamorphic garnet indicates that it went through the same Cretaceous garnet amphibolite-facies metamorphism as the older rocks of the Ecstall belt. Primary minerals include plagioclase, quartz, hornblende, biotite, and varying amounts of magnetite.

Textural and compositional variations in the main pluton are gradational. It is cut by leucotonalite (trondhjemite) dikes (Fig. 10e). The main phase ranges from coarse grained equigranular to plagioclase-megacrystic (Fig. 10f). Rafts of mafic xenoliths occur rarely (Fig. 10g). In a few cases, trains of shape-oriented plagioclase megacrysts parallel mafic schlieren, indicating magmatic flow. Fine-grained diorite occurs locally at the edge of the intrusion. The Foch pluton is much more homogeneous than either the Kleanza suite or the Shames River intrusive complex. Its plagioclase megacrystic textures are unique.

Numerous planar, fracture-controlled epidote-quartz zones cut the pluton (Fig. 10h). Some are cored by narrow, planar quartz veins. The zones tend to localize foliation and shearing (Fig. 10h). In some, small garnets developed at the expense of epidote. These zones probably formed during late stage cooling of the pluton. Because of the original fracture control and abundance of fine-grained secondary hydrous minerals, they likely focused strain during Cretaceous deformation. These low-temperature post-magmatic zones suggest that the Foch pluton was emplaced at fairly shallow depths in the upper crust, and does not represent the deep root of an Early Jurassic magma chamber. The pluton, along with older stratified rocks of the Ecstall belt, was tectonically buried and metamorphosed under garnet amphibolite facies conditions in the Cretaceous.

### 2.2.2.4. Geochemistry

A set of 17 samples was submitted for major and trace element analysis (Table 1; see Nelson and Friedman, 2017 for full geochemical data and analytical techniques). Given that the Early Jurassic suites are primarily coarse-grained plutonic rocks, geochemical interpretation focuses on major element chemistry for classification and comparison (see Frost et al., 2001). Trace element signatures give approximate evidence of tectonic setting, but must be interpreted with caution because of likely extensive fractionation and possible multi-phase melting.

On the Modified Alkali-Lime Index (MALI) vs. silica diagram (Fig. 7), most samples from the three Early Jurassic suites plot as a single continuous sequence within or just below the calc-alkalic field. Two samples from the Shames River intrusive complex are more calcic. On the Fe\* vs. silica diagram (Fig. 8), the combined suite shows a progression from magnesian to weakly ferroan at highest contents of SiO<sub>2</sub>, a pattern typical of Cordilleran granites (Frost et al., 2001). Figure 11 shows Aluminum Saturation Index vs. silica for the suite, which plots as a narrow, single trend from metaluminous to weakly peraluminous at highest contents of SiO<sub>2</sub>. This pattern resembles that of the Tuolumne pluton in the Sierra Nevada, a typical differentiated Cordilleran calc-alkalic continental arc intrusion (Frost and Frost, 2014). In all three Harker-type (X vs. silica) diagrams, some Shames gabbros are the lowest in SiO<sub>2</sub>, and Foch tonalite analyses plot in the centre of the wide range of silica values of Kleanza and Shames samples. This is consistent with the relatively homogeneous intermediate character of the Foch pluton, as opposed to the great compositional and textural

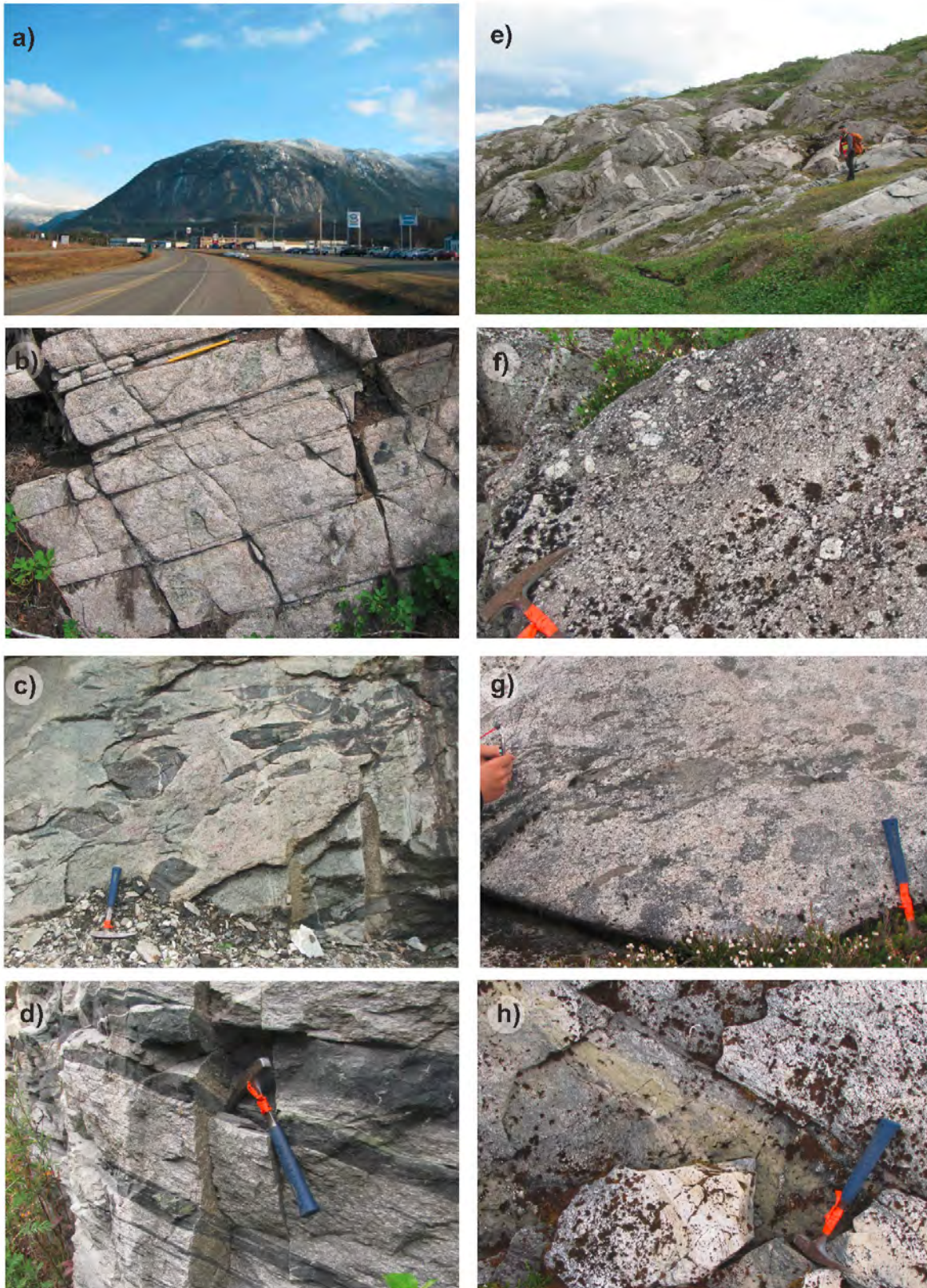


**Fig. 10.** Early Jurassic intrusive bodies. **a)** View of southwest face of Copper Mountain from Highway 16, Thornhill. **b)** Kleanza granite, north of Zymoetz River, 05EK01-01, 542077 E, 6039548 N. **c)** Amphibolite and gabbro xenoliths in Shames River intrusion, Dasque Creek, 507286 E, 6025714 N. **d)** Interlayered tonalite and gabbro, Shames River, 506497 E, 6029206 N. **e)** Leucotonalite dikes in Foch tonalite, 484548 E, 5951111 N. **f)** Plagioclase megacrysts, Foch pluton, 484116 E, 5951478 N. **g)** Swarm of mafic xenoliths in Foch tonalite, 483465 E, 5952518 N. **h)** Sheared epidote-rich zone in Foch pluton, 483414 E, 5953006 N.

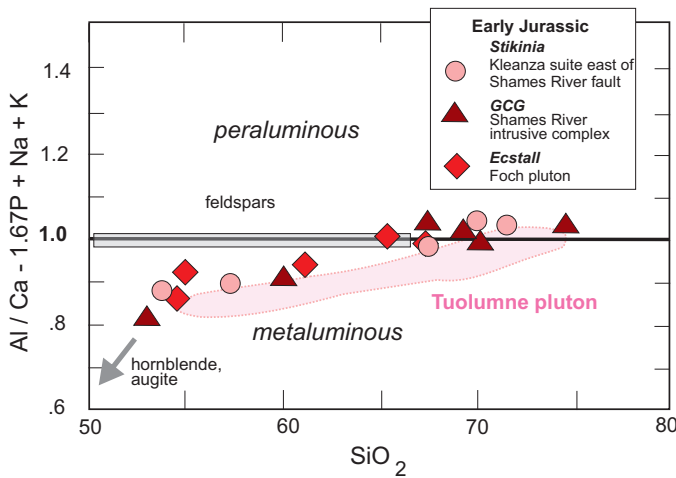


**Fig. 11.** ASI (aluminum saturation index) vs.  $SiO_2$  for Early Jurassic suite, using modified ASI formula of Frost et al. (2001). Mineral compositions and Tuolumne pluton field from Frost and Frost (2014).

range of phases in the Kleanza and Shames suites. The two lowest silica values from the Foch pluton are from its fine-grained marginal diorite phase.

Primitive mantle-normalized spider plots further illustrate the character of the Early Jurassic suites (Fig. 12). All show the negative Nb, Ti, V, and Sc deflections characteristic of arc-derived igneous rocks, in most accompanied by negative slopes reflecting strong enrichment of LREE. Rocks containing a high modal percentage of plagioclase show positive Eu and Al anomalies that identify them as plagioclase cumulates. Plots of samples from the Foch pluton (Fig. 12a) are consistent, in keeping with the observed homogeneous nature of the body. Most likely, the main Foch pluton formed from a single, differentiating magma phase. In contrast, the Kleanza (Fig. 12b) and Shames (Figs. 12c, d) suites each show significant internal variation in terms of REE slopes, varying enrichment of Al and Zr-Hf, and degree of depletion of Nb and Ti. This suggests that both suites formed through similar processes of cooling of multiple magma batches, each phase with a somewhat different origin and differentiation history. Notably, the spectra of variations in the Kleanza and Shames suites are similar, suggesting common sources and similar differentiation processes.

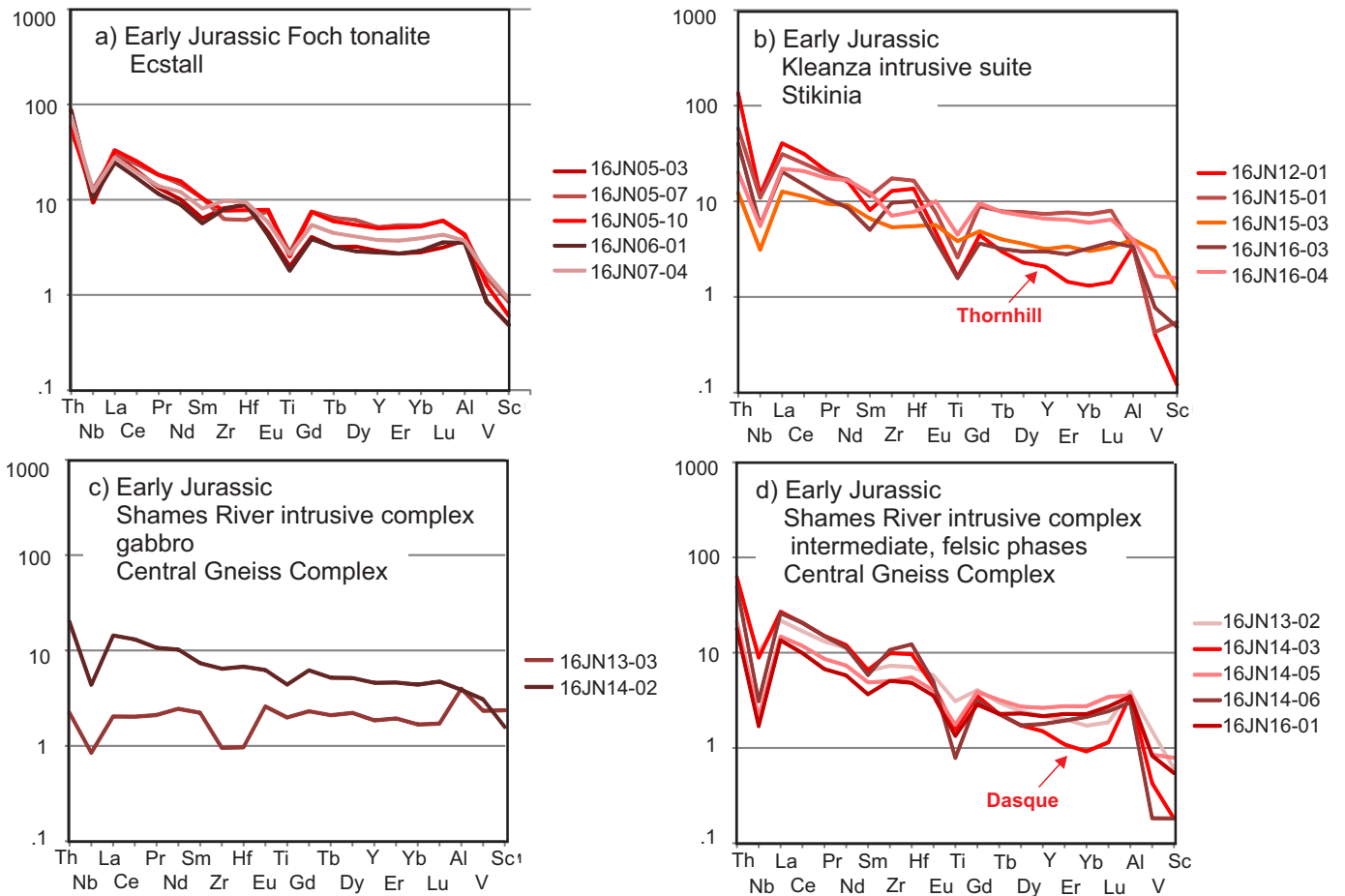


**Fig. 12.** Spider plots of immobile trace elements for Early Jurassic samples, normalized against primitive mantle values of Sun and McDonough (1989). Choice and order of elements from most to least compatible after Piercy et al. (2006).

Crystal-melt partition coefficients for the rare earth elements display distinct patterns for amphibole relative to garnet (Davidson et al., 2007). For garnet, crystal-melt coefficients correlate negatively with ionic size, decreasing from nearly 10 for Yb to 0.1 for La, whereas hornblende-melt coefficients fall to lower values for LREE and HREE from a MREE peak at Dy (Davidson et al., 2007). Therefore plots of La/Yb and Dy/Yb vs. silica for igneous suites can be used to determine refractory minerals either in residua or as fractionating phases. Most of the Early Jurassic samples from all three suites show increasing La/Yb and decreasing Dy/Yb with increasing silica (Fig. 13). The trends lie close to an amphibole fractionation trend (Smith, 2014). All of these rocks contain hornblende, with modal amounts generally decreasing with higher silica. Thus, in addition to plagioclase fractionation, field observations and trace element behaviour point to hornblende fractionation as an important process.

Two samples stand out as highly anomalous on Figure 13, with very high La/Yb and Dy/Yb ratios, and similar overall trace element profiles on Figure 12. They include: a) the Thornhill granodiorite phase of the Kleanza pluton (16JN12-01); and b) a Shames River suite mafic-poor, well-foliated

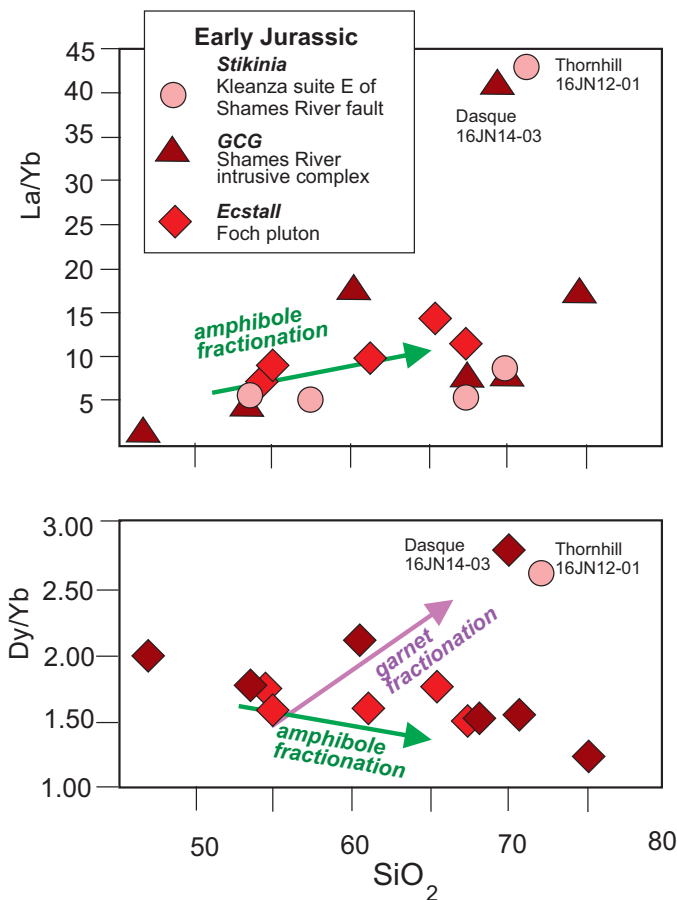


**Fig. 13.** La/Yb and Dy/Yb vs. for Early Jurassic suite. Amphibole fractionation arrow from Smith (2014). Garnet fractionation arrow from Davidson et al. (2007).

granodiorite (16JN14-03). Their extreme LREE and MREE enrichment is consistent with abundant garnet in a residual phase. Strong depletion in compatible elements V and Sc and high values of incompatible Th identify these rocks as more evolved than the rest of the suite. Their chemistry is consistent with a complex origin. The strong LREE enrichment and depletion of compatible elements suggests a parent with a much smaller degree of partial melting than the rest of the Early Jurassic suite. These rocks could have evolved through multiple crystallization-remelting cycles at the base of a thick crust or in the sub-arc mantle.

#### 2.2.2.5. Telkwa rhyolite with Precambrian inheritance

A sample of red, coherent dacite from the Telkwa Formation, 05TB26-10, yielded three discordant zircon fractions (Fig. 14). Two-point discordia, based on the youngest fraction and each of the two oldest fractions have Early Jurassic lower intercepts and Paleoproterozoic upper intercepts. The lower intercepts,  $204.0 \pm 5.4$  Ma and  $205.5 \pm 4.4$  Ma, are close to the actual age of the dacite, because it lies stratigraphically above a  $204.29 \pm 0.45$  Ma rhyolite and below a  $194.35 \pm 0.32$  Ma rhyolite (Barresi et al., 2015). The upper intercepts at ca. 1605 and 1779 Ma reflect Precambrian cores in igneous zircons.

### 2.3. Discussion

New data presented above test potential correlation and continuity of late Paleozoic and Early Jurassic units from Stikinia near Terrace into the Coast Mountains orogen to the west. Ages of late Paleozoic volcanic and intrusive units near Terrace (325-323 Ma) agree with a previously reported, less precise age of 331-317 Ma (Heah, 1991). These ages are somewhat younger than the single age available from the Ecstall belt ( $336.8 \pm 17.7$  Ma), but overlap within error. Late Paleozoic igneous suites in both Stikinia and the Ecstall belt are bimodal. Mafic rocks are of non-arc origin, E-MORB in Ecstall

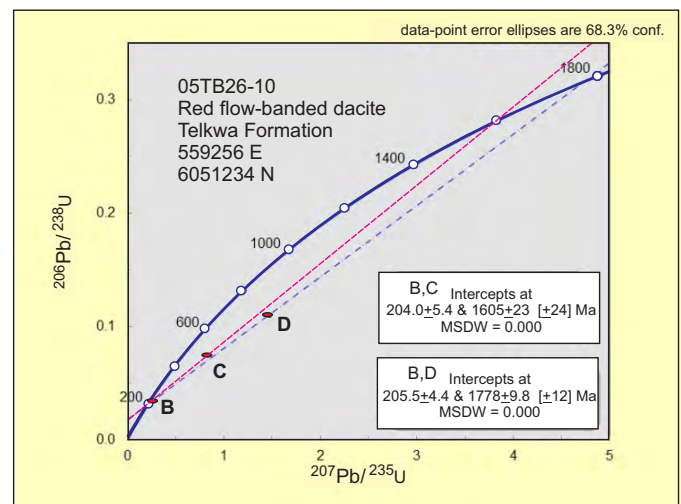


**Fig. 14.** Concordia plot for zircons from Telkwa Formation rhyolite, 05TB26-10. Proterozoic upper intercepts are from cores in two zircon fractions.

and BABB in Stikinia, whereas felsic rocks are calc-alkaline. Coexisting felsic arc and mafic non-arc suites are common in late Paleozoic assemblages of the Yukon-Tanana terrane, where rocks of non-arc affinity have been attributed to back-arc extension (Piercey et al., 2006). The similar age and character of these suites suggests late Paleozoic commonalities between Stikinia and the Ecstall belt. However, because late Paleozoic igneous rocks are throughout northern Stikinia (Gunning et al., 2006), they do not constitute a precise link.

Early Jurassic intrusions such as the Kleanza suite (western Stikinia), the Shames River orthogneiss (Coast Mountains orogen) and the Foch pluton (Ecstall belt) form a continuum of major element compositions that define them as a calc-alkalic, mainly magnesian, metaluminous magmatic suite that evolved to slightly ferroan and peraluminous at highest SiO<sub>2</sub> values. For most of the suite, increase of La/Yb at higher SiO<sub>2</sub> with corresponding decrease of Dy/Yb is consistent with hornblende fractionation. Positive Al and Eu peaks in spider plots indicate plagioclase fractionation. Minor element profiles for the Kleanza and Shames River suites show similar degrees of internal variability, suggesting involvement of multiple melts. Notably, one sample from each suite shows extreme LREE enrichment, characteristic of strong influence by residual garnet.

Based on their petrologic and geochemical similarities, it is likely that the Shames River intrusive complex represents deeper levels of the Kleanza intrusive suite (Fig. 3). Restoring normal displacement on the Shames River fault and the Shames River detachment zone places the Terrace region structurally above the Central Gneiss Complex in the Late Cretaceous. This configuration was partly created by Cretaceous crustal shortening and west-vergent ductile deformation in the Coast Mountains orogen. However, the parallels between the Kleanza and Shames River intrusive suites suggest that an earlier link existed, at least as deep as the base of the Shames River complex.

The Foch pluton is coeval with the Kleanza intrusive suite and forms part of a geochemical continuum with it. The position of the Foch and Johnson plutons on a western continuation of the east-northeasterly trend of the Kleanza intrusive suite (Figs. 1, 2) is consistent with emplacement of all these bodies into a set of magma chambers controlled by a system of structurally controlled lower crustal conduits. The east-northeast trend of the Early Jurassic intrusive suite coincides with the Skeena arch (Fig. 1), a long-lived crustal discontinuity oriented at a high angle to Stikinia. Association of the Foch and Johnson plutons with the Kleanza suite suggests that the same basement discontinuity extends underneath the Ecstall belt. The deep structures that accommodated Early Jurassic intrusions of the Kleanza and related suites may have played a role equivalent to strands of the Pitman fault array farther north, notably the Boundary fault, which hosts the Red stock and Red Chris porphyry deposit. Long-lived, recurrent uplift of the Stikine and Skeena arches was triggered by differential movement across these deep crustal discontinuities. These discontinuities

also likely provided conduits at times of high magmatic flux, most notably during development of the Hazelton arc and its associated intrusions in the latest Triassic-Early Jurassic.

### 3. Mt. Clashmore supracrustal rocks

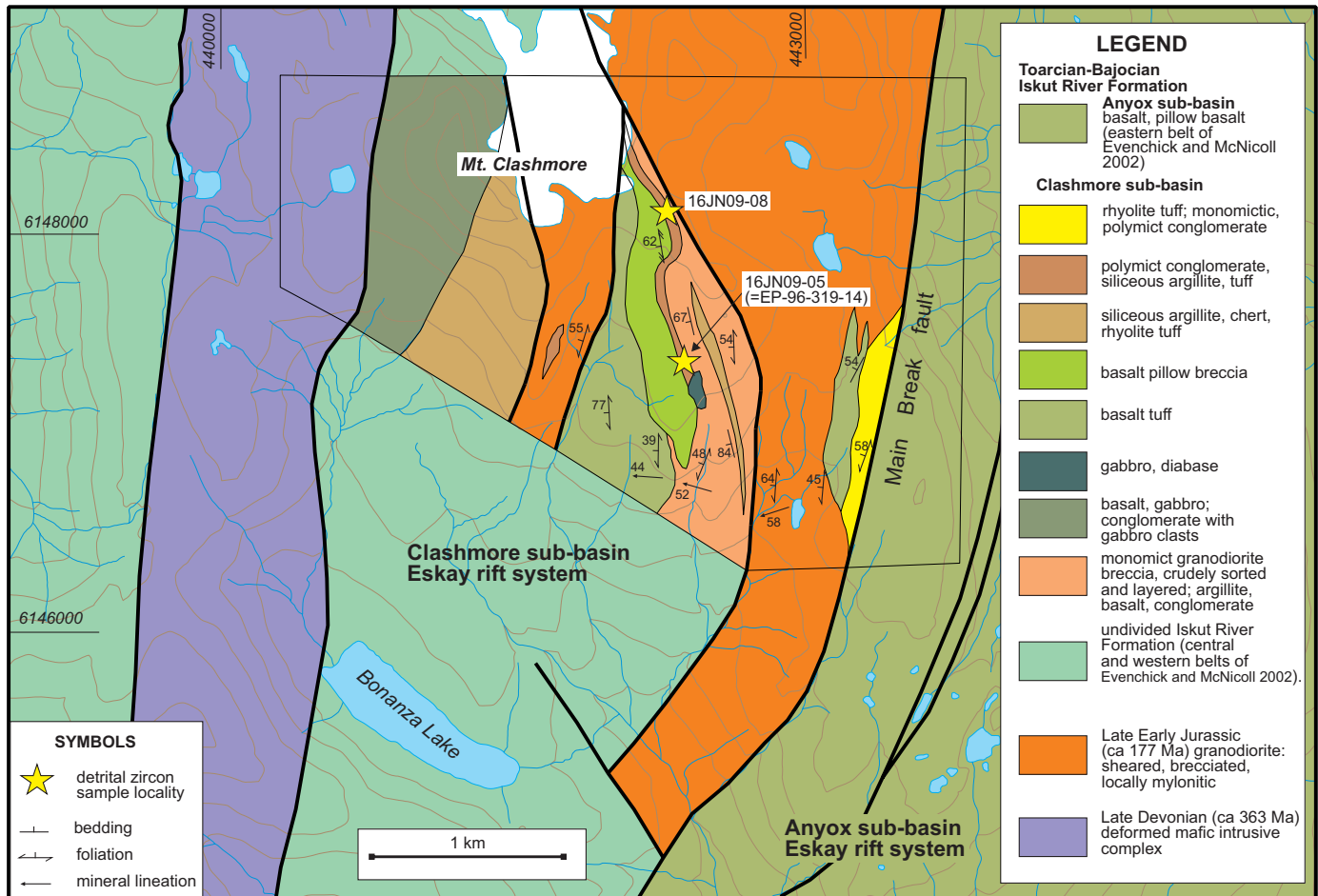
Building on mapping and geochronologic studies by Evenchick and McNicoll (2002), fieldwork near Mt. Clashmore in 2016 focused on remapping Lower to Middle Jurassic supracrustal rocks (Fig. 15) and resampling conglomeratic rocks for detrital zircon geochronology. Below I consider the possible relationship between these supracrustal rocks and deposits in the main Eskay rift; geochronologic results are pending.

Evenchick and McNicoll (2002) mapped across the southernmost exposures of the Eskay rift, where a predominantly basalt succession hosts Anyox, a Cu-rich volcanogenic deposit. Supracrustal rocks in the rift and near Mount Clashmore to the west (Fig. 15) both yielded zircons as young as late Early to Middle Jurassic, which they recognized as coeval with host rocks of the Eskay Creek volcanogenic orebody (186-173 Ma; Evenchick and McNicoll, 2002). Although they considered the Jurassic successions part of the Hazelton Group, they assigned those west of Anyox (central and western belts) to the Mt. Clashmore complex, a tectonically-defined unit that also contains fault-bounded panels of deformed Late Devonian and late Early Jurassic intrusive rocks (Fig. 15).

Of 11 zircons from a conglomerate sample analyzed by Evenchick and McNicoll (2002) from Mt. Clashmore (EP-96-319-14, Fig. 15), seven yielded Precambrian-Cambrian ages (SHRIMP; 1058, 1023, 987, 918, 612, 560, and 517 Ma), which have not been found to the north, in the Yukon-Tanana terrane.

Stratified units on Mt. Clashmore include basalt pillow breccia (Fig. 16a) and mafic tuff, siliciclastic strata, and minor rhyolite and rhyolite tuff, cut by coeval basalt, diabase, and gabbro dikes (Fig. 15). They occur in two panels, in steep fault contact with intervening sheared late Early Jurassic (ca. 177 Ma) granodiorite. Igneous rocks are bimodal, with a basalt:rhyolite ratio of >100:1. The only rhyolite body of mappable size is on the eastern margin of the assemblage, next to the Main Break fault (Fig. 15). At the margins of this body, large, angular rhyolite clasts float in a black argillite matrix (Fig. 16b). Fine-grained sedimentary layers consist of thinly bedded siliceous argillite and chert with pale felsic tuff laminae (Fig. 16c). East of the Mt. Clashmore summit, the polymictic conglomerate sampled by Evenchick and McNicoll (2002) forms a single, continuous layer stratigraphically above coarse, poorly layered monomictic breccia derived from the granodiorite (Fig. 16d). The conglomerate contains white felsic volcanic clasts, dark grey mudstone wisps and intraclasts, and rare grey chert and limestone clasts (Figs. 16e, f). Except for the chert and limestone, the clasts are probably intraformational. Farther west, on the southern slope of Mt. Clashmore, polymictic breccia/conglomerate contains clasts of basalt and fine-grained gabbro in a dark argillaceous matrix.

Evenchick and McNicoll (2002) concluded that the Jurassic



volcanosedimentary strata at Mt. Clashmore accumulated in graben adjacent to active normal faults, and that erosional stripping of intervening horsts provided clasts to conglomeratic units. The Grenville to Neoproterozoic to Cambrian detrital zircons were likely derived from horsts or rift-flank uplifts within or adjacent to the Eskay rift in the late Early to Middle Jurassic. The argillite-matrix rhyolite breccia, like rhyolite peperites in the northern part of the rift (Alldrick et al., 2004), is interpreted as the collapsed carapace of a subaqueous dome or cryptodome.

The association of late Early to Middle Jurassic bimodal volcanic and subvolcanic rocks with intervals of thinly bedded, fine-grained sedimentary strata and thickly bedded conglomeratic units favours correlation with the Iskut River Formation, a sequence of basalt, rhyolite, fine-grained siliceous argillite with pale tuff laminae ('pyjama beds') and siliciclastic deposits that form the fill of the Eskay rift in Iskut area, west-central Stikinia (Gagnon et al., 2012). The minimum detrital ages reported by Evenchick and McNicoll (2002) are coeval with the Iskut River Formation. Supracrustal rocks near Mt. Clashmore are separated from the mainly basaltic sequence that hosts the Anyox deposit only a few km to the east by the Main

Break fault (Alldrick, 2003). The two sequences were probably deposited in separate sub-basins of the Eskay rift system. I propose that all of the Jurassic supracrustal rocks in the Mt. Clashmore area be assigned to the Iskut River Formation, and that the term 'Clashmore complex' be abandoned.

Detrital zircon populations comparable to the Grenvillian or Neoproterozoic to Cambrian suite at Mt. Clashmore have not been reported from the Yukon-Tanana terrane, where Late Devonian and younger arc-related igneous assemblages are superimposed on continent margin strata with Archean to Paleoproterozoic zircon populations probably sourced from northwestern Laurentia (Nelson et al., 2006a). With a non-northwestern Laurentian zircon population, immediately adjacent Precambrian source rocks interpreted to have fed sediment directly into the southern Eskay rift contrast strongly with the Yukon-Tanana terrane that underpins the far northern part of Stikinia. Analysis of samples collected from this conglomerate in 2016 will provide a statistically valid data set to evaluate local basement sources.

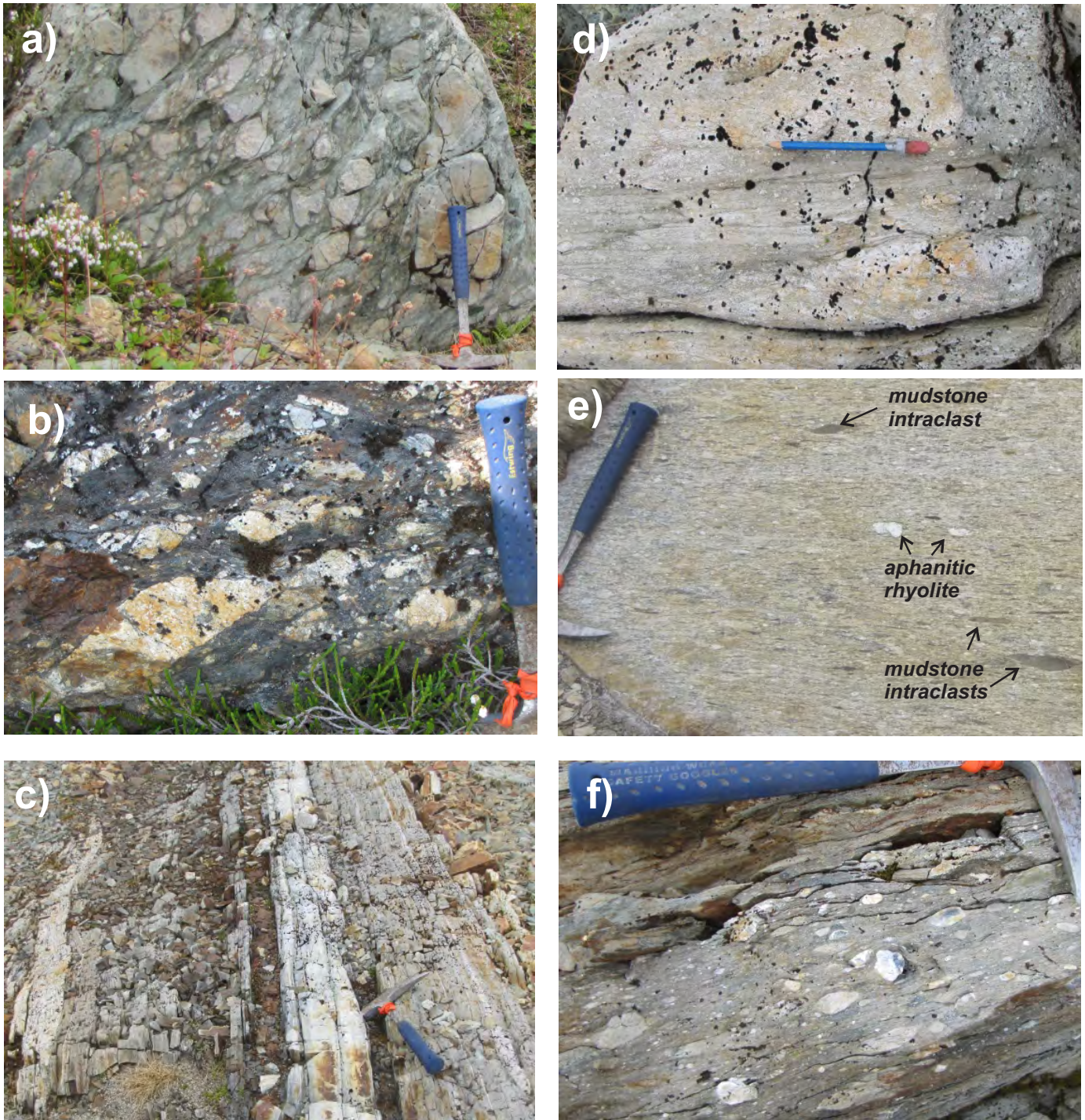


**Fig. 16.** Photos of Iskut River Formation units on Mt. Clashmore. **a)** Pillow breccia, 442435 E, 6147087 N. **b)** Rhyolite fragments in black argillite matrix, 443230 E, 6147529 N. **c)** Thin-bedded to laminated siliceous argillite and felsic tuff, 442408 E, 6147132 N. **d)** Sheared monomictic granodiorite breccia, 442478 E, 6146918 N. **e)** Heterolithic conglomerate at detrital zircon sample site 16JN09-06, 442380 E, 6147465 N. **f)** Heterolithic conglomerate with light grey chert clasts at detrital zircon sample site 16JN09-08, 442283 E, 6148076 N.

#### 4. Conclusions

Early Jurassic plutons east of and within the Coast Mountains orogen between Terrace and Prince Rupert show strong geochemical similarities and were probably parts of a single magmatic system emplaced along a structurally controlled corridor related to the Skeena arch. Furthermore, similarities in

age and chemistry of Mississippian igneous rocks of the Ecstall belt to those of Stikinia suggest that the Ecstall belt formed part of the pre-mid Paleozoic basement of the terrane. The structural corridor was certainly of pre-Jurassic origin, and may have existed before the Devonian, the age of the oldest known rocks of the Ecstall belt.

Late Early to Middle Jurassic supracrustal rocks near Mt. Clashmore, west of Anyox, represent a different facies compared to the immediate host rocks of the Anyox deposit and likely record separate sub-basin development in the southern Eskay rift. The succession at Mt. Clashmore has not been previously considered to have potential for volcanogenic occurrences. Correlation with the Iskut River Formation in the main Eskay rift and small rhyolite centres within it favour further exploration.

The Middle Devonian arc assemblage of the Ecstall belt and the cryptic Grenvillian-Cambrian source to the Mt. Clashmore conglomerate each represent distinct components within the pre-late Paleozoic basement of Stikinia. They differ from each other and from the Yukon-Tanana terrane, which underlies the Stikine assemblage at the far northern end of the terrane. The extreme contrasts between them, compared to the more homogeneous and continuous younger units, support the idea that these disparate crustal fragments amalgamated in a cryptic mid-Paleozoic collision before deposition of the Stikine assemblage and intrusion of cogenetic plutons such as More Creek and Forrest Kerr. The N-S and E-W fault arrays cut across all basement components. They probably initiated after accretion and before or during the first onset of Stikine assemblage magmatic activity.

Detrital zircon studies now in progress for samples from Mt. Clashmore are anticipated to shed additional light on the nature of Paleozoic and Precambrian basement units of west-central Stikinia.

### Acknowledgments

Joel Knickle provided excellent assistance in the field. This paper benefitted from a thorough review by Bram van Straaten.

### References cited

- Angen, J.J. 2009. Geospatial structural analysis of the Terrace area, west-central British Columbia (NTS 103I/08, 09, 10, 16). In: Geological Fieldwork 2008, British Columbia Ministry of Energy and Mines, British Columbia Geological Survey Paper 2009-1, pp. 21-33.
- Barresi, T., Nelson, J.L. and Friedman, R., 2015. Evolution of the Hazelton arc near Terrace, British Columbia: Stratigraphic, geochronological and geochemical constraints on a Late Triassic – Early Jurassic arc and Cu-Au porphyry belt. *Canadian Journal of Earth Sciences* 52, 466-494.
- Cecil, M.R., Gehrels, G., Ducea, M.N. and Patchett, P.J. 2011. U-Pb-Hf characterization of the central Coast Mountains batholith: Implications for petrogenesis and crustal architecture. *Lithosphere*, 3, 247-260.
- Cui, Y., Miller, D., Nixon, G., and Nelson, J., 2015. British Columbia digital geology. BC Ministry of Energy and Mines, British Columbia Geological Survey, Open File 2015-2.
- Currie, L.D. and Parrish, R.R. 1997. Paleozoic and Mesozoic rocks of Stikinia exposed in northwestern British Columbia: Implications for correlations in the northern Cordillera. *Geological Society of America Bulletin* 109, 1402-1420.
- Davidson, J., Turner, S., Handley, H., Macpherson, C. and Dosseto, A. 2007. Amphibole “sponge” in arc crust? *Geology*, 35, 787-790.
- Evenchick, C.A., 2001. Northeast-trending folds in the western Skeena Fold Belt, northern Canadian Cordillera: a record of Early Cretaceous sinistral plate convergence. *Journal of Structural Geology*, 23, 1123-1140.
- Evenchick, C.A., and McNicoll, V.J., 2002. Stratigraphy, structure, and geochronology of the Anyox pendant, northwest British Columbia, and implications for mineral exploration. *Canadian Journal of Earth Sciences*, 39, 1313-1332.
- Frost, B.R. and Frost, C.D. 2014. *Essentials of Igneous and Metamorphic Petrology*. Cambridge University Press, 305 p.
- Frost, B.R., Barnes, C.G., Collins, W.J., Arculus, R.J., Ellis, D.J. and Frost, C.D. 2001. A geochemical classification for granitic rocks. *Journal of Petrology*, 42, 2033-2048.
- Gabrielse, H., 1985. Major dextral transcurrent displacements along the Northern Rocky Mountain Trench and related lineaments in north-central British Columbia. *Geological Society of America Bulletin*, 96, 1-14.
- Gagnon, J.F., Barresi, T., Waldron, J.W.F., Nelson, J.L., Poulton, T.P., and Cordey, F. 2012. Stratigraphy of the upper Hazelton Group and Jurassic evolution of the Stikine terrane, British Columbia. *Canadian Journal of Earth Sciences*, 49, 1027-1052.
- Gareau, S.A. 1991. Geology of the Scotia-Quaal metamorphic belt, Coast Plutonic Complex, British Columbia. Ph.D. thesis, Carleton University, 391 p.
- Gareau, S.A. and Woodsworth, G.J. 2000. Yukon-Tanana terrane in the Scotia-Quaal belt, Coast Plutonic Complex, central-western British Columbia. In: Stowell, H.H. and McClelland, W.C., (Eds.), *Tectonics of the Coast Mountains, southeastern Alaska and British Columbia*, Geological Society of America Special Paper 343, pp. 23-44.
- Gareau, S.A., Friedman, R.M., Woodsworth, G.J., Childe, F. 1997. U-Pb ages from the northeastern quadrant of Terrace map area, west-central British Columbia. In: *Current Research 1996*, Geological Survey of Canada Paper 1997-A/B, 31-40.
- Gehrels, G.E., McClelland, W.C., Samson, S.D., Patchett, P.J. and Jackson, J.L. 1990. Ancient continental margin assemblage in the northern Coast Mountains, southeast Alaska and northwest Canada. *Geology*, 18, 208-211.
- Gehrels, G., Rusmore, M., Woodsworth, G., Crawford, M., Andronicos, C., Hollister, L., Patchett, J., Ducea, M., Butler, R., Klepeis, K., Davidson, C., Friedman, R., Haggart, J., Mahoney, B., Crawford, W., Pearson D., and Girardi, J., 2009. U-Th-Pb geochronology of the Coast Mountains batholith in north-coastal British Columbia: Constraints on age and tectonic evolution. *Geological Society of America Bulletin* 121, 1341-1361.
- Gunning, M.H., Hodder, R.W.H., and Nelson, J.L. 2006. Contrasting volcanic styles within the Paleozoic Stikine assemblage, western Stikine terrane, northwestern British Columbia. In: Colpron, M., and Nelson, J.L., (Eds.), *Paleozoic Evolution and Metallogeny of Pericratonic Terranes at the Ancient Pacific Margin of North America*, Canadian and Alaskan Cordillera. Geological Association of Canada Special Paper 45, pp. 201-227.
- Heah, T.S.T. 1991. Mesozoic ductile shear and Paleogene extension along the eastern margin of the Central Gneiss Complex, Coast belt, Shames River area, near Terrace, British Columbia. M.Sc. thesis, University of British Columbia, 155 p.
- Hill, M.L. 1985. Remarkable fossil locality: Crinoid stems from migmatite of the Coast Plutonic Complex, British Columbia. *Geology*, 13, 825-826.
- Hollister, L.S. and Andronicos, C. 2000. The Central Gneiss Complex, Coast Mountains, British Columbia. In: Stowell, H.H. and McClelland, W.C., (Eds.), *Tectonics of the Coast Mountains, southeastern Alaska and British Columbia*, Geological Society of America Special Paper 343, pp. 45-60.
- Kirkham, R.V. and Margolis, J. 1995. Overview of the Sulphurets area, northwestern British Columbia. In: Schroeter, T.G., (Ed.), *Porphyry Deposits of Western North America*, Canadian Institute of Mining and Metallurgy Special Volume 46, pp. 473-523.
- Kyba, J. and Nelson, J. 2015. Stratigraphic and tectonic framework of the Khyber-Sericite-Pins mineralized trend, lower Iskut River,

- northwest British Columbia. In: Geological Fieldwork 2014, British Columbia Ministry of Energy and Mines, British Columbia Geological Survey Paper 2015-1, pp. 41-58.
- Logan, J. M., Drobe J. R. and McClelland W. C. 2000. Geology of the Forrest Kerr-Mess Creek area, northwestern British Columbia (NTS 104B/10, 15 & 104G/2 & 7W). British Columbia Ministry of Energy and Mines, British Columbia Geological Survey Bulletin 104, 163 p.
- Mihalynuk, M.G., 1999, Geology and mineral resources of the Tagish Lake (NTS 104M/8,9,10E and 104N/12W) area, northwestern British Columbia. British Columbia Ministry of Energy and Mines, British Columbia Geological Survey Bulletin 105, 217 p.
- Mihalynuk, M.G., Smith, M.T., Hancock, K.D., and Dudka, S. 1994. Regional and economic geology of the Tulsequah River and Glacier areas. In: Geological Fieldwork 1993, British Columbia Ministry of Energy and Mines, British Columbia Geological Survey Paper 1994-1, pp. 171-197.
- Mihalynuk, M.M., Erdmer, P., Ghent, E.D., Cordey, F., Archibald, D.A., Friedman, R.M., and Johannson, G.G., 2004, Coherent French Range blueschist: Subduction to exhumation in <2.5 m.y.? Geological Society of America Bulletin, 116, 910-922.
- Nelson, J.L., 2009. Terrace Project Year 4: Extension of Paleozoic volcanic belt and indicators of VMS-style mineralization near Kitimat, NTS 103I/02, 07. In: Geological Fieldwork 2008, British Columbia Ministry of Energy and Mines, British Columbia Geological Survey Paper 2009-1, pp. 7-20.
- Nelson, J. 2014. Reactivated basement structures controlled emplacement of Triassic-Jurassic Stikine Cu-Au porphyries. Abstract, Paper No. 240-5, Geological Society of America Annual Meeting.
- Nelson, J.L. and Friedman, R. 2017. U-Pb and geochemical data from late Paleozoic and Jurassic rocks of western Stikinia and the Coast Mountains. British Columbia Ministry of Energy and Mines, British Columbia Geological Survey GeoFile 2017-1.
- Nelson, J.L. and Kyba, 2014. Structural and stratigraphic control of porphyry and related mineralization in the Treaty Glacier – KSM – Brucejack – Stewart trend of northwestern Stikinia. In: Geological Fieldwork 2013, British Columbia Ministry of Energy and Mines, British Columbia Geological Survey Paper 2014-1, pp. 111-140.
- Nelson, J.L., Barresi, T., Knight, E. and Boudreau, N. 2006a. Geology and mineral potential of the Usk map area (103I/09) near Terrace, British Columbia. In: Geological Fieldwork 2005, British Columbia Ministry of Energy and Mines, British Columbia Geological Survey Paper 2006-1, pp. 117-134.
- Nelson, J.L., Colpron, M., Piercey, S.J., Dusel-Bacon, C., Murphy, D.C., and Roots, C.F., 2006b. Paleozoic tectonic and metallogenic evolution of pericratonic terranes in Yukon, northern British Columbia and eastern Alaska. In: Colpron, M., and Nelson, J.L., (Eds.), Paleozoic Evolution and Metallogeny of Pericratonic Terranes at the Ancient Pacific Margin of North America, Canadian and Alaskan Cordillera. Geological Association of Canada, Special Paper 45, pp. 323-360.
- Nelson, J.L., Kyba, J., McKeown, M. and Angen, J. 2008. Terrace regional mapping project, Year 3: Contributions to stratigraphic, structural and exploration concepts, Zymoetz River to Kitimat River, east-central British Columbia. In: Geological Fieldwork 2007, British Columbia Ministry of Energy and Mines, British Columbia Geological Survey Paper 2008-1, pp.159-174.
- Nelson, J.L., Colpron, M. and Israel, S., 2013. The Cordillera of British Columbia, Yukon and Alaska: Tectonics and metallogeny. In: Colpron, M., Bissig, T., Rusk, B.G. and Thompson, J.F., (Eds.), Tectonics, Metallogeny and Discovery: The North American Cordillera and Similar Accretionary Settings. Society of Economic Geologists Special Publication, 17, Chapter 3, pp. 53-103.
- Pecha, M.E., Gehrels, G.E., McClelland, W.C., Giesler, M., White, C. and Yokelson, I. 2016. Detrital zircon geochronology and Hf isotopic geochemistry of the Yukon-Tanana terrane, Coast Mountains, southeast Alaska. *Geosphere*, 12, 1556-1574. DOI: 10.1130/GES01303.1.
- Piercey, S.J., Nelson, J.L., Colpron, M., Dusel-Bacon, C. Murphy, D.C., Simard, R-L, and Roots, C.F., 2006. Paleozoic magmatic, tectonic, and crustal recycling history of the ancient Pacific margin of North America: Geochemical constraints from the Yukon-Tanana terrane in British Columbia, Yukon, and Alaska. In: Colpron, M., Nelson, J.L. and Thompson, R.I., (Eds.), Paleozoic evolution and metallogeny of pericratonic terranes at the ancient Pacific margin of North America, Canadian and Alaskan Cordillera, Geological Association of Canada Special Paper 45, pp. 281-322.
- Rees, C., Riedell, K.B., Proffett, J., Macpherson, J. and Robertson, S. 2015. The Red Chris porphyry copper-gold deposit, northern British Columbia, Canada: Igneous phases, alteration and controls of mineralization. *Economic Geology*, 110, 857-888.
- Rusmore, M.E., Gehrels, G.E. and Woodsworth, G.J. 2001. Southern continuation of the Coast shear zone and Paleocene strain partitioning in British Columbia – southeast Alaska. *Geological Society of America Bulletin*, 113, 961-975.
- Rusmore, M.E., Woodsworth, G.J. and Gehrels, G.E. 2005. Two-stage exhumation of midcrustal arc rocks, Coast Mountains, British Columbia. *Tectonics*, 24, TC5013, 25 p.
- Samson, S.D., McClelland, W.C., Patchett, P.J., Gehrels, G. and Anderson, R.G. 1989. Evidence from neodymium isotopes for mantle contributions to Phanerozoic crustal genesis in the Canadian Cordillera. *Nature*, 337, 705-709.
- Smith, D.J. 2014. Clinopyroxene precursors to amphibole sponge in arc crust. *Nature Communications* 5:4329. DOI: 10.1038/ncomms5329. 6 p.
- Sun, S.S. and McDonough, W.F. 1989. Chemical and isotopic systematics of oceanic basalts: implications for mantle composition and processes. In: A.D. Saunders and M.J. Norry, (Eds.), *Magmatism in Ocean Basins*, Geological Society of London Special Publication 42, pp. 313-345.

# Late Early to Middle Jurassic Hazelton Group volcanism and mineral occurrences in the McBride-Tanzilla area, northwest British Columbia



Bram I. van Straaten<sup>1, a</sup>, and Rohanna Gibson<sup>1</sup>

<sup>1</sup>British Columbia Geological Survey, Ministry of Energy and Mines, Victoria, BC, V8W 9N3

<sup>a</sup>corresponding author: Bram.vanStraaten@gov.bc.ca

Recommended citation: van Straaten, B.I., and Gibson, R., 2017. Late Early to Middle Jurassic Hazelton Group volcanism and mineral occurrences in the McBride-Tanzilla area, northwest British Columbia. In: Geological Fieldwork 2016, British Columbia Ministry of Energy and Mines, British Columbia Geological Survey Paper 2017-1, pp. 83-115.

## Abstract

A previously poorly understood volcanic succession (Horn Mountain Formation) on the northeastern margin of Stikinia hosts several early-stage porphyry copper exploration projects. Stratigraphic and structural data based on 1:20,000-scale mapping, and preliminary geochronology indicate that the oldest units in the McBride-Tanzilla area are mafic volcanic rocks of the Stuhini Group (Triassic) that are cut by the Cake Hill pluton (Late Triassic). Separated by a regional unconformity, these units are overlain by the Spatsizi Formation (Hazelton Group, late Pliensbachian to Toarcian), a sedimentary succession up to 1 km thick. The unconformity provides one of the few well-documented examples of unroofed Stuhini arc in northern Stikinia. The Spatsizi Formation grades laterally and vertically to a volcanic succession (about 4.5 km thick), recently defined as the Horn Mountain Formation (late Early to Middle Jurassic) in the upper part of the Hazelton Group. This succession is unusual because it postdates typical Late Triassic to Early Jurassic arc volcanism in northern Stikinia, and is concurrent with accretion of the Stikine and Cache Creek terranes. Units in the lower part of the Horn Mountain Formation include massive green augite-plagioclase-phyric volcanic breccia and rare grey coarse platy plagioclase-phyric lapilli tuff and pillows that were, at least in part, deposited in a subaqueous environment. Overlying units of interlayered maroon augite-plagioclase-phyric flows, volcanic breccia and tuff suggest increasingly greater volumes of volcanism and the formation of a subaerial volcanic edifice. During a hiatus in volcanism, these rocks were cut and hydrothermally altered by a 173 Ma (Aalenian) porphyry. An unconformity separates these units from Bajocian mafic volcanic flows in the upper part of the Horn Mountain Formation. The Horn Mountain Formation is cut by the Three Sisters pluton (ca. 173-169 Ma, Aalenian-Bajocian), and is unconformably overlain by sedimentary rocks of the Bowser Lake Group (Bajocian). In the northern part of the map area, folded Takwahoni Formation siliciclastic rocks deposited in the Whitehorse trough (Laberge Group, Pliensbachian) are in the hanging wall of the south-verging Kehlechoa thrust fault, and structurally overlie the Horn Mountain volcanic succession. Regionally, these sedimentary rocks record unroofing of the Stuhini arc. The Snowdrift Creek pluton (Late Jurassic) cuts the Kehlechoa fault and constrains movement on the foreland thrust of the Stikinia-Quesnellia accretionary welt to ca. 170-160 Ma.

At least three magmatic-hydrothermal events are recognized in the map area. Late Triassic porphyry-style copper mineralization occurs at the Gnat Pass developed prospect and nearby Moss showing. The Horn Mountain Formation hosts aerielly extensive gossans at Tanzilla and McBride (both early-stage porphyry projects) interpreted as Middle Jurassic in age. Molybdenum mineralization is locally in the Snowdrift Creek pluton (Late Jurassic) and its immediate wall rocks, and in a satellite stock to the south. At Tanzilla, an advanced argillic lithocap overlies porphyry-style alteration at depth. Quartz-sericite-pyrite to potassic alteration with anomalous copper and molybdenum is hosted by a syn-mineral 173 Ma plagioclase porphyry. Our mapping extends the advanced argillic alteration at Tanzilla for at least 17 km along strike. It is interpreted as a lithocap formed by acidic hydrothermal fluid flow along an unconformity or fault in the upper Horn Mountain Formation. At the McBride showing, widespread quartz-sericite-pyrite and local potassic alteration hosts elevated copper and gold.

The Horn Mountain Formation and Three Sisters plutonic suite are coeval with accretion of the Stikine and Quesnel island arcs. The syncollisional Middle Jurassic magmatic event represents a potential new metallogenic epoch for the Canadian Cordillera and is prospective for porphyry- and epithermal-style mineralization.

**Keywords:** Horn Mountain Formation, Spatsizi Formation, Hazelton Group, Stuhini Group, Cake Hill pluton, Three Sisters pluton, Snowdrift Creek pluton, Takwahoni Formation, Kehlechoa fault, Jurassic, McBride, Tanzilla, lithocap, advanced argillic alteration, Stikine terrane

## 1. Introduction

This paper describes a volcano-sedimentary succession southeast of Dease Lake (northern Stikinia; Fig. 1) that hosts the McBride and Tanzilla porphyry copper mineral occurrences. Previously, this succession was poorly

understood. In published maps, part of it was assigned to the Takwahoni Formation (Lower Jurassic), part to the Stuhini Group (Triassic), and part to a unit of Triassic-Jurassic volcanic rocks that could correlate with either the Stuhini Group or the Hazelton Group (Gabrielse, 1998). Detailed mapping by van

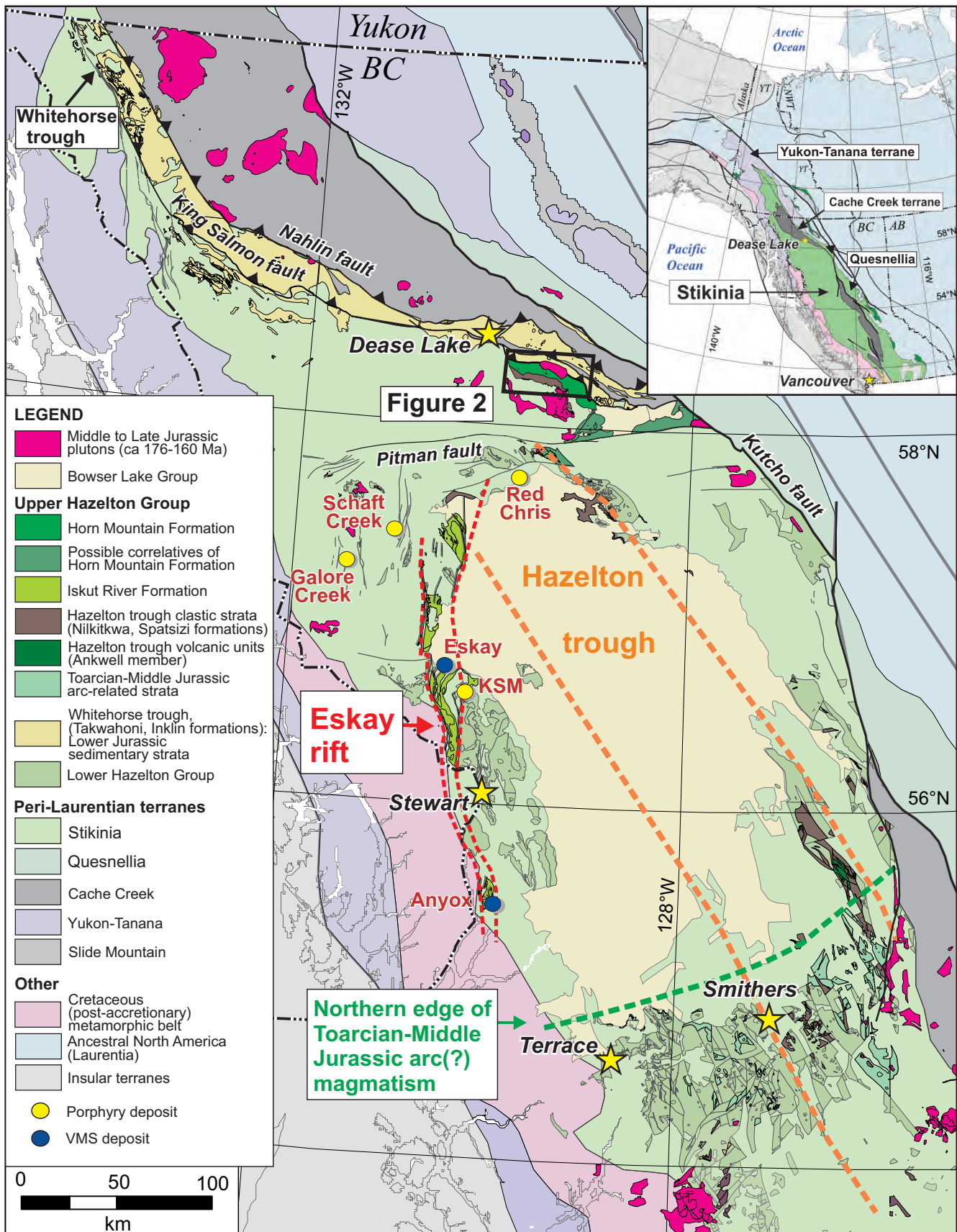


Fig. 1. Geology of northern Stikinia with emphasis on Middle to Late Jurassic geology and tectonic elements. Boundary of Hazelton trough from Marsden and Thorkelsen (1992); boundary of Eskay rift from Gagnon et al. (2012). Modified from van Straaten and Nelson (2016).

Straaten and Nelson (2016) studied a complete cross section of this enigmatic volcano-sedimentary sequence in the Tanzilla area (Fig. 1), and identified a volcanic succession (ca. 5.4 km thick) overlying a sedimentary succession (up to 1 km thick). They found the units to be late Early to Middle Jurassic, and defined the volcanic unit as the Horn Mountain Formation (part of the upper Hazelton Group). Herein we present the results of two months of 1:20,000-scale mapping carried out by two field teams between Gnat Pass and the McBride River (Fig. 2). The study was aimed at constraining the age, nature and along-strike stratigraphy of this volcano-sedimentary sequence and establishing a geological framework for alteration and mineralization.

## 2. Geological setting

The study area is in the Intermontane belt of the Canadian Cordillera, near the northeastern margin of the Stikine terrane (Stikinia; Fig. 1). Stikinia represents a volcanic island arc complex that was accreted to ancestral North America during the Middle Jurassic (Nelson and Mihalynuk, 1993; Mihalynuk et al., 1994; Evenchick et al., 2007; Nelson et al., 2013). Volcanic and sedimentary rocks of the Stikine assemblage (Devonian to Permian), basement to Stikinia, are overlain by volcanic and related sedimentary rocks of the Stuhini Group (Triassic) and the Hazelton Group (Early to Middle Jurassic; Tipper and Richards, 1976; Marsden and Thorkelson, 1992). Also in the Intermontane belt, the Quesnel terrane (Quesnellia), is a volcanic island arc with a similar Devonian to Early Jurassic history. The two volcanic arcs are separated by the Cache Creek terrane, an accretionary complex of oceanic crustal rocks, primitive arc ophiolites, pelagic rocks, and carbonate rocks (Fig. 1). The northeastern margin of Stikinia and adjacent Cache Creek terrane are covered by Early Jurassic siliciclastic rocks of the Whitehorse trough (Fig. 1; Colpron et al., 2015). Combined, Stikinia and Quesnellia host most of the porphyry copper deposits in the Canadian Cordillera (Logan and Mihalynuk, 2014).

A volcano-sedimentary succession assigned to the Spatsizi and Horn Mountain formations is in Stikinia, forming a westerly trending belt, about 50 km long and 10 km wide, north and northeast of the Hotailuh batholith (Figs. 1, 2). The succession unconformably overlies Late Triassic rocks of the Cake Hill pluton. Previous workers considered it part of the Takwahoni Formation (Lower Jurassic), structurally overlain by volcano-sedimentary rocks of the Stuhini Group (Triassic) above an inferred thrust (Hotailuh fault; Anderson, 1983; Gabrielse, 1998). However, Iverson et al. (2012) demonstrated that rocks previously mapped as part of the Stuhini Group contain an Early to Middle Jurassic detrital zircon population (ca. 176 Ma peak), leading to the interpretation that the entire volcano-sedimentary succession is part of the Hazelton Group, and removing the need for the putative Hotailuh thrust (Fig. 2). The Hazelton Group volcano-sedimentary succession is bounded to the north and northeast by the Kehlechoa thrust fault, which separates it from rocks of the Whitehorse trough (Takwahoni

Formation), and to the west by the Gnat Pass and related faults; its southeastern extent is unknown. Farther north, Cache Creek terrane rocks in the hanging wall of the King Salmon thrust (north dipping) structurally overlie the Takwahoni Formation (Figs. 1, 2).

## 3. Lithostratigraphic units

Rocks in the study area lie within two tectonostratigraphic domains. Stratigraphic units in the footwall (south) of the Kehlechoa thrust fault are part of Stikinia; those in the hanging wall (north) are part of the Whitehorse trough (Figs. 2, 3; Table 1). Classifications for sedimentary rocks (Hallsworth and Knox, 1999) and igneous rocks (Gillespie and Styles, 1999) are used throughout the following.

### 3.1. Stikinia

#### 3.1.1. Stuhini Group (Triassic)

Mafic volcanic rocks of the Stuhini Group are exposed in the southwest corner of the map area. They comprise flows, massive volcanic breccia and lapilli tuff (Figs. 2, 4; Table 1). The rocks are commonly chlorite-epidote altered, a feature that may distinguish them from the generally weakly altered Horn Mountain volcanic rocks. Crosscutting relationships with the Gnat Pass plagioclase±quartz porphyry ( $216.5 \pm 1.4$  Ma, U-Pb zircon, van Straaten et al., 2012) confirms they are Triassic rather than Jurassic. The succession likely represents Late Triassic arc construction.

An atypical unit of clast-supported polymictic volcanic breccia with sea green-grey amygdaloidal aphanitic, lesser green plagioclase-augite-phyric and maroon aphanitic clasts outcrops northeast to east of the Bell showing. It extends for at least 800 metres in a northwest to southeast direction.

At the western edge of the map area, a volcanic breccia and lapilli tuff unit (TrSTvm? in Fig. 2) contains clasts with 10-30% fresh euhedral augite (1-4 mm) and 10-40% lath-shaped plagioclase (0.5-1 mm). The volcanic rocks appear to overlie a NNE-dipping volcanoclastic sandstone and siltstone unit (TrSTs? in Fig. 2). Farther south, these sedimentary rocks are cut by a clinopyroxene-rich diorite to gabbro (Triassic to Jurassic; Section 4.1.). Limited field observations and a lack of ages prevent us from confidently assigning this succession. Following mapping by Logan et al. (2012a; b) to the west, we tentatively assign these rock units to the Stuhini Group rather than the Hazelton Group. We interpret that a NNW-trending fault separates these rocks from the Horn Mountain and Spatsizi formations (Fig. 2; Section 5.3.).

#### 3.1.2. Hazelton Group (Lower to Middle Jurassic)

Volcano-sedimentary rocks of the upper part of the Hazelton Group are exposed in the central part of the map area, forming an east-trending, north-dipping belt about 10 km wide (Fig. 2). The belt contains a lower sedimentary sequence (Spatsizi Formation) and an upper volcanic sequence (Horn Mountain Formation; Fig. 3). In the southwestern part of the map area, the Hazelton Group is inferred to unconformably overlie the





Fig. 2. Continued.

**Table 1.** Summary of volcano-sedimentary units. Mineral abbreviations after Kretz (1983).

Age	Unit	Description	Position
Miocene-Pleistocene	Tuya Formation	<b>Olivine basalt (MPTvm; Gabrielse, 1998)</b>	Overlap
Lower Jurassic	Laberge Group	<b>Siltstone (JTs).</b> Dark grey to black parallel laminated to massive siltstone unit. Interbedded with 5-25%, 5-40 cm thick, fine- to medium-grained feldspathic arenite and rare feldspathic wacke beds containing 5-10% Qtz and 10% lithic grains. Recessive, crumbly to platy, brownish grey weathering. <b>Greywacke (JTW).</b> Interbedded sandstone and siltstone. Fine- to medium-grained (rare coarse-grained) feldspathic arenite to feldspathic wacke in 10-400 cm-thick internally massive, lesser fining upward and rare parallel-laminated beds. Sandstone contains 5-15% Qtz and 10-15% lithic grains. Rare calcareous feldspathic arenite. Interbedded with 0-25%, recessive, dark grey to black, laminated, non-calcareous siltstone. Fairly resistant, grey to orange weathering, well-stratified. Contains (early) Pliensbachian macrofossils (Gabrielse, 1998).	Whitehorse trough
	Bowler Lake Group	<b>Sandstone and conglomerate (mJBLs)<sup>1</sup>.</b> Interbedded calcareous (locally fossiliferous) sandstone, cross-bedded sandstone, and polymictic conglomerate containing mafic volcanic, Pl-phyric, hypabyssal, and pyritic clasts. Moderately resistant, brownish weathering. Contains a probable Toarcian ammonite (T. Poulton, pers. comm., 2015); Middle Jurassic detrital zircon population.	
Middle Jurassic		<b>Upper mafic volcanic rocks (mJHMUvm); &gt;650 m thick.</b> Predominantly Aug-Pl-phyric coherent rocks (15-20%, 2-3 mm Aug; 40%, 1-3 mm equant Pl; locally amygdaloidal) interpreted as flows. Minor volcanic breccia, medium to very thickly bedded lapilli tuff, lapillistone and tuff. Fragmental volcanic rocks contain cm-sized angular Aug-Pl-phyric clasts in an Aug and Pl crystal-rich matrix. Very rare volcanic breccia with minor felsic, Pl-phyric and grey siliceous clasts <sup>1</sup> . Very rare flows, volcanic breccia and tuff with coarse platy Pl crystals. Resistant, dark grey weathering. Middle Jurassic detrital zircon population.	
		<b>Upper felsic volcanic rocks (mJHMUvf)<sup>1</sup>; 235 m thick.</b> Relatively well-stratified crystal tuff, fine tuff, and pyroclastic breccia of sparsely Pl-phyric clasts in a grey glassy groundmass, medium-dark grey aphanitic to glassy clasts and lesser (Aug-Hbl-)Pl-phyric clasts. Common bomb sags. Includes rare pebble conglomerate with well-rounded clasts, and calcareous sandstone (locally fossiliferous).	
Early-Middle Jurassic	Upper part of Hazelton Group	<b>Middle maroon volcanic rocks (lmJHMVp); ≤3000 m thick.</b> Interlayered flows, volcanic breccia, tuff and lapilli-tuff; upper volcanoclastic subunit. Aug-Pl-phyric flows (maroon, medium grey, rarely green) transition to monomictic autoclastic breccia. Rare glassy felsic (?) flows (blood-red to maroon) <sup>1</sup> . Massive maroon volcanic breccia with angular-subangular varicoloured 0.2-100 cm Aug-Pl-phyric clasts, common maroon aphyric clasts and very rare platy Pl-phyric clasts. Reddish-maroon laminated to medium-bedded tuff, crystal tuff, lapillistone, and rare welded lapilli tuff with sub-cm fiamme and lithic fragments. Upper subunit of laminated to thinly bedded maroon volcanoclastic sandstone and tuff. Resistant to moderately resistant, dark grey to maroon weathering, moderately to crudely stratified.	Stikinia
	Horn Mountain Formation	<b>Lower mafic volcanic rocks (lmJHMLvm); 850-1500 m thick.</b> Massive monomictic volcanic breccia and lapilli tuff; predominantly clast-supported. Subangular, Aug-Pl-phyric, 1-10 cm (locally up to 100 cm) clasts in a sand- to granule-sized Aug and Pl crystal matrix. Rare volcanoclastic sandstone, Aug-Pl crystal tuff and tuff interbeds. Very resistant, dark grey to green and hackly weathering. <b>Lower mafic volcanic rocks with felsic clasts (lmJHMLvm,fc)<sup>1</sup>; 0-75 m thick.</b> Similar to lower mafic volcanic rocks, but contains flow-banded Pl-phyric clasts, epidote-altered clasts, and fine-grained to aphyric off-white felsic clasts. <b>Lower mafic volcanic rocks with epidote-altered clasts (lmJHMLvm,ep)<sup>1</sup>; 0-220 m thick.</b> Massive volcanic breccia with epidote-altered clasts, Aug diorite clasts (15-20%, 2-3 mm Aug; 80-85%, 0.5-1 mm Pl) and moderately crystalline Aug-Pl-phyric clasts (15%, 2-3 mm Aug; 20-40%, 0.5-1 mm Pl). Resistant, dark green to green weathering. <b>Lower volcanoclastic sandstone (lmJHMLvs); 0 to &gt;150 m thick.</b> Laminated to thickly bedded volcanoclastic sandstone with abundant Pl grains, lesser siltstone. Minor lapilli tuff and Aug-Pl crystal tuff. Recessive, brown weathering.	

Table 1. Continued.

Age	Unit	Description	Position
Lower-Middle Jurassic	Upper part of Hazelton Group	<p><b>Lowermost platy plagioclase-phyric volcanic rocks (lmJHMLMvpo); 0-350 m thick.</b> Coarse platy Pl-rich lapilli tuff, lesser lapillistone, tuff breccia and volcanic breccia. Local 0.5-2 m circular to elongate pillows with a light coloured centre, dark rim and inter-pillow laminated tuff, volcanoclastic sandstone and calcareous sandstone. Medium grey to creamy-grey volcanic clasts and pillows contain 20-35% platy Pl (0.5-2 cm), 0-5% Aug (0.5-1 mm) and common vesicles. Very resistant, dark grey weathering, moderately to crudely stratified.</p> <p><b>Felsic volcanic rocks (lmJHMLMvf); 0-70 m thick.</b> Clast-supported volcanic breccia. Clasts are angular to subangular, 0.5-30 cm, commonly vesicular, aphyric to Pl-phyric and sea green to light grey to creamy-purple. Some flow banded clasts. Moderately resistant, medium grey weathering.</p>	Stikinia
		<p><b>Lowermost mafic volcanic rocks (lmJHMLMvm); 0-1000 m thick.</b> Clast-supported volcanic breccia with subangular Aug-Pl-phyric 1-100 cm clasts. Clasts vary in colour (light green, medium green, dark green, maroonish grey, maroon), Pl abundance (15-65%, 0.5-2 mm, lath to equant), Aug abundance (5-30%, 1-4 mm, equant) and amygdules (0-25%). Very thick (~70 m) internally massive beds of volcanic breccia are locally separated by well-stratified, rusty brown, recessive siltstone and sandstone. Breccia at the base of the unit and base of the second very thick bed contains subrounded to subangular 0.5-30 cm (locally 2-4 m) clasts of Hbl Qtz monzodiorite, Hbl Qtz monzonite and Hbl monzogranite. Resistant, dark grey and hackly weathering.</p> <p><b>Volcanoclastic sandstone (lmJSPsv); 0-300 m thick.</b> Fine- to coarse-grained volcanoclastic sandstone interbedded with lesser siltstone. Common interlayers of monomictic volcanic breccia with Aug-Pl-phyric clasts. Subordinate light grey fine tuff laminae. Local granule conglomerate with angular pale grey fine tuff rip-up clasts (up to 3 cm) in a matrix of angular to euhedral Pl and Aug crystals. Common soft-sediment deformation structures. Common parallel laminae and local normal grading. Moderately resistant, medium-dark brown weathering and well-stratified.</p> <p><b>Argillite, siltstone and sandstone (lmJSPs); 0-560 m thick.</b> Interbedded argillite, siltstone and fine-grained sandstone. Rare to locally common medium- to coarse-grained sandstone, granule conglomerate and clast-supported volcanic breccia. Conglomerate and breccia are mono- to polymictic and contain Aug-Pl-phyric, Pl-phyric, coarse platy Pl-phyric, aphyric and local siltstone clasts. Minor grey tuff laminae; rare volcanoclastic sandstone. Generally recessive, rusty orange-brown weathering, well-stratified. Contains late Pliensbachian to Toarcian ammonites and bivalves (T. Poulton, pers. comm., 2016); Early to Middle Jurassic detrital zircon population (Iverson et al., 2012).</p> <p><b>Platy plagioclase-phyric volcanic rocks (lmJSPvpo)<sup>1</sup>; 0-75 m thick.</b> Monomictic clast-supported volcanic breccia with medium grey coarse platy Pl-phyric and pale grey aphyric, common vesicular clasts. Resistant, medium grey weathering.</p> <p><b>Mafic volcanic rocks (lmJSPvm); 0-60 m thick.</b> Polymictic clast-supported volcanic breccia with Aug-Pl-phyric and aphyric clasts. Resistant, dark grey-green weathering.</p>	
Triassic	Stuhini Group	<p><b>Basal sandstone and conglomerate (lmJSPcg); 0-140 m thick.</b> Qtz-rich feldspathic arenite and clast-supported conglomerate containing Hbl Qtz monzonite to Hbl Qtz monzodiorite (and locally Hbl monzogranite) clasts similar to subjacent Cake Hill pluton. Local Aug-Pl-phyric, Aug-phyric, Pl-phyric and aphyric volcanic clasts set in a matrix of medium sand to grit-sized Fsp and Qtz grains. Rare fossiliferous calcareous sandstone and siltstone. Subfeldspathic arenite (likely grus) unconformably overlies the Cake Hill pluton. Recessive, orange-brown weathering. Contains early Toarcian fossils (Henderson and Perry, 1981); Late Triassic detrital zircon population.</p>	
		<p><b>Mafic volcanic rocks (TrSTvm).</b> Volcanic breccia and lapilli tuff with (Pl-)Aug-phyric clasts. (Pl-)Aug-phyric flows. Minor (Aug-)Pl-phyric coherent rocks may represent flows.</p> <p><b>Sedimentary rocks (TrSTs).</b> Sandstone, volcanoclastic sandstone and argillite (Gabrielse, 1998; van Straaten et al., 2012).</p>	

Note: <sup>1</sup> van Straaten and Nelson (2016)

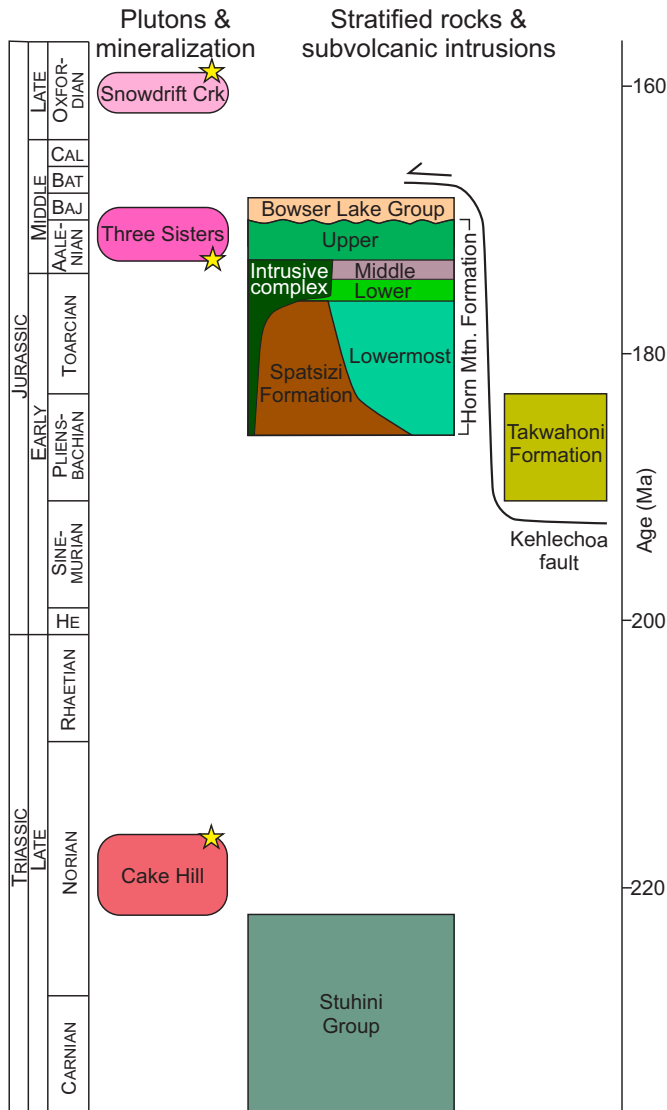


**Fig. 3.** Schematic stratigraphic, plutonic and structural relationships for Triassic to Jurassic rocks in the map area. Main mineralization events indicated by yellow star. Jurassic stage abbreviations: Hettangian (He), Bajocian (Baj), Bathonian (Bat), Callovian (Cal). Chronostratigraphic ages from International Commission on Stratigraphy, version December 2016 (Cohen et al., 2013).

Stuhini Group (Triassic), in the remainder of the field area it rests unconformably on the Cake Hill pluton (Late Triassic). The Spatsizi Formation is up to 1 km thick in the southwestern part of the map area. It thins and pinches out to the southeast, where the Horn Mountain Formation rests unconformably on the Cake Hill pluton. Farther southeast, the stratigraphic level occupied by the unconformity, Spatsizi Formation and lower Horn Mountain Formation is cut by the Three Sisters pluton (Middle Jurassic).

**3.1.2.1. Spatsizi Formation**

A succession of predominantly sedimentary rocks (up to 1 km thick) is exposed in the central and western parts of the map area (Fig. 2). We correlate this sequence with the Spatsizi



**Fig. 4.** Stuhini Group mafic volcanic unit (TrSTvm). Volcanic breccia with augite-plagioclase-phyric clasts.

Formation, as defined by Thomson et al. (1986) and modified by Evenchick and Thorkelson (2005) and Gagnon et al. (2012). It unconformably overlies the Cake Hill pluton (Late Triassic) in most of the map area, except in the far west where it is inferred to rest unconformably on the Stuhini Group (Triassic). It is conformably overlain by volcanic rocks of the Horn Mountain Formation. We recognize three main Spatsizi Formation units in the study area (Table 1).

In the basal unit, subfeldspathic arenite, clast-supported conglomerate, and quartz-rich feldspathic arenite unconformably overlie the Cake Hill pluton (Table 1). The unit contains abundant hornblende quartz monzonite to quartz monzodiorite clasts similar to the subjacent Cake Hill pluton; locally, volcanic clasts are common. South of Glacial Mountain, the Spatsizi Formation is generally absent between the Cake Hill pluton and Horn Mountain Formation, except for a 800 by 250 m zone of monomictic conglomerate to breccia interbedded with rare siltstone and sandstone (Figs. 2, 5). The conglomerate contains abundant hornblende monzogranite clasts similar in composition and texture to the pluton exposed directly to the south and east (Fig. 2; Section 4.1.). It likely represents the fill of a paleodepression cut into the Cake Hill pluton.

The basal unit fines upward to a unit of argillite, siltstone, and fine-grained sandstone (Fig. 6) with rare to locally common medium- to coarse-grained sandstone, granule conglomerate, and clast-supported volcanic breccia. This middle unit contains two volcanic subunits, coarse platy plagioclase-phyric volcanic breccia northeast of the Tanzilla River (van Straaten and Nelson, 2016), and mafic volcanic breccia southwest of the Tanzilla River, south of Horn Mountain and south of Glacial Mountain.

At the top of the Spatsizi Formation in the centre of the map area, a volcaniclastic unit consists mainly of fine- to coarse-grained volcaniclastic sandstone (Fig. 7) with lesser siltstone and fine tuff laminae. Rare augite-plagioclase-phyric coherent rocks are interpreted as sills. This unit gradationally overlies



**Fig. 5.** Spatsizi Formation basal sandstone and conglomerate unit (lmJSPcg). Conglomerate with sandstone interbeds; granitic clasts in conglomerate have a similar composition to the immediately underlying Cake Hill pluton.



**Fig. 6.** Spatsizi Formation argillite, siltstone, and sandstone unit (lmJSPs). Interbedded siltstone and fine- to medium-grained sandstone displaying syn-sedimentary deformation.

siliciclastic rocks of the middle unit (van Straaten and Nelson, 2016).

New geochronological data and fossil collections confirm the age and provenance of the Spatsizi Formation in the study area. A detrital zircon sample from the basal sandstone and conglomerate unit yielded a Late Triassic zircon population (Section 7.1.), complementing the results of Iverson et al., (2012) who reported Late Triassic and Early-Middle Jurassic zircon populations from the middle argillite, siltstone and sandstone unit. A tan to grey weathering, fine-grained calcareous sandstone at the base of this middle unit (Fig. 8) contains common bivalves and rare ammonites. Based on preliminary study, T. Poulton (pers. comm., 2016) suggests that ammonites may be as old as late Pliensbachian (*Protogrammoceras*) or as young as late Toarcian (*Pseudogrammoceras*) and that bivalves (*Bositra buchi*) are also late Pliensbachian to Toarcian. Henderson and Perry (1981) reported early Toarcian



**Fig. 7.** Spatsizi Formation volcanoclastic sandstone unit (lmJSPsv). Bedded volcanoclastic sandstone.

fossils from the basal unit in the western part of the map area, including bryozoa faunas interpreted to record shallow-marine conditions. Fossils from the same unit in the central part were interpreted as late Toarcian (Anderson, 1983) or, more recently, as early to middle Toarcian (Gabrielse, 1998).

The base of the Spatsizi Formation marks the change from Stuhini arc uplift and erosion to subsidence and sedimentation. The basal unconformity represents one of the few well-documented examples of unroofed Stuhini arc in northern Stikinia. It spans at least 30 m.y., and includes the latest Triassic and Early Jurassic porphyry copper metallogenic epochs farther south (e.g., Galore Creek, Red Chris, KSM; Fig. 1). The overall fining upward of the Spatsizi Formation, from basal conglomerate and sandstone to thick sections of argillite and siltstone suggests basin deepening. Regionally, the Spatsizi Formation is correlated with the predominantly siliciclastic Nilkitkwa Formation east and northeast of Smithers. The north-northwest trend of the Spatsizi and Nilkitkwa formations records Pliensbachian to Toarcian marine sedimentation in a back-arc or intra-arc depression (Hazelton trough; Fig. 1; Tipper and Richards, 1976; Marsden and Thorkelson, 1992; Gagnon et al., 2012).

### 3.1.2.2. Horn Mountain Formation

The Horn Mountain Formation, defined by van Straaten and Nelson (2016), is a volcanic succession (approximately 5.4 km thick) exposed between Gnat Pass and the McBride River (Figs. 2, 3; Table 1). Along its 50 km strike length, this succession displays relatively consistent stratigraphy and lithological

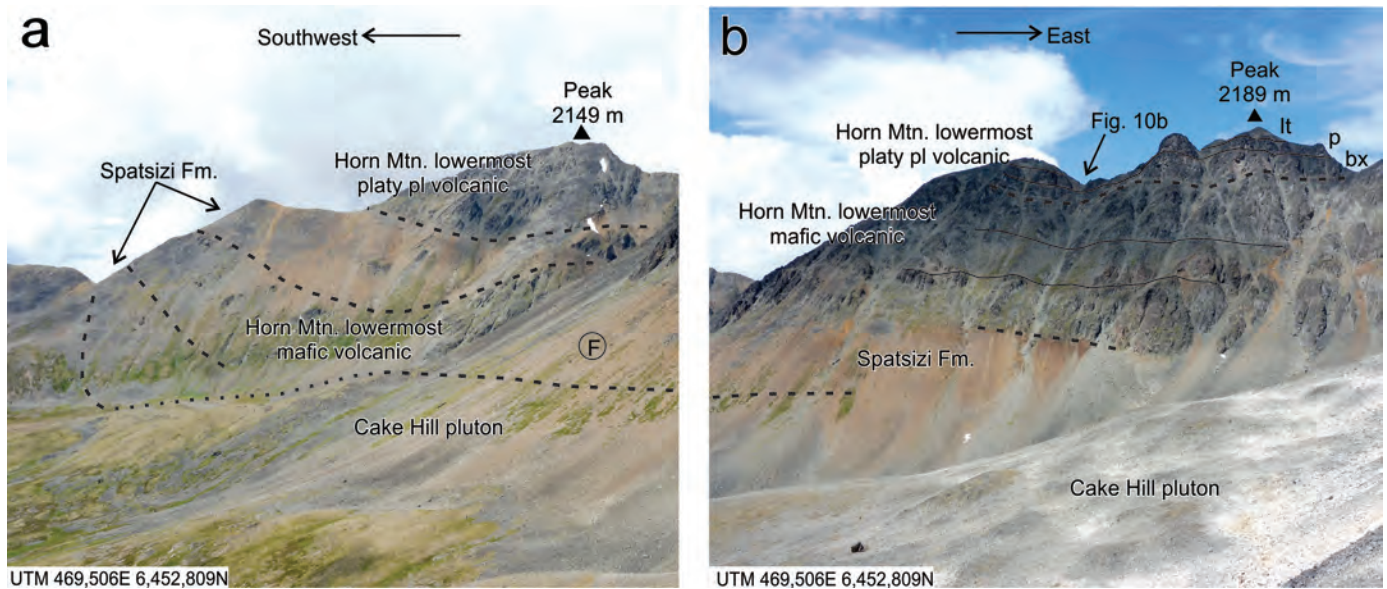


**Fig. 8.** Outcrop character and interfingering relationships between the Spatsizi and Horn Mountain formations. In far left background (a) and foreground (a, b) is Cake Hill quartz monzodiorite (LrCHqm). **a)** In left background are recessive, orange-brown weathering, well-bedded Spatsizi Formation sedimentary rocks (lmJSPcg, lmJSPs) overlain by resistant, cliff-forming, crudely bedded grey coarse platy plagioclase-phyric volcanic rocks (lmJHMLMv.po) on the right. Within the Spatsizi Formation sedimentary rocks is a tongue of moderately resistant, dark grey mafic volcanic rocks of the Horn Mountain Formation (lmJHMLMvm). **b)** Continuation of a), to the east. On the left, recessive, orange-brown weathering, well-bedded Spatsizi Formation argillite, siltstone, and sandstone unit (lmJSPs) overlain by Horn Mountain Formation. Thick dashed lines represent contacts between units, thin solid lines represent lithologic contacts within units. Three very thick beds are identified in the lowermost mafic volcanic rock unit (lmJHMLMvm); the first and second bed are separated by a several m-thick recessive orange-brown weathering siltstone and sandstone bed. Three very thick beds are identified within the platy plagioclase-phyric volcanic unit (lmJHMLMv.po); they comprise a basal tuff breccia (bx), middle pillow (p) and upper lapilli tuff (lt) bed. F = fossil sample location (late Pliensbachian-Toarcian).

characteristics. In this study we significantly expand the known extent of this unit. Originally subdivided into four informal subdivisions (van Straaten and Nelson, 2016), herein we describe an additional two subdivisions exposed at the base of the formation in the east-central part of the map area.

**The lowermost mafic volcanic unit** contains augite-plagioclase-phyric volcanic breccia (Fig. 9a). The unit is only present in the east-centre of the map area. In the east the unit is up to 1 km thick and unconformably overlies the Cake Hill pluton. Immediately southwest of Peak 2189 m it is 310 m thick and conformably overlies a 150 m-thick Spatsizi Formation section (Fig. 8b). In both cases the unit is overlain by the lowermost platy plagioclase-phyric volcanic unit (see below). Two kilometres west of Peak 2189 m the lowermost mafic volcanic unit thins to 65 m, where it forms an apparently conformable tongue within the Spatsizi Formation argillite, siltstone and sandstone unit (Fig. 8a). South of Peak 2189 m very thick (~70 m) internally massive beds of mafic volcanic breccia are locally separated by well-stratified, rusty brown, recessive siltstone and sandstone (Fig. 8b). Here, breccias at the base of the unit and the base of the second very thick bed contain subrounded to subangular 0.5-30 cm clasts of hornblende quartz monzodiorite to quartz monzonite. The clasts have a similar texture and composition as the Cake Hill pluton exposed to the south. One of these plutonic clasts yielded a K-Ar hornblende age of  $227 \pm 14$  Ma (Anderson, 1983),

within error of ages for the Cake Hill pluton (Table 2). South of Glacial Mountain, the base of the unit contains common hornblende monzogranite clasts, similar to the subjacent hornblende monzogranite intrusion (Figs. 2, 9b; Section 4.1.). A bed of lapilli tuff with aphyric felsic clasts and a bed of pale greenish-grey felsic fine tuff were sampled for U-Pb zircon geochronology (Section 7.1.). The lowermost volcanic units appear to represent relatively low volume volcanic eruptions with rapid lateral facies transitions. The interfingering fine-grained sedimentary rocks indicate that at least some of the volcanic rocks were deposited in a subaqueous setting.

**The lowermost platy plagioclase-phyric volcanic unit**, the second additional unit we recognize (Table 1), forms a distinct 200 to 350 m-thick marker above the lowermost mafic volcanic unit in the centre of the map area (Fig. 8). It consists of medium- to very thickly bedded lapilli tuff, lesser lapillistone, tuff breccia and volcanic breccia (Fig. 10a). On the high ridges of Peak 2189 m, tuff breccia beds are overlain by a 35 m-thick bed of pillows, in turn overlain by lapilli tuff (Figs. 8b, 10b). Volcanic clasts and pillows contain coarse platy plagioclase, amygdules, and local rare augite. A felsic volcanic breccia subunit is exposed at two locations, west and northwest of Peak 2189 m; it contains light-coloured aphyric, plagioclase-phyric and rare flow banded clasts (Table 1). Immediately southwest of Peak 2189 m, the unit directly overlies augite-plagioclase-phyric volcanic breccia of the lowermost mafic volcanic unit



**Fig. 9.** Horn Mountain Formation, lowermost mafic volcanic unit (ImJHMLMvm). **a)** Massive, clast-supported volcanic breccia with augite-plagioclase-phyric clasts. **b)** Granitic and volcanic clasts at base of unit. Granitic clasts have a similar composition to the immediately underlying Cake Hill pluton.

with a sharp but conformable contact (Fig. 8b). Eight hundred and fifty metres west of Peak 2189 m, it conformably overlies 5 m of rusty weathered siltstone and fine-grained sandstone above the lowermost mafic volcanic unit. About 1.5 km west of Peak 2189 m, the unit conformably overlies a 250 m-thick section of Spatsizi Formation granule to pebble conglomerate, sandstone, argillite and clast-supported volcanic breccia above the lowermost mafic volcanic unit (Fig. 8a). North of Peak

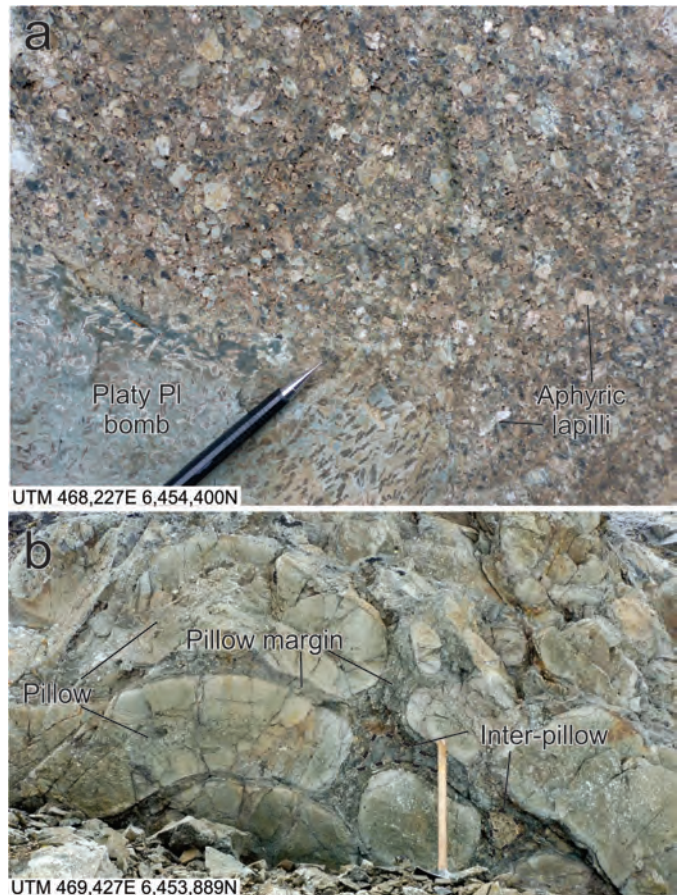


**Fig. 10.** Horn Mountain Formation, lowermost platy plagioclase-phyric volcanic unit (ImJHMLMv.po). **a)** Massive, clast-supported lapilli tuff with angular aphyric to plagioclase-phyric lapilli and platy plagioclase-phyric bomb. **b)** Elongate to circular pillows (in 2D) of coarse platy plagioclase-phyric mafic flow.

2189 m, wavy laminated Spatsizi Formation volcanoclastic siltstones directly overlie the platy plagioclase-phyric volcanic unit with a sharp but conformable contact. In the east, the platy plagioclase-phyric volcanic unit is overlain by the lower mafic volcanic unit (see below). Conformable contacts and interfingering between the platy plagioclase-phyric volcanic unit and Spatsizi Formation sedimentary rocks indicate that the two units are coeval. The platy plagioclase-phyric volcanic subunit in the Spatsizi Formation (Table 1) is likely a lateral facies equivalent of the Horn Mountain lowermost platy plagioclase-phyric volcanic unit.

The pillows at Peak 2189 m suggest subaqueous deposition and the overlying very thick lapilli tuff beds indicate volcanic eruptions with a high fragmentation intensity. A lack of change in litho-geochemistry (B. van Straaten et al., unpublished data), mineralogy, crystal content or vesicularity suggests the shift from effusive to explosive volcanism is unlikely to have resulted from a change in magma composition. The lapilli tuff may have formed by phreatomagmatic eruptions.

**The lower mafic volcanic unit** (Table 1) is 850-1500 m thick and consists predominantly of massive dark green monomictic

**Table 2.** Summary of intrusive units. Mineral abbreviations after Kretz (1983).

Age	Phase	Description	Timing relationships	Geochronology
Late Jurassic	Snowdrift Creek subalkaline	<b>Snowdrift Creek pluton (LJSCgd)</b> . Medium-grained (3-5 mm) equigranular Bt-bearing Hbl to Hbl-bearing Bt granodiorite. A fine-grained (1-3 mm) equigranular (Hbl-bearing) Bt Qtz diorite at the Joyce showing is interpreted as a satellite stock. Recessive to moderately resistant, medium grey weathering.	Cuts Takwahoni greywacke unit <sup>1</sup> , mafic intrusive complex and Horn Mountain upper mafic volcanic unit. At contact, metamorphosed Takwahoni greywacke unit <sup>1</sup> , mafic intrusive complex, and Horn Mtn upper mafic volcanic unit. Interpreted to cut Kehlechoa fault.	U-Pb zircon: 160.43 ±0.16 Ma
		<b>Hornblende diorite (LJdr)</b> . Hbl diorite dikes and possible sills. Contains 1-6 mm (generally acicular) Hbl and equant 1-4 mm Pl. Resistant, light grey to white weathering.	Cuts Takwahoni greywacke unit; Spatsizi argillite, siltstone & sandstone unit; Spatsizi platy Pl-phyric volcanic and volcanoclastic sandstone units <sup>1</sup> ; Horn Mtn lower mafic volcanic and middle maroon volcanic units <sup>1</sup> ; mafic intrusive complex. Follows faults.	
Middle Jurassic	Three Sisters subalkaline	<b>Potassic phase (MJTSgr)</b> . Bt-bearing Hbl monzogranite with 20% Pl phenocrysts (1-3 mm) set in a fine-grained (0.1-1 mm) sugary groundmass. Moderately resistant, pink to pink-grey weathering.	Dikes cut Horn Mtn lower mafic and middle maroon volcanic units; Three Sisters central phase. Interpreted to cut mafic intrusive complex.	U-Pb zircon: 171 ±1 Ma <sup>4</sup> 169.1 ±0.8 Ma <sup>3</sup> 168.57 ±0.54 Ma <sup>2</sup>
		<b>Central felsic phase (MJTSqm)</b> . Medium-grained (2-4 mm) equigranular (Bt-bearing) Hbl Qtz monzodiorite, rare granodiorite. Local microdiorite xenoliths. Resistant, medium grey to pink-grey weathering.	Apophyses cut Three Sisters mafic phase. Interpreted to cut Cake Hill pluton and Horn Mtn lower mafic volcanic unit.	U-Pb zircon: 177.13 ±0.59 Ma <sup>2</sup> 172.75 ±0.87 Ma <sup>2</sup> 169.0 ±1.3 Ma <sup>3</sup>
	<b>Mafic phase (MJTSqd)</b> . Medium-grained (2-3 mm) equigranular Hbl-Cpx to Cpx-Hbl diorite, rare Qtz diorite. Resistant, dark greenish-grey weathering.	Interpreted to cut Cake Hill pluton and Horn Mountain lowermost mafic volcanic unit.	Ar-Ar Hbl: 171.9 ±1.7 Ma <sup>3</sup>	
	<b>Augite quartz diorite (MJqd)</b> . Medium-grained equigranular Aug Qtz diorite (and diorite?) <sup>2</sup> .	Cuts Horn Mountain middle maroon volcanic and upper felsic volcanic units <sup>1</sup> ; Aug-bearing Pl porphyry <sup>1</sup> .		
Early-Middle Jurassic	Spatsizi & Horn Mountain alkaline	<b>Augite-bearing plagioclase porphyry (MJap)</b> . Aug-bearing Pl porphyry dikes and stocks with 40% tabular to equant Pl (1-4 mm), 3-5% equant Aug (<2 mm), minor Mag <sup>2</sup> .	Interpreted to cut Horn Mtn middle maroon volcanic unit, mafic intrusive complex, and Horn Mtn upper felsic volcanic unit <sup>1</sup> .	U-Pb zircon: 173.25 ±0.13 Ma <sup>1</sup>
		<b>Felsic intrusive (EMJf)</b> . Felsic dikes with common dike margin-parallel flow bands and wispy Qtz ribbons. Local m-wide tabular to 100 m-wide bulbous bodies of intrusive breccia containing angular to amoeboid Pl-phyric (20%, 1-2 mm) clasts, aphyric clasts, Aug-Pl-phyric clasts and minor flow-banded autoclasts.	Cuts Horn Mountain lower mafic volcanic unit <sup>1</sup> . Interpreted to cut mafic intrusive complex.	
		<b>Hornblende monzonite (EMJmz)</b> . Hbl to Hbl-Bt monzonite dikes, Pl-porphyrific; contains minor Mag.	Cuts mafic intrusive complex.	

Table 2. Continued.

Age	Phase	Description	Timing relationships	Geochronology
Early-Middle Jurassic	Spatsizi & Horn Mountain alkaline	<b>Platy plagioclase porphyry (EMJm-po)</b> . Pl-phyrlic dikes, sills, and stocks. Coarse Pl plates (0.5-4 cm, 5:4:1 aspect ratio) and locally rare Aug (<2 mm) set in a dark green to dark purple-grey aphanitic groundmass. Locally amygdaloidal. Rare breccia textures. Resistant, dark grey weathering.	Cuts Horn Mountain lower mafic volcanic and middle maroon volcanic units. Cuts mafic intrusive complex, locally with gradational contacts <sup>1</sup> .	
		<b>Mafic intrusive complex (EMJm)</b> . Aug-Pl-phyrlic sills, dikes and intrusive bodies. Contains 30% equant Pl (0.5-2 mm), 20% Aug (1-4 mm, locally up to 10 mm) and rare amygdules. Local Aug microdiorite. Resistant, dark grey to green weathering.	Cuts Spatsizi volcanoclastic sandstone unit, Horn Mountain lower mafic volcanic and middle maroon volcanic units.	
Triassic-		<b>Cpx-rich diorite to gabbro (TrJgb)</b> . Medium-grained (1-4 mm) equigranular Cpx-rich diorite to gabbro. Highly magnetic. Resistant, dark grey to black weathering.	Cuts sedimentary rocks assigned to Stuhini Group. Interpreted to cut Horn Mtn maroon volcanic unit.	
Late Triassic	Stikine subalkaline	<b>Gnat Pass porphyry (LTrGP)</b> . Porphyritic hypabyssal intrusive with euhedral-subhedral Pl (2 mm), rare Qtz (2-4 mm) and Hbl <sup>4</sup> .	Cuts Stuhini Group mafic volcanic unit.	U-Pb zircon: 216.5 ± 1.4 Ma <sup>3</sup>
		<b>Cake Hill quartz-rich phase (LTrCHgr)</b> . Medium-grained (3-5 mm) equigranular Hbl monzogranite, often with Qtz eyes (5-7 mm) and tabular Hbl. Correlated with the Cake Hill quartz-rich phase of van Straaten et al. (2012). Moderately resistant, greyish-white weathering.	Interpreted to be unconformably overlain by Spatsizi basal sandstone and conglomerate unit; Horn Mtn lowermost mafic volcanic unit.	U-Pb zircon: 216.2 ± 1.2 Ma <sup>3</sup>
		<b>Cake Hill pluton (LTrCHqm)</b> . Medium-grained (3-4 mm) equigranular (Bt-bearing) Hbl Qtz monzodiorite to Qtz monzonite with local granodiorite and Qtz diorite. Contains accessory Tm and Mag. Locally foliated. Resistant, pale grey weathering.	Cuts Gnat Lakes intrusive <sup>3</sup> . Unconformably overlain by Spatsizi basal conglomerate unit and Horn Mtn lowermost mafic volcanic unit. Interpreted to cut Stuhini volcanic and sedimentary units.	U-Pb zircon: 221 ± 3 Ma <sup>4</sup> , 218.2 ± 1.3 Ma <sup>3</sup>
	Stikine alkaline	<b>Gnat Lakes intrusive (LTrGLum)</b> . Medium-grained (3-4 mm) equigranular Pl-bearing hornblende to Cpx Hbl-rich gabbro. Moderately resistant, black weathering.	Interpreted to cut Stuhini volcanic and sedimentary units <sup>3</sup> .	

Note: <sup>1</sup> van Straaten and Nelson (2016); <sup>2</sup> Takaichi (2013a; b); <sup>3</sup> van Straaten et al. (2012); <sup>4</sup> Anderson and Bevier (1992)

volcanic breccia and lapilli tuff (Fig. 11). Volcaniclastic sandstone, augite-plagioclase crystal tuff, and tuff, although rarely observed, are locally common southeast of Glacial Mountain. Minor augite-plagioclase-phyric coherent rocks are interpreted as sills. The unit displays a gradational lower contact with the Spatsizi Formation in the western and central parts of the map area. Farther east, it overlies the lowermost platy plagioclase-phyric volcanic unit; both a gradational and a sharp but conformable contact were observed. The unit is texturally and compositionally similar to the lowermost mafic volcanic unit described above, but can be distinguished by its stratigraphic position, lateral extent, and lack of interbedded fine-grained siliciclastic rocks and plutonic clasts near its base. Based on gradational contacts with underlying sedimentary rocks and lateral transitions to volcaniclastic sandstones (see below), at least some of the volcanic rocks may have been deposited in a submarine setting.

The mafic volcanic rocks grade westward into a volcaniclastic sandstone subunit at Gnat Pass (Fig. 2, Table 1). Resistant volcanic breccias near Peak 2096 m transition to intervals of alternating resistant volcanic breccia and recessive volcaniclastic sandstone on its western slopes. In the Gnat Pass area, limited outcrop shows both volcanic breccia and volcaniclastic sandstone. Along Tsenaglode Creek, rocks currently considered part of the volcaniclastic subunit consist of lithic arenite and pebbly granular conglomerate interbedded with laminated siltstone. The conglomerate contains angular-subrounded dark grey very fine-grained (volcanic?) and rare grey siliceous clasts in a feldspar-rich matrix with up to 2%



**Fig. 11.** Horn Mountain Formation, lower mafic volcanic unit (1mJHMLvm). Massive, monomictic, clast-supported tuff breccia with augite-plagioclase-phyric volcanic clasts.

quartz. These rocks are cut by platy plagioclase-augite- and plagioclase-phyric mafic intrusions.

**The middle maroon volcanic unit** overlies the lower mafic volcanic unit everywhere but in the centre of the map area, where it is obscured by the mafic intrusive complex (Fig. 2). The lower contact of the unit is not exposed. The unit is up to 3 km thick and contains interlayered flows, volcanic breccia, tuff and lapilli tuff (Figs. 12, 13). Flows and clasts are predominantly augite-plagioclase-phyric. Interlayering of flows, tuff, and volcanic breccia is common and well-illustrated in exposures north of the McBride mineral occurrence (Fig. 12). The uppermost part of this unit in the Tanzilla area and immediately north of the Wolf showing contains well-stratified volcaniclastic sandstone and tuff. Rare welded lapilli tuff beds are developed at several locations. At one locale, a poorly sorted pyroclastic breccia with concave downward-shaped gas cavities above larger clasts grades upward into welded lapilli tuff (Figs. 12d, e), suggesting deposition as a hot, gas-rich pyroclastic density current.

The middle maroon volcanic unit formed in a predominantly subaerial environment as indicated by massive lava flows, local welded tuff and rare pyroclastic flow deposits. During formation of this unit, volcanic deposition rates outpaced subsidence rates, leading to the formation of a large subaerial volcanic edifice. Volcaniclastic sandstone and tuff in the upper part of the unit may indicate the end of widespread volcanism. The middle maroon volcanic unit is cut by a 173 Ma augite-bearing plagioclase porphyry (Table 2) which, when combined with the ca. 176 Ma detrital zircon peak from the top of the Spatsizi Formation (Iverson et al., 2012), suggests that the 4.5 km thick section of the lower and middle volcanic units were deposited within an 3 m.y. interval.

**The upper felsic volcanic unit** overlies the middle maroon volcanic unit in the Tanzilla area, (Table 1). Silica-altered plagioclase-phyric, possibly flow banded volcanic rocks 6 km east of Glacial Lake are tentatively assigned to this unit, and may include strong texturally destructive quartz-sericite-clay±lazulite altered rocks at the new Straight-across mineral occurrence (Section 6.2.3.3.). Contact relationships with the underlying unit were not observed. Bomb sags indicate subaerial deposition, and minor conglomerate beds and rare fossiliferous sandstone suggest local erosion within this unit.

**The upper mafic volcanic unit** caps the upper felsic volcanic unit, middle maroon volcanic unit and mafic intrusive complex (Fig. 2). The unit consists mostly of augite-plagioclase-phyric coherent rocks interpreted as flows and minor volcanic breccia, lapilli tuff, and tuff. Mafic coherent rocks and rare volcanic breccia north of the Gopher zone mineral occurrence, previously assigned to the mafic intrusive complex (van Straaten and Nelson, 2016), are reinterpreted here as the upper mafic volcanic unit. Barresi (2008) described drill core from the Mo showing with similar massive to well-bedded lapilli-tuff and crystal tuff containing plagioclase and augite crystals, providing further support for a mafic extrusive unit between the Gopher zone and Straight-up mineral occurrences. Given

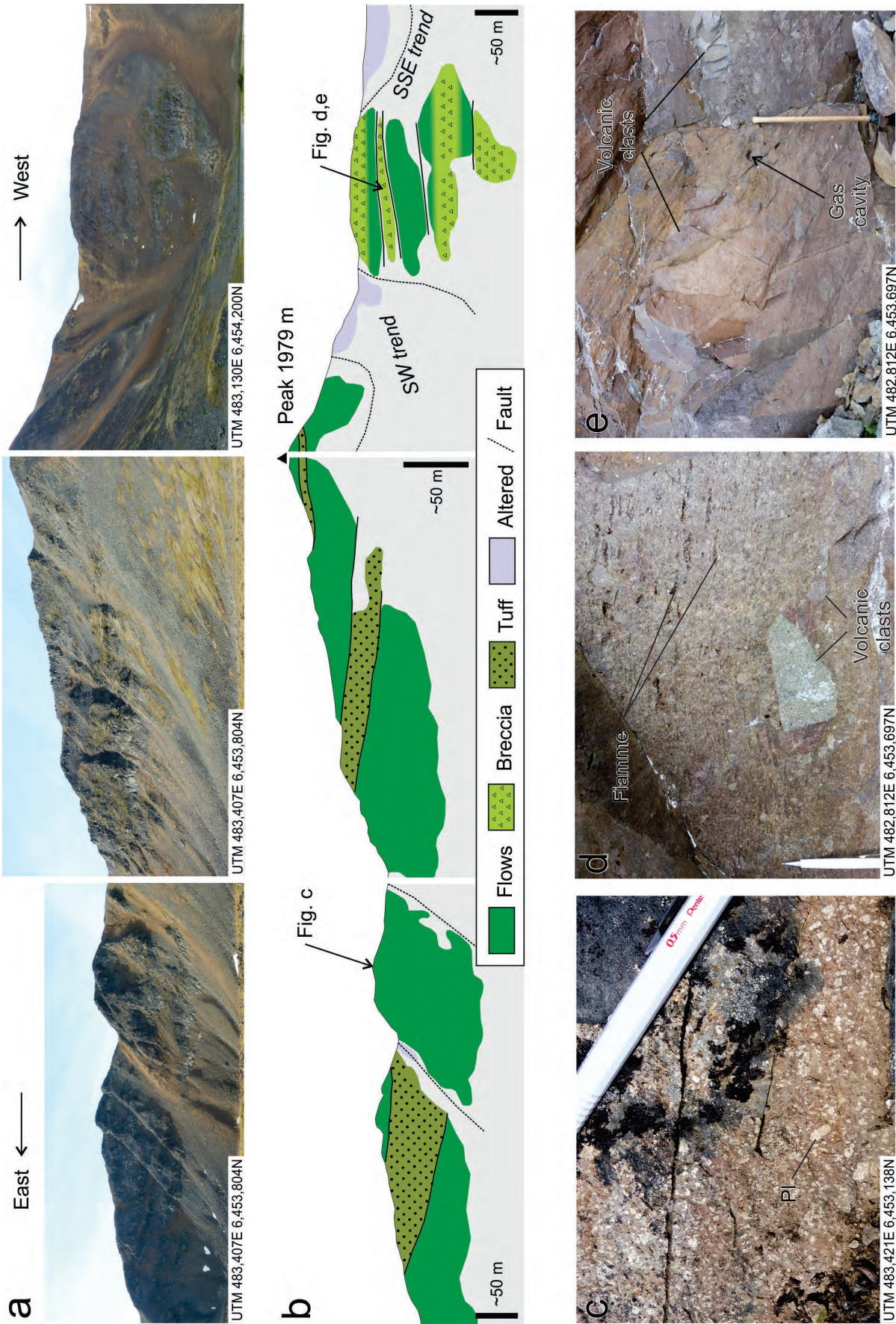


**Fig. 12.** Horn Mountain Formation, middle maroon volcanic unit (lmJHMMv) immediately north of the McBride mineral occurrence. **a)** Panorama of locally altered interlayered flows, volcanic breccia, and tuff. **b)** Diagram of rock types in a). **c)** Maroon plagioclase-phyric coherent rock interpreted as a volcanic flow. Relatively coarse plagioclase laths (4–6 mm, ~1:2.3 aspect ratio) characterize many flows of the unit near the McBride mineral occurrence. **d)** Maroon polymictic welded lapilli tuff with fiamme. **e)** Very poorly sorted maroon tuff breccia with concave-down gas cavities immediately above volcanic clasts.



**Fig. 13.** Horn Mountain Formation. Maroon polymictic tuff breccia in middle maroon volcanic unit (1mJHMMv). Clasts are typically sub-angular, varicoloured, and (augite)-plagioclase-phyric to aphyric.

the abundance of coherent mafic rocks, the unit is difficult to distinguish from the mafic intrusive complex (cf. Tables 1, 2). On the ridge west of Tanzilla, the contact with rocks of the underlying upper felsic volcanic unit is gradational. Contact relationships in all other areas are obscured by alteration and/or shearing. At Tanzilla, the unit overlies strongly quartz-sericite-clay altered rocks interpreted as the upper felsic volcanic unit. In the centre of the map area the unit overlies a northwest-dipping zone (at least 275 m wide) of generally strongly quartz-sericite-clay altered and variably sheared rocks (Fig. 14, Section 5.1.). Locally recognizable textures suggest a platy plagioclase-phyric porphyry protolith (Fig. 2). A down-dropped fault block west of Glacial Lake contains a gently north-dipping sequence of augite-plagioclase-phyric flows, and rare platy plagioclase-phyric flows, platy plagioclase-phyric volcanic breccia, and tuff with coarse platy plagioclase crystals; it is assigned to the upper mafic volcanic unit. Here, the succession overlies platy plagioclase-phyric coherent rocks interpreted as sills; the



**Fig. 14.** Horn Mountain Formation upper mafic volcanic unit (mJHMUvm) overlies strongly altered platy plagioclase porphyry (EMJm.po). Horn Mountain upper mafic volcanic unit is dark grey and moderately resistant. Gossans of the Straight-up mineral occurrence are visible underneath. View to the north-northeast.

intervening contact was not observed. A detrital zircon sample from a polymictic breccia in the upper mafic volcanic unit at Tanzilla yielded a Middle Jurassic maximum depositional age (Section 7.1.).

### 3.1.3. Bowser Lake Group

Gently north-dipping sedimentary rocks assigned to the Bowser Lake Group unconformably overlie Horn Mountain Formation upper volcanic rocks in the northwestern part of the map area (Figs. 2, 3); east of the map area, the Bowser Lake Group is in conformable contact with the middle maroon volcanic unit (van Straaten and Nelson, 2016). The section at Tanzilla contains an ammonite of probable Toarcian age (T. Poulton, pers. comm., 2015), which is at odds with a Middle Jurassic (Bajocian) maximum depositional age indicated by U-Pb analysis of detrital zircons from the same location (Section 7.1.), and middle Bajocian fossils collected east of the map area (Gabrielse, 1998). Regionally, deposition of Cache Creek-derived chert clast-bearing conglomerate in the Bowser basin records the onset of erosion from the Stikinia – Cache Creek tectonic welt (Evenchick et al., 2007).

## 3.2. Whitehorse trough

### 3.2.1. Takwahoni Formation (Early Jurassic)

Sedimentary rocks of the Takwahoni Formation (Laberge Group; Table 1) are exposed in a 5 km-wide belt between the Kehlechoa and King Salmon thrust faults (Figs. 2, 3). The most common lithology is interbedded quartz-bearing (5–15%) feldspathic arenite, feldspathic wacke and lesser siltstone (Fig. 15). Several fossil collections date this succession as (early) Pliensbachian (Gabrielse, 1998). Local basement to the Whitehorse trough strata is not exposed.

A recessive siltstone unit was observed in the northeastern part of the map area (Figs. 2, 16; Table 1). It is generally interbedded with minor fine- to medium-grained feldspathic arenite and feldspathic wacke. The contact between the north-dipping, right-way-up siltstone sequence and underlying sandstone unit is covered. The presence of the siltstone unit in the two eastern fault panels is inferred from regional aeromagnetic data (Aeroquest Airborne, 2012).

Regionally, the Whitehorse trough records progressive erosion of the Stuhini volcanic arc to plutonic levels, accompanied by input from Pliensbachian lower Hazelton arc volcanism to the south; it has been interpreted as a forearc basin (Johannson et al., 1997; Mihalynuk et al., 2004) or, more recently, a synorogenic basin (Colpron et al., 2015).

## 3.3. Overlap unit

### 3.3.1. Tuya Formation (Miocene to Pleistocene)

Gabrielse (1998) mapped several exposures of olivine basalt in the area. The volcanic centres are all on or near major faults (Fig. 2), and show a characteristic dipole signature on the regional aeromagnetic survey (Aeroquest Airborne, 2012).



**Fig. 15.** Fault propagation fold within interbedded sandstone and siltstone (Takwahoni Formation, sandstone unit, IJTgw). Arrows show tops; view to the southeast.

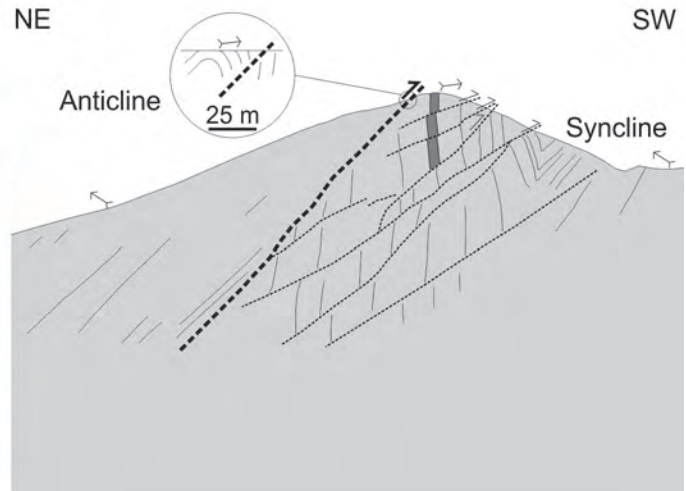


**Fig. 16.** Takwahoni Formation; recessive, orange-brown weathering, and well stratified siltstone unit (IJTs). View to the northeast.

## 4. Intrusive units

### 4.1. Late Triassic intrusions

The margin of the Cake Hill pluton, part of the 2275 km<sup>2</sup> composite Hotailuh batholith (van Straaten et al., 2012), is exposed in the southern part of the map area (Fig. 2). The main phase comprises hornblende quartz monzodiorite to quartz monzonite with accessory titanite and magnetite. Generally massive, it is locally foliated in the western part of the map area near Gnat Pass (Table 2). At its western contact, the Cake Hill pluton cuts Triassic Stuhini mafic volcanic rocks (van Straaten et al., 2012). Results from two U-Pb zircon samples indicate a ca. 221-218 Ma age (Anderson and Bevier, 1992; van Straaten et al., 2012). The northern margin of the pluton is unconformably overlain by Hazelton Group volcano-sedimentary rocks (Figs. 2, 8).

A small (~4 km<sup>2</sup>) intrusive body of medium-grained (3-5 mm) equigranular hornblende monzogranite is exposed in the

southeast of the map area (Fig. 2). It can be distinguished from the main phase of the Cake Hill pluton by a higher abundance of K-feldspar and quartz, and 5-7 mm quartz eyes (Fig. 17; Table 2). Contact relationships with the Hazelton Group to the north are equivocal. However, the presence of texturally-similar hornblende monzogranite clasts in basal Hazelton Group suggests an unconformity. Based on textural similarities and a probable pre-Early Jurassic age, the intrusion is correlated with the Cake Hill quartz-rich phase (Late Triassic) of van Straaten et al. (2012). The locally abundant hornblende monzogranite clasts suggest the quartz-rich phase may be (or may have been) more extensive than currently recognized.

The Gnat Pass porphyry consists of numerous small (<0.2 km<sup>2</sup>) plagioclase±quartz±hornblende porphyritic intrusions in the northwest of the map area (Fig. 2; Table 2). These rocks host K-feldspar-tourmaline alteration and local chalcopyrite-

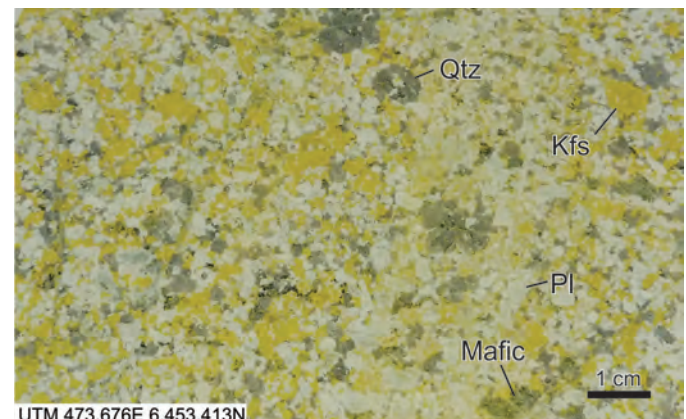


**Fig. 17.** Cake Hill pluton, quartz-rich phase (LTrCHgr). Medium-grained, equigranular, massive hornblende monzogranite. Slab is stained for K-feldspar.

pyrite mineralization at the Gnat Pass developed prospect and Moss showing (Section 6.1.).

A clinopyroxene-rich diorite to gabbro body of uncertain age was mapped in two areas in the western part of the map area (Fig. 2; Table 2). It is highly magnetic and has a concomitant high aeromagnetic response (Aeroquest Airborne, 2012). The unit intrudes sedimentary rocks tentatively assigned to the Stuhini Group (Fig. 2). A narrow (~100 m wide) diorite-gabbro body in the Horn Mountain middle maroon volcanic unit is assigned to this unit; contacts are not exposed. A similar pyroxenite, hornblende gabbro to monzodiorite unit (Triassic to Jurassic) was mapped ~30 km west of the map area by Logan et al. (2012a; b).

#### 4.2. Early to Middle Jurassic subvolcanic intrusions

The mafic intrusive complex forms two bodies (37 km<sup>2</sup> and 26 km<sup>2</sup>) in the central and eastern part of the map area (Fig. 2). It consists of augite-plagioclase-phyric mafic coherent rocks (Fig. 18; Table 2) and minor microdiorite. Rare volcanic breccia is interpreted as Horn Mountain Formation wall rock. The complex consists of irregular intrusive bodies, sills, and dikes that cut the Spatsizi volcanoclastic unit, and Horn Mountain lower mafic volcanic and middle maroon volcanic units (Fig. 2). The intrusions are likely coeval with high-volume volcanism during formation of the lower and middle Horn Mountain volcanic units based on their textural, mineralogical, and lithogeochemical similarities and because they cross-cut only the lower and middle Horn Mountain units (van Straaten and Nelson, 2016; this study). This implies that the contact between the mafic intrusive complex and the Horn Mountain upper mafic volcanic unit is either a local unconformity or a fault. The central location of the complex in the volcanic belt indicates a possible feeder relationship.

Dikes and sills of coarse platy plagioclase porphyry commonly cut the mafic intrusive complex and Horn Mountain

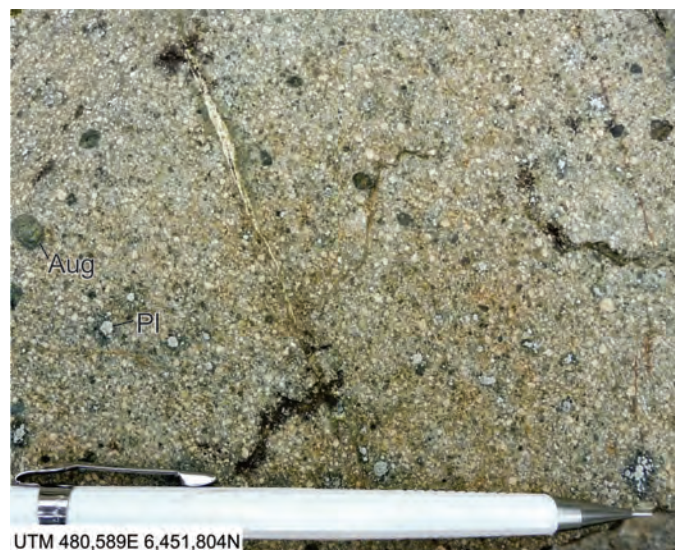


**Fig. 18.** Mafic intrusive complex, massive augite-plagioclase-phyric coherent rock (EMJm).

lower mafic and middle maroon units (Fig. 2; Table 2). A south-dipping zone of generally strongly quartz-sericite-clay altered and variably sheared rocks is structurally below the Horn Mountain upper mafic volcanic unit northwest of Glacial Lake (Sections 5.1., 6.2.). Locally recognizable textures at the southern end of the 275 m-wide zone suggest a platy plagioclase porphyry protolith (Fig. 2). In a down-dropped fault block west of Glacial Lake, platy plagioclase-phyric coherent rocks that underlie the upper mafic volcanic unit are interpreted as sills.

Near the Joyce showing, rare pale-grey plagioclase-phyric felsic dikes and a felsic breccia body are at the contact between a quartz diorite intrusion (Late Jurassic, see below) and the mafic intrusive complex (Figs. 2, 19). The breccia body contains (augite)-plagioclase-phyric and aphyric clasts in a pale grey flow-banded coherent groundmass (Table 2). Similar felsic dikes and a felsic intrusive breccia body cut the Horn

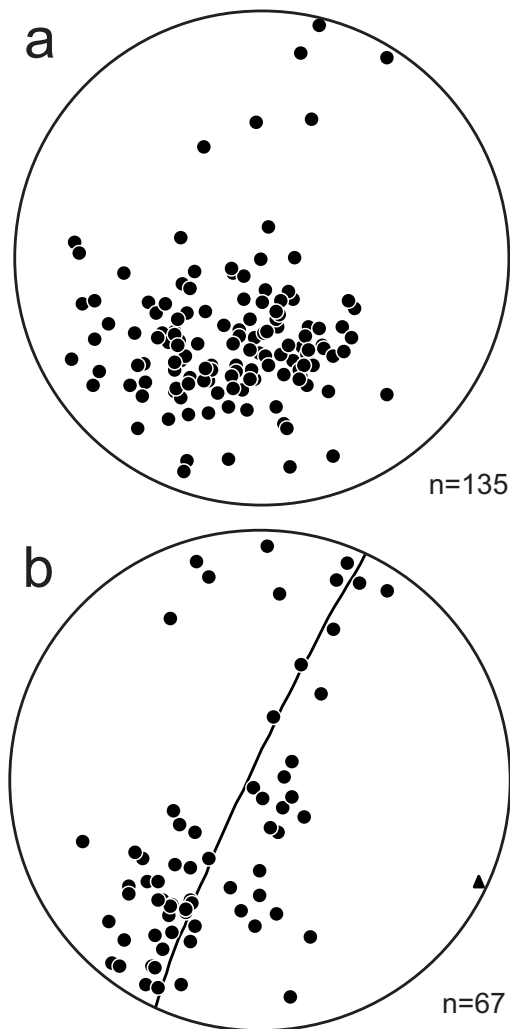


**Fig. 19.** Stereonet plots with poles to bedding for **a**) southern structural domain (upper part of Hazelton Group, Stikinia), and **b**) northern structural domain (Takwahoni Formation, Whitehorse trough). Great circle in **b**) shows cylindrical best fit, triangle represents corresponding fold axis. Lower hemisphere equal area projections.

Mountain lower mafic volcanic unit 5.5 km west of the Joyce showing (van Straaten and Nelson, 2016).

Several metre-wide monzonite dikes near the McBride mineral occurrence contain plagioclase, hornblende, and biotite crystals in a very fine-grained, pink groundmass. These dikes display alteration and porphyry-style veining internally and along their margins (Section 6.2.1.2.). Texturally and mineralogically similar dikes were observed east of Tanzilla (van Straaten and Nelson, 2016). They may represent alkaline intrusions (Early-Middle Jurassic) coeval with the Horn Mountain volcanic rocks, or subalkaline intrusions (Middle Jurassic) related to the potassic phase of the Three Sisters pluton.

#### 4.3. Middle Jurassic intrusions

The Three Sisters pluton in the southeast of the map area consists of a main central felsic phase and marginal mafic and potassic phases (Fig. 2; Table 2). Crosscutting relationships (van Straaten et al., 2012; this study) and geochronological data (Table 2) suggest an evolutionary path from mafic towards more evolved compositions between ca. 173 and 169 Ma.

The mafic phase is a small (<2 km<sup>2</sup>) hornblende-clinopyroxene diorite intrusion in the southeast of the map area. It is highly magnetic and has a high aeromagnetic response (Aeroquest Airborne, 2012).

Small (<0.2 km<sup>2</sup>) intrusive bodies of (augite-bearing) plagioclase porphyry at the Tanzilla prospect and Straight-across mineral occurrences are generally surrounded by highly altered rocks interpreted as the Horn Mountain middle maroon volcanic unit. These intrusions are interpreted to be coeval with porphyry-style alteration at the Tanzilla prospect, and a U-Pb zircon age of 173.25 ± 0.13 Ma indicates that the intrusions are coeval with the mafic phase of the Three Sisters pluton.

The central felsic phase consists of hornblende quartz monzodiorite to biotite-bearing hornblende quartz monzodiorite. Part of this body was previously mapped as the Cake Hill pluton (Gabrielse, 1998). It is re-interpreted here as Three Sisters central felsic phase based on Middle Jurassic U-Pb zircon ages (Takaichi 2013a; b; see Section 7.2). Local minor biotite, presence of common diorite xenoliths, and the lack of accessory titanite confirm this assignment. Apophyses of the central felsic phase cut the mafic phase, and diorite xenoliths similar to the mafic phase are common in the central felsic phase (Table 2). Fluidal-shaped mafic domains and mafic domains with chilled margins in central felsic phase rocks (van Straaten et al., 2012) suggest the central felsic and mafic phases are roughly coeval.

The potassic phase comprises biotite-bearing hornblende monzogranite. It occurs immediately east of the central phase, and as a ~700 m wide apophysis cutting the mafic intrusive complex, Horn Mountain lower mafic and Horn Mountain middle maroon volcanic unit (Fig. 2; Table 2). Pale pink hornblende-plagioclase-phyric dikes correlated with the potassic phase cut Horn Mountain lower mafic and middle maroon volcanic rocks, and appear to cut the central felsic

phase.

The Three Sisters pluton is part of a Middle Jurassic quartz-bearing calc-alkaline plutonic belt that trends northwest to east-southeast for at least 300-400 km, spanning the Cache Creek and Stikine terranes (Fig. 1; van Straaten et al., 2012). In the far northwest of this belt, the Fourth of July batholith (ca. 171 Ma) cuts deformed rocks of the Cache Creek terrane (Mihalynuk et al., 1992). These plutons extend into the Yukon, where they are referred to as the Bryde suite (ca. 172-168 Ma; Colpron et al., 2016a; b).

#### 4.4. Late Jurassic intrusions

The Snowdrift Creek pluton is a mostly recessive 96 km<sup>2</sup> hornblende-bearing biotite granodiorite body (Table 2; Fig. 2). Apophyses of the pluton cut Takwahoni sandstone and augite-plagioclase-phyric coherent rocks interpreted as the Horn Mountain upper mafic volcanic unit. Moderate to intense biotite hornfels, with up to 25% very fine-grained (0.02-0.2 mm) black biotite replacement, occurs up to one kilometre away from the southern margin of the pluton. It affects the Horn Mountain upper mafic volcanic rocks, mafic intrusive complex, platy plagioclase porphyry and augite-bearing plagioclase porphyry. Along the northeastern margin of the pluton, fine-grained brown biotite hornfels extends at least several hundred metres into Takwahoni sandstone. We interpret that the Snowdrift Creek pluton cuts the Kehlechoa fault, the thrust that places sedimentary rocks of the Whitehorse trough structurally above Stikinia (Fig. 2).

A ~5 km<sup>2</sup> intrusive body of fine-grained hornblende-bearing biotite quartz diorite cuts the mafic intrusive complex at the Joyce showing (Fig. 2). Based on its composition, texture and crosscutting relationships we consider it a satellite stock of the Snowdrift Creek pluton. A small (0.1 km<sup>2</sup>) hornblende quartz monzodiorite intrusion crops out 2 km south of the Snowdrift Creek pluton and a small granodiorite body is interpreted from drill logs from the Mo prospect (Barresi, 2008; Fig. 2).

Hornblende diorite dikes and sills correlated with the Snowdrift Creek pluton occur throughout the map area. They cut the Takwahoni Formation and most units in the upper part of the Hazelton Group (Table 2).

The Snowdrift Creek pluton yielded a U-Pb zircon age of 160.43 ± 0.16 Ma. Plutons of this age are rare in the northern Canadian Cordillera. However, recent studies in the Yukon suggest that the McGregor pluton is of roughly similar age (ca. 163-160 Ma, Colpron et al., 2016a; b).

### 5. Structure

The map area can be divided into southern and northern structural domains, separated by the Kehlechoa thrust fault (Fig. 2). In the southern domain, the Spatsizi and Horn Mountain formations define a moderately NNE-dipping homocline that is cut by northeast-striking normal faults and northwest-striking dextral and normal faults. In the northern domain, sedimentary rocks of the Whitehorse trough in the hanging wall of the Kehlechoa thrust are deformed by south-

vergent folds and thrusts that are offset by NNE-striking tear faults. In the western part of the map area between Gnat Pass and Dease Lake, both domains are cut by NNW-striking faults that were active from the Late Triassic to late Middle Jurassic.

### 5.1. Southern structural domain

Bedding in the Spatsizi and Horn Mountain formations defines a generally NNE-dipping homocline (Fig. 19a). Local east-dipping bedding coincides with the eastern margin of the Cake Hill pluton, and may reflect heterogeneous strain around the margins of a rigid body. Rare steeply south-dipping bedding in the Horn Mountain lower mafic volcanic unit west of Highway 37 (Fig. 19a) may represent open upright folds with east-trending hinge lines, similar to those in the northern structural domain (see below).

Several northeast-striking faults cut the Spatsizi and Horn Mountain formations with apparent right- and left-lateral offset. They are interpreted as normal faults with both east-side and west-side down movement (Fig. 2). These faults are truncated to the north by the Snowdrift Creek pluton and the Kehlechoa fault.

Northwest-striking faults cut the Spatsizi and Horn Mountain formations. The regional-scale (10-20 km) northwest-striking Tanzilla River fault and a fault south of Peak 2096 m display an apparent dextral offset and cut the northeast-striking faults. Short (<4 km) northwest-striking dextral and north-side down normal faults are cut by the northeast-striking faults. A steeply north-dipping fault 3 km south-southwest of Glacial Lake juxtaposes a hanging wall of Horn Mountain Formation lowermost mafic volcanic rocks with a footwall of Cake Hill quartz monzonite. A normal sense is inferred based on the juxtaposition of younger over older rocks. In the hanging wall of an inferred north-side down, northwest-striking normal fault immediately west of Glacial Lake, moderately to gently north-dipping Horn Mountain Formation upper mafic volcanic flows lie above a footwall of moderately to steeply north-dipping Horn Mountain middle maroon volcanic rocks (Fig. 2). This fault is defined by a 2 m-wide zone of steeply north-dipping quartz-clay schist. The lack of foliation development in other northwest-striking faults suggests the foliation may have formed as a result of subsequent reverse movement, similar to the shear zone at the Straight-up mineral occurrence (see below).

At the Gopher zone and Straight-up mineral occurrences (Fig. 2), well-developed foliation generally dips moderately to steeply to the northeast, or steeply to the southwest. It is best developed in a zone (at least 275 m wide) of strongly quartz-sericite-clay-pyrite altered rocks (see Section 6.2.). This zone likely extends for 12 km along strike, from the Gopher zone to the Straight-up mineral occurrence, based on 1) subcrop and float of altered and/or foliated rocks at the Mo east mineral occurrence, and 2) similar chargeability anomalies along the Gopher zone and Mo east occurrences (Andrzejewski and Bui, 2012). Although kinematic indicators were not observed and the structure does not appear to duplicate or omit stratigraphy,

a reverse shear sense is inferred based on a roughly similar orientation as regional-scale thrust faults and its crosscutting relationship with respect to the alteration system at Tanzilla. It likely formed along a zone of weakness created by earlier hydrothermal alteration. The shear zone has a similar orientation to both bedding and normal faults in the map area, as such it may represent 1) a decollement surface developed within altered rocks below an unconformity at the base of the upper mafic volcanic unit, and/or 2) a southwest-verging thrust fault reactivating a northeast-side down normal fault, which previously focussed hydrothermal fluids and resultant advanced argillic alteration. The shear zone appears to be offset across two northeast-striking left-lateral tear faults (Fig. 2).

Local biotite schists form steeply NNE-dipping metre-wide domains of limited lateral continuity in the Horn Mountain upper mafic volcanic unit. At two locations, fabrics in the schists are cut by pink felsic dikelets (2 cm wide) attributed to the Snowdrift Creek pluton.

### 5.2. Northern structural domain

Two regional SSW-vergent thrust faults define the boundaries of the northern structural domain (Fig. 2). In the north, the King Salmon fault places rocks of the Cache Creek terrane over the Takwahoni Formation (Whitehorse trough; Gabrielse, 1998). To the south, the Kehlechoa fault places Takwahoni Formation rocks over younger Horn Mountain Formation and Bowser Lake Group (Stikinia) rocks. The Kehlechoa fault is inferred from 1) the juxtaposition of Pliensbachian Takwahoni Formation over younger, Toarcian-Bajocian Bowser Lake Group and Horn Mountain Formation; 2) the presence of folds and internal imbrication in the hanging wall; and 3) a well-defined aeromagnetic lineament (Aeroquest Airborne, 2012). The absence of internal imbrication and folding in the homoclinal footwall sequence suggests the Kehlechoa fault is the foreland thrust of the Cache Creek-Stikinia orogenic welt. Geochronological data (see Section 7) indicate that the fault moved between ca. 170 and 160 Ma.

Bedding in the Takwahoni Formation is predominantly right-way-up and moderately north- to northeast-dipping (Fig. 2). The folds are open to tight, with subhorizontal fold axes (Fig. 19b), and have wavelengths of up to 1 km. Folds, small-scale thrusts and a 100s of metre-scale fault propagation fold (Fig. 15) verge to the south-southwest. Rare axial planar cleavage in fine-grained units dips moderately to steeply north to north-northeast and locally, steeply south. The orientation and vergence of structural elements in the northern structural domain are similar to the Kehlechoa and King Salmon faults, and agree with results from other studies in the region (Gabrielse, 1998; Logan et al., 2012a).

Northeast-striking faults, with apparent right-lateral and left-lateral slip cut the Takwahoni Formation in the northeast part of the map area (Fig. 2). They terminate a thrust fault and km-scale fold patterns, and offset the Takwahoni siltstone unit.

### 5.3. NNW-trending faults between Gnat Pass and Dease Lake

Regional-scale NNW-trending faults cut the southern and northern structural domains in the western part of the map area. A NNW-striking fault is inferred to cut across Tsenaglade Creek in the westernmost part of the map area (Fig. 2). The base of the Takwahoni Formation shows a 6 km right-lateral offset along the northern segment of this fault. West of the fault, the basal contact of the Takwahoni Formation is inferred as depositional on top of Stuhini Group (Logan et al., 2012a; b). East of this fault, the Takwahoni Formation occupies the hanging wall of a thrust fault above the Horn Mountain Formation. Our mapping extends the Horn Mountain Formation to at least the lower reaches of Tsenaglade Creek. Here, the NNW-trending fault is interpreted to juxtapose Stuhini Group and Horn Mountain Formation (Fig. 2). On the west side of the inferred fault, the age of volcano-sedimentary rocks is uncertain; following mapping by Logan et al. (2012b) farther west we tentatively assign this succession to the Stuhini Group. The southernmost 6 km of the fault manifests as a well-defined aeromagnetic lineament; the remainder of the fault lacks a clear aeromagnetic expression (Aeroquest Airborne, 2012).

Along Highway 37 (Fig. 2), the Gnat Pass structure is defined by a zone of foliated rocks up to 1 km wide at the contact of the Stuhini Group and Cake Hill pluton (Late Triassic). These rocks are interpreted as a syn-intrusion east-side-up reverse shear zone (van Straaten et al., 2012). East-west continuity of Spatsizi and Horn Mountain units, and the Gnat Pass to Moss alteration system (see Section 6.1.) suggest minimal, if any, strike-slip movement. The structure is inferred to extend northward and merge with an adjacent fault to the east.

A northwest-striking fault passes ~1-2 km east of Gnat Pass (Fig. 2). The northern segment of the fault is defined by an aeromagnetic lineament. Based on the 1.7 km apparent right-lateral offset of an east-west aeromagnetic lineament ascribed to the Kehlechoa fault, it is interpreted as a tear fault. In the south, this fault shows a relatively well-constrained 2 km apparent right-lateral offset of the Spatsizi basal sandstone and conglomerate unit, and appears to structurally juxtapose altered rocks of the Gnat Pass developed prospect against Spatsizi basal sandstone and conglomerate. We interpret this segment of the fault as an Early Jurassic growth fault, based on 1) abrupt thickening of the Spatsizi Formation across the fault (Fig. 2), 2) abundant small-scale syn-sedimentary faults and soft-sediment deformation in the Spatsizi Formation (Fig. 6), and 3) an up-section decrease in displacement of contacts in the overlying Horn Mountain Formation.

## 6. Mineral occurrences

Mineral occurrences in the map area (Fig. 20) can be subdivided according to age of formation, age of host rocks, mineralization characteristics, and alteration style. Late Triassic porphyry-style copper mineralization occurs at the Gnat Pass developed prospect and nearby Moss showing. The Horn Mountain Formation hosts aerially extensive

gossans at Tanzilla and McBride and epithermal veins with elevated copper values near Glacial Lake. A trend of argillic to advanced argillic altered rocks (at least 17 km long) is exposed at high stratigraphic levels of the Horn Mountain Formation. Molybdenum mineralization is present locally in the Snowdrift Creek pluton and its immediate wall rocks, and in a satellite stock to the south.

Preliminary assay data from ten altered and/or mineralized rock samples collected in 2016 are presented in Table 3. Samples were jaw crushed and pulverized at the British Columbia Geological Survey, and analyzed at Bureau Veritas in Vancouver. The samples were dissolved using an aqua regia digestion before being analyzed by ICP-ES/MS. Results of external standards and duplicates were monitored to ensure analytical reproducibility and accuracy. Detailed methods and complete results will be reported elsewhere.

### 6.1. Mineral occurrences in Triassic rocks

The two porphyry copper mineral occurrences in the southwestern part of the map area are hosted in Stuhini Group mafic volcanic rocks and Gnat Pass plagioclase porphyry.

#### 6.1.1. Gnat Pass (MINFILE 104I 001)

Drilling at the Gnat Pass porphyry copper developed prospect (Fig. 20) in the 1960s defined a non NI 43-101-compliant resource of 30 million tonnes grading 0.389% copper (Lytton Minerals Ltd., 1972, reported in MINFILE 104I 001; British Columbia Geological Survey, 2016). Limited diamond drilling was carried out in 1989 and 2012 (Smith and Garagan, 1990; Roberts et al., 2013). Chalcopyrite is in black tourmaline veins and disseminations, and is commonly accompanied by pink K-feldspar alteration (van Straaten et al., 2012; Roberts et al., 2013). Mineralization is mainly in the Gnat Pass plagioclase porphyry, but is also in Stuhini Group mafic volcanic rocks adjacent to the porphyry. Sheeted subvertical, northwest-striking black tourmaline±chalcopyrite±magnetite veins were observed near Gnat Pass. A NNW-trending fault juxtaposes altered Stuhini Group and unaltered Spatsizi Formation rocks (Figs. 2, 20). A northeast-trending fault bounds the Gnat Pass deposit to the south. Surface mapping and drilling indicates that it separates altered Stuhini Group and Gnat Pass porphyry in the hanging wall from Spatsizi basal sandstone and conglomerate overlying the Cake Hill pluton in the footwall (Bowen, 2013; Roberts et al., 2013).

#### 6.1.2. Moss (MINFILE 104I 029)

The Moss porphyry copper showing is 2.3 km west-northwest of the Gnat Pass developed prospect (Fig. 20). Geologic, geochemical, and geophysical surveys, trenching, and percussion drilling were conducted in conjunction with work on the Gnat Pass developed prospect in the late 1960s to early 1970s. Chalcopyrite is in a northwest-trending zone of tourmaline veins and breccias with pink K-feldspar alteration (Bowen, 2013). Results from trenching returned 122 metres at 0.10% copper (Lytton Minerals Ltd., 1969). Recent

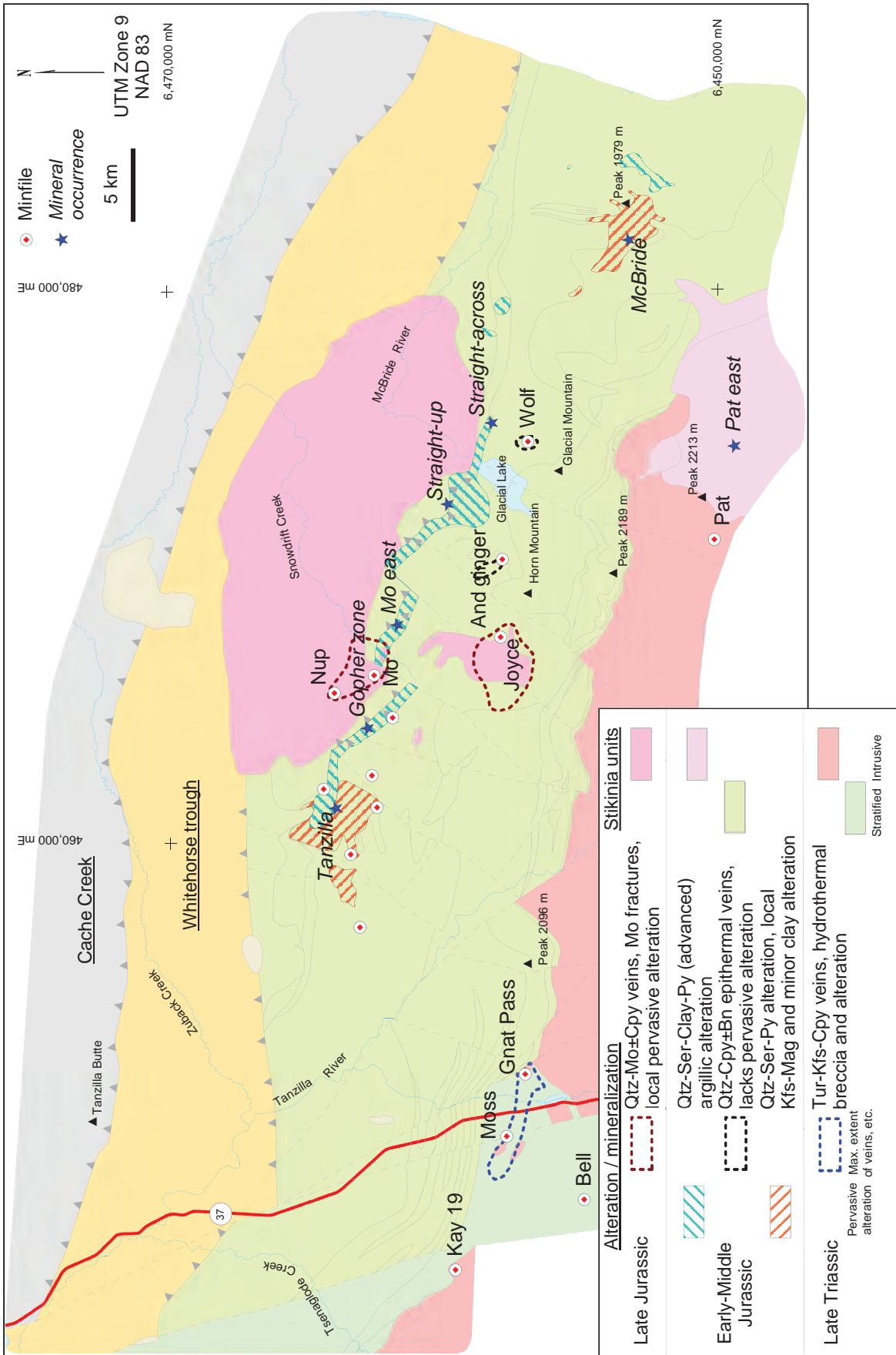


Fig. 20. Simplified geologic map highlighting mineral occurrences, and generalized extent of characteristic alteration and mineralization domains. For detailed geology and legend see Figure 2.



trench grab samples returned up to 2.1% copper and 0.7 g/t gold (Andrzejewski and Bui, 2012). Similar to the Gnat Pass developed prospect, the Moss showing is spatially coincident with Gnat Pass porphyry intrusions (Figs. 2, 20; Bowen, 2013). Including the Gnat Pass developed prospect, tourmaline and/or K-feldspar alteration and chalcopyrite mineralization extend for 4.3 km along a west-northwest trend (Fig. 20; van Straaten et al., 2012; Bowen, 2013). The tourmaline vein and breccia zones at the Moss showing and sheeted tourmaline veins at Gnat Creek suggest a strong structural control.

## 6.2. Mineral occurrences in Early to Middle Jurassic rocks

Early to Middle Jurassic rocks in the map area host porphyry-style occurrences, local epithermal-style veins, and a laterally extensive argillic to advanced argillic alteration zone.

### 6.2.1. Porphyry-style occurrences

#### 6.2.1.1. Tanzilla (MINFILE 104I 142)

The Tanzilla occurrence is in a zone of quartz-sericite-clay±pyrite alteration measuring at least 5 by 2 km (Fig. 20). The altered area includes the Gopher zone (see Section 6.2.3.1.) and other MINFILE occurrences (Fig. 20). Recent work includes geophysical surveys, a terraspec alteration mineral study, and diamond drilling (Luckman et al., 2013; Barresi et al., 2014). In addition to phyllic, argillic and intermediate argillic alteration, the terraspec-aided field study identified an advanced argillic alteration assemblage of alunite, pyrophyllite and topaz (Luckman et al., 2013). Diamond drilling in 2014 and 2015 tested for porphyry-style alteration and mineralization below the strongly advanced argillic altered lithocap exposed at the surface (Barresi et al., 2014). Drill holes intersected advanced argillic alteration overlying porphyry-style alteration with local anomalous copper and molybdenum concentrations (Barresi et al., 2014; Kaizen Discovery Inc., 2015; van Straaten and Nelson, 2016). An augite-bearing plagioclase porphyry (173 Ma; Section 7.4.) was affected by pervasive quartz-sericite-pyrite and potassic alteration. van Straaten and Nelson (2016) interpreted this porphyry as syn-mineral because it hosts porphyry-style alteration and veining, and lacks the advanced argillic alteration of adjacent volcanic rocks. The alteration system at Tanzilla is cut by unaltered hornblende diorite dikes, correlated with the Snowdrift Creek pluton (Table 2).

#### 6.2.1.2. McBride

The first recorded exploration activities near the McBride occurrence (Fig. 20) were by Teck Resources Limited (2011 to 2014) and included geophysical surveys, stream-sediment, soil and rock sampling, and geologic mapping (Takaichi and Johnson, 2012; Takaichi, 2013a; Jutras et al., 2014). The occurrence is in interlayered augite-plagioclase-phyric flows, tuffs, and volcanic breccias of the Horn Mountain middle maroon unit (Figs. 2, 12). A gossan (~1.5 by 1.5 km) immediately west of Peak 1979 m shows abundant float, subcrop, and local outcrop of moderately to strongly quartz-sericite-pyrite altered rocks, and local cm-scale quartz-pyrite

veins. A magnetite breccia (75 by 100 m) described by Jutras et al. (2014) in the western part of this gossan is in a probable intrusive rock containing plagioclase phenocrysts set in a pink, very fine-grained K-feldspar-rich groundmass. The K-feldspar, likely in part hydrothermal, is accompanied by common magnetite-pyrite alteration, and magnetite, biotite, and rare quartz-magnetite veinlets. Rock samples from this location returned up to 0.07% copper and 0.25 g/t gold (Jutras et al., 2014). The close spatial relationship of potassic alteration and hydrothermal veins with monzonite intrusions (EMJmz, Table 2) suggest they may be cogenetic. Several narrow (<50-100 m) alteration zones extend north-northwest to northeast from the gossanous zone (Figs. 12a, 20) and are likely related to pre-existing faults. A zone of weak to moderate quartz-sericite-pyrite alteration extends along the creek west of Peak 1979 m for at least 1 km (Fig. 20). The zone contains several northwest- to north-trending pink hornblende-biotite monzonite dikes (EMJmz; Table 2) with rare quartz-pyrite veins and local magnetite veinlets in the adjacent mafic intrusive. Farther east, on the hillside above the McBride River, a northeast-trending zone, 1.8 km long by 0.3 km wide, with variable alteration characteristics is exposed. Hydrothermal mineral assemblages vary from quartz-sericite-clay-pyrite to quartz-clay-pyrite and massive grey silica-pyrite. Medium grey massive silica-pyrite altered rock is exposed at an isolated outcrop 2.4 km north-northeast of Peak 1979 m (Fig. 20). The local potassic alteration and porphyry-style veining within a broader quartz-sericite-pyrite altered zone may represent the upper levels of a porphyry system (Jutras et al., 2014). The eastern and north-northeastern exposures appear to display more distal argillic to advanced argillic alteration assemblages.

### 6.2.2. Epithermal-style mineral occurrences

Several small copper-bearing veins in the centre and south-centre of the map area generally lack significant alteration envelopes and are likely relatively low-temperature, shallow epithermal in origin.

#### 6.2.2.1. And Ginger (MINFILE 104I 140)

The And Ginger copper-silver showing, 2 km west of Glacial Lake, was discovered in 2008 during geologic mapping and prospecting near the Joyce property (Barresi, 2009; Fig. 20). The showing includes quartz-calcite-epidote-chlorite-bornite±chalcopyrite veins and pods hosted in sea green aphanitic rhyolite dikes and mafic volcanic rocks (Barresi, 2009). Grab samples returned up to 3% copper and 69 g/t silver (Barresi, 2009). Nearby we observed similar chalcopyrite- and malachite-bearing quartz veins that show open-space vein-fill textures and lack significant alteration envelopes.

#### 6.2.2.2. Wolf (MINFILE 104I 056)

The Wolf copper showing is 1 km southeast of Glacial Lake (Fig. 20). Prospecting and geologic mapping identified a restricted (45 by 45 m) zone of copper mineralization (Noel, 1972). Abundant cm- to rarely 0.5 m-wide quartz-chlorite-

carbonate-chalcopyrite-bornite veins locally have slickenfibres developed along their surfaces. Mineralization is along the margin of, and locally within, a NNE-NE-trending, steeply dipping hornblende diorite dike that is up to 12 m wide. The dike is equigranular, medium grained (3-4 mm), and contains 15% euhedral hornblende and 85% euhedral, concentrically zoned plagioclase. It cuts augite-plagioclase-phyric flows of the Horn Mountain middle maroon volcanic unit and is considered part of the Snowdrift Creek suite. The veining and mineralization at Wolf are comparable to And ginger, but contrast strongly to those at occurrences in Late Jurassic rocks (see below).

#### 6.2.2.3. Pat East

Subcrop and float of a brecciated malachite-stained quartz vein was observed in a 5-10 m wide northwest-trending recessive zone with common disseminated pyrite in central felsic phase quartz monzodiorite of the Three Sisters pluton. An assay sample returned 0.35% copper and anomalous molybdenum and gold (Table 3). The vein is 3 km east-southeast of the Pat copper-molybdenum showing (MINFILE 104I 043; Fig. 20).

### 6.2.3. Argillic to advanced argillic alteration zones

A 17 km-long zone of quartz-sericite-clay-pyrite alteration extends across the central part of the map area (Fig. 20). It includes alteration at Tanzilla, the Gopher zone, Mo east, Straight-up and the newly discovered Straight-across occurrence. At Tanzilla and the Gopher zone, terraspec analyses confirmed advanced argillic alteration assemblages (Luckman et al., 2013). Based on textural and mineralogical similarities, we postulate that advanced argillic alteration extends across the entire zone. Similar alteration may be present east and northeast of the McBride occurrence, 10 km east of the Straight-across occurrence.

#### 6.2.3.1. Gopher zone (MINFILE 104I 141)

The Gopher zone mineral occurrence, 2.5 km east-southeast of Tanzilla, trends northwest and is at least 275 m wide. It consists of strongly sheared silicified rocks and quartz-sericite-clay schist, and commonly contains blue lazulite (an anhydrous phosphate mineral). A terraspec-aided field study identified an advanced argillic alteration assemblage of pyrophyllite±topaz (Luckman et al., 2013). Texturally destructive alteration generally prevents protolith identification, but near the southern end of the zone is coarse platy plagioclase porphyry.

#### 6.2.3.2. Mo East

A broad saddle on the ridge east of the Snowdrift Creek valley shows a pronounced chargeability high on an induced polarization survey (Andrzejewski and Bui, 2012). Although exposure is generally poor, rare subcrop and float indicate massive to strongly foliated quartz-sericite-clay altered rocks. Abundant iron oxide coated fractures, iron oxide lined cavities, and only rare disseminated pyrite, suggest extensive surface leaching of pyritiferous rocks. A sample of coarse platy plagioclase-phyric coherent rock with disseminated

pyrite and a quartz-pyrite±molybdenite vein, returned 117 ppm molybdenum (Table 3).

#### 6.2.3.3. Straight-up

The Straight-up mineral occurrence consists of extensive gossans on the ridges northwest of Glacial Lake (Figs. 14, 20). This occurrence was first described by Barresi (2009), who reported highly variable alteration intensity, alteration minerals, and planar fabric development. Alteration minerals include quartz, clay, chlorite, sericite, pyrite, hematite and rare kaolinite, andalusite, lazulite and titanite. Barresi (2009) described the rocks as being highly leached, and reported that samples failed to yield significant base or precious metal concentrations. He considered alteration mineralogy, strong apparent leaching, and high aluminum concentrations consistent with strong acidic alteration. We confirmed the presence of quartz-sericite-clay altered rocks, commonly with a well-developed foliation. At the north end of the zone protoliths were not identifiable due to strong texturally destructive alteration; at the south end, the protolith is variably altered and sheared platy plagioclase porphyry. The valleys to the southwest and east contain ferricrete deposits and, together with the abundant iron oxide coated fractures and vugs, indicate extensive pyrite leaching.

#### 6.2.3.4. Straight-across

We mapped massive grey silica±sericite altered rocks containing minor blue lazulite, 1.5 km east-southeast of the outlet of Glacial Lake and herein name the occurrence 'Straight-across' (Fig. 20). It displays similar argillic to advanced argillic alteration as Tanzilla, Gopher zone, Mo east and Straight-up. Leached cavities are common, except in rare areas where abundant (<5-10%) disseminated pyrite is preserved. A sample did not return significant base or precious metal concentrations (Table 3). The southern part of the occurrence, and an isolated outcrop 300 m to the east, consist of biotite hornfelsed and locally quartz-pyrite altered augite-bearing plagioclase porphyry, similar to the syn-mineral porphyry at Tanzilla. The area surrounding the Straight-across occurrence is covered by thick overburden.

### 6.3. Mineral occurrences in Late Jurassic rocks

#### 6.3.1. Mo and Nup (MINFILE 104I 146, 104I 059)

The Mo and Nup mineral occurrences are in the overburden-filled Snowdrift Creek valley (Fig. 20). Anomalous molybdenum and copper in stream-sediment, soil, and rock samples were identified by Stevenson (1973a; b), Ball and Ashton (1982), Graham (1982), and Bradford (2008). Drilling by Paget Moly Corporation in 2008 intersected volcanic tuff, platy plagioclase porphyritic intrusion, and biotite granodiorite of the Snowdrift Creek pluton (Barresi, 2008). Anomalous molybdenum values were intersected in several drill holes, generally coincident with widely spaced molybdenite and trace chalcopyrite in quartz veins with pink K-feldspar envelopes (Barresi, 2008). Most likely, this mineralization is a molybdenum (copper) porphyry system genetically related to the Snowdrift Creek pluton.

### 6.3.2. Joyce (MINFILE 104I 049)

The Joyce showing is 2 km northwest of Horn Mountain (Fig. 20). In the late 1960s low-grade molybdenum-copper mineralization was identified by prospecting, geologic mapping, induced polarization surveys and trenching (Woolverton, 1967). Diamond-drill holes intersected variable chlorite-sericite, clay, and silica alteration accompanied by molybdenite, but mineralization was not deemed economic (James and Westervelt, 1970). Recent rock geochemical analyses confirmed elevated molybdenum and copper (Barresi, 2009). We observed molybdenite, pyrite, and rare chalcopyrite in quartz veins, fracture coatings, and as disseminations in altered wall rock. Mineralization is hosted in a biotite quartz diorite intrusion interpreted as a satellite stock of the Snowdrift Creek pluton (Fig. 20). Historical trenches in areas of overburden contain gossanous and yellow clay altered rocks; gossanous exposures extend ~1 km east and west of the showing.

## 7. Geochronology

U-Pb zircon and Ar-Ar mica analyses were carried out at the Pacific Centre for Isotopic and Geochemical Research (University of British Columbia). Re-Os molybdenite analyses were carried out at the Canadian Centre for Isotopic Microanalysis (University of Alberta). Preliminary results are presented in Table 4; detailed methods and final results will be reported elsewhere. Preliminary maximum depositional ages are calculated for LA-ICP-MS detrital zircon analyses using the weighted mean age of the youngest zircon population (excluding outliers). Future work will use methods of Ludwig (2012), and Dickinson and Gehrels (2009) to further constrain maximum depositional ages.

Takaichi (2013a; b) reported U-Pb zircon results from three Middle Jurassic intrusive rock samples; herein we also provide detailed field descriptions from the sample sites to accompany the geochronological data.

### 7.1. Lower to middle Jurassic stratified units

We sampled the Spatsizi Formation basal sandstone and conglomerate unit northwest of the Tanzilla River (Fig. 2). The sample (15BvS-03-14) returned a unimodal detrital zircon peak at  $214.8 \pm 1.5$  Ma (Fig. 21a), which overlaps with ages for the youngest phases of the Stikine plutonic suite (Table 2).

A sample of felsic lapilli tuff from the Horn Mountain lowermost mafic volcanic breccia unit (Fig. 2; Table 4) yielded a preliminary age age of  $215.5 \pm 1.4$  Ma (R. Friedman, pers. comm., 2016), which overlaps with ages from the youngest phases of the Stikine plutonic suite. Based on the presence of Early Jurassic fossils and zircon populations (Table 1) along strike we interpret the Late Triassic zircons as detrital.

A bed of polymictic conglomerate in a section of mafic volcanic breccias and flows of the Horn Mountain upper mafic volcanic unit was sampled in 2014 (sample 14MT-03-04). The conglomerate is quartz-sericite-chlorite altered, locally foliated, and contains white plagioclase-phyric clasts, dark grey augite-

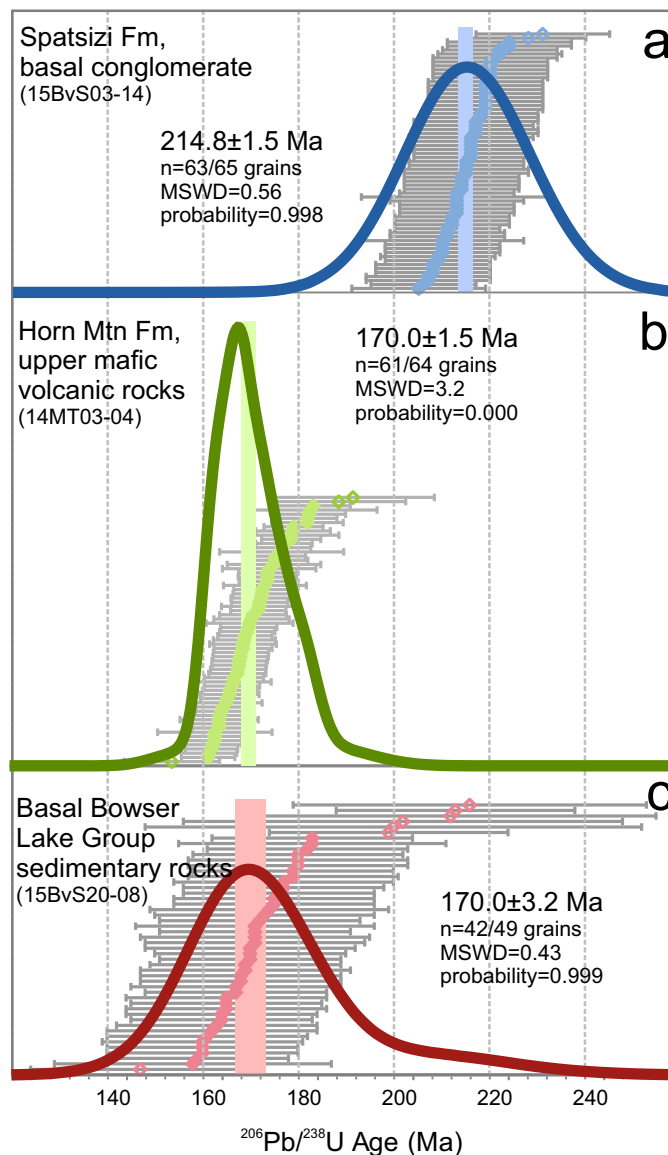


**Fig. 21.** Detrital zircon  $^{206}\text{Pb}/^{238}\text{U}$  age distribution plots, probability curves, and preliminary maximum depositional ages for: **a)** Spatsizi Formation basal sandstone and conglomerate unit (1mJSPcg); **b)** Horn Mountain Formation upper mafic volcanic unit (mJHMUvm); and **c)** Bowser Lake Group sandstone and conglomerate unit (mJBLs). The  $^{206}\text{Pb}/^{238}\text{U}$  ages are marked with coloured diamonds (open symbols are outliers excluded from age calculation) with two standard deviation analytical error represented by grey bars. The probability distribution is plotted with bold coloured lines and the mean age listed on the plots is represented by the coloured vertical line.

plagioclase-phyric mafic clasts, and cream-coloured silicified clasts. The latter clast type is likely derived from the Tanzilla alteration system. The sample returned an apparent unimodal detrital zircon peak with a preliminary maximum depositional age of  $170.0 \pm 1.5$  Ma (Fig. 21b). The preliminary maximum depositional age has a larger Mean Square Weighted Deviation (MSWD = 3.2) than expected for such a population (target MSWD = 1.37). This indicates that the scatter is greater than expected based on the precision of individual measurements,

**Table 4.** Geochronology results, sample descriptions and coordinates.

Sample no.	Unit	UTM	Type	Description	Population	Statistics	Age (Ma)
1	14MT-03-04 ( <i>lmJHMUvm</i> )	461,900E 6,464,420N	U-Pb Zrn LA-ICP-MS	Polymictic conglomerate with white (felsic/silicified) clasts and Aug-Pl-phyrlic clasts	61/64 analyses	MSWD=3.2 p=0.000	170.0 ±1.5 (MDA)
2	15BvS-02-04 ( <i>lmJSPv.po</i> )	461,753E 6,456,072N	-	Monomictic volcanic breccia with pale grey coarse platy Pl-phyrlic clasts	-	-	No Zrn
3	15BvS-03-14 ( <i>lmJSPcg</i> )	461,607E 6,455,278N	U-Pb Zrn LA-ICP-MS	Polymictic conglomerate with plutonic clasts and pale aphyric volcanic clasts	63/65 analyses	MSWD=0.56 p=0.998	214.8 ±1.5 (MDA)
4	15BvS-14-05 ( <i>LJSCgd</i> )	464,005E 6,463,656N	U-Pb Zrn CA-TIMS	Medium-grained equigranular Hbl-Bt tonalite	4/4 grains	MSWD=1.02 p=0.38	160.43 ±0.16
5	15BvS-20-07 ( <i>MJqd</i> )	461,054E 6,464,384N	Ar-Ar white mica	Intensely Qtz-Ser altered rock with coarse white mica	4/14 steps 39.4% <sup>39</sup> Ar	MSWD=1.01 p=0.39	135.83 ±0.44
6	15BvS-20-08 ( <i>mJBLs</i> )	461,225E 6,464,919N	U-Pb Zrn LA-ICP-MS	Polymictic conglomerate and sandstone	5/14 steps 16% <sup>39</sup> Ar	MSWD=0.97 p=0.42	144.6 ±1.9
7	TZ15-01 352.26-373.43m ( <i>MJap</i> )	461,335E 6,464,490N	U-Pb Zrn CA-TIMS	Syn-hydrothermal Pl porphyry with 25% 1-3 mm Pl, locally 1-2 mm equant mafic grains visible. Chl-Ser-Py altered	42/49 analyses	MSWD=0.43 p=0.999	170.0 ±3.2 (MDA)
7	TZ15-01 488.65-489.00m ( <i>MJap</i> )	461,335E 6,464,490N	Re-Os Mo	Anh-Py-Mo vein in Qtz-Ser-Py altered Pl porphyry	5/5 grains	MSWD=0.94 p=0.44	173.25 ±0.13
8	16BvS-15-111a ( <i>lmJHMLMvm</i> )	468,732E 6,454,418N	U-Pb Zrn LA-ICP-MS	Felsic lapilli tuff with abundant aphyric to Pl-phyrlic clasts	20/20 analyses	MSWD=0.80 p=0.71	Ages did not replicate 215.5 ±1.4 (MDA)

Sample numbers 1-8 correspond to labels in Fig. 2. UTM coordinates in NAD 83, zone 9 north. Mineral abbreviations after Kretz (1983); Ser = sericite; MDA = maximum depositional age. Age for TZ15-01 488.65-489.00 m reported in van Straaten and Nelson (2016).

suggesting that 1) all grains are not of the same true age, or 2) uncertainty is underestimated. The peak on the probability curve for this sample is ca. 168 Ma, suggesting that the maximum depositional age for this sample is at least as young as ca. 168 Ma.

A conglomerate near the base of the Bowser Lake Group north of Tanzilla (sample 15BvS-20-08) contains abundant clasts of plagioclase porphyry, some of which are pyritic. Analytical results show a unimodal detrital zircon peak with a preliminary maximum depositional age of  $170.0 \pm 3.2$  Ma (Fig. 21c).

### 7.2. Middle Jurassic intrusive units

Below we present field descriptions from three U-Pb LA-ICP-MS zircon geochronological sample locations reported by Takaichi (2013a; b).

Takaichi (2013a; b) described sample CNJ-0059 as a monzonite with propylitic chlorite alteration and reported an age of  $172.75 \pm 0.07$  Ma. The sample site exposes an unaltered equigranular medium-grained (2-4 mm) biotite-bearing hornblende quartz monzonite with microdiorite xenoliths that we consider part of the Three Sisters pluton central felsic phase.

Sample CNJ-0043, which was described as an unaltered syenite, yielded an age of  $177.13 \pm 0.59$  Ma (Takaichi, 2013a; b). At the sample site is an equigranular medium-grained (2-4 mm) biotite-bearing hornblende quartz monzodiorite with local weak epidote and chlorite alteration that we also consider part of the Three Sisters pluton central felsic phase. The reported age is unusually old for the Three Sisters plutonic suite, which has a typical age range of ca. 173-169 Ma (Table 2).

Takaichi (2013a; b) described sample CNJ-0054 as a monzonite with propylitic epidote alteration, and reported an age of  $168.57 \pm 0.54$  Ma. The lithology at the sample site is a biotite-bearing hornblende monzogranite with plagioclase, hornblende and biotite phenocrysts set in a fine-grained sugary groundmass that we include in the potassic phase of the Three Sisters pluton.

### 7.3. Late Jurassic intrusive units

A sample of medium-grained equigranular hornblende-biotite tonalite from the southwestern part of the Snowdrift Creek pluton returned a preliminary age of  $160.43 \pm 0.16$  Ma (Fig. 22).

### 7.4. Tanzilla alteration and mineralization

We attempted to establish the timing of alteration and mineralization at the Tanzilla prospect using U-Pb, Re-Os, and Ar-Ar geochronology. A syn-mineral augite-bearing plagioclase porphyry at Tanzilla (sample TZ15-01 352.26-373.43 m) returned a U-Pb zircon age of  $173.25 \pm 0.13$  Ma (Table 4; see van Straaten and Nelson; 2016).

We collected a sample of anhydrite-pyrite-molybdenite vein in quartz-sericite-pyrite altered plagioclase porphyry from drill hole TZ15-01 for Re-Os analysis (sample TZ15-01 488.65-489.00 m, Table 4; van Straaten and Nelson, 2016).

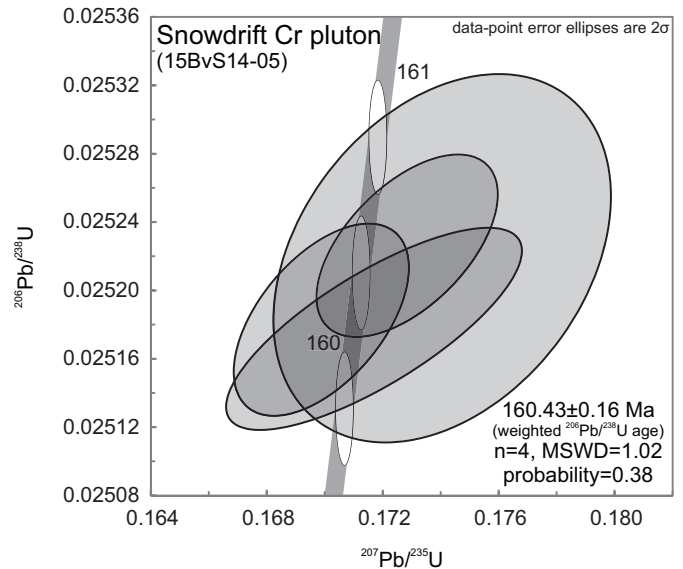


**Fig. 22.** Uranium-lead zircon concordia diagram showing chemical abrasion thermal ionization mass spectrometry results from the Snowdrift Creek pluton.

The analytical results did not properly replicate, and no final age could be calculated (R. Creaser, pers. comm., 2016). This indicates a heterogeneous molybdenite separate, which could have resulted from more than one molybdenite crystallization event.

A strongly quartz-sericite altered rock with coarse white mica was submitted for Ar-Ar analysis. The sample was collected 375 m northwest of the peak at Tanzilla, in a large advanced argillic alteration zone. The sample did not yield a robust plateau age (Fig. 23), suggesting that the rock has been disturbed. A

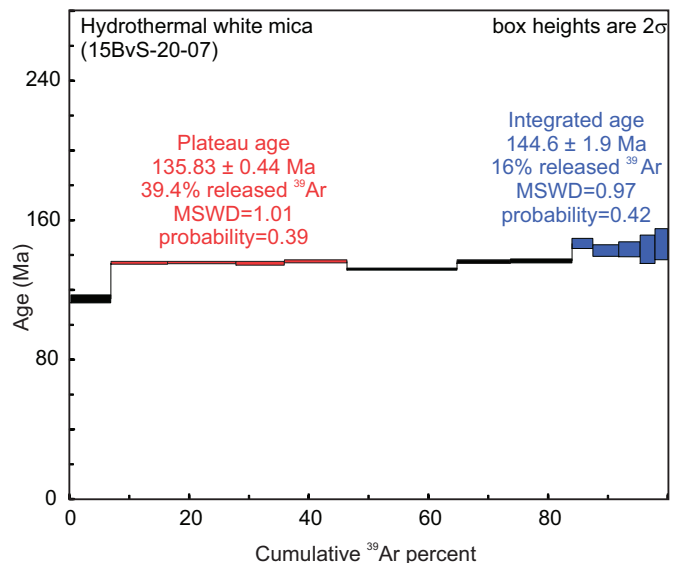


**Fig. 23.** White mica argon-argon step-heating spectrum from strongly quartz-sericite altered rocks at Tanzilla. This sample did not yield a robust plateau age. Weighted mean ages for younger and older steps are identified in red and blue, respectively.

preliminary plateau age of the younger steps ( $135.83 \pm 0.44$  Ma) probably indicates the disturbance. An integrated age of the last five steps ( $144.60 \pm 1.9$  Ma) only comprises 16% of the total  $^{39}\text{Ar}$  released, but may be related to the original age. These ages do not correlate with known Middle Jurassic (ca. 177-169 Ma), Late Jurassic (ca. 160-152 Ma) and Upper Cretaceous to Paleocene (ca. 65-63 Ma) intrusive ages in the region (see Table 2 and references therein). The closest age determinations are K-Ar cooling ages for the Snowdrift Creek pluton, which range from  $160.8 \pm 2.5$  Ma (hornblende),  $157.8 \pm 2.4$  Ma (biotite; Gabrielse, 1998), to  $147 \pm 5$  Ma (biotite; Stevens et al., 1982). We tentatively interpret that the disturbed ages represent resetting due to intrusion of the nearby Snowdrift Creek pluton, possibly followed by slow cooling.

## 8. Discussion

### 8.1. Regional extent and significance of the Horn Mountain Formation

The Horn Mountain Formation postdates widespread arc volcanism recorded in lower part of the Hazelton Group. Volcanic rocks are rare in the upper part of the Hazelton Group. In northern Stikinia, the upper part of the Hazelton Group consists mainly of Pliensbachian and younger sedimentary rocks assigned to the Nilkitkwa and Smithers formations in the south and the Spatsizi Formation in the north; both are succeeded by the Quock Formation (Gagnon et al., 2012). Volcanic rocks are mainly in a narrow, north-south oriented belt of tholeiitic pillow basalts, sedimentary rocks, and minor rhyolites assigned to the Iskut River Formation (Gagnon et al., 2012; Barresi et al., 2015a). This Middle Jurassic (Aalenian to Bajocian) succession is interpreted to have formed in a series of sub-basins that define the Eskay rift (Fig. 1). The Iskut River Formation contrasts markedly with the Horn Mountain Formation in lithology, depositional style, structural setting and litho-geochemistry (van Straaten and Nelson, 2016). The Horn Mountain Formation represents a unique volcanic sequence in the upper part of the Hazelton Group. It is coeval with accretion of the Stikine and Cache Creek terranes, and so far, similar volcanic successions have not been documented elsewhere in northern Stikinia. Evaluation of the regional literature indicates that the Horn Mountain Formation may continue for up to 110 km, as a west-northwest to east-southeast trending belt along and near the northeastern margin of Stikinia (Fig. 1; van Straaten and Nelson, 2016).

### 8.2. Alteration and mineralization

At least three magmatic-hydrothermal events are recognized in the map area. The first event was responsible for porphyry copper mineralization in the Gnat Pass and Moss area (Fig. 20). The occurrences are in, or immediately adjacent to, plagioclase porphyry intrusions (Late Triassic; Table 2). Porphyry-style tourmaline-K-feldspar alteration and chalcopyrite mineralization extends for 4.3 km in a west-northwest direction. The WNW-trending hydrothermal veins and breccia zones, east-west elongate Cake Hill pluton, and north-trending

Gnat Pass reverse shear zone are compatible with north-south extension. The 1.2 billion tonne Schaft Creek porphyry copper deposit (Fig. 1; Scott et al., 2008; Farah et al., 2013) shares several characteristics with the Gnat Pass and Moss porphyry occurrences. Both have a Late Triassic age, contain copper and minor molybdenum and gold, host appreciable tourmaline, are located immediately adjacent to a several thousand square kilometre Late Triassic pluton, and show veins and hydrothermal breccia zones that trend parallel to the long axis of the adjacent batholith.

Several alteration zones in Horn Mountain volcanic rocks are attributed to a Middle Jurassic magmatic-hydrothermal event, including porphyry-style alteration at Tanzilla and McBride (Fig. 20). At Tanzilla, advanced argillic alteration overlies intermediate argillic, argillic and phyllic assemblages. In deep drilling, rare potassic mineral assemblages and anomalous copper and molybdenum values were intersected. The McBride mineral occurrence displays widespread surface quartz-sericite-pyrite alteration with local potassic alteration. The zone of advanced argillic alteration at Tanzilla is at the contact between the middle maroon volcanic and upper felsic volcanic unit (van Straaten and Nelson, 2016). This year's mapping found that the zone of advanced argillic alteration extends for at least 17 km from Tanzilla to the new Straight-across mineral occurrence (Fig. 20). The Gopher zone, Mo east to Straight-up segment of the alteration zone is variably sheared, and – where identifiable – the protolith is a coarse platy plagioclase porphyry. We tentatively interpret the Gopher, Mo east, Straight-up and Straight-across zones to be formed by fluid channelling along a local unconformity or fault zone. The advanced argillic lithocap formed by acidic fluids related to possible porphyry-fertile intrusions at depth. In addition to porphyry-style and advanced argillic alteration zones, epithermal veins are found at the And ginger and Wolf showings. They may have been cogenetic with the porphyry occurrences.

Before studies in the Tanzilla and McBride area, no Middle Jurassic porphyry-style mineral occurrences had been documented in the Canadian Cordillera. Based on mapping and geochronological studies at Tanzilla, van Straaten and Nelson (2016) proposed that this magmatic event represents a potential new metallogenic epoch prospective for porphyry- and epithermal-style mineralization. Notably, copper-gold mineralization hosted in the Teslin Crossing pluton at Mars (65 km northeast of Whitehorse, Yukon; New Dimension Resources Ltd., 2012) has recently been reported to be Middle Jurassic (Colpron et al., 2016a); it may provide further support for a Middle Jurassic porphyry-style metallogenic epoch in the Canadian Cordillera.

A third magmatic-hydrothermal event is represented in the Snowdrift Creek pluton (Late Jurassic) and an interpreted satellite stock. These include the Nup, Mo and Joyce showings (Fig. 20); all are characterized by quartz-molybdenite±chalcopyrite veins and molybdenite-coated fractures associated with variable alteration styles.

### 8.3. Tectonic evolution and origin of the Horn Mountain Formation

During the Mesozoic, three main phases of magmatic arc development took place in Stikinia, punctuated by collisional events. The Stuhini arc (Late Triassic) was succeeded by the latest Triassic to Early Jurassic main-stage Hazelton arc. The youngest, Toarcian to Late Jurassic, arc is represented by widespread volcanic rocks in southern and central Stikinia (Fig. 1).

During the Late Triassic, voluminous magmatism was predominant along the northern to eastern margin (current reference frame) of Stikinia, resulting in eruption of Stuhini Group augite-phyric mafic volcanic rocks and intrusion of the Stikine plutonic suite (Woodsworth et al., 1991). The arc likely formed as a result of subduction below the northern to eastern margins of Stikinia (Nelson and Mihalynuk, 1993; Mihalynuk et al., 1994; Colpron et al., 2015). Profound plate rearrangement at the end of the Triassic is marked by the cessation of volcanism on the northern margin of Stikinia, followed by arc uplift and erosion. At this time, the northern end (present coordinates) of Stikinia collided with far northern Quesnellia and the Yukon-Tanana terrane, with strata of the Whitehorse trough deposited across all three terranes and adjacent parts of the Cache Creek terrane (Johannson et al., 1997; Mihalynuk et al., 2004; Colpron et al., 2015).

Reconfigured subduction in the latest Triassic to Early Jurassic created two belts of arc-related lower Hazelton Group volcanic rocks in north-central Stikinia south of the Pitman fault. The volcanic arcs are interpreted to have formed by opposing subduction on either side of the Stikinia microplate, creating a western and eastern volcanic belt separated by a central belt of predominantly sedimentary rocks interpreted as the Hazelton trough (Fig. 1; Marsden and Thorkelson, 1992). Volcanism waned in the Pliensbachian and ended in the late Toarcian (Alldrick, 1993; Brown et al., 1996; Barresi et al., 2015b) as Stikinia accreted with neighbouring terranes to the east and west (Nelson et al., 2013). A final episode of arc-related volcanism in Toarcian-Callovia time created a belt of volcanic and intrusive rocks in central and southern Stikinia (Fig. 1; Tipper and Richards, 1976; Diakow and Webster, 1994; MacIntyre et al., 2001). The Horn Mountain Formation rocks are coeval with the youngest arc succession, but the formation is near the northeastern margin of the terrane, close to the Cache Creek-Stikinia suture.

Timing of the Cache Creek-Stikinia collision is constrained as late Early to Middle Jurassic. The youngest Cache Creek cherts that have been overprinted by blueschist-facies, sodic amphibole-bearing metamorphic assemblages are Pliensbachian to Toarcian (Mihalynuk et al., 2004). Argon-argon cooling ages on phengite in blueschist mineral assemblages indicate that the central part of the orogenic welt was exhumed by  $173.7 \pm 0.8$  Ma (Aalenian; Mihalynuk et al., 2004). Deposition of Cache Creek-derived chert clast-bearing conglomerate in the Bowser Basin started in the early Bajocian (Ricketts et al., 1992). Thus, the Cache Creek accretionary complex became the site of a

southwest-vergent tectonic welt that began to shed debris into the Bowser foreland basin in the early Bajocian (ca. 169 Ma).

The Horn Mountain Formation volcanic rocks and their local correlatives were probably not the products of normal subduction-related arc magmatism for several reasons. First, subduction was not taking place below northern Stikinia at the time of collision. Subduction below the northern margin of Stikinia ceased in the Late Triassic, followed by slab breakoff soon thereafter (Logan and Mihalynuk, 2014). Subduction below the western and eastern margins of Stikinia waned in the Pliensbachian and ended in the Toarcian. Second, the Horn Mountain Formation rocks are younger than any known volcanic successions of arc affinity in northern Stikinia. In the north, rocks of the upper part of the Hazelton Group are either mainly sedimentary (Spatsizi and Quock formations), or of bimodal volcanic-sedimentary character (Iskut River Formation in the Eskay rift). Third, the Horn Mountain volcanic succession is in the foreland adjacent to the Stikinia-Cache Creek collisional boundary (King Salmon fault), and was erupted between ca. 176 and 169 Ma, during collision. They interfinger with synorogenic clastic strata of the Bowser Lake Group (van Straaten and Nelson, 2016), and are intruded by a 173-160 Ma belt of plutons that cut the Stikinia-Cache Creek suture zone. Lithogeochemical data show that the Middle Jurassic calc-alkaline plutons (Mihalynuk et al., 1992; van Straaten et al., 2012) and Horn Mountain Formation (Logan and Iverson, 2013; B. van Straaten et al., unpublished data) are of volcanic arc chemistry. We put forward the preliminary hypothesis that the Horn Mountain Formation formed by re-melting of subduction-modified lithosphere due to collision between the Stikine and Quesnel terranes. Similar to typical subduction-related arc volcanism, postsubduction (syncollisional) arc-like volcanism has been shown to produce porphyry- and epithermal-style mineral deposits (Richards, 2009).

### 9. Conclusions

The Horn Mountain Formation, a previously poorly understood volcanic succession on the northeastern margin of Stikinia, hosts several early-stage porphyry copper exploration projects. Geological mapping and preliminary geochronology indicate that the oldest rocks in the field area are mafic volcanic rocks of the Stuhini Group (Triassic), cut by the Cake Hill pluton (Late Triassic). An at least 50 km-long regional unconformity cuts into the Cake Hill pluton. It represents one of the few well-documented examples of unroofed Stuhini arc in northern Stikinia.

The erosional surface is overlain by a moderately north-northeast dipping volcano-sedimentary succession assigned to the upper part of the Hazelton Group. It includes a lower (up to 1 km-thick) sedimentary sequence grouped with the Spatsizi Formation, and an upper (up to 5.4 km-thick) volcanic sequence assigned to the Horn Mountain Formation. The volcanic rocks are unusual within northern Stikinia as they postdate widespread arc volcanism of the lower part of the Hazelton Group, are coeval with deposition of predominantly

sedimentary rocks of the upper part of the Hazelton Group, and are concurrent with accretion of the Stikine and Cache Creek terranes. Sedimentary rocks of the Spatsizi Formation (late Pliensbachian to Toarcian) grade laterally and vertically to mafic volcanic breccia and rare pillows of the lower part of the Horn Mountain Formation. They were, at least in part, deposited in a subaqueous environment. Overlying interlayered flows, volcanic breccia and tuff of the middle maroon volcanic unit represent increasingly higher volume volcanism that led to formation of a subaerial volcanic edifice. Lower and middle units are cut by cogenetic feeder dikes and intrusions. During an erosional hiatus in volcanism the volcanic units were cut and hydrothermally altered by a 173 Ma (Aalenian) porphyry intrusion. An upper mafic volcanic unit (Bajocian) caps the succession. The Horn Mountain Formation is unconformably overlain by Bowser Lake Group conglomerates (Bajocian) and cut by the Three Sisters pluton (ca. 173-169 Ma)

The Horn Mountain Formation hosts two early-stage porphyry projects. At Tanzilla, an advanced argillic lithocap overlies porphyry-style alteration at depth. At the McBride mineral occurrence widespread quartz-sericite-pyrite and local potassic alteration is associated with elevated copper and gold. Our field studies have extended the advanced argillic alteration at Tanzilla for at least 17 km along strike. It is interpreted as a lithocap formed by acidic hydrothermal fluid flow along an unconformity or fault in the upper part of the Horn Mountain Formation.

The Kehlechoa thrust fault places siliciclastic rocks of the Whitehorse trough (Takwahoni Formation, Pliensbachian) above the Horn Mountain Formation and Bowser Lake Group. The hanging wall panel is internally folded and imbricated. Regionally, the sedimentary rocks record unroofing of the Stuhini arc. The Snowdrift Creek pluton (Late Jurassic) cuts the Kehlechoa fault, and constrains movement on the foreland thrust of the Stikine-Quesnel accretionary belt to ca. 170-160 Ma.

The Horn Mountain Formation and Three Sisters plutonic suite are coeval with accretion of the Stikine and Quesnel island arcs. The syncollisional Middle Jurassic magmatic event represents a potential new metallogenic epoch for the Canadian Cordillera and is prospective for porphyry- and epithermal-style mineralization.

### Acknowledgments

We thank Erin Bros and Carly Smythe for their capable and enthusiastic assistance during the field season, and Lakelse Air for safe flying. Quartz Mountain Resources Ltd. and Bearclaw Capital Corp. are acknowledged for permission to use field data collected by the first author in 2012 while employed by Hunter Dickinson Inc. Special thanks to JoAnne Nelson for her mentorship, initiating the Tanzilla project in 2015, and constructive commentary that significantly improved the manuscript. We also thank Terry Poulton (Geological Survey of Canada, Calgary) for providing preliminary macrofossil age determinations, Andrew Caruthers and Christopher McRoberts

for discussions regarding ammonite and bivalve collections, and Richard Friedman and Janet Gabites (University of British Columbia, Vancouver) for providing preliminary U-Pb zircon and Ar-Ar geochronology results.

### References cited

- Aeroquest Airborne, 2012. Report on a helicopter-borne magnetic survey (Aeroquest Job #11-046) for Geoscience BC. Geoscience BC Report 2012-2, 11p.
- Alldrick, D.J., 1993. Geology and metallogeny of the Stewart mining camp, northwestern British Columbia. British Columbia Ministry of Energy, Mines and Petroleum Resources, British Columbia Geological Survey Bulletin 85, 105p.
- Anderson, R.G., 1983. Geology of the Hotailuh batholith and surrounding volcanic and sedimentary rocks, north-central British Columbia. Unpublished Ph.D. thesis, Carleton University, Ottawa, Ontario, Canada, 669p.
- Anderson, R.G., and Bevier, M.L., 1992. New late Triassic and early Jurassic U-Pb zircon ages from the Hotailuh Batholith, Cry Lake map area, North - Central British Columbia. In: Radiogenic age and isotopic studies: Report 6, Geological Survey of Canada Paper 92-02, pp. 145-152.
- Andrzejewski, A., and Bui, P., 2012. Geochemical, and Geophysical Work on the GALAXIE Property. British Columbia Ministry of Energy and Mines, Assessment Report 33659, 39p.
- Ball, C.W., and Ashton, J.M., 1982. Geochemical report on Drift group mineral claims. British Columbia Ministry of Energy and Mines, Assessment Report 10356, 20p.
- Barresi, T., 2008. Diamond drilling report on the MO property (MO mineral claims). British Columbia Ministry of Energy and Mines, Assessment Report 30933, 22p.
- Barresi, T., 2009. Rock and Stream Sediment Geochemistry on the JD Mineral Claims (JD 1-4, 6-9, 13-14, & 19-27 Mineral Claims). British Columbia Ministry of Energy and Mines, Assessment Report 30590, 18p.
- Barresi, T., Bradford, J., and Luckman, N., 2014. 2014 Diamond drilling report on the Tanzilla property, northwestern British Columbia. British Columbia Ministry of Energy and Mines, Assessment Report 35471, 46p.
- Barresi, T., Nelson, J.L., and Dostal, J., 2015a. Geochemical constraints on magmatic and metallogenic processes: Iskut River Formation, volcanogenic massive sulfide-hosting basalts, NW British Columbia, Canada. *Canadian Journal of Earth Sciences*, 52, 1-20.
- Barresi, T., Nelson, J.L., Dostal, J., and Friedman, R., 2015b. Evolution of the Hazelton arc near Terrace, British Columbia: stratigraphic, geochronological, and geochemical constraints on a Late Triassic – Early Jurassic arc and Cu–Au porphyry belt. *Canadian Journal of Earth Sciences*, 52, 466-494.
- Bowen, B.K., 2013. Technical report on the Galaxie project. Liard Mining Division, British Columbia, Canada. NI 43-101 Report prepared for Quartz Mountain Resources Ltd., 140p.
- Bradford, J., 2008. Rock, silt and soil geochemistry on the MO property (MO mineral claims). British Columbia Ministry of Energy and Mines, Assessment Report 29545, 16p.
- British Columbia Geological Survey, 2016. MINFILE - British Columbia mineral inventory database. Available from <http://minfile.gov.bc.ca/>.
- Brown, D.A., Gunning, M.H., and Greig, C.J., 1996. The Stikine project: Geology of western Telegraph Creek map area, northwestern British Columbia. British Columbia Ministry of Employment and Investment, British Columbia Geological Survey Bulletin 95, 130p.
- Cohen, K.M., Finney, S.C., Gibbard, P.L., and Fan, J.-X., 2013. The ICS International Chronostratigraphic Chart. *Episodes*, 36, 199-204. Updated version (December, 2016) available from <http://>

- www.stratigraphy.org/.
- Colpron, M., Crowley, J.L., Gehrels, G., Long, D.G.F., Murphy, D.C., Beranek, L., and Bickerton, L., 2015. Birth of the northern Cordilleran orogen, as recorded by detrital zircons in Jurassic synorogenic strata and regional exhumation in Yukon. *Lithosphere*, 7, 541–562.
- Colpron, M., Israel, S., and Friend, M., 2016b. Yukon plutonic suites. Yukon Geological Survey, Open File 2016-37, scale: 1:750,000.
- Colpron, M., Sack, P.J., Crowley, J.L. and Murray M.A., 2016a. Late Triassic to Middle Jurassic magmatism in the Intermontane terranes of Yukon. The Geological Society of America, Annual Meeting, Denver, Colorado, USA. doi:10.1130/abs/2016AM-280151.
- Diakow, L.J., and Webster, I.C.L., 1994. Geology of Fawnie Creek map area (NTS 93F/3). In: *Geological Fieldwork 1993*, British Columbia Ministry of Energy, Mines and Petroleum Resources, British Columbia Geological Survey Paper 1994–1, pp. 15–26.
- Dickinson, W.R., and Gehrels, G.E., 2009. Use of U–Pb ages of detrital zircons to infer maximum depositional ages of strata: A test against a Colorado Plateau Mesozoic database. *Earth and Planetary Science Letters*, 288, 115–125.
- Evenchick, C.A., and Thorkelson, D.J., 2005. Geology of the Spatsizi River map area, north-central British Columbia. *Geological Survey of Canada Bulletin 577*, 276p.
- Evenchick, C.A., McMechan, M.E., McNicoll, V.J., and Carr, S.D., 2007. A synthesis of the Jurassic-Cretaceous tectonic evolution of the central and southeastern Canadian Cordillera: Exploring links across the orogen. In: *Sears, J.W., Harms, T.A., and Evenchick, C.A., (Eds.), Whence the Mountains? Inquiries into the Evolution of Orogenic Systems: A Volume in Honour of Raymond A. Price*: Geological Society of America, Special Paper 433, 117–145.
- Farah, A., Friedman, D., Yang, D., Pow, D., Trout, G., Ghaffari, H., Stoyko, H.W., Huang, J., Karrei, L., Danon-Schaffer, M., Morrison, R.S., da Palma Adanjo, R., and Hafes, S.A., 2013. Feasibility study on the Schaft Creek Project, BC, Canada. NI 43-101 Report prepared for Copper Fox Metals Inc., 604p.
- Gabrielse, H., 1998. Geology of Cry Lake and Dease Lake map areas, North-Central British Columbia. *Geological Survey of Canada Bulletin 504*, 147p.
- Gagnon, J.-F., Barresi, T., Waldron, J.W.F., Nelson, J.L., Poulton, T.P., and Cordey, F., 2012. Stratigraphy of the upper Hazelton Group and the Jurassic evolution of the Stikine terrane, British Columbia. *Canadian Journal of Earth Sciences*, 49, 1027–1052.
- Gillespie, M.R., and Styles, M.T., 1999. BGS rock classification scheme. Volume 1. Classification of igneous rocks. *British Geological Survey Research Report RR99-06*, 52p.
- Gladney, E.S., and Roelands, I., 1990. 1988 Compilation of Elemental Concentration Data for USGS Geochemical Exploration Reference Materials GXR-1 to GXR-6. *Geostandards Newsletter*, 14, 21–118.
- Graham, J.D., 1982. Geochemical report on Drift group mineral claims. British Columbia Ministry of Energy and Mines, Assessment Report 10923, 11p.
- Hallsworth, C.R., and Knox, R.W.O., 1999. BGS rock classification scheme. Volume 3. Classification of sediments and sedimentary rocks. *British Geological Survey Research Report RR99-03*, 44p.
- Henderson, C.M., and Perry, D.G., 1981. A Lower Jurassic heteropodid bryozoan and associated biota, Turnagain Lake, British Columbia. *Canadian Journal of Earth Sciences*, 18, 457–468.
- Iverson, O., Mahoney, J.B., and Logan, J.M., 2012. Dease Lake geoscience project, part IV: Tsaybahe group: Lithological and geochemical characterization of Middle Triassic volcanism in the Stikine arch, north-central British Columbia. In: *Geological Fieldwork 2011*, British Columbia Ministry of Energy, Mines and Natural Gas, British Columbia Geological Survey Paper 2012–1, pp. 17–22.
- James, G.L., and Westervelt, R.D., 1970. West joint venture 1970 summary field report Gnat Creek area, British Columbia. British Columbia Ministry of Energy and Mines, Property File 650340, 14p.
- Johannson, G.G., Smith, P.L., and Gordey, S.P., 1997. Early Jurassic evolution of the northern Stikinian arc: evidence from the Laberge Group, northwestern British Columbia. *Canadian Journal of Earth Sciences*, 34, 1030–1057.
- Jutras, G., Bickerton, L., Stock, L., Thompson, V., and Beckman, S., 2014. Assessment report on geological, geochemical and geophysical work conducted during July and August 2014 on the McBride mineral tenure. British Columbia Ministry of Energy and Mines, Assessment Report 35038, 40p.
- Kaizen Discovery Inc., 2015. Kaizen reports 2015 exploration drill results from its British Columbia projects. News release, November 3, 2015. Available from <http://www.kaizendiscovery.com/>.
- Kretz, R., 1983. Symbols for rock-forming minerals. *American Mineralogist*, 68, 227–279.
- Logan, J.M., and Iverson, O., 2013. Dease Lake geoscience project: Geochemical characterization of Tsaybahe, Stuhini and Hazelton volcanic rocks, northwestern British Columbia (NTS 104I, J). In: *Summary of Activities 2012*, Geoscience BC Report 2013–1, pp. 11–32.
- Logan, J.M., and Mihalynuk, M.G., 2014. Tectonic controls on Early Mesozoic paired alkaline porphyry deposit belts (Cu–Au±Ag–Pt–Pd–Mo) within the Canadian Cordillera. *Economic Geology*, 109, 827–858.
- Logan, J.M., Moynihan, D.P., and Diakow, L.J., 2012a. Dease Lake geoscience project, Part I: Geology and mineralization of the Dease Lake (NTS 104J/08) and East-Half of the Little Tuya River (NTS 104J/07E) map sheets, northern British Columbia. In: *Geological Fieldwork 2011*, British Columbia Ministry of Energy, Mines and Natural Gas, British Columbia Geological Survey Paper 2012–1, pp. 23–44.
- Logan, J.M., Moynihan, D.P., Diakow, L.J., and van Straaten, B.I., 2012b. Dease Lake - Little Tuya River geology (NTS 104J/08, 07E). British Columbia Ministry of Energy, Mines and Natural Gas, British Columbia Geological Survey Open File 2012-04, scale: 1:50,000.
- Luckman, N., Celiz, M.A.D., Wetherup, S., and Walcott, P., 2013. Induced polarization, terraspec and structural surveys on the Tanzilla property. British Columbia Ministry of Energy and Mines, Assessment Report 34550, 24p.
- Ludwig, K.R., 2012. Isoplot 3.75 – A geochronological toolkit for Microsoft Excel. *Berkley Geochronology Center Special Publication 5*, 75p.
- Lytton Minerals, 1969. Moss property geology of trenches 3, 4, 5, 6, 7, 8, 9. British Columbia Ministry of Energy and Mines, Property File 19795, 1p.
- MacIntyre, D.G., Villeneuve, M.E., and Schiarizza, P., 2001. Timing and tectonic setting of Stikine Terrane magmatism, Babine-Takla lakes area, central British Columbia. *Canadian Journal of Earth Sciences*, 38, 579–601.
- Marsden, H., and Thorkelson, D.J., 1992. Geology of the Hazelton Volcanic Belt in British Columbia: Implications for the Early to Middle Jurassic evolution of Stikinia. *Tectonics*, 11, pp. 1266–1287.
- Mihalynuk, M.G., Erdmer, P., Ghent, E.D., Cordey, F., Archibald, D.A., Friedman, R.M., and Johannson, G.G., 2004. Coherent French Range blueschist: Subduction to exhumation in <2.5 m.y.? *Geological Society of America Bulletin*, 116, 910.
- Mihalynuk, M.G., Nelson, J., and Diakow, L.J., 1994. Cache Creek terrane entrapment: Oroclinal paradox within the Canadian Cordillera. *Tectonics*, 13, 575.
- Mihalynuk, M.G., Smith, M.T., Gabites, J.E., Runkle, D., and Lefebure, D., 1992. Age of emplacement and basement character of the Cache Creek terrane as constrained by new isotopic and

- geochemical data. *Canadian Journal of Earth Sciences*, 29, 2463–2477.
- Nelson, J., and Mihalynuk, M., 1993. Cache Creek ocean: Closure or enclosure? *Geology*, 21, 173–176.
- Nelson, J., Colpron, M., and Israel, S., 2013. The Cordillera of British Columbia, Yukon and Alaska: tectonics and metallogeny. In: Colpron, M., Bissig, T., Rusk, B., and Thompson, J.F.H. (Eds.), *Tectonics, metallogeny and discovery: the North American cordillera and similar accretionary settings.*, Society of Economic Geologists, Special Publication 17, pp. 53–109.
- New Dimension Resources Ltd., 2012. New Dimension Receives Encouraging Drill Results at Mars Project, Yukon. News release, January 11, 2012. Available from: <http://www.newdimensionresources.com/>.
- Noel, G.A., 1972. Geological-geochemical report on the Wolf 1-18 claims. British Columbia Ministry of Energy and Mines, Assessment Report 4498, 11p.
- Richards, J.P., 2009. Postsubduction porphyry Cu-Au and epithermal Au deposits: Products of remelting of subduction-modified lithosphere. *Geology*, 37, 247–250.
- Ricketts, B.D., Evenchick, C.A., Anderson, R.G., and Murphy, D.C., 1992. Bowser basin, northern British Columbia: Constraints on the timing of initial subsidence and Stikinia-North America terrane interactions. *Geology*, 20, 1119–1122.
- Roberts, K., Lang, J., van Straaten, B.I., Galicki, M., Takahashi, A., and Jessen, K.E.H., 2013. Assessment report on drilling program on the Galaxie property. British Columbia Ministry of Energy and Mines, Assessment Report 34230, 37p.
- Scott, J.E., Richards, J.P., Heaman, L.M., Creaser, R.A., and Salazar, G.S., 2008. The Schaft Creek porphyry Cu-Mo-(Au) deposit, northwestern British Columbia. *Exploration and Mining Geology* 17, 163–96.
- Smith, G., and Garagan, T., 1990. Summary report on the 1989 exploration program on the Gnat Pass property. British Columbia Ministry of Energy and Mines, Assessment Report 20408, 27p.
- Stevens, R.D., DeLabio, R.N., and Lachance, G.R., 1982. Age determinations and geological studies. In: K-Ar isotopic ages, report 15. Geological Survey of Canada Paper 81–2, p. 56.
- Stevenson, R.W., 1973a. Kennco Explorations, (Western) Limited, Report on geochemical survey. British Columbia Ministry of Energy and Mines, Assessment Report 4645, 6p.
- Stevenson, R.W., 1973b. Report on silt and rock geochemical survey. British Columbia Ministry of Energy and Mines, Assessment Report 4661, 9p.
- Takaichi, M., 2013a. Assessment Report on the 2012 Geological, Geochemical, Program at the McBride Property, BC, Canada. British Columbia Ministry of Energy and Mines, Assessment Report 34265, 17p.
- Takaichi, M., 2013b. Assessment Report on the 2012 Geological, Geochemical, and Geophysical Program at the Eagle Property, BC, Canada. British Columbia Ministry of Energy and Mines, Assessment Report 34266, 22p.
- Takaichi, M., and Johnson, C., 2012. Assessment report on the 2011/2012 geological and geophysical program at the Pitman property, BC, Canada. British Columbia Ministry of Energy and Mines, Assessment Report 33340, 23p.
- Thomson, R.C., Smith, P.L., and Tipper, H.W., 1986. Lower to Middle Jurassic (Pliensbachian to Bajocian) stratigraphy of the northern Spatsizi area, north-central British Columbia. *Canadian Journal of Earth Sciences*, 23, 1963–1973.
- Tipper, H.W., and Richards, T.A., 1976. Jurassic stratigraphy and history of north-central British Columbia. *Geological Survey of Canada Bulletin 270*, Geological Survey of Canada, 82p.
- van Straaten, B.I., and Nelson, J.L., 2016. Syncollisional late Early to early Late Jurassic volcanism, plutonism, and porphyry-style alteration on the northeastern margin of Stikinia. In: *Geological Fieldwork 2015*, British Columbia Ministry of Energy and Mines, British Columbia Geological Survey Paper 2016–1, pp. 113–143.
- van Straaten, B.I., Logan, J.M., and Diakow, L.J., 2012. Mesozoic magmatism and metallogeny of the Hotailuh Batholith, northwestern British Columbia. British Columbia Ministry of Energy, Mines and Natural Gas, British Columbia Geological Survey Open File 2012-06, 58p.
- Woodsworth, G.J., Anderson, R.G., Armstrong, R.L., Struik, L.C., and van der Heyden, P., 1991. Chapter 15: Plutonic Regimes. In: *Geology of the Cordilleran Orogen in Canada*. Gabrielse, H. and Yorath, C.J. (Eds.), Geological Survey of Canada, *Geology of Canada*, 4, pp. 491–531.
- Woolverton, R.W., 1967. West joint venture 1967 summary field report Gnat Creek area, British Columbia. British Columbia Ministry of Energy and Mines, Property File 650340, 21p.



# The Mount Hickman ultramafic complex: An Fe-rich Alaskan-type ultramafic intrusion



Dejan Milidragovic<sup>1, 2, a</sup>, Alex Zagorevski<sup>3</sup>, and John B. Chapman<sup>2</sup>

<sup>1</sup> present address, British Columbia Geological Survey, Ministry of Energy and Mines, Victoria, BC, V8W 9N3

<sup>2</sup> Geological Survey of Canada, 1500-605 Robson Street, Vancouver, BC, V6B 5J3

<sup>3</sup> Geological Survey of Canada, 601 Booth Street, Ottawa, ON, K1A 0E8

<sup>a</sup> corresponding author: Dejan.Milidragovic@gov.bc.ca

Recommended citation: Milidragovic, D., Zagorevski, A., and Chapman, J.B., 2017. The Mount Hickman ultramafic complex: An Fe-rich Alaskan-type ultramafic intrusion. In: Geological Fieldwork 2016, British Columbia Ministry of Energy and Mines, British Columbia Geological Survey Paper 2017-1, pp. 117-132.

**Abstract**

The Mount Hickman ultramafic complex (Triassic) is a composite Alaskan-type ultramafic pluton in Stikine terrane, northwestern British Columbia. Cumulate rocks in the complex are mainly olivine ± magnetite clinopyroxenite, but include subordinate serpentized dunite, wehrlite, and gabbro. Magnetite is a volumetrically significant primary phase, especially in magnetite-olivine clinopyroxenite, where it may constitute up to 40% by volume. In contrast to most other Alaskan-type intrusions, and terrestrial ultramafic plutons in general, the Mount Hickman ultramafic complex has an unusually high concentration of FeO<sup>TOT</sup>, including ~21 wt.% in dunite. We currently favour a model in which the high contents of FeO<sup>TOT</sup> in the Mount Hickman ultramafic complex reflect mixing of two types of magma: a relatively primitive ultramafic (picritic/basaltic silicate magma, and a dense Fe-Ti-P-rich highly oxidized magma.

**Keywords:** Hickman ultramafic complex, Alaskan-type intrusion, Triassic, Stikinia, cumulate

**1. Introduction**

The Stikine terrane (Paleozoic to Mesozoic) of the Canadian Cordillera (Fig. 1) experienced a period of arc building and extensive mineralization during the Middle to Late Triassic. This period was marked by ultramafic to intermediate volcanism and related sedimentation (Stuhini and Lewes River groups; Mihalynuk et al., 1999; Logan et al., 2000) and intermediate to felsic plutonism of both calc-alkaline (~228-215 Ma Stikine suite) and alkaline (~215-200 Ma; Copper Mountain suite) affinities (Woodsworth et al., 1991; Zagorevski et al., 2016). Alaskan-type mafic-ultramafic intrusions, defined by the association of olivine, clinopyroxene, and hornblende, and complete lack of orthopyroxene (Taylor, 1967; Nixon et al., 2015) represent a volumetrically minor component of this period. Nonetheless, their petrogenetic significance and relationship to coeval igneous rocks of Stikine terrane are poorly understood.

Woodsworth et al. (1991) introduced the term ‘Polaris suite’ for Late Triassic Alaskan-type intrusions in the northern Cordillera. However, more recent work has demonstrated that these intrusions formed from the Middle Triassic to the Early Jurassic (237 ± 2 Ma, Lunar Creek complex, Nixon et al., 1997; 186 ± 2 Ma, Polaris complex, Nixon et al., 1997; 190 ± 1 Ma Turnagain intrusion, Scheel, 2007) in both Stikine and Quesnel terranes. Because of potential confusion about use of ‘Polaris suite’, we avoid the term in this paper.

The Mount Hickman ultramafic complex is an Alaskan-type intrusion exposed on the southeastern margin of the Hickman pluton (Fig. 2; ~220-222 Ma; Holbek 1988; Nixon et al., 1989;

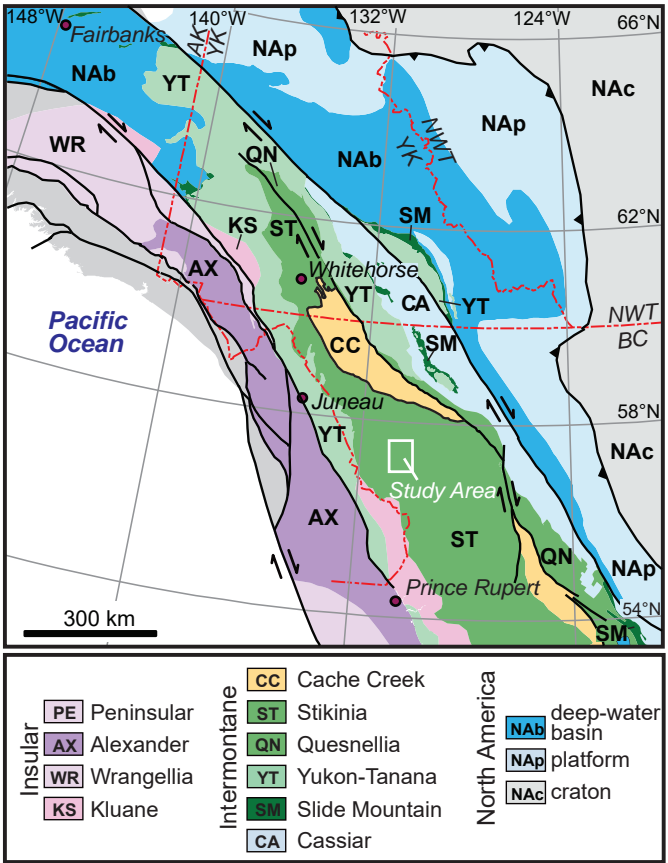
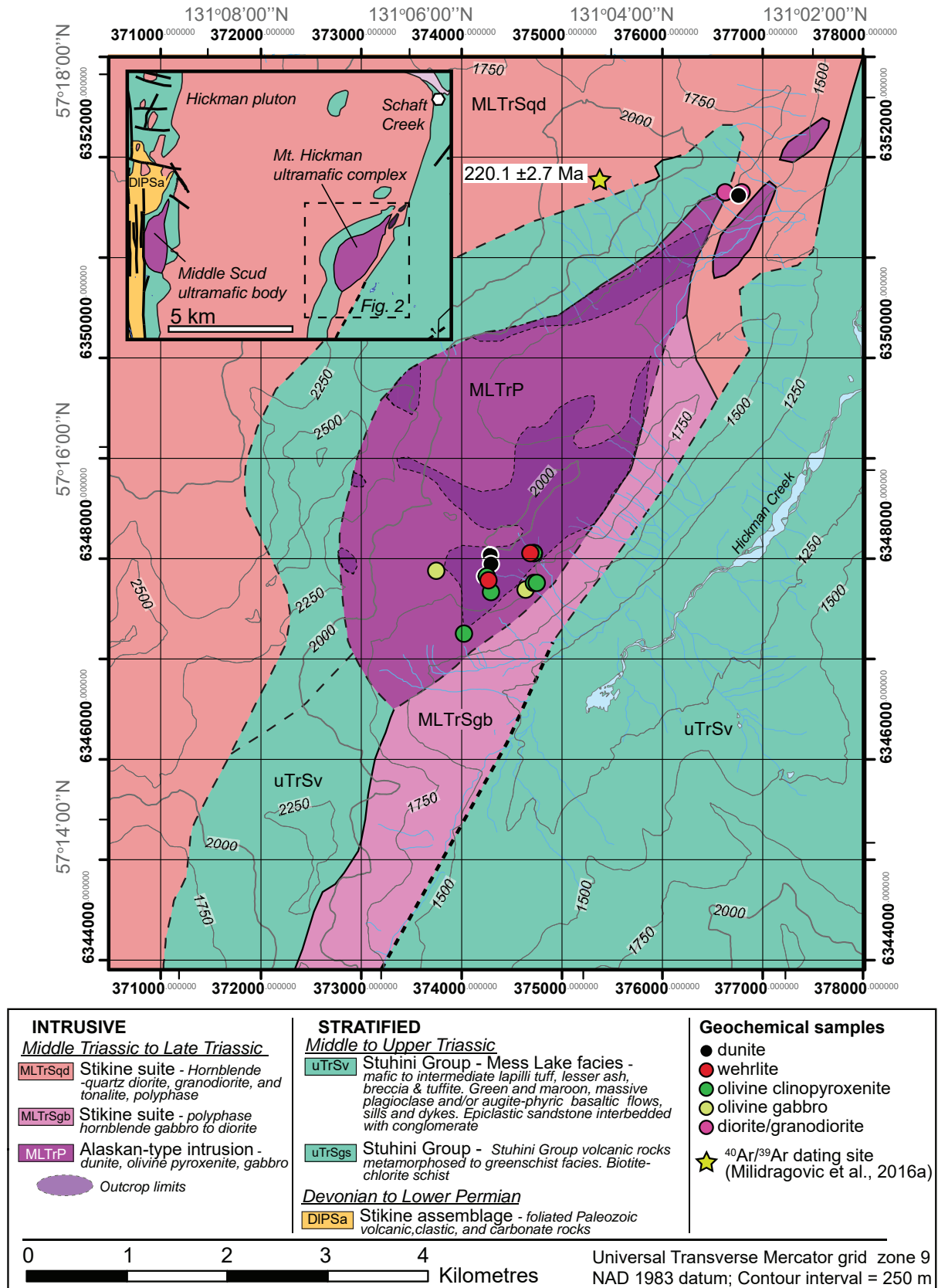


Fig. 1. Terrane map of the northern Canadian Cordillera showing the location of the study area (modified from Nelson et al., 2013).



**Fig. 2.** Geological map of the Mount Hickman ultramafic complex (modified after Brown et al., 1996, Mihalynuk et al., 1996, and Milidragovic et al., 2016a), showing the locations of samples analyzed for geochemistry (Table 1). Inset: regional geology map, showing the location of the Mount Hickman ultramafic complex, the Middle Scud ultramafic body, and the Schaft Creek exploration camp.

Milidragovic et al., 2016a). This report provides a petrographic and geochemical description of the principal rock types in the Mount Hickman ultramafic complex, and a comparison to the nearby Middle Scud ultramafic body on the west side of the Hickman pluton (Fig. 2 inset).

## 2. Geological setting

The Stikine terrane is a composite Devonian to Jurassic volcanic arc consisting mainly of volcanosedimentary and plutonic rocks. The first of three episodes of island-arc formation is recorded by the Stikine assemblage (Paleozoic; Monger, 1977). The second is recorded by the Stuhini Group (Middle-Upper Triassic), which unconformably overlies the Stikine assemblage and consists of predominantly subaqueous mafic to felsic volcanic and related sedimentary rocks. Unconformably above the Stuhini Group, the Hazelton Group (Lower-Middle Jurassic) represents the third episode, and contains subaqueous to subaerial, volcano-sedimentary rocks (e.g., Brown et al., 1996; Logan et al., 2000; Barresi et al., 2015). Plutonic suites coeval with these episodes include: Forrest Kerr (Late Devonian); More Creek (Early Mississippian); Stikine, Alaskan-type and Copper Mountain (Late Triassic); Texas Creek, Aishihik, and Long Lake (Early Jurassic); and Three Sisters (Middle Jurassic; Logan et al., 2000; Zagorevski et al., 2016). The Hickman pluton, north and west of the Mount Hickman ultramafic complex (Fig. 2), is a composite intrusion and part of the Stikine suite (Brown et al., 1996; Logan et al., 2000).

The Mount Hickman ultramafic complex is an elongate, northeast-trending, ultramafic intrusion, approximately 6 km long and 3 km wide (Fig. 2; Holbek, 1988; Brown and Gunning, 1989; Nixon et al., 1989). Previous work described the Mount Hickman ultramafic complex as a zoned intrusion containing minor serpentized dunite, (olivine) clinopyroxenite, and gabbro (Holbek, 1988; Nixon et al., 1989). The range of observed rock types qualifies the Mount Hickman ultramafic complex as an Alaskan-type intrusion, (see Taylor, 1967; Nixon et al., 2015). Along its western margin, the Mount Hickman ultramafic complex is in contact with plagioclase-phyric andesite of probable Stuhini Group affinity (Brown and Gunning, 1989; Nixon et al., 1998; Brown et al., 1996). Brown and Gunning (1989) and Nixon et al. (1989) interpreted this contact as intrusive, implying that complex is Middle Triassic or younger. The northern margin of the Mount Hickman ultramafic complex is truncated by the main phase of the Hickman pluton (Brown and Gunning, 1989; Nixon et al., 1989). Rubidium-Strontium, K-Ar and  $^{40}\text{Ar}/^{39}\text{Ar}$  ages of ~220-222 Ma on biotite and hornblende from the Hickman pluton (Holbek, 1988; Milidragovic et al., 2016a) indicate that the Mount Hickman ultramafic complex is Late Triassic or older.

The Middle Scud ultramafic body is ~15 km west of the Mount Hickman ultramafic complex, separated from it by the Mount Hickman pluton (Fig. 2 inset). The Middle Scud body intrudes mafic metavolcanic rocks of probable Stuhini Group affinity and is intruded by the main phase of the Hickman

Pluton (Brown et al., 1996). The Middle to Late Triassic age, the predominantly olivine and clinopyroxene mineralogy, and proximity to the Mount Hickman complex suggest that the Middle Scud ultramafic body may be genetically related to the Mount Hickman complex.

## 3. Analytical methods

Nineteen samples collected in 2015 were analyzed at Activation Laboratories (Ancaster, ON) for whole-rock major and trace element compositions (Table 1), using the 4Lithores analytical package. Samples, pulverized using an agate mill, were mixed with a flux of lithium metaborate/tetraborate, fused, and dissolved in nitric acid. The concentrations of major and selected trace elements (Sc, V, Be, Ba, Sr, and Zr) were measured by inductively coupled plasma-optical emission spectrometry (ICP-OES). The remaining trace elements, including REE, were determined by inductively coupled plasma-mass spectrometry (ICP-MS). The relative uncertainty in measurement, at a 95% confidence interval, is  $\leq 6\%$  for most major elements. Due to low concentrations, the relative uncertainty in the measurement of  $\text{Na}_2\text{O}$ ,  $\text{K}_2\text{O}$ , and  $\text{P}_2\text{O}_5$  is larger; near the quantification limit (defined as 3.33 times the detection limit), the relative uncertainty is ~30% for  $\text{Na}_2\text{O}$  and  $\text{P}_2\text{O}_5$  and ~50% for  $\text{K}_2\text{O}$ . The uncertainty in most trace element concentrations varies between  $<5\%$  relative (Cr, Ni) to  $\leq 40\%$  relative (Nb, Ta, Hf) at the 95% confidence level. The relative uncertainty in concentration of rare earth elements (REE), Y, Zr, Th, and U is  $\leq 25\%$ , whereas the relative uncertainty in the measurement of large ion lithophile elements (LILE) varies from ~5% (Sr) to  $\leq 40\%$  (Ba).

The composition of olivine (Table 2) was measured at the University of British Columbia (Vancouver, BC) on a Cameca SX50 electron microprobe. Analyses by wavelength dispersive spectrometry (WDS) were performed using 20 kV accelerating voltage, 15 nA beam current, and 5 mm beam diameter. Errors in  $\text{SiO}_2$  and MgO measurements on olivine are  $<1\%$  relative ( $2\sigma$ ), whereas the uncertainty in FeO measurement is  $\leq 3\%$  relative. The relative uncertainty in minor oxide constituents of olivine (NiO, MnO) is typically  $<50\%$ . The concentrations of  $\text{TiO}_2$ ,  $\text{Al}_2\text{O}_3$ ,  $\text{Cr}_2\text{O}_3$ , and CaO in olivine are near or below detection limit.

## 4. Main rock types of the Mount Hickman ultramafic complex

Glaciers and scree obscure large parts of the Mount Hickman ultramafic complex, which consists of serpentized dunite, wehrlite, olivine clinopyroxenite, and olivine gabbro. Olivine clinopyroxenite is volumetrically the most abundant rock type; pods and slivers of dunite (Fig. 3) and wehrlite are volumetrically minor and exposed in the southeastern and northeastern parts of the intrusion. Olivine gabbro is limited to isolated outcrops in the southern part of the intrusion. Concentric zoning from a dunite core, through peridotite and clinopyroxenite ( $\pm$ hornblende  $\pm$ magnetite), to a feldspathic rim, which is sometimes considered as a defining characteristic

**Table 1.** Major and trace element compositions of the Mount Hickman ultramafic complex and the Middle Scud ultramafic body.

Sample #	ZE15DM 4-03A <sup>a</sup>	ZE15DM 4-05A <sup>a</sup>	ZE15DM 4-06A <sup>a</sup>	ZE15DM 4-08B <sup>a</sup>	ZE15DM 4-01A <sup>a</sup>	ZE15DM 4-04A <sup>a</sup>	ZE15DM 4-01B <sup>a</sup>	ZE15DM 4-02A <sup>a</sup>	ZE15DM 4-03B <sup>a</sup>	ZE15SB 53A <sup>a</sup>	ZE15SB 53B <sup>a</sup>	ZE15DM 4-01C <sup>a</sup>	ZE09 062 <sup>a</sup>
Easting	374195	374253	374251	376720	374648	374196	374648	374267	374195	374699	374699	374648	374025
Northing	6347831	6347922	6348013	6351625	6348059	6347802	6348059	6347682	6347831	6347776	6347776	6348059	6347258
Lithology	dunite	dunite	dunite	dunite	wehrlite	wehrlite	ol. cpxite	mt. ol. cpxite	mt. ol. cpxite	mt. ol. cpxite	mt. ol. cpxite	mt. ol. cpxite	mt. ol. cpxite
Major elements (wt.%)													
SiO <sub>2</sub>	33.66	33.74	34.90	32.45	44.98	44.30	49.48	44.78	45.59	44.91	43.56	43.14	44.25
TiO <sub>2</sub>	0.24	0.18	0.16	0.02	0.23	0.35	0.40	0.35	0.67	0.40	0.87	0.86	0.91
Al <sub>2</sub> O <sub>3</sub>	0.61	0.50	0.40	0.28	2.33	2.12	3.21	3.28	3.10	4.29	4.40	11.10	4.41
Fe <sub>2</sub> O <sub>3</sub>	20.92	20.33	21.11	12.70	12.50	12.62	8.88	15.42	15.41	17.76	19.47	15.25	18.62
MnO	0.22	0.21	0.15	0.12	0.26	0.22	0.20	0.22	0.20	0.23	0.22	0.22	0.20
MgO	32.69	33.02	32.68	31.56	23.20	22.26	16.70	17.41	15.71	13.63	12.91	10.93	13.69
CaO	0.09	0.09	0.09	7.07	12.45	13.43	20.06	17.05	18.92	17.21	17.16	15.02	16.81
K <sub>2</sub> O	<0.01	<0.01	<0.01	<0.01	0.03	<0.01	0.04	0.02	<0.01	0.11	0.02	1.07	0.45
Na <sub>2</sub> O	<0.01	<0.01	<0.01	<0.01	0.22	0.20	0.37	0.26	0.27	0.37	0.34	0.68	0.48
P <sub>2</sub> O <sub>5</sub>	0.01	0.02	<0.01	<0.01	0.01	0.02	0.03	0.02	0.01	0.02	<0.01	0.04	0.02
LOI	10.63	10.86	10.06	15.70	3.50	4.44	0.95	1.37	0.59	0.27	1.12	2.41	0.53
Total	99.09	98.96	99.55	99.91	99.72	99.96	100.30	100.50	100.50	99.74	100.10	100.70	100.40
<sup>c</sup> Mg#	0.76	0.76	0.75	0.83	0.79	0.78	0.79	0.69	0.67	0.60	0.57	0.59	0.59
Trace elements (ppm)													
Cs	<0.1	<0.1	<0.1	<0.1	0.1	<0.1	0.1	<0.1	0.1	0.3	<0.1	0.4	0.6
Rb	<1	<1	<1	<1	<1	<1	1	<1	<1	3	<1	19	10
Ba	4	<3	<3	5	12	<3	14	8	3	28	11	330	140
Th	<0.05	<0.05	<0.05	<0.05	<0.05	<0.05	0.16	<0.05	<0.05	0.08	<0.05	0.09	0.09
U	0.02	0.01	<0.01	1.57	0.03	0.02	0.03	0.03	0.02	0.03	0.03	0.07	0.29
Nb	<0.2	<0.2	<0.2	<0.2	<0.2	<0.2	<0.2	<0.2	<0.2	0.9	<0.2	<0.2	1.0
Ta	0.02	0.02	0.02	0.03	0.02	0.02	0.01	0.02	0.03	0.03	0.02	0.04	0.04
Pb	<5	<5	<5	<5	<5	<5	<5	<5	<5	<5	<5	<5	<5
Sr	4	4	3	94	53	37	75	49	46	89	52	327	113
Zr	2	2	2	2	8	8	14	12	11	12	13	17	20
Hf	<0.1	<0.1	<0.1	<0.1	0.2	0.3	0.4	0.4	0.3	0.5	0.6	0.4	0.7
Y	0.5	0.7	0.6	<0.5	5.5	4.9	9.3	7.2	6.9	10.1	9	10.2	8.9
Ga	2	2	2	1	4	5	5	7	8	14	12	12	11
Sc	8	12	10	4	43	61	70	77	84	76	77	53	76
V	142	105	91	24	94	145	158	305	325	481	497	410	461
Co	167	154	159	107	78	85	44	67	61	81	69	53	90
Zn	100	50	120	50	80	70	50	60	70	100	80	80	72
Cu	<10	<10	30	<10	<10	<10	<10	<10	<10	20	20	10	50
Cr	850	850	880	1970	1430	1080	1530	710	990	610	320	280	280
Ni	500	450	470	650	280	250	130	160	120	140	120	70	170
La	0.18	0.17	0.28	0.33	0.76	1.01	1.55	0.90	0.80	1.27	1.18	1.84	1.80
Ce	0.31	0.29	0.38	0.50	2.42	2.30	4.46	2.76	2.52	3.63	3.57	4.70	4.66
Pr	0.05	0.06	0.04	0.05	0.43	0.34	0.76	0.57	0.49	0.63	0.67	0.81	0.77
Nd	0.34	0.35	0.37	0.29	2.71	2.44	4.63	3.31	2.76	3.79	4.07	4.29	4.19
Sm	0.12	0.09	0.12	0.09	0.84	0.81	1.52	1.24	1.12	1.44	1.44	1.60	1.50
Eu	0.034	0.032	0.056	0.032	0.328	0.268	0.602	0.417	0.364	0.553	0.517	0.637	0.473
Gd	0.08	0.14	0.09	0.06	1.08	1.64	1.91	1.64	1.50	1.70	1.92	2.12	1.74
Tb	0.01	0.03	0.02	0.01	0.19	0.16	0.31	0.25	0.25	0.30	0.30	0.35	0.31
Dy	0.10	0.17	0.13	0.06	1.11	1.47	1.77	1.47	1.39	1.81	1.78	2.07	1.74
Ho	0.02	0.03	0.02	0.01	0.21	0.18	0.34	0.28	0.24	0.35	0.33	0.39	0.31
Er	0.08	0.08	0.07	0.05	0.54	0.49	0.94	0.75	0.65	0.94	0.90	1.03	0.88
Tm	0.012	0.012	0.014	0.007	0.074	0.071	0.130	0.101	0.092	0.129	0.122	0.152	0.133
Yb	0.08	0.09	0.11	0.05	0.47	0.44	0.82	0.63	0.63	0.82	0.77	1.01	0.82
Lu	0.014	0.016	0.016	0.01	0.071	0.071	0.125	0.099	0.102	0.130	0.120	0.145	0.113

Table 1. Continued.

Sample #	ZE15SB 54 <sup>a</sup>	ZE15SB 55A <sup>a</sup>	ZE15DM4 08C <sup>a</sup>	ZE15-DM4 09A <sup>a</sup>	ZE15DM4 08A <sup>a</sup>	ZE15DM7- 03D <sup>b</sup>	ZE15DM7- 03F <sup>b</sup>	ZE15DM7- 03E <sup>b</sup>	ZE15-DM7- 03C <sup>b</sup>
Easting	374611	373751	376720	376611	376720	361699	361699	361699	361699
Northing	6347728	6347894	6351625	6351660	6351625	6349640	6349640	6349640	6349640
Lithology	ol. gabbro	gabbro	hbl. diorite	hbl. diorite	Granodiorite dyke	wt. wehrlite	wehrlite	ol. hbl'd'te	bt. wehrlite
Major elements (wt.%)									
SiO <sub>2</sub>	46.08	46.08	57.96	55.93	67.84	39.55	41.49	44.15	42.56
TiO <sub>2</sub>	0.20	0.20	0.56	0.64	0.24	0.24	0.24	0.35	0.62
Al <sub>2</sub> O <sub>3</sub>	20.68	20.68	18.22	18.37	15.46	5.68	2.77	6.18	7.12
Fe <sub>2</sub> O <sub>3</sub>	4.65	4.65	5.63	8.05	2.68	11.27	10.63	10.31	10.78
MnO	0.10	0.10	0.14	0.16	0.04	0.16	0.15	0.15	0.14
MgO	8.58	8.58	5.84	3.19	1.00	26.90	31.64	25.37	22.76
CaO	12.70	16.78	5.10	4.99	1.96	6.49	6.07	7.34	9.09
K <sub>2</sub> O	1.18	3.02	2.95	2.07	3.61	0.70	0.02	0.47	2.25
Na <sub>2</sub> O	2.00	0.21	4.81	4.65	4.97	0.49	0.27	0.92	0.57
P <sub>2</sub> O <sub>5</sub>	0.07	<0.01	0.30	0.22	0.10	0.03	0.03	0.10	0.02
LOI	1.55	3.26	1.78	2.53	1.58	7.55	4.75	2.83	4.23
Total	100.10	100.80	99.88	100.50	99.47	99.40	98.07	98.19	100.10
<sup>c</sup> Mg#	0.57	0.71	0.46	0.44	0.43	0.83	0.85	0.83	0.81
Trace elements (ppm)									
Cs	0.5	1.1	0.5	1.1	0.4	0.1	<0.1	0.3	0.5
Rb	19	72	53	46	58	8	<1	17	14
Ba	329	902	799	552	1178	42	10	322	348
Th	0.15	<0.05	2.20	1.08	2.80	<0.05	<0.05	0.21	<0.05
U	0.09	0.03	1.43	0.62	3.87	0.01	<0.01	0.2	0.01
Nb	0.7	<0.2	4.8	1.7	6.0	0.4	<0.2	0.3	0.3
Ta	0.07	0.04	0.30	0.15	0.34	0.06	0.04	0.05	0.07
Pb	<5	<5	<5	<5	<5	<5	<5	<5	<5
Sr	771	515	689	598	395	38	71	168	58
Zr	14	7	81	69	91	14	6	17	14
Hf	0.6	0.2	1.8	1.7	1.9	0.4	0.2	0.5	0.5
Y	9.6	4.4	13.5	17.4	5.9	7.7	4.1	6.9	8.5
Ga	13	10	18	16	16	6	3	6	7
Sc	45	46	10	12	2	31	18	23	30
V	346	117	171	147	48	158	106	151	181
Co	44	20	10	14	5	80	85	75	72
Zn	70	<30	40	60	30	60	60	60	50
Cu	40	170	30	20	10	10	<10	70	<10
Cr	170	170	30	20	30	1350	1920	1770	1200
Ni	70	40	<20	<20	<20	960	1320	950	810
La	2.57	1.58	13.10	9.11	9.36	0.61	0.59	2.10	0.95
Ce	5.76	2.52	24.20	19.10	15.90	2.51	1.33	4.27	2.76
Pr	0.86	0.31	2.95	2.38	1.73	0.50	0.25	0.64	0.57
Nd	5.04	1.70	12.70	11.40	6.68	2.82	1.41	3.28	3.03
Sm	1.69	0.68	2.83	2.68	1.18	1.38	0.50	1.04	1.22
Eu	0.582	0.319	0.946	0.995	0.469	0.372	0.197	0.333	0.421
Gd	1.84	0.82	2.70	3.24	1.08	1.42	0.67	1.20	1.49
Tb	0.33	0.14	0.43	0.49	0.14	0.14	0.12	0.19	0.25
Dy	1.98	0.83	2.39	2.88	0.91	1.39	0.82	1.14	1.50
Ho	0.36	0.15	0.48	0.58	0.19	0.28	0.16	0.24	0.29
Er	0.95	0.39	1.34	1.72	0.59	0.76	0.40	0.68	0.82
Tm	0.139	0.054	0.195	0.264	0.094	0.104	0.058	0.098	0.117
Yb	0.85	0.33	1.41	1.80	0.71	0.63	0.36	0.60	0.74
Lu	0.119	0.048	0.210	0.265	0.131	0.095	0.057	0.086	0.107

<sup>a</sup> Mount Hickman ultramafic complex. <sup>b</sup> Middle Scud ultramafic body. <sup>c</sup> Minimum Mg-number defined as Mg/(Mg+Fe<sup>2+</sup>), where all Fe is expressed as Fe<sup>2+</sup>.

**Table 2.** Average olivine compositions from the Mount Hickman ultramafic complex and the Middle Scud ultramafic body.

Sample:	ZE15-DM4-01B	ZE15-DM4-01A	ZE15-SB53	ZE15-DM7-03F
<sup>1</sup> n	3	8	9	14
Area	Hickman	Hickman	Hickman	
Rock	ol. cpxite	wehrlite	mt. ol. cpxite	wehrlite
<sup>2</sup> WR Mg#	0.79	0.79	0.57	0.85
SiO <sub>2</sub>	39.2 ±0.3	39.2 ±0.4	38.9 ±0.6	41.0 ±0.5
TiO <sub>2</sub>	<0.06	<0.06	<0.06	<0.06
Al <sub>2</sub> O <sub>3</sub>	<0.04	<0.04	<0.04	<0.04
MgO	39.8 ±0.4	40.3 ±0.4	38.8 ±0.6	47.8 ±0.4
FeO	20.1 ±0.1	19.7 ±0.5	21.6 ±0.7	10.7 ±0.3
MnO	0.41 ±0.06	0.45 ±0.04	0.55 ±0.06	0.20 ±0.05
CaO	0.06 ±0.02	0.06 ±0.04	<0.06	<0.06
NiO	<0.15	<0.15	<0.15	<0.15
Cr <sub>2</sub> O <sub>3</sub>	<0.12	<0.12	<0.12	0.30 ±0.07
Total	99.7 ±0.7	99.9 ±0.7	99.9 ±0.8	100.0 ±0.8
Fo	0.77 ±0.00	0.78 ±0.00	0.76 ±0.01	0.89 ±0.00
Ni (ppm)	-	-	-	1573 ±426
100Mn/Fe	2.0 ±0.3	2.3 ±0.2	2.5 ±0.2	1.9 ±0.5

<sup>1</sup>n=number of analyses/sample. <sup>2</sup>WR Mg# = whole rock Mg-number. Reported uncertainties are 2σ deviations from the mean calculated from n samples.

of Alaskan-type intrusions (Taylor, 1967; Guillou-Frottier, 2014), is not well developed (Fig. 2).

#### 4.1. Serpentinized dunite

Volumetrically minor, serpentinized dunite forms light brown to beige weathering, strongly magnetic, irregularly shaped pods in wehrlite or olivine clinopyroxenite. These pods are elongate irregular bodies, metres to 10s of metres long, that locally pinch out in surrounding pyroxenite (Fig. 3a). The geometry of the pods suggests that dunite flowed plastically through the more competent wehrlite and olivine clinopyroxenite.

Dunite is completely replaced by serpentine and is, along with surrounding pyroxenite, cut by mm- to cm-wide veins of magnetite. Serpentinized dunite is predominantly composed of lizardite and veins of chrysotile ±talc, and has a density of ~2.9 g/cm<sup>3</sup>. All samples are cut by a pervasive network of magnetite microveins (Fig. 4a). Trace amounts of phlogopite, and minor, strongly-altered grains of clinopyroxene (<15% modal) occur as irregularly shaped interstitial crystals.

#### 4.2. Wehrlite

Mesocumulate wehrlite weathers brown and appears massive and black on fresh surfaces. Olivine has undergone variable degrees of serpentinization (40-90%), whereas clinopyroxene is largely fresh and unaltered.

Wehrlite is typically medium grained and contains highly fractured and irregular shaped olivine, and euhedral to subhedral clinopyroxene (0.5-0.8 cm across). Olivine grain boundaries and fractures are lined by thin coatings of secondary magnetite. Individual clinopyroxene grains commonly contain multiple inclusions of olivine, indicating early olivine crystallization (Fig. 4b). However, predominantly cotectic crystallization of the two minerals is indicated by their subequal proportions and similar crystal size, as well as the subhedral to euhedral crystal habit of clinopyroxene.

#### 4.3. Olivine ±magnetite clinopyroxenite

Brown weathering, dark green olivine clinopyroxenite is the predominant lithology of the Mount Hickman ultramafic complex (Fig. 3b). Meso- to orthocumulate olivine clinopyroxenite is medium grained, and composed chiefly of euhedral clinopyroxene (>80%), pseudomorphed olivine, and magnetite (2-10%). Well saussuritized plagioclase and biotite form local intercumulus crystals.

Clinopyroxene is generally fresh, and contains inclusions of olivine and magnetite. Cores of clinopyroxene, delineated by needles of fine magnetite, are rare. Magnetite also occurs both as irregular shaped interstitial crystals and blebby cumulus grains (Figs. 4c-d). Rare, magnetite-enriched olivine clinopyroxenite contains up to 40% interstitial, net-textured magnetite (Figs. 3c and 4e-f).

#### 4.4. Magnetite olivine gabbro

Brown weathering, mottled, medium-grained olivine gabbro was observed along the southwestern margin of the Mount Hickman ultramafic complex. The gabbro contains subequal proportions of euhedral clinopyroxene and saussuritized plagioclase (>90%), heavily altered (iddingsite) olivine (~5%), and interstitial magnetite (Fig. 4g).

A green-weathering olivine gabbro was also identified along the western margin of the exposed ultramafic. The gabbro is extensively altered, with chlorite veins (<1 mm), pervasively saussuritized plagioclase, and significant replacement of clinopyroxene by chlorite ±actinolite. Trace olivine (~1%) is completely replaced by iddingsite.

#### 4.5. Middle Scud wehrlite

The ultramafic rocks of the Middle Scud body are weakly to strongly foliated, brown to dark grey weathering, fine-grained meta-wehrlites. Metamorphism and recrystallization at the Middle Scud body vary from intensely recrystallized, fine-



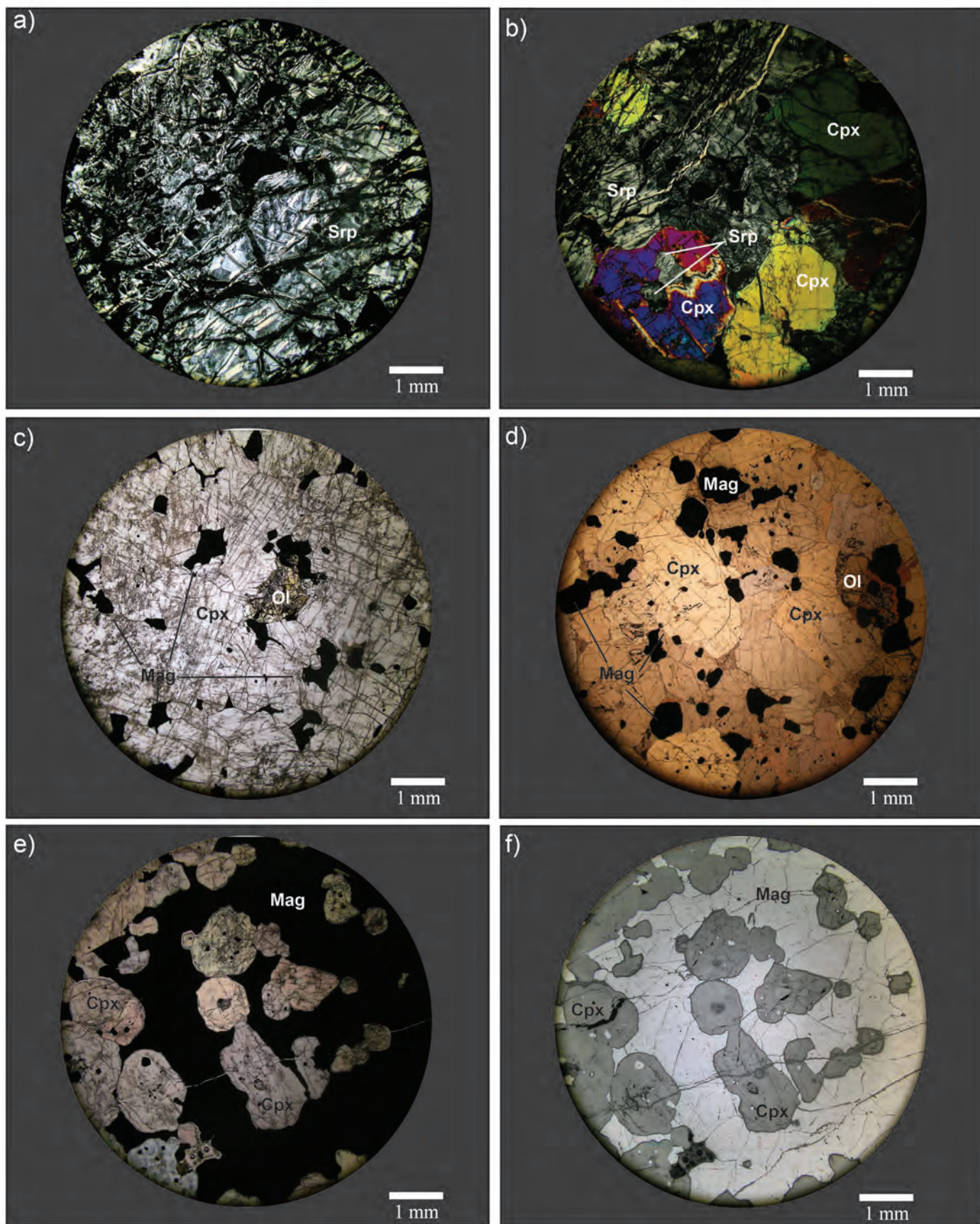
**Fig. 3.** **a)** Irregularly-shaped serpentinized dunite pod surrounded by olivine clinopyroxenite. Plates of magnetite, interpreted to be remnants of a vein are visible on the exposed serpentinized dunite surface. **b)** Brown to rust-stained rubbly outcrop of olivine clinopyroxenite. **c)** Close-up of a weathered surface of an extreme-end member of orthocumulate magnetite olivine clinopyroxenite. Cumulus crystals of beige-weathering clinopyroxene and olivine (not discernible) are hosted in intercumulus magnetite; see also Fig. 4c). A magnetite vein is visible on the right side of the photo. **d)** Black, recessive, sheared serpentinized dunite between hornblende diorite. A late basaltic dike cuts the outcrop ca. 10 m above the dunite.

grained amphibolite, composed predominantly of granoblastic polygonal amphibole and clinopyroxene, to wehrlite with well-preserved igneous cumulate textures composed predominantly of clinopyroxene and serpentinized olivine (Fig. 4h). All samples contain magnetite and variable amounts of phlogopite (up to 15%).

## 5. Geochemistry

### 5.1. Mount Hickman mafic-ultramafic complex

The rocks of the Mount Hickman ultramafic complex are crystal cumulates; consequently their geochemical composition is mainly governed by the relative proportions of constituent mafic minerals. In addition to having the highest MgO (>37 wt.%) and MgO + FeO<sup>TOT</sup> (51 wt.%) concentrations



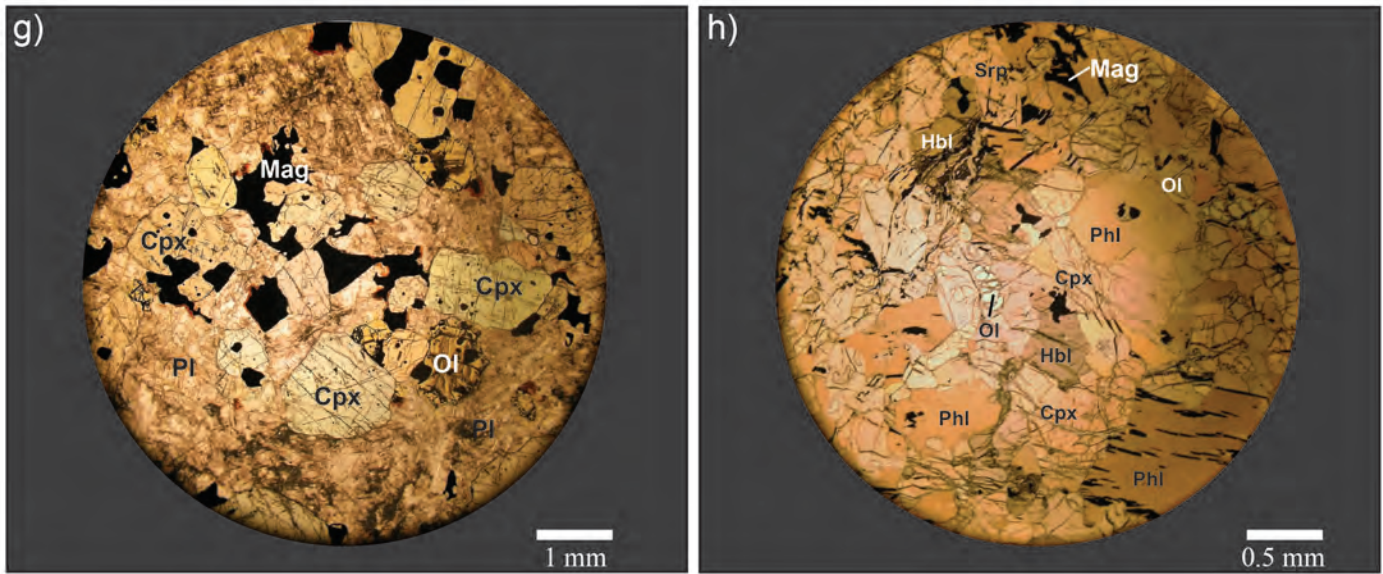


**Fig. 4.** **a)** Cross-polarized photomicrograph of a pervasively serpentinized (Srp) dunite, (sample ZE15-DM4-05A). **b)** Cross-polarized light image of wehrlite (sample ZE15-DM4-04A) consisting of mainly fresh clinopyroxene (Cpx) and serpentine. Note the euhedral inclusions of serpentinized olivine in the clinopyroxene crystal in the lower left quadrant. **c)** Plane-polarized light image of mesocumulate olivine clinopyroxenite (sample ZE15-DM4-03B), containing relatively fresh clinopyroxene, pervasively serpentinized olivine (Ol), and interstitial magnetite (Mag). **d)** Plane-polarized light image of magnetite olivine clinopyroxenite (sample ZE09-062). In contrast to the interstitial habit of magnetite grains in c), magnetite is blebby and sub-equant, suggesting cotectic crystallization with olivine and clinopyroxene. **e)** Plane-polarized light image of an orthocumulate magnetite clinopyroxenite (sample ZE15-DM04-03C). This extreme end member contains  $\leq 40\%$  magnetite. **f)** Reflected light image of e). **g)** Plane-polarized image of an olivine gabbro (sample ZE15-SB54A), comprising iddingsitized olivine, clinopyroxene, magnetite, and plagioclase (Pl). **h)** Plane-polarized light image of a phlogopite (Phl)-rich meta-wehrlite (sample ZE15-DM7-03C) from the Middle Scud ultramafic body. In addition to phlogopite, metamorphosed wehrlites from the Middle Scud body contain abundant hornblende (Hbl) after clinopyroxene, and partially serpentinized olivine.

(LOI-free), which approach those of pure olivine, dunite has the lowest abundances of  $\text{Al}_2\text{O}_3$  ( $<1$  wt.%), CaO,  $\text{Na}_2\text{O}$ , and  $\text{K}_2\text{O}$  (below detection limit), and incompatible trace elements (Figs. 5 and 6) among the Mount Hickman complex rock types. Sample ZE15-DM4-08B contains ubiquitous carbonate and higher concentrations of CaO (8.5 wt.%), Sr, and LOI (16 wt.%) than other dunites (CaO  $\sim 0.10$  wt.%; LOI = 10-11 wt.%), and is thus interpreted to be significantly metasomatized. The remaining dunite samples have FeO concentrations of  $\sim 21$  wt.%, which exceed those of all other rock types, including the carbonate metasomatized dunite, and Mg-numbers (defined here as  $\text{Mg}/(\text{Mg}+\text{Fe}^{\text{TOT}})$ ) of  $\leq 0.76$ . In dunite, the concentration of Ni ranges from 450-650 ppm; Cr ranges from 850 to 2000 ppm. The concentrations of Ni in the serpentinized dunite are notable because they are significantly lower than those of most cumulate dunite samples, globally (Fig. 7a). The abundance of incompatible trace elements is low, typically between 0.1 and 1 x PM (Primitive Mantle concentrations; Palme and O'Neill, 2003), although Nb and most large ion lithophile elements (LILE) are below detection limit. Due, in part, to low absolute abundances, which approach analytical detection limits, the PM-normalized trace element profiles of the Mount Hickman complex dunite samples display significant spread and appear jagged (Fig. 6). Notably, the FeO-rich serpentinized dunites also display strong, PM-normalized, relative enrichments in  $\text{TiO}_2$  (0.2-0.3 wt.%) and may also be relatively enriched in  $\text{P}_2\text{O}_5$ .

However, the positive P anomalies (Fig. 6) are equivocal, given the low (below quantification limit) absolute abundance of  $\text{P}_2\text{O}_5$  in the dunites. In contrast to the FeO-rich dunite samples, the carbonate-metasomatized serpentinized dunite lacks the marked relative  $\text{TiO}_2$  enrichment (Fig. 6).

Abundances of MgO (20-25 wt.%) and  $\text{FeO}^{\text{TOT}}$  (12 wt.%) in wehrlite are consistent with subequal proportions of olivine and clinopyroxene. In contrast to dunite, wehrlite samples have higher concentrations of  $\text{Al}_2\text{O}_3$  (2.0-2.5 wt.%), CaO (13-14 wt.%),  $\text{Na}_2\text{O}$ ,  $\text{K}_2\text{O}$ , and incompatible trace elements (Fig. 6), and higher Mg-numbers (0.78-0.79). They contain  $\sim 300$  ppm Ni and 1100-1400 ppm Cr. As in dunite, the abundance of Nb and LILE is typically below detection limit. Despite the low levels of Nb, the high field strength elements (HFSE) display a clear depletion trend relative to the similarly compatible rare earth elements (REE), reflecting in part, the greater incompatibility of +4 charged HFSE relative to +3 charged REE in clinopyroxene (e.g., Wood and Blundy, 2001; Francis and Minarik, 2008). Rare earth elements define a convex upward profile (Fig. 6) with middle REE (MREE) enrichments relative to heavy (HREE) and light REE (LREE). Microprobe analyses of olivine from one wehrlitic sample indicate uniform Fo content (0.78), similar to the whole-rock Mg-number, and low Ni concentrations below the detection limit of  $\sim 700$  ppm.

Samples of olivine  $\pm$  magnetite clinopyroxenite have lower abundances of MgO (11-18 wt.%) and higher abundances

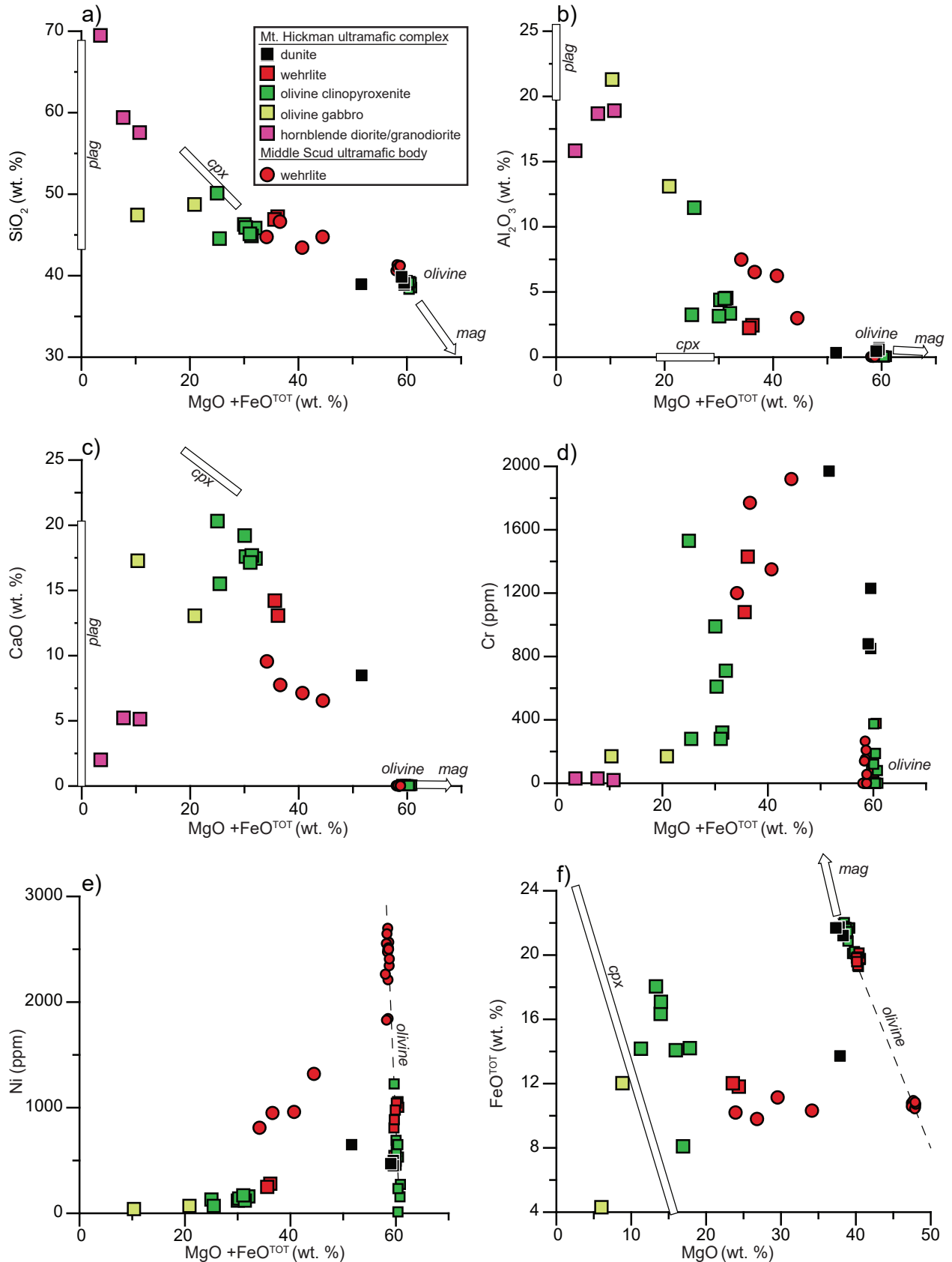


**Fig. 5.** Major and compatible trace element geochemistry of the Mount Hickman ultramafic complex and the Middle Scud ultramafic body normalized to LOI-free compositions. **a)** SiO<sub>2</sub> vs. MgO + FeO<sup>TOT</sup>. **b)** Al<sub>2</sub>O<sub>3</sub> vs. MgO + FeO<sup>TOT</sup>. **c)** CaO vs. MgO + FeO<sup>TOT</sup>. **d)** Cr vs. MgO + FeO<sup>TOT</sup>. **e)** Ni vs. MgO + FeO<sup>TOT</sup>. **f)** FeO<sup>TOT</sup> vs. MgO.

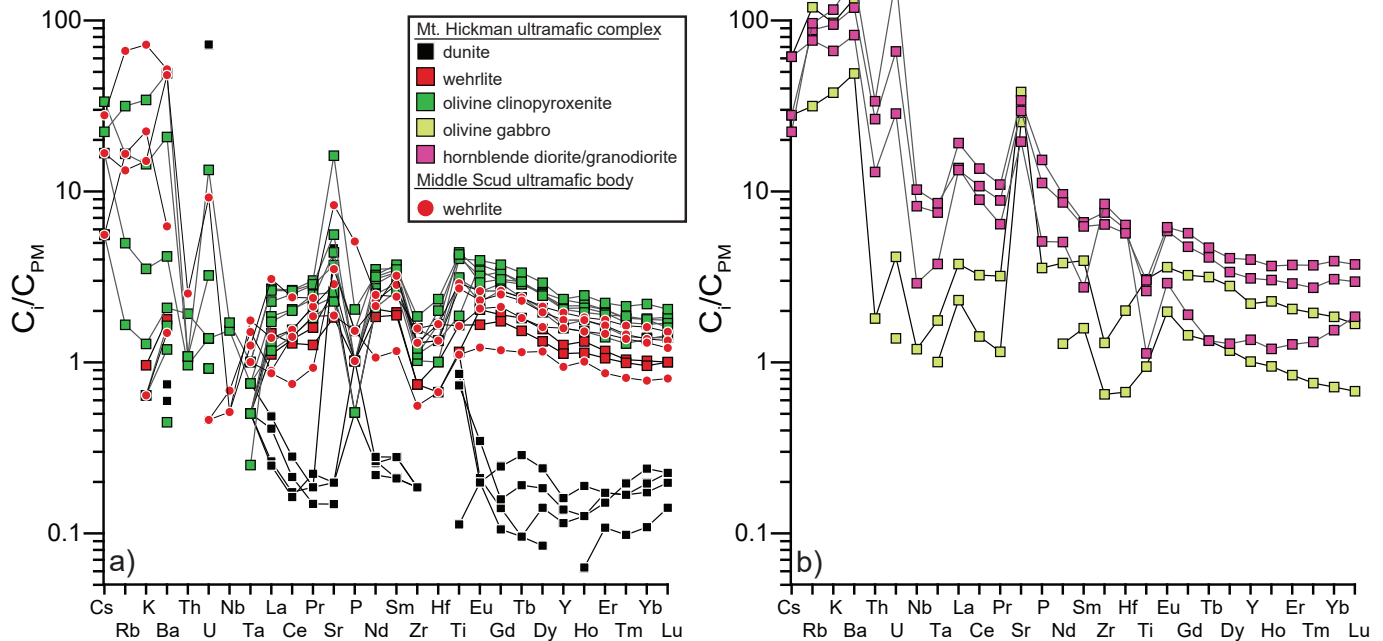


**Fig. 6.** Primitive mantle (Palme and O'Neill, 2003) normalized trace element profiles for **a)** ultramafic rocks of the Mount Hickman complex and Middle Scud body and **b)** gabbroic to granitic rocks of the Mount Hickman complex.

of  $\text{FeO}^{\text{TOT}}$  (8-17 wt.%),  $\text{Al}_2\text{O}_3$  (3-11 wt.%), and CaO (15.5-20.5 wt.%) than wehrlites, consistent with greater modal abundances of clinopyroxene and magnetite. Increasing FeO contents in olivine clinopyroxenite are accompanied by concomitant increases in  $\text{TiO}_2$  (0.4-1.0 wt.%), V, Sc, and Co. The incompatible trace element profiles of olivine  $\pm$ magnetite clinopyroxenites broadly resemble those of wehrlites, albeit at higher absolute concentrations. However, olivine clinopyroxenites show greater relative enrichments in MREE. Furthermore, the abundances of Ni (70-170 ppm) and Cr (300-1500 ppm) are lower than those in dunite and wehrlite. Olivine from one olivine clinopyroxenite has Fo content of 0.77 and olivine from one magnetite-rich olivine clinopyroxenite has Fo content of 0.76 Fo; both have Ni contents below detection limit.

Two samples of olivine gabbro have relatively low concentrations of MgO (6-9 wt.%) and  $\text{FeO}^{\text{TOT}}$  (4-12 wt.%), but relatively high concentrations of  $\text{Al}_2\text{O}_3$  (13-21 wt.%) and CaO (13-17 wt.%). The trace element profile of the relatively magnesian olivine gabbro is similar to those of olivine clinopyroxenite samples. However, the gabbro displays strong enrichment of Sr relative to similarly compatible trace elements. The less magnesian, relatively aluminous gabbro, shows strong relative depletion in HREE, and low absolute abundances of incompatible trace elements (except Sr), consistent with significant accumulation of plagioclase.

### 5.2. Middle Scud wehrlite

The Middle Scud ultramafic body wehrlite samples have 23-32 wt.% MgO, spanning the compositional gap between the Mount Hickman complex dunites and wehrlites. However,

the  $\text{FeO}^{\text{TOT}}$  concentrations (10-11 wt.%) of the Middle Scud wehrlites are less than those of the ultramafic rocks of the Mount Hickman complex, and require a parental magma with a higher Mg/Fe ratio, thus precluding a simple closed-system genetic relationship between the two intrusions. Three wehrlite samples (Fig. 7) have trace element profiles that overlap with those of the olivine clinopyroxenites from the Mount Hickman complex. In contrast, one sample (ZE15-DM-03F), has lower absolute incompatible trace element abundances, and displays the least relative MREE enrichment.

## 6. Discussion

The most striking characteristic of the ultramafic rocks of the Mount Hickman ultramafic complex is their relatively high  $\text{FeO}^{\text{TOT}}$  content (Fig. 8) which, at a given MgO concentration, exceeds that of most Alaskan-type intrusions in the North American Cordillera (see Findlay, 1969; Himmelberg and Loney, 1985; Scheel, 2007) and most terrestrial ultramafic rocks in general. These elevated Fe contents, however, are approached by the Duke Island Alaskan-type intrusion (Irvine, 1974) and resemble ferropicrites, a rare class of rocks whose emplacement is mainly limited to the Archean (e.g., Milidragovic and Francis, 2016). In contrast, the Middle Scud ultramafic body has relatively low whole-rock  $\text{Fe}^{\text{TOT}}$  contents and contains relatively Fo-rich olivine ( $\text{Fo}_{89}$ ), and thus resembles most Alaskan-type ultramafic intrusions. In the following we focus on dunite as the most primitive magmatic cumulate and the closest representative of the magma parental to the Mount Hickman ultramafic complex, and consider four permissible petrologic explanations for the unusually Fe-rich

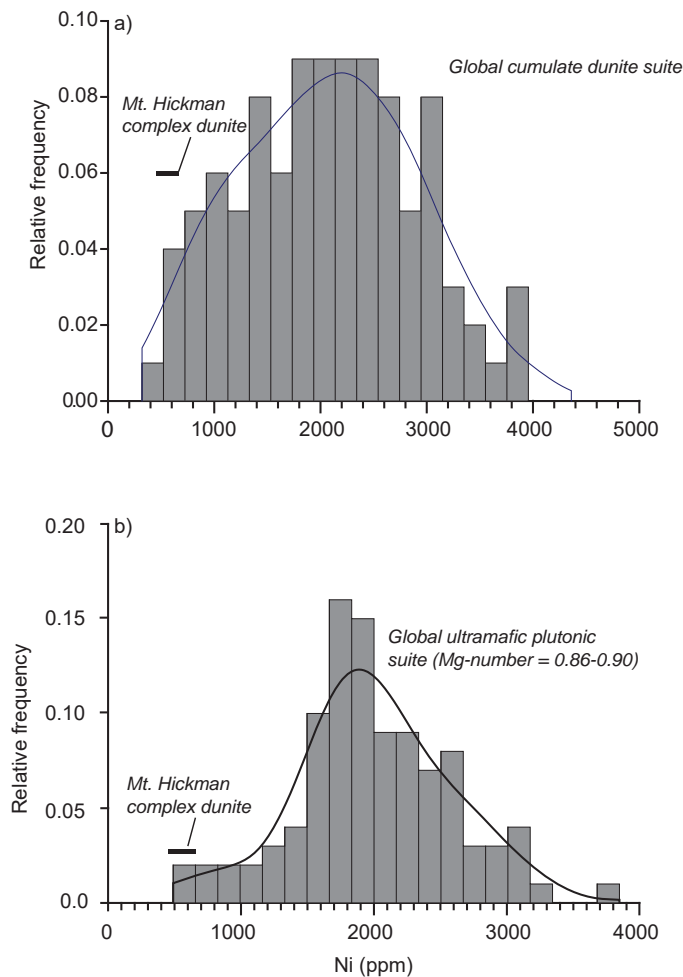


**Fig. 7.** Relative probability histogram of whole-rock Ni content from the global compilation of **a)** cumulate dunites ( $n=242$ ) and **b)** high Mg-number (0.86-0.90) cumulates ( $n=170$ ; MgO > 27 wt.%). Source: GEOROC database (<http://georoc.mpch-mainz.gwdg.de>), accessed on Nov. 15<sup>th</sup>, 2016.

character of the complex: 1) alteration and element mobility; 2) evolution of a primary magma towards Fe-enrichment; 3) remobilization of cumulates from original Fe-rich olivine layers; and 4) magma mixing.

### 6.1. Alteration and element mobility

The ultramafic rocks of the Mount Hickman ultramafic complex have been extensively serpentinized and contain widespread veins of magnetite raising the possibility of significant element mobility, including Fe and Ni. Therefore, one possible explanation for the high content of FeO<sup>TOT</sup> in dunites from the Mount Hickman ultramafic complex is metasomatic enrichment by Fe-rich melts and fluids. The relative enrichment of Ti  $\pm$  P in dunites (Fig. 6), further suggests metasomatism by Fe-Ti-P-rich fluids or immiscible melts, similar to those attributed to late-stage magmatic liquid immiscibility in slowly cooled mafic intrusions elsewhere (Philpotts, 1982; Jakobsen et al., 2005; Zhou et al., 2013). Similarly, mobility of Ni to form secondary Ni-sulphide (millerite, heazlewoodite), Ni-arsenide

(nickeline) or Ni-Fe alloy (awaruite) may account for the low absolute concentrations of Ni (<650 ppm) in serpentinized dunites of the Mount Hickman ultramafic complex. However, mass balance calculations indicate that metasomatism alone may not account for FeO-rich rocks in the complex.

Mass balance calculations, based on the assumption that serpentinization of Mount Hickman dunites did not directly result in MgO-loss or FeO-gain, indicate that the observed high FeO<sup>TOT</sup> concentrations of the Mount Hickman complex dunite would require the addition of 6-10 mol.% FeO as magnetite to 'normal' dunite with Mg-number of 0.86-0.90 (Fig. 8). Assuming average serpentine and magnetite density of 2.55 g/cm<sup>3</sup> and 5.2 g/cm<sup>3</sup>, respectively (Deer et al., 1969), such metasomatically Fe-enriched dunites would comprise ~10-20 vol.% magnetite; modal magnetite abundance in samples collected for geochemical analysis is significantly lower than this. Furthermore, the density of analyzed dunite samples (~2.9 g/cm<sup>3</sup>) suggests that the maximum magnetite content (assuming pure Mg-serpentine) and no clinopyroxene and/or chromite is ~10%.

Based on these considerations, the origin of the FeO-rich dunite of the Mount Hickman ultramafic complex solely through post-crystallization metasomatic enrichment of 'normal' dunite (Mg-number=0.86-0.90) appears unlikely. Instead, metasomatic addition of FeO, if significant, operated on a dunitic precursor with a relatively low Mg-number ( $\leq 0.86$ ; Fig. 8). Regardless of the exact amount of metasomatic FeO addition, the FeO-rich nature of the Mount Hickman ultramafic rocks must, in part, reflect the original FeO-rich character of their parental magmas.

### 6.2. Evolution of primary magma towards Fe-enrichment

The Fe-rich, Ni-poor character of the Mount Hickman complex dunite may reflect an earlier history of magmatic differentiation and olivine fractionation. Although fractionation of sulphide  $\pm$  Cr-spinel results in efficient Ni removal from melts, extensive fractionation of either phase is inconsistent with the Fe-rich character of dunite. The exact amount of fractionation necessary for the observed Fe-enrichment is impossible to determine. However, some robust inferences using olivine-liquid Fe-Mg equilibria (cf. Roeder and Emslie, 1970) and the minimum MgO-content of the parental liquid saturated in olivine only (~10 wt.% MgO), may be drawn. An olivine-saturated magma, parental to the Fe-rich dunite of the Mount Hickman mafic-ultramafic complex, requires an Mg/(Mg+Fe<sup>2+</sup>) ratio of 0.49, and a corresponding minimum FeO<sup>TOT</sup> concentration of 19 wt.% to produce adcumulate dunite with a whole-rock Mg-number of ~0.76. Such Fe-rich magmas are restricted to Archean ferropicrites and cannot be produced by olivine fractionation from primary liquids generated by melting of normal pyrolitic mantle (Milidragovic and Francis, 2016). Consequently, it is unlikely that dunites of the Mount Hickman ultramafic complex formed by accumulation of olivine from an evolved residual magma derived from high Mg-number (>0.65) primary melts by closed system fractional crystallization.

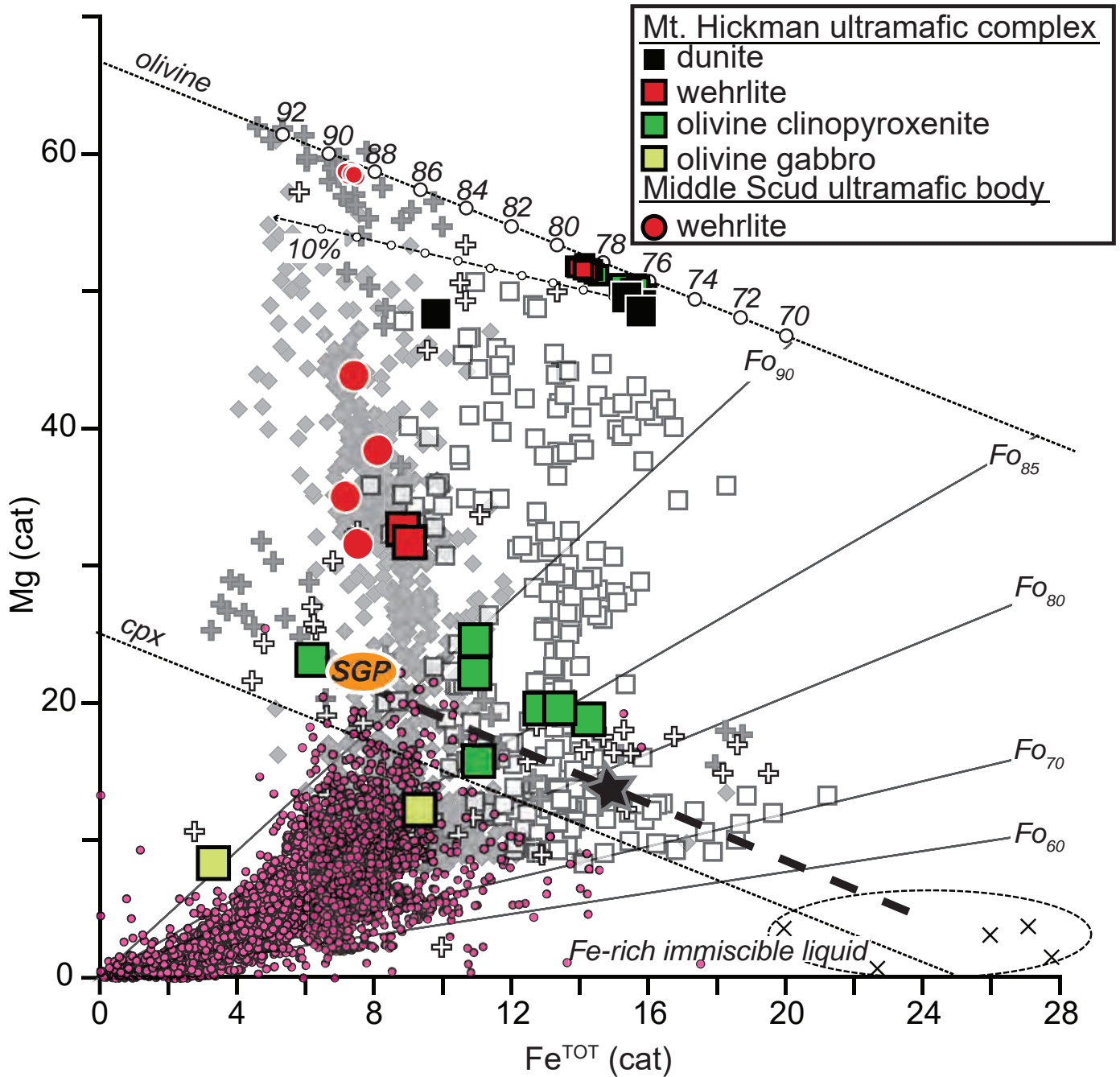


**Fig. 8.** Mg vs.  $Fe^{TOT}$  in cation units, showing the compositions of rocks (large symbols) and olivine (small symbols) from the Mount Hickman complex and the Middle Scud body. Electron microprobe-determined olivine compositions are shown by the smaller symbols along the olivine stoichiometric line (negatively sloping dashed line near the top of diagram). Also shown is the clinopyroxene stoichiometric line (cpx), and the isopleths of constant Fo content coexisting with liquids as determined by the Fe-Mg exchange coefficient ( $K_D=0.30$ ) and adjusted for  $Fe^{3+}/Fe^{TOT}=0.15$ . The effect of post accumulation magnetite metasomatism (0-10%) is illustrated by the dashed line emanating from the Mount Hickman complex dunite. Other data: pink circles – calcalkaline volcanic suite from Andes arc ( $n=5339$ ; <http://georoc.mpch-mainz.gwdg.de>); grey diamonds – mafic and ultramafic rocks with pyroclitic (Mg-number=0.88-0.92) mantle provenance (Milidragovic and Francis, 2016); white squares – Archean ferropicrites from the Superior Province (Milidragovic and Francis, 2016); grey crosses – Alaskan-type intrusions (Findlay, 1969; Himmelberg and Loney, 1995; Scheel, 2007); white crosses – Fe-rich Alaskan-type intrusions (Irvine, 1974; Himmelberg and Loney, 1995); x – average Fe-rich immiscible liquids compiled by Jakobsen et al. (2005); SGP=parental composition of the Stuhini Group picrite determined by Milidragovic et al. (2016b). Black star – hypothetical magma in equilibrium with  $Fo_{76}$  and parental to the Mount Hickman complex dunites, formed by mixing between an olivine-saturated basalt and an Fe-rich immiscible liquid (thick dashed line).

### 6.3. Remobilization of transient Fe-rich dunite layers

The decimetre to metre-scale serpentized dunite units observed in the complex (see above) could conceivably represent remobilized olivine-rich layers within wehrlite or olivine clinopyroxenite, thus explaining the lack of a well-developed dunite core. Macro-scale layering is a signature of large layered intrusions (e.g., Muskox Intrusion; Irvine and Smith, 1967); remobilization of olivine-rich cumulate layers has been inferred at the Turnagain and Tulameen complexes (Nixon et al., 1997; Scheel, 2007, Nixon et al., 2012). Layers of dunite with relatively low Mg-number may be generated by mixing of relatively evolved, clinopyroxene-saturated liquids with primitive, olivine-saturated, magmas (e.g., Irvine, 1979), and thus represent transient deviations from the olivine-clinopyroxene cotectic. Mixing between differentiated and primitive liquids may also explain the low concentrations of Ni in dunite without invoking Ni mobility and secondary Ni mineralization.

We consider that such remobilization is unlikely because the high Fe content of Mount Hickman complex dunites appears to require a parental magma with low Mg-number and  $\text{FeO}^{\text{TOT}} \geq 19$  wt.%, and the calc-alkaline magma (indicated by the observed crystallization sequence of olivine, clinopyroxene, magnetite, plagioclase) would have been unable to reach the implied level of Fe-enrichment (Fig. 8). Furthermore, mixing between primitive and evolved magmas fails to readily explain the relative enrichment of  $\text{TiO}_2$  in serpentized dunites, because neither the primitive or differentiated liquids would be enriched in Ti relative to the similarly incompatible elements. The problem would be further compounded if the differentiated liquids were co-saturated in magnetite, whose fractionation would result in relative  $\text{TiO}_2$  depletion.

### 6.4. Magma mixing

We favour a model in which the Mount Hickman mafic-ultramafic complex was generated by two fundamentally different and unrelated, magma types. The abundant, fresh to pervasively altered, olivine and clinopyroxene cumulus crystals indicate crystallization from a silicate, mafic to ultramafic, parental liquid. However, the rounded and embayed clinopyroxene crystals in intercumulus magnetite (Figs. 4e-f), suggest that clinopyroxene was not in equilibrium with the Fe-oxide -saturated magma that occupied the interstitial space. Based on these observations, we infer the coexistence of a relatively evolved (Ni-poor), olivine  $\pm$ clinopyroxene-saturated picritic to basaltic silicate magma and magma with high normative magnetite content. Accordingly, we attribute the Fe-rich character of the ultramafic rocks to mixing of these two fundamentally different magmas at different stages of the complex's evolution. The Fe-rich oxide magma, was also likely enriched in Ti  $\pm$ P, accounting for the marked relative enrichments of these elements in the otherwise refractory dunite.

Fe-Ti-P rich glassy globules and melt inclusions, resulting from immiscible separation of Fe- and Si-rich melts from

relatively evolved tholeiitic and alkaline magmas have been observed from a range of volcanic suites (Philpotts, 1982) and mafic intrusions (Jakobsen et al., 2005; Zhou et al., 2013). Based on work in Skaergaard intrusion, Jakobsen et al. (2005) proposed mixing of dense Fe-rich liquids with primitive basaltic magmas to explain the origin of ferropicrites. However, immiscible separation of Fe-rich liquids, requires relatively reducing conditions, which inhibit early magnetite crystallization (Philpotts, 1982). Furthermore, magmatic evolution towards Fe-rich liquid immiscibility is unlikely to be achieved through a calc-alkaline (olivine-clinopyroxene-plagioclase) crystallization sequence, which is exhibited by the Mount Hickman ultramafic complex, and is instead more consistent with tholeiitic (olivine-plagioclase-clinopyroxene) differentiation.

The mixing process proposed herein requires the separation of a dense, immiscible Fe-rich liquid from a relatively evolved, dry, and reduced magma at low pressure, where plagioclase, rather than clinopyroxene, is stable (see Grove and Baker, 1984). However, the calc-alkaline crystallization sequence exhibited by the Mount Hickman complex, indicates a relatively hydrous and oxidizing ultramafic magma (see Sisson and Grove, 1993). Thus we propose that the immiscible Fe-rich liquid sank into the crust, as proposed by Jakobsen et al. (2005) for the genesis of ferropicrites, and mixed with liquid to partially crystalline picritic to basaltic magma to form an Fe-rich, olivine-saturated hybrid magma that was parental to the dunites of the Mt. Hickman ultramafic complex.

## 7. Conclusions

The Mount Hickman ultramafic complex is a composite, Middle to Late Triassic, Alaskan-type intrusion comprising dunite, wehrlite, olivine clinopyroxenite and gabbro. With pervasively serpentized dunite and nearly fresh olivine  $\pm$ magnetite clinopyroxenite, the intrusion is variably altered. The ultramafic rocks have  $\text{FeO}^{\text{TOT}}$  contents that exceed most terrestrial ultramafic rocks, including other Alaskan-type intrusions from the North American Cordillera. The high whole-rock  $\text{FeO}^{\text{TOT}}$  concentrations are in stark contrast to the nearby (~15 km) Middle Scud ultramafic body. Of the four possibilities considered (metasomatism, magmatic differentiation, remobilization of cumulates from original Fe-rich olivine layers, and magma mixing), field, petrographic, and geochemical evidence leads us to favour a preliminary model in which the unusual Fe-enrichment of the Mount Hickman ultramafic complex resulted from mixing of two magma types: a relatively evolved picritic/basaltic magma and a Fe-Ti-P-rich liquid similar to the glassy globules and melt inclusions reported from elsewhere by Philpotts (1982) and Jakobsen et al. (2005). The proposed model may be tested by in-situ analysis of melt inclusions hosted in clinopyroxene crystals from the Mount Hickman ultramafic complex and identification of a population with strong Fe enrichment, similar to that reported by Jakobsen et al. (2005) and references therein (Fig. 8). An expanded global geochemical database of Alaskan-type intrusions combined

with further study of magnetite, clinopyroxene, and trapped melt inclusions from the Mount Hickman Complex will help address the origin of ultramafic intrusions at convergent margins and aid understanding, and exploring for, magmatic Ni-Cu-PGE mineralization of Alaskan-type intrusions.

### Acknowledgments

This study was funded by the Government of Canada's Geomapping for Energy and Minerals program (ESS contribution number 20160198). Logistical support was generously provided by Teck Resources, and we with particularly thank Klaus Hepe, Gabe Jutras, and Leif Bailey. The authors benefited from excellent field assistance by Simon Carroll and Sebastian Bichlmaier. We thank Graham Nixon for perceptive comments to a first draft and, in particular, for pointing out misconceptions tied to the term 'Polaris suite' and for challenging us with possible alternative origins.

### References cited

- Barresi, T., Nelson, J.L., Dostal, J., and Friedman, R., 2015. Evolution of the Hazelton arc near Terrace, British Columbia: stratigraphic, geochronological, and geochemical constraints on a Late Triassic-Early Jurassic arc and Cu-Au belt. *Canadian Journal of Earth Sciences*, 52, 466-494.
- Brown, D.A. and Gunning, M.H., 1989. Geology of the Scud River area, northwestern British Columbia (104G/5 and 6). In: *Geological Fieldwork 1988*, British Columbia Ministry of Energy, Mines and Petroleum Resources, British Columbia Geological Survey Paper 1989-1, pp. 251-267.
- Brown, D.A., Gunning, M.H., and Greig, C.J., 1996. The Stikine project: geology of the western Telegraph Creek map area, Northwestern British Columbia (NTS 104G/5, 6, 11W, 12 and 13). *British Columbia Ministry of Energy, Mines and Natural Gas, British Columbia Geological Survey Bulletin 95*, 175 p.
- Deer, W.A., Howie, R.A., Zussman, J., 1969. *An introduction to the rock forming minerals*, 4<sup>th</sup> Edition, John Wiley and Sons Inc., New York, 528 p.
- Findlay, D.C., 1969. Origin of the Tulameen ultramafic-gabbro complex, southern British Columbia. *Canadian Journal of Earth Sciences*, 6, 399-425.
- Francis, D. and Minarik, W., 2008. Aluminum-dependent trace element partitioning in clinopyroxene. *Contributions to Mineralogy and Petrology*, 156, 439-451.
- Grove, T. and Baker, M.B., 1984. Phase equilibrium controls on the tholeiitic versus calc-alkaline differentiation trends. *Journal of Geophysical Research*, 89, 3253-3274.
- Guillou-Frottier, L., Burov, E., Augé, T., Gloaguen, E., 2014. Rheological conditions for emplacement of Ural-Alaskan-type ultramafic complexes. *Tectonophysics*, 631, 130-145.
- Himmelberg, G.R. and Loney, R.A., 1995. Characteristics and petrogenesis of Alaskan-type ultramafic-mafic intrusions, southeastern Alaska. *U.S. Geological Survey Professional Paper 1564*, 51 p.
- Hirth, G. and Guillot, S., 2013. Rheology and tectonic significance of serpentinite. *Elements*, 9, 107-113. In: *Geological Fieldwork 1988*, British Columbia Ministry of Energy, Mines and Petroleum Resources, British Columbia Geological Survey Paper 1989-1, pp. 429-442.
- Holbek, P.M., 1988. *Geology and mineralization of the Stikine Assemblage, Mess Creek Area, northwestern British Columbia*. Unpublished M.Sc. thesis, The University of British Columbia, 184 p.
- Irvine, T.N., 1974. Petrology of the Duke Island ultramafic complex, southeastern Alaska. *The Geological Society of America Memoir* 138, 240 p.
- Irvine, T.N., 1979. Rocks whose composition is determined by crystal accumulation and sorting. In: H.S.Jr., Yoder (Ed.), *The Evolution of Igneous Rocks: Fiftieth Anniversary Perspectives*. Princeton University Press, Princeton, pp. 245-306.
- Irvine, T.N. and Smith, C.H., 1967. The ultramafic rocks of the Muskox intrusion, Northwest Territories, Canada. In: P.J. Wyllie (Ed.), *Ultramafic and Related Rocks*. John Wiley and Sons Inc., New York, pp. 38-49.
- Jakobsen, J.K., Veksler, I.V., Tegner, C., and Brooks, C.K., 2005. Immiscible iron- and silica-rich melts in basalt petrogenesis documented in Skaergaard intrusion. *Geology*, 33, 885-888.
- Mihalynuk, M.G., Bellefontaine, K.A., Brown, D.A., Logan, J.M., Nelson, J.L., Legun, A.S. and Diakow, L.J., 1996. *Geological compilation, northwest British Columbia (NTS 94E, L, M; 104F, G, H, I, J, K, L, M, N, O, P; 114J, O, P)*. BC Ministry of Energy and Mines, British Columbia Geological Survey Open File 1996-11.
- Milidragovic, D. and Francis, D., 2016. Ca. 2.7 Ga ferropicritic magmatism: A record of Fe-rich heterogeneities during Neoproterozoic global mantle melting. *Geochimica et Cosmochimica Acta*, 185, 44-63.
- Milidragovic, D., Joyce, N.L., Zagorevski, A., and Chapman, J.B., 2016a. Petrology of explosive Middle-Upper Triassic ultramafic rocks in the Mess Creek area, northern Stikine terrane. In: *Geological Fieldwork 2015*, British Columbia Ministry of Energy and Mines, British Columbia Geological Survey Paper 2016-1, pp. 95-111.
- Milidragovic, D., Chapman, J.B., Bichlmaier, S., Canil, D., and Zagorevski, A., 2016b. H<sub>2</sub>O-driven generation of picritic melts in the Middle to Late Triassic Stuhini arc of the Stikine terrane, British Columbia, Canada. *Earth and Planetary Science Letters* 454, 65-77.
- Nixon, G.T., Ash, C.H., Connely, J.N., and Case, G., 1989. Alaskan-type mafic-ultramafic rocks in British Columbia: the Gnat Lakes, Hickman, and Menard Creek complexes. In: *Geological Fieldwork 1988*, British Columbia Ministry of Energy, Mines and Petroleum Resources, British Columbia Geological Survey Paper 1989-1, pp. 429-442.
- Nixon, G.T., Hammack, J.L., Ash, C.H., Cabri, L.J., Case, G., Connely, J.N., Heaman, L.M., Laflamme, J.G.H., Nuttall, C., Paterson, W.P.E., and Wong, R.H., 1997. Geology and platinum-group-element mineralization of Alaskan-type ultramafic-mafic complexes in British Columbia. *British Columbia Ministry of Employment and Investment, British Columbia Geological Survey Bulletin 93*, 141 p.
- Nixon, G.T., Hitchens, A.C., Ross, G.P., 2012. Geology of the Turnagain ultramafic intrusion, Northern British Columbia; BC Ministry of Energy and Mines, Open File 2012-05, map 1:10,000 scale.
- Nixon, G.T., Manor, M.J., Jackson-Brown, S., Scoates, J.S., and Ames, D.E., 2015. Magmatic Ni-Cu-PGE sulphide deposits at convergent margins, In: D.E. Ames and M.G. Houlé (Eds.), *Targeted Geoscience Initiative 4: Canadian Nickel-Copper-Platinum Group Elements-Chromium Ore Systems — Fertility, Pathfinders, New and Revised Models*. Geological Survey of Canada, Open File 7856, pp. 17-34.
- Palme, H. and O'Neill, H.St.C., 2003. Cosmochemical estimates of mantle composition. In: Holland, H.D., Turekian, K.K., Davis, A.M. (Eds.), *Treatise on Geochemistry*, vol. 2. Elsevier, Amsterdam, The Netherlands, pp. 1-38.
- Philpotts, A.R., 1982. Compositions of immiscible liquids in volcanic rocks. *Contributions to Mineralogy and Petrology*, 80, 201-218.
- Roeder, P.L. and Emslie, R.F., 1970. Olivine-liquid equilibrium. *Contributions to Mineralogy and Petrology*, 29, 275-289.
- Scheel, J.E., 2007. Age and origin of the Turnagain Alaskan-type

- intrusion and associated Ni-sulphide mineralization, north-central British Columbia, Canada. Unpublished M.Sc. thesis, The University of British Columbia, 211 p.
- Sisson, T.W. and Grove, T.L., 1993. Experimental investigations of the role of H<sub>2</sub>O in calc-alkaline differentiation and subduction zone magmatism. *Contributions to Mineralogy and Petrology*, 113, 143-166.
- Taylor, H.P.Jr., 1967. The zoned ultramafic complexes of southeastern Alaska. In: P.J. Wyllie (Ed.), *Ultramafic and Related Rocks*. John Wiley and Sons Inc., New York, p. 97-121.
- Wood, B.J. and Blundy, J.D., 2001. The effect of cation charge on crystal-melt partitioning of trace elements. *Earth and Planetary Science Letters*, 188, 59-71.
- Woodsworth, G. J., Anderson, R. G., and Armstrong, R. L., 1991. Plutonic regimes, in Gabrielse, H., and Yorath, C. J., (Eds.), *Geology of the Cordilleran Orogen in Canada, Volume Geology of Canada 4*, Geological Survey of Canada, p. 491-531.
- Zagorevski, A., Mihalynuk, M.G., Milidragovic, D., Joyce, N., Kovacs, N., Allan, M., and Kellett, D., 2016. Characterization of volcanic and intrusive rocks across the British Columbia - Yukon border, GEM2 Cordillera. Geological Survey of Canada, Open File 8141, 13 p. doi:10.4095/299198.
- Zhou, M.-F., Chen, W.T., Wang, C.Y., Prevec, S.A., Liu, P.P., and Howarth, G.H., 2013. Two stages of immiscible liquid separation in the formation of Panzhihua-type Fe-Ti-V oxide deposits, SW China. *Geoscience Frontiers* 4, 481-502.

# Late Cretaceous magmatism in the Atlin-Tagish area, northern British Columbia (104M, 104N)



A. Zagorevski<sup>1, a</sup>, M.G. Mihalynuk<sup>2</sup>, N. Joyce<sup>1</sup>, and R.G. Anderson<sup>3</sup>

<sup>1</sup>Geological Survey of Canada, Ottawa, ON, K1A 0E8

<sup>2</sup>British Columbia Geological Survey, Ministry of Energy and Mines, Victoria, BC, V8W 9N3

<sup>3</sup>Geological Survey of Canada, Vancouver, BC, V6B 5J3

<sup>a</sup>corresponding author: alex.zagorevski@canada.ca

Recommended citation: Zagorevski, A., Mihalynuk, M.G., Joyce, N., and Anderson, R.G., 2017. Late Cretaceous magmatism in the Atlin-Tagish area, northern British Columbia (104M, 104N). In: Geological Fieldwork 2016, British Columbia Ministry of Energy and Mines, British Columbia Geological Survey Paper 2017-1, pp. 133-152.

## Abstract

The Cache Creek and Stikine terranes in northern British Columbia are unconformably overlain by Upper Cretaceous volcanic, hypabyssal, and sedimentary rocks of the Montana Mountain complex and Windy-Table suite and cut by intrusive rocks of the Surprise Lake plutonic suite. Although these rocks are commonly spatially and temporally associated with mineral prospects, their regional distribution and inter-relationships are not well understood. Herein we present three new U-Pb zircon ages for Upper Cretaceous volcanic and plutonic rocks and new geochemical data. A sample of Peninsula Mountain rhyolite yielded a  $85.0 \pm 1.6$  Ma age indicating that it forms part of the Windy-Table suite. Mafic volcanic rocks previously assigned to Peninsula Mountain suite have the same geochemical characteristics as ophiolitic rocks of the Graham Inlet suite (Cache Creek terrane). These data indicate that the stratigraphy of the area requires significant revision. Ages from the Surprise Lake batholith of  $79.70 \pm 0.15$  Ma and from a granite near Tutshi Lake of  $76.5 \pm 1.3$  Ma are slightly younger than the Windy-Table suite volcanism. The age of these volcanic and plutonic rocks overlaps the age of magmatism and prolific mineralization in northern British Columbia and Yukon.

**Keywords:** Late Cretaceous magmatism, Windy-Table suite, Peninsula Mountain suite, Surprise Lake batholith, Graham Inlet suite, ophiolite

## 1. Introduction

The Cretaceous is a tectonically complex and economically important period in the development of the northern Cordilleran orogen. It marks the end of a high-flux magmatic episode (DeCelles et al., 2009) that led to the emplacement of mid-Cretaceous magmas throughout the Cordillera. Many workers have presumed a back-arc to arc setting for this episode (ca. 115-90 Ma; Hart et al., 2004) and thus for mineral deposits and prospects such as copper skarns of the Whitehorse Copper belt (108-112 Ma; Hart, 1996; Hart, 1997). This magmatic-metallogenic epoch is broadly coeval with the end of dextral transpression inboard of the Intermontane superterrane, and cessation of motion on faults such as the Teslin-Thibert-Kutcho fault (Fig. 1), which are thought to have accommodated major translations only until mid-Cretaceous (Gabrielse et al., 2006). Subsequent Late Cretaceous magmatism was characterized by emplacement of low volume stocks and minor volcanic eruptions in a presumed arc setting and is associated with economic mineralization in British Columbia, Yukon and Alaska (Allan et al., 2013; Nelson et al., 2013; Simmons et al., 2005; Smith and Arehart, 2010).

Upper Cretaceous rocks are common in northwestern British Columbia (Fig. 2; Mihalynuk et al., 1999; Simmons et al., 2005; Smith and Arehart, 2010) and Yukon (Hart and Pelletier, 1989). Although these rocks host many mineral prospects, their stratigraphy, age, and distribution have not been considered

collectively since the work of Hart (1997). Herein we present new U-Pb geochronological and geochemical data from the Atlin and Tagish lakes area (Figs. 2, 3) and consider their stratigraphic, magmatic, and metallogenic implications.

## 2. Regional geology

Atlin and Tagish lakes are the principal physiographic features in the study area (Fig. 2). Areas surrounding these lakes are underlain by rocks of the Stikine and Cache Creek terranes (Fig. 1), parts of which have been the subject of systematic regional studies by various workers (Gwillim, 1901; Watson and Mathews, 1944; Aitken, 1959; Monger, 1975, 1977; Bultman, 1979; Lefebure and Gunning, 1988; Bloodgood et al., 1989; Bloodgood and Bellefontaine, 1990; Ash, 1994; Mihalynuk et al., 1999, 2003). Stikine terrane comprises Late Devonian to Early Permian and Middle Triassic to Early Jurassic volcanic arc successions that, in Atlin area, are represented by volcano-sedimentary rocks of the Stuhini Group (Upper Triassic), plutonic rocks of Stikine plutonic suite (Upper Triassic), volcanic rocks of the Hazelton Group (Lower Jurassic) and sedimentary rocks of the Laberge Group (Lower to Middle Jurassic, Fig. 2). Cache Creek terrane comprises a diverse assemblage of Carboniferous to Lower Jurassic rocks (e.g., Monger, 1975; Golding et al., 2016).

The oldest dated Cache Creek units are the Horsefeed Formation limestone (Carboniferous to Permian) and

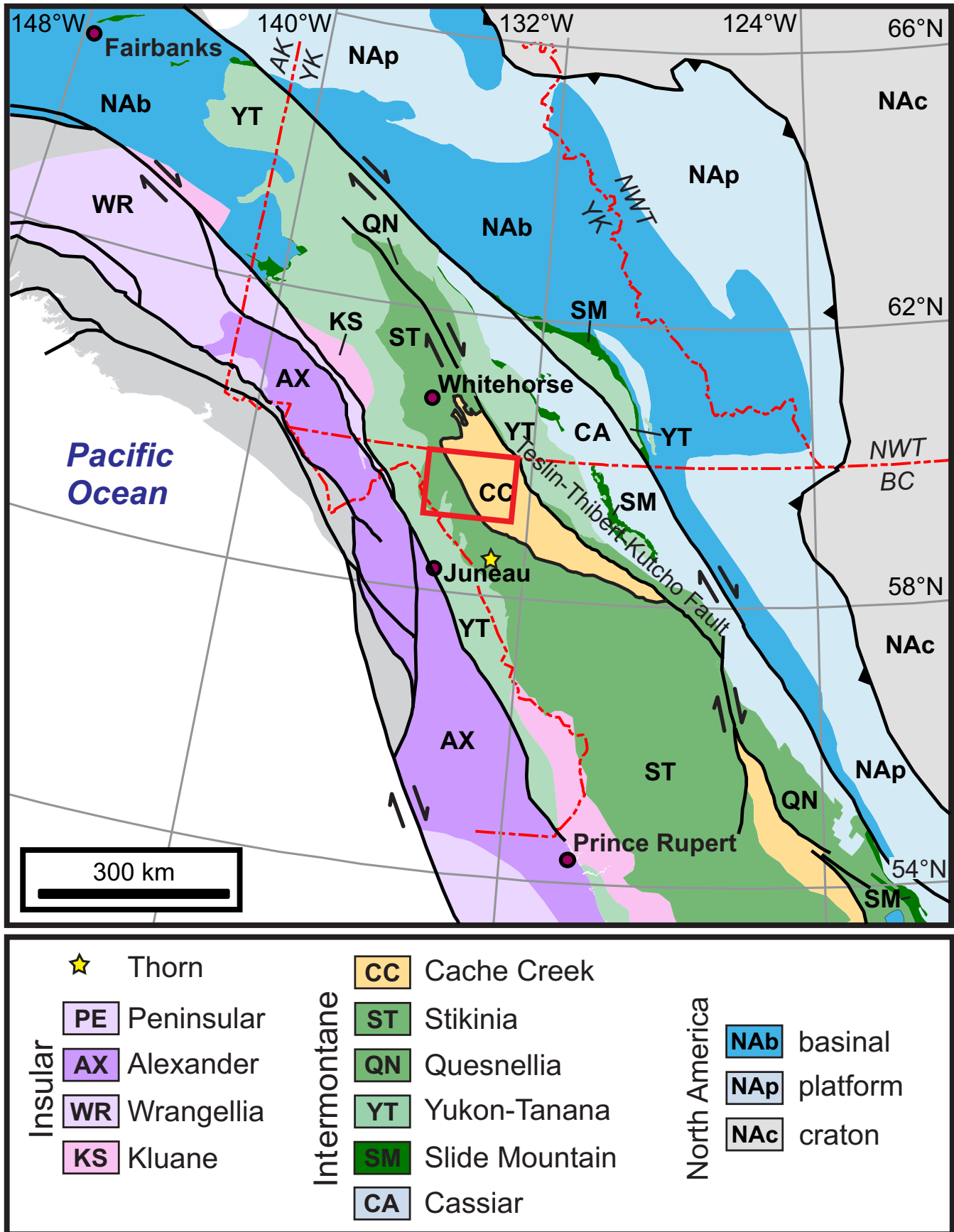
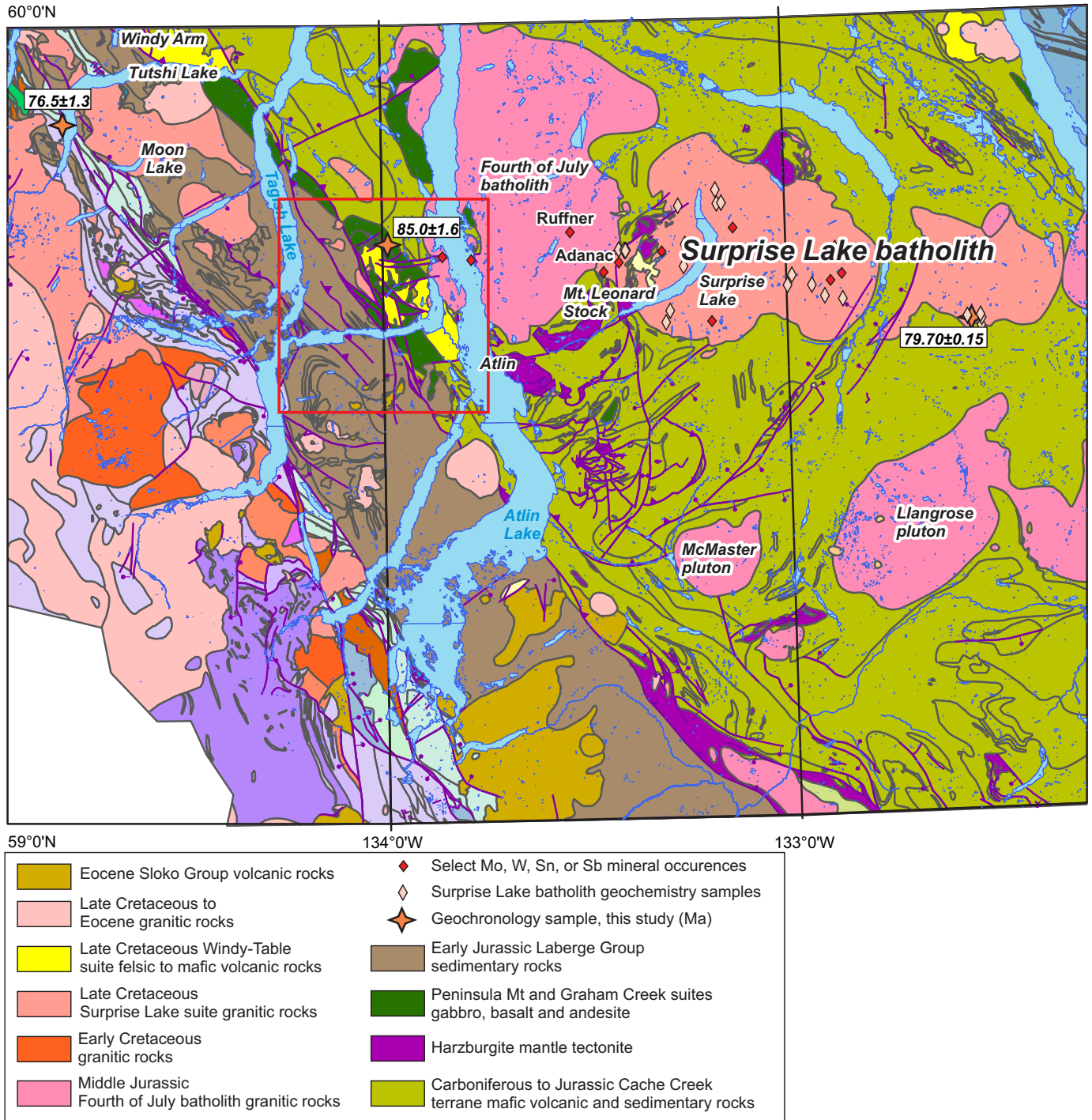


Fig. 1. Northern Cordillera terranes (from Colpron and Nelson, 2011). Atlin-Tagish Lake area outlined by solid red box.



**Fig. 2.** Simplified geology of Atlin-Tagish Lake area (from Massey et al., 2005). Graham Inlet area outlined by solid red box.

siliclastic rocks and chert of the Kedahda Formation (Early Carboniferous to Early Jurassic). Ophiolitic rocks once thought to form the basement of the terrane (e.g., Monger, 1975) are now known to be Upper Permian to Middle Triassic (Nakina formation, Graham Inlet suite, Peninsula Mountain suite, Mitchie Formation: Gordey et al., 1998; Mihalynuk et al., 1999, Mihalynuk et al., 2003; Bickerton et al., 2013). Triassic to Lower Jurassic siliclastic and chemical sedimentary rocks

once included in the Kedahda Formation have been recognized in some areas as a separate unit (Mihalynuk et al., 2003; Fig. 2). Stikine and Cache Creek terranes are juxtaposed along the Nahlin fault, which commonly places ophiolitic mantle on its eastern side against sedimentary rocks of the Laberge Group (Early to Middle Jurassic) to the west.

Stikine and Cache Creek terrane rocks were deformed, locally intensely, before emplacement of the Three Sisters plutonic

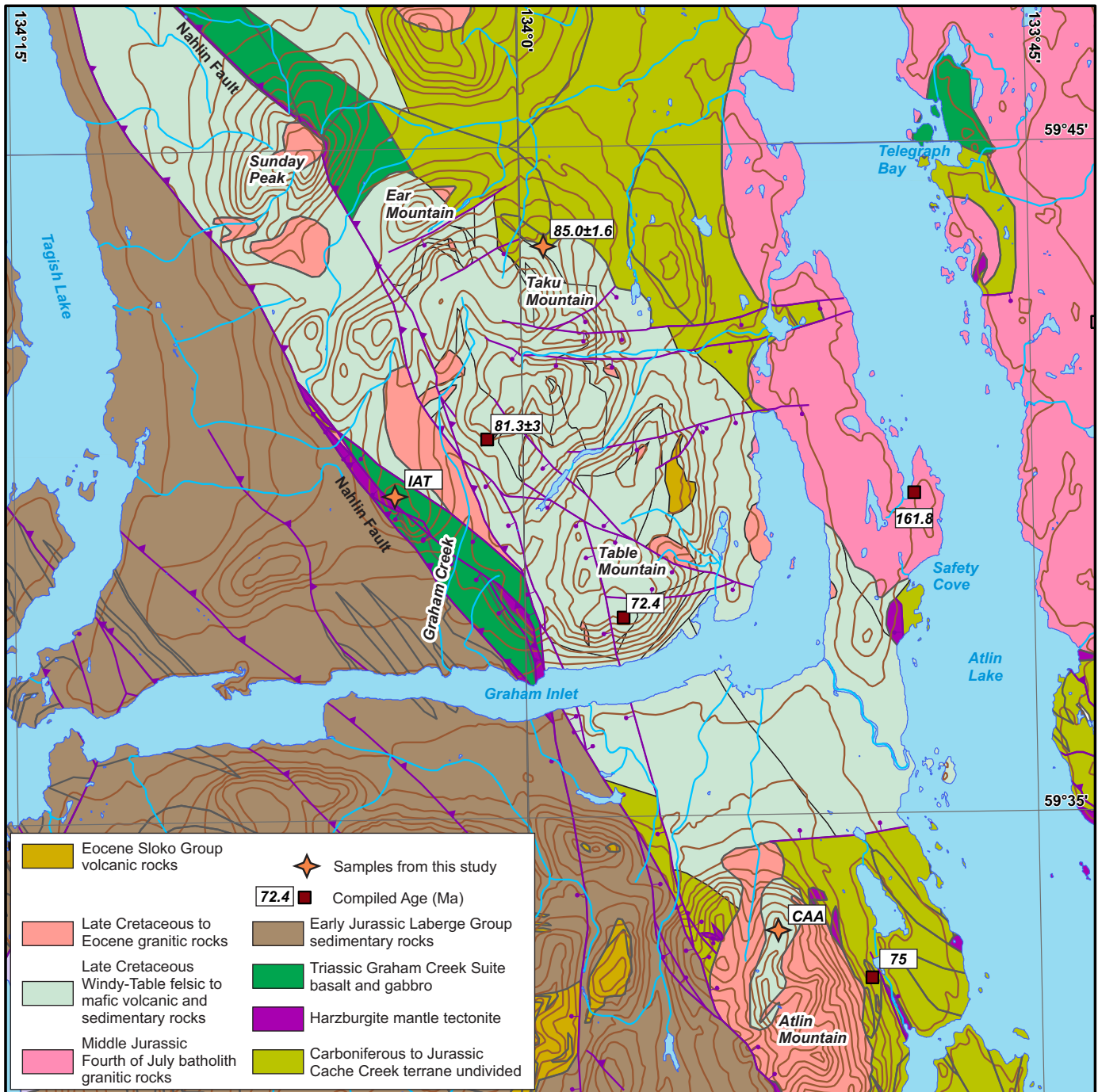


**Fig. 3.** Revised geology of the Graham Inlet area (modified from Massey et al., 2005) on the basis of new data. IAT- island arc tholeiite, CAA – calc-alkaline andesite. Ages from Breitsprecher and Mortensen (2004).

suite (Middle Jurassic). Intrusions belonging to this suite are the Fourth of July batholith, Llangorse and McMaster plutons and coeval satellite stocks, which intrude on both sides of the Nahlin fault and thermally metamorphose previously deformed rocks of the Cache Creek terrane and Whitehorse Trough (Fig. 2; ca. 172 Ma: Mihalynuk et al., 1992). A magmatic lull followed Three Sisters plutonic suite magmatism with low magmatic productivity lasting from ~165 to 115 Ma (Mihalynuk et al., 1999). Resumption of high-flux magmatism in the mid-

Cretaceous is marked by emplacement of voluminous Coast Plutonic Complex intrusions to the west (Massey et al., 2005) and Whitehorse plutonic suite to the north of the study area (Colpron et al., 2016). Coeval volcanic strata are preserved in the lower part of the Montana Mountain complex (ca. 95 Ma: Hart, 1996). This episode was followed by deposition of volcano-sedimentary rocks in the upper part of the Montana Mountain complex and the Windy-Table suite (ca. 84 Ma: Hart, 1996; ca. 81 Ma: Mihalynuk et al., 1992), and emplacement of

coeval plutonic rocks of the Surprise Lake plutonic suite and its correlatives (Fig. 2; ca. 83-78 Ma: Mihalynuk et al., 1992; Smith and Arehart, 2010).

### 2.1. Permian to Early Jurassic rocks

The Cache Creek terrane (Fig. 1) contains aerially extensive mafic-ultramafic ophiolitic rocks and overlying siliciclastic and chemical sedimentary rocks. Crustal ophiolitic rocks have been included in the Nakina Formation, Graham Inlet suite, and Peninsula Mountain suite (Late Permian to Middle Triassic: Mihalynuk et al., 1999, Mihalynuk et al., 2003). Triassic to Lower Jurassic siliciclastic and chemical sedimentary rocks of the Kedadha Formation (e.g., Golding et al., 2016) are locally interlayered with ophiolitic rocks but are generally mapped as a separate unit. In the study area, the Graham Creek suite contains ultramafic rocks, gabbro and tholeiitic pillow basalt (Mihalynuk et al., 1999). The Peninsula Mountain suite is inferred to overlie ophiolitic rocks of the Graham Creek suite. The Peninsula Mountain suite consists of conglomeratic rocks, pyritic rhyolite, calc-alkaline andesite breccia, polyolithic breccia, pillow basalt, and interbedded chert and wacke (Mihalynuk et al., 1999).

### 2.2. Montana Mountain complex and older

Lower Cretaceous volcanic rocks are spatially restricted in northern British Columbia. Lower Cretaceous intermediate to felsic volcanic rocks were deposited paraconformably on Laberge Group (Jurassic) strata west of Tutshi Lake. These rocks yielded a  $124.9 \pm 0.5$  Ma crystallization age based on the two most-concordant zircon fractions (Mihalynuk et al., 2003). Deposition of these rocks was followed by deposition of the Montana Mountain complex, which at its type locality in Yukon, comprises two units separated by ca. 10 m.y. (Hart, 1996). The lower unit consists of green to maroon andesite and mafic flows that yielded a  $95 \pm 1$  Ma U-Pb zircon age (Hart, 1996). These are overlain by rhyolite flows, breccia and andesite that yielded a  $84 \pm 1$  Ma U-Pb zircon age (Hart, 1996). The Montana Mountain complex was interpreted by Mihalynuk et al. (1999) to extend from Yukon to Windy Arm. For the purposes of mapping and to retain consistency with BC nomenclature, Mihalynuk et al. (1999) used Montana Mountain complex for andesitic rocks at Windy Arm but assigned other felsic and andesitic rocks to the Windy-Table suite (see below).

### 2.3. Windy-Table suite

The Windy-Table suite (Mihalynuk et al., 1999: Hutshi Formation of Bultman, 1979) comprises andesite to rhyodacite flows and tuff, and minor basalt that are discontinuously exposed from Windy Arm to Atlin Mountain (Figs. 3, 4). The Windy-Table suite was deposited on Jurassic and older rocks in the area above an unconformity surface with more than a kilometre of relief (Bultman, 1979). At Table Mountain, felsic volcanic rocks near the top of the Windy-Table suite yielded a  $81.3 \pm 0.3$  Ma U-Pb zircon crystallization age (Mihalynuk et al., 1992).

### 2.4. Surprise Lake plutonic suite

The Surprise Lake plutonic suite (Late Cretaceous) consists of texturally heterogeneous biotite granites that form two aerially extensive bodies (Surprise Lake batholith), the Mount Leonard stock, and several small plutons west of Atlin Lake (Fig. 2; Aitken, 1959; Ballantyne and Littlejohn, 1982; Mihalynuk et al., 1999). The granites include irregularly distributed phases that are equigranular, seriate, megacrystic, or porphyritic. They commonly contain biotite, alkali feldspar, lesser plagioclase, and smoky quartz, although some zones are aplitic or pegmatitic with miarolitic cavities (Lowe et al., 2003). Mihalynuk et al. (1992) obtained a crystallization age of  $83.8 \pm 5$  Ma (U-Pb zircon) from the marginal phase of the Surprise Lake batholith southeast of Surprise Lake. Detailed study of the Mount Leonard stock, host to the Adanac molybdenum deposit east of Surprise Lake, yielded U-Pb age determinations ranging from  $81.6 \pm 1.1$  to  $77.5 \pm 1.0$  Ma, and significantly younger molybdenum Re/Os ages, from  $70.87 \pm 0.36$  to  $69.72 \pm 0.35$  Ma (Smith and Arehart, 2010), similar to previous K-Ar and Rb-Sr age determinations (Christopher and Pinsent, 1982; Mihalynuk et al., 1992). Coeval intrusions west of Atlin Lake, including the Racine and Atlin Mountain plutons, are compositionally distinctive, relatively homogeneous quartz diorite to granodiorite. All were included with what Mihalynuk et al. (1999) termed the 'Carmacks magmatic epoch', constrained mainly by cooling ages of ~85 to 70 Ma (mostly by Bultman, 1979).

### 3. U-Pb geochronology

We collected samples of granitic rocks from the Surprise Lake batholith (CL01-094) and from a pluton near Tutshi Lake (MMI15-18-3) and a sample of rhyolite from the Peninsula Mountain suite (ZE10-248). Zircon separates were prepared by standard crushing, disk mill, Wilfley™ table, and heavy liquid techniques. Mineral separates were sorted by magnetic susceptibility using a Frantz™ isodynamic separator.

For the Surprise Lake batholith sample, zircons were analyzed using U-Pb TIMS as outlined in Parrish et al. (1987). Multigrain zircon fractions analyzed were very strongly air abraded following the method of Krogh (1982). Treatment of analytical errors follows Roddick et al. (1987), with errors on the ages reported at the  $2\sigma$  level (Table 1).

Zircons from samples ZE10-248 and MMI15-18-3 were analyzed on separate mounts using the Sensitive High Resolution Ion Microprobe (SHRIMP) at the Geological Survey of Canada in Ottawa. Analytical procedures and calibration details for the SHRIMP followed those described by Stern (1997) and Stern and Amelin (2003). Zircons were cast in 2.5 cm diameter epoxy mounts along with the Temora2 zircon primary standard, the accepted  $^{206}\text{Pb}/^{238}\text{U}$  age of which is  $416.8 \pm 0.33$  Ma (Black et al., 2005). Fragments of the GSC laboratory zircon standard (z6266, with  $^{206}\text{Pb}/^{238}\text{U}$  age = 559 Ma) were also included on the mounts as a secondary standard, analyses of which were interspersed among the sample analyses throughout the data sessions to verify the accuracy of the U-Pb calibration. The

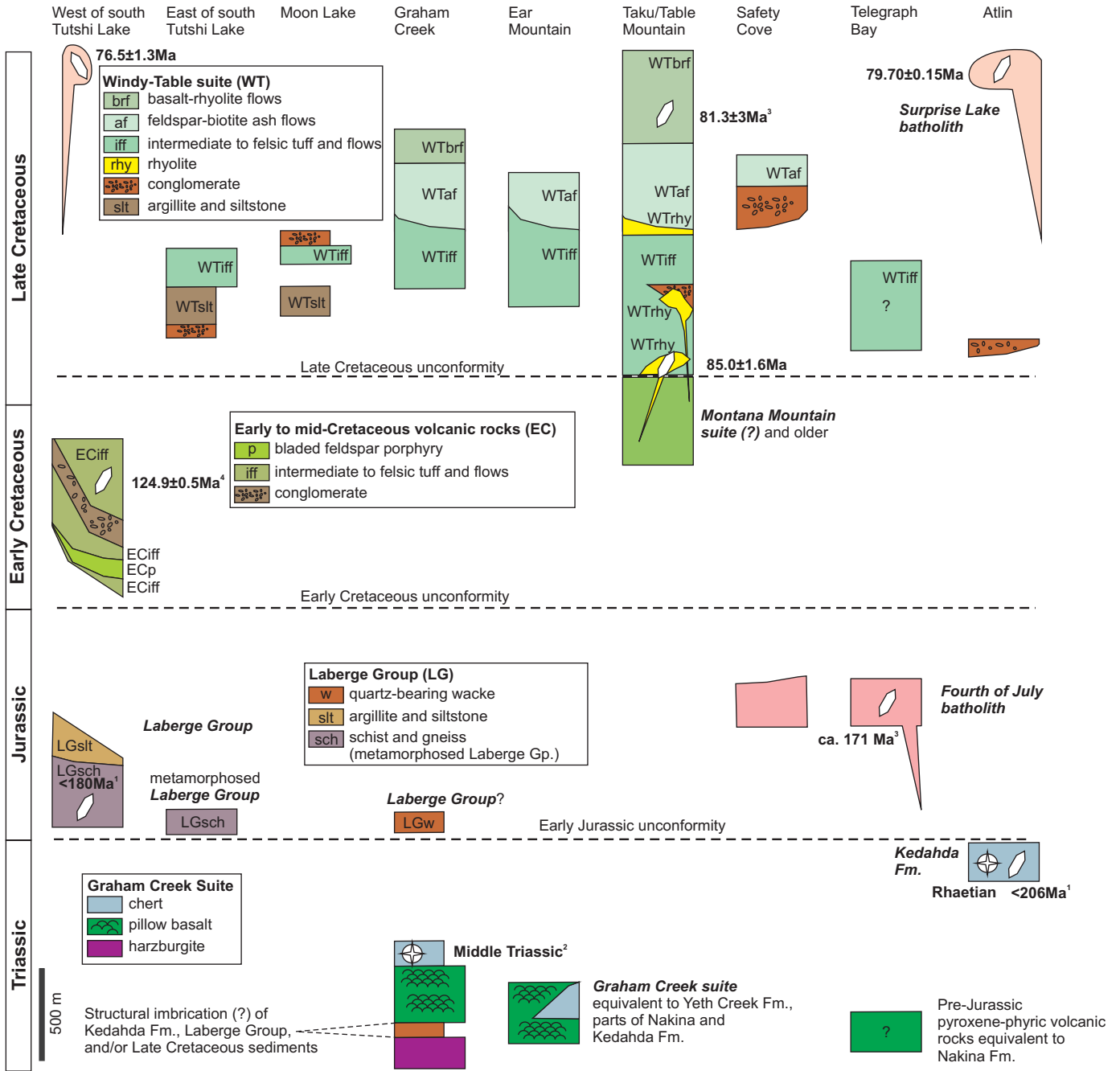


**Fig. 4.** Revised schematic stratigraphy of Triassic to Cretaceous rocks in the Atlin-Tagish area (modified from Mihalynuk et al., 1999). <sup>1</sup>Zagorevski, Joyce, and Cordey (unpublished data); <sup>2</sup>Mihalynuk et al.(1999); <sup>3</sup>Mihalynuk et al. (1992); <sup>4</sup> Mihalynuk et al. (2003).

mid-sections of the zircons were exposed using 9, 6, and 1 μm diamond compound, and internal features (e.g., zoning, structures, and alteration) were examined in both back-scattered electron mode (BSE) and cathodoluminescence mode (CL) using a Zeiss Evo 50 scanning electron microscope. The mount surfaces were evaporatively coated with 10 nm of high purity Au. Analyses were conducted during two separate data sessions, using an 160- primary beam, projected onto the zircons at 10 kV. Before analysis, the ion beam was rastered over the area of interest for 2 minutes to remove the Au coating and eliminate

effects of surface common lead. The sputtered area used for analysis was ca. 16 μm in diameter with beam currents of ~4 nA-7.5 nA. The count rates at ten masses including background were sequentially measured over 6 scans with a single electron multiplier and a pulse counting system with a deadtime of 11 ns (for sample ZE10-248) and 20 ns (for sample MMI15-18-3). The 1σ external errors of <sup>206</sup>Pb/<sup>238</sup>U ratios reported in Table 2 incorporate a ±0.80 - 1.60% error in calibrating the standard Temora2 zircon. Age errors are at the 2σ uncertainty level, and encompass the combined statistical uncertainty of

**Table 1.** ID-TIMS U-Pb zircon geochronological data.

Fraction Descr. <sup>12</sup>	#	Size µm	Wt ug	U ppm	Pb <sup>3</sup> ppm	Isotopic Ratios <sup>6</sup>								Ages (Ma) <sup>8</sup>								
						<sup>206</sup> Pb <sup>4</sup> 204Pb	Pb <sup>5</sup> pg	<sup>208</sup> Pb 206Pb	<sup>207</sup> Pb 235U	±1SE Abs	<sup>206</sup> Pb 238U	±1SE Abs	Corr. <sup>7</sup> Coeff.	<sup>207</sup> Pb 206Pb	±1SE Abs	<sup>206</sup> Pb 238U	±2SE	<sup>207</sup> Pb 235U	±2SE	<sup>207</sup> Pb 206Pb	±2SE	% Disc
<b>CL01-094 (Z7208): Surprise Lake batholith (granite)</b> 08V 635587E 6611708N NAD 83																						
Z1-El,Fg	43	74-200	52.0	404	5	1971	8.33	0.09875	0.081457	0.000199	0.012447	0.000022	0.624800	0.04746	0.00009	79.74	0.28	79.51	0.37	72.6	9.1	-10
Z2-El,Fg	82	<74	17.6	506	6	991.3	7.09	0.09990	0.082182	0.000360	0.012469	0.000027	0.433062	0.04780	0.00019	79.88	0.34	80.19	0.68	89.5	18.7	11
Z3-Eq,Fg,St	164	<74	50.6	584	7	2951	7.84	0.09811	0.082423	0.000133	0.012514	0.000014	0.807573	0.04777	0.00005	80.17	0.18	80.42	0.25	87.8	4.6	8.8
Z4-Eq,Fg,St	56	74-105	59.7	519	6	2883	8.36	0.09420	0.081802	0.000147	0.012426	0.000017	0.709603	0.04774	0.00006	79.61	0.21	79.84	0.28	86.6	6	8.1

<sup>1</sup>Z=zircon fraction; All fractions were air abraded following the method of Krogh (1982); <sup>2</sup>Zircon descriptions: all zircon fractions are abraded, colourless to pale yellow, with few clear to opaque inclusions from Frantz non-magnetic fraction at 0° sideslope and magnetic fraction at 0° sideslope, El=Elongate, Eq=Equant, Fg=Fragment, St=Stubby Prism; <sup>3</sup>Radiogenic Pb; <sup>4</sup>Measured ratio, corrected for spike and fractionation; <sup>5</sup>Total common Pb in analysis corrected for fractionation and spike; <sup>6</sup>Corrected for blank Pb and U and common Pb, errors quoted are 1 sigma absolute; procedural blank values for this study were from 0.1 pg U and 1 pg Pb for zircon analyses; <sup>7</sup>Correlation Coefficient; <sup>8</sup>Corrected for blank and common Pb, errors quoted are 2 sigma in Ma; The error on the calibration of the GSC 205Pb-233U-235U spike utilized in this study is 0.22% (2s).

the weighted mean age for the population and the 2σ error of the mean of the Temora2 zircon calibration standard. Off-line data processing was accomplished using customized in-house software. Isoplot v. 3.00 (Ludwig, 2003) was used to generate concordia plots and to calculate weighted means. Errors for isotopic ratios in Table 2 are given at 1σ uncertainty, as are the apparent SHRIMP ages. No fractionation correction was applied to the Pb-isotope data; common Pb correction used the Pb composition of the surface blank (Stern, 1997). All ages are reported as the <sup>207</sup>Pb-corrected weighted mean <sup>206</sup>Pb/<sup>238</sup>U age. The error ellipses on the concordia diagrams and the weighted mean errors are reported at 2σ.

### 3.1. CL01-094 (Z7208) Surprise Lake batholith granite (79.70 ±0.15 Ma)

Sample CL01-094 is a biotite monzogranite to alkali-feldspar granite from the southern margin of the Surprise Lake batholith in the Snowdon Range (Fig. 2). Zircons from this sample are equant to stubby to elongate prisms 70–200 µm long. Most are euhedral to subhedral faceted prisms and fragments with square cross sections. In transmitted light, the crystals range from clear and colourless to pale yellow, with minor clear and opaque inclusions and fractures. Four fractions were analyzed, all of which overlap concordia (Fig. 5a, Table 1). Fraction Z3 comprises 164 equant to stubby prismatic grains and yields a <sup>206</sup>Pb/<sup>238</sup>U age of 80.2 ±0.2 Ma. This is slightly older than the other three fractions, and is thus considered to reflect an inherited component. Fractions Z1, Z2, and Z3 consist of elongate, stubby prismatic to equant grains. All three fractions overlap each other on concordia, and their weighted average <sup>206</sup>Pb/<sup>238</sup>U age is 79.70 ±0.15 Ma (MSWD = 0.97, POF = 0.38). This is considered to be the crystallization age of the Surprise Lake batholith granite.

### 3.2. ZE10-248 (Z10297) Rhyolite northeast of Taku Mountain (85.0 ±1.6 Ma)

Sample ZE10-248 is from an altered, white to grey weathering, aphyric flow-banded rhyolite on the north side of Taku Mountain, previously included in the Peninsula Mountain suite (Mihalyuk et al., 1999). Most zircons from this sample

are fragments of stubby to semi-elongate prisms 50–200 µm long, and are clear and colourless to pale yellow. Although most grain fragments have preserved facets, others are slightly rounded, with grain surfaces that are pitted and chipped. Fractures and clear bubble-shaped inclusions are common. SEM-CL images reveal two contrasting grain types (Fig. 5b). Type I zircons are bright in CL (relatively low U), with distinct oscillatory and/or sector-zoning. Type II zircons are dark grey in CL (relatively high U), and grains are either homogeneous and unzoned or oscillatory-zoned. In transmitted light, types I and II zircon are indistinguishable.

Type I grains have a broad range of low to high U content (105–594 ppm) and moderate Th/U (0.23–0.55). The weighted mean <sup>207</sup>Pb-corrected <sup>206</sup>Pb/<sup>238</sup>U age of this sample is 174 ±2 Ma (n = 14, MSWD = 0.64; Fig. 5b). Type II zircon contain higher amounts of U (635–3491 ppm) and moderate Th/U (0.28–0.60). Nine Type II zircon grains yield a <sup>207</sup>Pb-corrected <sup>206</sup>Pb/<sup>238</sup>U age of 85.0 ±1.6 Ma (n = 9, MSWD = 1.5; Fig. 5b). One analysis, spot 10297-9.1, yields an age of 146 Ma; this result is interpreted to record mixing of differently aged zircons and was excluded from age calculations and interpretations. The age from the type II zircon of 85.0 ±1.6 Ma is interpreted as the rhyolite crystallization age. Type I zircon grains are interpreted as inherited from the Fourth of July batholith or coeval rocks.

### 3.3. MMI15-18-3 (Z11799) biotite monzogranite near Tutshi Lake (76.5 ±1.3 Ma)

Sample MMI15-18-3 is from a medium-grained, K-feldspar porphyritic biotite monzogranite to alkali feldspar granite (Figs. 2 and 5c) from highway outcrops along the west shore of Tutshi Lake. This granite is chilled against deformed Laberge Group strata along the east shore of southern Tutshi Lake where it yielded a poor-quality K-Ar biotite age of ~80 Ma (Bultman, 1979; recalculated).

Zircons from this sample are large (125–300µm) euhedral stubby to elongate prisms. In transmitted light, the grains are clear and colourless, with abundant colourless bubble- and rod-shaped inclusions. In SEM-CL images, central regions of most grains exhibit sector-zoned or striped growth, mantled by igneous oscillatory-zoned zircon of varying thickness. The

Table 2. SHRIMP U-Pb zircon geochronological data.

Spot	U ppm	Th ppm	$\frac{Th}{U}$	$^{206}Pb^*$ ppm	$\frac{^{204}Pb}{^{206}Pb}$	$\pm$	f(206) %	$\frac{^{208}Pb}{^{206}Pb}$	$\pm$	$\frac{^{238}U}{^{206}Pb}$	$\pm$	$\frac{^{207}Pb}{^{206}Pb}$	$\pm$
<b>ZE10-248 - Rhyolite (NAD83 Zone 8: 556929 E 6621288 N; Z10297; Mount IP579)</b>													
<b>Type II Zircon</b>													
7.1	797	309	0.40	8.5	0.0001339	0.0001339	0.24	0.1140	0.0142	80.443	2.309	0.0452	0.0028
25.1	1612	467	0.30	18.0	0.0004022	0.0001520	0.73	0.0665	0.0091	76.550	1.238	0.0493	0.0017
21.1	635	368	0.60	7.1	0.0001176	0.0001176	0.21	0.2128	0.0171	76.201	1.497	0.0487	0.0025
32.1	648	343	0.55	7.3	0.0002715	0.0001920	0.49	0.1774	0.0177	75.662	1.415	0.0519	0.0028
11.1	2014	536	0.28	23.1	<i>bdl</i>		0.00	0.0883	0.0066	75.001	1.210	0.0497	0.0015
24.1	1328	386	0.30	15.1	0.0003711	0.0001515	0.67	0.0893	0.0100	75.167	1.334	0.0474	0.0018
2.1	1633	517	0.33	18.8	<i>bdl</i>		0.00	0.1027	0.0078	74.761	1.244	0.0489	0.0017
17.1	1420	428	0.31	16.4	0.0001253	0.0000886	0.23	0.0802	0.0085	74.210	1.203	0.0452	0.0018
15.1	3491	2013	0.60	41.1	0.0000834	0.0000401	0.15	0.1843	0.0063	72.854	1.180	0.0480	0.0010
9.1	1711	729	0.44	33.8	-0.000032	-0.000032	-0.06	0.1257	0.0066	43.553	0.71	0.0488	0.0013
<b>Type I Zircon</b>													
31.1	578	130	0.23	13.2	0.0002605	0.0001504	0.47	0.0631	0.0103	37.516	0.618	0.0490	0.0046
30.1	105	28	0.28	2.4	0.0004340	0.0004340	0.78	0.1159	0.0314	36.766	0.683	0.0589	0.0054
26.1	454	219	0.50	10.5	0.0000911	0.0000911	0.16	0.1453	0.0127	37.058	0.612	0.0514	0.0041
28.1	369	163	0.46	8.5	0.0002632	0.0001861	0.48	0.1367	0.0162	36.998	0.618	0.0496	0.0027
23.1	396	195	0.51	9.2	<i>bdl</i>		0.00	0.1435	0.0132	36.783	0.646	0.0513	0.0025
20.1	525	270	0.53	12.2	0.0000819	0.0000819	0.15	0.1825	0.0135	36.936	0.607	0.0476	0.0020
19.1	169	56	0.34	3.9	0.0006648	0.0003839	1.20	0.0744	0.0215	36.751	0.855	0.0504	0.0035
29.1	274	145	0.55	6.4	0.0008911	0.0003986	1.61	0.1561	0.0241	36.331	0.717	0.0567	0.0033
16.1	138	50	0.38	3.2	0.0008055	0.0004652	1.45	0.0949	0.0258	36.695	0.777	0.0455	0.0037
18.1	313	136	0.45	7.4	<i>bdl</i>		0.00	0.1495	0.0142	36.403	0.607	0.0507	0.0025
27.1	452	225	0.51	10.7	0.0005190	0.0002119	0.94	0.1478	0.0148	35.929	0.686	0.0554	0.0022
14.1	407	172	0.44	9.6	0.0003908	0.0001954	0.71	0.1194	0.0207	35.994	0.594	0.0494	0.0039
13.1	203	105	0.53	4.8	0.0007214	0.0004166	1.30	0.0913	0.0231	35.628	0.909	0.0516	0.0037
19.2	594	174	0.30	14.3	0.0002626	0.0001313	0.47	0.0941	0.0097	35.486	0.619	0.0535	0.0033
<b>MMI15-18-3 - Granodiorite (NAD83 Zone 8: 511777 E 6634078 N; Z11799; Mount IP824)</b>													
6.1	294	111	0.39	3.0	0.0002032	0.0001437	0.35	0.1366	0.0138	85.133	1.299	0.0513	0.0020
34.1	206	106	0.53	2.1	0.0004876	0.0002816	0.85	0.1619	0.0209	84.883	2.845	0.0537	0.0027
7.1	150	58	0.40	1.5	0.0004128	0.0002920	0.72	0.1229	0.0206	85.186	1.863	0.0463	0.0028
16.1	415	196	0.49	4.2	0.0002220	0.0001282	0.38	0.1288	0.0113	85.107	0.887	0.0466	0.0016
32.1	557	475	0.88	5.6	0.0003115	0.0001393	0.54	0.2926	0.0156	84.887	1.232	0.0468	0.0016
10.1	295	104	0.36	3.0	0.0006008	0.0002454	1.04	0.1096	0.0150	84.694	0.787	0.0474	0.0019
2.1	168	59	0.36	1.7	<i>bdl</i>		0.00	0.1160	0.0156	84.979	2.371	0.0442	0.0025
9.1	407	190	0.48	4.1	0.0001542	0.0001091	0.27	0.1561	0.0124	84.370	1.320	0.0489	0.0017
3.1	345	197	0.59	3.5	0.0004334	0.0001939	0.75	0.1811	0.0157	83.686	1.910	0.0518	0.0019
1.1	328	207	0.65	3.3	0.0005748	0.0002348	1.00	0.1912	0.0170	84.117	0.758	0.0467	0.0018
38.1	267	115	0.45	2.7	0.0004778	0.0002390	0.83	0.1211	0.0162	83.737	1.477	0.0476	0.0021
4.1	202	112	0.57	2.1	0.0004122	0.0002381	0.71	0.1488	0.0177	83.527	1.975	0.0461	0.0023
8.1	168	66	0.40	1.8	-0.000358	-0.000253	-0.62	0.1240	0.0173	82.815	1.638	0.0477	0.0026
31.1	352	154	0.45	3.7	-0.000269	-0.000156	-0.47	0.1450	0.0128	82.844	1.884	0.0457	0.0018
17.1	370	174	0.49	3.9	-0.000155	-0.000109	-0.27	0.1645	0.0121	82.252	1.163	0.0474	0.0017
18.1	322	200	0.64	3.4	0.0002998	0.0001731	0.52	0.1736	0.0158	81.979	0.748	0.0474	0.0019
33.1	395	209	0.55	4.2	0.0002263	0.0001307	0.39	0.1808	0.0134	81.207	1.181	0.0459	0.0016

Notes (see Stern, 1997): Mount IP579, K100b spot size (13x16µm), 2 minute raster, 6 mass scans, Primary beam intensity ~4nA; weighted mean  $^{207}Pb$ -corrected  $^{206}Pb/^{238}U$  age of secondary standard z6266 zircon was  $569 \pm 6$  Ma, MSWD=0.56, n=25 (2 rejections); error in  $^{206}Pb/^{238}U$  calibration 1.60% (included). Standard Error in Standard calibration was 0.42% (not included in above errors). Mount IP824, K100b spot size (13x16µm), 2 minute raster, 6 mass scans; Primary beam intensity ~7.5nA; Weighted mean  $^{207}Pb$ -corrected  $^{206}Pb/^{238}U$  age of secondary standard z6266 zircon was  $558 \pm 8$  Ma, MSWD=1.4, n=25 (2 rejections) (accepted  $^{206}Pb/^{238}U$  age is 559 Ma); Error in  $^{206}Pb/^{238}U$  calibration 0.80% (included); Standard Error in Standard calibration was 0.72% (not included in above errors).

Table 2. Continued.

Spot	$\frac{^{207}\text{Pb}}{^{235}\text{U}}$		$\frac{^{206}\text{Pb}}{^{238}\text{U}}$		Corr Coeff	$\frac{^{207}\text{Pb}}{^{206}\text{Pb}}$		$^{206}\text{Pb}/^{238}\text{U}$ apparent age (Ma)			
		±		±			±	204 corrected Age	±	207 corrected Age	±
<b>ZE10-248</b>											
<b>Type II Zircon</b>											
7.1	0.074	0.006	0.0124	0.0004	0.344	0.0432	0.0034	79.5	2.3	<b>79.9</b>	<b>2.3</b>
25.1	0.078	0.005	0.0130	0.0002	0.241	0.0434	0.0029	83.1	1.4	<b>83.5</b>	<b>1.4</b>
21.1	0.085	0.006	0.0131	0.0003	0.292	0.0470	0.0030	83.9	1.6	<b>83.9</b>	<b>1.7</b>
32.1	0.087	0.007	0.0132	0.0003	0.224	0.0479	0.0040	84.2	1.6	<b>84.2</b>	<b>1.6</b>
11.1	0.091	0.003	0.0133	0.0002	0.463	0.0497	0.0015	85.4	1.4	<b>85.2</b>	<b>1.4</b>
24.1	0.076	0.005	0.0132	0.0002	0.251	0.0419	0.0029	84.6	1.5	<b>85.2</b>	<b>1.5</b>
2.1	0.090	0.003	0.0134	0.0002	0.436	0.0489	0.0017	85.7	1.4	<b>85.5</b>	<b>1.4</b>
17.1	0.080	0.004	0.0134	0.0002	0.301	0.0433	0.0022	86.1	1.4	<b>86.6</b>	<b>1.4</b>
15.1	0.088	0.003	0.0137	0.0002	0.550	0.0468	0.0011	87.8	1.4	<b>87.9</b>	<b>1.4</b>
9.1	0.156	0.005	0.0230	0.0004	0.505	0.0493	0.0014	146.4	2.4	146.4	2.4
<b>Type I Zircon</b>											
31.1	0.165	0.019	0.0265	0.0004	0.145	0.0452	0.0052	168.8	2.8	<b>169.7</b>	<b>2.9</b>
30.1	0.195	0.032	0.0270	0.0005	0.125	0.0525	0.0084	171.7	3.4	<b>171.0</b>	<b>3.4</b>
26.1	0.186	0.016	0.0269	0.0004	0.190	0.0501	0.0043	171.4	2.8	<b>171.3</b>	<b>2.9</b>
28.1	0.170	0.015	0.0269	0.0005	0.198	0.0457	0.0039	171.1	2.9	<b>171.9</b>	<b>2.9</b>
23.1	0.192	0.010	0.0272	0.0005	0.336	0.0513	0.0025	172.9	3.0	<b>172.5</b>	<b>3.0</b>
20.1	0.173	0.009	0.0270	0.0004	0.309	0.0464	0.0024	172.0	2.8	<b>172.6</b>	<b>2.8</b>
19.1	0.150	0.025	0.0269	0.0007	0.143	0.0405	0.0068	171.0	4.1	<b>172.9</b>	<b>4.1</b>
29.1	0.163	0.026	0.0271	0.0006	0.132	0.0436	0.0069	172.3	3.6	<b>173.5</b>	<b>3.5</b>
16.1	0.124	0.030	0.0269	0.0006	0.095	0.0335	0.0080	170.8	3.8	<b>174.2</b>	<b>3.7</b>
18.1	0.192	0.010	0.0275	0.0005	0.318	0.0507	0.0025	174.7	2.9	<b>174.5</b>	<b>2.9</b>
27.1	0.181	0.015	0.0276	0.0005	0.233	0.0477	0.0039	175.3	3.4	<b>175.7</b>	<b>3.4</b>
14.1	0.166	0.019	0.0276	0.0005	0.150	0.0436	0.0049	175.4	2.9	<b>176.7</b>	<b>3.0</b>
13.1	0.156	0.028	0.0277	0.0007	0.147	0.0409	0.0073	176.2	4.6	<b>178.0</b>	<b>4.6</b>
19.2	0.192	0.015	0.0280	0.0005	0.222	0.0497	0.0038	178.3	3.1	<b>178.3</b>	<b>3.2</b>
<b>MMI15-18-3</b>											
6.1	0.078	0.005	0.0117	0.0002	0.2	0.0484	0.0029	75.0	1	<b>74.9</b>	<b>1.2</b>
34.1	0.075	0.008	0.0117	0.0004	0.3	0.0466	0.0050	74.9	3	<b>74.9</b>	<b>2.5</b>
7.1	0.065	0.008	0.0117	0.0003	0.2	0.0402	0.0052	74.7	2	<b>75.3</b>	<b>1.7</b>
16.1	0.070	0.004	0.0117	0.0001	0.2	0.0434	0.0025	75.0	0.8	<b>75.4</b>	<b>0.8</b>
32.1	0.068	0.004	0.0117	0.0002	0.2	0.0422	0.0026	75.1	1	<b>75.6</b>	<b>1.1</b>
10.1	0.062	0.007	0.0117	0.0001	0.1	0.0385	0.0042	74.9	0.8	<b>75.7</b>	<b>0.7</b>
2.1	0.072	0.005	0.0118	0.0003	0.4	0.0442	0.0025	75.4	2	<b>75.7</b>	<b>2.1</b>
9.1	0.076	0.004	0.0118	0.0002	0.3	0.0467	0.0024	75.8	1	<b>75.8</b>	<b>1.2</b>
3.1	0.074	0.006	0.0119	0.0003	0.3	0.0454	0.0034	76.0	2	<b>76.2</b>	<b>1.7</b>
1.1	0.062	0.006	0.0118	0.0001	0.1	0.0381	0.0040	75.4	0.7	<b>76.3</b>	<b>0.7</b>
38.1	0.066	0.007	0.0118	0.0002	0.2	0.0405	0.0041	75.9	1	<b>76.5</b>	<b>1.4</b>
4.1	0.066	0.007	0.0119	0.0003	0.2	0.0400	0.0042	76.2	2	<b>76.8</b>	<b>1.8</b>
8.1	0.089	0.008	0.0122	0.0002	0.2	0.0529	0.0045	77.9	2	<b>77.4</b>	<b>1.5</b>
31.1	0.083	0.005	0.0121	0.0003	0.4	0.0496	0.0029	77.7	2	<b>77.5</b>	<b>1.8</b>
17.1	0.083	0.004	0.0122	0.0002	0.3	0.0497	0.0023	78.1	1	<b>77.9</b>	<b>1.1</b>
18.1	0.072	0.005	0.0121	0.0001	0.1	0.0429	0.0032	77.8	0.7	<b>78.2</b>	<b>0.7</b>
33.1	0.072	0.004	0.0123	0.0002	0.2	0.0426	0.0025	78.6	1	<b>79.1</b>	<b>1.2</b>

Notes (continued): Calibration standard Temora2 age = 416.8 +/-0.33 Ma (Black et al., 2004).

Uncertainties reported at 1s and are calculated by using SQUID 2.50.11.10.15, rev. 15 Oct 2011.

f(206) refers to mole percent of total  $^{206}\text{Pb}$  that is due to common Pb, calculated using the  $^{204}\text{Pb}$ -method; common Pb composition used is the surface blank (4/6: 0.05770; 7/6: 0.89500; 8/6:

2.13840). \* refers to radiogenic Pb (corrected for common Pb). Ages in bold are used in weighted mean age. bdl: below detection limit

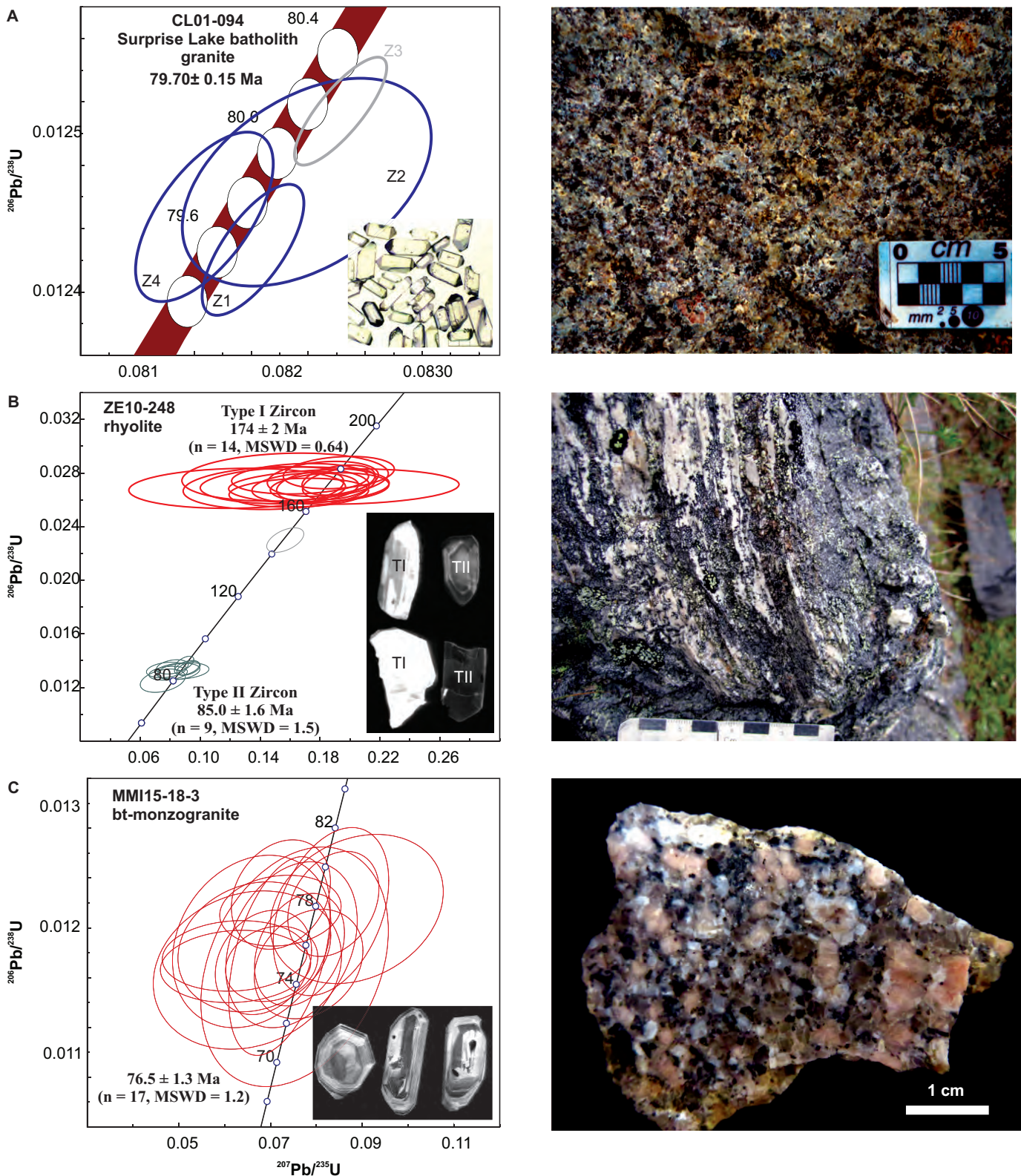


**Fig. 5.** U-Pb zircon concordia diagrams and representative photographs of Late Cretaceous samples. a) Surprise Lake batholith biotite alkali-feldspar granite. b) Rhyolite northeast of Taku Mountain. c) Biotite monzogranite near Tutshi Lake.

grains have a broad range of low to high U content (150-557 ppm) and moderate Th/U (0.36-0.88). The weighted mean  $^{207}\text{Pb}$ -corrected  $^{206}\text{Pb}/^{238}\text{U}$  age of this sample is  $76.5 \pm 1.3$  Ma ( $n = 17$ , MSWD = 1.2; Fig. 5c) and is interpreted as the crystallization age of the intrusion.

#### 4. Geochemistry

Previously published whole-rock geochemical analyses of Mesozoic plutonic rocks in the Atlin map are either incomplete analyses or summary data (White et al., 1976; Ballantyne and Littlejohn, 1982; Mihalynuk et al., 1992, 1999; Ray et al., 2000). Twenty eight Surprise Lake batholith samples collected by Lowe et al. (2003) were analyzed at the Geological Survey of Canada (Ottawa, ON) for whole-rock major and trace element compositions (2002-2003; Table 3). Pulverized samples were mixed with a flux of lithium metaborate, fused, and dissolved using four acid digestions. The concentration of major elements was measured using x-ray fluorescence (XRF) on fused disks. For trace elements and rare-earth elements, samples were dissolved using four acid digestion followed by lithium metaborate fusion of the residue. Select trace elements (Ba, Be, Co, Cr, Cu, Ni, Sc, Sr, V and Zn) were measured by inductively coupled plasma-optical emission spectrometry (ICP-OES). The remaining trace elements, including rare earth elements (REE), were determined by inductively coupled plasma-mass spectrometry (ICP-MS). The uncertainty in measurement relative to concentration is <1% relative for major elements. The uncertainty in most trace and rare earth element concentrations measured by ICP-OES and ICP-MS is <10% relative. An additional 2 samples were collected during regional reconnaissance mapping in 2010 and analysed at Activation Laboratories (Ancaster, ON; using the 4Lithores analytical package, see Milidragovic et al. (2016) for analytical procedure and uncertainties).

The Surprise Lake batholith samples display high  $\text{SiO}_2$  (average 73.43 wt.%) and  $\text{K}_2\text{O}$  (average 5.37 wt.%) and, on the basis of geochemistry are classified as alkali-feldspar granite to syenogranite (equivalent to rhyolite; Fig. 6a) typical of highly fractionated or minimum granitic melts generated in post-orogenic and anorogenic settings (Whalen and Frost, 2013). These samples are generally peraluminous and corundum normative (Fig. 6b), and plot in the alkalic to alkali-calcic fields on modified alkali-lime index (MALI) plots (Fig. 6c). On tectonic discrimination diagrams, Surprise Lake plutonic suite samples plot in within-plate granite fields (Fig. 6d). On MORB and chondrite-normalized REE and extended trace element and REE plots, the samples show significant Ba, Sr, Eu depletion indicative of plagioclase fractionation, and are highly enriched in Cs, Rb, Th, U and Pb (Figs. 6e, f).

Two samples of volcanic rocks were sampled from Peninsula Mountain suite of Mihalynuk et al. (1999). A sample of basalt was collected west of Graham Creek, from Peninsula Mountain suite pillow basalt sequence immediately adjacent to the Graham Creek suite (Fig. 3). The basalt (52.48 wt.%  $\text{SiO}_2$ ) contains relatively high  $\text{TiO}_2$  (1.35 wt.%) and displays a flat,

MORB-like REE profile on an extended trace element plot, with slight Nb depletion and Th enrichment (Fig. 7b). It plots on the boundary between volcanic arc tholeiite, back-arc basin basalt, and normal mid-ocean ridge on a tectonic discrimination diagram (Fig. 7c). A sample of andesite was sampled from the Peninsula Mountain suite andesite sequence on the north side of Atlin Mountain (Fig. 3). The andesite (61.56 wt.%  $\text{SiO}_2$ , Fig. 7a) is enriched in Th, Ba, Sr, Pb, LREE and depleted in Nb, Ti and P on an extended N-MORB normalized trace element plot (Fig. 7d). It plots in calc-alkaline field on a Y-La-Nb tectonic discrimination diagram (Fig. 7c).

#### 5. Discussion

Previous mapping in the area identified several Triassic to Cretaceous lithostratigraphic units (Bultman, 1979; Mihalynuk et al., 1999). Paucity of distinctive lithological characteristics, and general lack of age and geochemical constraints necessitated several revisions to the stratigraphy as new data became available, including reassignments of rocks between the Peninsula Mountain and Windy-Table suites and their equivalents (Mihalynuk et al., 1999). Data presented herein necessitate further revisions and indicate that Late Cretaceous magmatism and sedimentation are more widespread than previously thought. In particular, voluminous plutons east of Atlin have extensive volcanic and hypabyssal equivalents west of Atlin Lake (Fig. 2).

##### 5.1. Peninsula Mountain suite

Rhyolite from the base of the Peninsula Mountain suite yielded a Late Cretaceous age (Fig. 5b), indicating that Peninsula Mountain suite to the north of Taku Mountain is actually part of the Windy-Table suite. This implies that andesitic rocks that appear to stratigraphically overlie the rhyolites must also form part of the Late Cretaceous supracrustal sequence (Figs. 3, 4). Whole-rock geochemical analyses from the andesitic and rhyolitic rocks (Mihalynuk et al., 1999) indicate strong LREE enrichment relative to MORB. Andesite on the northern flank of Atlin Mountain yields a similar LREE enrichment and is also likely part of the Windy-Table suite (Fig. 3).

Peninsula Mountain suite pillow basalts west of Graham Creek display a geochemistry that differs from other Peninsula Mountain suite volcanic rocks (Fig. 7) but is identical to the Graham Creek suite (Triassic). These are back-arc tholeiites with flat, MORB-like REE profile (Fig. 7b). However, our new data indicate that these rocks are not MORBs but rather back-arc basin basalts or primitive island arc tholeiites. Although Mihalynuk et al. (1999) noted that these rocks were distinctly different than the Cache Creek terrane, subsequent work demonstrated that island arc and back-arc tholeiite geochemical signatures are characteristic of both the Nakina and Yeth Creek formations (Fig. 7b; English et al., 2010) in the Cache Creek terrane. As such, this pillow basalt is more appropriately included in the Graham Creek suite (Figs. 3, 4), and likely marks the western limit of the Cache Creek terrane.

**Table 3.** Whole rock geochemistry of Late Cretaceous rocks.

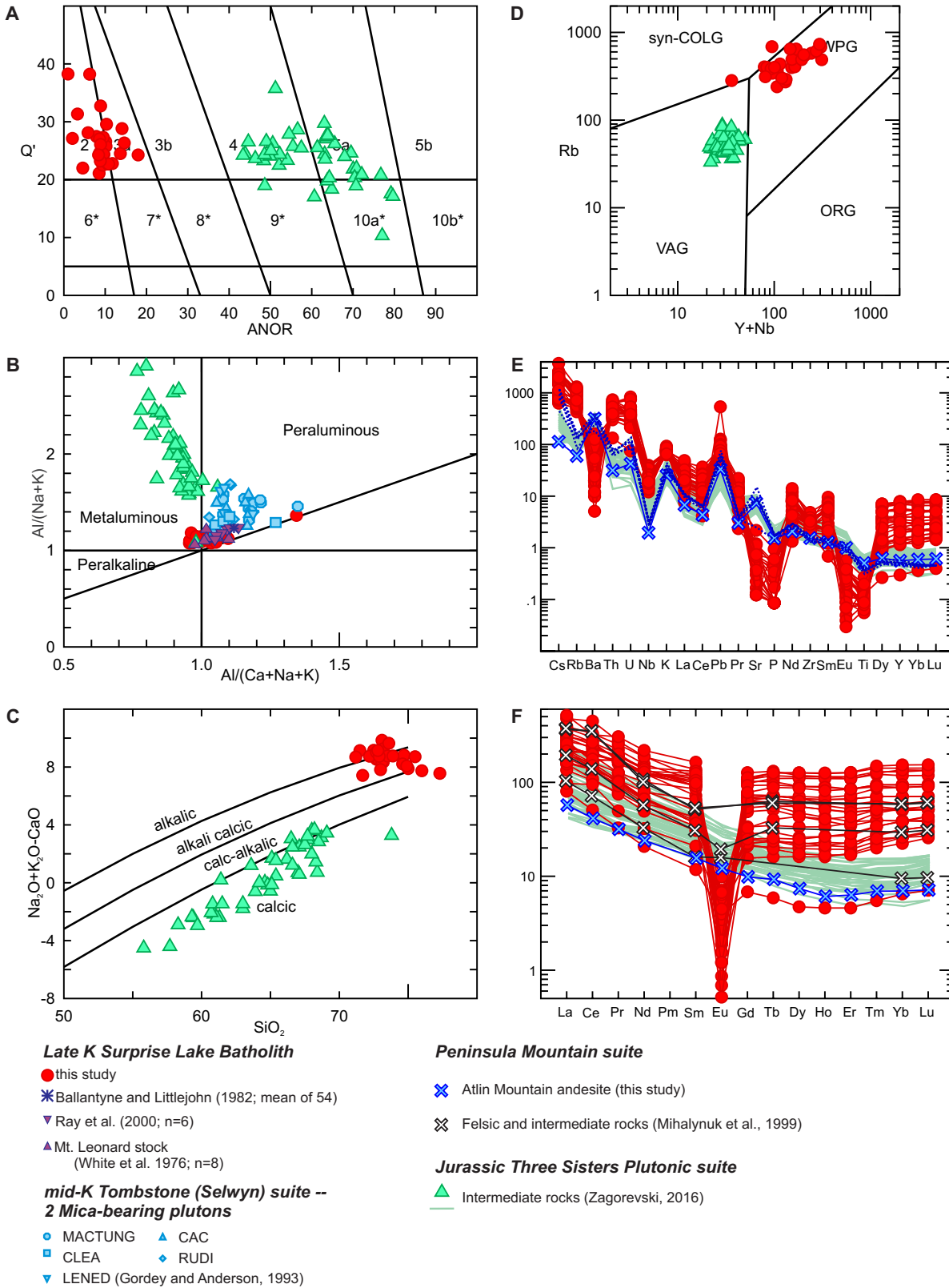
Sample	CL-01-94	AT02-01-01A	AT02-01-03A	AT02-02-02A	AT02-02-04A	AT02-02-05A	AT02-12-01A	AT02-12-02A	AT02-12-04A	AT02-14-07A
Laboratory	GSC	GSC	GSC	GSC	GSC	GSC	GSC	GSC	GSC	GSC
Latitude	59.6217	59.6166	59.6184	59.6055	59.6151	59.6191	59.7103	59.7078	59.7008	59.6626
Longitude	-132.5942	-132.5546	-132.5554	-132.5208	-132.5197	-132.5224	-132.8591	-132.8790	-132.8776	-132.9388
Rocktype	granite	granite	granite	granite	granite	granite	granite	granite	granite	granite
SiO <sub>2</sub>	77.30	74.70	74.60	71.50	72.90	72.70	72.50	72.80	73.20	72.50
Al <sub>2</sub> O <sub>3</sub>	11.80	13.40	13.30	14.50	14.30	14.30	14.40	14.00	14.00	14.30
Fe <sub>2</sub> O <sub>3</sub> (T)	1.40	1.40	1.10	1.10	1.70	1.30	1.50	2.00	1.70	1.90
MnO	0.01	0.01	0.01	0.01	0.02	0.01	0.01	0.04	0.01	0.02
MgO	0.10	0.06	0.05	0.03	0.08	0.07	0.07	0.23	0.07	0.03
CaO	0.40	0.65	0.70	0.84	0.66	0.75	0.70	1.05	0.73	0.66
Na <sub>2</sub> O	3.10	3.70	3.90	4.70	4.00	3.80	4.30	4.10	4.10	4.30
K <sub>2</sub> O	4.86	5.77	5.01	5.27	5.69	5.48	5.55	5.52	5.29	5.19
TiO <sub>2</sub>	0.08	0.11	0.12	0.21	0.16	0.17	0.14	0.21	0.14	0.10
P <sub>2</sub> O <sub>5</sub>	0.01	0.01	0.01	0.00	0.01	0.01	0.01	0.05	0.01	0.00
LOI	0.5	0.4	0.6	0.5	0.4	0.8	0.6	0.3	0.5	0.5
Total	99.8	100.2	99.5	98.7	100.0	99.5	99.9	100.5	99.7	99.5
Ba	260	213	159	73	273	142	119	336	127	62
Be	5.0	7.8	5.4	7.3	6.9	5.5	13.0	9.1	7.3	5.1
Cr	35	22	22	20	26	21	25	26	25	19
Cs	10.00	17.00	14.00	14.00	11.00	13.00	18.00	7.20	16.00	16.00
Ga	25.00	28.00	30.00	39.00	30.00	36.00	30.00	23.00	31.00	37.00
Hf	8.00	10.00	10.00	12.00	12.00	15.00	12.00	8.90	12.00	10.00
Mo	0.7	0.9	0.3	1.7	0.4	1.3	0.2	0.8	0.3	1.0
Nb	34.00	53.00	51.00	92.00	44.00	45.00	43.00	46.00	47.00	88.00
Pb	21	24	20	38	25	15	28	20	29	23
Rb	240	397	406	488	357	546	492	435	578	680
Sb	0.2	0.7	0.4	0.9	0.4	0.6	1.5	0.4	0.5	0.2
Sc	3.0	2.5	2.6	2.5	3.5	2.9	2.0	1.8	2.1	2.5
Sn	4.5	5.7	5.8	4.9	2.9	22.0	5.0	6.0	4.3	3.5
Sr	15	20	12	-10	27	-10	11	52	11	-10
Ta	4.30	5.50	5.80	8.80	4.30	5.00	5.50	7.00	7.80	16.00
Th	38.00	50.00	49.00	76.00	50.00	42.00	60.00	56.00	65.00	76.00
U	13.00	18.00	20.00	39.00	18.00	13.00	20.00	21.00	17.00	16.00
Y	73.00	99.00	113.00	220.00	64.00	163.00	110.00	69.00	196.00	217.00
Zr	183.0	250.0	213.0	195.0	309.0	358.0	284.0	235.0	251.0	185.0
La	73.0	89.0	70.0	49.0	113.0	93.0	74.0	59.0	122.0	65.0
Ce	164.0	184.0	140.0	130.0	274.0	202.0	154.0	118.0	196.0	146.0
Pr	16.00	21.00	18.00	15.00	26.00	24.00	17.00	12.00	29.00	18.00
Nd	58.0	73.0	64.0	57.0	88.0	87.0	59.0	38.0	102.0	67.0
Sm	11.00	16.00	15.00	18.00	17.00	21.00	14.00	7.70	25.00	20.00
Eu	0.19	0.20	0.14	0.05	0.22	0.11	0.11	0.34	0.13	0.04
Gd	10.00	15.00	15.00	22.00	13.00	21.00	14.00	6.90	26.00	22.00
Tb	1.90	2.70	2.70	4.40	2.10	3.80	2.70	1.30	4.90	4.70
Dy	11.00	17.00	17.00	29.00	12.00	23.00	17.00	8.50	30.00	32.00
Ho	2.20	3.40	3.70	6.50	2.40	5.10	3.70	1.90	6.50	7.00
Er	5.70	9.60	11.00	19.00	6.30	14.00	11.00	6.10	18.00	21.00
Tm	1.00	1.60	1.80	3.30	1.00	2.40	1.80	1.20	3.10	3.60
Yb	6.60	10.00	12.00	22.00	6.60	16.00	12.00	8.90	20.00	24.00
Lu	0.97	1.60	1.80	3.40	1.00	2.40	1.80	1.40	3.00	3.60

Table 3. Continued.

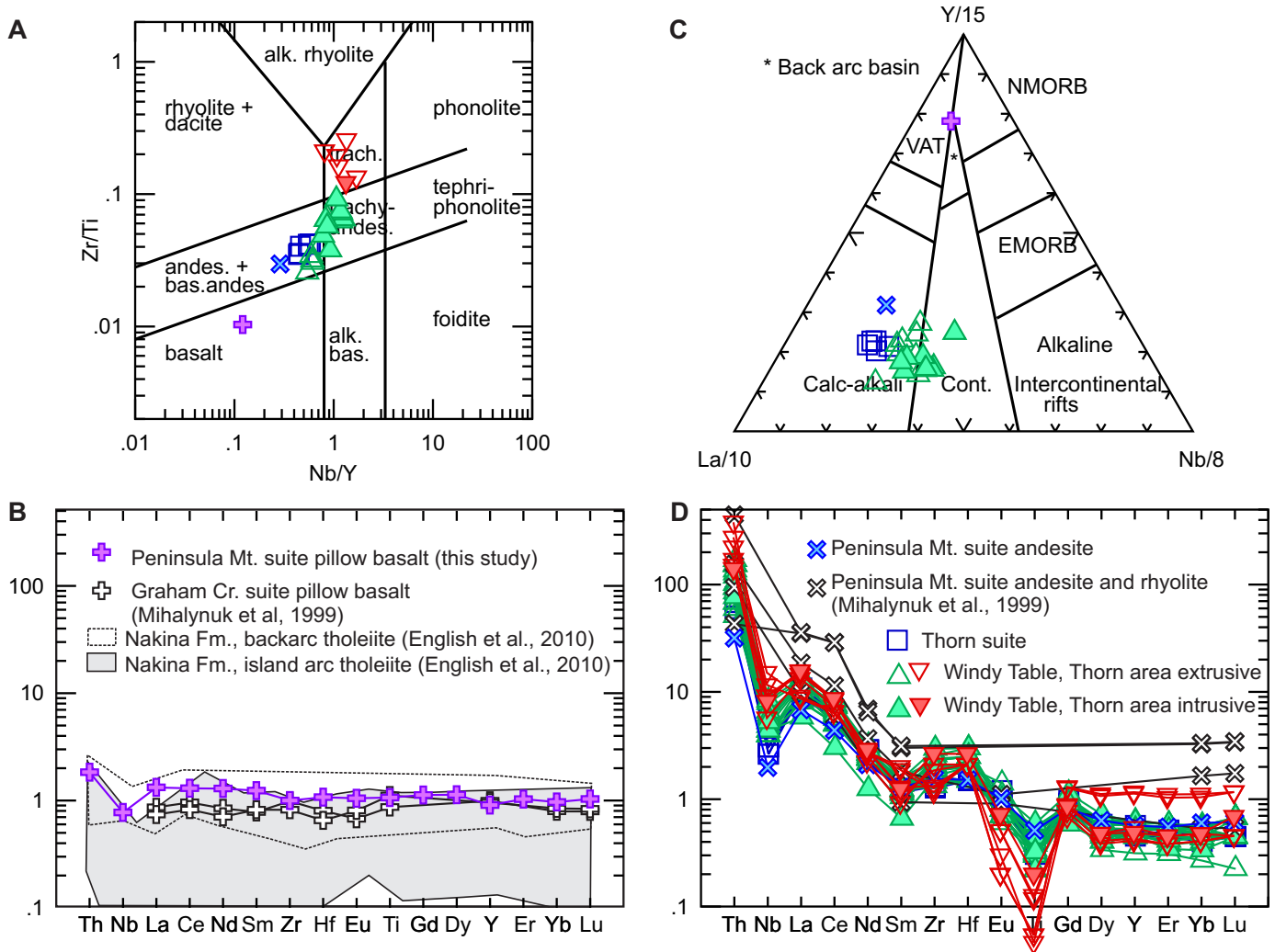
Sample	AT02-15-01A	AT02-15-04A	AT02-15-05A	AT02-16-03A	AT02-17-01A	AT02-17-06A	AT02-18-01A	AT02-18-03A	AT02-19-01A	AT02-19-01B
Laboratory	GSC									
Latitude	59.7859	59.7683	59.7692	59.7666	59.6908	59.7185	59.6351	59.6206	59.7117	59.7117
Longitude	-133.1737	-133.1707	-133.1591	-133.2674	-133.2569	-133.2526	-133.2925	-133.3038	-133.4027	-133.4027
Rocktype	granite									
SiO <sub>2</sub>	73.20	72.20	75.00	73.10	71.20	74.90	72.70	73.20	73.10	73.50
Al <sub>2</sub> O <sub>3</sub>	14.40	14.40	13.60	14.80	14.80	14.10	14.60	14.40	13.40	12.90
Fe <sub>2</sub> O <sub>3</sub> (T)	1.70	1.30	1.10	1.30	1.70	0.60	1.20	1.40	1.90	2.40
MnO	0.05	0.02	0.01	0.01	0.02	0.00	0.04	0.02	0.05	0.04
MgO	0.22	0.10	0.09	0.07	0.06	0.17	0.14	0.06	0.35	0.28
CaO	1.00	0.97	0.95	0.30	0.81	0.08	0.83	0.65	1.02	0.82
Na <sub>2</sub> O	4.40	4.50	4.30	4.90	4.40	2.70	4.50	4.40	3.30	2.90
K <sub>2</sub> O	4.95	5.22	4.54	5.25	5.10	5.45	5.35	5.51	6.08	6.68
TiO <sub>2</sub>	0.18	0.12	0.10	0.07	0.10	0.16	0.11	0.13	0.20	0.17
P <sub>2</sub> O <sub>5</sub>	0.05	0.01	0.01	0.00	0.00	0.01	0.03	0.01	0.06	0.05
LOI	0.5	0.5	0.2	0.5	0.7	1.6	0.3	0.3	0.5	0.4
Total	100.6	99.4	100.1	100.3	98.8	99.8	99.9	100.1	100.0	100.3
Ba	355	205	200	126	99	1010	392	406	423	447
Be	10.0	10.0	8.1	16.0	5.6	2.9	6.7	6.4	8.9	7.5
Cr	25	24	23	21	22	20	30	28	20	27
Cs	16.00	11.00	5.70	18.00	26.00	4.40	6.00	7.10	5.00	5.70
Ga	21.00	31.00	25.00	32.00	38.00	17.00	21.00	30.00	20.00	20.00
Hf	7.10	11.00	11.00	13.00	12.00	4.70	5.70	8.10	5.60	4.90
Mo	0.4	0.3	0.5	0.2	1.4	2.0	0.2	0.3	47.0	101.0
Nb	39.00	81.00	40.00	56.00	80.00	28.00	31.00	42.00	54.00	46.00
Pb	25	37	31	35	17	161	28	30	17	20
Rb	404	611	272	645	731	282	361	291	342	399
Sb	0.4	0.2	0.4	0.7	1.0	0.8	-0.2	0.4	0.3	-0.2
Sc	1.6	1.8	1.3	1.9	3.5	1.6	1.7	2.0	2.3	2.0
Sn	11.0	3.2	3.5	2.0	9.8	2.8	5.4	6.3	5.2	5.7
Sr	64	33	33	11	-10	71	61	33	107	102
Ta	4.50	12.00	3.80	9.60	14.00	3.40	3.80	3.00	7.60	7.40
Th	55.00	74.00	66.00	88.00	73.00	16.00	44.00	40.00	42.00	41.00
U	17.00	35.00	16.00	22.00	18.00	3.50	12.00	12.00	17.00	22.00
Y	40.00	193.00	91.00	113.00	216.00	8.30	54.00	91.00	42.00	38.00
Zr	219.0	200.0	216.0	230.0	199.0	151.0	167.0	186.0	169.0	145.0
La	53.0	55.0	38.0	65.0	53.0	19.0	43.0	46.0	32.0	37.0
Ce	98.0	125.0	83.0	102.0	120.0	31.0	83.0	99.0	64.0	67.0
Pr	10.00	16.00	10.00	17.00	16.00	3.10	9.00	12.00	7.40	7.10
Nd	32.0	57.0	37.0	57.0	61.0	9.7	30.0	47.0	26.0	23.0
Sm	5.90	17.00	10.00	14.00	19.00	1.80	6.40	13.00	5.20	4.70
Eu	0.37	0.16	0.20	0.09	0.07	0.23	0.32	0.31	0.41	0.37
Gd	5.00	20.00	11.00	13.00	23.00	1.40	5.80	14.00	4.60	4.30
Tb	0.90	4.10	2.10	2.60	4.70	0.22	1.10	2.50	0.89	0.76
Dy	5.60	28.00	14.00	18.00	32.00	1.20	6.60	16.00	5.30	5.00
Ho	1.30	6.20	2.90	3.90	7.10	0.26	1.50	3.20	1.20	1.10
Er	3.70	18.00	8.00	12.00	21.00	0.76	4.50	8.60	3.40	3.20
Tm	0.72	3.20	1.30	2.20	3.80	0.14	0.86	1.40	0.69	0.60
Yb	5.30	23.00	8.70	15.00	26.00	1.10	6.60	8.80	5.30	4.50
Lu	0.86	3.40	1.30	2.30	3.90	0.18	1.10	1.30	0.86	0.76

Table 3. Continued.

Sample	AT02-19-02A	AT02-19-04A	AT-02-19-03A	AT-02-19-05A	ATLH-02-05-07A	ATMH-02-04-01A	AT02-12-04Adup	ZE09-033B	ZE10-249
Laboratory	GSC	GSC	GSC	GSC	GSC	GSC	GSC	Actlabs(2009)	Actlabs(2011)
Latitude	59.7136	59.7126	59.7131	59.7120	59.6632	59.6488	59.7008	59.5550	59.6638
Longitude	-133.4172	-133.3990	-133.4032	-133.4009	-132.9997	-132.9074	-132.8776	-133.8780	-134.0622
Rocktype	granite	granite	granite	granite	granite	granite	granite	andesite	basalt
SiO <sub>2</sub>	73.90	72.90	76.00	71.70	73.60	73.00	73.30	61.56	52.48
Al <sub>2</sub> O <sub>3</sub>	13.80	14.30	12.40	14.30	14.20	13.80	14.00	17.17	15.27
Fe <sub>2</sub> O <sub>3</sub> (T)	0.90	1.20	1.50	2.10	1.40	2.20	1.70	6.53	8.07
MnO	0.01	0.03	0.02	0.06	0.02	0.04	0.01	0.073	0.132
MgO	0.06	0.20	0.13	0.49	0.07	0.29	0.06	2.23	6.5
CaO	0.69	0.67	0.92	1.52	0.17	1.12	0.75	3.85	8.68
Na <sub>2</sub> O	3.90	4.10	3.40	4.30	3.60	4.20	4.20	3.69	3.93
K <sub>2</sub> O	5.55	5.31	5.26	4.64	6.21	4.74	5.56	1.85	0.31
TiO <sub>2</sub>	0.12	0.17	0.15	0.34	0.11	0.25	0.11	0.648	1.351
P <sub>2</sub> O <sub>5</sub>	0.05	0.04	0.02	0.11	0.01	0.07	0.01	0.18	0.16
LOI	0.7	0.7	0.3	0.4	0.6	0.4	0.5	2.02	2.61
Total	99.8	99.8	100.3	100.1	100.2	100.2	100.2	99.8	99.48
Ba	126	299	569	785	152	338	173	2024	33
Be	7.4	7.8	5.9	8.0	5.8	7.7	7.3	<1	<1
Cr	21	23	23	34	24	24	26	50	210
Cs	13.00	5.10	6.10	5.40	14.00	7.90	16.00	0.8	0.2
Ga	30.00	20.00	24.00	20.00	31.00	22.00	32.00	18	15
Hf	11.00	5.60	8.90	6.80	10.00	8.30	11.00	3.1	2.2
Mo	2.0	7.8	15.0	9.2	0.2	0.9	0.4	<2	<2
Nb	48.00	61.00	32.00	48.00	53.00	44.00	47.00	4.6	1.8
Pb	24	23	16	16	23	20	26	10	<5
Rb	489	384	302	312	688	399	628	34	4
Sb	2.7	0.2	0.4	0.8	0.5	0.5	0.7	0.9	0.4
Sc	2.1	1.7	3.3	3.0	2.1	1.9	2.1	16	39
Sn	5.9	2.7	2.5	5.8	4.8	5.6	4.3	1	<1
Sr	11	62	61	195	11	66	-10	673	195
Ta	5.00	8.00	2.80	4.90	6.10	5.70	7.70	0.39	0.14
Th	79.00	46.00	36.00	42.00	64.00	47.00	64.00	3.81	0.22
U	35.00	19.00	10.00	17.00	25.00	18.00	16.00	2.01	0.46
Y	145.00	32.00	88.00	33.00	42.00	57.00	197.00	15.9	25.4
Zr	230.0	158.0	251.0	193.0	208.0	239.0	239.0	115	74
La	57.0	23.0	81.0	48.0	48.0	51.0	119.0	17	3.31
Ce	122.0	58.0	163.0	89.0	86.0	92.0	194.0	32.8	9.75
Pr	16.00	4.70	19.00	9.40	9.80	9.60	29.00	4	1.68
Nd	58.0	15.0	64.0	31.0	31.0	31.0	102.0	15.3	9.43
Sm	16.00	3.20	14.00	5.60	5.60	5.60	24.00	3.4	3.25
Eu	0.12	0.26	0.39	0.57	0.07	0.39	0.12	1.03	1.07
Gd	19.00	3.20	13.00	4.50	4.60	5.10	25.00	3.02	4.14
Tb	3.50	0.60	2.30	0.73	0.88	0.95	4.80	0.52	0.82
Dy	23.00	4.10	14.00	4.40	5.80	6.30	31.00	2.88	5.15
Ho	5.00	0.91	2.90	0.95	1.20	1.50	6.40	0.54	1.08
Er	14.00	2.90	7.90	2.80	3.80	4.70	19.00	1.63	3.06
Tm	2.40	0.55	1.30	0.51	0.64	0.87	2.90	0.273	0.456
Yb	16.00	4.40	8.50	3.80	4.40	6.50	20.00	1.83	2.95
Lu	2.40	0.74	1.30	0.65	0.68	1.10	2.90	0.28	0.47



**Fig. 6.** Geochemical characteristics of the Surprise Lake batholith. **a)**  $Q'$  ( $100 \times \text{Quartz} / (\text{Quartz} + \text{Orthoclase} + \text{Albite} + \text{Anorthite})$ ) – ANOR (Anorthite/(Orthoclase+Anorthite)) plot (Whalen and Frost, 2013). **b)** Shand's index plot (Maniar and Piccoli, 1989). **c)** Modified alkali-lime index (MALI) plot (Frost et al., 2001). **d)** Tectonic discrimination plot (Pearce et al., 1984). **e)** N-MORB normalized extended trace element plot. **f)** Chondrite-normalized rare-earth element plot (normalization factors from Sun and McDonough, 1989). Tombstone plutonic suite major element data are from Anderson (1983). Surprise Lake batholith data are compiled from White et al., (1976), Ballantyne and Littlejohn (1982), Ray et al. (2000). Three Sisters Plutonic suite data are from Zagorevski (2016).



**Fig. 7.** Geochemical characteristics of Peninsula Mountain suite volcanic rocks. **a)** Rock type discrimination plot (Pearce, 1996). See **b)** and **d)** for symbol legend. **b)** N-MORB normalized trace element plot of Peninsula Mountain pillow basalt near headwaters of Graham Creek. **c)** Tectonic discrimination plot (Cabanis and Lecolle, 1989). **d)** N-MORB normalized (Sun and McDonough, 1989) trace element plot of Atlin Mountain andesite. Data compiled from Mihalyuk et al. (1999), Simmons et al. (2005) and English et al. (2010). N-MORB – normal mid-ocean ridge basalt, E-MORB – enriched mid-ocean ridge basalt, VAT – volcanic arc tholeiite.

## 5.2. Late Cretaceous magmatism, sedimentation, and tectonism

Evidence of Late Cretaceous magmatism is widespread in northwestern British Columbia and adjacent Yukon. The area to the east of Atlin Lake is mainly underlain by highly fractionated alkali-feldspar granite and monzogranite. West of Tagish Lake, Late Cretaceous magmatism is represented by relatively homogenous granodiorite. Between Tagish and Atlin lakes, Late Cretaceous volcanic and hypabyssal rocks, locally more than 1 km thick, were deposited on a high-relief angular unconformity (Bultman, 1979). East of Atlin Lake, Cretaceous supracrustal sequences are not obvious, although isolated outcrops of polymictic conglomerate containing flow-banded rhyolite clasts overlying Kedahda Formation chert may represent remnants of the basal unconformity (Fig. 4).

Existing data on Late Cretaceous volcanic rocks are sparse, but indicate an andesitic arc-like setting (Simmons et al., 2005;

Fig. 7). The Surprise Lake batholith is much more evolved than the Windy-Table suite andesitic rocks and has undergone significant fractionation of plagioclase, indicated by depletion of Sr, Ba and Eu. Due to paucity of data on volcanic rocks and the highly fractionated chemistry of plutonic rocks, comparisons between the Surprise Lake batholith and coeval volcanic rocks to the west is not meaningful. Data presented herein clearly distinguish the Late Cretaceous Surprise Lake batholith from the adjacent Jurassic Fourth of July batholith and related Mount McMaster and Langrose Mountain stocks, providing a guide for regional comparisons (Fig. 6). These data highlight problems arising from tectonic discrimination of highly fractionated granites. Surprise Lake suite analyses plot in the within-plate field on the Pearce et al. (1984) diagram (Fig. 6d), yet coeval andesitic rocks suggest a calc-alkaline arc setting (Figs. 6, 7).

In the Sutlahine River area, ~150 km southeast of our study

area, volcanic strata at the Thorn developed prospect may be equivalent to the Windy-Table suite. Based on U-Pb zircon age determinations, Simmons et al. (2005) identified three Late Cretaceous magmatic peaks at: ca. 93-87 Ma (Thorn suite); ca. 87 Ma (early Windy-Table suite); and ca. 82 Ma (late Windy-Table suite). The initiation of felsic magmatism in the early Windy-Table suite appears to be broadly coeval at Table Mountain ( $85.0 \pm 1.6$  Ma: this study) and at Thorn ( $87.5 \pm 1.2$  Ma dacite flow; SHRIMP, Simmons et al., 2005). At the Thorn developed prospect (Fig. 1), volcanic strata are as young as  $81.1 \pm 1.5$  Ma (trachyte flow, U-Pb zircon, SHRIMP; Simmons et al., 2004) and  $82.8 \pm 0.6$  Ma (rhyolite breccia U-Pb zircon, TIMS, Mihalynuk et al., 2003), overlapping the youngest felsic volcanic U-Pb zircon crystallization age at Table Mountain ( $81.3 \pm 0.3$  Ma: Mihalynuk et al., 1992). The youngest Windy-Table suite felsic magmatism is coeval with the emplacement of the oldest phases of the Surprise Lake batholith ( $83.8 \pm 5$  Ma: Mihalynuk et al., 1992;  $81.6 \pm 1.1$  Ma: Smith and Arehart, 2010). The youngest phases of the Surprise Lake batholith ( $77.5 \pm 1.0$  Ma: Smith and Arehart, 2010) overlap the age of the biotite monzogranite near Tutshi Lake ( $76.5 \pm 1.3$  Ma: this study).

The emplacement of the Windy-Table and Surprise Lake suites immediately precedes and, in part, overlaps the economically important Late Cretaceous Casino suite plutonism in Yukon (~78-72 Ma: Johnston, 1995, Selby and Creaser, 2001; Bennett et al., 2010; Allan et al., 2013; Nelson et al., 2013; Ryan et al., 2013; Mortensen et al., 2016). The Casino suite comprises volumetrically small hypabyssal rocks that yield very limited information on the processes in the underlying crust or in the now eroded volcanic carapaces. As such, more detailed investigation of the Windy-Table and Surprise Lake suites can improve the geological constraints on the late Cretaceous magmatism, including the nature and tectonic setting of the Intermontane terranes immediately before outpouring of the regionally extensive Carmacks Group basalt in Yukon (e.g., Johnston et al., 1996).

### 5.3. Late Cretaceous mineralization

The Surprise Lake suite and its metamorphic aureole host numerous molybdenum and granophile mineral occurrences. Mount Leonard stock hosts the Ruby Creek molybdenum deposit (also known as Adanac: 275,354,000 tonnes grading 0.067% molybdenum, measured and indicated; MINFILE 104N 052) and is possibly the source of precious metal and polymetallic base metal sulphide mineralization at the past-producing Atlin Ruffner mine. Tin and tungsten skarns adjacent to the Surprise Lake batholith (Ray et al., 2000) and cassiterite and wolframite in placer streams underlain by the batholith indicate W-Sn mineralization potential in addition to defined resources at the Ruby Creek deposit. The Surprise Lake batholith is compositionally similar to other W-Sn bearing plutonic suites, such as the Tombstone-Tungsten plutonic suite in Yukon (96-90 Ma, Anderson, 1983; Gordey and Anderson, 1993). Both suites are highly fractionated, peraluminous granites, with high

alkali concentrations. Key geochemical differences between Surprise Lake and Tombstone-Tungsten suites is the more fractionated character of the Surprise Lake suite, indicated by higher  $K_2O$  and lower  $FeO_{total}$ ,  $MgO$  and  $Sr$ . Late Cretaceous volcanic rocks of the Windy-Table suite host high sulphidation epithermal to transitional porphyry-style precious and base metal sulphide-rich mineralization at the Thorn developed prospect, about 150 km southeast of the present study area. This mineralization is hosted by the Thorn suite plutons (ca. 93-87 Ma) and was emplaced contemporaneously with Windy-Table suite rocks (Simmons et al., 2005, Simmons et al., 2005). Highly evolved phases similar to the Surprise Lake batholith appear to be absent near Thorn (Fig. 7; Simmons et al., 2005).

Placer gold streams in the Atlin camp border the Surprise Lake batholith (e.g., Mihalynuk et al., 2017). Some streams contain tin and tungsten placers in addition to gold. Boulder Creek is known for its rich gold and wolframite placers and has its headwaters in the batholith, where tungsten showings are concentrated (Ray et al., 2000). A study of placer gold from Feather Creek (Fig. 2) identified cassiterite and thorite intergrown with gold nuggets. Both cassiterite and thorite occur within the highly fractionated Surprise Lake suite and associated skarns, but not with Jurassic Three Sisters plutonic suite or ultramafic rocks of the Cache Creek complex. Such observations led Sack and Mihalynuk (2003) to suggest a Surprise Lake batholith source for the Atlin placer gold in addition to altered ultramafic rocks (Ash, 1994; Ash et al., 2001). Subsequent collections of nuggets from other placer creeks failed to find gold intergrown with minerals of unambiguous origin (Mihalynuk et al., 2011), but did recover gold nuggets with attached phyllite from Otter Creek. In 2016, placer mining on Otter Creek discovered quartz-gold veins cutting calcareous black phyllite bedrock (Mihalynuk et al., 2017) proving that regardless of the ultimate gold source, ultramafic rocks are not a prerequisite for lode gold deposition. A placer showing on Graham Creek, west of Atlin, may also be genetically related to the Late Cretaceous magmatism rather than ultramafic rocks.

Affiliation of placer gold workings with evolved, mineralized Late Cretaceous intrusions is well established in the Yukon. For example, such placers are found in the Nansen Creek and Klaza River headwaters north of Mt. Nansen, where Yukon Tanana terrane basement rocks are cut by Early Cretaceous rocks of the Whitehorse suite plutons (Dawson Range batholith) and are overlain by coeval Mount Nansen suite volcanic strata (Yukon Geological Survey, 2016). Similarly, placer workings are directly underlain by the Mount Nansen porphyry complex and Klaza area gold-silver mineralization (Hart and Langdon, 1997; Wengzynowski et al., 2015) associated with stocks and feldspar porphyry dikes that have returned ca. 78.2-76.3 Ma U-Pb zircon crystallization ages (Mortensen et al., 2016). Placer-lode gold links in the Klaza area have also been made on the basis of detrital grain morphology and chemistry (Chapman et al., 2016).

## 6. Conclusion

New geochronologic and geochemical data require stratigraphic revisions in the Atlin-Tagish area (Fig. 4). New age determinations for the Surprise Lake batholith yield a crystallization age that falls in the middle of 78-82 Ma cluster determined by modern techniques. Surprise Lake batholith and comagmatic volcanic strata are part of a mineralized belt that extends into Yukon and ca. 150 km to the southeast into the Sutlahine River area. In Yukon, mineralizing Casino suite intrusions in the Klaza area are age equivalent to the mineralized Mount Leonard stock of the Surprise Lake batholith ( $81.6 \pm 1.1$  to  $77.5 \pm 1.0$  Ma, Smith and Arehart, 2010). Re-Os ages for molybdenite mineralization in the Mount Leonard stock cluster around 70 Ma, significantly younger than most crystallization ages, but overlapping published cooling ages and youngest parts of the Casino suite. In the Sutlahine River area, the ~87-80 Ma Windy-Table suite is coeval with high sulphidation mineralization at the Thorn developed prospect.

## Acknowledgments

Discovery Helicopters (Atlin) are gratefully acknowledged for providing logistical support and transportation in the field. This is a contribution to the Geomapping for Energy and Minerals 2, Cordillera project. Legacy data were obtained during the Targeted Geoscience Initiative: Atlin project (2001-2003). P. Sack and L. Aspler provided valuable comments that improved this manuscript.

## References cited

- Aitken, J.D., 1959. Atlin map-area, British Columbia. Geological Survey of Canada, Memoir 307, 89p.
- Allan, M.M., Mortensen, J.K., Hart, C.J.R., Bailey, L.A., Sanchez, M.G., Ciolkiewicz, W., McKenzie, G.G., and Creaser, R.A., 2013. Magmatic and metallogenic framework of west-central Yukon and eastern Alaska. In: Colpron, M., Bissig, T., Rusk, B. G., and Thompson, J. F. H. (Eds.), *Tectonics, Metallogeny, and Discovery: The North American Cordillera and similar accretionary settings*. Society of Economic Geologists, Special Publication 17, 111-168.
- Anderson, R.G., 1983. Selwyn plutonic suite and its relationship to tungsten skarn mineralization, southeastern Yukon and District of Mackenzie. Geological Survey of Canada, Paper 83-1B, 151-163.
- Ash, C.H., 1994. Origin and tectonics setting of ophiolitic ultramafic and related rocks in the Atlin area, British Columbia (NTS 104N). Ministry of Energy, Mines and Petroleum Resources, British Columbia Geological Survey, Bulletin 94, 54p.
- Ash, C.H., MacDonald, R.W., and Reynolds, P.R., 2001. Relationship between ophiolites and gold-quartz veins in the North American Cordillera. British Columbia, Ministry of Energy and Mines. British Columbia Geological Survey. Bulletin 108, 140p.
- Ballantyne, S.B., and Littlejohn, A.L., 1982. Uranium mineralization and litho-geochemistry of the Surprise Lake batholith, Atlin, British Columbia. Geological Survey of Canada, Paper 81-23, 145-155.
- Bennett, V., Schulze, C., Ouellette, D., and Pollries, B., 2010. Deconstructing complex Au-Ag-Cu mineralization, Sonora Gulch project, Dawson Range: A Late Cretaceous evolution to the epithermal environment. In: MacFarlane, K.E., Weston, L.H., and Blackburn, L.R. (Eds.), *Yukon Exploration and Geology 2009*, Yukon Geological Survey, pp. 23-45.
- Bickerton, L., Colpron, M., and Gibson, D., 2013. Cache Creek terrane, Stikinia, and overlap assemblages of eastern Whitehorse (NTS 105D) and western Teslin (NTS 105C) map areas. In: MacFarlane K.E., Nordling, M.G., and Sack P.J. (Eds.), *Yukon Exploration and Geology 2012*, Yukon Geological Survey, pp. 1-17.
- Black, L.P., Kamo, S.L., Allen, C.M., Davis, D.W., Aleinikoff, J.N., Valley, J.W., Mundil, R., Campbell, I.H., Korsch, R.J., Williams, I.S., and Foudoulis, C., 2005. Improved  $^{206}\text{Pb}/^{238}\text{U}$  microprobe geochronology by the monitoring of a trace-element-related matrix effect; SHRIMP, ID-TIMS, ELA-ICP-MS and oxygen isotope documentation for a series of zircon standards. *Chemical Geology*, 205, 115-140.
- Bloodgood, M.A., and Bellefontaine, K.A., 1990. The geology of the Atlin area (Dixie Lake and Teresa Island) (104N/6 and parts of 104N/5 and 12). In: *Geological Fieldwork*, Ministry of Energy, Mines and Petroleum Resources, British Columbia Geological Survey, Paper 1990-1, pp. 205-215.
- Bloodgood, M.A., Rees, C.J., and Lefebvre, D.V., 1989. Geology of the Atlin area; NTS 104N/11W, 12E. Ministry of Energy, Mines and Petroleum Resources, British Columbia Geological Survey Open File 1989-15.
- Breitsprecher, K., and Mortensen, J.K., 2004. BCAGE 2004A - a database of isotopic age determinations for rock units from British Columbia. British Columbia Ministry of Energy and Mines, British Columbia Geological Survey Open File 2004-3 (Release 2.0)
- Bultman, T.R., 1979. Geology and tectonic history of the Whitehorse Trough west of Atlin, British Columbia. Ph.D. thesis, Yale University, 296p.
- Cabanis, B., and Lecolle, M., 1989. Le diagramme  $\text{La}/10\text{-Y}/15\text{-Nb}/8$ ; un outil pour la discrimination des series volcaniques et la mise en evidence des processus de melange et/ou de contamination crustale. *Comptes Rendus de l'Academie des Sciences, Serie 2, Mecanique, Physique, Chimie, Sciences de l'Univers, Sciences de la Terre*, 309, 2023-2029.
- Chapman, R., Cook, M., Grimshaw, M., and Myles, S., 2016. Placer-lode gold relationships in the Nansen placer district, Yukon. In: MacFarlane, K.E., and Nordling, M.G. (Eds.), *Yukon Exploration and Geology*, Yukon Geological Survey, pp. 63-78.
- Christopher, P.A., and Pinsent, R.H., 1982. Geology of the Ruby Creek and Boulder Creek area near Atlin (104N/11W). Ministry of Energy, Mines and Petroleum Resources, British Columbia Geological Survey, Preliminary Map 52, 10p.
- Colpron, M., and Nelson, J.L., 2011. A Digital Atlas of Terranes for the Northern Cordillera. Ministry of Energy and Mines, British Columbia Geological Survey GeoFile 2011-11.
- Colpron, M., Israel, S., Murphy, D., Pigake, L., and Moynihan, D., 2016. Yukon bedrock geology map. Yukon Geological Survey Open File 2016-1, scale 1:1,000,000.
- DeCelles, P.G., Ducea, M.N., Kapp, P., and Zandt, G., 2009. Cyclicity in Cordilleran orogenic systems. *Nature Geoscience*, 2, 251-257.
- English, J.M., Mihalynuk, M.G., and Johnston, S.T., 2010. Geochemistry of the northern Cache Creek Terrane and implications for accretionary processes in the Canadian Cordillera. *Canadian Journal of Earth Sciences*, 47, 13-34.
- Frost, B.R., Barnes, C.G., Collins, W.J., Arculus, R.J., Ellis, D.J., and Frost, C.D., 2001. A geochemical classification for granitic rocks. *Journal of Petrology*, 42, 2033-2048.
- Gabrielse, H., Murphy, D.C., and Mortensen, J.K., 2006. Cretaceous and Cenozoic dextral orogen-parallel displacements, magmatism, and paleogeography, north-central Canadian Cordillera. In: Haggart, J.W., Enkin, R.J., and Monger, J.W.H. (Eds.), *Paleogeography of the Northern American Cordillera: Evidence for and against large-scale displacements*. Geological Association of Canada, Special Paper 46, 255-276.
- Golding, M.L., Orchard, M.J., and Zagorevski, A., 2016. Microfossils from the Cache Creek Complex in northern British Columbia and southern Yukon. Geological Survey of Canada,

- Open File 8033, 25p.
- Cordey, S.P., and Anderson, R.G., 1993. Evolution of the northern Cordilleran miogeocline, Nahanni map area [105I], Yukon and Northwest Territories. Geological Survey of Canada, Memoir 428, 214p.
- Cordey, S.P., McNicoll, V.J., and Mortensen, J.K., 1998. New U-Pb ages from the Teslin area, southern Yukon, and their bearing on terrane evolution in the northern Cordillera. In: Radiogenic age and isotopic studies, Geological Survey of Canada, Report 11, 129-148.
- Gwillim, J.C., 1901. Atlin mining district; Geological Survey of Canada, Annual Report 1899, Volume 12, pp. B5-B48.
- Hart, C.J.R., 1996. Magmatic and tectonic evolution of the Intermontane Superterrane and Coast Plutonic Complex in southern Yukon Territory. M.Sc. thesis, University of British Columbia.
- Hart, C.J.R., 1997. A transect across Northern Stikinia: Geology of the Northern Whitehorse map area, Southern Yukon Territory (105D/13-16). Exploration and Geological Services Division, Yukon region, Bulletin 8, 113p.
- Hart, C.J.R., and Pelletier, K.S., 1989. Geology of Carcross (105D/2) and part of Robinson (105D/7) Map Areas. Indian and Northern Affairs Canada, Open File 1989-1, 84p.
- Hart, C.J.R., Goldfarb, R.J., Lewis, L.L., and Mair, J.L., 2004. The Northern Cordilleran mid-Cretaceous plutonic province: ilmenite/magnetite-series granitoids and intrusion-related mineralisation. *Resource Geology*, 54, 253-280.
- Hart, C.J.R., and Langdon, M., 1997. Geology and mineral deposits of the Mount Nansen camp, Yukon. In: Roots, C.F. (Ed.), *Yukon Exploration and Geology 1997*, Exploration and Geological Services Division, Yukon, Indian and Northern Affairs Canada, 129-138.
- Johnston, S.T., 1995. Geological compilation with interpretation from geophysical surveys of the northern Dawson Range, central Yukon (115-J/9 and 115-J/10, 115-J/12, 1: 100 000 scale map). Exploration and Geological Services Division, Yukon, Indian and Northern Affairs Canada, Open File 2.
- Johnston, S.T., Wynne, P.J., Francis, D., Hart, C.J.R., Enkin, R.J., and Engebretson, D.C., 1996. Yellowstone in Yukon; the Late Cretaceous Carmacks Group. *Geology*, 24, 997-1000.
- Johnston, S.T., Enkin, R.J., Baker, J., Francis, D., Colpron, M., and Larson, K., 2001. Solitary Mountain, Yukon, in Cook, F. and Erdmer, P., (Eds.), *Preliminary paleomagnetic results strengthen the correlation with the Carmacks Formation*. Lithoprobe SNORCLE – Cordilleran Tectonics Workshop, Victoria, Canada. 79, p. 85.
- Krogh, T.E., 1982. Improved accuracy of U-Pb zircon ages by the creation of more concordant systems using an air abrasion technique. *Geochimica et Cosmochimica Acta*, 46, 637-649.
- Lefebvre, D.V., and Gunning, M.H., 1988. Yellowjacket. In: *Exploration in British Columbia; 1987*, Exploration in British Columbia 1987, B87-B95.
- Lowe, C., Mihalynuk, M.G., Anderson, R.G., Canil, D., Cordey, F., English, J.M., Harder, M., Johnson, S.T., Orchard, M., Russell, K., Sano, H., and Villeneuve, M.E., 2003. Overview of the Atlin Integrated Geoscience Project, northwestern British Columbia, year three. *Current Research - Geological Survey of Canada*, 7p.
- Ludwig, K.R., 2003. User's manual for Isoplot/Ex rev. 3.00. a Geochronological Toolkit for Microsoft Excel, Berkeley Geochronology Center, Berkeley, Special Publication 4, 70p.
- Maniar, P.D., and Piccoli, P.M., 1989. Tectonic discrimination of granitoids. *Geological Society of America Bulletin*, 101, 635-643.
- Massey, N.W.D., MacIntyre, D.G., Desjardins, P.J., and Cooney, R.T., 2005. Digital Map of British Columbia: Whole Province, B.C. Ministry of Energy and Mines, GeoFile 2005-1.
- Mihalynuk, M.G., Johnston, S.T., English, J.M., Cordey, F., Villeneuve, M.E., Rui, L., and Orchard, M.J., 2003a. Atlin TGI; Part II, Regional geology and mineralization of the Nakina area (NTS 104N/2W and 3). In: *Geological Fieldwork 2002*, British Columbia Ministry of Energy and Mines, British Columbia Geological Survey, pp. 9-37.
- Mihalynuk, M.G., Devine, F.A.M., and Friedman, R.M., 2003b. Marksmen partnership - potential for shallow submarine VMS (Eskay-style) and intrusive-related gold mineralization, Tutshi Lake Area. British Columbia Ministry of Energy and Mines, British Columbia Geological Survey, Geofile 2003-9.
- Mihalynuk, M.G., Mountjoy, K.J., Smith, M.T., Currie, L.D., Gabites, J.E., Tipper, H.W., Orchard, M.J., Poulton, T.P., and Cordey, F., 1999. Geology and mineral resources of the Tagish Lake area (NTS 104M/8,9,10E, 15 and 104N/12W), northwestern British Columbia. British Columbia Ministry of Energy and Mines, Energy and Minerals Division, Geological Survey Branch, Bulletin 105, 202p.
- Mihalynuk, M.G., Smith, M.T., Gabites, J.E., Runkle, D., and Lefebvre, D., 1992. Age of emplacement and basement character of the Cache Creek Terrane as constrained by new isotopic and geochemical data. *Canadian Journal of Earth Sciences*, 29, 2463-2477.
- Mihalynuk, M.G., Smyth, W.R., Mountjoy, K.J., McMillan, W.J., Ash, C.H., and Hammack, J.L., 1991. Highlights of 1990 fieldwork in the Atlin area. In: *Geological Fieldwork, 1990* Ministry of Energy, Mines and Petroleum Resources, British Columbia Geological Survey Paper 1991-1, pp. 145-152.
- Mihalynuk, M.G., Ambrose, T.K., Devine, F.A.M., and Johnston, S.T., 2011. Atlin placer gold nuggets containing mineral and rock matter: implications for lode gold exploration. In: *Geological Fieldwork 2010*, British Columbia Ministry of Energy and Mines, British Columbia Geological Survey Paper 2010-1, pp. 65-72.
- Mihalynuk, M.G., Zagorevski, A., Orchard, M.J., English, J.M., Bidgood, A.K., Joyce, N., and Friedman, R.M., 2017. Geology of the Sinwa Creek area (104K/14). In: *Geological Fieldwork 2016*, British Columbia Ministry of Energy and Mines, British Columbia Geological Survey Paper 2017-1, this volume.
- Milidragovic, D., Joyce, N.L., Zagorevski, A., and Chapman, J.B., 2016. Petrology of explosive Middle-Upper Triassic ultramafic rocks in the Mess Creek area, northern Stikine terrane. In: *Geological Fieldwork 2015*, British Columbia Ministry of Energy and Mines, British Columbia Geological Survey Paper 2016-1, pp. 95-111.
- Monger, J.W.H., 1975. Upper Paleozoic rocks of the Atlin Terrane, northwestern British Columbia and south-central Yukon. Paper 74-47, Geological Survey of Canada, 73p.
- Monger, J.W.H., 1977. Upper Paleozoic rocks of northwestern British Columbia. Geological Survey of Canada, Paper 77-1A, 255-262.
- Mortensen, J.K., Hart, C.J.R., Tarswell, J., and Allan, M.M., 2016. U-Pb zircon age and Pb isotopic constraints on the age and origin of porphyry and epithermal vein mineralization in the eastern Dawson Range, Yukon. In: *Yukon Exploration Geology 2015*, MacFarlane, K.E., and Nordling, M.G., (Eds.), Yukon Geological Survey, pp. 165-185, including appendices.
- Nelson, J.L., Colpron, M., and Israel, S., 2013. The Cordillera of British Columbia, Yukon, and Alaska: tectonics and metallogeny. In: Colpron, M., Bissig, T., Rusk, B.G., and Thompson, J.F.H., (Eds.), *Tectonics, Metallogeny, and Discovery: The North American Cordillera and similar accretionary settings*, Society of Economic Geologists, Special Publication 17, 53-109.
- Parrish, R.R., Roddick, J.C., Loveridge, W.D., and Sullivan, R.W., 1987. Uranium-lead analytical techniques at the Geochronology Laboratory, Geological Survey of Canada. Geological Survey of Canada, Paper 87-2, 3-7.
- Pearce, J.A., 1996. A user's guide to basalt discrimination diagrams. In: Wyman, D. A., (Ed.), *Trace element geochemistry of volcanic rocks: Applications for massive sulphide exploration*, Geological

- Association of Canada, Short Course, Volume 12, 79-113.
- Pearce, J.A., Harris, N.B.W., and Tindle, A.G., 1984. Trace element discrimination diagrams for the tectonic interpretation of granitic rocks. *Journal of Petrology*, 25, 956-983.
- Ray, G.E., Meinert, L.D., Webster, I.C.L., Ballantyne, S.B., Kilby, C.E., Cornelius, S.B., Lentz, D.R., and Newberry, R.J., 2000. The geochemistry of three tin-bearing skarns and their related plutonic rocks, Atlin, northern British Columbia. *Economic Geology*, 95, 1349-1365.
- Roddick, J.C., Loveridge, W.D., and Parrish, R.R., 1987. Precise U/Pb dating of zircon at the sub-nanogram Pb level. *Chemical Geology, Isotope Geoscience Section*, 66, 111-121.
- Ryan, J.J., Zagorevski, A., Williams, S.P., Roots, C., Ciolkiewicz, W., Hayward, N., and Chapman, J.B., 2013. *Geology, Stevenson Ridge (northeast part), Yukon: Geological Survey of Canada, Canadian Geoscience Map 116.*
- Sack, P.J., and Mihalynuk, M.G., 2003. Proximal gold-cassiterite nuggets and composition of the Feather Creek placer gravels: clues to a lode source near Atlin, B.C. In: *Geological Fieldwork 2003, British Columbia Ministry of Energy and Mines, British Columbia Geological Survey Paper 2003-1*, pp. 147-161.
- Selby, D., and Creaser, R.A., 2001. Late and Mid-Cretaceous mineralization in the northern Canadian Cordillera: constraints from Re-Os molybdenite dates. *Economic Geology*, 96, 1461-1467.
- Simmons, A.T., Tosdal, R.M., Baker, D., Friedman, R., and Ullrich, T.D., 2005. Late Cretaceous volcanoplutonic arcs in northwestern British Columbia: implications for porphyry and epithermal deposits. In: *Geological Fieldwork 2004, British Columbia Ministry of Energy, Mines and Petroleum Resources, British Columbia Geological Survey Paper 2005-1*, pp. 347-360.
- Smith, J.L., and Arehart, G.B., 2010. Isotopic investigation of the Adanac porphyry molybdenum deposit in northwestern British Columbia (NTS 104N/11); final project report. *Geoscience BC Report*, 2010-1, 115-126.
- Stacey, J.S., and Kramers, J.D., 1975. Approximation of terrestrial lead isotope evolution by a two-stage model. *Earth and Planetary Science Letters*, 26, 207-221.
- Stern, R.A., 1997. The GSC Sensitive High Resolution Ion Microprobe (SHRIMP); analytical techniques of zircon U-Th-Pb age determinations and performance evaluation. In: *Current Research, Geological Survey of Canada Paper 1997-F, 1-3.1.*
- Stern, R.A., and Amelin, Y., 2003. Assessment of errors in SIMS zircon U-Pb geochronology using a natural zircon standard and NIST SRM 610 glass. *Chemical Geology*, 197, 111-142.
- Sun, S.S., and McDonough, W.F., 1989. Chemical and isotopic systematics of oceanic basalts; implications for mantle composition and processes. *Geological Society Special Publication*, 42, 313-345.
- Watson, K.D., and Mathews, W.H., 1944. The Tuya-Teslin area, northern British Columbia. *British Columbia Department of Mines. British Columbia Geological Survey Bulletin 19*, 52p.
- Wengzynowski, W.A., Giroux, G.H., and Martin, C.J., 2015. NI43-101 technical report describing geology, mineralization, geochemical surveys, geophysical surveys, diamond and percussion drilling, metallurgical testing and mineral resources on the Klaza property Yukon, Canada. SEDAR filing, and [https://www.rockhavenresources.com/assets/projects/2015-06-19\\_Klaza\\_NI-43-101.pdf](https://www.rockhavenresources.com/assets/projects/2015-06-19_Klaza_NI-43-101.pdf) [accessed November, 2016].
- Whalen, J., and Frost, C., 2013. The Q-ANOR diagram: A tool for the petrogenetic and tectonomagmatic characterization of granitic suites. *Geological Society of America Abstracts with Programs*, 45, 24.
- White, W.H., Stewart, D.R., and Ganster, M.W., 1976. Adanac (Ruby Creek). *Canadian Institute of Mining and Metallurgy, Special Volume 15*, pp. 476-483.
- Zagorevski, A., 2016. Geochemical data of the northern Cache Creek and Stikine terranes and their overlap assemblages, British Columbia and Yukon; Geological Survey of Canada, Open File 8039, 1 .zip file.

# Geology of the Sinwa Creek area, northwest BC (104K/14)



Mitchell G. Mihalynuk<sup>1, a</sup>, Alexandre Zagorevski<sup>2</sup>, Joseph M. English<sup>3</sup>,  
Michael J. Orchard<sup>2</sup>, Anna K. Bidgood<sup>4</sup>, Nancy Joyce<sup>2</sup>, and Richard M. Friedman<sup>5</sup>

<sup>1</sup> British Columbia Geological Survey, Ministry of Energy and Mines, Victoria, BC, V8W 9N3

<sup>2</sup> Geological Survey of Canada, Ottawa, ON, K1A 0E8

<sup>3</sup> Geoscience Consultant, Clonskeagh, Dublin, D14, Ireland

<sup>4</sup> Department of Earth Sciences, University of Oxford, Oxford, United Kingdom, OX1 3AN

<sup>5</sup> Pacific Centre for Geochemical and Isotopic Research, University of British Columbia, Vancouver, BC, V6T 1Z4

<sup>a</sup> corresponding author: Mitch.Mihalynuk@gov.bc.ca

Recommended citation: Mihalynuk, M.G., Zagorevski, A., English, J.M., Orchard, M.J., Bidgood, A.K., Joyce, N., and Friedman, R.M., 2017. Geology of the Sinwa Creek area, northwest BC (104K/14). In: Geological Fieldwork 2016, British Columbia Ministry of Energy and Mines, British Columbia Geological Survey Paper 2017-1, pp. 153-178.

## Abstract

Stikine terrane is one of the largest crustal blocks in the Cordillera, measuring more than 1100 km long and 250 km wide. In northern British Columbia it is well known for its large porphyry Cu-Au ±Mo-Ag deposits. Stikine terrane tapers northward, replaced by a broadening wedge of oceanic crustal rocks of the Cache Creek terrane, interpreted to have overthrust Stikine terrane reducing its exposed width to ~10 km at 60°N. This overthrust region is where Triassic-Jurassic magmatic belts with known porphyry deposits disappear, and it is mostly underlain by Triassic-Jurassic arc-derived clastic rocks of the Whitehorse trough. Overthrusting has traditionally been attributed to the northwest-trending King Salmon fault, which carries conspicuous Late Norian Sinwa Formation limestone in its hanging wall. On many terrane maps, the Sinwa Formation marks the western margin of the oceanic Cache Creek terrane. However, clast provenance, biochronology, conodont fossil fauna, and sedimentary facies carried by the King Salmon fault are inconsistent with this interpretation. Instead, these data suggest that rocks in the hangingwall of the King Salmon fault were deposited in the Triassic forearc of the Stikine terrane, isolated from the subducting Cache Creek oceanic lithosphere by an intervening trench. Thus, the King Salmon fault is not a terrane boundary, and although regionally important, it is but one of several faults that carry Sinwa Formation limestone. Complicating this simple tectonic picture are detrital zircons from one sample collected in the footwall of the King Salmon fault. They form a nearly unimodal population with a main peak at 242 Ma, an age unknown in Stikinia but common within volcanic and plutonic rocks of the Kutcho-Sitlika-Venables arc, which have historically been included in the Cache Creek terrane. If this provenance link is correct, it supports the Kutcho-Sitlika-Venables arc as a separate terrane, distinct from the Cache Creek, and juxtaposed with the Stikine forearc before the Bajocian (~173 Ma) juxtaposition of Cache Creek terrane. King Salmon and adjacent fault panels carry steep northeast plunging folds having southeast-dipping axial surfaces, consistent with a top to the north component of motion (or sinistral if originally steep) that may be related to a phase of deformation during latest Triassic Kutcho-Sitlika-Venables arc collision.

**Keywords:** Sinwa Formation, Stuhini Group, Lewes River Group, Whitehorse Trough, Cache Creek terrane, Stikine terrane, Kutcho-Sitlika-Venables arc, Whitehorse trough fold and thrust belt

## 1. Introduction

A prolific belt of porphyry copper deposits tracks northward in British Columbia to the Sheslay River area where it seems to disappear (Fig. 1). South of this latitude (~58.5°N) the Late Triassic – Early Jurassic Stuhini and Hazelton volcanic arcs that spawned the porphyry deposits are coextensive and have east-west dimensions of ~250 km. Between 58.5°N and the BC-Yukon border (60°N), the map extent of the Triassic arc thins to less than 10 km, and Early Jurassic volcanic rocks are unknown. In their place is a northward-widening wedge of oceanic crustal and accretionary complex rocks of the Cache Creek terrane and an intervening belt of marine sedimentary strata known as the Whitehorse trough (Wheeler, 1961; Fig. 1). At the southern apex of the wedge, Cache Creek and Whitehorse trough rocks are structurally interleaved (Monger and Thorstad, 1978) leading to inclusion of the Whitehorse trough with the Cache Creek terrane (Wheeler and McFeely, 1991; Gabrielse et al.,

1992). Thus defined, the Cache Creek terrane is bounded to the west by a belt of Late Triassic carbonate rocks called the Sinwa Formation, which are carried by a regional structure, the King Salmon fault. In the Sinwa Creek area, the King Salmon fault is mainly a southwest verging thrust (Monger, 1975; Souther, 1971). Just how this crustal-scale thrust has interacted with the metalliferous Triassic-Jurassic arcs is critically important to tracking the porphyry belts farther north. Did the thrust cut off the Triassic and younger arc edifices, or did it tectonically bury the mineralized arc? If buried, do windows exist in the thrust sheet through which the underlying arc may be accessed, or nearly so? Or, is the thrust coincident with a northward arc submergence and regionally diminished arc edifices, as might be inherited from Mesozoic trench geometry.

In 2015, we conducted regional mapping in the Sinwa Creek map area, where the King Salmon fault is well exposed and where the Sinwa Formation was first defined (Fig. 2). Here

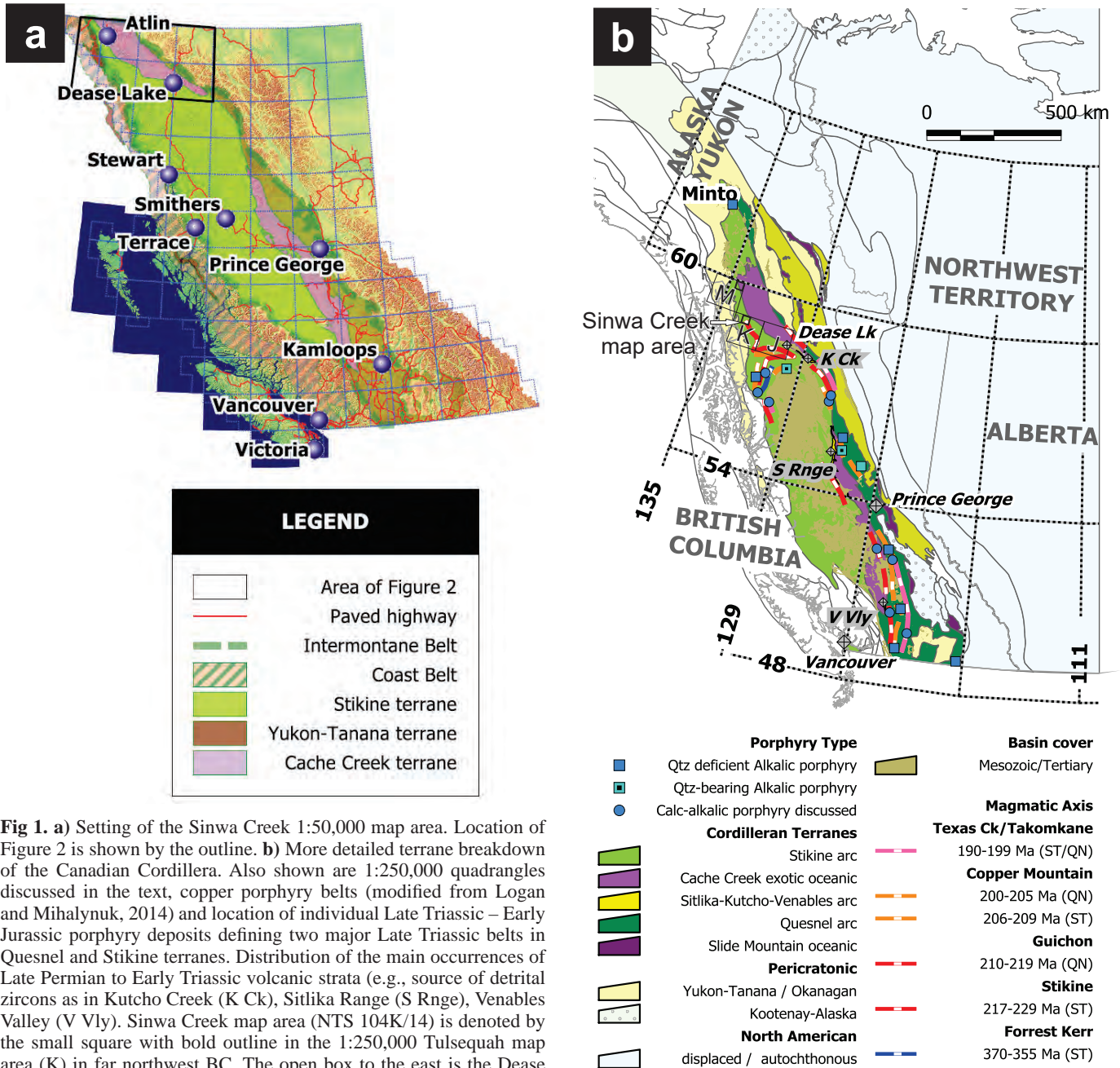


**Fig 1. a)** Setting of the Sinwa Creek 1:50,000 map area. Location of Figure 2 is shown by the outline. **b)** More detailed terrane breakdown of the Canadian Cordillera. Also shown are 1:250,000 quadrangles discussed in the text, copper porphyry belts (modified from Logan and Mihalynuk, 2014) and location of individual Late Triassic – Early Jurassic porphyry deposits defining two major Late Triassic belts in Quesnel and Stikine terranes. Distribution of the main occurrences of Late Permian to Early Triassic volcanic strata (e.g., source of detrital zircons as in Kutcho Creek (K Ck), Sitlika Range (S Rnge), Venables Valley (V Vly). Sinwa Creek map area (NTS 104K/14) is denoted by the small square with bold outline in the 1:250,000 Tulsequah map area (K) in far northwest BC. The open box to the east is the Dease Lake sheet (J), and to the northwest is the Bennett sheet (M).

we present findings from this mapping and geochronological analysis of two key units, tuff from the southeast corner of the map area (arc proximal) and strata immediately below an unconformity near the top of the Triassic section, as they pertain to the stratigraphic and structural evolution of the region.

## 2. Physiography and access

Sinwa Creek map area covers nearly 900 square kilometres at the transition between the coastal Boundary Ranges and the drier, more interior Taku Plateau. Southeast-flowing Sinwa Creek drains the center of the map area, merging with the Taku River about 6 km downstream of the Taku-Inklin River

confluence (Fig. 3; also shown as Nakina-Inklin confluence on some maps). There are no roads or permanent settlements in the area, although buildings near the mouth of the Inklin River may be occupied during the fishing and hunting seasons. Shallow-draft boats can be used to access Taku and Inklin River valleys, but the most practical means of access is via helicopter with the nearest base 80 km to the north-northwest in Atlin. Juneau, Alaska is 90 km southwest.

## 3. Regional geology and previous work

Exploration of the area dates to 1887-1888 with the passage of prospectors up the Taku River en route to the Klondike

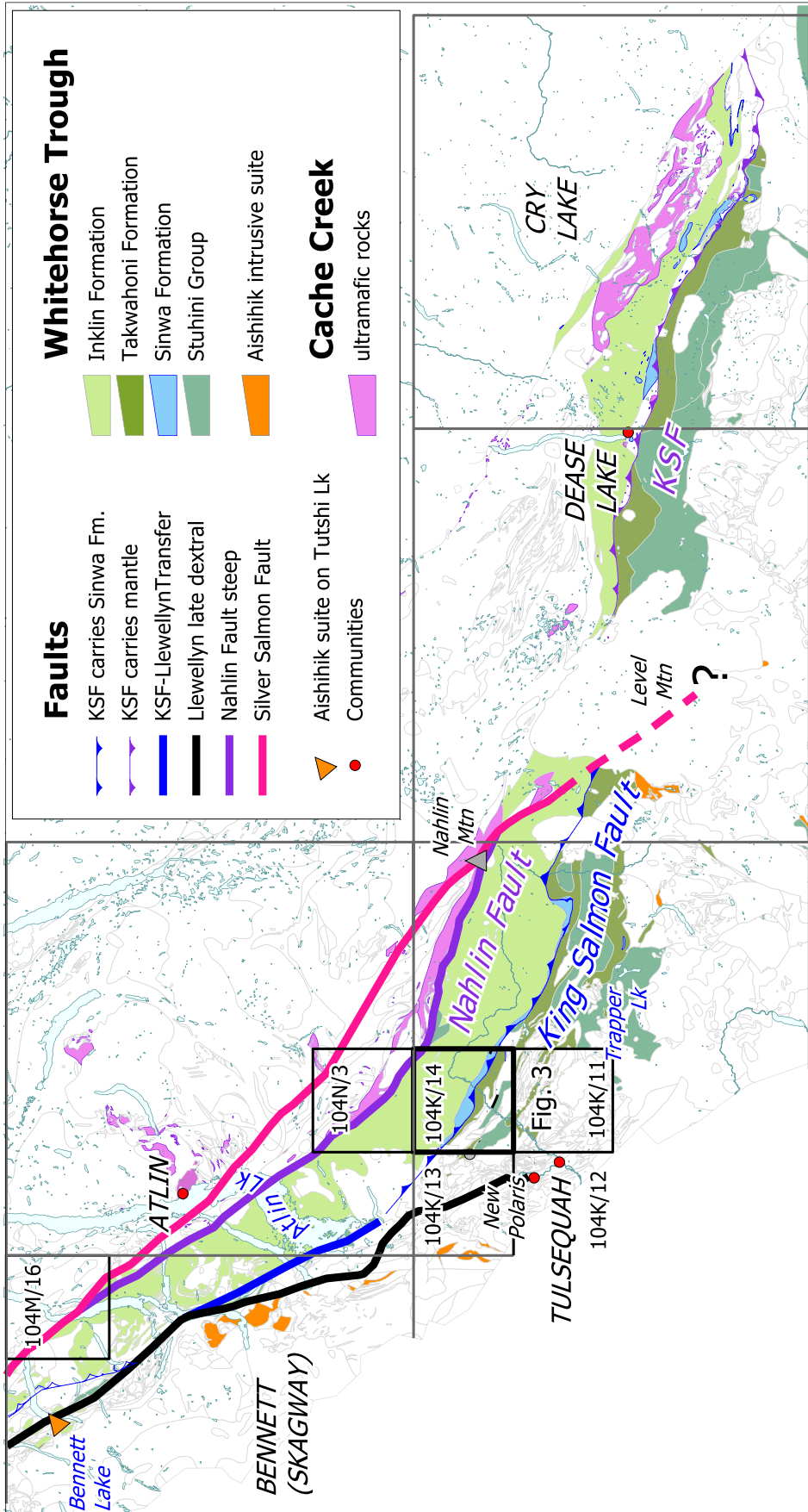


**Fig. 2.** Location of the Sinwa Creek map area in northwest BC with respect to crustal scale faults and key geological elements; Whitehorse trough strata of the Stikine terrane, and ultramafic rocks of the Cache Creek terrane (other units in these terranes are shown as grey outlines, no outlines for geology units comprising terranes to the east). Quadrangles discussed in text are shown. Large grid includes 1:250,000-scale quadrangles of Bennett, Atlin, Tulsequah, Dease Lake and Cry Lake map areas. Small quadrangles are 1:50,000 sheets: Sinwa Creek (104K/14, the focus of this paper); Turtle Lake (104M/16); and other sheets referred to in the text. King Salmon Fault is shown in two colours; where coloured blue it carries Sinwa Formation in its hangingwall, and where coloured purple (KSF) it also carries slivers of mantle rocks.

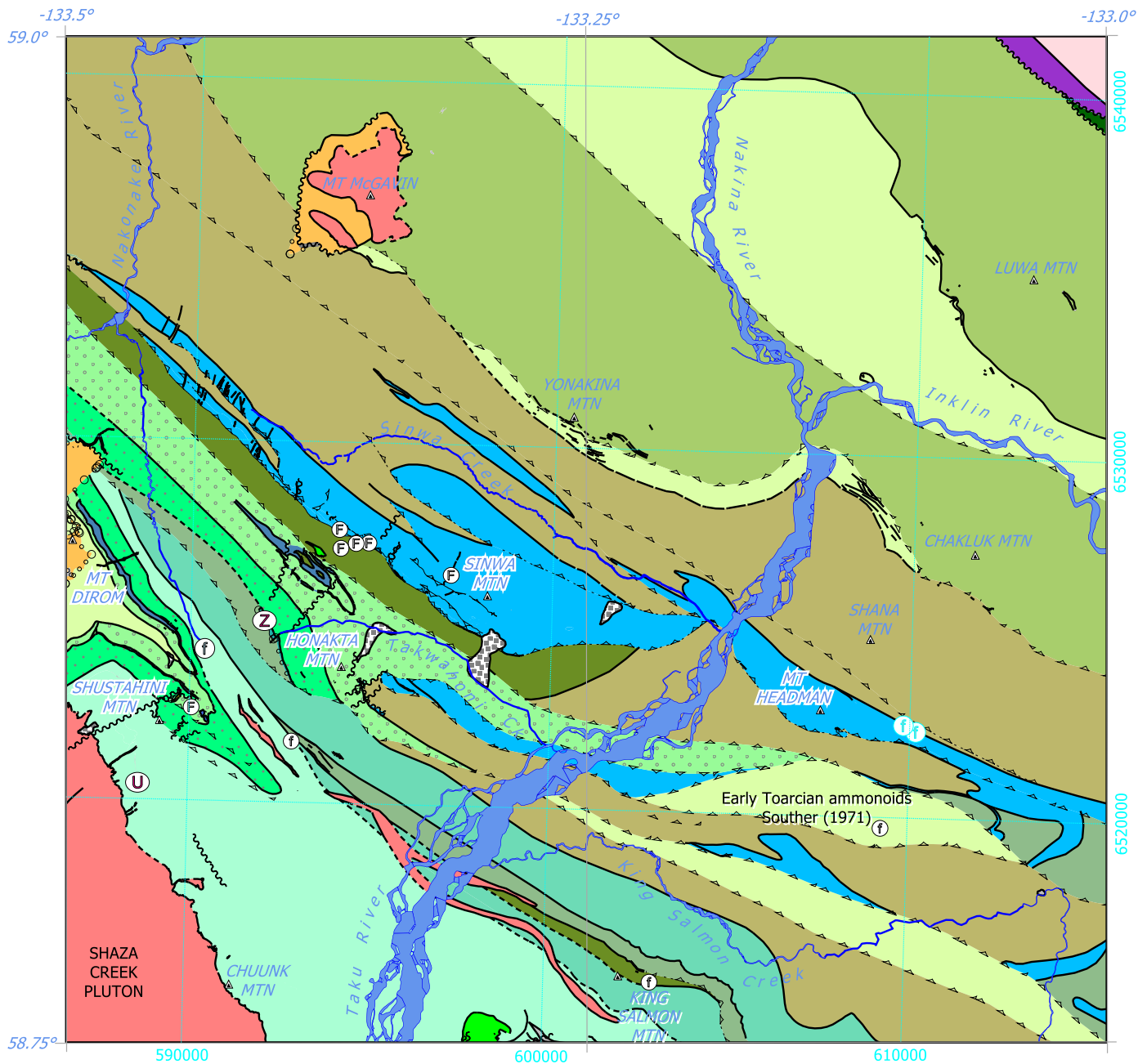


Fig. 3. Preliminary geology of the Sinwa Creek map area (104K/14).

goldfields. In 1923 and 1929, discovery of the Tulsequah Chief and Polaris Taku deposits led to establishment of a permanent mining town, complete with bowling alley, just 8 km from the southwest corner of the Sinwa Creek map area (Fig. 2). Systematic regional mapping of the region began with investigations by Kerr (1931a, b, 1948), followed by 1:250,000-scale mapping of the entire Tulsequah sheet in 1958 to 1960 by Souther (1971). Parts of the northeastern Sinwa Creek area were mapped by Monger (1975) who focused on Upper Paleozoic stratigraphy. Systematic 1:50,000-scale mapping in the area began in 1991 with reconnaissance surveys

leading to coverage of the Tulsequah Glacier and Tulsequah River areas (104K/12 and 13; Mihalynuk et al., 1994 a, b), Stuhini Creek (104K/11, Mihalynuk et al., 1995 a, b) and Sloko River (104N/3, Mihalynuk et al., 2003a, b). These mapsheets surround the Sinwa Creek map area on all but its eastern side (Fig. 2). Unpublished mapping conducted as part of a Ph.D. thesis by English (2004) covered much of the alpine area northeast and within ~10 km of the prominent northwest-trending belt of Sinwa Formation limestone that bisects the Sinwa Creek map area.

Most of the Sinwa Creek map area is underlain by Late Triassic

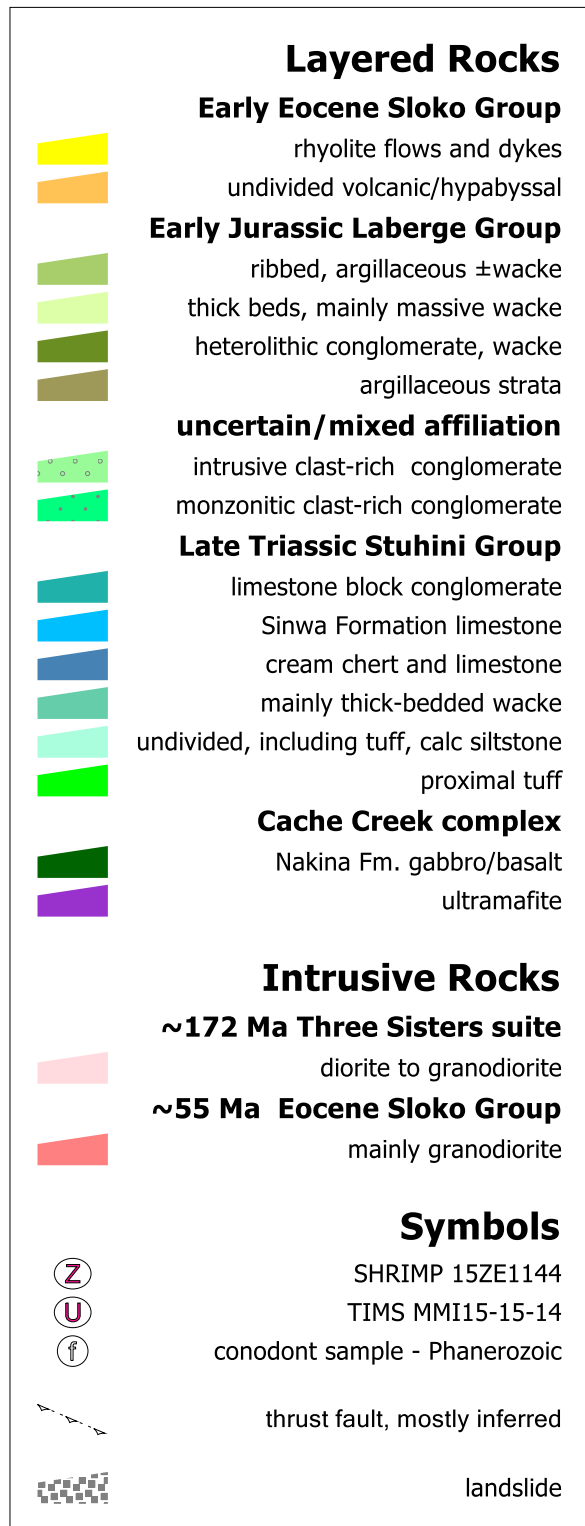


Fig. 3. Continued.

and Early Jurassic strata of the Whitehorse Trough (as defined by Wheeler, 1961; Figs. 2, 3). In the far southwest corner of the area is Eocene granodiorite of the Shaza Creek pluton (Souther, 1971; Mihalynuk et al., 1994), in the far northeast corner are oceanic crustal rocks and mantle rocks (Monger, 1975) of the

Cache Creek terrane. In the northwest part of the map area, an outlier of Sloko Group volcanic rocks (Early Eocene) rests unconformably on deformed Jurassic strata and is cut by a presumably comagmatic quartz-monzonitic intrusion that underlies Mount McGavin (Fig. 3).

### 3.1. Terrane boundary constraints

Whitehorse trough marks the boundary between two major crustal terranes (Coney et al., 1980) of the Canadian Cordillera (Figs. 1, 2). To the northeast are oceanic crustal and mantle rocks together with exotic Paleozoic Tethyan marine strata of the Cache Creek terrane (Monger, 1977); to the southwest are the Paleozoic and Mesozoic arc strata of the Stikine terrane (Brown et al., 1991). However, the location of the terrane boundary within the Whitehorse Trough is debatable. Based on clast compositions in conglomeratic units that lie southwest of the King Salmon fault, affiliation with Stikinia has been argued (Johannson, 1993; Mihalynuk et al., 1995; Hart et al., 1995; Dickie and Hein, 1988; Johannson et al., 1997; Mihalynuk et al., 2004). These are rocks considered part of the Takwahoni Formation (Souther, 1971) which, together with more distal strata northeast of the fault (Inklin Formation) form the Laberge Group. Inklin Formation rocks have a less certain terrane affiliation. West of Atlin, the Inklin Formation is structurally interleaved with mid-ocean ridge-type pillow basalt and slivers of gabbro and serpentinized ultramafite (Mihalynuk et al., 1999).

Most workers have concluded that the Inklin Formation was deposited in the Stikine forearc (Dickie and Hein, 1995; Hart et al., 1995; Johannson et al., 1997; Bultman, 1979; Mihalynuk et al., 1999; Colpron et al., 2015), but evidence for arc construction spanning the Early Jurassic is lacking near 60°N, except for a magmatic pulse between 180-190 Ma represented in the Inklin Formation by layers of Nordenskiöld dacite (Cairnes, 1910; Nordenskiöld formation of Bostock and Lees, 1938; Colpron and Friedman, 2007; 186 - 188 Ma) or by their coeval and presumably comagmatic intrusive counterparts intruding basement rocks that flank the Whitehorse trough to the west, which include the Aishihik (Johnston and Erdmer, 1995; Johnston et al., 1996; see also, Fig. 2) and Long Lake (Woodsworth et al., 1992; Johnston et al., 1996) intrusive suites, and the Tagish intrusive suite in BC (Currie and Parrish, 1997). Detrital zircon age distribution peaks at 201 to 196 Ma have also been reported from the Laberge Group (Early Jurassic) in Yukon (Colpron et al., 2015), suggesting contributions from either nearby magmatic source rocks of this age, or ash from a more distal volcanic arc. We know of no discrete ash beds in the Laberge Group that have been isotopically dated as older than the Nordenskiöld dacite. Approximately coeval with these dacite tuffite layers are concentrations of feldspar porphyry clasts with a 'sooty' black matrix that Canil et al. (2006) found in some of the most inboard portions of the trough where ultra-high pressure (UHP) eclogite clasts (MacKenzie et al., 2005) of unknown provenance are also locally abundant in ~181 Ma Laberge Group strata (Zagorevski et al., 2015).

#### 4. Stratigraphy

Late Triassic and Early Jurassic strata of the Whitehorse trough interfinger with and overlie volcanic rocks of the Stuhini arc (Late Triassic), which underlie parts of southwestern Sinwa Creek map area and Stuhini Creek map area to the south. Although folds and thrust faults complicate relations, strata generally become less proximal, dip regionally, and young to the northeast, away from the apparent arc axis. The stratigraphic and facies progression from mainly Late Carnian volcanic Stuhini Group (Souther, 1971) is: coeval flanking and overlying volcano-sedimentary rocks, capped by the Upper Norian Sinwa Formation, unconformably (?) overlain by Pliensbachian to Toarcian conglomeratic Takwahoni Formation (southwest of the King Salmon fault), and wacke and argillite of the Sinemurian to Pliensbachian Inklin Formation (northeast of the King Salmon fault). Conglomeratic units including those dominated by monzonitic volcanic and intrusive clasts overlap units originally mapped by Souther (1971) as Stuhini Group (including volcanic rocks and his 'King Salmon Formation' clastic strata). These conglomeratic units apparently overlie a Late Triassic unconformity, and on that basis, are probably Early Jurassic in age, but conclusive age data are lacking. Until such data are available, we refer to the conglomerate units as having 'uncertain/mixed affiliation' (Fig. 3). Youngest strata of the Laberge Group, Middle Jurassic (Aalenian to Bajocian) chert pebble conglomerate derived from Cache Creek terrane (Souther, 1971; Mihalynuk et al., 2004), are known to the south, but have yet to be identified in the Sinwa Creek area. Early Eocene volcanic strata of the Sloko Group unconformably overly the Whitehorse trough as scattered outliers at high elevations. These volcanic strata have been described where they extensively crop out in adjacent map areas (Mihalynuk et al., 1994; Mihalynuk et al., 1995); therefore, descriptions are not repeated here.

#### 4.1. Stuhini Group

West-northwest-trending limestone beds of the Sinwa Formation (Late Norian, Souther, 1971) form a conspicuous unit that caps the Stuhini Group and divides the Sinwa Creek map area diagonally in two. Structurally below the Sinwa Formation are distinctive conglomeratic, volcanogenic and minor, but prominent, limestone strata that may correlate regionally. Units mapped in the Sinwa Creek area are described here, from southwest to northeast, mainly from oldest to youngest, except for probable thrust duplication (see below, King Salmon fault).

##### 4.1.1. Tuff at Chuunk Mtn.

Stuhini Group in the Chuunk Mountain area (Fig. 3) consists of light green to maroon interlayered andesitic tuff breccia to crystal tuff. Tuff breccia horizons are poly lithic and include massive, vesicular, feldspar and/or hornblende porphyritic andesite blocks that range from angular to amoeboid. Within the same beds, the colour of the clasts varies from green to maroon. Finer tuff layers are locally pervasively hematized and contain angular, white feldspar crystal-rich laminae that

exhibit both normal and reverse grading. Laminae are locally truncated by volcanic blocks, and also exhibit local sags and/or draping. Massive tuff beds >4 m thick, amoeboid blocks, apparent volcanic bombs, and inversely graded layers suggest an explosive, vent-proximal volcanic environment. Hematized blocks and beds are common, consistent with oxidizing conditions in subareal or shallow marine settings. A sample of massive lapilli tuff collected for U-Pb isotopic analysis (15ZE1144) returned an age of 217.49 +0.31/-0.44 Ma (see below, Geochronology).

##### 4.1.2. Well-bedded calcareous siltstone

Orange-weathering, well-bedded calcareous siltstones occur at several stratigraphic levels and are generally included in Figure 3 as part of the 'undivided' Stuhini Group. In the region near Shustahini and Honakta mountains, brown to orange-weathering, well-bedded calcareous siltstone is the predominant unit. Planar interbeds of massive wacke and lenses of conglomerate containing boulders of coarse augite porphyry and beds of impure, orange-weathering limestone, all from ~1 m to ~10m thick, are locally important constituents. Siltstone beds are typically 1-10cm thick with parallel laminae; although they can display good cross stratification. Marley beds are common. Where bedding planes part cleanly, well-preserved ammonites and paper clams (*Halobia?*) can be found with a little searching. Where this unit occurs structurally above the monzonitic clast-rich conglomerate it contains distinctive layers of gastropod packstone. At their thickest, these layers form ~20 cm beds packed with gastropods 2-3 cm across (Fig. 4).

Owing to their distinctive and easily recognized appearance, these beds, and the carbonate-rich siliciclastic interval in which they occur, could make a useful regional marker. However, the two localities where this lithology has been observed are both structurally disrupted and their stratigraphic position is uncertain. Thus, on Figure 3 we include them in the "undivided,



**Fig. 4.** Distinctive, orange-weathering gastropod packstone with matrix composed of volcanic sand grains in micrite.

including tuff, calc siltstone” unit, designating the fossil rich layers with an “F” (at Shustahini Mountain, where the unit is too restricted to show at the map scale).

Based on previous fossils reported from this part of the map area (Souther, 1971) and unconfirmed field identification, we suspect that this unit is Late Triassic. However, changes in younging directions within the mainly homoclinal succession at Honakta Mountain (Fig. 3) suggests that cryptic isoclinal folds repeat at least parts of the unit.

Generally fine grain size suggests deposition as some distance from source terrains, and possibly in relatively deep water. However, based on modern analogues, gastropods are photic zone grazers and such abundant fossil remains points to a shallow-water environment. Lack of broken shells suggests a quiet, possibly lagoonal or estuarine setting with siliciclastic input. High carbonate content may represent background carbonate productivity. Relatively pure carbonate accumulated when siliciclastic input waned, as indicated by gradations on metre scales from siltstone to limestone.

#### 4.1.3. Black, friable argillite

Dark brown to black, locally petroliferous argillite underlies the main Sinwa Formation carbonate layer west of Sinwa Mountain. Thin bedding tends to break into centimetre-scale pieces creating friable, recessive outcrops. Black argillite probably grades into orange- and black-weathering, finely bedded argillite and siltstone structurally down section. However, abundant low- and high-angle faults preclude establishing stratigraphic continuity. About 200m structurally down section are coarse wacke and intrusive clast-rich conglomerate layers (Fig. 5). No macrofossils were recovered from the argillite-siltstone section.

The black argillite unit may have been a detachment surface during thrust repetition of the apparently overlying Sinwa Formation. On the southeast flank of Sinwa Mountain, the main mass of carbonate rocks can be seen in imagery to grade into underlying dark siliciclastic strata, probably equivalents of this unit. Thrust slivers of the unit are too thin to portray on Fig. 3.

#### 4.1.4. Sinwa Formation

Sinwa Formation limestone is beautifully exposed on the glacially sculpted ridges (Fig. 6) underlying Sinwa Mountain, extending northwest to the Nakonake valley, and more than 50 km southeast to the headwaters of the Inklin River. Typically light grey-weathering and massive, well-bedded sections occur near the base and middle of the formation (Fig. 6). Some distinctive horizons, such as a petroliferous, colonial coral packstone (Fig. 7a), can be traced for kilometres, commonly terminating at faults. We estimate that the Sinwa Formation is at least 2000 m thick, but structural disruption leading to thickening and stratigraphic omission can be cryptic, and detailed sections were not measured. Extensive karsting has led to modern collapse features, sinkholes, and influent or disappearing streams.

Massive limestones are predominant and locally contain

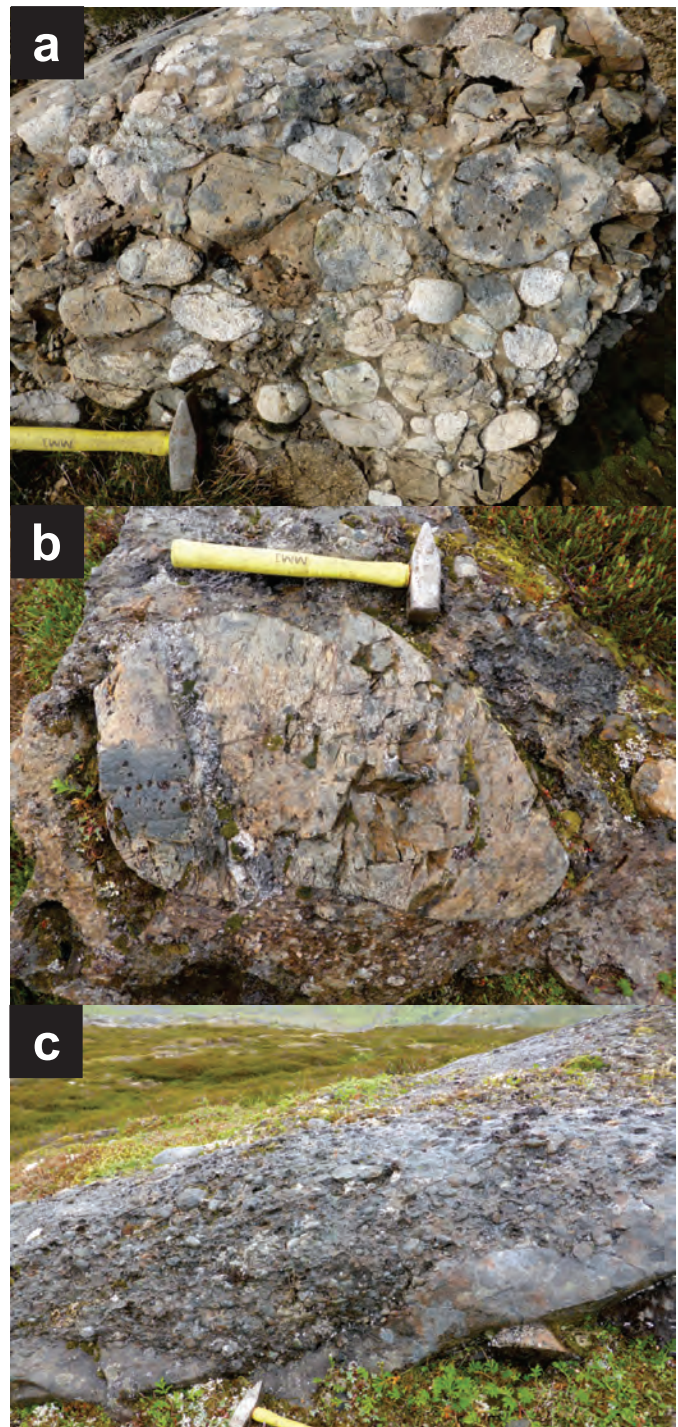


**Fig. 5.** Intrusive clast-rich conglomerate. **a)** Near Takwahoni Creek. **b)** Near Sinwa Mountain. **c)** Also near Sinwa Mountain, a conglomerate bed with erosional base cutting underlying coarse wacke beds.

nodular chert in crudely layered zones tens of metres thick. These massive limestone units form the top of at least two major depositional cycles and are locally coralline (Fig. 7b). In the lower cycle, dark fine-grained siliciclastic strata grade to limestones, with the number and thickness of limestone beds increasing upsection. The cycle is capped by sparsely bioclastic limestone beds, locally with colonial corals, metres to about ten



**Fig. 6.** View to the east, oblique to the strike, with light grey-weathering Sinwa Formation limestone in the near horizon. White-weathering mountain face in the centre, far horizon is Mt. Sinawa Eddy, mainly Permian Tethyan limestone of the Cache Creek terrane. Cream-weathering chert-limestone unit at the left center cores a southwest-verging fold outlined by dark grey-weathering intrusive clast-rich conglomerate (chert-limestone enclosed by cyan dashed line). Light weathering rocks in the foreground are monzonitic clast-rich conglomerate.

metres thick. At the base of the second cycle, limestones are abruptly overlain by siliciclastic rocks that weather dark grey, brown and locally maroon (Fig. 8). Breccia zones are common. Some are localized along faults, but others form lobes that may be hundreds of metres across. Breccia lobes truncate adjacent strata and are draped by overlying limestone beds (Fig. 8). Rare laminated, cream coloured cherty beds less than 1m thick are similar to those that predominate a cream chert and limestone unit structurally below (southwest of) the main belt of Sinwa Formation.

Few fossil collections from the Sinwa Formation at its type locality have been sufficiently well studied to yield ages to the stage level. Souther (1971) noted only two such collections, neither from Mount Sinwa (from near King Salmon Lake, southeast of the Sinwa Creek map area), both 'Upper Norian'. Late Norian to Rhaetian (*Epigondolella englandi*) conodonts have also been recovered from a discontinuous belt of limestone bodies extending from the Yukon border to southern Atlin Lake

(Mihalynuk, et al., 1999). This belt continues into Yukon where reef mound buildups are well exposed, such as at the famously fossiliferous Lime Peak reef, north of Whitehorse (Yarnell et al., 1998; Reid and Tempelman, 1987).

#### 4.1.5. Cream chert and limestone

Distinctive cream-colouration of a chert and limestone unit together with extensive talus fans permit them to be easily distinguished at a distance from limestones of the Sinwa Formation (Figs. 6, 9a). Thickness varies from ~110 to 180 m, although structural thickening and thinning are likely. The chert and limestone form discrete interbeds a decimetre or more thick (Fig. 9b). Resistant laminae are common on chalky weathered surfaces of the chert beds.

A stratigraphic contact between the cream chert-limestone unit and an underlying intrusive clast-rich conglomerate unit (see below) cannot be unequivocally demonstrated, but if depositional, an abrupt change in environment is implied. The

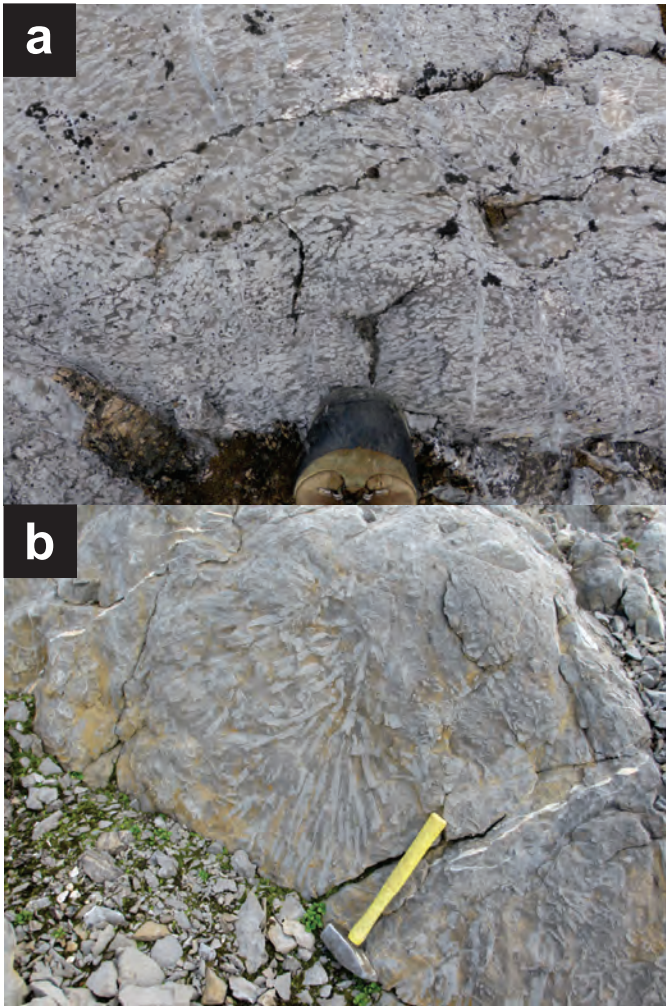


**Fig. 7. a)** Colonial coral packstone, probably *phaceloid Retiophyllia* sp., based on similarity with samples identified by G. Stanley (written communication) from a petroliferous, well-bedded Sinwa Formation sample. **b)** Branching coral.

age of the unit is unknown, but based on similar sparse beds in the Sinwa Formation, a Norian age is inferred.

#### 4.1.6. Limestone block conglomerate

On the northwest flank of Honakta Mountain, a distinctive limestone block conglomerate (Figs. 10a, b) marks the unconformable contact between a well-bedded predominantly siltstone section and overlying volcanic sandstone and conglomerate. Light grey-weathering bioclastic limestone blocks comprise 70-90% of the clasts and can be more than a metre across (Fig. 10a), far larger than any other clast type. However, in the cirque face to the north, light grey blocks ~5m in long dimension can be seen from afar (Fig. 10c). Coral, crinoid, bivalve and fish bone fossils are well preserved in many of the blocks. Identification of these fossils is pending.

Other common clasts include porphyritic intrusive clasts, with mainly feldspar, lesser hornblende  $\pm$  pyroxene, and quartz grains. Attaining boulder size, they are typically well rounded, in contrast to many of the limestone clasts, which can be highly

angular or even have delicate appendages (Fig. 10b).

Based on paper clams in underlying strata and *Halobia* identified on the west side of Honakta Creek, as well as Early Jurassic fossils in strata correlated with the overlying conglomerates of Takwahoni Creek (Souther, 1971), a Late Triassic, probably Late Norian age is suggested. A medium-grained sandstone bed beneath the conglomerate was collected for detrital zircon age determination to test this age assignment, but unexpectedly returned a nearly unimodal population of Middle Triassic zircons with a peak at ~242 Ma (see below, Geochronology) which requires special circumstances for deposition in a Late Triassic forearc environment (see below, Discussion).

Some limestone blocks show evidence of post deposition compaction and may have been deposited in a semi-lithified state (Fig. 10b). Semi-lithified limestone blocks metres across are most likely olistostromal deposits. Admixture of rounded boulders of monzonite point to the combination of sediments from intra and extra-basinal sources, as may have occurred during collision and uplift of the carbonate bank. Rounding of boulders is not necessarily an indication of long distance alluvial transport because spheroidal weathering of jointed rocks in tropical environments produces rounded blocks at the outcrop source (e.g., Hall and Smyth, 2008).

#### 4.2. Uncertain/mixed affiliation

Conglomerate units here grouped as 'uncertain/mixed affiliation' have been mapped by Souther (1971) as Takwahoni Formation (Early Jurassic) and as Stuhini Group (Late Triassic).

##### 4.2.1. Monzonitic clast-rich conglomerate

Conglomerate containing predominantly monzonitic clasts is well exposed at the headwaters of Takwahoni Creek where a structural thickness of ~1.2 km is exposed. Although low-angle faults cut the section, the amount of structural thickening is unknown. Conglomerate beds are tabular to lensoid. The unit can be easily identified based on characteristic white to pale pink-weathering, porphyritic clasts (locally maroon to green), which weather lighter than the matrix. Clasts are commonly acicular hornblende and tabular feldspar porphyry (Fig. 11a). Fine-grained to aphanitic green and maroon clasts may comprise up to ~2% of typical outcrops. Clasts are pebble and cobble sized, ranging to boulder sized (Fig. 11b). Interbeds of sandstone and tuffite display both sharp and gradational contacts with conglomerate. Within dense conglomerate bed interiors, the tuffaceous sandy matrix is weakly- to non-calcareous, but where the unit becomes orange-tinged, it is commonly calcareous. Viewed from a distance, layers containing megaclasts up to ~7 m across, can be identified (Fig. 11c). Near contacts with the underlying limestone block conglomerate (see above) this unit includes ~10 m sections of green volcanic sandstone with white alteration spots.

To the east, in the headwaters of Sinwa Creek, beds with lapilli and ash-sized monzonitic fragments are interpreted as distal equivalents of the conglomerate. Green argillaceous layers



**Fig. 8.** View to the northeast of a megabreccia lobe that truncates well-bedded limestone of the Sinwa Formation. Dashed red line follows the approximate base of the unit and beginning of successive depositional cycle with massive limestone near its base.

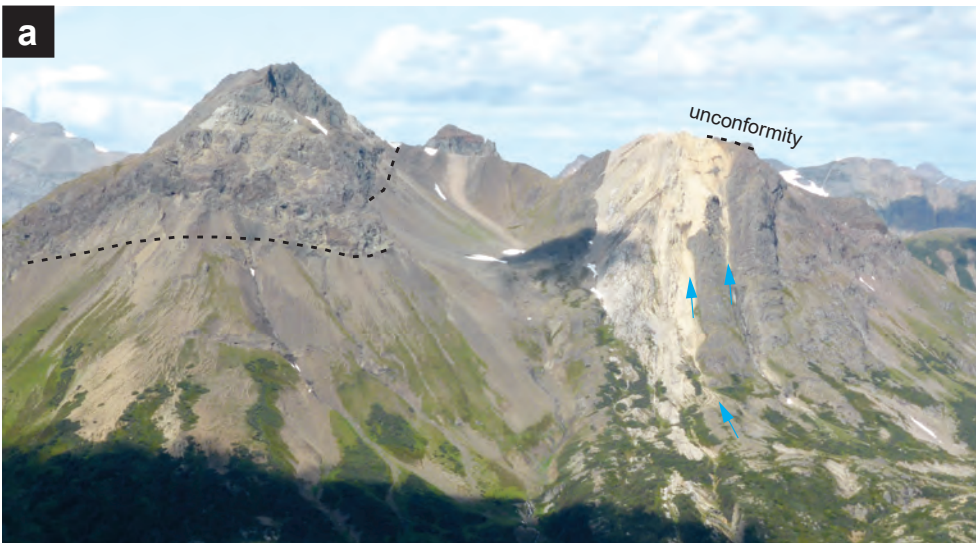


**Fig. 9. a)** View along strike to the northwest of cream-weathering chert and lesser carbonate at Mt. Dirom dip steeply to the west and are unconformably overlain by dark brown to maroon flow and interflow breccia of the Sloko Group (Eocene; Nakonake formation (above dotted lines) cf. Mihalynuk et al., 1994). In addition to the distinctive cream colour, this unit produces talus slopes (blue arrows), unlike the relatively pure carbonate rocks of the Sinwa Formation, which tend to erode by dissolution. Massive thick units enclosing the chert are intrusive boulder conglomerate layers, stained deep maroon by iron oxides below the unconformity. Recessive strata in the col at the centre of the photo are thinly bedded argillaceous strata of uncertain, but presumed Early Jurassic age. Thick conglomerate beds east of the chert and lesser carbonate unit appear truncated by the unit, perhaps by an east-directed back thrust. **b)** Close-up of laminated, cream chert beds and a light grey interbed of fine-grained, recrystallized limestone.

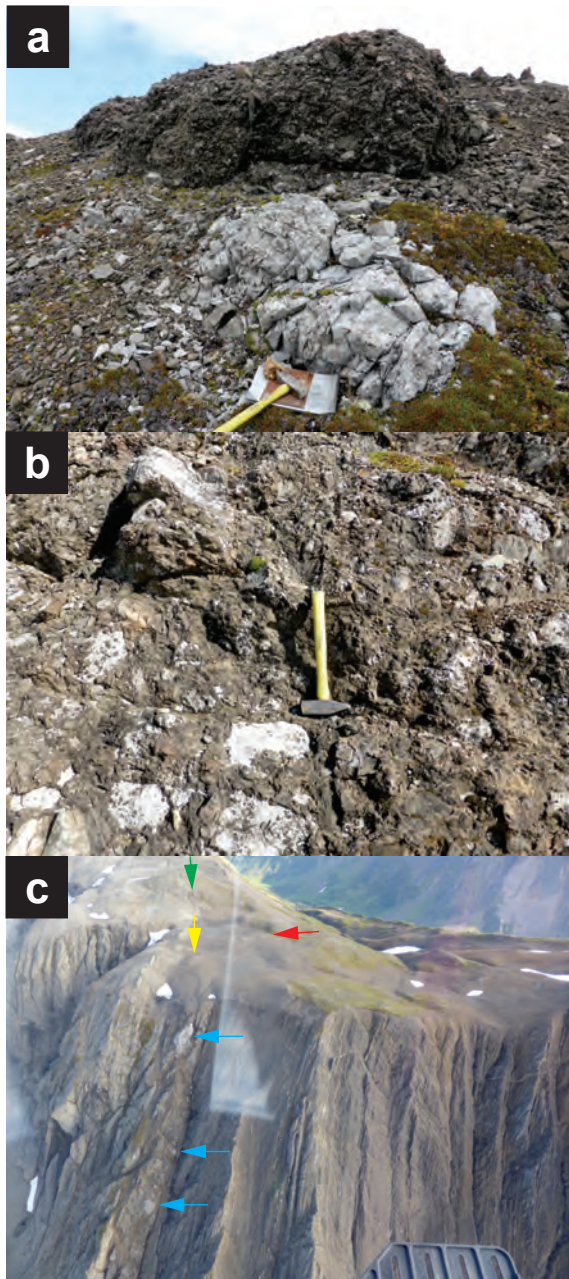


**Fig. 10.** a) Limestone boulder conglomerate that contains blocks more than a metre across (e.g., light grey limestone clast that the clipboard is resting against). Rubble of slope is composed of boulders weathered out of the conglomerate. b) Many limestone clasts have irregular outlines (e.g., below left of hammer) suggesting deposition in a semi-lithified state. In contrast, most intrusive boulders are well rounded (e.g., see top of outcrop in a). c) Southward overview through helicopter window (note reflections) of the unconformity between calcareous Late Triassic *Halobia*-bearing argillite (brown on right) and siltstone and monzonite clast-rich conglomerate and volcanic sandstone (grey, to left). Blue arrows point to very large limestone blocks in the conglomeratic unit. Green arrow shows location of coarse conglomerate as it strikes southwest across the plateau. Yellow arrow is approximate site of sample collected for detrital zircon age determination (MMI15-15-14). Red arrow denotes a dike that cuts section (continues to behind yellow arrowhead), part of an extensive dike set that can also be seen farther west on the plateau and cutting well-bedded Late Triassic strata in the cliff section.

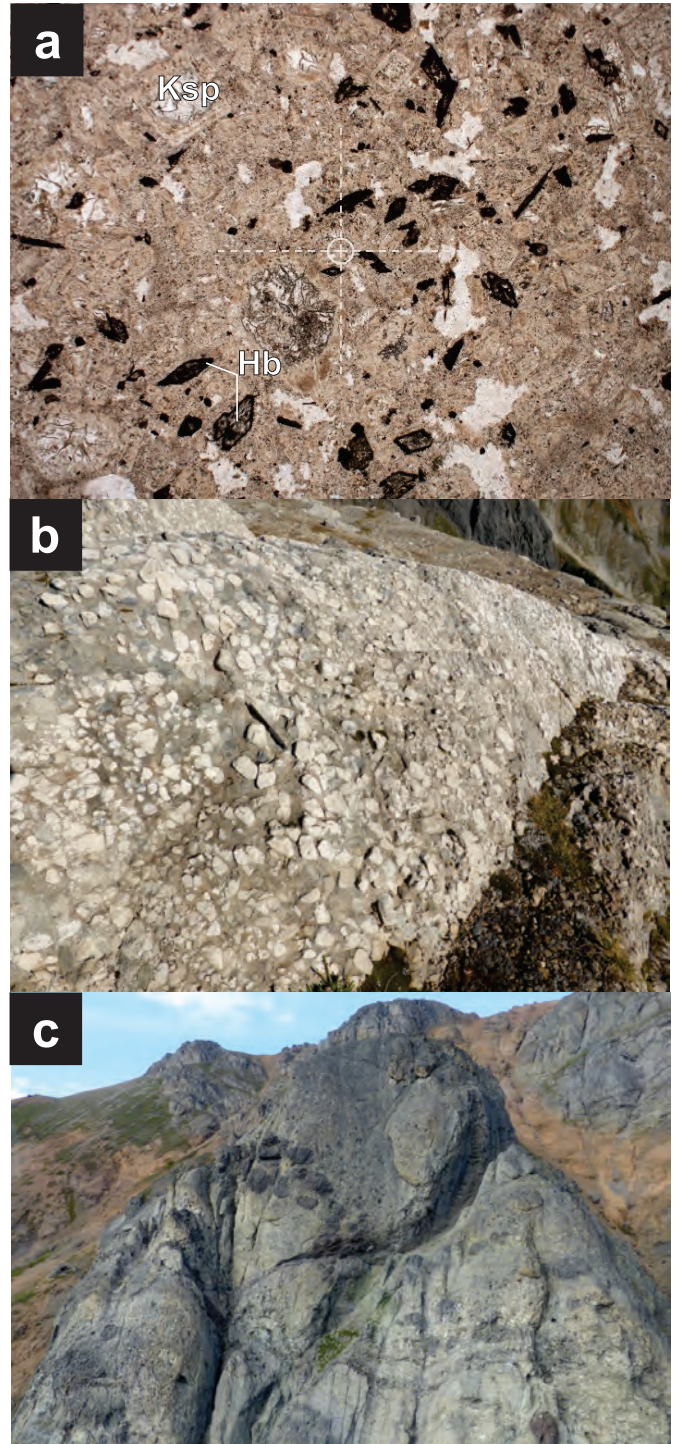


**Fig. 11.** a) Thin section of monzonite clast conglomerate. Hb=hornblende, Ksp=K-feldspar, in plane-polarized light; width of photomicrograph represents ~4 mm. The circle at the cross hairs has a radius of 100 microns. b) Outcrop of monzonite clast-rich conglomerate showing typical white to light tan pebbles, cobbles and boulders. c) View eastward of megaclast conglomerate in the monzonite clast conglomerate. Height of the near cliff face is about 30 m (aerial reconnaissance not confirmed by on-the-ground observations). Megaclasts in the cliff face are both darker and lighter (largest clast, ~7 m, near peak) than the enclosing strata. A megaclast-bearing unit outside the field of view to the right (southwest) contains mainly limestone blocks (not the same layer as shown in Figure 10).

millimetres thick display possible desiccation cracks infilled by volcanic sandstone (Fig. 12). The coarse conglomerates were derived from a restricted, relatively homogenous igneous source area and probably deposited in a fan-type submarine to locally subaerial setting.



**Fig. 12.** Carbonate-altered tuffaceous sandstone with mud interlayer that appears to have been cracked (view of top of muddy layer), possibly due to desiccation during subaerial exposure.

#### 4.2.2. Intrusive clast-rich conglomerate

Thick sections of intrusive clast-rich conglomerate crop out extensively west of the Sinwa Formation. Internally, bedded layers can be more than 260m thick (e.g., the northeast flank of Mount Dirom). Clasts range from coarse K-feldspar-rich granitoids to medium-grained plagioclase, and quartz-eye and plagioclase quartz-eye porphyries (Figs. 5a, b). Hornblende can comprise up to ~15% of the porphyritic clasts and is generally intensely chloritized. The unit locally contains volcanic sandstone beds and thin maroon beds with variegated lapilli- and ash-sized fragments in a fine tuffite matrix. Some tabular beds display erosional, channeled bases (Fig. 5c). At Mt. Dirom and along strike at Shustahini Mountain, conglomerates are in contact with a cream-coloured limestone-chert unit, or nearly so (Fig. 9a). Unfortunately, a lack of clear sedimentary younging indicators and concentration of strain along the contact, renders the stratigraphic relationship ambiguous. A complete lack of cream chert clasts in the adjacent boulder conglomerate unit where it has been mapped suggests that either the chert-limestone unit was deposited atop the conglomerate, or the contact is a bedding-parallel fault with considerable offset. Abrupt lateral truncation of conglomerate layers on the east flank of Mt. Dirom points to an east-directed thrust fault (Fig. 9a).

#### 4.2.3. Mainly thick-bedded wacke

Dark olive-brown wacke beds up to ~10m thick can form featureless cliff bands. Volcanic-lithic and feldspar grains are the most common constituents. In some localities fine-grained feldspar porphyry clasts with indistinct clast outlines

comprise a significant proportion of the beds. Angularity of these volcanic clasts suggests a proximal source with minor reworking; some accumulations of volcanic debris may be subaqueous tuff. Sets of massive wacke beds form resistant ribs that extend northward into the Nakonake River valley and are readily visible on satellite images.

This unit was mainly mapped as Stuhini Group by Souther (1971), but is lithologically similar to wacke of the Laberge Group. Nevertheless, until fossil or isotopic data confirm an Early Jurassic age, we retain this unit as part of the Stuhini Group.

### 4.3. Laberge Group

Structurally and stratigraphically above the Sinwa Formation, most sections are composed of varying proportions of massive wacke, argillite, siltstone and minor conglomerate, all with variable matrix carbonate contents, which we include with the Inklin Formation of the Laberge Group (as did Souther, 1971). The Inklin Formation can be divided into two major units: predominantly massive volcanic wacke which is thick-bedded and blocky; and argillaceous strata ± wacke, which is medium to thin-bedded and weathers into strongly ribbed outcrops. Distinctive, eclogite-clast-bearing beds that occur in the massive wacke unit along strike to the northwest (English et al., 2005; Canil et al., 2006; MacKenzie et al., 2005) are apparently lacking in the Sinwa Creek area.

Less abundant units include, argillite-siltstone couplets, and coarse conglomerates, and these can locally be the principal rock type over tens of metres of section. Limestone is uncommon, occurring as thin interbeds in argillaceous strata, and rarely, as massive beds tens of metres thick, as at Mount Luwa (Fig. 3). Along strike to the northwest, Inklin Formation units have been thoroughly described by previous workers (Dickie et al., 1992; Mihalynuk et al., 1999; Hart, 1997; Johannson et al., 1997) and only the main units are summarized briefly below.

#### 4.3.1. Massive to well-bedded wacke

Feldspathic wacke forms massive beds decimetres to metres thick, with rare beds 10 or more metres thick. Beds tend to be planar, but can also be lensoid. Scoured bases are locally well developed, and lower parts of the beds may contain abundant wacke intraclasts. Individual beds display graded bedding and rare ripple or trough cross stratification near their tops. Granules and pebbles of finely-porphyritic volcanic and intrusive derivation commonly form diffuse layers, typically less than a few pebbles thick, within otherwise massive wacke beds. Detrital quartz can locally comprise 10% of beds, typically together with orthoclase and detrital biotite, indicating a granitoid source terrain. Propylitic alteration of some igneous clasts indicate derivation from an altered source.

Interbeds of coarse feldspathic sandstone, siltstone, and shale can range from centimetres to many metres thick (Fig. 13). Wacke is also interbedded with, and less commonly grades into, cobble conglomerate across bedding widths of decimeters to metres. Argillaceous wacke-supported conglomerate beds

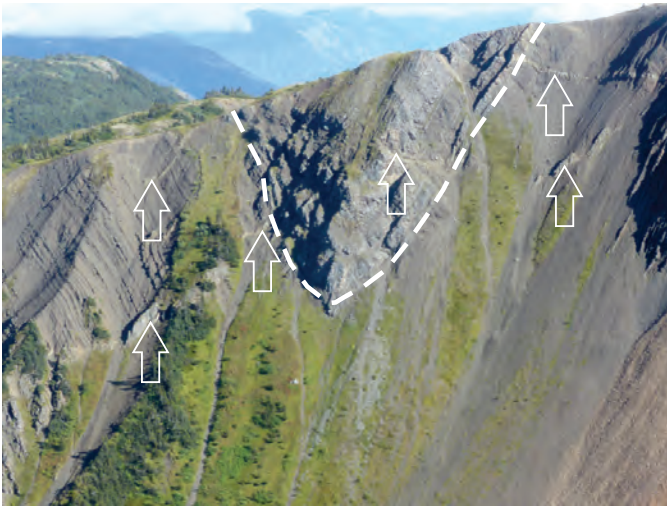


**Fig. 13.** Thick-bedded wacke in core of syncline (white dashed line) enveloped by dark brown, argillaceous siltstone. Cutting the section are two light-weathering sets of dikes (white arrows, probably Eocene).

commonly contain well-rounded limestone, granite and rare chert clasts, suggesting recycling of the Triassic sedimentary rocks.

#### 4.3.2. Argillite – siltstone

Well-bedded siltstone sections commonly display beautiful cross stratification, both trough cross stratification and climbing ripples (Fig. 14). Beds are generally 0.5-5 cm thick and tend to be laminated. They weather orange and black and are typically strongly calcareous. In some sections, abundant 2-3 mm wide wormy trace fossils cover bedding surfaces. Sparse paleoflow directions, as determined from trough axes, tend to be from the northwest or west.

Sections of tan and black rhythmites (Fig. 15) have been mapped northwest, west and south of Atlin (Mihalynuk et al., 1999; Johansson et al., 1997; English et al., 2003, 2005; Wight



**Fig. 14.** Trough cross stratification in calcareous siltstone of the Laberge Group indicating paleoflow to the east or southeast.



**Fig. 15.** Black and tan rhythmite in the Whitehorse trough. This is a characteristic lithology of the Richthofen formation in the Yukon, which has been mapped southward into BC to ~59.5°N (Johnston et al., 1999).

et al., 2004) and are known in Yukon as one of the diagnostic rock types in the Richthofen formation (Tempelman-Kluit, 1984; Lowey, 2003, 2004). Siltstone-argillite couplets form graded layers 1-5 cm thick; some layers have bases of fine- to medium-grained sandstone. Vermicular trace fossils are locally well preserved in the argillite. Cleavage is commonly well-developed in this lithology, leaving only fragmentary bedding surfaces preserved. These rhythmites were interpreted by Lowey (2004) as distal turbidites deposited in a submarine fan complex, representing outer-fan levee and interchannel/interlobe sedimentation.

#### 5. Sloko (?) dikes

Porphyritic dark greenish-grey, orange to green-weathering, subvertical dikes (2.5-6 m thick) are interpreted to be subvolcanic equivalents of the regionally extensive Sloko Group. The dikes are most obvious where they cut the Sinwa Formation (Fig. 3) where they have sharp, chilled contacts. They are medium grained (lesser coarse grained) and contain tabular and glomeroporphyritic feldspar (30-40%) and ~2-5% equant chlorite clots, probably derived from fine-medium grained pyroxene. Dike interiors commonly weather recessively (Fig. 16a). Silicification of limestone adjacent to the dikes can be intense, and some silicified zones contain bladed calcite characteristic of epithermal alteration (Fig. 16b). Preliminary geochemical analyses do not indicate precious or base metal enrichment. Further analyses are pending.

Dike orientations are predominantly north-northeast, and they probably fed a volcanic carapace that has been eroded away, except for a ~15 km<sup>2</sup> relict underlying the flanks of Mount McGavin. Sloko Group volcanic rocks are more extensive in map areas to the west and south where they have been described in detail (see Mihalynuk et al., 1994; Mihalynuk et al., 1995).

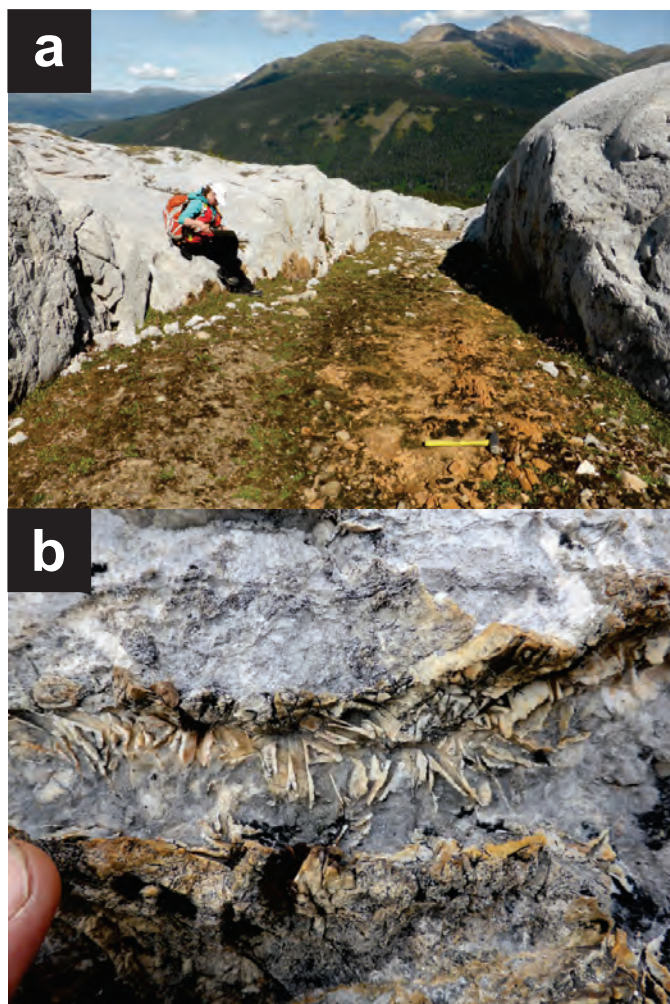


**Fig. 16. a)** North-trending, sub-vertical, orange-weathering, recessive, mafic dike (presumably Early Eocene) cuts Sinwa Formation (Fig. 3). It is part of a regional swarm interpreted to have fed Sloko volcanic strata, such as the those capping Mt. McGavin on the horizon. **b)** Joints in adjacent wallrocks above where the dykes solidified display evidence of hydrothermal activity. Bladed calcite in a matrix of finer-grained calcite may indicate boiling, which can cause gold and other metals to precipitate. Samples collected from this bladed calcite carried neither elevated Au nor other metal values.

## 6. Geochronology

Between the Taku River area and Yukon, strata in the hangingwall of the King Salmon fault (Hart et al., 1995; Johansson et al., 1997; Mihalynuk et al., 1999; Colpron et al., 2015) are well-dated. In contrast, age control in the footwall are relatively sparse (Souther, 1971; Mihalynuk et al., 1995). To address this imbalance, we collected samples with fossil invertebrates and material for microfossil determination (identifications are pending). We also collected two samples for U-Pb geochronology, one from tuffaceous strata north of Chuunk Mountain (Fig. 3; see Section 4.1.1.), and one from a coarse, quartz-rich sandstone unconformably below the limestone block conglomerate unit (see Section 4.1.6.) near the headwaters of Takwahoni Creek. The Chuunk volcanic tuff

sample was dated by Chemical Abrasion Thermal Ionization Mass Spectroscopy (CA-TIMS, Fig. 17) and detrital zircons from the sandstones were analyzed by the Sensitive High Resolution Ion Microprobe (SHRIMP, Fig. 18).

## 6.1. Methods

### 6.1.1. CA-TIMS

CA-TIMS procedures described here are modified from Mundil et al., (2004), Mattinson (2005) and Scoates and Friedman (2008). After rock samples have undergone standard mineral separation procedures zircons were handpicked in alcohol. The clearest, crack- and inclusion-free grains were selected, photographed and then annealed in quartz glass crucibles at 900°C for 60 hours. Annealed grains were transferred into 3.5 mL PFA screwtop beakers, ultrapure HF (up to 50% strength, 500 mL) and HNO<sub>3</sub> (up to 14 N, 50 mL) were added and caps were closed finger tight. The beakers were placed in 125 mL PTFE liners (up to four per liner) and about 2 mL HF and 0.2 mL HNO<sub>3</sub> of the same strength as acid within beakers containing samples were added to the liners. The liners were then slid into stainless steel Parr™ high pressure dissolution devices, which were sealed and brought up to a maximum of 200°C for 8-16 hours (typically 175°C for 12 hours). Beakers were removed from liners and zircon was separated from leachate. Zircons were rinsed with >18 MΩ.cm water and subboiled acetone. Then 2 mL of subboiled 6N HCl was added and beakers set on a hotplate at 80°-130°C for 30 minutes and again rinsed with water and acetone. Masses were estimated from the dimensions (volumes) of grains. Single grains were transferred into clean 300 mL PFA microcapsules (crucibles), and 50 mL 50% HF and 5 mL 14 N HNO<sub>3</sub> were added. Each was spiked with a <sup>233-235</sup>U-<sup>205</sup>Pb tracer solution (EARTHTIME ET535), capped and again placed in a Parr liner (8-15 microcapsules per liner). HF and nitric acids in a 10:1 ratio, respectively, were added to the liner, which was then placed in Parr high-pressure device, and dissolution was achieved at 240°C for 40 hours. The resulting solutions were dried on a hotplate at 130°C, 50 mL 6N HCl was added to microcapsules and fluorides were dissolved in high-pressure Parr devices for 12 hours at 210°C. HCl solutions were transferred into clean 7 mL PFA beakers and dried with 2 mL of 0.5 N H<sub>3</sub>PO<sub>4</sub>. Samples were loaded onto degassed, zone-refined Re filaments in 2 mL of silicic acid emitter (Gerstenberger and Haase, 1997).

Isotopic ratios were measured a modified single collector VG-54R or 354S (with Sector 54 electronics) thermal ionization mass spectrometer equipped with analogue Daly photomultipliers. Analytical blanks were 0.2 pg for U and up to 1 pg for Pb. U fractionation was determined directly on individual runs using the EARTHTIME ET535 mixed <sup>233-235</sup>U-<sup>205</sup>Pb isotopic tracer and Pb isotopic ratios were corrected for fractionation of 0.25%/amu, based on replicate analyses of NBS-982 reference material and the values recommended by Thirlwall (2000). Data reduction employed the Excel-based program of Schmitz and Schoene (2007). Standard concordia diagrams (Fig. 17a) were constructed and regression intercepts, weighted averages

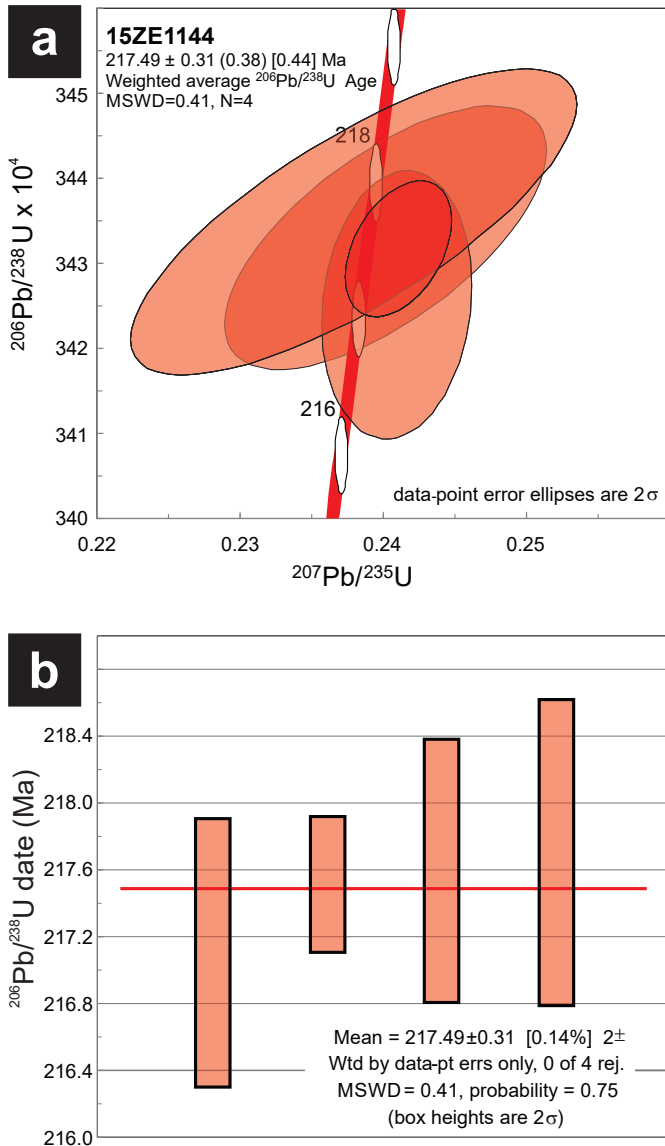


**Fig. 17.** CA-TIMS geochronology results for sample 15ZE1144, lapilli tuff from Chuunk Mountain. **a)** Concordia plot showing concordant analyses from four grains at 217.49 ± 0.31 Ma (weighted average  $^{206}\text{Pb}/^{238}\text{U}$  age). **b)** Statistical treatment of the four analyses.

calculated with Isoplot (Ludwig, 2003). Unless otherwise noted all errors are quoted at the  $2\sigma$  or 95% level of confidence (Table 1). Isotopic ages were calculated with the decay constants  $\lambda_{238}=1.55125\text{E}-10$  and  $\lambda_{235}=9.8485\text{E}-10$  (Jaffey et al., 1971). EARTHTIME U-Pb synthetic solutions were analyzed on an on-going basis to monitor the accuracy of results.

### 6.1.2. SHRIMP

Zircon separates for sandstone sample MMI15-15-14 were prepared by standard crushing, disk mill, Wilfley™ table, and heavy liquid techniques. Mineral separates were sorted by magnetic susceptibility using a Frantz™ isodynamic separator. Zircons were analyzed on a mount using the SHRIMP at

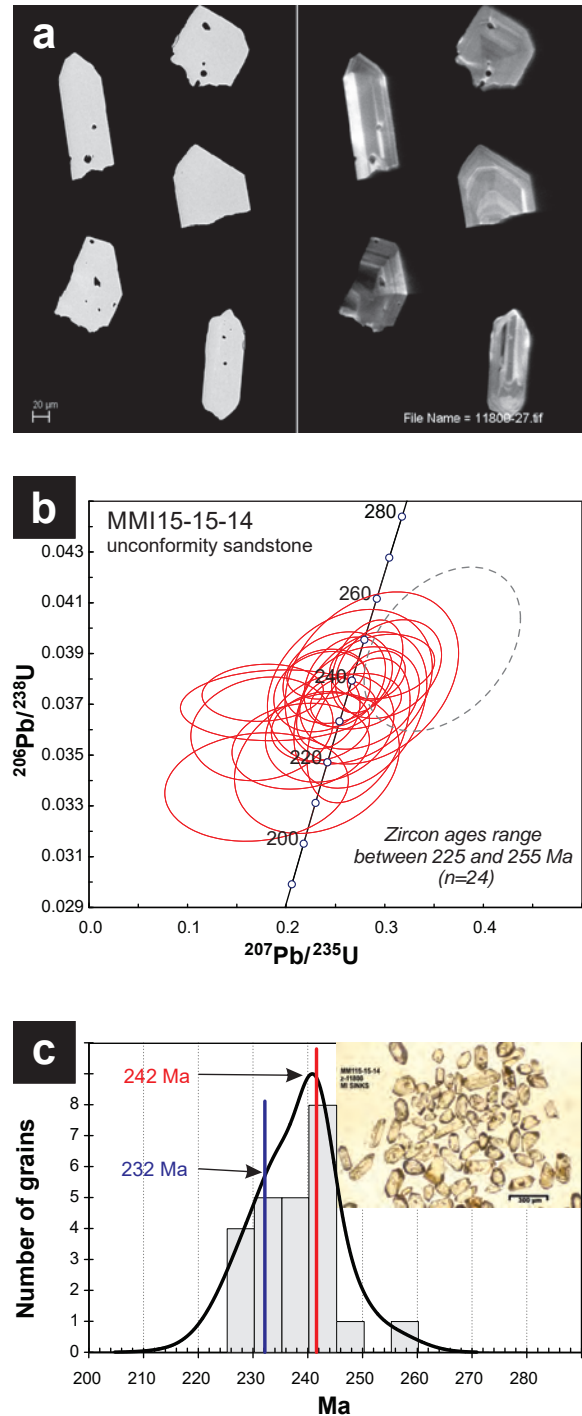


**Fig. 18.** SHRIMP geochronology results for sample MMI15-15-14, quartz-rich sandstone unconformably below the limestone block conglomerate unit near the headwaters of Takwahoni Creek. **a)** Back-scattered electron mode (left) and cathodoluminescence mode (right) images of a subset of grains analyzed (Scale bar is 20µm). **b)** Concordia plot of the entire set of grains analyzed. The grey dotted ellipse is discordant and not included in age calculations. **c)** age distribution plot: histogram and two age populations resolved using Unmix function in Isoplot 3.00 (Ludwig, 2003). Populations of 232 Ma (blue line) and 242 Ma (red line) are suggested using this function. The youngest grain was 225 ± 4 Ma. Inset photomicrograph in transmitted, plane polarized light shows the character of zircons analyzed.

**Table 1.** TIMS analytical results for U-Th-Pb abundance and isotopic composition of zircons from sample 15ZE1144.

Sample	Compositional Parameters									Radiogenic Isotope Ratios					Isotopic Ages								
	Wt. mg (a)	U ppm (b)	Pb ppm (c)	Th U (d)	<sup>206</sup> Pb* x10 <sup>-13</sup> mol (e)	mol % (e)	Pb* (e)	Pb <sub>c</sub> (pg) (e)	<sup>206</sup> Pb (f)	<sup>208</sup> Pb / <sup>206</sup> Pb (g)	<sup>207</sup> Pb / <sup>206</sup> Pb (g)	% err (h)	<sup>207</sup> Pb / <sup>235</sup> U (g)	% err (h)	<sup>206</sup> Pb / <sup>238</sup> U (g)	% err (h)	corr. coef. (h)	<sup>207</sup> Pb / <sup>206</sup> Pb (i)	± (h)	<sup>235</sup> U / <sup>238</sup> U (i)	± (h)	<sup>206</sup> Pb / <sup>238</sup> U (i)	± (h)
<b>15ZE1144</b>																							
B	0.0015	306	10.6	0.272	0.6632	99.01%	29	0.54	1878	0.087	0.051017	1.761	0.240934	1.774	0.034252	0.378	0.140	242	41	219.2	3.5	217.10	0.81
C	0.0017	87	3.7	0.726	0.2072	95.72%	7	0.76	432	0.229	0.050236	5.028	0.237914	5.351	0.034349	0.429	0.769	206	117	216.7	10.4	217.71	0.92
D	0.0010	330	11.5	0.245	0.4828	98.67%	21	0.54	1389	0.079	0.050943	1.187	0.241048	1.254	0.034318	0.192	0.418	238	27	219.3	2.5	217.51	0.41
E	0.0017	73	2.8	0.362	0.1794	96.70%	9	0.50	561	0.116	0.050731	3.587	0.240135	3.821	0.034331	0.369	0.663	229	83	218.5	7.5	217.59	0.79

the Geological Survey of Canada in Ottawa. Analytical procedures and calibration details for the SHRIMP followed those described by Stern (1997) and Stern and Amelin (2003). Briefly, zircons were cast in a 2.5 cm diameter epoxy mount along with the Temora2 zircon primary standard, the accepted <sup>206</sup>Pb/<sup>238</sup>U age of which is 416.8 ± 0.33 Ma (Black et al., 2004). Fragments of the GSC laboratory zircon standard (z6266, with <sup>206</sup>Pb/<sup>238</sup>U age=559 Ma) were also included on the mount as a secondary standard, analyses of which were interspersed among the sample analyses throughout the data session to verify the accuracy of the U-Pb calibration. The mid-sections of the zircons were exposed using 9, 6, and 1 μm diamond compound, and the internal features of the zircons (such as zoning, structures, and alteration) were characterized in both back-scattered electron mode (BSE) and cathodoluminescence mode (CL) using a Zeiss Evo 50 scanning electron microscope (Fig. 18a). The mount surface was evaporatively coated with 10 nm of high purity Au. Analyses were conducted during two separate data sessions, using an <sup>16</sup>O- primary beam, projected onto the zircons at 10 kV. Before analysis, the ion beam was rastered over the area of interest for 2 minutes to locally remove the Au coating and eliminate effects of surface common lead. The sputtered area used for analysis was ca. 16 μm in diameter with a beam current of ~7.5 nA. The count rates at ten masses including background were sequentially measured over 6 scans, with a single electron multiplier and a pulse counting system with a deadtime of 20 ns. The 1σ external errors of <sup>206</sup>Pb/<sup>238</sup>U ratios reported in the data table incorporate a ±0.80% error in calibrating the standard Temora2 zircon. Age errors reported in the text are at the 2σ uncertainty level, and encompass the combined statistical uncertainty of the weighted mean age for the population and the 2σ error of the mean of the Temora2 zircon calibration standard. Additional details of the analytical conditions and instrument settings are presented in the footnotes of Table 2. Off-line data processing was accomplished using customized in-house software. Isoplot v. 3.00 (Ludwig, 2003) was used to generate concordia plots and to calculate weighted means. Errors for isotopic ratios in Table 2 are given at 1σ uncertainty, as are the apparent SHRIMP ages. No fractionation correction was applied to the Pb-isotope data; common Pb correction used the Pb composition of the surface blank (Stern, 1997). All ages are reported as the <sup>207</sup>Pb-corrected weighted mean <sup>206</sup>Pb/<sup>238</sup>U age. The error ellipses on the concordia diagram (Fig. 18b) and the weighted mean errors are reported at 2σ.

## 6.2. Geochronological results

### 6.2.1. 15ZE1144: Chuunk Mountain volcanic tuff

Four zircons from the Chuunk Mountain tuffaceous rock were analyzed (Table 1). Analyses form a single overlapping population falling on concordia (Fig. 17a) with a weighted <sup>206</sup>Pb/<sup>238</sup>U age of 217.49 +0.38/-0.44 Ma (Fig. 17b). This age is considered the best age for the sample.

### 6.2.2. MMI15-15-14 (Z11800): Quartz-rich sandstone unconformably below limestone block conglomerate unit

Zircons from this sample are large (100-300μm), zoned, and euhedral stubby to semi-elongate prisms (Fig. 18a). Twenty-four grains were analyzed (Fig. 18b). Although most grains have well-preserved facets, ~35% of the grains have subrounded and/or irregular grain boundaries. In transmitted light, the grains are clear and colourless (Fig. 18c, inset), with abundant colourless and brown bubble- and rod-shaped inclusions. In SEM-CL images (Fig. 18a, right), most grains exhibit igneous oscillatory zoning. Approximately 10% of the grains show broad sector zoning. U-Th compositions and U-Th-Pb isotopic ratios of the grains analyzed are shown in Table 2. The grains are generally low in U (39-193 ppm) and low to moderate in Th/U (0.18-0.50). The zircon ages are distributed between 225 and 255 Ma (Figs. 18b, c), with an asymmetric peak at 241 Ma when data are plotted on a conventional probability distribution diagram (not shown). Using the Unmix routine of Isoplot (Ludwig, 2003), the composite peak consists of two possible age populations: 232 Ma and 242 Ma (Fig. 18c). The youngest grain was 225 Ma (grain 100). Two analyses initially yielded younger apparent ages of 217 ± 5 Ma (spot 11800-33.1, Table 2) and 220 ± 7 Ma (spot 11800-11.1, Table 2). However, replicate analyses on grains 33 and 11 yielded ages of 232 and 238 Ma, respectively, which are indistinguishable from the main populations.

## 7. Deformation

### 7.1. King Salmon fault and Whitehorse trough fold and thrust belt

In the Tulsequah area, King Salmon fault is delineated by the main body of Sinwa Formation limestone in its immediate hangingwall as recognized by Souther (1971) who called it the “King Salmon Thrust” (and “King Salmon thrust fault”). Closer to Dease Lake (Fig. 2), Monger and Thorstad (1978) referred to it as the “King Salmon Fault”; and this more generic name is preferred because of evidence for a significant strike-slip

**Table 2.** SHRIMP U-Pb zircon results for sample MMI15-15-14.

Spot name	U (ppm)	Th (ppm)	Th/U	<sup>206</sup> Pb* (ppm)	<sup>208</sup> Pb/ <sup>206</sup> Pb	<sup>238</sup> U/ <sup>206</sup> Pb ±	<sup>207</sup> Pb/ <sup>206</sup> Pb ±	<sup>207</sup> Pb/ <sup>235</sup> U ±	<sup>206</sup> Pb/ <sup>238</sup> U ±	Corr Coeff ±	<sup>207</sup> Pb/ <sup>206</sup> Pb ±	Apparent Ages (Ma)									
												<sup>204</sup> corrected <sup>206</sup> Pb/ <sup>238</sup> U	<sup>207</sup> corrected <sup>206</sup> Pb/ <sup>238</sup> U								
<i>Sample Number: MMI15-15-14 - Takwahoni Formation sandstone (NAD83 Zone 8: 592039 E 6525006 N)</i>																					
11800-033.1 <sup>a</sup>	48	8	0.18	1.48	0.0587	0.0250	29.234	0.719	0.0490	0.0033	0.1688	0.03823	0.0337	0.0009	0.1	0.0363	0.0082	214	5	217	5
11800-011.1 <sup>a</sup>	62	14	0.24	0.72	0.0548	0.0173	28.653	0.930	0.0542	0.0055	0.2299	0.03438	0.0346	0.0011	0.2	0.0481	0.0070	220	7	220	7
11800-100.1	92	27	0.31	1.34	0.0852	0.0194	27.938	0.523	0.0553	0.0026	0.2135	0.02865	0.0353	0.0007	0.1	0.0439	0.0058	224	4	225	4
11800-032.1	67	22	0.34	-0.33	0.1019	0.0156	27.920	0.906	0.0522	0.0028	0.2726	0.02142	0.0359	0.0012	0.4	0.0590	0.0039	228	7	226	7
11800-009.1	61	23	0.38	0.71	0.1152	0.0202	27.554	0.654	0.0549	0.0031	0.2433	0.02679	0.0360	0.0009	0.2	0.0490	0.0053	228	5	229	5
11800-031.1	102	28	0.28	0.67	0.0755	0.0139	27.508	0.415	0.0525	0.0023	0.2335	0.02040	0.0361	0.0006	0.2	0.0469	0.0040	229	3	230	3
11800-033.2	57	11	0.21	-0.47	0.0839	0.0171	27.342	0.934	0.0502	0.0033	0.2743	0.02766	0.0367	0.0013	0.3	0.0541	0.0051	233	8	232	8
11800-018.1	73	23	0.33	1.38	0.0834	0.0195	27.391	0.616	0.0469	0.0024	0.1741	0.02967	0.0360	0.0008	0.1	0.0351	0.0059	228	5	232	5
11800-099.1	187	71	0.39	0.45	0.1011	0.0100	27.182	0.425	0.0517	0.0016	0.2418	0.01325	0.0366	0.0006	0.3	0.0479	0.0025	232	4	233	4
11800-017.1	96	33	0.35	0.45	0.1109	0.0146	26.833	0.315	0.0565	0.0024	0.2697	0.01888	0.0371	0.0005	0.2	0.0527	0.0036	235	3	234	3
11800-106.1	122	43	0.36	0.73	0.0955	0.0138	26.664	0.586	0.0595	0.0025	0.2735	0.02492	0.0372	0.0008	0.2	0.0533	0.0047	236	5	235	5
11800-011.2	68	25	0.38	1.45	0.0822	0.0225	26.677	0.365	0.0499	0.0048	0.1905	0.04073	0.0369	0.0006	0.1	0.0374	0.0080	234	4	238	3
11800-027.1	78	22	0.30	0.65	0.0851	0.0173	26.372	0.866	0.0562	0.0050	0.2635	0.03437	0.0377	0.0012	0.3	0.0507	0.0064	238	8	238	8
11800-001.1	106	21	0.21	0.75	0.0762	0.0138	26.484	0.450	0.0519	0.0021	0.2354	0.02014	0.0375	0.0007	0.2	0.0455	0.0038	237	4	239	4
11800-019.1	39	7	0.18	0.60	0.0514	0.0196	26.148	0.945	0.0596	0.0042	0.2861	0.03615	0.0380	0.0014	0.3	0.0546	0.0066	241	9	240	9
11800-005.1	174	64	0.38	-0.24	0.1310	0.0103	26.297	0.273	0.0533	0.0017	0.2907	0.01199	0.0381	0.0004	0.3	0.0553	0.0022	241	2	240	3
11800-101.1	90	23	0.27	0.24	0.0913	0.0129	26.339	0.500	0.0516	0.0024	0.2588	0.01697	0.0379	0.0007	0.3	0.0496	0.0031	240	5	240	5
11800-008.1	72	26	0.38	0.31	0.1183	0.0178	25.979	0.537	0.0599	0.0030	0.3031	0.02202	0.0384	0.0008	0.3	0.0573	0.0040	243	5	241	5
11800-071.1	150	50	0.34	1.04	0.0696	0.0134	26.015	0.494	0.0567	0.0022	0.2512	0.02281	0.0380	0.0007	0.2	0.0479	0.0042	241	5	242	5
11800-007.1	141	67	0.50	1.78	0.1062	0.0160	26.234	0.295	0.0492	0.0018	0.1747	0.02527	0.0374	0.0005	0.1	0.0338	0.0049	237	3	242	3
11800-035.1	53	12	0.24	-0.34	0.1011	0.0156	26.084	0.343	0.0531	0.0029	0.2968	0.02185	0.0385	0.0005	0.2	0.0560	0.0040	243	3	242	3
11800-037.1	135	49	0.38	0.29	0.1212	0.0116	25.915	0.502	0.0555	0.0019	0.2814	0.01482	0.0385	0.0008	0.4	0.0530	0.0026	243	5	243	5
11800-015.1	193	62	0.33	0.84	0.0992	0.0112	25.976	0.263	0.0526	0.0016	0.2391	0.01608	0.0382	0.0004	0.2	0.0454	0.0030	241	3	243	2
11800-012.1 <sup>b</sup>	52	18	0.36	-0.77	0.1378	0.0217	25.732	0.862	0.0599	0.0034	0.3580	0.03254	0.0392	0.0013	0.4	0.0663	0.0056	248	8	243	8
11800-013.1	71	23	0.33	-0.59	0.1133	0.0163	25.851	0.627	0.0516	0.0050	0.3031	0.03337	0.0389	0.0010	0.2	0.0565	0.0061	246	6	245	6
11800-016.1	127	41	0.34	0	0.1108	0.0105	25.587	0.400	0.0507	0.0019	0.2732	0.01120	0.0391	0.0006	0.4	0.0507	0.0019	247	4	247	4
11800-103.1	77	32	0.44	-1.01	0.1667	0.0180	24.765	0.501	0.0511	0.0025	0.3344	0.02806	0.0408	0.0009	0.2	0.0595	0.0048	258	5	255	5

Notes (see Stern, 1997):

Mount IP824, K100b spot size (13x16µm), 2 minute raster, 6 mass scans

Primary beam intensity ~7.5nA, Weighted mean <sup>207</sup>Pb-corrected <sup>206</sup>Pb/<sup>238</sup>U age of the analyses of secondary standard z6266 zircon was determined to be 558 ± 8 Ma, MSWD=1.4, n=25 (2 rejections) (accepted <sup>206</sup>Pb/<sup>238</sup>U age is 559 Ma)

Spot name follows the convention x-y-z; where x = lab number, y = grain number and z = spot number

Uncertainties reported at 1s and are calculated by using SQUID 2.50.11.10.15, rev. 15 Oct 2011

<sup>204</sup>Pb and f(<sup>206</sup>)<sup>204</sup> are not reported here due to space limitations. For complete data set please contact the corresponding author.

\* refers to radiogenic Pb (corrected for common Pb)

Calibration standard Temora2; Age = 416.8 ± 0.33 Ma (Black et al., 2004)

Error in <sup>206</sup>Pb/<sup>238</sup>U calibration 0.80% (included)

Standard Error in Standard calibration was 0.72% (not included in above errors but required when comparing data from different mounts).

Apparent ages shown in bold font are those which were included in weighted mean age calculations

*bdl*: below detection limit

**a.** indicates an analysis that was younger than other grains in the sample, but a second replicate analysis yielded a result that was indistinguishable from the older population  
**b.** analysis was discordant and thus not included in any age interpretation

component. Although many regional scale maps portray the King Salmon fault as single southwest-verging strand, Souther (1971) identified an additional thrust strand southwest of what he mapped as the main fault trace. This strand extends from the headwaters of King Salmon Creek, where it carries Stunini Group sedimentary rocks, to near its confluence with the Taku River, northwest of which it rapidly dies out into the contact between “Sinwa Formation” and underlying Triassic strata.

In agreement with Souther (1971), our mapping in the Sinwa Creek area delineated more than one thrust fault carrying Sinwa Formation strata southwest over undated, but presumably younger rocks. However numerous thrust faults appear to cut and thicken the Sinwa Formation internally and repeat less distinctive strata in both the hangingwall and footwall of the King Salmon fault (Figs. 3, 19). Hence the King Salmon fault is just one of many faults comprising a regionally extensive fold and thrust belt mapped in the area (English et al., 2005) and to the northwest (Mihalynuk et al., 1999), which we herein call the ‘Whitehorse trough fold and thrust belt’. Earlier works also documented thrust faults in the Laberge Group (e.g., Souther, 1971; and in Yukon, Wheeler, 1961), but the thrust shortening implied by this work is not as great as that suggested by more recent work in Yukon (e.g., Colpron, 2011) and northernmost BC (Mihalynuk et al., 1999). In the Sinwa Creek area, most of the regional and mountain scale fold hinges parallel the King Salmon fault and other faults in the Whitehorse trough fold and thrust belt, but a sparsely developed fold set displays steeply plunging hinges (Fig. 20).

Early Middle Jurassic deformation in the Whitehorse trough was protracted, (Mihalynuk et al., 2004), starting from the Cache Creek in the northeast and migrating southwest toward Stikine terrane. This deformation has been attributed to oblique (dextral, south-southwest) overthrusting of Cache Creek above Stikine terrane as extrapolated from the Dease Lake area (Fig. 21b; Mihalynuk et al., 1999). However, Whitehorse trough fold and thrust belt fold orientations in the Sinwa Creek area indicate more west-directed shortening direction (Fig. 21a), and a less obvious geometric and kinematic link to dextral offset on the Llewellyn fault zone. In addition, steeply plunging folds with hinges nearly orthogonal to the fold belt (Figs. 20, 21a) are unlikely to have been formed by dextral oblique underthrusting.

## 7.2. Steep fold hinges

Outcrop- to mountain-scale folds of the Sinwa Formation in the hangingwall of the main strands of the King Salmon fault (Fig. 19) locally display hinges that plunge steeply northeast and axial surfaces that dip southeast (Figs. 20, 21a). Within these folds, fossils as strain markers show one of three characteristics: no deformation, flattening parallel to the fold axial surfaces (uncommon), or bedding-parallel flattening within hinge zones of concentric folds (Fig. 20b). Conglomerate clasts show the same strain characteristics. West of Sinwa Mountain peak, the core of one such steep fold is exposed in outcrops of intrusive boulder conglomerate scattered over an area of about 10 m<sup>2</sup> (Fig. 19c). Strain gradients are high. Within a few metres,

undeformed, subround cobbles pass into strongly flattening clasts displaying width-to-thickness ratios of >8. This clast flattening is concentrated in the steeply plunging concentric fold hinge (e.g., 354°/62°-90°). Similar folds are observed in the footwall strata, including sandstone (Fig. 20 a) and intrusive cobble conglomerate. The relationship of the steep folds to the main phase of shortening in the Whitehorse trough fold and thrust belt is unknown. Although some steep fold limbs appear to be truncated by thrust faults (Fig. 21a), sense of motion on these faults has not been determined unequivocally. Regardless of relative timing of the thrusts and steep folds, the steep fold hinge plane orientations are consistent with a sinistral, not dextral component of oblique motion in the fault zone. Implied sense of motion is lower plate southward relative to the upper plate, opposite of that expected of south- or southwestward-directed thrusting (Figs. 2, 21).

## 8. Discussion

Our primary aim was to address the nature of the King Salmon fault and its effect on the Late Triassic-Early Jurassic porphyry deposits that track northwards through BC into the Yukon. Our mapping in the Sinwa Creek mapsheet relied heavily on rapid field data collection techniques and remote imagery; it does not conform to BC Geological Survey 1:50,000-scale map data coverage standards. Some fossil identifications and isotopic age determinations are pending and detailed sections and age control that are necessary to conclusively constrain structural duplication are currently lacking. Although much of the area falls within the 805 km<sup>2</sup> Taku River conservancy and adjacent 1673 km<sup>2</sup> Nakina-Inklin River conservancy (Figs. 2, 3) established in 2012, the Sinwa Creek area occupies a pivotal position to understanding the regional geological history and mineral potential in adjacent areas. It is here that the King Salmon fault is best exposed and associated deformation is most apparent, and so it is likely the best place to constrain the degree of overthrusting and tectonic burial of the Late Triassic-Jurassic porphyry belts.

### 8.1. King Salmon fault

Expression of the King Salmon fault in the Sinwa Creek area, where it carries Sinwa Formation in its hangingwall, contrasts with the fault expression in the eastern Dease Lake and Cry Lake areas, where its trace is defined by lenses of serpentinized peridotite and chert in the hangingwall (Fig. 2; Gabrielse, 1998; Monger and Thorstad, 1978). Such contrast in crustal level of the hangingwall begets the question: Are these the same fault? The amount of shortening, the crustal level of the thrust sole, the possibility of different basement to the Whitehorse Trough in these two regions, and the uncertainty in the Stikinia – Cache Creek terrane boundary location are all considerations.

#### 8.1.1. Amount of overthrusting

The Triassic arc narrows from >250 to <10 km between 58.5°N and the BC-Yukon border (60°N) suggesting either: structural excision to the west along the Llewellyn fault, burial

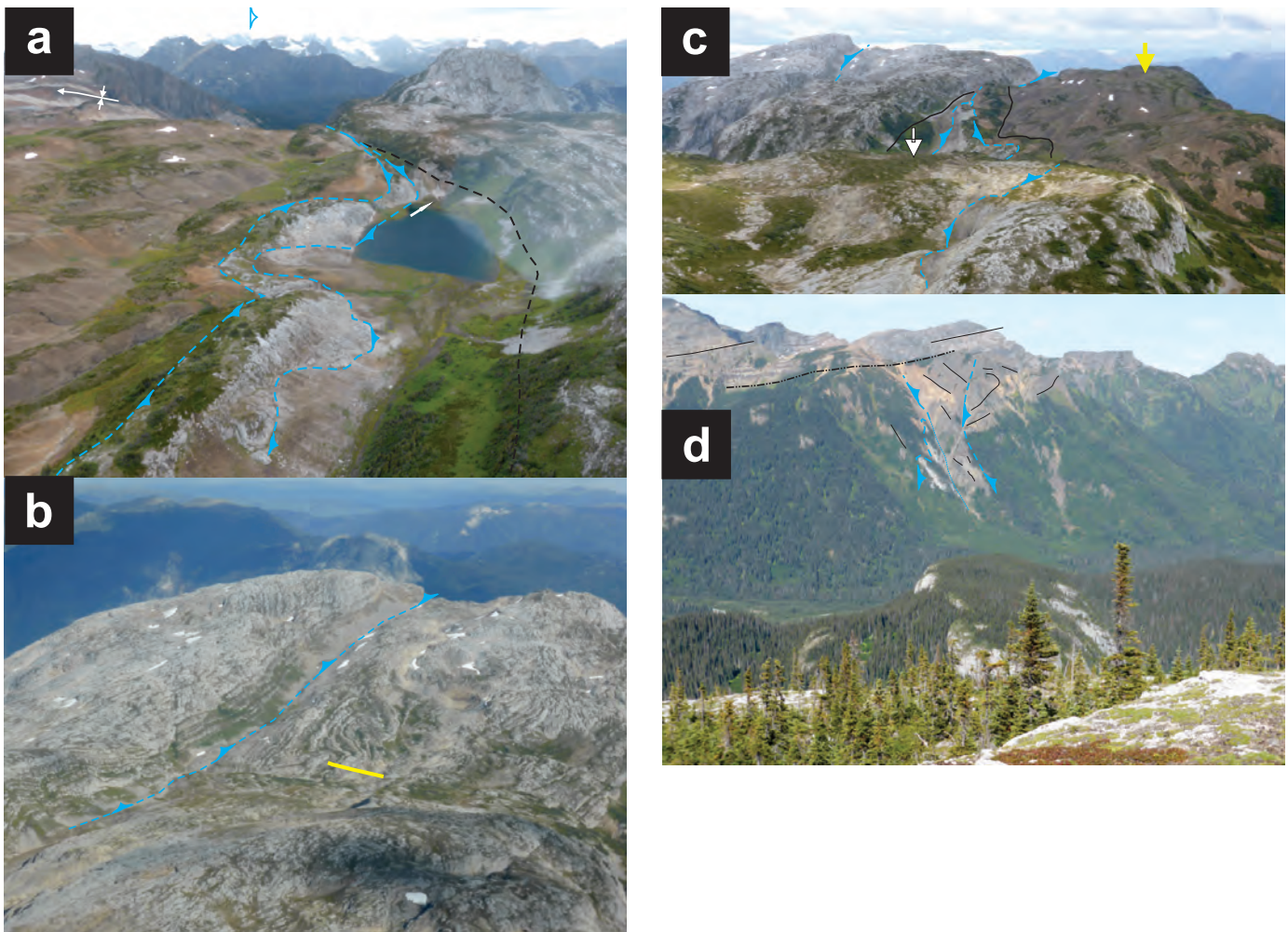


**Fig. 19. a)** View northwest along the leading edge of the main Sinwa Fm. limestone which is interpreted as the hangingwall of the principal strand of the King Salmon Fault. A karst lake sits mainly atop black argillite that forms the valley bottom toward the photographer and drains into a limestone cavern to the northeast (white arrow). A thin limestone layer between the black argillite and an orange-weathering, broken argillite and siltstone unit is interpreted as a separate thrust sheet. **b)** View southeast along the Sinwa Fm. limestone from near Sinwa Mountain. Strata southwest of the valley (occupied by blue thrust symbols) display significant shortening, in sharp contrast to strata to the northeast which dip steeply, but are not significantly folded, indicating that a detachment surface (thrust) occupies the valley. Yellow line shows the approximate location of a section sampled in 2016 for conodont biogeochronology. **c)** View to the southeast along the King Salmon Fault zone. Blue barbed lines outline faults shown in a and b. White arrow points to karst lake of Figure 19a hidden behind near horizon. Black lines are the approximate contacts between recessive black shale and limestone to the left (northeast) and, to the right, between orange weathering argillaceous siltstone and wacke and intrusive conglomerate unit of Figs. 5b, c. Yellow arrow shows the approximate location of a steep fold hinge within the boulder conglomerate where hinges defined by flattened and folded clasts measure  $354^{\circ}/62^{\circ}$  to nearly vertical. **d)** view to the north-northwest of the northern termination of the main belt of Sinwa Fm. limestone. Solid black lines highlight layering. A considerable thickness of light grey Sinwa Fm. in foreground terminates in gully to north, apparently truncated by a thrust that cuts up section through footwall and hangingwall strata (thrusts shown by blue dashes with barbs in hangingwall; dotted blue is interpreted stratigraphic top of the Sinwa Fm.). The hangingwall is interpreted to be cut by another thrust that is overturned as it cuts up section and carries an overturned antiform, probably also cored by a thrust (not shown). Sloko Group volcanic strata unconformably overlie the thrust panels (unconformity approximated by black dash, double dot) and gently dip to the west.

by the Jurassic strata of the Whitehorse trough, or significant overthrusting along the King Salmon fault. The King Salmon fault in the Sinwa Creek area has significant apparent offset because the ~70 m-thick carbonate-cream chert with over- and underlying boulder conglomerate in the footwall of the fault contrasts strongly with the hundreds of metres-thickness of main carbonate and underlying petroliferous silty mudstone at Sinwa Mountain. Intervening fault panels with carbonate

rocks of intermediate thickness and underlying clastic strata with intermediate grain size are lacking. If the cream chert is correlative with the main belt of Sinwa Formation, then transitional faces have been overthrust to juxtapose distinct facies. However, it is possible that the chert unit and main carbonate unit did not originate as widely separated facies, limiting the need for significant bedding-parallel shortening for their juxtaposition. In order to quantify the amount of

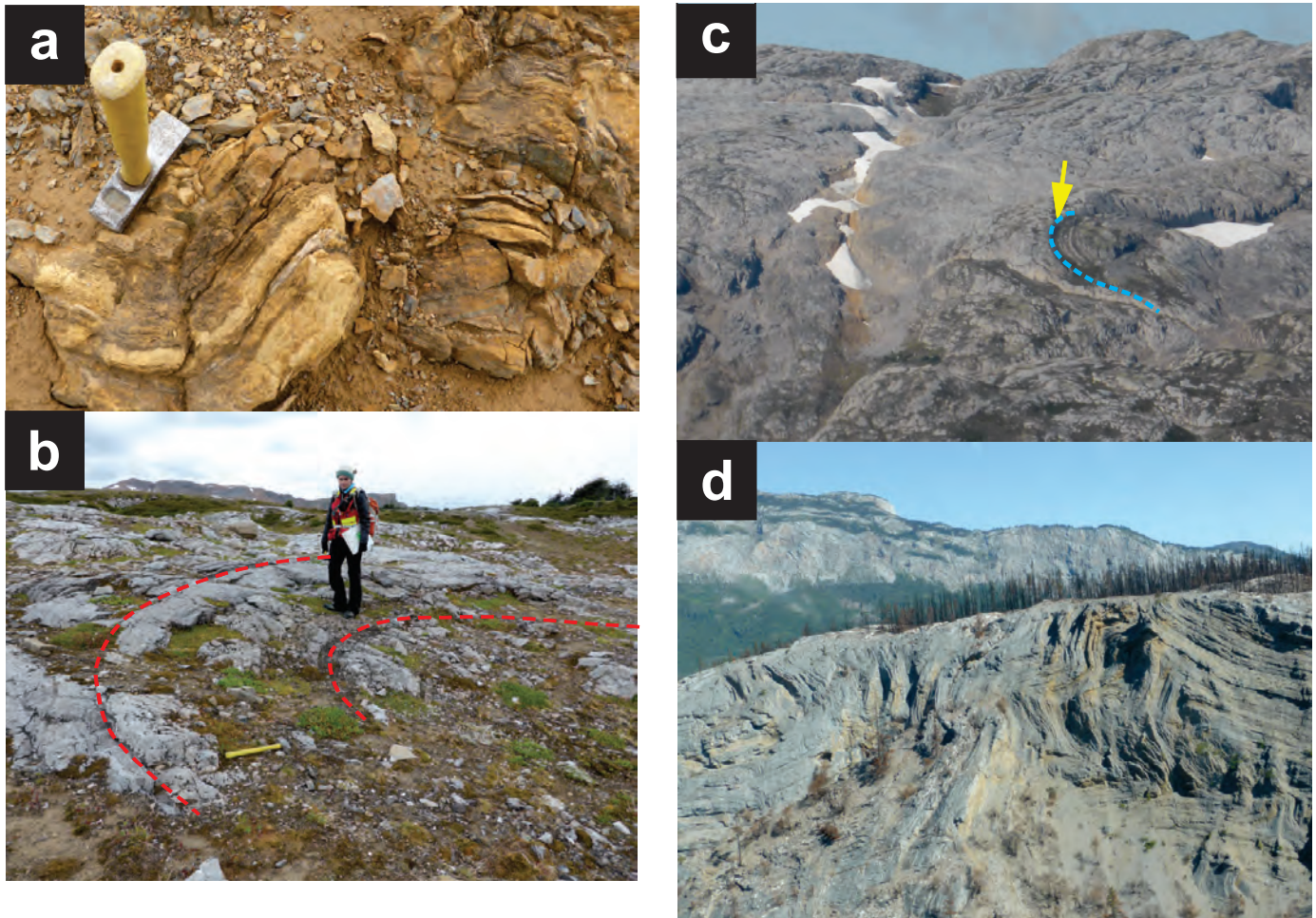


**Fig. 20.** Moderately plunging to vertical fold hinges occur at all scales within and near the Sinwa Formation. **a)** About 2 km within the footwall of the King Salmon fault, steeply plunging folds in calcareous sandstone (fold hinge is approximately parallel to the hammer handle). **b)** View to the south of a nearly vertical fold hinge outlined by beds of fossiliferous Sinwa Formation limestone. This fold appears to be cylindrical, with a hinge trending  $\sim 015^\circ/85^\circ$ . **c)** dark, argillaceous strata are cut along a fault outlined by snow patches, and in the centre of the photo a steeply-plunging fold is well displayed. **d)** Views of Sinwa Formation limestone cliffs from south of the Taku River northward to the south flank of Sinwa Mountain (in distance, north of the Taku River). Fold hinges plunge moderately to the northeast and folds verge northwest, suggest transport oblique to the regional trace of the King Salmon fault.

overthrusting, the stratigraphy of hangingwall and footwall sections and structural cut-offs need to be established. If previous workers who have suggested a forearc setting for the Whitehorse Trough are correct, then estimates for original facies distributions can be guided by modern oceanic forearc environments. For example, the Sunda arc, which forms above the subducting oceanic lithosphere of the Australian plate, and extends for >6000 km. Along its length, forearc basins between the magmatic arc and outer-arc ridge are 50-100 km wide and segmented into sub-basins  $\sim 100$  km long (Van der Werff, 1996). West of central Sumatra, the forearc basin shelf is underlain by two shallow water carbonate successions 700-800 m thick separated by a  $\sim 200$  m coaly volcanic conglomerate and tuffite facies that was deposited during a Miocene lowstand (Beaudry and Moore, 1981). The upper carbonate succession is corallgal detrital limestone deposited from upper Pliocene to present. Relatively clean carbonate is able to accumulate because the

basin has continually subsided, resulting in the trapping of arc-derived clastics near the un-filled basin margin, except for the Middle Miocene. Based on seismic stratigraphy, juxtaposition of Sunda arc coarse clastic facies with carbonate bank deposits might only require  $\sim 10$  km of overthrusting, consistent with the 16 km minimum estimate of King Salmon fault overthrusting based on an interpreted klippe of Sinwa Formation. east of Trapper Lake (Fig. 2; Souther, 1971).

### 8.1.2. Boundary of the Cache Creek terrane?

Souther's mapping and interpretation of the King Salmon fault predated the mobilist framework of plate tectonics (e.g., Vine and Hess, 1970), identification of the exotic nature of the Cache Creek terrane (Coney et al., 1980; Monger, 1975), and quantitative estimates of the huge horizontal displacements along plate margins (e.g., Kreemer et al., 2014; Sigloch and Mihalynuk, 2013). Mobilist notions helped to

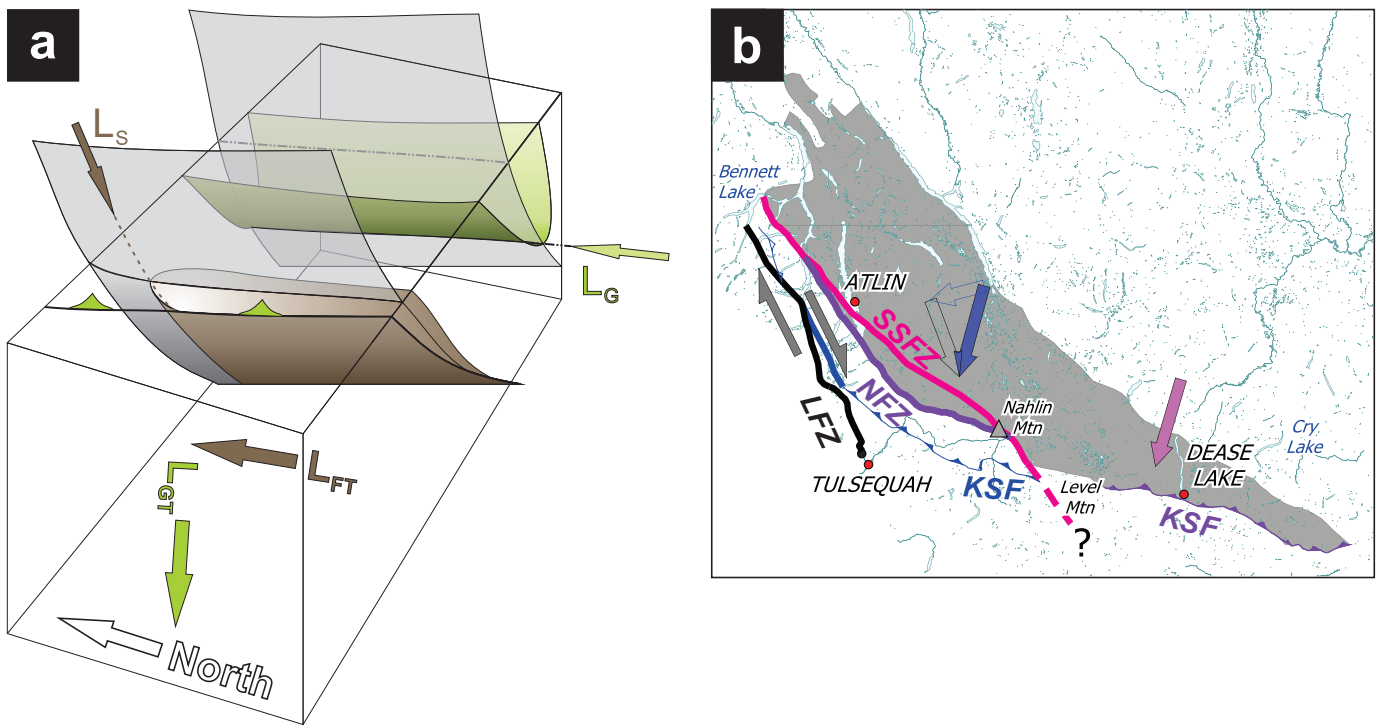


**Fig. 21. a)** Block diagram representation of the sparse steeply plunging fold lineations ( $L_s$ , brown) in comparison with the typical gently plunging fold lineations ( $L_g$ , green) and thrust faults (with green bars) of the Whitehorse trough fold and thrust belt. Interpreted transport directions during formation of the gentle ( $L_{GT}$ ) and steep ( $L_{FT}$ ) folds are shown. In this representation, the thrust is interpreted to cut the  $L_s$  fold at depth, but such a relationship has not yet been observed (e.g., outlasts  $L_{FT}$  deformation). Nevertheless, if the  $L_s$  fold is restored to a pre- $L_g$  orientation it verges northerly (axial surface dips southerly). **b)** Geometry of major faults in northwestern British Columbia modified after Mihalynuk et al. (1999). Convergence vectors were extrapolated from those unambiguously determined in the Dease Lake area (purple vector) and assumed to be consistent across the northern Cache Creek terrane. North over south transport on the southern portion of the Nahlin fault zone (NFZ) was interpreted to change northward to predominantly dextral motion as the fault orientation changes. So too for the King Salmon fault as it converges with the Llewellyn fault zone (LFZ) north of Atlin Lake, where strike slip motion is dominant. Components of convergence that are parallel and normal to the Llewellyn fault zone are shown by the black and blue vector outlines. Although major folds and faults parallel the King Salmon fault, steep folds within the thrust sheets are consistent with a sinistral, not dextral component of motion during, or immediately before thrusting (see Discussion).

formulate the tectonic assemblage and terrane maps of the Canadian Cordillera, which show the King Salmon thrust as the southwestern boundary of the Cache Creek terrane, and as such, a suture zone (Wheeler and McFeely, 1991; Wheeler et al., 1988). However, various lines of evidence argue against the King Salmon fault forming the southwest boundary of the oceanic Cache Creek terrane. Some of the strongest evidence is that correlatives of the Sinwa Formation, which mark the hangingwall of the King Salmon fault, are in stratigraphic contact with Stikine terrane rocks between Atlin Lake and  $60^\circ$  N (Wight et al., 2004; Mihalynuk and Mountjoy, 1990) and farther north, in Yukon (e.g., Wheeler, 1961; Colpron, 2011). In addition, the Takwahoni facies of the Laberge Group occur in both the footwall and hanging wall of the King Salmon fault, suggesting that the fault juxtaposes different facies of the same basin(s) rather than bounding terranes. North of Nahlin Mountain, the absence of any exotic rock types along the King Salmon fault, or its splays, is consistent with it rooting at the base of the Sinwa Formation or in underlying argillaceous strata, rather than in the exotic Cache Creek terrane (with the

possible exception of the quartz-rich sandstone with unmixed age population of  $\sim 242$  Ma detrital zircons; see above). In addition, Cache Creek did not appear to contribute detritus throughout the Early Jurassic evolution of the Whitehorse trough and was either tectonically or stratigraphically buried or geographically isolated during the Early Jurassic.

### 8.1.3. Shared identity at fault

Unlike the Sinwa Creek-Tulsequah area, the King Salmon thrust in the eastern Dease and Cry Lake areas (Fig. 2) is marked by Cache Creek terrane rocks in the hangingwall. The difference between the nature of the thrust in these areas may be explained in two ways.

The first explanation is that the King Salmon fault in these areas represents two fundamentally different faults. Accordingly, in the Dease and Cry Lake areas it is a crustal-scale fault that carries Cache Creek terrane mantle in the hanging wall and roots into the Nahlin fault south of Nahlin Mountain; whereas in the Sinwa Creek-Tulsequah area, it belongs to a thin-skinned thrust belt where it carries Sinwa Formation in its hangingwall

for about 90km, forming an almost unbroken limestone belt centred on King Salmon Lake (Fig. 2).

The second explanation is that the King Salmon and Nahlin faults form two major loci of Middle Jurassic displacement in the same thrust and fold belt, which imbricates a Latest Triassic-Middle Jurassic Stikinia-Cache Creek suture that was overlapped by the Whitehorse trough. Implicit in this explanation is that the Cache Creek terrane formed incrementally, as many accreted microterranes, atop of which the Late Triassic forearc of the Stikine terrane was locally constructed. Both of these explanations involve changes in the composition of the hangingwall across a curious appendage of Cache Creek terrane southeast of Nahlin Mountain (Fig. 2) that extends into the Whitehorse Trough. The idea that the boundary of the Cache Creek terrane changes from the Nahlin fault northwest of Nahlin Mountain, to the KSF to the southeast has been incorporated into the terrane map of Colpron and Nelson (2011), but evaluation of alternate explanations for this change will require mapping the remote areas southeast of Nahlin Mountain and in the Cry Lake areas. Regardless of the nature of the mode of Cache Creek – Whitehorse Trough juxtaposition, reconnaissance investigations as part of GEM indicate significant modification of the contact by transcurrent faulting (Zagorevski, unpublished data).

## 8.2. Regional fault network and kinematics

Northward projection of the King Salmon fault connects it with the crustal-scale Llewellyn fault zone (Figs. 2, 21b; Bultman, 1979; Mihalynuk et al., 1999; see also discussion in Wight et al., 2004). Assumed south(west)ward thrusting of the King Salmon fault is consistent with its overall thrust fault geometry and orientation, paralleled by major folds that can be traced for kilometres. All suggest a kinematic link with late dextral motion on the Llewellyn fault zone (Mihalynuk et al., 1999). Inconsistent with such a link are outcrop to mountain-scale folds within thrust panels that have moderate to steeply northeast-plunging fold hinges and southeast dipping axial surfaces, pointing to a sinistral, not dextral component of motion along the King Salmon fault (Fig. 21a, see above). An alternative explanation for steep fold axes is strongly inhomogeneous transport of previously developed hinge lines in the direction of thrusting, but ductile fabrics supporting such flow are lacking. Polyphase deformation is another possible explanation for the steep hinges, but clear evidence of refolding of early structures has not been observed, and flattening fabrics, which seem largely confined to the steep fold hinges, likely developed during progressive, rather than polyphase, deformation. Observations from these sparsely developed, steeply plunging folds are not sufficiently numerous to warrant statistical treatment and key crosscutting relationships have not been observed. Their significance is still poorly understood, but they appear to indicate a phase of sinistral strain in the Whitehorse trough fold and thrust belt, the relative timing of which is not constrained.

North of Atlin Lake, the King Salmon fault is interpreted to

join the dextral Llewellyn fault (Figs. 2, 21b), which separates the Whitehorse Trough from metamorphosed rocks to the west. West of the junction, metamorphic rocks include the strongly deformed Hale Mountain granodiorite (Mihalynuk and Mountjoy, 1990), a K-feldspar augen gneiss which is part of the Aishihik plutonic suite (Fig. 2; Woodsworth et al., 1992; Johnston et al., 1996). The gneissic fabric is steep, penetrative, pervasively affects the granodiorite and displays sinistral shear sense indicators (Mihalynuk et al., 1999). It is crosscut by an aplitic dike swarm that is offset by, and locally intrudes, pervasive brittle fractures with dextral offsets. U-Pb zircon crystallization ages of the granodiorite and cross-cutting aplite dikes are  $186.5 \pm 1.5$  Ma and  $178.8 \pm 0.9$  Ma (Mihalynuk et al., 1999). About 20 km to the south, the ductile fabric overprints a quartz monzodiorite body and is in turn overprinted by metamorphic monazite; the intrusion and monazite are U-Pb dated as  $180.9 \pm 3.1$  and  $177.5 \pm 1.5$  Ma (Currie, 1994; Currie and Parrish, 1997). It is unknown if the granodiorite and quartz monzonite were intruded into an already active deformation zone, but ductile sinistral shear ceased by  $\sim 178$  Ma. Immediately following, at  $\sim 177$  Ma (Currie, 1994), metamorphism peaked at upper amphibolite facies within the metamorphic rocks west of the Llewellyn fault, suggesting tight interdependency.

Sinistral offset related to ductile deformation within the Llewellyn fault zone (older and deeper deformation, which is overprinted by young and shallower, brittle fabrics, (Mihalynuk et al., 1999; Ootes et al., 2017) is suggested by a new, preliminary U-Pb crystallization age of  $\sim 185$  Ma (Friedman, unpublished) from a 2.5 km-long lens of protomylonitic granodiorite along the Llewellyn fault (Fig. 2) where it crosses southern Tutshi Lake (Mihalynuk et al., 1999). It is possible that this body intruded into the fault near its present location and intrusive contacts were obscured by later deformation, but we suggest that it is a part of the Hale Mountain granodiorite border that was offset sinistrally, by about 70 km.

Sinistral fabrics are also observed within conglomerate facies of the Laberge Group in northernmost BC (Mihalynuk et al., 1999) where fossil age constraints limit deformation age to younger than 183 Ma. Regional constraints on youngest (western) Whitehorse trough fold and thrust belt deformation come from the Tulsequah and Dease Lake areas where Laberge Group strata as young as Bajocian ( $\sim 170$  Ma) and are deformed by nearly syndepositional folds and thrusts (Mihalynuk et al., 1995). Structures correlated with the old eastern Whitehorse trough fold and thrust belt, emplace 174 Ma blueschist along with Cache Creek strata and are cut by 172 Ma intrusions (M. Mihalynuk et al., 2004).

## 8.3. Disruption during Latest Triassic carbonate deposition

Preservation of carbonate is not solely controlled by depositional facies arising from the interplay of paleogeography, climate, and ocean chemistry. Evolution too plays an important role, especially in Triassic and Jurassic times, when reef forming organisms were recovering from two global extinction crises. During the Permo-Triassic mass extinction event,

carbonate reef-formers were wiped out and did not widely reappear until the Middle Triassic. It was not until the Norian that corals became important reef-formers, especially the Scleractinians (Stanley, 2003; Flügel, 2002). Reef-formers were similarly hard-hit by the end Triassic extinction event and did not rebound until the third stage of the Early Jurassic (Pliensbachian, Stanley, 2003; although rare reefs from the first two Jurassic stages are known, Hodges and Stanley Jr, 2015). As a result of evolution, lack of reefal carbonate accumulation during the Early-Middle Triassic and first half of the Early Jurassic in the Sinwa Creek area does not necessarily indicate inappropriate depositional environment (e.g., too deep) or climate (e.g., too cool).

Against this backdrop, it is not surprising that Sinwa Formation is largely restricted to the Norian. Spatial distribution of Sinwa Formation is from southeast of Sinwa Creek map area to north of Whitehorse, where warm water carbonate reef mounds are fringed by inter-mound carbonate sandstone, as at the well-studied Lime Peak locality (Reid, 1985; Reid and Tempelman, 1987; Yarnell et al., 1998). The Sinwa Formation in these areas are relicts of what was probably a much more widespread reef-mound-sandstone complex before Late Norian uplift and erosion. Latest Triassic uplift of the western side of the Whitehorse Trough between southern Atlin Lake and Yukon is marked by an unconformity developed late during carbonate deposition, roughly synchronous with late arc alkalic volcanism (Mihalynuk et al., 1999; Logan and Mihalynuk, 2014) and predating onset of Laberge Group deposition in Early Jurassic. Within the Sinwa Creek area, this event may be represented by limestone block conglomerates (see above). Widespread occurrence of Norian carbonate and Late Triassic igneous boulders in Late Triassic conglomerate is consistent with exposure of the Sinwa Formation or a similar limestone unit and the underlying Late Triassic Stuhini arc, starting in the Late Triassic as indicated by probable *Halobia* bivalves in strata below the limestone block conglomerate which is inferred to be composed of Late Norian carbonate, like all limestone clasts dated within the Whitehorse trough. The age of strata overlying the unconformity is unknown; although, Souther (1971) reported an Early Toarcian ammonite collected from strata along strike, and in the Stuhini Creek area, volcanic conglomerate is commonly Pliensbachian in age (Mihalynuk et al., 2004; igneous conglomerate is Pliensbachian to Toarcian). North of the Sinwa Creek map area, this period of uplift and exposure may have extended through to the Early Jurassic as recorded by detrital zircons ranging from Late Triassic through Early Jurassic and boulders of Norian carbonate in the Laberge Group (Early Jurassic; Colpron et al., 2015). Southeast of the Sinwa Creek area, Souther (1971) mapped Laberge Group in contact with Stuhini arc strata without intervening Sinwa Formation, and ~80 km southeast of Sinwa Mountain, Laberge Group strata are mapped in stratigraphic contact with Triassic intrusive rocks.

The underlying causes of the Late Norian uplift are not known, but Logan and Mihalynuk (2014) have suggested that

collision of the Kutcho-Sitlika arc with the Quesnel-Stikine arc at this time initiated a pulse of alkalic magmatism with high Cu-Au-Ag tenor, and generated economically important porphyry deposits along the length of the province. Such an event may explain the main 242 Ma detrital zircon population (resolved from a 232 Ma subpeak using Unmix routine of Isoplot; Ludwig, 2003) in the strata at the unconformity, a magmatic age unknown in adjacent Stikinia, but predominant in the Kutcho-Sitlika arc (Childe and Thompson, 1995; Mihalynuk et al., 2003; Schiarizza, 2013). Magmatic ages of ~232 Ma are also not known within Stikine terrane; although in the Quesnel arc, felsic magmatism seems to have been underway by ~239 Ma (Mihalynuk et al., 2016) and crystallization ages of 230.2 ± 0.8 Ma have been reported (Erdmer et al., 2002). However, it seems unlikely that a unimodal population of zircons could transit from the outer arc ridge collision site to the interior of the pre-collision platform without contamination from other detrital zircon sources. A reassessment of the currently accepted Stikine subduction polarity may be warranted.

Regardless of tectonic model, a widespread unconformity is indicated and implications are that the Stuhini arc was eroded to its plutonic roots between the latest Triassic and Early Jurassic. Consequences for preservation of Late Triassic – Early Jurassic porphyry deposits in these areas would thus appear dire, unless the mineralized arc was tectonically buried during Middle Jurassic collapse of the Whitehorse Trough or decapitated during the Late Triassic arc disruption and preserved at a structural level below the current erosional surface. Careful delineation of the mineralized arc axes will be required before such options can be properly evaluated.

## 9. Summary

Reconnaissance mapping in the Sinwa Creek map area (104K/14) of northwest British Columbia (59°N) was conducted in 2015 to determine what happens at this latitude to a Triassic-Jurassic magmatic belt that is mineralized with Cu-Au porphyry deposits as far north as ~58.5°. Sinwa Creek map area is mostly underlain by Triassic and Jurassic volcanosedimentary strata of the Whitehorse trough, which parallels the western boundary of the exotic, oceanic Cache Creek terrane in BC and extends along strike into central Yukon (~500 km in total). The area is diagonally bisected by a belt of massive to well-bedded limestone, the Sinwa Formation, that defines the King Salmon fault. At this latitude, the King Salmon fault is a northeast-dipping thrust, part of the Whitehorse trough fold and thrust belt that includes folds recording sinistral transpression. Many previous workers have included the Sinwa (and Whitehorse trough strata northeast of the Sinwa Formation) with the Cache Creek terrane, which lacks known porphyry deposits. We favour an alternative hypothesis, supported by stratigraphic, biochronologic (conodont), clast compositions, detrital zircon populations, and rock types in the immediate hangingwall of the King Salmon fault, which places the Whitehorse trough above the Stuhini forearc. If correct, the King Salmon fault within, or north of, the Sinwa Creek area is not the Cache Creek

terrane boundary. However, southeast of Nahlin Mountain, the King Salmon fault as currently defined **does** carry Cache Creek terrane rocks in its hangingwall, placing Cache Creek terrane and structurally overlying parts of the distal Whitehorse trough over its arc-proximal facies. Thus, we speculate that King Salmon fault segments north and south of Nahlin Mountain may be two fundamentally different faults. If they are different faults, then the manner in which they have interacted with Triassic-Jurassic magmatic belts may also vary along strike.

In the Sinwa Creek area, the Whitehorse trough is most likely underlain by the Cu-Au porphyry-rich Stikine terrane, but clear evidence that the porphyry belt extends beneath the trough in the near sub-surface is currently lacking. A full accounting of the crustal level and amount of Middle Jurassic shortening across the Whitehorse Trough as well as both earlier and later translational offsets will be required before the implications for Cu-Au porphyry exploration are known.

### Acknowledgments

This work was carried out under the auspices of a collaborative GSC-BCGS program delivered as a component of Geomapping for Energy and Minerals (GEM). Field studies were aided by the keen observations of S. Bichlmaier, S. Carroll, K. Sigloch, Y. Cui, D. Miller, and M.A. Henderson. Thanks to G. Stanley for preliminary identification of fossil corals. Isotopic analyses at the Pacific Centre for Isotopic and Geochemical Research were aided by H. Lin who did the mineral separation, and T. Ockerman who conducted activities in the clean lab, as well as C. Wall, H. Lin and N. Moerhius who all assisted with mass spectrometry. Safe, reliable and efficient helicopter support was provided by P. Vera and N. Graham of Discovery Helicopters, Atlin.

### References cited

- Beaudry, D., and Moore, G.F., 1981. Seismic-stratigraphic framework of the forearc basin off central Sumatra, Sunda Arc. *Earth and Planetary Science Letters*, 54, 17-28.
- Bostock, H.S., and Lees, E.J., 1938. Laberge map-area, Yukon. Department of Mines and Resources Canada, Geological Survey of Canada, Memoir 217, 32p.
- Black, L.P., Kamo, S.L., Allen, C.M., Davis, D.W., Aleinikoff, J.N., Valley, J.W., Mundil, R., Campbell, I.H., Korsh, R.J., Williams, I.S., and Foudoulis, C., 2004. Improved  $^{206}\text{Pb}/^{238}\text{U}$  microprobe geochronology by monitoring of a trace-element-related matrix effect: SHRIMP, ID-TIMS, ELA-ICP-MS and oxygen isotope documentation for a series of zircon standards. *Chemical Geology*, 205, 115-140.
- Brown, D.A., Logan, J.M., Gunning, M.H., Orchard, M.J., and Bamber, W.E., 1991. Stratigraphic evolution of the Paleozoic Stikine Assemblage in the Stikine and Iskut rivers area, northwestern British Columbia. In: *Contributions to the geology and geophysics of northwestern British Columbia and southeastern Alaska*, Canadian Journal of Earth Sciences 28, 958-972.
- Bultman, R.B., 1979. Geology and tectonic history of the Whitehorse Trough west of Atlin, British Columbia. Unpublished Ph.D. thesis, Yale University, 284p.
- Cairnes, D.D., 1910. Preliminary Memoir on the Lewes and Nordenskiöld Rivers Coal District, Yukon Territory. Geological Survey of Canada, Memoir 5, 70p.
- Canil, D., Mihalynuk, M., and Charnell, C., 2006. Sedimentary record for exhumation of ultrahigh pressure (UHP) rocks in the northern Cordillera, British Columbia, Canada. *Geological Society of America Bulletin*, 118, 1171-1184. doi: 10.1130/b2592.1.
- Childe, F., and Thompson, J.F.H., 1995. U-Pb age constraints and Pb isotopic signature of the Kutcho VMS deposit; implications for the terrane affiliation of the Kutcho Formation, north central British Columbia. In: *Geological Association of Canada - Mineralogical Association of Canada - Canadian Geophysical Union, Joint Annual Meeting, Program with Abstracts 20*, p. 17.
- Colpron, M., 2011. Geological compilation of Whitehorse trough-Whitehorse (105D), Lake Laberge (105E), and part of Carmacks (115J), Glenlyon (105L), Aishihik Lake (115H), Quiet Lake (105F) and Teslin (105C). Yukon Geological Survey, Geoscience Map, 2011-1, scale 1:250,000.
- Colpron, M., and Friedman, R.M., 2007. U-Pb zircon ages for the Nordenskiöld formation (Laberge Group) and Cretaceous intrusive rocks, Whitehorse Trough, Yukon. In: *Yukon Exploration and Geology 2007*, 139-151.
- Colpron, M., and Nelson, J.L., 2011. A Digital atlas of terranes for the northern Cordillera. British Columbia Ministry of Energy and Mines, BC Geological Survey, GeoFile 2011-11. [http://www.geology.gov.yk.ca/pdf/terrane\\_readme.pdf](http://www.geology.gov.yk.ca/pdf/terrane_readme.pdf) accessed October 14, 2014.
- Colpron, M., Crowley, J.L., Gehrels, G., Long, D.G., Murphy, D.C., Beranek, L., and Bickerton, L., 2015. Birth of the northern Cordilleran orogen, as recorded by detrital zircons in Jurassic synorogenic strata and regional exhumation in Yukon. *Lithosphere*, 7, 541-562.
- Coney, P.J., Jones, D.L., and Monger, J.W.H., 1980. Cordilleran suspect terranes. *Nature (London)*, 288, 329-333.
- Crowley, J.L., Schoene, B., and Bowering, S.A., 2007. U-Pb dating of zircon in the Bishop Tuff at the millennial scale. *Geology*, 35, 1123-1126.
- Currie, L.D., 1994. The geology and Mid-Jurassic amalgamation of Tracy Arm Terrane and Stikinia of northwestern British Columbia. Unpublished Ph.D. thesis, Carleton University, 385p.
- Currie, L.D., and Parrish, R.R., 1997. Paleozoic and Mesozoic rocks of Stikinia exposed in northwestern British Columbia; implications for correlations in the northern Cordillera. *Geological Society of America Bulletin*, 109, 1402-1420.
- Dickie, J.R., Grist, A.M., and Donelick, R.A., 1992. Differential uplift across the Coast plutonic complex-northern Stikine Terrane contact, Yukon; preliminary evidence from apatite fission-track thermochronometry. In: *Yukon Geology, Exploration and Geological Services Division, Yukon Indian and Northern Affairs Canada*, 160-166.
- Dickie, J.R., and Hein, F.J., 1995. Conglomeratic fan deltas and submarine fans of the Jurassic Laberge Group, Whitehorse Trough, Yukon Territory, Canada; fore-arc sedimentation and unroofing of a volcanic island arc complex. In: *Fan deltas; depositional styles and controls*. *Sedimentary Geology*, 98, 263-292.
- Dickie, J.R., and Hein, F.J., 1988. Facies and depositional setting of Laberge Conglomerates (Jurassic), Whitehorse Trough, Yukon. In: *Yukon Geology, Exploration and Geological Services Division, Yukon Indian and Northern Affairs Canada*, 2, 26-32.
- English, J.M., Mihalynuk, M.G., Johnston, S.T., Orchard, M.J., Fowler, M., and Leonard, L.J., 2003. Atlin TGI, Part VI: Early to Middle Jurassic sedimentation, deformation and a preliminary assessment of hydrocarbon potential, central Whitehorse Trough and northern Cache Creek terrane. In: *Geological Fieldwork 2002*, British Columbia Ministry of Energy, Mines and Petroleum Resources, BC Geological Survey, Paper 2003-1, 187-201.
- English, J.M., 2004. Convergent margin tectonics in the North American Cordillera: implications for continental growth and orogeny. Unpublished Ph.D. thesis, University of Victoria, Victoria, Canada, 191p.
- English, J.M., Johansson, G.G., Johnston, S.T., Mihalynuk, M.G.,

- Fowler, M., and Wight, K.L., 2005. Structure, stratigraphy and petroleum resource potential of the Central Whitehorse Trough, Northern Canadian Cordillera. *Bulletin of Canadian Petroleum Geology*, 53, 130–153. doi: 10.2113/53.2.130.
- Erdmer, P., Moore, J.M., Heaman, L., Thompson, R.I., Daughtry, K.L., and Creaser, R.A., 2002. Extending the ancient margin outboard in the Canadian Cordillera: record of Proterozoic crust and Paleocene regional metamorphism in the Nicola horst, southern British Columbia. *Canadian Journal of Earth Sciences*, 39, 1605-1623.
- Flügel, E., 2002. Triassic reef patterns. In: *Phanerozoic Reef Patterns*; Wolfgang, Kiessling, Erik, Flügel, and Jan. Golonka (Eds.), *Society for Sedimentary Geology, Special Publication*, 72, 391-463. DOI: 10.2110/pec.02.72.
- Gabrielse, H., 1998. Geology of the Cry Lake and Dease Lake map areas, north-central British Columbia. *Geological Survey of Canada, Bulletin* 504, 147p.
- Gabrielse, H., Monger, J.W.H., Wheeler, J.O., and Yorath, C.J., 1992. Tectonic framework; Part A, Morphogeological belts, tectonic assemblages and terranes. In: *Geology of the Cordilleran Orogen in Canada*, 15-28.
- Gerstenberger, H., and Haase, G., 1997. A Highly effective emitter substance for mass spectrometric Pb isotopic ratio determinations. *Chemical Geology*, 136, 309-312.
- Hall, R., and Smyth, H.R., 2008. Cenozoic arc processes in Indonesia: identification of the key influences on the stratigraphic record in active volcanic arcs. *Geological Society of America Special Papers*, 436, 27-54.
- Hart, C.J.R., 1997. A transect across northern Stikinia: Geology of the northern Whitehorse map area, southern Yukon Territory (105D/13-16). *Exploration and Geological Services Division, Yukon Region, Indian and Northern Affairs Canada, Bulletin*, 8, 112p.
- Hart, C.J.R., Dickie, J.R., Ghosh, D.K., and Armstrong, R.L., 1995. Provenance constraints for Whitehorse Trough conglomerate; U-Pb zircon dates and initial Sr ratios of granitic clasts in Jurassic Laberge Group, Yukon Territory. In: *Jurassic magmatism and tectonics of the North American Cordillera*, Geological Society of America, *Special Paper* 299, 47-63.
- Hodges, M.S., and Stanley Jr, G.D., 2015. North American coral recovery after the end-Triassic mass extinction, New York Canyon, Nevada, USA. *GSA Today*, 25, 4-7.
- Jaffey, A.H., Flynn, K.F., Glendenin, L.E., Bentley, W.C., and Essling, A.M., 1971. Precision measurement of half-lives and specific activities of  $^{235}\text{U}$  and  $^{238}\text{U}$ . *Physical Review*, C4, 1889-1906.
- Johannson, G.G., 1993. Preliminary report on the stratigraphy, sedimentology, and biochronology of the Inklin Formation in the Atlin Lake area, northern British Columbia. In: *Current Research, Cordillera and Pacific margin*, Geological Survey of Canada, *Paper* 93-1A, 37-42.
- Johannson, G.G., Smith, P.L., and Gordey, S.P., 1997. Early Jurassic evolution of the northern Stikinian arc; evidence from the Laberge Group, northwestern British Columbia. *Canadian Journal of Earth Sciences*, 34, 1030-1057.
- Johnston, S.T., and Erdmer, P., 1995. Hot-side-up aureole in Southwest Yukon and limits on terrane assembly of the northern Canadian Cordillera. *Geology* (Boulder), 23, 419-422.
- Johnston, S.T., Mortensen, J.K., and Erdmer, P., 1996. Igneous and metaigneous age constraints for the Aishihik metamorphic suite, Southwest Yukon. *Canadian Journal of Earth Sciences*, 33, 1543-1555.
- Johnston, S.T., Mihalynuk, M.G., Brew, D.A., Hart, C.J.R., Erdmer, P., Gehrels, G.E., Currie, L.D., and Parrish, R.R., 1999. Paleozoic and Mesozoic rocks of Stikinia exposed in northwestern British Columbia; implications for correlations in the northern Cordillera; discussion and reply. *Geological Society of America Bulletin*, 111, 1103-1106.
- Kerr, F.A., 1931a. Some of the mineral properties in the Taku District, British Columbia. *Geological Survey of Canada, Summary Report* 1930, Part A, 17-40.
- Kerr, F.A., 1931b. Explorations between Stikine and Taku Rivers, B.C., *Geological Survey of Canada, Summary Report* 1930, Part A, 41-55.
- Kerr, F.A., 1948. Taku River map-area, British Columbia. *Geological Survey of Canada, Memoir* 248, 84p.
- Kreemer, C., Blewitt, G., and Klein, E.C., 2014. A geodetic plate motion and global strain rate model. *Geochemistry, Geophysics, Geosystems*, 15, 3849-3889.
- Logan, J.M., and Mihalynuk, M.G., 2014. Tectonic controls on early Mesozoic paired alkaline porphyry deposit belts (Cu-Au  $\pm$ Ag-Pt-Pd-Mo) within the Canadian Cordillera. *Economic Geology*, 109, 827-858.
- Lowey, G.W., 2003. Preliminary lithostratigraphy of the Laberge Group (Jurassic), south-central Yukon: Implications concerning the petroleum potential of the Whitehorse Trough. *Yukon Exploration and Geology, Yukon Geological Survey*, 129-142.
- Lowey, G.W., 2004. Sedimentology, stratigraphy and source rock potential of the Richthofen formation (Jurassic), northern Whitehorse Trough, Yukon. *Yukon Exploration and Geology, Yukon Geological Survey*, 177-191.
- Ludwig, K.R., 2003. User's manual for Isoplot/Ex rev. 3.00: a Geochronological Toolkit for Microsoft Excel. *Special Publication*, 4, Berkeley Geochronology Center, Berkeley, 70p.
- MacKenzie, J.M., Canil, D., Johnston, S.T., English, J., Mihalynuk, M.G., and Grant, D.B., 2005. First evidence for ultrahigh-pressure garnet peridotite in the North American Cordillera. *Geology*, 33, 105-108.
- Mattinson, J.M., 2005. Zircon U-Pb chemical abrasion ("CA-TIMS") method: Combined annealing and multi-step partial dissolution analysis for improved precision and accuracy of zircon ages: *Chemical Geology*, 220, 47-66.
- Mihalynuk, M.G., and Mountjoy, K.J., 1990. Geology of the Tagish Lake area (104M/ 8, 9E). In: *Geological fieldwork, 1989*, British Columbia Ministry of Energy, Mines and Petroleum Resources, BC Geological Survey, *Paper* 1990-1, 181-196.
- Mihalynuk, M.G., Smith, M.T., Hancock, K.D., and Dudka, S., 1994a. Regional and economic geology of the Tulsequah River and Glacier areas (104K/12 & 13). In: *Geological fieldwork 1993*, British Columbia Ministry of Energy, Mines and Petroleum Resources, BC Geological Survey, *Paper* 1994-1, 171-197.
- Mihalynuk, M.G., Smith, M.T., Hancock, K.D., Dudka, S., and Payne, J., 1994b. Geology of the Tulsequah River and Glacier areas (NTS 104K/12 & 13). *British Columbia Ministry of Energy, Mines and Petroleum Resources, British Columbia Geological Survey, Open File* 1994-03.
- Mihalynuk, M.G., Meldrum, D., Sears, S., and Johannson, G., 1995a. Geology and mineralization of the Stuhini Creek area (104K/ 11). In: *Geological fieldwork 1994*; British Columbia Ministry of Energy, Mines and Petroleum Resources, BC Geological Survey, *Paper* 1995-1, 321-342.
- Mihalynuk, M.G., Meldrum, D., Sears, S., Johannson, G., Madu, B.E., Vance, S., Tipper, H.W., and Monger, J.W.H., 1995b. Geology and geochemistry of the Stuhini Creek map area (NTS 104K/11). *British Columbia Ministry of Energy, Mines and Petroleum Resources, British Columbia Geological Survey, Open File* 1995-5.
- Mihalynuk, M.G., Mountjoy, K.J., Smith, M.T., Currie, L.D., Gabites, J.E., Tipper, H.W., Orchard, M.J., Poulton, T.P., and Cordey, F., 1999. Geology and mineral resources of the Tagish Lake area (NTS 104M/ 8,9,10E, 15 and 104N/ 12W), northwestern British Columbia. *British Columbia Ministry of Energy and Mines, BC Geological Survey, Bulletin* 105, 201p.
- Mihalynuk, M.G., Johnston, S.T., English, J.M., Cordey, F.,

- Villeneuve, M.J., Rui, L., and Orchard, M.J., 2003a. Atlin TGI Part II: Regional geology and mineralization of the Nakina area (NTS 104N/2W and 3). In: Geological Fieldwork 2002, British Columbia Ministry of Energy, Mines and Petroleum Resources, BC Geological Survey, Paper 2003-1, 9-37.
- Mihalynuk, M.G., Villeneuve, M.E., and Cordey, F., 2003b. Atlin TGI, Part III: Geological setting and style of mineralization at the Joss'alun occurrence, Atlin area (NTS 104N/2SW), MINFILE 104N136. In: Geological Fieldwork 2002, British Columbia Ministry of Energy, Mines and Petroleum Resources, BC Geological Survey, Paper 2003-1, 39-49.
- Mihalynuk, M.G., Erdmer, P., Ghent, E.D., Cordey, F., Archibald, D.A., Friedman, R.M., and Johannson, G.G., 2004. Coherent French Range blueschist: Subduction to exhumation in < 2.5 m.y.? *Geological Society of America Bulletin*, 116, 910-922. doi: 10.1130/b25393.
- Mihalynuk, M.G., Diakow, L.J., Friedman, R.M., and Logan, J.M., 2016. Chronology of southern Nicola arc stratigraphy and deformation. In: Geological Fieldwork 2015, British Columbia Ministry of Energy and Mines, British Columbia Geological Survey, Paper 2016-1, 31-64.
- Monger, J., 1975. Upper Paleozoic rocks of the Atlin Terrane, northwestern British Columbia and south-central Yukon. Geological Survey of Canada, Paper 74-47, 63p.
- Monger, J.W.H., 1977. Upper Paleozoic rocks of the western Canadian Cordillera and their bearing on Cordilleran evolution. *Canadian Journal of Earth Sciences*, 14, 1832-1859.
- Monger, J.W.H., and Thorstad, L., 1978. Lower Mesozoic stratigraphy, Cry Lake and Spatsizi map-areas, British Columbia. In: Current research, part A., Geological Survey of Canada, Paper 78-1a, 21-24.
- Mundil, R., Ludwig, K. R., Metcalfe, I., and Renne, P. R., 2004. Age and timing of the Permian Mass Extinctions: U/Pb Dating of Closed-System Zircons, *Science*, 305, 1760-1763.
- Ootes, L., Elliott, J.M., and Rowins, S.M., 2017. Testing the relationship between the Llewellyn fault, gold mineralization, and Eocene volcanism in northwest British Columbia: A preliminary report. In: Geological Fieldwork 2016, British Columbia Ministry of Energy and Mines, British Columbia Geological Survey Paper 2017-1, this volume.
- Reid, R.P., 1985. The Facies and Evolution of an Upper Triassic Reef Complex in Northern Canada (convergent Margin, Yukon, Lime Peak). Unpublished Ph.D. thesis, University of Miami, URL <http://scholarlyrepository.miami.edu/dissertations/1504/> accessed December 11, 2015.
- Reid, R.P., and Tempelman, K.D.J., 1987. Upper Triassic Tethyan-type reefs in the Yukon. *Bulletin of Canadian Petroleum Geology*, 35, 316-332.
- Schiarizza, P., 2013. The Wineglass assemblage, lower Chilcotin River, south-central British Columbia: Late Permian volcanic and plutonic rocks that correlate with the Kutcho assemblage of northern British Columbia. In: Geological Fieldwork 2012, British Columbia Ministry of Energy, Mines and Natural Gas, BC Geological Survey, Paper 2013-1, 53-70.
- Scoates, J.S., and Friedman, R.M., 2008. Precise age of the platinumiferous Merensky Reef, Bushveld Complex, South Africa, by the U-Pb ID-TIMS chemical abrasion ID-TIMS technique, *Economic Geology*, 103, 465-471.
- Schmitz, M.D., and Schoene, B., 2007. Derivation of isotope ratios, errors, and error correlations for U-Pb geochronology using  $^{205}\text{Pb}$ - $^{235}\text{U}$ -( $^{233}\text{U}$ )-spiked isotope dilution thermal ionization mass spectrometric data. *Geochemistry, Geophysics, Geosystems* (G-cubed), 8, Q08006. doi:10.1029/2006GC001492.
- Sigloch, K., and Mihalynuk, M.G., 2013. Intra-oceanic subduction shaped the assembly of Cordilleran North America. *Nature*, 496, 50-56.
- Souther, J.G., 1971. Geology and mineral deposits of Tulsequah map-area, British Columbia. Geological Survey of Canada, Memoir 362, 84p.
- Stacey, J.S., and Kramers, J.D., 1975. Approximation of terrestrial lead isotopic evolution by a two-stage model. *Earth and Planetary Science Letters*, 26, 207-221.
- Stanley, G.D., 2003. The evolution of modern corals and their early history. *Earth-Science Reviews*, 60, 195-225.
- Stern, R.A., 1997. The GSC Sensitive High Resolution Ion Microprobe (SHRIMP): analytical techniques of zircon U-Th-Pb age determinations and performance evaluation in Radiogenic age and Isotopic Studies, Report 10, Geological Survey of Canada, Current Research 1997-F, 1-31.
- Stern, R.A., and Amelin, Y., 2003. Assessment of errors in SIMS zircon U-Pb geochronology using a natural zircon standard and NIST SRM 610 glass: *Chemical Geology*, 197, 111-142.
- Tempelman-Kluit, D.J., 1984. Geology, Leberge (105E) Carmacks (115), Yukon Territory. Geological Survey of Canada, Open File 1101, 10p. doi:10.4095/129923.
- Thirlwall, M.F., 2000. Inter-laboratory and other errors in Pb isotope analyses investigated using a  $^{207}\text{Pb}$ - $^{204}\text{Pb}$  double spike. *Chemical Geology*, 163, 299-322.
- Van der Werff, W., 1996. Variation in forearc basin development along the Sunda Arc, Indonesia. *Journal of Southeast Asian Earth Sciences*, 14, 331-349.
- Vine, F.J., and Hess, H.H., 1970. Sea floor spreading. In: Maxwell, A.E. (Ed.), *The Sea*, Volume 4, part 2: Wiley, New York, New York, 587-622.
- Wheeler, J.O., Brookfield, A.J., Gabrielse, H., Monger, J.W.H., Tipper, H.W., and Woodsworth, G.J., 1988. Terrane map of the Canadian Cordillera. Geological Survey of Canada, Map 1713A, scale 1:2,000,000, 9p.
- Wheeler, J.O., 1961. Whitehorse map-area, Yukon Territory, 105D. Department of Mines and Technical Surveys, Geological Survey of Canada, Memoir 312, 156p.
- Wheeler, J.O., and McFeely, P., 1991. Tectonic assemblage map of the Canadian Cordillera and adjacent parts of the United States of America. Geological Survey of Canada Map 1712A, scale 1: 2,000,000.
- Wight, K.L., English, J.M., and Johnston, S.T., 2004. Structural relationship between the Laberge Group and Sinwa Formation on Copper Island, southern Atlin Lake, northwest British Columbia. In: Summary of Activities, 2004, British Columbia Ministry of Energy and Mines, Resource Development and Geoscience Branch, 113-120.
- Woodsworth, G.J., Anderson, R.G., Armstrong, R.L., Struik, L.C., and van der Heyden, P., 1992. Plutonic regimes. In: *Geology of the Cordilleran Orogen in Canada*, 493-531.
- Yarnell, J.M., Stanley, G.D., and Hart, C.J., 1998. New paleontological investigations of Upper Triassic shallow-water reef carbonates (Lewes River Group) in the Whitehorse area, Yukon. In: Yukon Exploration and Geology 1998, Exploration and Geological Services Division, Yukon, Indian and Northern Affairs Canada, 179-184.
- Zagorevski, A., Mihalynuk, M.G., Joyce, N., Kellett, D.A., and Milidragovic, D., 2015. Characterization of volcanic and intrusive rocks across the British Columbia – Yukon border, GEM 2 Cordillera. Geological Survey of Canada, Open File 7956, 13p. doi:10.4095/297272.

# A new lode gold discovery at Otter Creek: Another source for the Atlin placers



Mitchell G. Mihalynuk<sup>1, a</sup>, Alexandre Zagorevski<sup>2</sup>, Fionnuala A.M. Devine<sup>3</sup>, and Elaine Humphrey<sup>4</sup>

<sup>1</sup>British Columbia Geological Survey, Ministry of Energy and Mines, Victoria, BC, V8W 9N3

<sup>2</sup>Geological Survey of Canada, 601 Booth Street, Ottawa, ON, K1A 0E8

<sup>3</sup>Merlin Geosciences Inc., Atlin, BC, V0W 1A0

<sup>4</sup>Department of Mechanical Engineering, University of Victoria, Victoria, BC, V8P 5C2

<sup>a</sup>corresponding author: Mitch.Mihalynuk@gov.bc.ca

Recommended citation: Mihalynuk, M.G., Zagorevski, A., Devine, F.A.M., and Humphrey, E., 2017. A new lode gold discovery at Otter Creek: Another source for the Atlin placers. In: Geological Fieldwork 2016, British Columbia Ministry of Energy and Mines, British Columbia Geological Survey Paper 2017-1, pp. 179-193.

## Abstract

Primary exploration targets for lode gold near Atlin, northwestern British Columbia have historically been quartz-carbonate-mariposite-altered ('listwanite') ultramafic and mafic bedrocks. These have long been considered the source of nearby placer deposits, and locally do contain fine visible gold. However, despite more than a century of searching, coarse gold such as found in the placer gravels has never been discovered. This has prompted the belief that the 'listwanites' are mere erosional remnants of bedrock sources of the coarse placer gold, and that these sources have been almost entirely lost to erosion. An alternative hypothesis argues that, although gold is found with listwanite, it was not the only bedrock source. Streams with placer deposits are distributed around the evolved Surprise Lake batholith (Sn-U-Th-Mo-W-F rich) and rare gold nuggets contain Sn- and Th-rich mineral intergrowths (cassiterite and thorite), demonstrating that at least some of the placer gold may be related to the batholith. Discovery of coarse lode gold (>5 mm) in graphitic and quartz-rich phyllitic bedrock beneath placer deposits along Otter Creek in 2016 confirms that listwanite-altered mafic and ultramafic rocks are not required for lode gold mineralization. At the discovery site, native gold is intergrown with quartz-albite veins and occurs as open space fillings. Rutile in quartz veins, and perhaps altered titanite in the adjacent phyllite may have grown along with gold deposition. Geochemical analysis of pyrite-rich phyllite adjacent to the gold veins yields no appreciable gold, but is slightly elevated in Cu (11-54 ppm), Pb (~33 ppm) and zinc (60-70 ppm). These results are consistent with petrographic observations that show abundant chalcopyrite inclusions but no gold inclusions in pyrite. Discovery of coarse gold in quartz veins cutting graphitic and quartz-rich phyllitic country rocks significantly expands the lode gold exploration target in the Atlin placer camp.

**Keywords:** Lode gold, placer gold, Surprise Lake batholith, Fourth of July batholith, Kedahda Formation, listwanite, Cache Creek terrane, Otter Creek, Slonski, Atlin

## 1. Introduction

Near the turn of the 20<sup>th</sup> century, the newly discovered placer creeks of the Atlin camp (northwest British Columbia) attracted miners who had abandoned the lode gold mines of California. Placer gold claims in the Atlin camp were first staked on Pine Creek, east of the future Atlin townsite, in 1898 (Robertson, 1898; Debicki, 1984; Figs. 1, 2). Atlin camp placers were spatially associated with quartz-carbonate-mariposite-altered (listwanite) ultramafic rocks (Figs. 2, 3). Prospectors noted similarity to the ultramafic rock associated with the rich ore streaks in the Alleghany district in California where, for example, 35,600 ounces were recovered from one ~4 x 7 m vein section in the Oriental Mine (Ferguson and Gannett, 1932). Aiming to duplicate the lode mining success in California, the ultramafic rocks near Atlin became the prime gold exploration target. Yet, despite intense exploration, only about 3 kg of lode gold was produced in the century following the placer discovery (Imperial Mine, MINFILE 104N 008, BC Geological Survey, 2016; for a summary of lode occurrences

see Bloodgood et al., 1989). This lack of lode gold prompted previous workers to conclude that any rich lodes in altered ultramafic and mafic rocks of the Atlin area had been removed by erosion, leaving only gold placers behind (Aitken, 1959; Ash et al., 2001).

Drilling in the listwanite-altered Pine Creek bedrock underlying the historic placers at the Yellowjacket property (Fig. 2) delineated an inferred gold resource of 184,000 tonnes grading 4.4 g/t (781 kg total Au, 0.5 g/t cut-off, Price and Dandy, 2010). Although the gold production and resource are relatively small, they do demonstrate that gold is associated with altered ultramafic rocks. However, this association is lacking in most other places. For example, aerially extensive altered ultramafic rocks southeast of Atlin (Nahlin ultramafic complex; Fig. 1) lack lode and placer gold deposits. Furthermore, coarse gold nuggets in Atlin placers are much coarser than sporadic, barely visible gold in known bedrock-hosted showings (e.g. Spruce Creek holds the provincial record for the largest nugget, weighing 2.6 kilograms (85 ounces) and

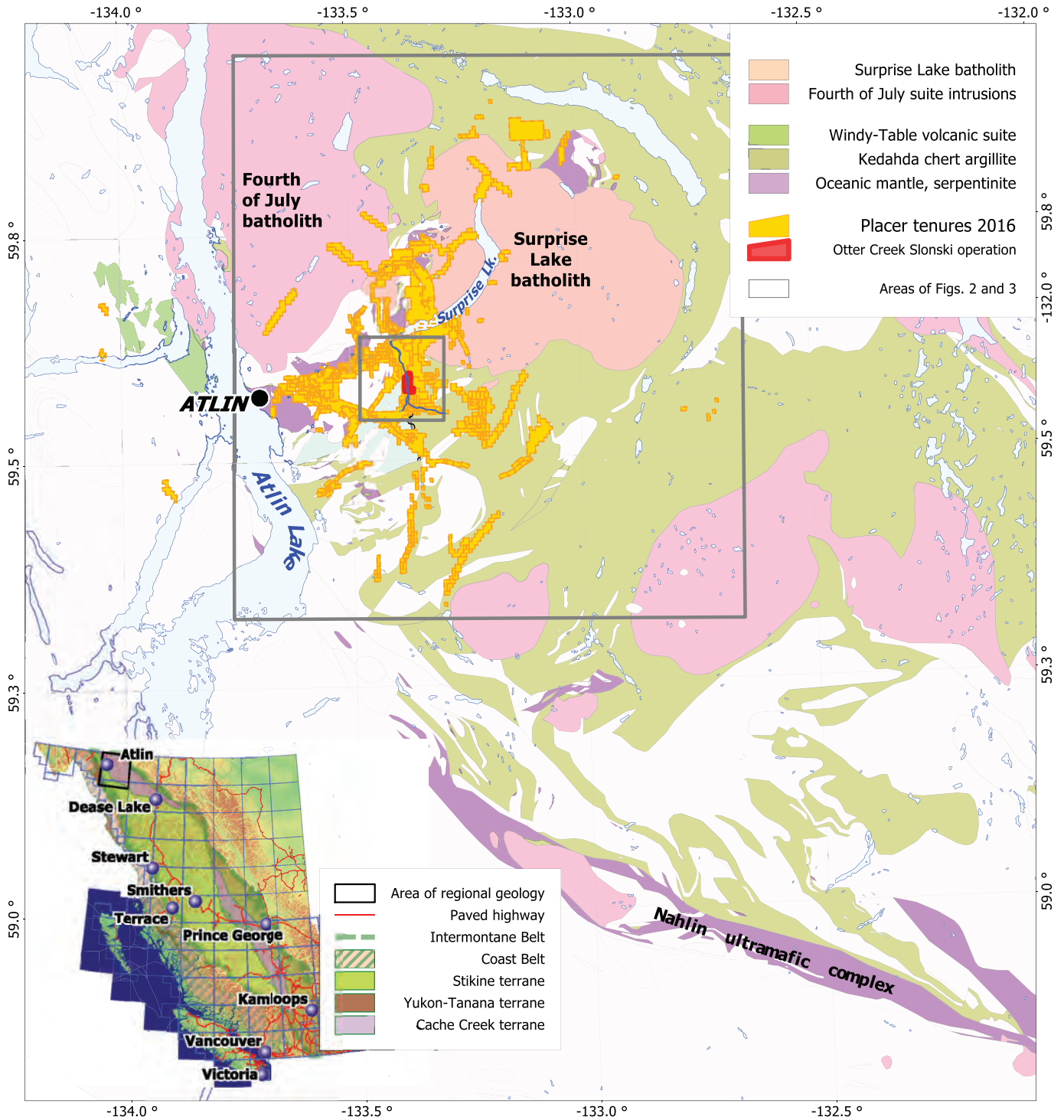


**Fig. 1.** Distribution of placer claims (yellow and red blocks) around the Surprise Lake batholith. Location of Otter Creek Slonski operation within the Atlin camp (red claim blocks). Geology base modified from Cui et al. (2015). Inset shows location of the study area with respect to major terranes in British Columbia.

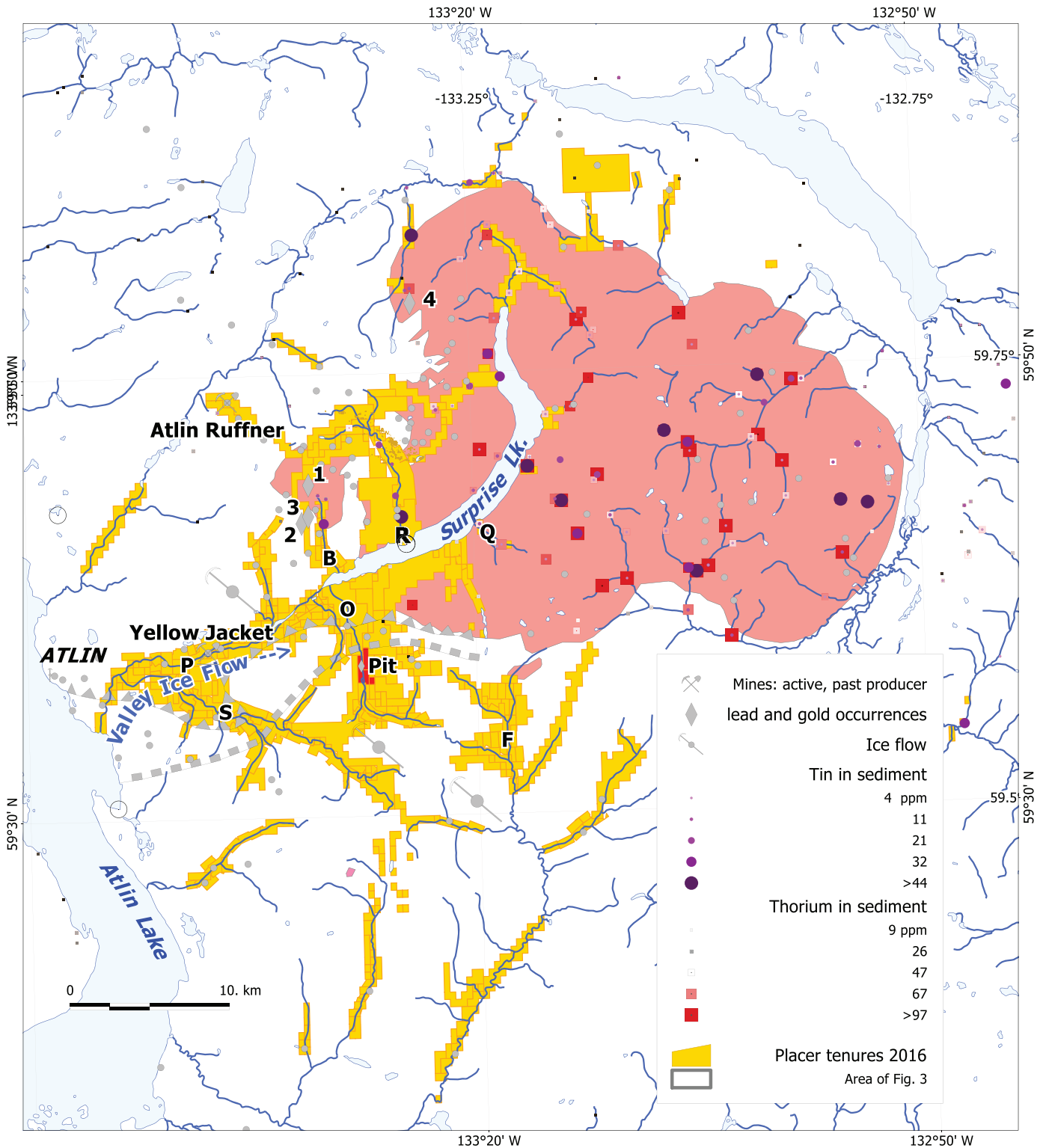


**Fig. 2.** Map of the Atlin placer camp showing placer tenures as of November, 2016. Almost all of the placer streams or their headwaters are underlain by the Surprise Lake batholith (pink) or its thermal metamorphic halo. There is a direct spatial relationship of regional stream sediment geochemical survey results for thorium (squares in shades of red) and tin (circles in shades of purple) with the areas underlain by the Surprise Lake batholith, showing that these elements are derived from the batholith. Creeks discussed in the text are denoted by the letters: B = Boulder, F = Feather, O = Otter, P = Pine, Q = Quartz, R = Ruby, S = Spruce.

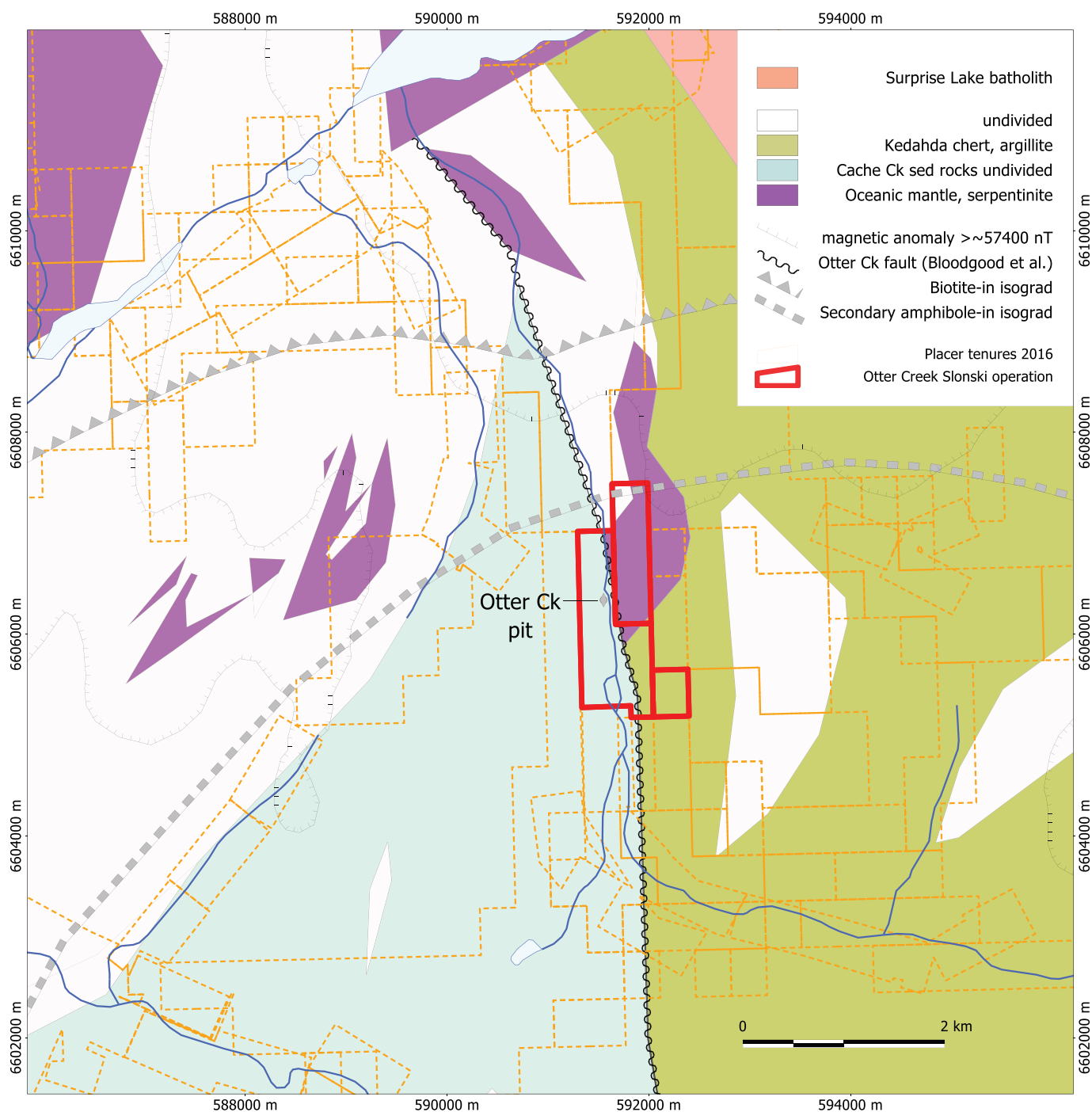


**Fig. 3.** Geology of the Otter Creek area, from Cui et al. (2015). Map shows Otter Creek fault following lower Otter Creek valley. Ultramafic bodies are broadly outlined by the  $>\sim 57400$  nT contour (ticks on high side of contour). Also shown are locations of the biotite-in and amphibole-in isograds (after Aitken, 1959). Sparse outcrops west of Otter Creek on the Slonski operation placer claims are metachert-argillite, like the Kedahda unit east of the fault. Universal Transverse Mercator grid designations, zone 8, NAD83.

for placer gold production; Levson, 1992), indicating that the source of the coarse placer gold is yet to be discovered. One possible alternative source is suggested by the distribution of placer streams. Their headwaters are underlain by the Surprise Lake batholith (Cretaceous), or country rock in its thermal metamorphic halo (cf. Aitken, 1959; Figs. 1, 2), suggesting a first-order relation between the batholith and placer gold.

In 2016, gold-quartz-albite-muscovite veins were discovered in graphitic phyllite bedrock in the Atlin placer camp. This discovery, on the middle section of Otter Creek amidst active placer operations (Figs. 2, 3), confirms a local source for the placer gold. The lode gold - graphitic phyllite association in Otter Creek valley is significant because it demonstrates that listwanite or mafic-ultramafic rock associations are not necessary for lode gold deposition in the Atlin camp. This expands the prospects for lode gold exploration adjacent to the Surprise Lake batholith, and perhaps beyond.

## 2. Atlin geology and previous work

Gwillim (1901) and Cairnes (1913) conducted the initial systematic regional geological surveys of the Atlin region. Subsequent mapping by Aitken (1959; 1:250,000 scale) established the regional framework for modern geological studies that is still in use today. More detailed studies of the area around Otter Creek were conducted by Bloodgood et al. (1989, Fig. 3) at 1:50,000 scale and in the area west of Otter Creek, by Ash (2004) at 1:25,000 scale.

Bedrocks of the Atlin area are predominantly Carboniferous to Early Jurassic oceanic crustal and sedimentary strata that were structurally imbricated and then cut by Mesozoic magmatic rocks of the Fourth of July batholith (Middle Jurassic) and Surprise Lake batholith (Late Cretaceous). Oceanic rock units of Cache Creek terrane originally formed at mantle to shallow-marine levels and have been fault juxtaposed such that lenses of ultramafic and mafic rocks are commonly interleaved with limestone, chert, and wacke at all scales. Early juxtaposition of contrasting rock packages probably originally occurred in multiple episodes at an accretionary margin (Monger, 1975; Monger et al., 1982). This has produced confounding geological relationships between rock types, hindering geological understanding and challenging standard practices of stratigraphic nomenclature in the Atlin area (see Monger, 1975; Mihalynuk et al., 1999).

Regionally, the youngest folded rocks are fossiliferous Aalenian to Bajocian strata (Mihalynuk et al., 1995; Shirmohammad et al., 2011). Following deformation, these early Middle Jurassic strata (~174 - ~169 Ma, time scale of Cohen et al., 2013) were intruded by the Fourth of July batholith at ~172 Ma, which is part of the Three Sisters suite. Plutonic members of this suite cut structures affecting correlative strata from Atlin to Dease Lake (Mihalynuk et al., 2004) and cooled within about 10 m.y. based on K/Ar cooling ages from the Fourth of July Batholith (Dawson, 1988, in Breitsprecher and Mortensen, 2004) and mariposite (Cr-mica) in listwanite-associated lode gold occurrences elsewhere in the Atlin camp

(Ash et al., 2001). Fourth of July and Cache Creek rocks were subsequently intruded by the highly evolved and geochemically distinct Surprise Lake batholith (Late Cretaceous; Zagorevski et al., 2017).

Sack and Mihalynuk (2003) evaluated the spatial association of gold and the geochemically anomalous Surprise Lake batholith (e.g., elevated Sn, Th, Fig. 2) by conducting a provenance study on non-quartz mineral intergrowths in placer gold nuggets. Their study focused on the placer deposits of Feather Creek (Fig. 2), known to contain abundant crystalline nuggets that are not rounded, presumably indicating nearby derivation. Nuggets collected from Feather Creek contain diagnostic mineral intergrowths of thorite (ThSiO<sub>4</sub>) and cassiterite (SnO<sub>2</sub>), providing an unambiguous genetic link to the Surprise Lake batholith, which is known to be enriched in U, Th, Sn, Mo, W, and F (Fig. 2), rather than to ultramafic rocks, which lack these elements. In a follow-up study, Mihalynuk et al. (2011) attempted to find similar intergrowths in nuggets from other creeks in the Atlin camp. Although this attempt was unsuccessful, Mihalynuk et al. (2011) found that rare gold nuggets from Otter Creek placers (Fig. 4a) are intergrown with phyllite similar to phyllitic metasedimentary rocks of the regionally extensive 'Kedahda Formation' (Watson and Mathews, 1944) that underlies the local Otter Creek drainage. Unfortunately, this type of country rock is common regionally, providing little help in pinpointing a lode gold source. Conceivably, these nuggets could have been transported by glaciers, either early valley ice that flowed up the Pine Creek drainage, or from continental ice sheets that flowed to the northwest (Fig. 2). However, most of the productive placer gravels in the Atlin camp are located stratigraphically below tills, proglacial outwash, postglacial debris flows, and Holocene channel gravels (Levson, 1992; Levson et al., 2003; Fig. 4b), suggesting that these phyllite-gold nuggets are locally derived.

Understanding the geology of the Otter Creek drainage, and other placer-bearing drainages, is hindered by lack of outcrop. For example, geology of the middle section of Otter Creek drainage was extrapolated by Bloodgood et al. (1989) from adjacent hillsides, which are underlain predominantly by chert and siliciclastic metasedimentary rocks, generally having uncertain contact relations with domains up to 2 km across of massive grey limestone, mafic volcanic, and ultramafic rocks. Bloodgood et al. (1989) also inferred that a south-trending, high-angle fault (Otter Creek fault) extends 9 km from the lower stretches of the drainage to beyond the main fork on the upper creek, where it is presumably beneath colluvial cover. It is extended farther south on the geological compilation of Figure 3.

## 3. Geology of the Otter Creek pit

Excavation during placer mining creates ephemeral bedrock exposures in the creek valleys (Fig. 4b). At active placer operations, these exposures can only be examined for brief periods when mining ceases. Active mining limited our investigation of bedrock at the Slonski operation pit in the



**Fig. 4.** **a)** View of Otter Creek Slonski operation pit on the central stretch of the creek as it appeared in autumn, 2015. Location of the 2015 pit is indicated, as is the future location of the 2016 (near pond) pit seen in b). Farther up the valley, a series of exploration roads are established for placer exploration drilling (drill rig is at the arrow head). **b)** View to the north of the pit bottom as it appeared in early August, 2016. Rusty pay gravels at the far end of the pit are overlain by tan to grey gravel and then dense, jointed basal till (immediately beneath yellow and red pump equipment). Dark grey-brown and tan layers above the till are channel gravels of probable Holocene age (cf. Levson, 1992). Yellow and grey bedrock at the left foreground are phyllites, dipping moderately to the west, an orientation that is common elsewhere in the pit.

middle part of the Otter Creek valley (henceforth referred to as “Otter Creek pit”). Immediately before our visit, gold-bearing veins were discovered in the pit by Doug (Gold Nuggie Dougie) Finlayson during a routine metal detector sweep of bedrock following stripping of pay gravels (Figs. 4, 5). Recovery of another 5-cm angular block of gold-phyllite during placer cleanup (Figs. 5e, f) suggests that gold in bedrock along this section of Otter Creek is not limited to the discovery site.

### 3.1. Graphitic phyllite

Bedrock in the Otter Creek pit is mostly graphitic and siliceous phyllite that typically contains less than 2%, but up to 5% euhedral pyrite cubes (Fig. 6a). Graphite content varies from strongly graphitic to almost graphite-free. Chlorite and muscovite are locally important foliation-defining constituents. However, where individual muscovite flakes are visible (up

to ~1 mm across where coarsest), they tend to be oblique to the foliation. Carbonate and silica contents also vary, probably reflecting differences in protolith compositions. This is consistent with relict interbedded (?) ribbon chert and cherty limestone that are exposed at adjacent mountainsides east and west of the pit (Bloodgood et al., 1989; Fig. 3). Outcrops southwest of the pit are sugary, silica-rich phyllite that is interpreted to be thermally altered interbedded chert and fine-grained siliciclastic strata.

Phyllite foliation orientation generally dips moderately to the west (~175°/50°; Fig. 4b), but does vary to east-southeast-dipping on an outcrop scale. The phyllitic foliation in the pit commonly preserves millimetre-scale intrafolial isoclinal folds indicating that it is a transposition fabric. Carbonate-rich layers commonly display an anastomosing foliation (Fig. 6b).

### 3.2. Dikes

Dikes cut phyllite in the pit (Figs. 7a, b, c) and form angular broken outcrop in the bank of a skid trail northwest of the pit that is coarser (medium grained) and less altered. The dike northwest of the pit is equigranular and light tan-weathering with medium grey fresh surfaces (Fig. 7d). A felted texture is well developed by intergrowth of elongate feldspar and hornblende and is overprinted by carbonate-chlorite alteration such that plagioclase is turbid and hornblende almost completely pseudomorphed by chlorite and epidote (Figs. 7e, f).

In the pit, dikes are cream coloured and form a steeply dipping, northeast-southwest striking set (225°-235°/80°-90°; 052°/79°). They range from a few centimeters to nearly a metre wide (Fig. 7a). Where least altered, they display a fine-grained felted texture. The dikes are strongly altered; the original minerals are replaced by chlorite and calcite (Figs. 7b, c) and only relicts remain. Secondary muscovite forms local booklets lacking a preferred orientation (Figs. 7b, c).

Dikes and local bedrock were analyzed by Inductively Coupled Plasma (ICP) / Mass Spectroscopy (MS) using the analytical package WRA + trace 4Lithoresearch at Activation Laboratories, Ancaster, Ontario. Samples were dissolved following lithium metaborate/tetraborate fusion and major elements were determined by fusion ICP and trace elements by fusion ICP/MS. Geochemical analyses show that, despite their light colour, these altered dikes have basaltic compositions (Fig. 8a). Although alteration resulted in almost complete replacement of igneous mineralogy, it does not appear to have resulted in extensive mobility of major or minor elements, with the exception of Rb. All samples plot in the basalt field with a trend toward trachybasalt on an immobile trace element rock classification plot (Fig. 8a; and basalt to trachybasalt field on major oxide rock classification plot SiO<sub>2</sub> versus Na<sub>2</sub>O+K<sub>2</sub>O of Le Bas et al., 1986, not shown). Dikes within and outside of the pit are chemically similar, especially their immobile trace element compositions (Figs. 8a-d).

Otter Creek dikes are geochemically similar to the mafic to intermediate phases of the Fourth of July batholith (Middle Jurassic) and to andesitic rocks at Atlin Mountain (west of

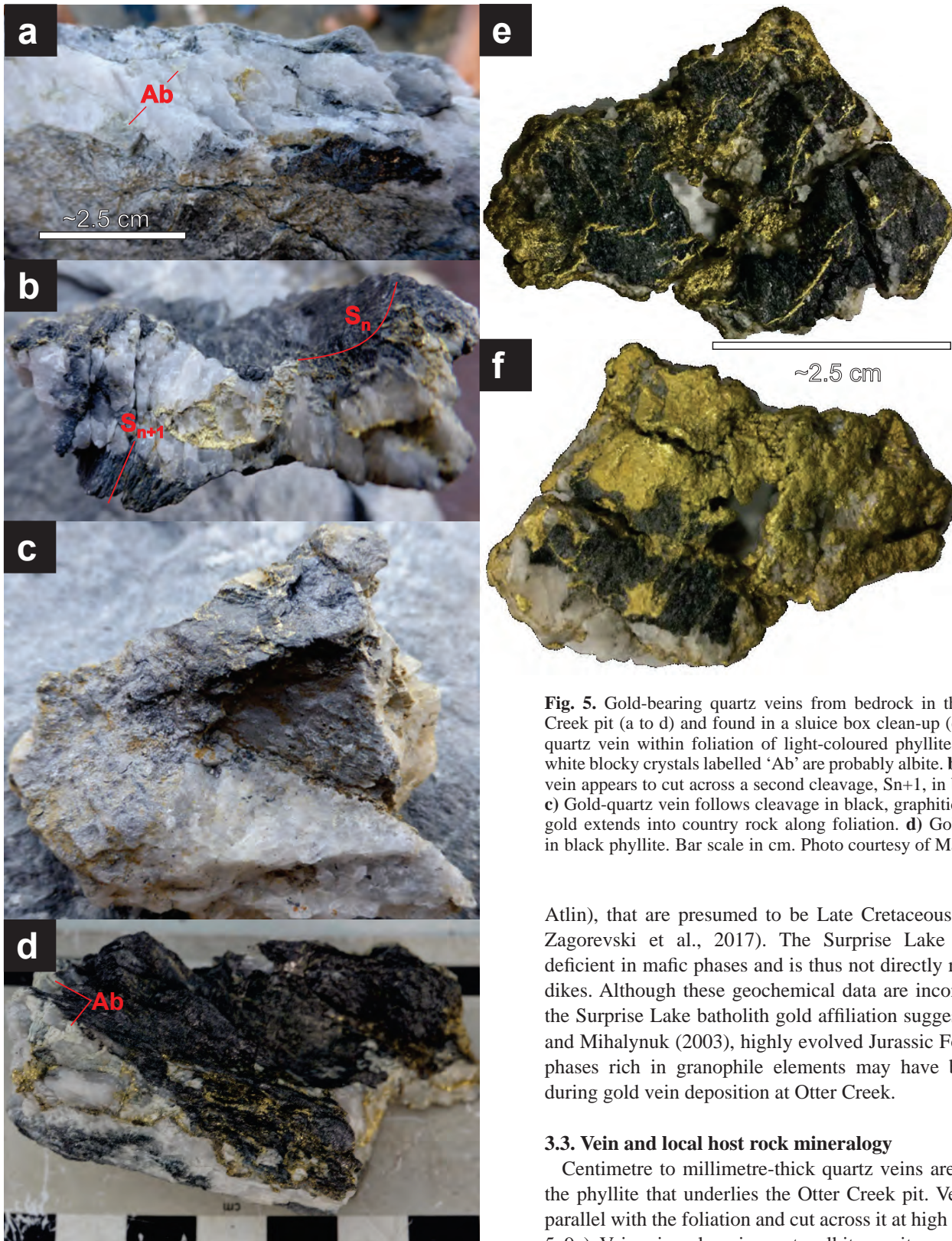


**Fig. 5.** Gold-bearing quartz veins from bedrock in the 2016 Otter Creek pit (a to d) and found in a sluice box clean-up (e, f). **a)** Gold-quartz vein within foliation of light-coloured phyllite. Green-tinted white blocky crystals labelled 'Ab' are probably albite. **b)** Gold-quartz vein appears to cut across a second cleavage,  $S_{n+1}$ , in black phyllite. **c)** Gold-quartz vein follows cleavage in black, graphitic phyllite, and gold extends into country rock along foliation. **d)** Gold-quartz vein in black phyllite. Bar scale in cm. Photo courtesy of Matt Fraser.

Atlin), that are presumed to be Late Cretaceous (Fig. 8, see Zagorevski et al., 2017). The Surprise Lake batholith is deficient in mafic phases and is thus not directly related to the dikes. Although these geochemical data are inconsistent with the Surprise Lake batholith gold affiliation suggested by Sack and Mihalynuk (2003), highly evolved Jurassic Fourth of July phases rich in granophile elements may have been present during gold vein deposition at Otter Creek.

### 3.3. Vein and local host rock mineralogy

Centimetre to millimetre-thick quartz veins are common in the phyllite that underlies the Otter Creek pit. Veins are both parallel with the foliation and cut across it at high angles (Figs. 5, 9a). Vein mineralogy is quartz–albite–pyrite–graphite  $\pm$ rutile

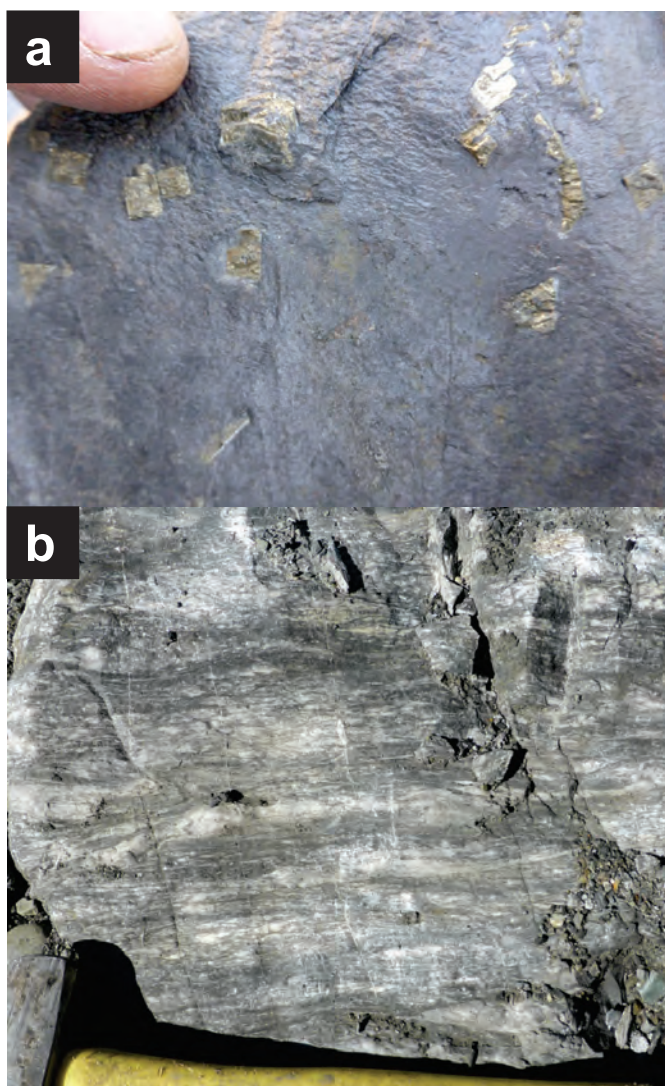


**Fig. 6.** a) Black graphitic phyllite displays zones where coarse euhedral pyrite cubes and aggregates are common. Pyrite grains show fracturing, embayments and deformation to varying degrees. b) Anastomosing fabric in carbonate-rich zone.

and possibly titanite. Both veins and the adjacent enclosing host rocks display this mineralogy. Gold was present in the only gold-bearing vein sample that could be obtained for destructive analyses. Like other veins, this gold-bearing vein contains a conspicuous medium- to coarse-grained, blocky white albite (confirmed by X-Ray Diffraction analysis; see below) that comprises ~5% of the vein volume (Figs. 5a, d, 9b). Albite cleavage planes are invaded by fine pyrite veins (<0.05 mm thick, Fig. 9b).

Phyllite hosting the gold veins commonly contains pyrite, most conspicuously as coarse euhedral cubes in graphitic country rocks. In samples containing gold, pyrite can form framboid-like aggregates (Fig. 9c) or corroded cubes, commonly with abundant irregular inclusions of chalcopyrite (Fig. 9d) and

sparse, minute pyrrhotite inclusions. Pyrite is also intergrown with slender prismatic white crystals that are interpreted as altered titanite (Figs. 9e, f). Graphite is a constituent of many, but not all, rock types that are cut by quartz veins near the lode gold occurrence in the Otter Creek pit. Although graphite can be easily identified in sooty hand samples, in none of our sectioned samples is graphite sufficiently well crystallized to permit it to be unequivocally identified petrographically. Instead, it occurs as a finely dispersed black discolouration of the rock (Fig. 9a). In places, similar dark discolouration seems to be introduced to a quartz-rich host along fractures (Fig. 9f).

Phyllite cut by quartz veins locally contains millimeter-size white mica booklets with no strongly-preferred orientation. They are confirmed by XRD analysis to be muscovite or phengite. Muscovite/phengite probably also defines the phyllitic fabric in some outcrops. XRD analysis of gold-bearing vein material also identified kaolinite, although this mineral has not been observed petrographically, so the relationship to gold-quartz veins is not yet known.

#### 4. Texture and composition of a gold nugget

In 2015, the Slonski placer operations at Otter Creek pit recovered a nugget with a 4 mm to 7 mm gold plate core enveloped by bladed carbonate and quartz. This sample was of particular interest because bladed calcite textures can be produced in hydrothermal veins, during boiling of CO<sub>2</sub>-supersaturated fluid in environments forming epithermal Au-Ag mineralization (Browne and Ellis, 1970; Simmons and Christenson, 1994; Simmons et al., 2005). Approximately two thirds of the surfaces of the gold plate are free of mineral intergrowths and shiny (Figs. 10a, b). Coarse bladed carbonate in the gold nugget is light tan to brown on the weathered surface and tan to white on fresh surfaces. Lesser amounts of milky anhedral quartz are also intergrown with the gold. Subordinate gold plates that grew perpendicular to the vein, between carbonate blades that have been eroded or dissolved, have been subjected to only minor alluvial rounding (Figs. 10a, b).

#### 4.1. SEM-EDS methods

Gold and carbonate of the gold nugget were investigated using Scanning Electron Microscope (SEM) – Energy Dispersive X-ray Spectroscopy (EDS). SEM-EDS analyses were conducted at the University of Victoria (British Columbia) Advanced Microscopy Facility using a Hitachi S-4800 scanning SEM fitted with a Bruker Quantax EDS system. Distilled water and acetone were used to clean the gold nugget sample, which was then dried in a vacuum chamber. Electrical conductivity of most parts of the sample surface are excellent, so conductive coating of the sample was not necessary. Elemental analyses reported here are semi-quantitative, calculated using ( $\rho z$ ) matrix corrections without using a standard. They were obtained using operating conditions optimized for EDS analysis of both points and fields on the grains. Working distance was set to ~15 mm with a beam voltage of 20kV.

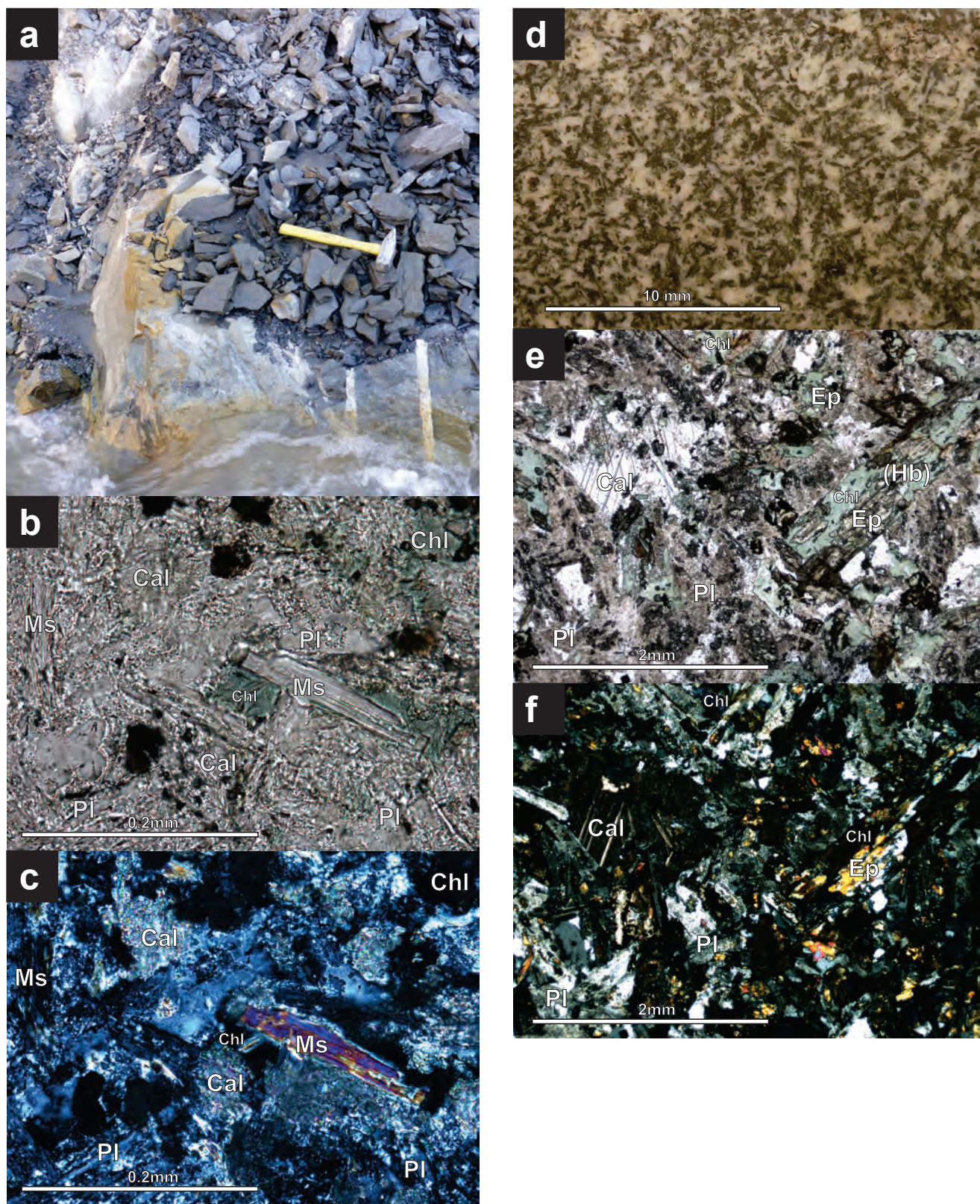


**Fig. 7.** **a**) View towards the northeast of a prominent set of white dikes (below and left of hammer) ranging from a few centimetres to ~0.75 m thick. Angular slabs of broken graphitic phyllite blanket the outcrop beneath hammer. **b**) Secondary muscovite booklets (Ms) have no preferred orientation. **c**) Same field of view as **b**) under cross-polarized light. **d**) Felted texture of blocky dike nearcrop from outside of the pit. **e**) Photomicrograph under transmitted, plane-polarized light, of altered dike shows carbonate (Cal), chlorite (Chl), and epidote (Ep) alteration. Plagioclase (Pl) is turbid from alteration to fine secondary minerals. Hornblende (Hb) is completely replaced by chlorite and epidote. **f**) Same field of view as **e**) under cross-polarized light.

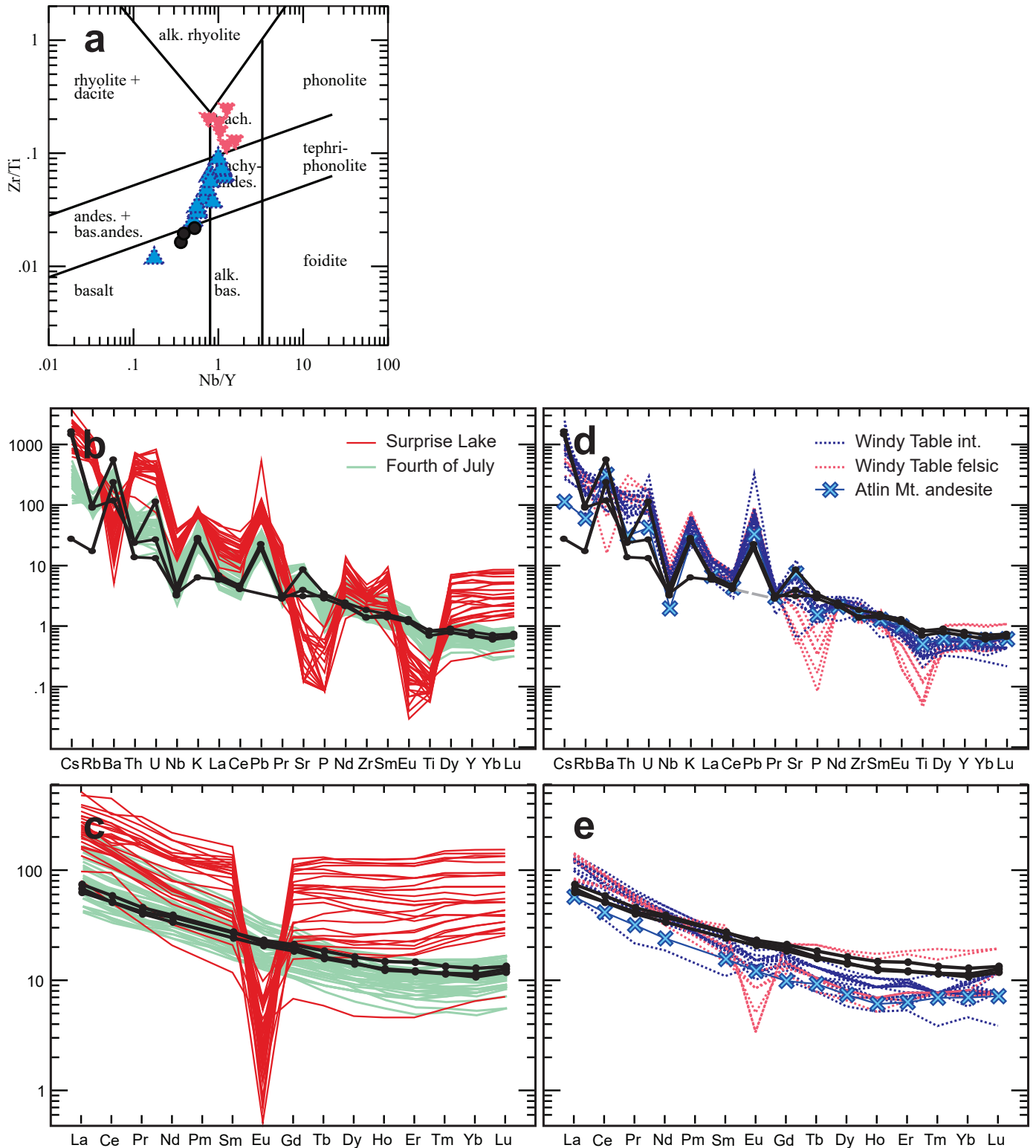


**Fig. 8.** Geochemistry of dikes inside and adjacent to the Otter Creek pit location (as of August, 2016). **a)** Dike compositions (black points) are plotted with respect to the compositional fields of Windy-Table felsic (red inverted triangles) and intermediate volcanic rocks (blue triangles). **b)** Otter Creek dikes (black) plotted on Primitive Mantle-normalized extended element plot with Surprise Lake (red) and Fourth of July (green) compositions. **c)** Like b), but for rare earth elements only. **d)** Like b), but showing Windy Table intrusive (blue dotted) and felsic volcanic (red dotted) compositions for comparison. **e)** Like c), but for rocks in legend of d). Data from all rocks other than Otter Creek dikes are from Zagorevski et al. (2017).

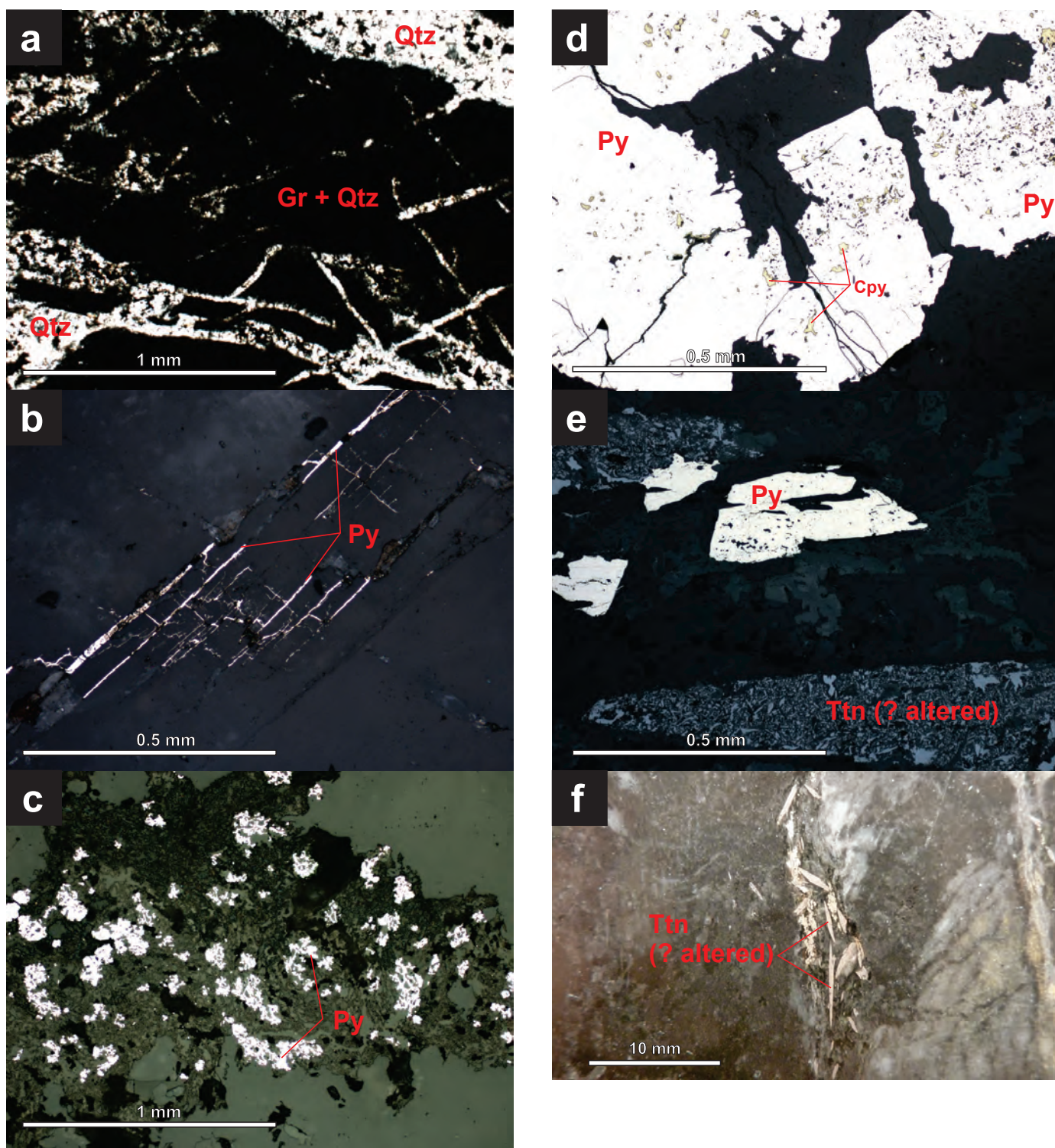


**Fig. 9.** Veins and vein mineralogy from bedrock in the Otter Creek pit. **a)** Plane polarized, transmitted light view of graphitic quartz-rich rock (black, Gr + Qtz) is cut by fine-grained quartz (Qtz). **b)** Reflected light view of albite with veinlets of pyrite (white, Py) along cleavage planes. **c)** Highly reflective (white, Py) framboid-like texture of pyrite in host rock adjacent to, and as patches in, gold-bearing veins. **d)** Reflected light view of corroded pyrite crystals (white, Py) containing abundant inclusions of yellow chalcopyrite (Cpy). Rare pyrrhotite inclusions are too small to see at this magnification. **e)** Corroded pyrite grains (cream, Py) in quartz-rich rock is intergrown with mineral tentatively identified as altered titanite (Ttn (?altered)), polycrystalline grey and black, upper left and lower). **f)** The slab of rock from which the polished section in e) was made. Irregular quartz veins along the right side and with slender, euhedral “Ttn? altered” cut the black (graphitic) and white quartz-rich rock.

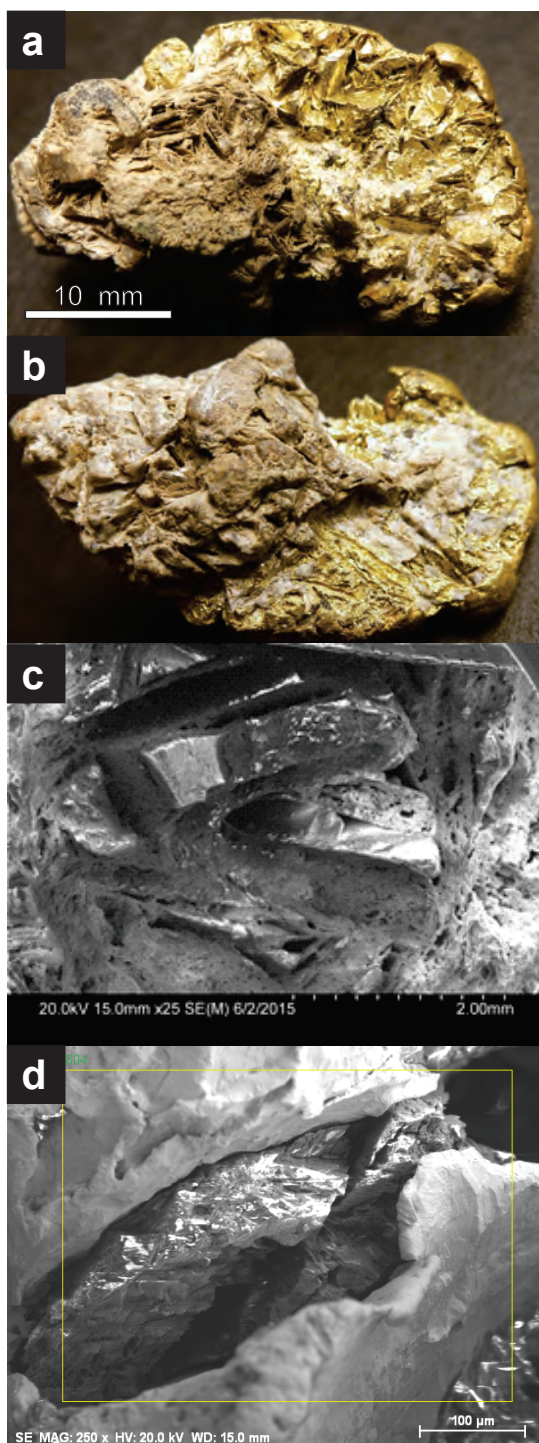


**Fig. 10.** a) Gold nugget with attached siliceous material shows evidence of bladed mineral moulds formed by gold and the siliceous rock material. Bladed calcite in hydrothermal deposits can take this form when crystallized rapidly from boiling fluids which leads to saturation and precipitation of metals carried in the fluid, including gold (thickness of the gold seam forming the nugget is 4 mm to 7 mm). b) Opposite side of nugget in a). c) Scanning Electron Microscope backscattered electron image showing a detailed view of the euhedral rhombic corner of the bladed mineral and moulds. d) Dissolution interface between carbonate displaying rhombic cleavage (dark grey with brightly highlighted crystal faces) and enclosing gold (light grey and amorphous).

#### 4.2. SEM-EDS results

Back Scatter Electron imaging (BSE) of the gold-carbonate intergrowths confirm the macroscopic relationships (Fig. 10c), but also shows that there was dissolution along the gold-carbonate interface (Figs. 10d, 11). EDS analysis shows that gold contains significant Ag, and traces of Hg (Figs. 11b, c). Silver contents are consistent with findings of Hora et al. (2012) from samples collected on Ruby and Wright creeks in the Altin placer camp (Fig. 2), where silver-in-gold values range up to 30 wt.%. Both copper and platinum may be present at concentrations of up to ~1 wt.%.

#### 5. Gold vein genesis

Chronology of the regional deformation fabrics cut by veins and dikes in the Otter Creek pit is bracketed by the age of the youngest deformed unit (Bajocian, south of the Otter Creek area) and the age of the oldest intrusions that cut the fabrics (~172 Ma). Chronology of the gold-bearing quartz vein emplacement is more difficult to constrain. These veins clearly cut the foliation in the phyllite in the Otter Creek pit and, if formed during regional deformation, this foliation pre-dates the Fourth of July batholith (~172 Ma; Mihalynuk et al., 2004; Harris et al., 2003). However, veining in the Otter Creek pit appears to be cut by the altered dikes that are geochemically similar to the Fourth of July batholith (Fig. 8).

Altered dikes, and country rocks contain muscovite lacking a preferred orientation and gold-quartz veins are intergrown with muscovite of similar character. A sample of coarse muscovite-pyrite-quartz vein (Fig. 12) derived from bedrock during mining was salvaged from the wash plant. A muscovite separate from this vein yielded a preliminary  $^{40}\text{Ar}/^{39}\text{Ar}$  age of ~160 Ma (A. Camacho, pers. comm., 2016) and efforts to refine this determination are ongoing. Muscovite from the sample of the gold-quartz vein collected from the Otter creek pit for destructive analyses will be evaluated for suitability of dating by the in-situ laser  $^{40}\text{Ar}/^{39}\text{Ar}$  technique.

It seems most likely that gold-quartz veins in the Otter Creek area immediately post-date ~174 Ma deformation and immediately predate, or are broadly synchronous with, cooling of the Fourth of July batholith. The batholith crystallized at ~172 Ma, was cut by comagmatic mafic and then possible lamprophyre dikes with  $^{40}\text{Ar}/^{39}\text{Ar}$  mineral closure ages between ~165 and ~162 Ma (Harris et al., 2003), and cooled through the K-Ar closure temperature of sericite by ~160 Ma (Dawson, 1988 in Breitsprecher and Mortensen, 2004). Establishing the exact relationship of gold-quartz veins with the dikes in Otter Creek and establishing the age of both will be necessary to fully understand lode gold deposition in the Otter Creek valley.

#### 6. Summary and implications for regional exploration

So far, only a single set of quartz veins containing coarse gold has been recorded in bedrock of the Otter Creek valley. From the existing evidence, it seems likely that the phyllite-hosted gold-bearing quartz veins in Otter Creek were emplaced following Jurassic regional deformation, and synchronous to,

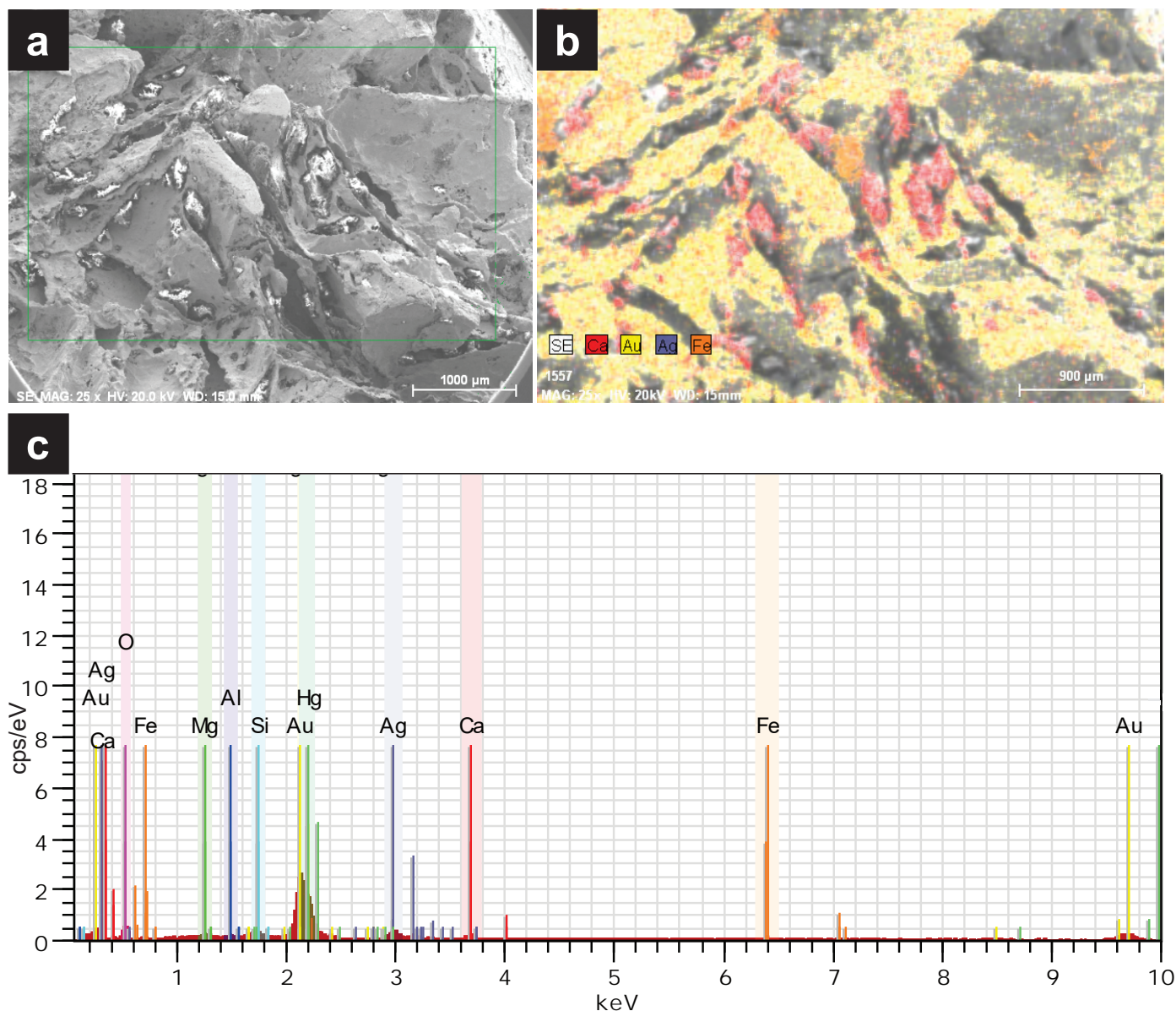


**Fig.11. a)** Scanning Electron Microscope backscattered electron image of corroded relicts of carbonate grains within gold. **b)** Elemental map of the same surface as shown in a). **c)** Induced X-ray energy spectrum of the area outlined in A, showing calcium, Ca-K $\alpha$  (characteristic X-rays emitted during transitions from K, L, and M shell induced vacancies are shown), gold, Au-MAB, silver, Ag-L $\alpha$ , silicon, Si-K $\alpha$ , aluminum, Al-K, O-K, iron, Fe-K $\alpha$ , magnesium, Mg-K, and mercury, Hg-M $\alpha$  counts. All peaks are accounted for. Notable are silver and mercury (Ag, Hg) as impurities in the gold. Accelerating voltage for this analysis was 20.0 kV.

or immediately preceding emplacement of crosscutting dikes that share geochemical characteristics with the Fourth of July batholith and other bodies of the Three Sisters suite (Fig. 8; see Zagorevski et al., 2017). Secondary muscovite in the dikes, gold veins, and unmineralized quartz veins lacks a strongly-preferred orientation. Preliminary  $^{40}\text{Ar}/^{39}\text{Ar}$  data indicate growth of this static muscovite at ca. 160 Ma, which is broadly coeval with cooling age determinations from the Fourth of July Batholith. In terms of phyllitic sedimentary host rocks, the Otter Creek lode occurrence is similar to well-known gold deposits like Maruntau (Uzbekistan) where nearby magmatic

rocks may be important (Kempe et al., 2016) or Macraes (New Zealand) where modern noble gas analytical techniques point to metamorphic fluid transport of gold (Goodwin et al., 2016).

Lode gold discovered along Otter Creek is in weakly metamorphosed sedimentary rocks of the Kedahda Formation, one of the most widespread units in the northern Cache Creek terrane. The Otter Creek discovery unequivocally demonstrates that lode gold mineralization is not restricted to zones in, or immediately adjacent to, listwanite-altered ultramafic or mafic rocks, significantly expanding areas near Atlin that are prospective for lode gold exploration.

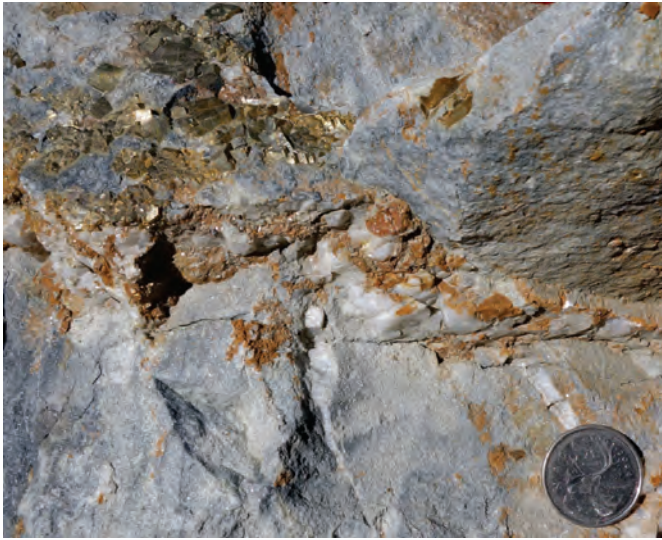


**Fig. 12.** Sample of quartz and coarse pyrite-muscovite veining in semi-schist from Otter Creek valley bedrock. This bedrock sample was collected from the placer washing plant and a sample of the coarse muscovite was submitted for  $^{40}\text{Ar}/^{39}\text{Ar}$  age determination, yielding a preliminary age of ~160 Ma (see text).

### Acknowledgments

Peter Shorts has been a generous supporter of our work, and together with Glen Slonski provided access to the Otter Creek Mining pits in 2015 and 2016, and donated gold-bearing quartz vein materials for destructive analyses. Peter Shorts, Glen Slonski and John Buckle provided editorial comments and clarifications on an earlier draft. Jean Pautler shared a collection of samples from the 2016 Otter Creek Mines pit. Discussions and correspondence with Jeff Kyba were illuminating and appreciated. We thank Atlin placer operators and supporters for their enduring encouragement, tolerance and willingness to share information in the furtherance of lode gold exploration in the region.

### References cited

- Aitken, J.D., 1959. Atlin map-area, British Columbia. Geological Survey of Canada, Memoir 307, 89p.
- Ash, C.H., 1994. Origin and tectonic setting of ophiolitic ultramafic and related rocks in the Atlin area, Northwestern British Columbia. BC Ministry of Energy, Mines and Petroleum Resources, British Columbia Geological Survey, Bulletin 94, 140p.
- Ash, C.H., 2004. Geology of the Atlin area, northwestern British Columbia. British Columbia Ministry of Energy and Mines, BC Geological Survey, Geoscience Map 2004-4, scale 1:25,000.
- Ash, C.H., MacDonald, R.W., and Reynolds, P.R., 2001. Relationship between ophiolites and gold-quartz veins in the North American Cordillera. BC Ministry of Energy and Mines, British Columbia Geological Survey, Bulletin 108, 140p.
- BC Geological Survey, 2016. MINFILE Mineral Inventory database. URL < <http://minfile.ca/> > November, 2016.
- Bloodgood, A., Rees, C.J., and Lefebvre, D.V., 1989. Geology of the Atlin area (NTS 104N/11W, 12E). BC Ministry of Energy, Mines and Petroleum Resources, British Columbia Geological Survey, Open File 1989-15, scale: 1:50,000.
- Breitsprecher, K., and Mortensen, J.K., 2004. BCAGE 2004A-1- a database of isotopic age determinations for rock units from British Columbia. BC Ministry of Energy and Mines, British Columbia Geological Survey, Open File 2004-03 (Release 2.0), 7766 records, 9.3 Mb.
- Browne, P.R.L., and Ellis, A.J., 1970. The Ohaki-Broadlands hydrothermal area, New Zealand; mineralogy and related geochemistry. *American Journal of Science*, 269, 97-131.
- Cairnes, D.D., 1913. Portions of Atlin District, British Columbia: with Special Reference to Lode Mining. Geological Survey of Canada, Memoir 37, 129p.
- Cohen, K.M., Finney, S.C., Gibbard, P.L., and Fan, J.X., 2013. The ICS International Chronostratigraphic Chart. *Episodes*, 36, 199-204.
- Cui, Y., Miller, D., Nixon, G., and Nelson, J., 2015. British Columbia digital geology. BC Ministry of Energy and Mines, British Columbia Geological Survey, Open File 2015-2.
- Debicki, R.L., 1984. An Overview of the Placer Mining Industry in Atlin Mining Division, 1978 to 1982. British Columbia Ministry of Energy, Mines and Petroleum Resources, Geological Branch, Paper 1984-2, 21p.
- Ferguson, H.G., and Gannett, R.W., 1932. Gold quartz veins of the Alleghany district, California. US Department of the Interior, Geological Survey Professional Paper 172, 139p.
- Goodwin, N.R., Burgess, R., Craw, D., Teagle, D.A., and Ballentine, C.J., 2016. Noble gases fingerprint a metasedimentary fluid source in the Macraes orogenic gold deposit, New Zealand. *Mineralium Deposita*, 1-13. doi:10.1007/s00126-016-0648-x.
- Gwillim, J.C., 1901. Atlin mining district. Annual Report 1899, Geological Survey of Canada, Volume 12, 48p. doi:10.4095/294883.
- Harris, M.J., Symons, D.T., Blackburn, W.H., Hart, C.J., and Villeneuve, M., 2003. Travels of the Cache Creek Terrane: a paleomagnetic, geobarometric and  $^{40}\text{Ar}/^{39}\text{Ar}$  study of the Jurassic Fourth of July Batholith, Canadian Cordillera. *Tectonophysics*, 362, 137-159.
- Hora, Z.D., Pivec, E., and Langrova, A., 2012. Irsasite (IrAsS), Osarsite (OsAsS) and Gold from Placer Black Sands, Ruby Creek and Wright Creek, Atlin, British Columbia. In: *Geological Fieldwork 2011*, BC Ministry of Energy, Mines and Petroleum Resources, Paper 2012-1, pp. 11-15.
- Kempe, U., Graupner, T., Seltmann, R., de Boorder, H., Dolgoplova, A., and van Emmichoven, M.Z., 2016. The Muruntau gold deposit (Uzbekistan)—A unique ancient hydrothermal system in the southern Tien Shan. *Geoscience Frontiers*, 7, 495-528.
- Le Bas, M.J.L., Maitre, R.W.L., Streckeisen, A., and Zanettin, B., 1986. A Chemical Classification of Volcanic Rocks Based on the Total Alkali-Silica Diagram. *Journal of Petrology*, 27, 745-750, doi: 10.1093/petrology/27.3.745.
- Levson, V.M., Kerr, D.E., Lowe, C., and Blyth, H., 2003. Quaternary geology of the Atlin area, British Columbia; BC Ministry of Energy, Mines and Petroleum Resources, British Columbia Geological Survey Branch, Geoscience Map 2003-1 and Geological Survey of Canada, Open File 1562. Scale 1:50,000.
- Levson, V.M., 1992. Quaternary Geology of the Atlin area; (104N/11W, 104N/12E). In: *Geological Fieldwork 1991*, BC Ministry of Energy and Mines, British Columbia Geological Survey Branch, Paper 1992-1, pp. 375-390.
- Mihalynuk, M.G., Ambrose, T.K., Devine, F.A.M., and Johnston, S.T., 2011. Atlin placer gold nuggets containing mineral and rock matter: implications for lode gold exploration. In: *Geological Fieldwork 2010*, BC Ministry of Energy, Mines and Petroleum Resources, British Columbia Geological Survey Branch, Paper 2010-1, pp. 56-72.
- Mihalynuk, M.G., Erdmer, P., Ghent, E.D., Cordey, F., Archibald, D.A., Friedman, R.M., and Johannson, G.G., 2004. Coherent French Range blueschist: Subduction to exhumation in < 2.5 m.y.? *Geological Society of America Bulletin*, 116, 910-922, 7-8. doi: 10.1130/b25393.

- Mihalynuk, M.G., Mountjoy, K.J., Smith, M.T., Currie, L.D., Gabites, J.E., Tipper, H.W., Orchard, M.J., Poulton, T.P., and Cordey, F., 1999. Geology and mineral resources of the Tagish Lake area (NTS 104M/ 8,9,10E, 15 and 104N/ 12W), Northwestern British Columbia. BC Ministry of Energy and Mines, British Columbia Geological Survey Branch, Bulletin 105, 202p.
- Mihalynuk, M.G., Meldrum, D., Sears, S., and Johannson, G., 1995. Geology and mineralization of the Stuhini Creek area (104K/ 11). In: Geological Fieldwork 1994, British Columbia Ministry of Energy, Mines and Petroleum Resources, Paper 1995-1, pp. 321-342.
- Monger, J., 1975. Upper Paleozoic rocks of the Atlin Terrane, northwestern British Columbia and south-central Yukon. Paper 74-47, Geological Survey of Canada, Paper 74-47, 73p.
- Monger, J.W.H., Price, R.A., and Tempelman-Kluit, D.J., 1982. Tectonic accretion and the origin of the two major metamorphic and plutonic belts in the Canadian Cordillera. *Geology*, 10, 70-75.
- Price, B.J., and Dandy, L., 2010. Yellowjacket gold project. 43-101 Technical report prepared for Eagle Plains Resources Ltd. and Prize Mining Corporation, January 27, 2010, 92p.
- Robertson, W.F., 1898. Cassiar district. In: Annual report of the Minister of Mines, Province of British Columbia, pp. 985-991.
- Sack, P.J., and Mihalynuk, M.G., 2003. Proximal gold cassiterite nuggets and composition of the Feather Creek placer gravels: clues to a lode source near Atlin, BC. In: Geological Fieldwork 2003, BC Ministry of Energy, Mines and Petroleum Resources, British Columbia Geological Survey Branch, Paper 2004-1 pp. 147-162.
- Shirmohammad, F., Smith, P., Anderson, R., and McNicoll, V., 2011. The Jurassic succession at Lisadele Lake (Tulsequah map area, British Columbia, Canada) and its bearing on the tectonic evolution of the Stikine terrane. *Volumina Jurassica*, 9, 43-60.
- Simmons, S.F., White, N.C., and John, D.A., 2005. Geological characteristics of epithermal precious and base metal deposits. In: *Economic Geology 100th Anniversary Volume*, Jeffrey W. Hedenquist, John F. H. Thompson, Richard J. Goldfarb, and Jeremy P. Richards (Editors), pp. 485-522.
- Simmons, S.F., and Christenson, B.W., 1994. Origins of calcite in a boiling geothermal system. *American Journal of Science*, 294, 361-400.
- Watson, K.D., and Mathews, W.H., 1944. The Tuya-Teslin area, northern British Columbia. British Columbia Department of Mines, Bulletin 19, 52p.
- Zagorevski, A., Mihalynuk, M.G., Joyce, N., and Anderson, R.G., 2017. Late Cretaceous magmatism in the Atlin-Tagish area, northern British Columbia (104M, 104N). In: Geological Fieldwork 2016, British Columbia Ministry of Energy and Mines, British Columbia Geological Survey Paper 2017-1, this volume.



# Geological setting of the Rock Canyon Creek REE-fluorite deposit, British Columbia, Canada



Craig Green<sup>1</sup>, George J. Simandl<sup>1,2,a</sup>, Suzanne Paradis<sup>3</sup>, Fiona Katay<sup>4</sup>, Mihoko Hoshino<sup>5</sup>, Yoshiaki Kon<sup>5</sup>, Shinsuke Kodama<sup>5</sup>, and Chris Graf<sup>6</sup>

<sup>1</sup>School of Earth and Ocean Sciences, University of Victoria, BC, V8P 5C2

<sup>2</sup>British Columbia Geological Survey, Ministry of Energy and Mines, Victoria, BC, V8W 9N3

<sup>3</sup>Geological Survey of Canada, Natural Resources Canada, Sidney, BC, V8L 4B2

<sup>4</sup>British Columbia Ministry of Energy and Mines, Cranbrook, BC, V1C 3P9

<sup>5</sup>Geological Survey of Japan, National Institute of Advanced Industrial Science and Technology

<sup>6</sup>Spectrum Mining Corporation, Wardner, BC, V0B 2J0

<sup>a</sup>corresponding author: George.Simandl@gov.bc.ca

Recommended citation: Green, C., Simandl, G.J., Paradis, S., Katay, F., Hoshino, M., Kon, Y., Kodama, S., and Graf, C., 2017. Geological setting of the Rock Canyon Creek REE-fluorite deposit, British Columbia, Canada In: Geological Fieldwork 2016, British Columbia Ministry of Energy and Mines, British Columbia Geological Survey Paper 2017-1, pp. 195-203.

## Abstract

The Rock Canyon Creek REE-fluorite deposit is in the Foreland Fold and Thrust belt of the Canadian Cordillera, 300 metres east of the Munroe Lake thrust fault which, in the deposit area, divides the Main Ranges from the Front Ranges of the Canadian Rocky Mountains. A literature review and preliminary fieldwork indicate that the deposit is hosted by Middle Devonian rocks of the Cedared and Burnais formations and consist mainly of dolostone, breccia, and laminated silty, calcareous gypsum. Fluorite-bearing outcrops extend across an area 3300 by 750 metres. The steeply dipping REE-fluorite zone was intersected by drilling. It may be more than 50 metres thick for more than 1100 metres along strike, and to a depth of 124 metres. It remains open along strike and dip, and its thickness locally exceeds 50 metres. Based on surface mapping and borehole logging, the deposit appears to be concordant with stratigraphy. Most of the mineralization occurs as breccias and fracture fillings in fluorite-impregnated dolostone. Fluorite concentrations vary from less than 1% to 13.5% by weight, and light REE (Ce+La+Nd) concentrations vary from trace to 2.8%. REE are hosted mainly by bastnasite-(Ce), parisite-(Ce), synchysite-(Ce), and REE-bearing phosphates. Ongoing work will focus on better characterizing the deposit to address questions about the origin of ore forming fluids and the temporal, structural, and stratigraphic relationship to Mississippi Valley-type and sparry magnesite deposits along the eastern flank of the Canadian Cordillera.

**Keywords:** Rare earth elements, fluorite, breccia, Cedared Formation, Burnais Formation

## 1. Introduction

The Rock Canyon Creek deposit, 90 kilometres northeast of Cranbrook (Fig. 1), contains rare earth elements (REE) and fluorite. The term REE is commonly used to cover lanthanides, yttrium and scandium. The geology of REE is summarized by Mariano (1989a, b, 2012), Simandl et al. (2012a), Simandl (2014), and market conditions are summarized by Simandl (2014) and Gambogi (2016 a, b). In 2015, more than 85% of REE production came from one jurisdiction (China). These elements are considered 'critical metals' due to the high risk of supply disruption, and the importance of REE for many industries, including national defense and those addressing greenhouse gas emissions (Simandl et al., 2015). Fluorspar, the commercial term for fluorite (CaF<sub>2</sub>) is an important industrial mineral with metallurgical applications.

Of the 44 known REE occurrences in British Columbia, all but one (Riddle Creek prospect, Trofanenko et al., 2013) are in the British Columbia alkaline province, along the boundary between the Omineca and Foreland belts (Fig. 1; Pell, 1994; Simandl et al., 2012a, b). The province consists of intrusive and extrusive carbonatites, nepheline and sodalite syenites,



**Fig. 1.** Location of the Rock Canyon Creek REE-fluorite deposit. The British Columbia alkaline province as defined by Pell (1994) is in red.

ijolite series rocks, kimberlite, and numerous ultramafic and lamprophyre diatremes, breccias, and dikes (Pell, 1994). Most, if not all, of these rocks intruded Cordilleran miogeoclinal strata. The Rock Canyon Creek REE-fluorite deposit is one of the most promising REE prospects in the alkaline province. Fluorite occurrences in British Columbia were inventoried and described by Pell (1992), and the Rock Canyon Creek is one of the deposits recommended for follow-up studies (Simandl, 2009).

The purpose of this paper is to summarize the tectonic, stratigraphic, and structural setting of the deposit, and its geometry and mineralogy. It is based on a review of the literature, a field reconnaissance, and logging of core from boreholes drilled by Spectrum Mining Corporation in 2009. The paper is a prelude to more detailed field and laboratory studies directed at establishing the origin of the Rock Canyon Creek deposit and possible relationships to other carbonate-hosted deposits in eastern British Columbia.

## 2. Tectonic setting

The Rock Canyon Creek deposit is in the Foreland Fold and Thrust belt of the Canadian Cordillera (e.g., Gabrielse et al., 1991; Monger and Price, 2002). It lies in the footwall of the Munroe Lake thrust (Fig. 2), which divides the Main Ranges from the Front Ranges of the southern Canadian Rocky Mountains (Mott, 1989). Late Jurassic to early Tertiary thin-skinned folding and thrusting in the Rocky Mountains affected miogeoclinal and foreland basin sedimentary rocks deposited on top of crystalline Precambrian basement (e.g., Price and Fermor, 1985; Monger and Price, 2002). Several diatremes and intrusions in the region may be related to deep transverse basement structural features (McMechan, 2012). Such intrusions have not been recognized near the Rock Canyon Creek REE-fluorite mineralization.

## 3. Geology of the Rock Canyon Creek area

The geology of the Rock Canyon Creek area (Figs. 2, 3) was mapped by Leech (1979), Mott (1989), and McMechan and Leech (2011). The interpretation shown in Figure 2 is based largely on the work of McMechan and Leech (2011). The location of the postulated Rock Canyon Creek fault is from Mott (1989). The distribution of fluorite occurrences is from Dix (1991), and Pell (1992), and the location and extent of the main zone is based on drill hole intersections (Pighin, 2010). The stratigraphic units and the orientation of the faults have a general northwest-southeast trend.

### 3.1. Stratigraphy

The oldest strata in the Rock Canyon Creek deposit area are part of the McKay Group Unit A (Fig. 2; Upper Cambrian-Lower Ordovician; Mott, 1989; McMechan and Leech, 2011). This 400-600 metre thick cliff-forming unit consists of dark grey, brown-weathering, limestone and dolostone with resistant siliceous or silty laminations. Local intraformational flat-pebble conglomerates and light blue-grey-weathering nodular

to lenticular chert horizons are in the upper 30 metres of the unit (McMechan and Leech, 2011). Fossil debris near the upper contact with the Glenogle Formation contains the Tremadocian (ca. 485-477 Ma) brachiopod *Nanorthis cf. N. putillus* (Mott, 1989).

The Glenogle Formation (Lower Ordovician) conformably overlies the McKay Group, and the contact is usually an abrupt planar surface (Mott, 1989). The Glenogle Formation is up to 175 metres thick, and grades upward from a graptolitic black shale to siltstone unit, to quartz arenite, to platy to thickly bedded mottled limestone and dolostone (Mott, 1989; McMechan and Leech, 2011). Black chert nodules are common in the upper carbonate rocks. The upper limestone and dolostone contain 1-2% crinoid, brachiopod, and gastropod fossil debris (Mott, 1989).

The Skoki Formation (Middle Ordovician) disconformably overlies carbonate rocks of the Glenogle Formation. About 150 metres thick, it consists of thickly bedded resistant, dark to pale grey dolostone with abundant chert nodules (10-30%), wavy laminae, and fossil debris (Mott, 1989; McMechan and Leech, 2011). The Skoki Formation is distinguished from the overlying Beaverfoot Formation by the absence of fossil coral (Mott, 1989).

The Skoki Formation is commonly overlain by a thin (<10 metres) but laterally persistent Upper Ordovician dolomite-quartz arenite unit. It may be the basal siliciclastic component of the Beaverfoot Formation (Mott, 1989) or a distinct formation, the Akanko Creek (McMechan and Leech, 2011). South of the map area, the contact between this siliciclastic unit and the underlying Skoki Formation is an angular unconformity (Mott, 1989).

A conglomerate unit (McMechan and Leech, 2011) at the base of the Beaverfoot Formation (Upper Ordovician-Lower Silurian) is overlain by pale grey, spheroidal weathering dolostones (Mott, 1989) with abundant corals (Pell and Hora, 1986) and silicified skeletal debris (crinoids and brachiopods; Mott, 1989). The combined thickness of the Akanko Creek unit and the Beaverfoot Formation is approximately 150 metres (Mott, 1989).

Hosting the Rock Canyon Creek deposit, the Cedared and Burnais formations (Middle Devonian) disconformably overlie the Beaverfoot Formation and have a combined thickness of 75-100 metres (Mott, 1989). They consist of orange-brown weathering dolostone, and pale-weathering quartz-bearing dolostone of the Cedared Formation (Fig. 4a), and breccia, and laminated grey to dark grey silty, calcareous gypsum of the Burnais Formation (Mott, 1989). The Cedared and Burnais are portrayed as a single unit on the map of McMechan and Leech (2011). Fossils and fossil debris include uncommon fish fragments, gastropod, crinoid and brachiopod debris (Mott, 1989). In the Rock Canyon Creek area they are separated from the Beaverfoot Formation by the Munroe Lake thrust fault.

The Fairholme Group (Upper Devonian), which is approximately 100 metres thick, disconformably overlies the Cedared and Burnais formations, and has been interpreted as an

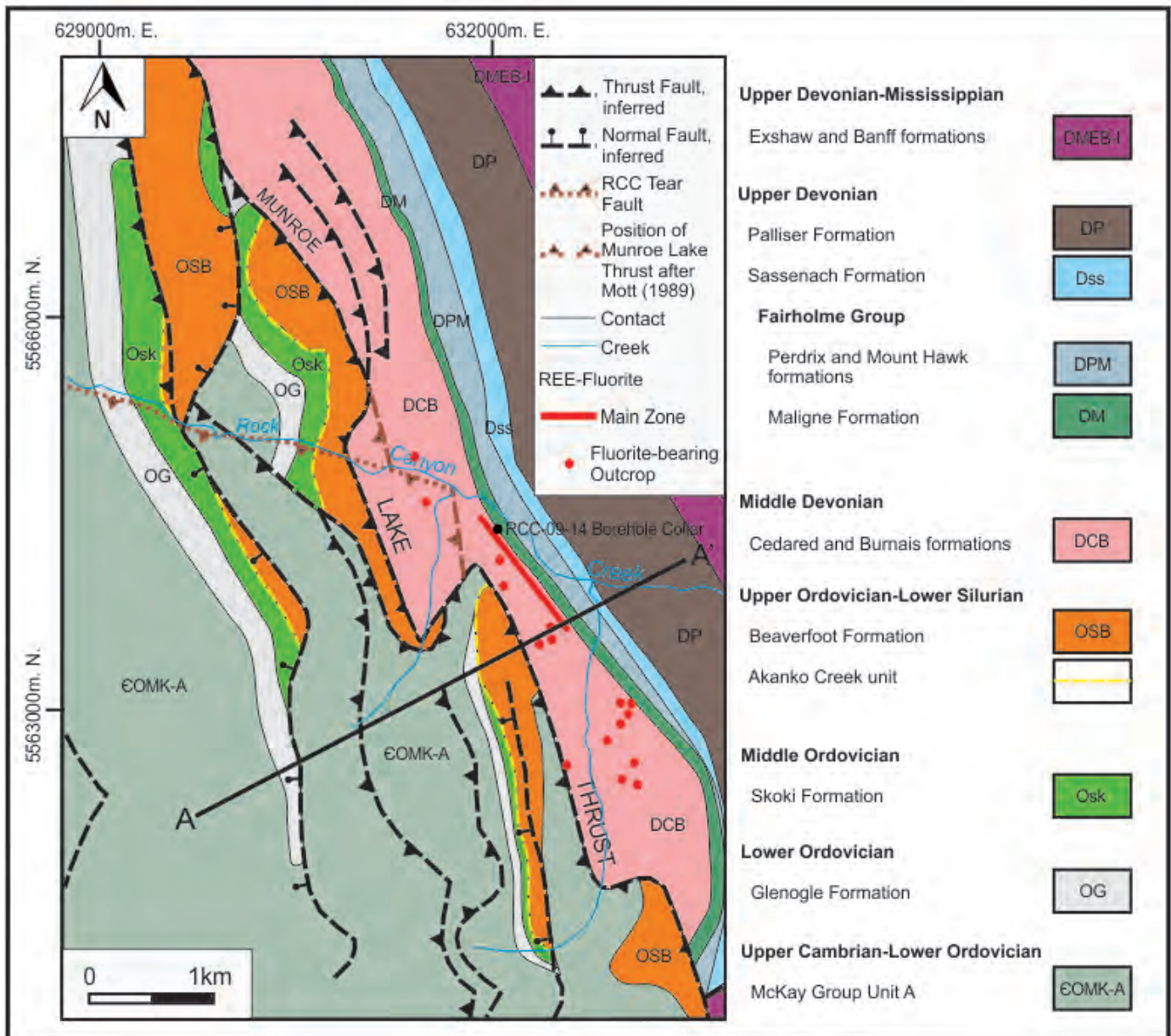


**Fig. 2.** Geological setting of the Rock Canyon Creek deposit. Modified after McMechan and Leech (2011). An alternative interpretation from Mott (1989) includes a west-northwest-trending fault (Rock Canyon Creek tear fault) in brown.

off-reef facies by McMechan and Leech (2011). The Fairholme Group has been further divided by McMechan and Leech (2011) into the basal Maligne Formation, and upper Perdrix and Mount Hawk formations (Fig. 2). The basal Maligne Formation is a dark-grey to black, buff weathering, fossiliferous, lime mudstone with a silty siliciclastic component. Mott (1989) also noted a late Givetian (late Middle Devonian) *disparilis* conodont zone at the base of the Fairholme in the Rock Canyon Creek area. The Perdrix and Mount Hawk formations are fissile dark grey to black calcareous, thinly bedded mudstones and shales with up to 1% fossil fragments (Mott, 1989; McMechan and Leech, 2011).

The Sassenach Formation, up to 200 metres thick at Rock

Canyon Creek, is Upper Devonian and consists of siltstone and sandstone, with local argillaceous limestone near its top and base (McMechan and Leech, 2011).

The Palliser Formation (Upper Devonian) is locally divided into a lower, cliff-forming unit and an upper recessive unit. The cliff-forming unit is a light grey weathering, massive micritic limestone and dolostone, that is locally peloidal and mottled by burrows. The recessive unit consists of grey weathering, thinly bedded lime mudstone, which is similar to the upper Fairholme Group (Mott, 1989; McMechan and Leech, 2011). Regionally, the Palliser Formation may be more than 600 metres thick (Mott, 1989).

Together, the Exshaw and Banff formations (Upper

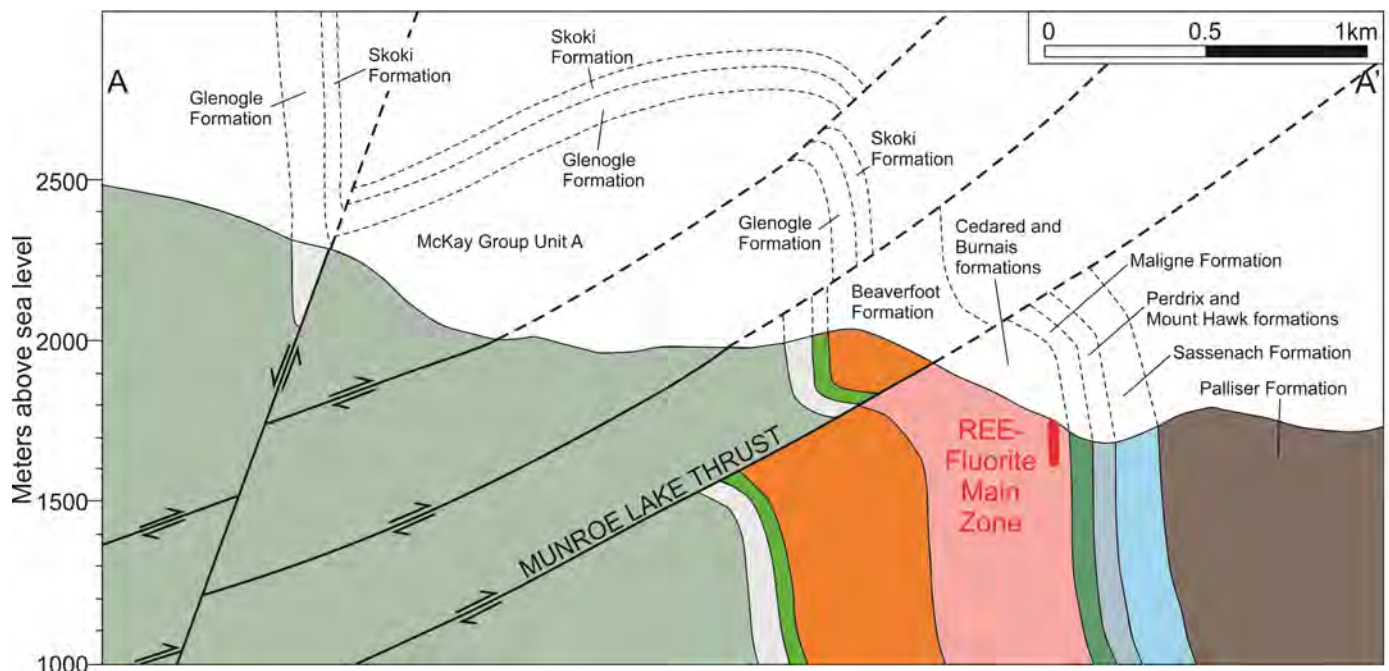


**Fig. 3.** Geological cross section of the Rock Canyon Creek deposit area. For section location and legend see Figure 2. No vertical exaggeration. Based on mapping by Mott (1989) and McMechan and Leech (2011).

Devonian-Mississippian) are about 1000 metres thick in the Rock Canyon Creek deposit area. The contact with the Palliser Formation is poorly exposed but sharp (Mott, 1989). The Exshaw-Banff formations consist of finely laminated, fissile shale with abundant pyrite nodules grading upwards into a brown-weathering limy shale and brown-grey shaly lime-mudstone (Mott, 1989). Regionally, the Exshaw Formation contains felsic tuffs with a ca. 363 Ma age (U-Pb zircon; Richards et al., 2002).

### 3.2. Structure

The predominant structural elements in the area are northeast-vergent thrusts and folds (Figs. 2, 3; Mott, 1989; McMechan and Leech, 2011). Thrust faults, including the Munroe Lake thrust, are oriented northwest-southeast and dip shallowly to the southwest (Fig. 3). A normal fault west of the Munroe Lake thrust has a similar strike to the thrusts (Fig. 2), but dips steeply southwest (Fig. 3).

Mott (1989) proposed that a northwest-striking, south-dipping tear fault (Rock Canyon Creek tear fault) follows the trend of Rock Canyon Creek, based on the observation that the Beaverfoot, Skoki, and Glenogle formations are exposed at lower elevations on the north side of the creek than on the south side. Although this putative tear fault was not included in the McMechan and Leech map (2011), its projection may connect to the Munroe Lake fault 200 metres northwest of the main REE-fluorite zone (Fig. 2). Because of the possible importance of the fault to mineralization, future fieldwork will attempt to resolve if the fault exists or not.

A pressure solution cleavage is best developed in argillaceous units of the McKay Group, and Cedared and Burnais formations.

In general, fracturing and veining (calcite and quartz) appears to be inversely proportional to the intensity of cleavage development for most units, with the exception of the Cedared and Burnais formations, which display both well-developed cleavage and fracturing (Mott, 1989). Different fracture sets crosscut one another, indicating multiple generations of fracturing. Fractured rocks probably acted as a sink for material removed from nearby units by pressure solution (Mott, 1989).

Breccias in the Cedared and Burnais formations in Beaverfoot, Brisco, and Stanford ranges consisting of angular fragments of limestone and dolostone in a sandy mudstone matrix, were interpreted by Belyea and Norford (1967) as the products of solution collapse. Similar breccias in the study area were also attributed to solution collapse (Mott, 1989; McMechan and Leech, 2011).

Breccias containing dolostone fragments, but of uncertain origin, coincide with the main mineralized REE-fluorite zone (see below). The elongate shape of the breccia zone suggests that it may be either a fault related ('crackle fault breccia') or a 'cave-ceiling crackle breccia' related to stratabound paleokarst development. Regardless of its origin, this breccia appears to be the main structural control on REE-fluorite mineralization, and for pyrite and sparry dolomite mineral growth.

### 4. Geology of the deposit

REE-fluorite mineralization coincides with a zone of dolostone-fragment crackle breccia hosted by the Cedared and Burnais formations (Figs. 2, 3). Fluorite-bearing outcrops extend across an area 3300 metres long and 750 metres wide. The main mineralized zone is approximately 50 metres from, and parallel to, the contact between the Cedared and Burnais

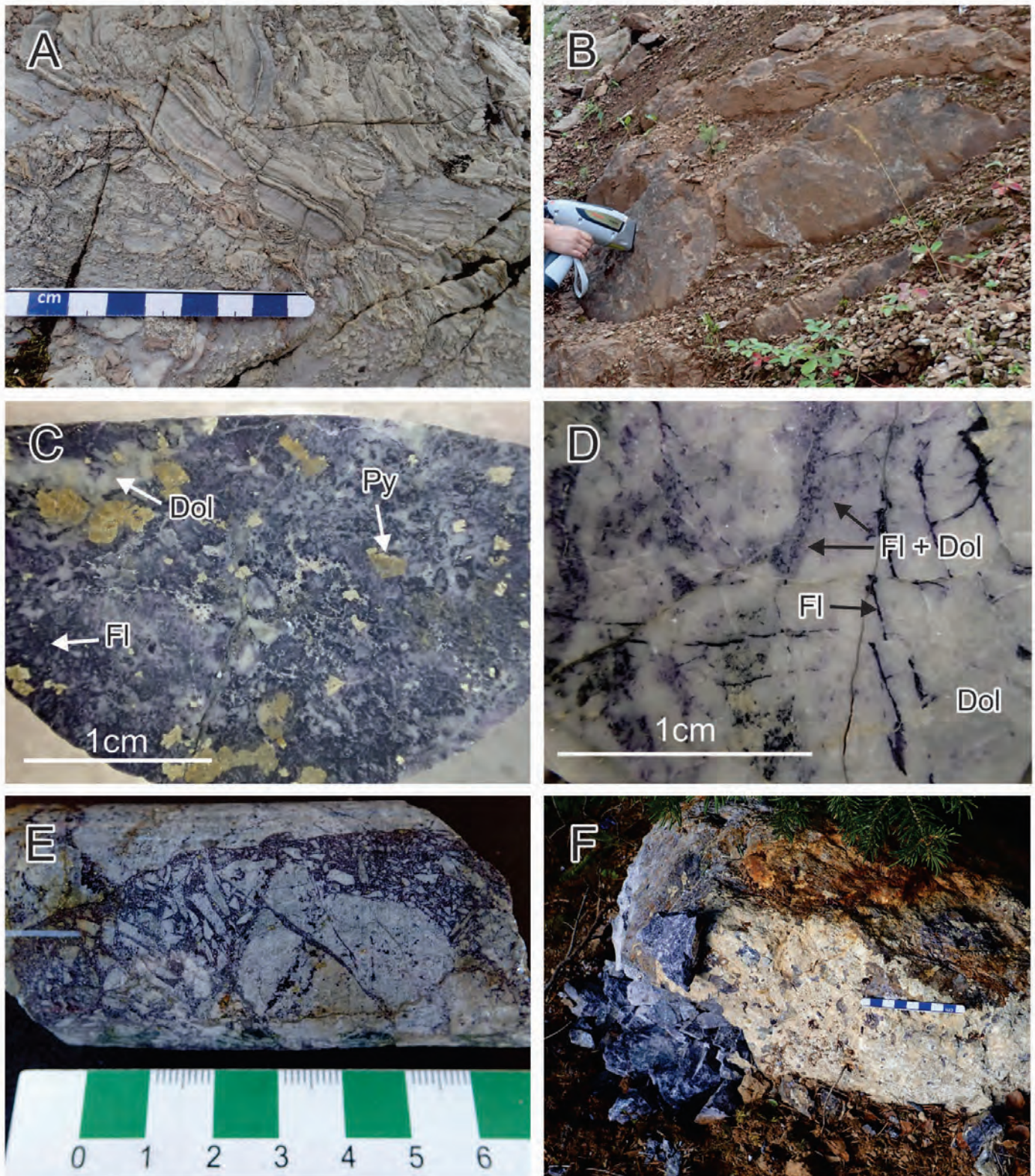


**Fig. 4.** Photographs from the Rock Canyon Creek deposit area. **a)** Intraformational breccia composed of evaporitic laminated gypsum of the Cedared and Burnais formations, weathered surface. **b)** REE-fluorite-bearing dolostone, the main zone, displaying characteristic red-brown weathering. **c)** Representative sample of mineralization consisting of purple fluorite (Fl) and pyrite (Py) in grey dolomite (Dol). REE-bearing minerals cannot be identified at this scale; however sample contains 1.8 weight % of Ce, La, and Nd combined. **d)** Example of 'crackle breccia' cemented by fluorite in the right portion of the photograph; open spaces filled by fluorite and dolomite (Fl + Dol). **e)** Monolithic dolostone breccia; larger fragments are cut by fluorite filled fractures; purple matrix of the breccia consists of fluorite, dolomite, barite, and pyrite. **f)** Fluorite-rich boulder suspected to contain cryolite found near the northwestern end of the main REE-fluorite zone.

formations and the Maligne Formation (Figs. 2, 3). Defined by drilling and illustrated in cross-section (Pighin, 2010), the zone appears to dip steeply along a strike length of more than 1100 metres, and appears to be stratabound, subparallel to the contact of the Cedared and Burnais formations with the overlying Maligne Formation. Mineralization was intersected to a depth of 124 metres; remains open at depth and along strike, and may be more than 50 metres thick. Based on fluorine concentrations reported by Pighin (2010) and assuming that most of the fluorine is contained in fluorite, we estimate that fluorite content varies from less than 1% to 13.5% by weight. Most of the fluorite is deep purple, although, red-wine coloured and colourless varieties were also observed. The main mineralized zone displays significant concentrations of REE. Light REE (Ce+La+Nd) concentrations vary from trace to 2.8% (Pighin, 2010). Spectrum Mining Corporation did not analyse for rare earth elements other than Ce, La, Nd, and Sm.

The main mineralized zone is dark red-brown on weathered surfaces (Fig. 4b), and grey and purple on fresh surfaces (Fig. 4c). Fluorite mineralization in the main zone is fracture controlled and as open space fillings (Fig. 4d). Early disseminated mineralization was reported in previous studies (Samson et al., 2001; Gagnon et al., 2003). Recent field observations suggest that disseminated fluorite forms envelopes around fluorite-filled fractures and breccia zones (Fig. 4e). The deepest purple fluorite appears to form haloes around radioactive grains (possibly monazite). Fluorite-filled hairline fractures cut the dolostone and dolostone breccia fragments. Coarser fractures (up to 1 cm thick) are commonly filled with fluorite ( $\pm$ carbonate and pyrite). Cross cutting relationships, symmetrically banded complex fracture fillings, and oscillatory growths in fluorite suggest multiple generations of fluid flow and fluid evolution with time. Based on a comparison of REE and fluorine content of analyzed drill core as reported by Pighin (2010), REE mineralization is spatially associated with fluorite. However, specific REE minerals are too fine grained to be identified macroscopically. Several generations of pyrite are in the mineralized zone. Pyrite occurs as cubes and pyritohedrons in aggregates and veinlets, and fine pyrite veinlets crosscut fluorite mineralization. The REE, fluorite, and pyrite content of other fluorite occurrences, which are hosted by white to pale gray carbonate, is significantly lower than that of the main REE-fluorite zone.

The mineralogy of the deposit (Table 1) was described by Hora and Kwong (1986), Pell (1992), Kerr (1995), Zhu (2000), and Samson et al. (2001). The studies by Hora and Kwong (1986) were largely based on samples of float. Pell (1992) complemented the data by describing some in-situ mineralization. Studies by Samson et al. (2001), Kerr (1995), and Zhu (2000) described both in-situ and float mineralization. Calcite, dolomite, fluorite, quartz, K-feldspar, barite, apatite (decomposed apatite), pyrite, REE carbonates [bastnaesite-(Ce), parisite-(Ce), synchysite-(Ce)], and a mixture of REE phosphates including monazite-(Ce) were identified by Hoshino et al. (2017). Rare earth element mineralization occurs

with hydrothermal stage fluorite and barite, and is crosscut by later-stage calcite veinlets (Hoshino et al., 2017). More detailed mineralogical studies on the drill core samples of the main REE-fluorite zone are in progress and will establish a paragenesis.

Cryolite, prosopite, and elpasolite have been observed in rounded and sub-rounded float boulders near the deposit (Fig. 4f). However, these minerals have not been found in samples collected from outcrops and drill core. These boulders may either indicate undiscovered mineralization on the property, or they may have been derived from as far as the Ice River complex and transported by glaciation. The second explanation is less likely because Spectrum Mining Corporation failed to locate boulders with similar characteristics in drainages north of Rock Canyon Creek and south of the Ice River complex.

### **5. Genetic considerations and possible genetic link to magnesite and MVT deposits in southeastern British Columbia**

The Rock Canyon Creek REE-fluorite deposit has historically been viewed as a being related to a carbonatite source (Graf, 1985; Hora and Kwong, 1986; Pell and Hora, 1987; Samson et al., 2001). Disseminated fluorite-REE mineralization was regarded as a result of interaction between F- and REE-bearing hydrothermal fluids of unspecified origin with carbonate wall rock (Gagnon et al., 2003). Differences in fluorite composition were interpreted either as progressive mixing of hydrothermal fluids or interaction of fluids with the country rock (Gagnon et al., 2003).

Although the deposit is in the British Columbia alkaline province (Pell, 1994), it is unusual in that it is not spatially associated with outcrops of carbonatite or alkaline rocks. Furthermore, it lacks primary monazite, although secondary monazite was recently reported in shallow drill core by Hoshino et al. (2017) from drill hole number RCC-09-14. Similarities between the Rock Canyon Creek REE-fluorite deposit, Mississippi Valley-type (MVT; e.g., Shag, Monarch, Kicking Horse, Munroe), and sparry magnesite deposits (e.g., Mount Brussilof Mine and related occurrences) in southeastern British Columbia were noted by Paradis and Simandl, in press. All the above deposits are in Paleozoic shelf carbonate rocks, which extend along the length of the Canadian Cordillera, and were likely generated by mineralizing processes operating in the absence of nearby magmatic sources of metals and heat. All of these deposit types are associated with breccias and zones of hydrothermal sparry carbonates, such as magnesite, calcite, and saddle dolomite, and contain sulphides (Paradis and Simandl, in press). Furthermore, Pell (1994) reported that the Rock Canyon Creek deposit was discovered as a result of geochemical exploration for MVT Zn-Pb deposits. Thus basinal fluids may have been responsible for, or at least partially contributed to, the formation of REE-fluorite mineralization at Rock Canyon Creek.

Possible links between the MVT and magnesite deposits and Rock Canyon Creek will be tested by future studies directed at establishing lithological, textural, mineralogical

**Table 1.** Mineralogy of the Rock Canyon Creek deposit. Sources: 1 - Hora and Kwong (1986), 2 - Pell (1992), 3 - Samson et al. (2001), and 4 - Hoshino et al. (2017).

		<b>Mineral</b>	<b>Formula</b>	<b>Sources</b>
<b>In-situ</b>	<b>Gangue</b>	Calcite	CaCO <sub>3</sub>	4
		Dolomite	CaMg(CO <sub>3</sub> ) <sub>2</sub>	3,4
		Ferroan Dolomite	CaMg(CO <sub>3</sub> ) <sub>2</sub>	3
		Pyrite	FeS <sub>2</sub>	2,4
		K-Feldspar	KAlSi <sub>3</sub> O <sub>8</sub>	3,4
		Quartz	SiO <sub>2</sub>	3,4
		Rutile	TiO <sub>2</sub>	3
		Magnetite	Fe <sup>2+</sup> Fe <sup>3+</sup> <sub>2</sub> O <sub>4</sub>	2
		Apatite	Ca <sub>5</sub> (PO <sub>4</sub> ) <sub>3</sub> (F,Cl,OH)	3,4
		Hematite	Fe <sub>2</sub> O <sub>3</sub>	3,4
	<b>Ore</b>	Fluorite	CaF <sub>2</sub>	2,3,4
		Barite	BaSO <sub>4</sub>	2,3,4
		Bastnaesite	(Ce,La,Y)CO <sub>3</sub> F	4
		Pyrochlore	(Na,Ca) <sub>2</sub> Nb <sub>2</sub> O <sub>6</sub> (OH,F)	3
		Parisite	Ca(Ce,La) <sub>2</sub> (CO <sub>3</sub> ) <sub>3</sub> F <sub>2</sub>	2,3,4
		Synchysite	CaCe(CO <sub>3</sub> ) <sub>2</sub> F	3,4
		Monazite	(Ce,La)PO <sub>4</sub>	4
		Sphalerite	(Zn,Fe)S	3
		Galena	PbS	3
		Cerussite	PbCO <sub>3</sub>	3
Smithsonite	ZnCO <sub>3</sub>	3		
<b>In-situ &amp; Float</b>	<b>Gangue</b>	Dolomite	CaMg(CO <sub>3</sub> ) <sub>2</sub>	1,3,4
		Pyrite	FeS <sub>2</sub>	1,2,4
		K-Feldspar	KAlSi <sub>3</sub> O <sub>8</sub>	1,3,4
		Quartz	SiO <sub>2</sub>	1,3,4
		Rutile	TiO <sub>2</sub>	1,3
	<b>Ore</b>	Bastnaesite	(Ce,La,Y)CO <sub>3</sub> F	1
		Fluorite	CaF <sub>2</sub>	1,2,3,4
Barite	BaSO <sub>4</sub>	1,2,3,4		
<b>Float</b>	<b>Gangue</b>	Limonite	FeO(OH)·nH <sub>2</sub> O	1
		Illite	(K,H <sub>3</sub> O)(Al,Mg,Fe) <sub>2</sub> (Si,Al) <sub>4</sub> O <sub>10</sub> [(OH) <sub>2</sub> ,(H <sub>2</sub> O)]	1
		Prosopite	CaAl <sub>2</sub> (F,OH) <sub>8</sub>	1,3
		Kaolinite	Al <sub>2</sub> Si <sub>2</sub> O <sub>5</sub> (OH) <sub>4</sub>	1,3
		Talc	Mg <sub>3</sub> Si <sub>4</sub> O <sub>10</sub> (OH) <sub>2</sub>	1
		Muscovite	KAl <sub>2</sub> (AlSi <sub>3</sub> O <sub>10</sub> )(F,OH) <sub>2</sub>	3
		Elpasolite	K <sub>2</sub> NaAlF <sub>6</sub>	3
		Goyazite	SrAl <sub>3</sub> (PO <sub>4</sub> )(PO <sub>3</sub> OH)(OH) <sub>6</sub>	3
		<b>Ore</b>	Gorceixite	BaAl <sub>3</sub> (PO <sub>4</sub> )(PO <sub>3</sub> OH)(OH) <sub>6</sub>
	Cryolite		Na <sub>3</sub> ·AlF <sub>6</sub>	3
	Ag-Sn-Te-S phase		Ag <sub>8</sub> Sn(TeS <sub>2</sub> ) <sub>2</sub>	3

and geochemical parameters, depositional conditions, mineralization ages, provenance of metals and sulphur, tectonic and structural controls, and variations in the C and O isotopes in carbonate rocks. Conceivably, Rock Canyon Creek mineralization may record interaction between carbonatite-related and basinal fluid mineralizing systems.

## 6. Ongoing and future work

Samples collected in 2016 are being analysed for major and trace elements including REE and fluorine and mineralogical studies are in progress. Our future work, focused on generating a dataset to enable comparisons with magnesite and MVT deposits in the area, includes the following.

- Fieldwork to determine the extent of the brecciated and mineralized zones, document changes in brecciation style, and establish the distribution and intensity of sparry dolomitization adjacent to the main mineralized zone.
- Developing a three dimensional model of the deposit based on geochemical analyses of core samples.
- Detailed petrography and mineral chemistry using the scanning electron microscope (SEM) and electron microprobe.
- LA-ICPMS studies for trace element analysis and fluid inclusion studies of fluorite to test for covariation in REE composition of fluorite, and temperature of the fluid.
- S-isotopes of sulphides and barite, and O, C and Sr isotopes of carbonate rocks.
- Re-Os (pyrite) and U-Pb (monazite) geochronology.
- Study of co-variation between fluorite, sulphur, major and trace elements relative to concentrations of REE.
- Comparison of REE normalized patterns of weathering-enriched mineralization relative to those corresponding to fresh mineralization.

## Acknowledgments

This study is part of the Targeted Geoscience Initiative 5, spearheaded by Natural Resources Canada, and in partnership with the Japan Geological Survey. We thank David Pighin for his perspectives on the geology of the district and for allowing us access to drill cores stored at the Vine property south of Cranbrook. We are grateful for improvements and suggestions of Dr. Margot McMechan of the Geological Survey of Canada in Calgary and JoAnne Nelson, British Columbia Geological Survey.

## References cited

- Belyea H.R., and Norford, B.S., 1967. The Devonian Cedared and Harrogate formations in the Beaverfoot, Brisco, and Stanford Ranges, Southeast British Columbia, Geological Survey of Canada, Bulletin 146, 64p.
- Dix, G.R., 1991. Report on the Stratigraphy, Structure, and Soil Geochemistry of the Fluorite-REE Prospect on the Deep Purple-Candy Claims (Minfile 082JSW018), Southeastern British Columbia. Unpublished Report, Active Minerals Ltd.
- Gabrielse, H., Monger, J.W.H., Wheeler, J.O., and Yorath, C.J., 1991. Chapter 2, Part A. Morphogeological belts, tectonic assemblages, and terranes, Geology of the Cordilleran Orogen in Canada. Geological Survey of Canada, pp. 15-28.
- Gagnon, J.E., Samson, I.M., Fryer, B.J., and Williams-Jones, A.E., 2003. Compositional heterogeneity in fluorite and the genesis of fluorite deposits - Insights from LA-ICP-MS analysis. *The Canadian Mineralogist*, 41, 365-382.
- Gambogi, J., 2016a. Yttrium, Mineral Commodity Summaries. US Geological Survey, pp. 188-189.
- Gambogi, J., 2016b. Rare Earths, Mineral Commodity Summaries. US Geological Survey, pp. 134-135.
- Graf, C., 1985. Geological Report on the D.P. 1,2,3 and Candy Claims REE-Ba-F-P Carbonatite Prospect, Golden Mining Division Southeastern British Columbia NTS 82J/3E. Geological Branch Assessment Report 14677.
- Hora, Z.D., and Kwong, Y.T.J., 1986. Anomalous rare earth elements (REE) in the Deep Purple and Candy claims. In: *Geological Fieldwork 1985*, British Columbia Ministry of Energy, Mines, and Petroleum Resources, British Columbia Geological Survey Paper 1986-1, pp. 241-242.
- Hoshino, M., Kon, Y., Kodama, S., Simandl, G.J., Paradis, S., Green, C., Namatame, C., Matsunaga, I., and Takagi, T., 2017. Mineralogy of the Rock Canyon Creek REE-Fluorite Deposit, British Columbia, Canada. In: *Geological Fieldwork 2016*, British Columbia Ministry of Energy and Mines, British Columbia Geological Survey Paper 2017-1, this volume.
- Kerr, I.D., 1995. Mineralogic and Paragenetic Studies of the Rock Canyon Creek Fluorite-Rare Earth Element Deposit, British Columbia. Unpublished BSc thesis, University of Windsor, 33p.
- Leech, G.B., 1979. Kananaskis Lakes Map Area, NTS 82J. Geological Survey of Canada, Open File 634.
- Mariano, A.N., 1989a. Economic geology of rare earth minerals. In: Lipman BR, McKay GA (Eds.), *Geochemistry and mineralogy of rare earth elements: reviews in mineralogy*, vol. 21. Mineralogical Society of America, Chantilly, pp. 303-337.
- Mariano, A.N., 1989b. Nature of economic mineralization in carbonatites and related rocks. In: Bell K (Ed.), *Carbonatites: genesis and evolution*. Unwin Hyman, London, pp. 149-176.
- McMechan, M.E., 2012. Deep transverse basement structural control of mineral systems in the southeastern Canadian Cordillera. *Canadian Journal of Earth Sciences*, 49, 693-708.
- McMechan, M.E., and Leech, G.B., 2011. Geology, Mount Peck, British Columbia; Geological Survey of Canada, Canadian Geoscience Map 9, scale 1:50,000.
- Monger, J., and Price, R.A., 2002. The Canadian Cordillera: Geology and Tectonic Evolution. *Canadian Society of Geophysicists Recorder*, 27, 7-36.
- Mott, J.A., 1989. Structural and stratigraphic relations in the White river region, eastern Main Ranges, southern Rocky Mountains, British Columbia; Unpublished Ph.D. thesis, Queen's University, Kingston, 404p.
- Paradis, S., Simandl, G.J., Keevil, H., and Raudsepp, M., 2016. Carbonate-Hosted Nonsulfide Pb-Zn Deposits of the Quesnel Lake District, British Columbia, Canada. *Economic Geology*, 111, 179-198.
- Paradis, S., and Simandl, G.J., in press. Is there a genetic link between the SEDEX and MVT deposits of the Canadian Cordillera? In: Rogers, N. (Ed.) *Targeted Geoscience Initiative – 2016 Report of Activities* (Ed.) N. Rogers; Geological Survey of Canada Open File.
- Pell, J., 1992. Fluorspar and Fluorine in British Columbia, British Columbia Ministry of Energy, Mines and Petroleum Resources, Open File 1992-16, 81p.
- Pell, J., 1994. Carbonatites, nepheline syenites, kimberlites and related rocks in British Columbia. British Columbia Ministry of Energy, Mines, and Petroleum Resources, Bulletin 88, 44p.
- Pell, J., and Hora, Z.D., 1986. Geology of the Rock Canyon Creek fluorite/rare earth element showing southern Rocky Mountains (82J/3E). In: *Geological Fieldwork 1986*, British Columbia

- Ministry of Energy, Mines and Petroleum Resources, British Columbia Geological Survey Paper 1987-1, pp. 255-258.
- Pighin, D.L., 2010. Assessment Report Rock Canyon Property, British Columbia Geological Survey Assessment Report 31435.
- Price, R.A., and Fermor, P.R., 1985. Structure section of the Cordilleran foreland thrust and fold belt west of Calgary, Alberta. Geological Survey of Canada, Paper 84-14, 1 sheet.
- Richards, B.C., Ross, G.M., and Utting, J., 2002. U – Pb geochronology, lithostratigraphy and biostratigraphy of tuff in the upper Famennian to Tournaisian Exshaw Formation: Evidence for a mid-Paleozoic magmatic arc on the northwestern margin of North America. In: L.V. Hills, C.M. Henderson and E.W. Bamber (Eds.), Carboniferous and Permian of the World. Canadian Society of Petroleum Geologists, Memoir 19, pp. 158–207.
- Samson, I.M., Kerr, I.D., and Graf, C., 2001. The Rock Canyon Creek Fluorite-REE deposit, British Columbia. In: Dunlop, S. and Simandl, G.J. (Eds.), Industrial Minerals in Canada, Special Volume 53, Canadian Institute of Mining and Metallurgy, pp. 35-44.
- Simandl, G.J., 2009. World Fluorspar Resources, Market and deposit examples from British Columbia, Canada. British Columbia Geological Survey, Information Circular 2009-4, 16p.
- Simandl, G., 2014. Geology and market-dependent significance of rare earth element resources. *Mineralium Deposita*, 49, 889-904.
- Simandl, G.J., Prussin, E.A., and Brown, N., 2012a. Specialty Metals In Canada. British Columbia Geological Survey Open File 2012-7, 48p.
- Simandl, G.J., Prussin, E.A., Hancock, K., and Meredith Jones, S., 2012b. Rare metal-bearing deposits in British Columbia with Selected Examples. British Columbia Ministry of Energy Mines, British Columbia Geological Survey, Geofile 2012-02.
- Simandl, G.J., Akam, C., and Paradis, S., 2015. Which materials are 'critical' and 'strategic'. In: Simandl, G.J. and Neetz, M., (Eds.), Symposium on Strategic and Critical Materials Proceedings, November 13-14, 2015, Victoria, British Columbia. British Columbia Ministry of Energy and Mines, British Columbia Geological Survey Paper 2015-3, pp. 1-4.
- Trofanenko, J., Williams-Jones, A.E., Simandl, G.J., and Reid, H.M., 2013. The Riddle Creek prospect, an unusual example of Sr-Ba-REE-F mineralization outside the Alkaline Province, British Columbia, Canada. In: Geological Fieldwork 2012, British Columbia Ministry of Energy, Mines and Natural Gas, British Columbia Geological Survey Paper 2013-1, pp. 139-148.
- Zhu, L., 2000. An isotopic and Fluid Inclusion Study of the Rock Canyon Creek, Fluorite-REE Deposit, southeastern British Columbia. Unpublished MSc thesis, University of Windsor, 114p.



# Mineralogy of the Rock Canyon Creek REE-fluorite deposit, British Columbia, Canada



Mihoko Hoshino<sup>1,a</sup>, Yoshiaki Kon<sup>1</sup>, Shinsuke Kodama<sup>1</sup>, George J. Simandl<sup>2,3</sup>, Suzanne Paradis<sup>4</sup>, Craig Green<sup>2</sup>, Chizu Namatame<sup>1</sup>, Izumi Matsunaga<sup>1</sup>, and Tetsuichi Takagi<sup>1</sup>

<sup>1</sup>Mineral Resource Research Group, National Institute of Advanced Industrial Science and Technology, Tsukuba, Japan

<sup>2</sup>School of Earth and Ocean Sciences, University of Victoria, BC, V8P 5C2

<sup>3</sup>British Columbia Geological Survey, Ministry of Energy and Mines, Victoria, BC, V8W 9N3

<sup>4</sup>Geological Survey of Canada, Natural Resources Canada, Sidney, BC, V8L 4B2

<sup>a</sup>corresponding author: hoshino-m@aist.go.jp

Recommended citation: Hoshino, M., Kon, Y., Kodama, S., Simandl, G.J., Paradis, S., Green, C., Namatame, C., Matsunaga, I., and Takagi, T., 2017. Mineralogy of the Rock Canyon Creek REE-Fluorite Deposit, British Columbia, Canada. In: Geological Fieldwork 2016, British Columbia Ministry of Energy and Mines, British Columbia Geological Survey Paper 2017-1, pp. 205-213.

## Abstract

The main REE-fluorite mineralized zone at the Rock Canyon Creek deposit was intersected by drilling along a strike length of 1100 metres and to a depth of more than 124 metres. Samples of drill core from this zone were analyzed by SEM-EDS, powder-XRD and Raman Spectroscopy. Mineralization consists of dolomite, fluorite, quartz, K-feldspar, barite, porous apatite, pyrite, REE-bearing fluorocarbonates [bastnäsite-(Ce), parisite-(Ce), synchysite-(Ce)], and REE-bearing phosphates [monazite-(Ce), crandallite group minerals] in various proportions. Barite and fluorite veinlets and those containing REE minerals, fluorite, barite and pyrite are cut by calcite-filled fractures. REE carbonates and REE phosphates are spatially associated with pyrite, barite and fluorite. Most of the pyrite in weathered surface samples is replaced by hematite. Preliminary results indicate that the bastnäsite-(Ce) contains 8.7 to 26.7 wt.% La, 24.3 to 34.4 wt.% Ce, from detection limit to 4.7 wt.% Pr, 8.2 to 24.1 wt.% Nd, undetected to 2.84 wt.% Sm, and undetected to 8.42 wt.% Th. Synchysite-(Ce) contains 5.2 to 17.4 wt.% La, 16.6 to 25.3 wt.% Ce, undetected to 8.3 wt.% Pr, 2.6 to 19.4 wt.% Nd, undetected to 2.13 wt.% Y, and undetected to 3.7 wt.% Th. Monazite contains 11.03 to 13.03 wt.% P, 14.15 to 18.95 wt.% La, 21.46 to 32.98 wt.% Ce, 4.01 to 8.80 wt.% Nd, and undetected to 3.55 wt.% Th. The monazite-(Ce) grains analyzed include impurity elements like Al, and Ca, suggesting that monazite-(Ce) is altered or formed in the supergene environment. Cross cutting relationships and replacement textures suggest that REE-bearing carbonates, fluorite, barite and pyrite are of hydrothermal origin.

**Keywords:** Rare earth elements, hydrothermal, bastnäsite, synchysite, parisite, crandallite group minerals, monazite, fluorite, barite

## 1. Introduction

The Rock Canyon Creek rare earth element (REE)-fluorite deposit, about 90 km north-northeast of Cranbrook is in the British Columbia alkaline province (Fig. 1). Most of the 44 REE occurrences reported in British Columbia (Simandl et al., 2012) are in this province which consists of carbonatites, nepheline and sodalite syenites, ijolite series rocks, kimberlite, and many ultramafic and lamprophyre diatremes, breccias, and dikes (Pell, 1994). The Rock Canyon Creek deposit is hosted by Middle Devonian carbonate rocks of the Cedared and Burnais formations (Pell and Hora, 1986; Green et al., 2017). The main REE-fluorite mineralized zone (Fig. 2) was investigated at depth by 17 diamond-drill holes totalling 1213.79 metres (Pighin et al., 2010). The steeply dipping REE-fluorite zone extends along strike for more than 1100 metres, to a depth greater than 124 metres; it remains open along strike and dip and, at least locally, is more than 50 metres thick. In this study, we carried out a detailed mineral identification of selected mineralized samples from the drill hole RCC-09-14 and report the results.

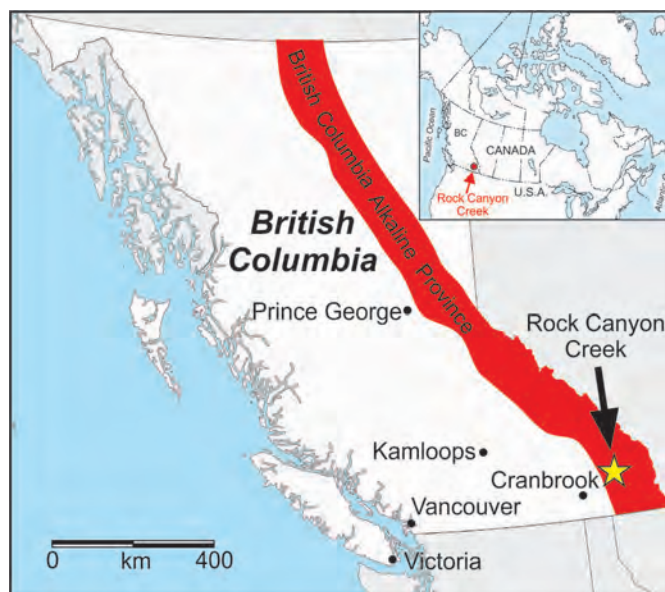


**Fig. 1.** Location of the Rock Canyon Creek REE-fluorite deposit. The British Columbia Alkaline Province, as defined by Pell (1994), is shown in red.

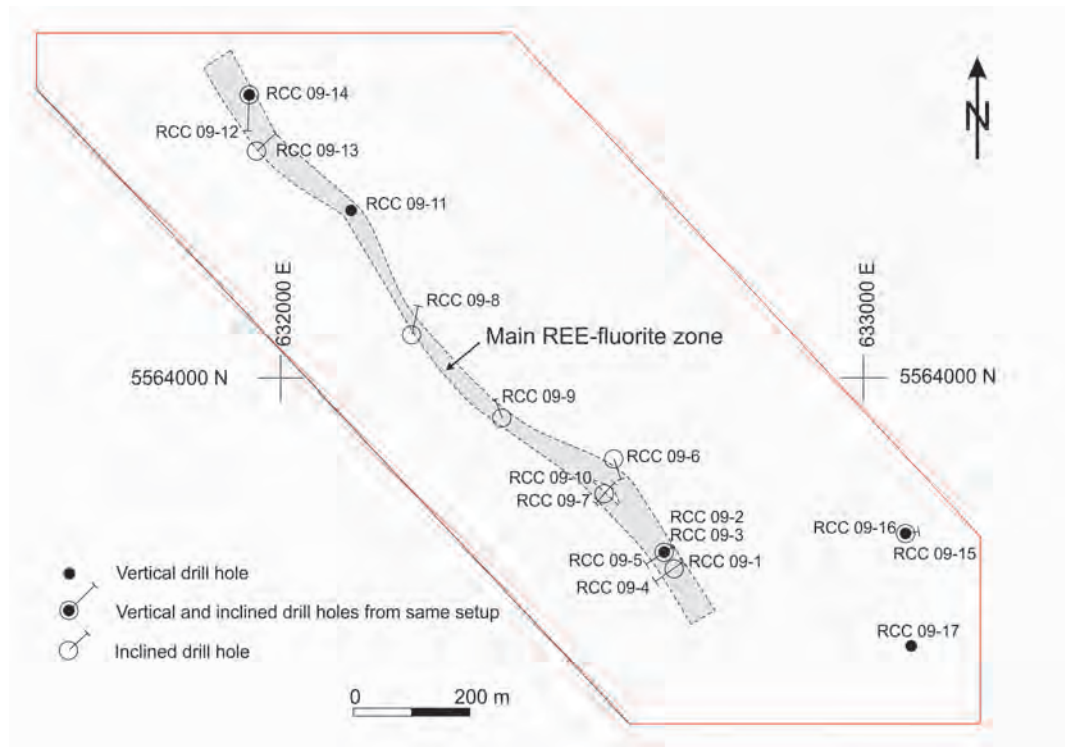


**Fig. 2.** Approximate vertical projection of the main REE-fluorite mineralized zone to the surface and locations of diamond-drill holes. Compiled from Pighin (2010). Mineralized zone is open at depth and along strike in both directions. Drill hole RCC-09-14, the main object of this study, intersected high-grade mineralization and is one of the two northernmost drill holes.

## 2. Analytical methods

Fifteen polished thin sections were prepared from core of the drill hole RCC-09-14. Selected minerals were analyzed using energy dispersive spectroscopy on a scanning electron microscope (SEM-EDS; JEOL JSM-6610LV) and Raman spectroscopy analysis (JASCO NRS-5100) was carried out for mineral identification on selected thin sections. Core samples, representing 3-metre drill core intervals, from drill hole RCC-09-14 were crushed, split, and milled to make powder samples for powder X-ray diffraction (Powder-XRD). Qualitative powder-XRD analyses were conducted on 38 powdered samples using the Rigaku Smart Lab X-ray diffractometer. The operating voltage and current were 40 kV and 200 mA, respectively, and samples were scanned from 3° to 70° 2θ at a step size of 0.02° and scan speed of 10° min<sup>-1</sup>. Mineral identification using the XRD data was conducted by using PDXL database fitting program (ver. 2.7.2). All analytical work was carried out at the Mineral Resource Research Group of National Institute of Advanced Industrial Science and Technology in Tsukuba, Japan.

## 3. Results

### 3.1. X-ray diffraction analysis

The main minerals identified by X-ray diffraction analysis (Powder-XRD) are dolomite, fluorite, barite and pyrite (Table 1). Quartz was in 30 of 38 samples. Bastnäsite was detected by Powder-XRD and SEM-EDS, and was identified as the

main REE mineral in 50% of the analyzed samples at depths of 1 to 6 m, 15 to 45 m and 114 to 124.7 m. The occurrence of bastnäsite is consistent with SEM-EDS results (Tables 1, 2). Monazite was only detected in two of the 3 metre-long samples. Apatite was detected from the 114-117 m and 123-124.7 m intervals.

### 3.2. SEM-EDS analysis

Following the qualitative analysis, quantitative analysis of minerals was conducted using SEM-EDS (JEOL JSM-6610LV). SEM-EDS analyses were carried out on 15 thin sections (Table 2). Cobalt (Co) standard was used for quantitative analysis. These analyses identified dolomite, fluorite, quartz, K-feldspar, barite, apatite, pyrite, REE-bearing fluorocarbonates [(bastnäsite-(Ce), parisite-(Ce) and synchysite-(Ce)], and REE phosphates [monazite-(Ce) and crandallite group minerals]. REE-bearing fluorocarbonates were identified in 14 samples, and REE phosphates in 9. Both REE carbonates and REE phosphates are commonly spatially associated with pyrite, barite and fluorite (Figs. 3a-f). Representative chemical compositions are summarized in Table 3 for bastnäsite-(Ce), Table 4 for synchysite-(Ce), Table 5 for parisite-(Ce), Table 6 for monazite-(Ce), and Table 7 for crandallite group minerals.

Pyrite is one of most common minerals in samples from drill hole RCC-09-14. It commonly occurs as aggregates of small euhedral pyrite grains (Figs. 3 a, d, e) with rims replaced by hematite (Fig. 3a). Barite and fluorite form crystals in

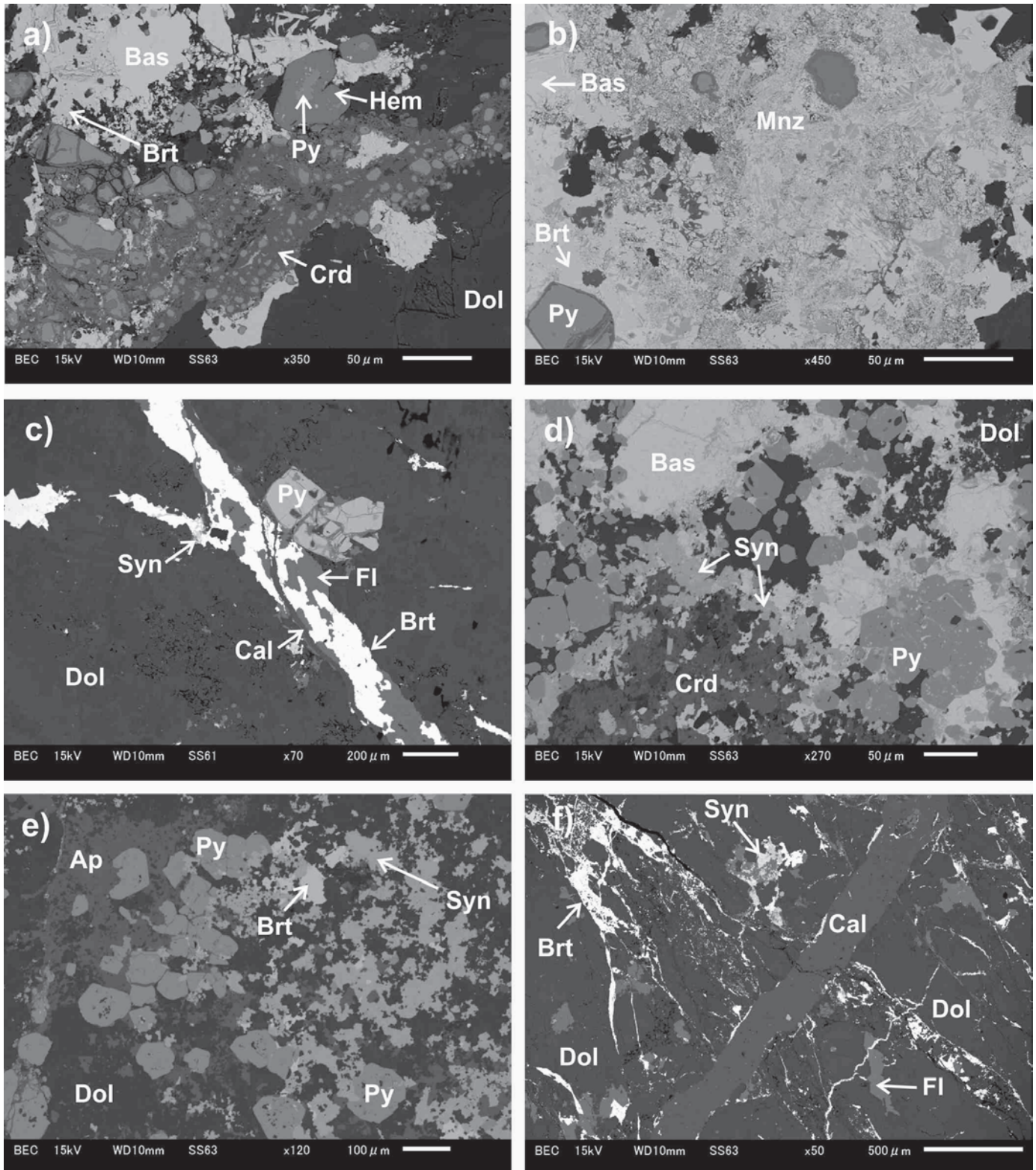


**Fig. 3.** Back-scatter-electron images of representative textures in drill hole RCC-09-14. **a)** RCC-09-14-1 m, bastnäsite-(Ce) with pyrite, hematite, barite, and crandallite. **b)** RCC-09-14-1 m, mixture of monazite-(Ce), bastnäsite-(Ce) and barite. **c)** RCC-09-14-1 m, late calcite-filled hairline fractures cut fractures filled with fluorite and barite. **d)** RCC-09-14-80.1 m, pyrite aggregates with bastnäsite-(Ce), crandallite and synchysite-(Ce). **e)** Euhedral pyrite aggregates with altered apatite, synchysite-(Ce) and barite in dolomite. **f)** RCC-09-14-121.2 m, late calcite veins cut barite and synchysite-(Ce) vein. Dol: dolomite, Fl: fluorite, Py: pyrite, Hem: hematite, Brt: barite, Bas: bastnäsite, Syn: synchysite, Crd: crandallite group mineral, Ap: apatite.

**Table 1.** List of minerals detected by Powder-XRD in samples from vertical drill hole RCC-09-14. Relative qualitative abundance of minerals is expressed in terms of height of their diagnostic peak.

Depth (m)	Dol	Cal	Fl	Brt	Py	Mc	Qtz	Ap	Bas	Mnz
1-6	+++	+	++	++	+		+		++	+
6-9	+++	++	++	+	++	+	+			
9-12	+++	++	++	+	++	+				
12-15	+++	++	++	+	++		+			
15-18	+++		++	+	+				++	
18-21	+++		++	++	+		+		++	
21-24	+++		++	++	+				++	+
24-27	+++		++	+	+				+	
27-30	+++		++	+	+				+	
30-33	+++		++	++	+				++	
33-36	+++		++	+	++		+		++	
36-39	+++		++	+	+	+	+		+	
39-42	+++		++	+	++	+	+			
42-45	+++		++	+	+	+	+		++	
45-48	+++		++	+	+		+			
57-60	+++		++	+	+		+		+	
60-63	+++		++	+	+	+	+		+	
63-66	+++		++	+	++		+			
66-69	+++		++	+	+		+		+	
69-72	+++		++	+	++		+		+	
72-75	+++		++	+	+		+			
75-78	+++		++	++	+		+			
78-81	+++		++	+	++		+			
81-84	+++		++	+	++					
84-87	+++		++	+	++		+		+	
87-90	+++		++	+	++		+			
90-93	+++		+	+	++					
93-96	+++		+	+	++					
96-99	+++		+	+	++		+			
99-102	+++		+	+	+		+			
102-105	+++		++	+	++		+			
105-108	+++		++	+	++		+			
108-111	+++		++	+	++		+			
111-114	+++			+	++		+			
114-117	+++		++	+			+	+	+	
117-120	+++		++	+			+		++	
120-123	+++		++	+			+		++	
123-124.7	+++		+	+			+	+	++	

Dol: dolomite, Cal: calcite, Fl: fluorite, Brt: barite, Py: pyrite, Mc: microcline,  
 Qtz: quartz, Ap: fluorapatite, Bas: bastnasite, Mnz: monazite  
 +++: peak high, ++: peak middle, +: peak low

**Table 2.** Sample descriptions and REE minerals detected by SEM-EDS in drill hole RCC-09-14. Mineral abundances: +++ major, ++ minor, + trace.

Sample Number	Rock Type	Microscopic observations	REE minerals	Other minerals	REE content
RCC-09-14_1	Dolostone (Fe oxide-stained), weathered	fg dolomitic limestone; REE carbonates and phosphates with pyrite, fluorite and barite; late calcite vein	REE carbonates++, REE phosphates+++	dolomite+++, barite+++, fluorite++, calcite++, pyrite+	high
RCC-09-14_2.8	Fluorite-bearing Fe oxide stained dolostone breccia	altered cg dolomitic limestone. REE carbonates and REE phosphates occur with pyrite, fluorite and barite; late calcite veinlets	REE carbonates++, REE phosphates+++	dolomite+++, barite++, fluorite+++, calcite++, pyrite+	high
RCC-09-14_5.8	Fluorite-bearing, Fe oxide stained dolostone	fg dolostone, REE carbonates and phosphates occur with pyrite, fluorite and barite; late stage fg pyrite aggregates; calcite vein is the latest	REE carbonates++, REE phosphates++	dolomite+++, barite++, fluorite+++, calcite++, pyrite+++	moderate
RCC-09-14_6.75	Fluorite-bearing, pale gray dolostone cut by calcite vein.	contact of altered fg dolostone with calcite vein; REE carbonates occur with pyrite, fluorite and barite; late veinlets consisting of fg pyrite aggregates	REE carbonates+	dolomite+++, barite++, fluorite+++, calcite+++, pyrite++	low
RCC-09-14_8.15	Fluorite-, pyrite-bearing pale gray dolostone cut by calcite vein	contact of altered fg dolostone with calcite vein. REE carbonates occur with pyrite, fluorite and barite; late veinlets containing fg pyrite aggregates	REE carbonates+	dolomite+++, barite+, fluorite+++, calcite+++, pyrite+++, K-feldspar+	low
RCC-09-14_8.5	Fluorite and pyrite-bearing whitish limestone, calcite vein	altered cg dolostone. REE carbonates and REE phosphates occur with pyrite, fluorite and barite; late veinlets containing fg pyrite aggregates	REE carbonates+, REE phosphates+	dolomite+++, barite+, fluorite+++, calcite+, pyrite+++	low
RCC-09-14_37.3	Fluorite-bearing dolostone; cut by cg calcite vein	altered fg dolostone; REE carbonates and phosphates with fluorite, barite, and pyrite	REE carbonates+, REE phosphates+	dolomite+++, barite+++, fluorite+++, quartz++, K-feldspar++, calcite+, pyrite++	low
RCC-09-14_40.4	Fluorite- and pyrite-bearing grey limestone	altered fg dolomitic limestone; apatite grains are cut by fluorite-filled fractures		dolomite+++, barite++, apatite+++, fluorite+++, quartz++, K-feldspar++, pyrite+++	low
RCC-09-14_69.6	Fluorite- and pyrite-bearing grey dolostone, calcite veinlets, with massive pyrite	altered fg dolostone; REE carbonates occur with fluorite, barite and pyrite. Late veinlets containing fg pyrite aggregates	REE carbonates++	dolomite+++, barite++, fluorite+++, quartz++, K-feldspar++, pyrite+++	moderate

Table 2. Continued.

<b>RCC-09-14_80.1</b>	Fluorite- and pyrite-bearing grey dolostone	altered fg dolostone; REE carbonates and phosphates occur with fluorite, barite, and pyrite; apatite is common; late fg pyrite aggregates	REE carbonates++, REE phosphates+	dolomite+++, barite++, apatite +++, fluorite++, K-feldspar++, pyrite+++	moderate
<b>RCC-09-14_108.6</b>	Fluorite and pyrite-rich grey dolostone	fg dolostone; REE carbonates accompanied by fluorite, pyrite and barite; fg pyrite aggregates	REE carbonates+++, REE phosphates+	dolomite+++, barite++, fluorite++, pyrite+++	high
<b>RCC-09-14_120</b>	Whitish dolostone	cg dolostone; REE carbonates and phosphates occur with fluorite, pyrite, and barite; apatite is common	REE carbonates++, REE phosphates+	dolomite+++, barite++, fluorite++, pyrite++	moderate
<b>RCC-09-14_121.2</b>	Whitish dolostone	fg dolostone; REE carbonates and phosphates occur with fluorite, pyrite, and barite; apatite is common; fg pyrite aggregates; late calcite veinlets	REE carbonates+++, REE phosphates+	dolomite+++, barite++, apatite +++, fluorite++, pyrite++	high
<b>RCC-09-14_121.6</b>	Fluorite-bearing whitish dolostone	cg dolostone; REE carbonates and REE phosphates with fluorite coexist pyrite and barite; fg pyrite aggregates; late calcite vein	REE carbonates+++, REE phosphates+++	dolomite+++, barite++, fluorite++, pyrite++	high
<b>RCC-09-14_124.7</b>	Whitish dolostone	cg recrystallized dolostone; REE carbonates with fluorite, pyrite and barite; apatite is common	REE carbonates+++	dolomite+++, barite++, apatite +++, fluorite++, pyrite++	high

cg-coarse grain, fg-fine grain

Table 3. Representative composition of bastnäsite from drill hole RCC-09-14. Concentrations of Si, Al, Na, Mg, Fe, Ba, and Y were not detected by SEM-EDS analysis. Results in wt.%, normalized to 100 wt.%.

(wt %)	RCC-09-14-1m	RCC-09-14-1m	RCC-09-14-1m	RCC-09-14-1m	RCC-09-14-1m	RCC-09-14-1m	RCC-09-14-80.1m	RCC-09-14-80.1m	RCC-09-14-108.1m	RCC-09-14-108.1m	RCC-09-14-108.1m	RCC-09-14-121.2m
Ca	-	-	0.72	0.67	0.90	-	1.76	2.01	2.13	2.81	1.90	1.19
Sr	1.63	2.07	-	2.03	-	-	-	-	-	1.01	-	-
Mn	-	-	-	-	-	-	-	-	-	-	0.79	-
As	-	-	-	0.93	-	-	-	-	-	-	-	-
La	19.81	22.1	20.8	18.47	22.09	26.7	8.72	9.37	20.28	19.05	19.47	24.93
Ce	33.83	34.41	30.77	29.97	33.45	33.56	24.31	24.69	28.53	27.92	28.84	32.44
Pr	3.38	-	2.53	2.33	-	-	4.72	4.27	-	-	-	2.81
Nd	10.6	10.86	11.68	10.61	10.27	8.18	24.06	22.61	8.38	8.69	10.62	8.32
Sm	-	-	-	-	-	-	2.84	2.56	-	-	-	-
Th	-	-	2.24	3.11	2.61	-	2.30	3.09	8.42	6.88	6.66	-
O	22.43	21.79	22.55	22.45	21.93	22.35	22.85	23.71	21.63	24.55	23.03	21.58
S	-	-	-	-	-	-	-	-	0.86	-	-	-
F	8.33	8.77	8.72	9.43	8.75	9.2	8.43	7.69	9.77	9.09	8.68	8.73
Total	100.0	100	100	100	100	100	100	100	100	100	100	100

**Table 4.** Representative composition of synchysite from drill hole RCC-09-14. Concentrations of P, Na, Mg, Sr, Mn, As, Fe, Ba, Sm and S were not detected by SEM-EDS analysis. Results in wt.%, normalized to 100 wt.%.

(wt %)	RCC-09-14-1m	RCC-09-14-1m	RCC-09-14-1m	RCC-09-14-1m	RCC-09-14-5.8m	RCC-09-14-80.1m	RCC-09-14-80.1m	RCC-09-14-80.1m	RCC-09-14-80.1m	RCC-09-14-121.2m	RCC-09-14-121.2m	RCC-09-14-121.2m								
Si	-	-	-	-	-	-	-	-	-	-	-	-	-	-	0.87	-	-	-	-	-
Al	-	-	-	-	-	-	-	-	-	-	-	-	-	-	-	-	0.51	-	-	-
Ca	14.42	14.45	12.83	14.97	14.56	15.46	15.5	16.12	14	15.7	13.66	13.66	15.53	14.59	14.25	14.37	14.07	14.61	11.19	
Y	-	-	-	-	2.13	1.44	-	-	-	-	-	-	-	-	-	-	-	-	-	-
La	12.82	12.32	17.41	13.03	11.16	13.00	14.75	12.3	15.61	15.36	15.53	16.07	5.23	5.82	14.4	13.85	15.94	15.55	20.23	
Ce	23.35	23.43	25.27	23.41	23.82	24.05	24.73	24.22	23.29	23.52	24.07	25.25	17.68	16.65	21.07	19.18	24.79	24.19	24.09	
Pr	-	-	-	-	2.92	-	-	-	-	-	8.3	7.27	-	-	-	-	-	2.77	-	
Nd	6.95	9.11	6.17	8.41	10.21	8.38	6.20	8.45	7.01	6.79	2.58	2.75	18.5	19.4	9.18	9.49	8.00	6.44	8.34	
Th	1.89	1.74	2.76	3.30	-	-	1.28	1.70	3.70	2.82	-	-	2.82	3.30	3.15	3.34	-	-	-	
O	33.72	32.59	27.99	30.52	28.64	31.35	31.8	31.41	30.34	30.28	30.58	28.56	33.49	33.67	31.35	33.27	31.31	30.06	29.18	
F	6.86	6.36	7.58	6.35	6.56	6.32	5.74	5.81	6.04	5.54	5.27	6.44	6.74	5.69	6.6	5.99	5.89	6.38	6.96	
Total	100	100	100	100	100	100	100	100	100	100	100	100	100	100	100	100	100	100	100	

**Table 5.** Representative composition of parisite from drill hole RCC-09-14. Concentrations of P, Si, Al, Na, Mg, Mn, As, Fe, Ba, Y, Sm and S were not detected by SEM-EDS analysis. Results in wt.%, normalized to 100 wt.%.

	RCC09-14-121.1m	RCC09-14-121.1m
Ca (wt %)	8.41	8.48
Sr	0.85	-
La	14.99	19.14
Ce	24.69	30.80
Pr	3.04	-
Nd	7.90	8.04
Th	5.40	-
O	22.44	26.04
F	12.27	7.50
Total	100	100

**Table 6.** Representative composition of monazite from drill hole RCC-09-14. Concentrations of Si, Na, Mg, Mn, As, Fe, Y, Pr, and Sm were consistently below the lower limit of detection. Results in wt.%, normalized to 100 wt.%.

	RCC09-14-1m	RCC09-14-1m	RCC09-14-5.8m	RCC09-14-5.8m	RCC09-14-5.8m	RCC09-14-5.8m	RCC09-14-5.8m
P (wt %)	11.17	13.03	11.03	12.69	12.33	12.31	12.75
Al	-	6.35	4.79	-	5.33	6.75	4.22
Ca	4.20	1.60	3.34	2.28	1.33	1.82	1.17
Sr	-	2.82	2.54	-	3.09	2.43	2.83
Ba	-	-	-	1.89	-	-	-
La	18.95	14.15	15.76	18.66	15.69	15.00	16.36
Ce	32.98	21.69	21.46	26.75	22.64	22.48	23.79
Nd	8.38	5.32	6.20	8.80	5.72	4.01	5.49
Th	3.55	-	-	1.99	1.54	-	1.75
O	20.78	34.28	33.4	26.94	31.55	34.28	31.21
S	-	0.76	0.52	-	0.78	0.92	0.43
F	-	-	0.95	-	-	-	-
Total	100	100	100	100	100	100	100

**Table 7.** Representative composition of crandallite group minerals from drill hole RCC-09-14. Concentrations of Na, Mg, Mn, As, Fe, Ba, Y, Pr, Sm and Th were consistently below the lower limit of detection. Results in wt.%, normalized to 100 wt.%.

	RCC09-14- 5.8m	RCC09-14- 80.1m	RCC09-14- 80.1m	RCC09-14- 121.2m	RCC09-14- 121.2m
P (wt %)	9.92	10.88	11.55	11.33	11.25
Si	-	1.72	-	-	-
Al	16.76	20.94	17.88	17.58	17.77
Ca	6.13	3.69	3.35	3.32	2.30
Sr	5.49	-	6.22	7.84	10.74
La	9.83	-	-	4.19	3.50
Ce	8.31	3.06	6.37	5.77	3.70
Nd	-	3.31	-	-	-
O	35.78	52.88	52.79	48.69	48.68
S	1.59	2.34	1.85	1.28	2.07
F	6.18	1.18	-	-	-
Total	100	100	100	100	100

veinlets. Late calcite veinlets cut fractures filled with fluorite and barite and also cut monomineralic pyrite veinlets that postdate fluorite-barite filled fractures (Fig. 3c). Apatite, with dissolution-induced porosity (Fig. 3e) was observed in 4 thin sections (RCC-09-14 40.4, 80.1, 121.2, 124.7).

Bastnäsite-(Ce) contains 8.7 to 26.7 wt.% La, 24.3 to 34.4 wt.% Ce and undetected to 4.7 wt.% Pr, 8.2 to 24.1 wt.% Nd, undetected to 2.8 wt.% Sm, and undetected to 8.4 wt.% Th (Table 3). Synchysite-(Ce) includes 5.2 to 17.4 wt.% La, 16.7 to 25.3 wt.% Ce, undetected to 8.3 wt.% Pr, 2.6 to 19.4 wt.% Nd, undetected to 2.1 wt.% Y and undetected to 3.7 wt.% Th (Table 4). Representative chemical compositions of parisite are shown in Table 5.

Monazite-(Ce) contains 11.03 to 13.03 wt.% P, 14.15 to 18.95 wt.% La, 21.46 to 32.98 wt.% Ce, 4.01-8.80 wt.% Nd, and undetected to 3.55 wt.% Th (Table 6).

The crandallite group mineral contains 9.9 to 11.6 wt.% P, 16.8 to 20.9 wt.% Al, 2.3 to 6.1 wt.% Ca, undetected to 10.7 wt.% Sr, undetected to 9.8 wt.% La, 3.1 to 8.3 wt.% Ce, and undetected to 3.3 wt.% Nd (Table 7). The Raman spectroscopy analysis of the crandallite group mineral shows a mixture of peaks attributable to crandallite, goyazite, and florencite. The crandallite group mineral displays a porous texture and variable chemical composition.

#### 4. Discussion

This mineralogical study supplements the summary of previously published data presented by Green et al. (2017) and confirms that fluorocarbonates and Al-containing phosphates of crandallite group are the main REE-carriers. Both REE carbonates and REE-bearing Al-phosphates are commonly spatially associated with pyrite, barite, and fluorite (Figs. 3a-f). Detailed paragenetic studies are ongoing.

#### 4.1. REE-bearing fluorocarbonates

Bastnäsite-(Ce), synchysite-(Ce) and parisite-(Ce) were identified at the Rock Canyon Creek deposit. Bastnäsite-(Ce) and synchysite-(Ce) are expected to have variable REE content (Fleisher, 1978; Hoshino et al., 2016). Concentrations exceeding 20 wt.% Nd in bastnäsite-(Ce) (sample RCC-09-14 80.1 m; Table 3) are uncommon in carbonatites, granites, and pegmatites but would be expected in hydrothermal deposits (Fleischer, 1978). Concentration of Nd in synchysite (sample RCC-09-14 80.1 m; Table 4) reaches more than 19 wt.%.

As generally reported in the literature, bastnäsite contains <0.3% Th, synchysite <0.8% Th and parisite <1.3% Th (Hoshino et al., 2016). Although REE fluorocarbonates from Rock Canyon Creek contain up to 8.4 wt.% Th, petrographic work failed to reveal visible Th-rich mineral inclusions in these minerals. If such inclusions exist, they must be submicroscopic. Alternatively, Th may be incorporated into the crystal structure of these REE-bearing fluorocarbonates.

#### 4.2. REE-bearing phosphates

Crandallite group minerals, apatite and monazite were identified in this study, and the importance of crandallite group minerals as REE-carriers was confirmed.

Unreported in previous studies (Green et al., 2017), the Monazite-(Ce) documented in this study is texturally and chemically heterogeneous, and incorporating substantial concentrations of Al, Ca and Sr (Table 6). Monazite-(Ce) is commonly mixed with REE fluorocarbonates, crandallite and/or barite (hydrothermal mineralization). It is anhedral, porous in appearance, and fractured. Zoning and embayed boundaries are shown on Figure 3b. Although identifying monazite solely by its chemical composition is difficult, its presence was confirmed by Raman spectroscopy. The composition of monazite is highly

variable and it is probably of secondary origin.

In the Rock Canyon Creek deposit, porous apatite occurs with pyrite, barite, fluorite and REE fluorocarbonates (Fig. 3e), and as disseminated porous grains in dolomite suggesting that it is a primary mineral. Regardless of its origin, apatite commonly contains less than 1 wt.% of  $\Sigma$ REE. The chemical composition of apatite from Rock Canyon Creek will be reported in future studies.

The crandallite group minerals belong to the crandallite-goyazite-florencite solid solution (Table 7). At Rock Canyon Creek, these minerals occur in veinlets. The porous texture and variable chemical composition suggest that the crandallite group minerals probably formed by relatively low-temperature hydrothermal, possibly retrograde, processes. Observed mineral associations suggest that most of the REE-bearing fluorocarbonates in drill hole RCC-09-14 are of hydrothermal origin, along with fluorite, barite, and pyrite. The crandallite group minerals, and possibly monazite, may be of retrograde or supergene origin. The variations in composition of individual REE-bearing minerals probably reflect changes in, for example, the temperature, alkalinity, and composition of hydrothermal fluids or position of the samples in the mineralizing system. Involvement of both hypogene and supergene fluids is possible.

### 5. Future laboratory work

Further mineralogical analyses of samples from drill holes RCC-09-14, RCC-09-10, and RCC-09-02 that intersected the Rock Canyon Creek mineralization will be performed at the Institute for Geo-resources and Environment, Geological Survey of Japan, National Institute of Advanced Industrial Science and Technology in Japan. The following methods will be used.

- Chemical analysis of REE-bearing minerals and major minerals by laser ablation inductively coupled plasma mass spectrometry (LA-ICP-MS).
- Determination of modal abundance of REE minerals in the representative thin sections by automated scanning electron microscope based mineral liberation analysis (MLA).
- Mg isotope analysis of fluorite, calcite and limestone by multi collector ICP-MS.

### Acknowledgments

This paper is a result of cooperation between the Geological Survey of Japan, British Columbia Geological Survey (also part of the Specialty Metal Component of the Targeted Geoscience Initiative 5; spearheaded by Natural Resources Canada), and Mr. Chris Graf and Spectrum Mining Corporation, the owners of the Rock Canyon Creek deposit. We thank Mr. Chris Graf for guidance in the field, permission to sample the core, and enriching discussions. Ms. Fiona Katay (British Columbia Ministry of Energy and Mines, Cranbrook) provided invaluable field survey and core logging support.

### References cited

- Green, C., Simandl, G.J., Paradis, S., Katay, F., Hoshino, M., Kon, Y., Kodama, S., and Graf, C., 2017. Geological setting of the Rock Canyon Creek REE-fluorite deposit, British Columbia, Canada. In: Geological Fieldwork 2016, British Columbia Ministry of Energy and Mines, British Columbia Geological Survey Paper 2017-1, this volume.
- Fleisher, M., 1978. Relative proportions of lanthanides in minerals of the bastnaesite group, *Canadian Mineralogist*, 16, 361-363.
- Hora, Z.D., and Kwong, Y.D.J., 1986. Anomalous rare earth elements (REE) in the Deep Purple and Candy claims. In: Geological Fieldwork 1985, British Columbia Ministry of Energy, Mines, and Petroleum Resources, British Columbia Geological Survey, Paper 1986-1, pp. 241-242.
- Hoshino, M., Sanematsu, K., and Watanabe, Y., 2016. REE mineralogy and resources. Handbook on the Physics and Chemistry of Rare Earths, Elsevier: Amsterdam, 49, Chapter 249, pp. 129-291.
- Pell, J., 1994. Carbonatites, nepheline syenites, kimberlites and related rocks in British Columbia. British Columbia Ministry of Energy, Mines, and Petroleum Resources, British Columbia Geological Survey, Bulletin 88, 44p.
- Pell, J., and Hora, Z.D., 1986. Geology of the Rock Canyon Creek fluorite/rare earth element showing southern Rocky Mountains (82J/3E). In: Geological Fieldwork, 1986, British Columbia Ministry of Energy, Mines and Petroleum Resources, British Columbia Geological Survey Paper 1987-1, pp. 255-258.
- Pighin, D.L., 2010. Assessment Report Rock Canyon Property, British Columbia Geological Survey Assessment Report 31435. 109p.
- Simandl, G.J., Prussin, E.A., and Brown, N., 2012. Specialty metals in Canada. British Columbia Ministry of Energy, Mines and Natural Gas, British Columbia Geological Survey Open File 2012-7, 48p.



# Using derived-stereo imagery to map macroscale ice-flow features



H. Arnold<sup>1, a</sup>, and A.S. Hickin<sup>1</sup>

<sup>1</sup>British Columbia Geological Survey, Ministry of Energy and Mines, Victoria, BC, V8W 9N3

<sup>a</sup>corresponding author: Holly.E.Arnold@gov.bc.ca

Recommended citation: Arnold, H., and Hickin, A.S., 2017. Using derived-stereo imagery to map macroscale ice-flow features. In: Geological Fieldwork 2016, British Columbia Ministry of Energy and Mines, British Columbia Geological Survey Paper 2017-1, pp. 215-229.

## Abstract

Understanding the extent, flow paths, and history of glaciers and ice sheets comes from interpreting landforms, some of which were created by subglacial processes. Subglacial streamlined landforms, such as crag-and-tails, drumlins, drumlinoids, and flutes (ice-flow features), form parallel to ice flow. Given the cost of fieldwork in remote regions, even the most recent compilations of these landforms in the Canadian Cordillera are incomplete. Derived-stereo imagery provides the ability to incorporate single-frame imagery into traditional stereo airphoto methods to remotely map these features at significantly less cost. A comparison of stereoscopic air photographs and two derived-stereo imagery types (Satellite Pour l'Observation de la Terre and orthomosaics) to map ice-flow features in the Atlin and Liard Plain areas of northern British Columbia indicates that derived-stereo orthomosaics provide government agencies, who can access the orthomosaics at no cost, the best value to map ice-flow features for the British Columbia Geological Survey ice-flow feature compilation. Although derived-stereo SPOT imagery is inferior to airphotos and derived-stereo orthomosaics, it may be adequate for regional ice-flow studies and, freely accessed, may be better suited to the general public.

**Keywords:** Derived-stereoscopic imagery, stereoscopic imagery, subglacial streamlined landforms, ice-flow feature compilation

## 1. Introduction

The Cordilleran Ice Sheet (CIS) refers to the mass of mountain ice caps and interconnected valley and piedmont glaciers that occupied western Canada, Alaska, Washington, Idaho, and Montana during major Quaternary glaciations (Jackson and Clague, 1991). The CIS formed and decayed several times, expanding from topographically controlled alpine glaciers that coalesced and reached sufficient thicknesses to flow independent of topography (Clague, 1989; Fulton, 1991; Jackson and Clague, 1991; Stumpf et al., 2000; Clague and Ward, 2011). Ice-flow landforms and ice sheet models indicate that ice in the interior of British Columbia was thick enough to flow west, across the Coast Mountains and onto the continental shelf, and east, across the Rocky Mountains onto the Canadian Interior Plains (Clague, 1989; Fig. 1). Understanding the extent, flow pathways, and history of the most recent CIS (Late Wisconsinan; ~22-10 ka; almost equivalent to marine isotopic stage 2) comes from interpreting landforms, some of which were created by subglacial processes (see Kleman, et al., 1997; Boulton et al., 2001; King et al., 2009; Clark et al., 2012; Stokes et al., 2015). Landforms, such as crag-and-tails, drumlins, drumlinoids, and flutes are streamlined along ice flow directions (referred to as ice-flow features) (Menziess, 1979; Boulton, 1987; Clark, 1993; Evans et al., 2006; Benn and Evans, 2010). Although Ferbey and Arnold, (2013), Ferbey et al. (2013) and Arnold et al. (2016) have compiled such ice-flow features formed in the Canadian Cordillera, mapping is incomplete. For example, the lack of ice-flow features in

large regions (Arnold et al., 2016) may merely reflect gaps in mapping. The British Columbia Geological Survey and the Geological Survey of Canada, under the Geo-mapping for Energy and Minerals (GEM) program, are collaborating to address some of the mapping inadequacies. In this paper, we evaluate a relatively inexpensive approach that uses small-scale imagery to map macroscale ice-flow features.

Most maps of ice-flow features in British Columbia have been generated using traditional stereoscopic aerial photography (Ferbey et al., 2013), in which sequential frames have significant overlap (60% along flight; 20-40% across flight; e.g., Aber et al., 2010). This overlap, needed for traditional stereo viewing, demands many images, which makes it expensive to map large areas with gaps in the Cordillera. As an alternative approach, digital derived-stereo imagery takes a single image and combines it with a digital elevation model (DEM) to generate a second offset image (DAT/EM, 2012). The original and generated images are combined using photogrammetric software to display a stereoscopic image (i.e., in 3D; DAT/EM, 2012). Because this approach does not require overlapping images, fewer are needed for regional mapping. Furthermore, fewer images or remote sensing scenes (e.g., Landgrebe, 2003) are needed because satellite imagery and orthomosaics commonly extend across large areas, although the resolution of this imagery is commonly lower than traditional digitized airphotos. Here we evaluate stereoscopic aerial photography and two derived-stereo imagery types (Satellite Pour l'Observation de la Terre or SPOT, and orthomosaics) for

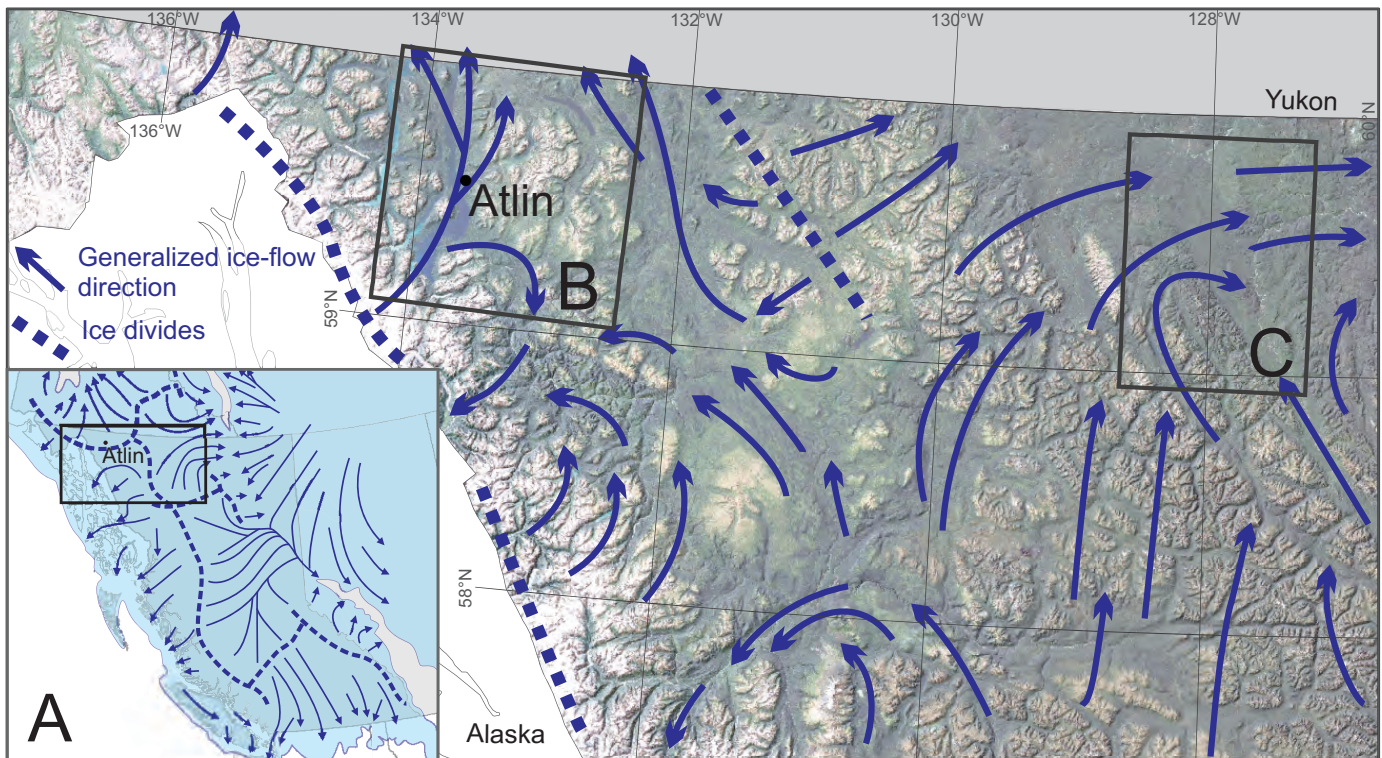


**Fig. 1.** a) Cordilleran ice sheet during the Late Wisconsinan and location of study areas (after Clague and Ward, 2011). Major Late Wisconsinan ice-flow directions in b) the Atlin area and c) the Liard Plain (summarized from Ryder and Maynard, 1991).

mapping ice-flow features in the Atlin and Liard Plain areas of northern British Columbia (Fig. 1).

## 2. Regional setting

The Atlin area was selected because overlapping remote sensing datasets (airphotos and SPOT) and maps depicting ice-flow features (Levson et al., 2003) are available. The Atlin area (Fig. 2a) is in the Teslin Plateau, with its gently sloping uplands and wide valleys. Peaks of the Snowdon, Lina, Johnson, Laurie, and Sloko ranges rise above the plateau surface. To the west, the Tahltan Highlands form the transition from the Teslin Plateau to the Coast Mountains (Holland, 1976). At glacial maximum, ice centres for the northern CIS were most likely over the Coast Mountains west of the Atlin area and in the Skeena Mountains and Stikine Plateau to the south (Figs. 1, 2a; Ryder and Maynard, 1991; Seguinot et al., 2016). Aitken (1959) interpreted that three ice streams flowed through the Atlin area. Accordingly, one flowed northeast from the Coast Mountains, north along Atlin Lake, then branched northwest through the Jones Lake valley (Aitken, 1959; Levson et al., 2003). The second flowed from the south end of Atlin Lake, east through the Pike and O'Donnell valley before deflecting south into the Taku Trench (Figs. 1, 2a). A third ice stream, probably sourced from ice caps in the Stikine Plateau, flowed through the broad valley now occupied by Gladys Lake and Hall Lake (Fig. 2a) and is part of the Teslin ice stream, which can be tracked more than 500 km from Tanzilla River in British Columbia, north into Yukon (Ryder and Maynard, 1991). Major

topographic features have had a profound influence on the ice-flow directions of both ice streams and valley glaciers (Ryder and Maynard, 1991). During deglaciation, topography and local relief likely controlled the flow of valley glaciers sourced in upland areas (Fig. 2a).

The Liard Plain was also selected because overlapping remote sensing datasets and maps depicting ice flow (Gabrielse, 1963) are available. The gently rolling lowlands of the Liard Plain rise in elevation to the southwest into the flat-topped ridges and rounded mountains of the Dease Plateau, southeast of which are the rugged mountains of the Ketchika Ranges (Fig. 2b; Holland, 1976). At glacial maximum, the northern CIS in British Columbia flowed north across the western Liard Plain into the Yukon (Jackson, 1994; Kennedy and Bond, 2004) and east through the Liard Plain to the edge of the Cordilleran deformation front, coalescing with the westward-flowing Laurentide Ice Sheet (Bednarski, 2008; Margold et al., 2013; Huntley et al., 2016; Figs. 1, 2b). In the final stages of deglaciation, ice diminished through active retreat rather than ice stagnation (Margold et al., 2013) and ice sourced in local uplands flowed down valleys and converged with montane glaciers that persisted in major trunk valleys.

## 3. Methods

### 3.1. Stereoscopic and derived-stereo imagery

Advances in 3D digital technology have enabled the transition from mapping using hardcopy aerial photographs to the digital environment. Specialized photogrammetric software is used

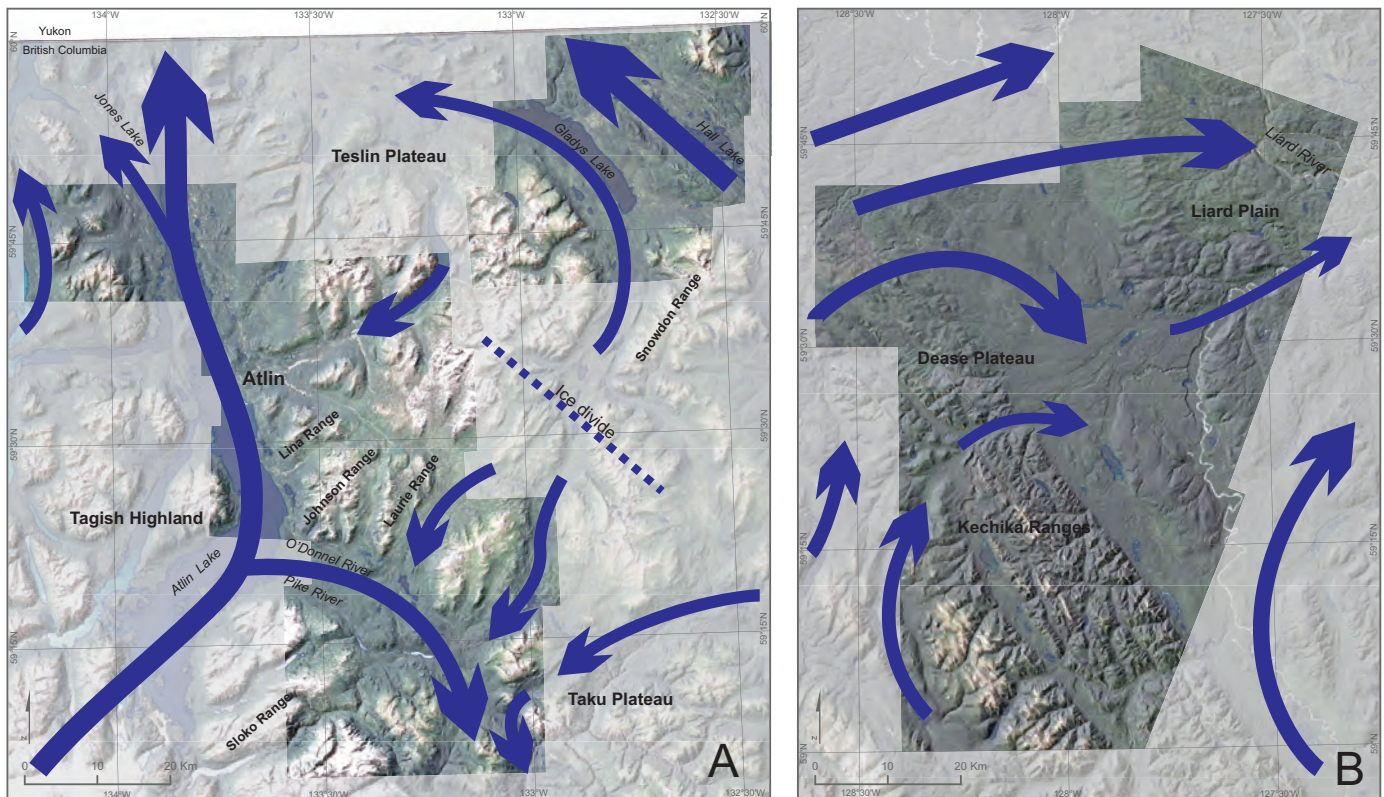


**Fig. 2.** Areas mapped (dark shading). **a)** Atlin area with ice-flow directions during the Late Wisconsinian, summarized from Aitken (1959), Ryder and Maynard (1991), Levson et al. (2003) and Clague and Ward (2011). **b)** Liard Plain area with ice-flow directions during the Late Wisconsinian, summarized from Gabrielse (1963) Jackson and Mackay (1990) Jackson et al. (1991) Ryder and Maynard (1991), and Margold et al. (2013).

to digitize 3D vectors directly into a geographic information system (GIS) and superimpose them on stereo imagery for immediate verification and editing. Stereo imagery (Fig. 3a), such as the airphotos used in this project, can be georeferenced and loaded for use in stereo photogrammetric software. We use SPOT and orthomosaic derived-stereo imagery to evaluate their value for mapping macroscale ice-flow features.

Like traditional stereo-paired airphotos, derived-stereo imagery requires two overlapping images for 3D display. However, unlike stereo-paired photographs, SPOT and orthomosaics are single frames with minimal overlap and must be digitally processed to render an offset image (Fig. 3b). The second, or derived image, is a duplicate of the original and is displaced in the direction of flight by a percent of the DEM resolution. The Shuttle Radar Topography Mission (SRTM) 1 Arc-second DEM was selected to produce derived-stereo imagery (SRTM, 2014). The amount of displacement (shift) selected between the derived and original images is 0.125 of the SRTM DEM resolution (1 Arc-second = ~30 m resolution;  $30 \text{ m} \times 0.125 = 3.75 \text{ m}$  horizontal shift in the direction of flight). The 'new' offset derived image is then draped over the DEM surface to spatially reference each of the pixels in the image. The edges of the new image are no longer straight, but instead pixels are warped to fit onto the DEM. This creates an image with a new perspective which, when combined with the original image, will appear in 3D (Fig. 4). We used DAT

EM's Summit Evolution photogrammetric software to create 3D stereo models. As with imagery flown in stereo, relief in the derived-stereo imagery is exaggerated. This exaggeration is a function of the horizontal offset between the original and derived images and the elevation range in the derived-stereo pair (Fig. 5).

### 3.2. Imagery types

We evaluated three imagery types: 1) traditional stereoscopic panchromatic 1:70,000-scale airphotos; 2) derived-stereo panchromatic SPOT imagery at 10 m resolution; and 3) derived-stereo panchromatic 1:20,000-scale orthomosaics. Fifty-nine digital aerial photographs were purchased from the Government of British Columbia for \$18.50 per photo. The photos were taken in 1987 and 1988 and cover an area of about 4,000 km<sup>2</sup>. A contractor georeferenced each image and digital stereo projects were created using Summit Evolution for \$20 per image (Table 1). Thirteen SPOT images were obtained from the Government of Canada at no cost (SPOT, 2010). Each SPOT image covers about 3,800 km<sup>2</sup> and has overlap of ~15 km west to east and ~5 km north to south (Fig. 3b). The images are from the SPOT 4 and SPOT 5 missions flown between 2005 and 2010. The derived-stereo SPOT imagery was produced by a contractor at a cost of \$20 per image (Table 1). Forty-one orthomosaics were obtained from the Government of British Columbia, at no cost for internal government use; the cost for external users is \$200

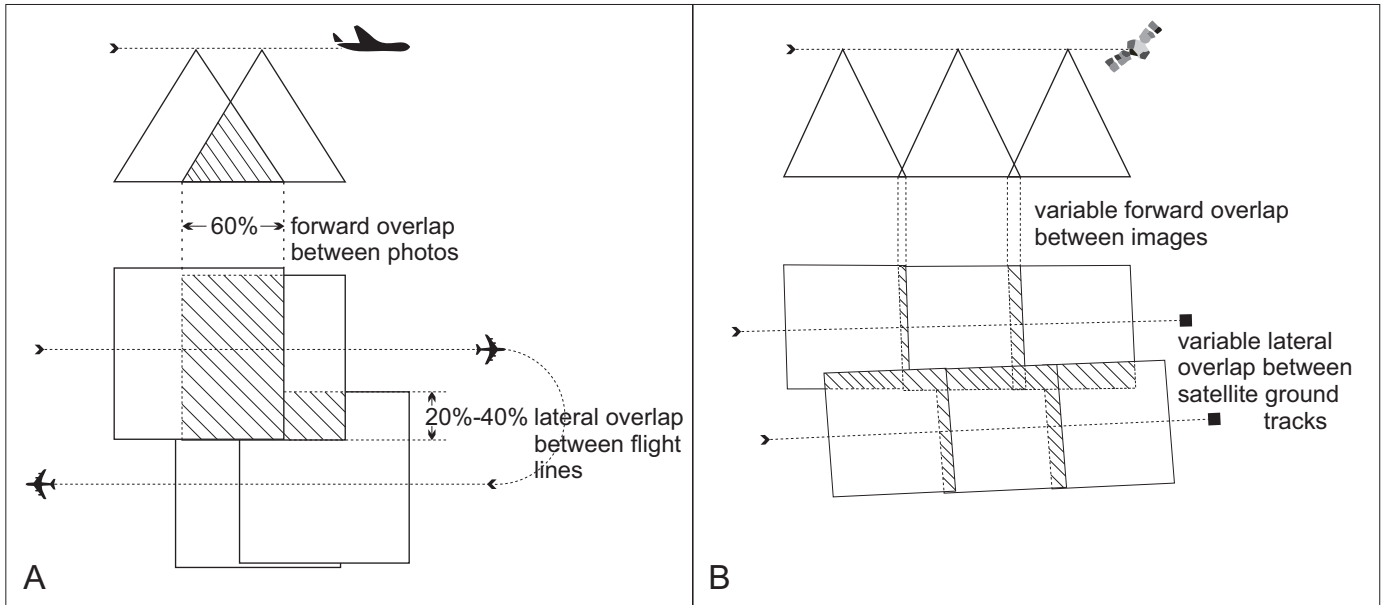


**Fig. 3. a)** Flight path for stereo imagery, with systematic overlap between sequential images. **b)** Flight path for non-stereo imagery, with variable overlap between sequential images. Modified after NRCAN (2016).

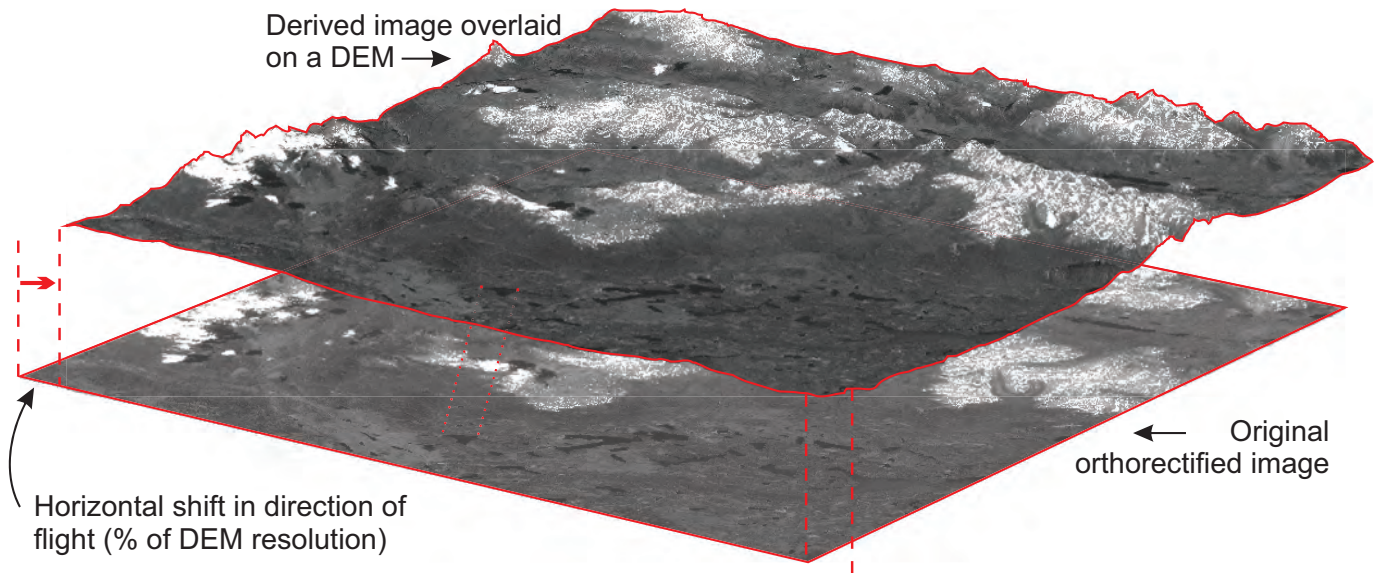


**Fig. 4.** Derived-stereo imagery is created by horizontally shifting a duplicate (derived image) in the flight direction. The derived image is then overlain on a DEM and georeferenced, providing a new perspective of the image based on topography. The amount of horizontal shift of the derived image is a percentage of the DEM resolution.

per frame. Each image covers about 130 km<sup>2</sup> with no overlap between images. The derived-stereo orthomosaic imagery was produced by a contractor for \$20 per image (Table 1).

**3.3. Ice-flow mapping**

We mapped ice-flow features for each imagery type, using Summit Evolution Lite running in tandem with ArcGIS, at scales of 1:4,000 (airphotos), 1:10,000 (SPOT imagery) and 1:4,000 (orthomosaics). Each feature was mapped manually

as a line (i.e., start node beginning up-ice and end node down-ice), recording length and directionality (unidirectional or bidirectional). Lines were converted to points and line azimuths were calculated and recorded. We then compared the data acquired from each imagery type. Where a feature was identified in different imagery types, we evaluated the consistency of location, length, azimuth, and if ice-flow directionality could be determined.

For the Atlin area, we compared features derived from:

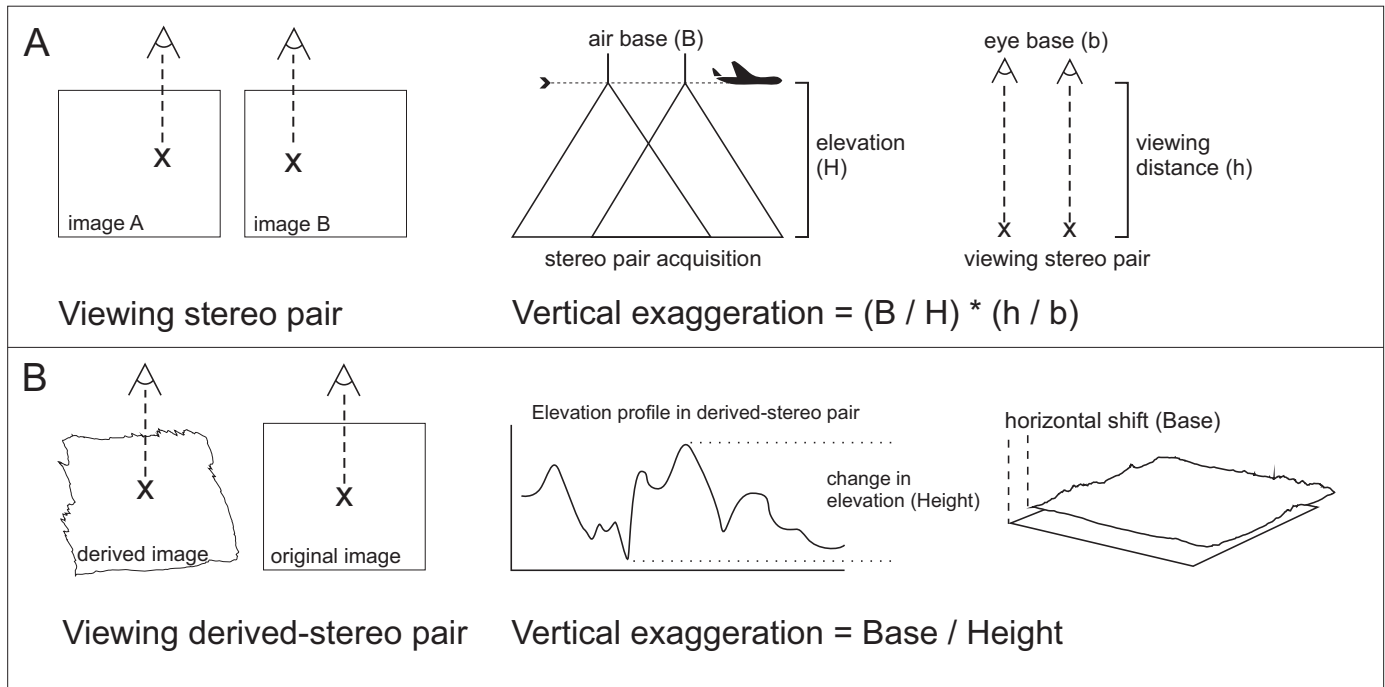


Fig. 5. Vertical exaggeration in a) Stereo imagery and b) Derived-stereo imagery. Modified from Sabins (1997) and Paine and Kiser (2012).

Table 1. Cost to create digital stereo and digital derived-stereo pairs for each imagery type.

Imagery type	Number of frames	Acquisition cost	Stereo/derived-stereo conversion (per frame)	Approximate area (km <sup>2</sup> )	Total		Cost per 100 km <sup>2</sup>
					cost	area (km <sup>2</sup> )	
Airphotos	59	\$ 18.50	\$ 20.00	68	\$ 2,271.50	4,000	\$ 56.79
SPOT	13	-	\$ 20.00	3,800	\$ 260.00	49,400	\$ 0.53
Orthomosaics	41	-	\$ 20.00	130	\$ 820.00	5,330	\$ 15.38

1) airphotos and mapping by Levson et al. (2003); 2) SPOT imagery and mapping by Levson et al. (2003); and 3) airphotos and SPOT imagery. For the Liard Plain area, we compared results from: 1) orthomosaic imagery and mapping by Gabrielse (1963); 2) SPOT imagery mapping by Gabrielse (1963); and 3) orthomosaic imagery and SPOT imagery.

Commonly, a single symbol is used to portray multiple streamlined features on surficial geology maps. Consequently, a single map symbol cannot be directly compared with a single ice-flow feature identified in the imagery. To enable more direct comparisons, we used buffers of 500 m and 1,000 m around each ice-flow map symbol in Levson et al. (2003) and Gabrielse (1963). In some cases ice-flow symbols in Levson et al. (2003) represent separations closer than 500 or 1000 m. In these situations, all ice-flow features in the imagery within 500 or 1,000 m of an ice-flow symbol were included in the comparison.

Levson et al. (2003) used hardcopy airphoto interpretation combined with field checks to produce earlier versions (see Levson, 1992; Levson and Kerr, 1992) of their map. Given that the same imagery type is used, significant differences

are unexpected when ice-flow features using digital airphotos are compared to those mapped by Levson et al. (2003). This comparison highlights the transition from hardcopy airphoto interpretation to the digital environment and provides a means of verifying the ice-flow features mapped using digital airphotos in part of the Atlin area (~780 km<sup>2</sup>). The methods used to produce Gabrielse (1963) map were not identified.

4. Results

4.1. Atlin area

4.1.1. Airphotos and features mapped by Levson et al. (2003)

Levson et al. (2003) shows 36 ice-flow symbols in an area of about 780 km<sup>2</sup> (Fig. 6; Table 2). Using the airphotos, 51 ice-flow features were identified in the same area. Of the ice-flow features recognized in the airphotos, 36 are within 500 m of 24 of the symbols in Levson et al. (2003). Therefore, within 500 m of where symbols were plotted, 12 of the ice-flow symbols in Levson et al. (2003) were not recognized on the airphotos (Fig. 7). Of the adjacent features, 47% on the airphotos have an ice-flow azimuth within 5° of the azimuth of the symbols

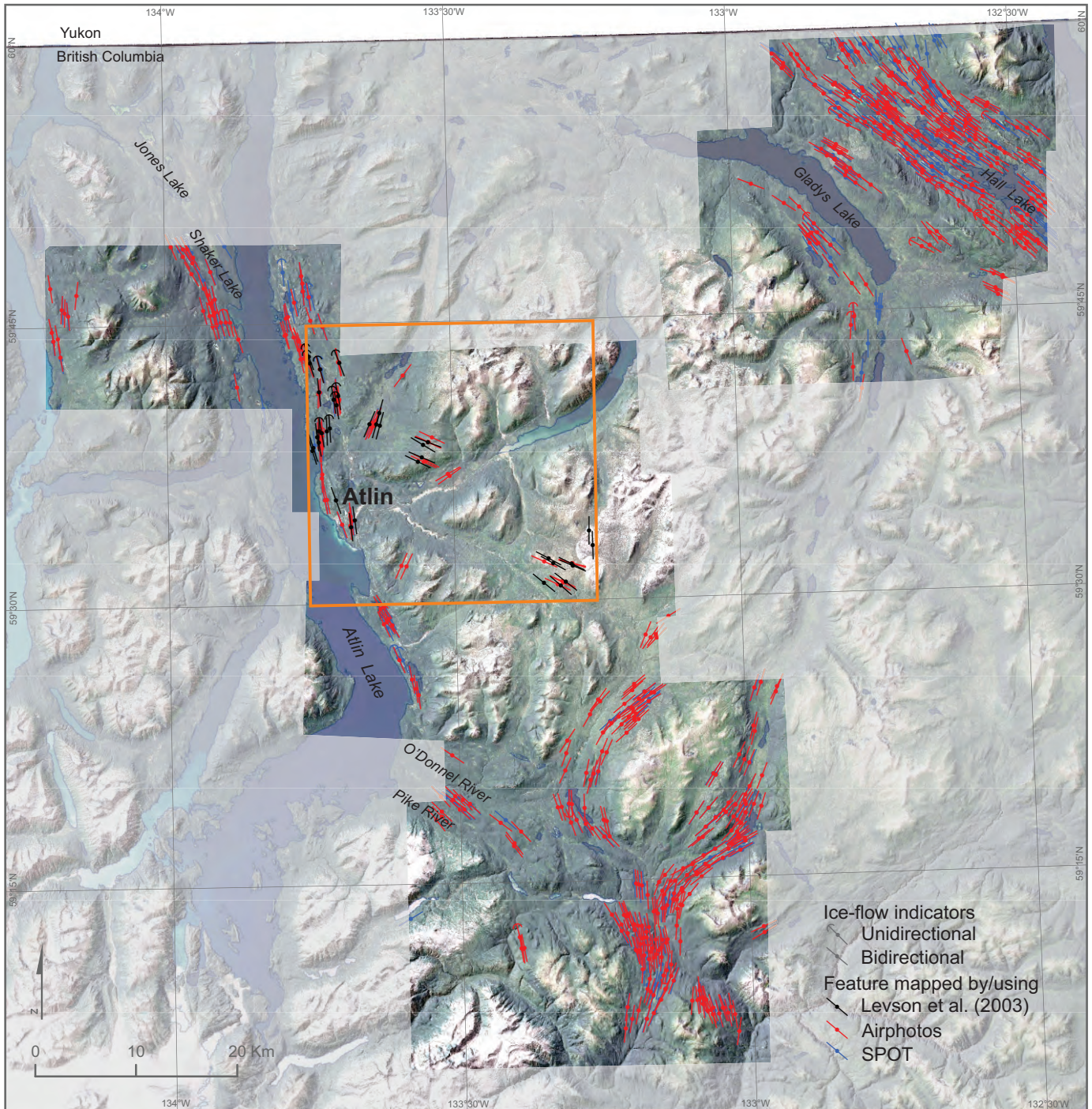


**Fig. 6.** Ice-flow feature mapping in the Atlin area. Orange box indicates area mapped by Levson et al. (2003).

on Levson et al. (2003) and 92% are within 10° (maximum discrepancy is 17°). The expanded 1,000 m buffer includes 42 ice-flow features identified in the airphotos. Thus, 33 of the 36 ice-flow symbols represented on the map have adjacent airphoto features within 1,000 m. Of the adjacent airphoto features, 43% have an ice-flow azimuth within 5° of symbols in Levson et al. (2003) and 83% are within 10° (maximum discrepancy of 18°; Table 3). Three ice-flow features identified by Levson et al. (2003) were not identified in the airphotos (Fig. 7, points

1-3). Two of these (Fig. 7, points 1-2) are in an area of high tonal saturation in the airphotos, which hampers identification. Levson et al. (2003) identified nine unidirectional features in the map area, but only one was identified in the airphotos, which underscores the importance of field checks.

#### 4.1.2. SPOT and features mapped by Levson et al. (2003)

Using the SPOT imagery, 21 ice-flow features were identified in the area mapped by Levson et al. (2003). Of these, 17 are

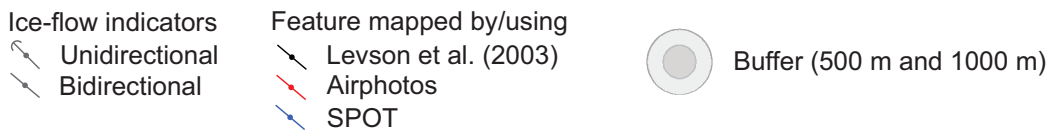
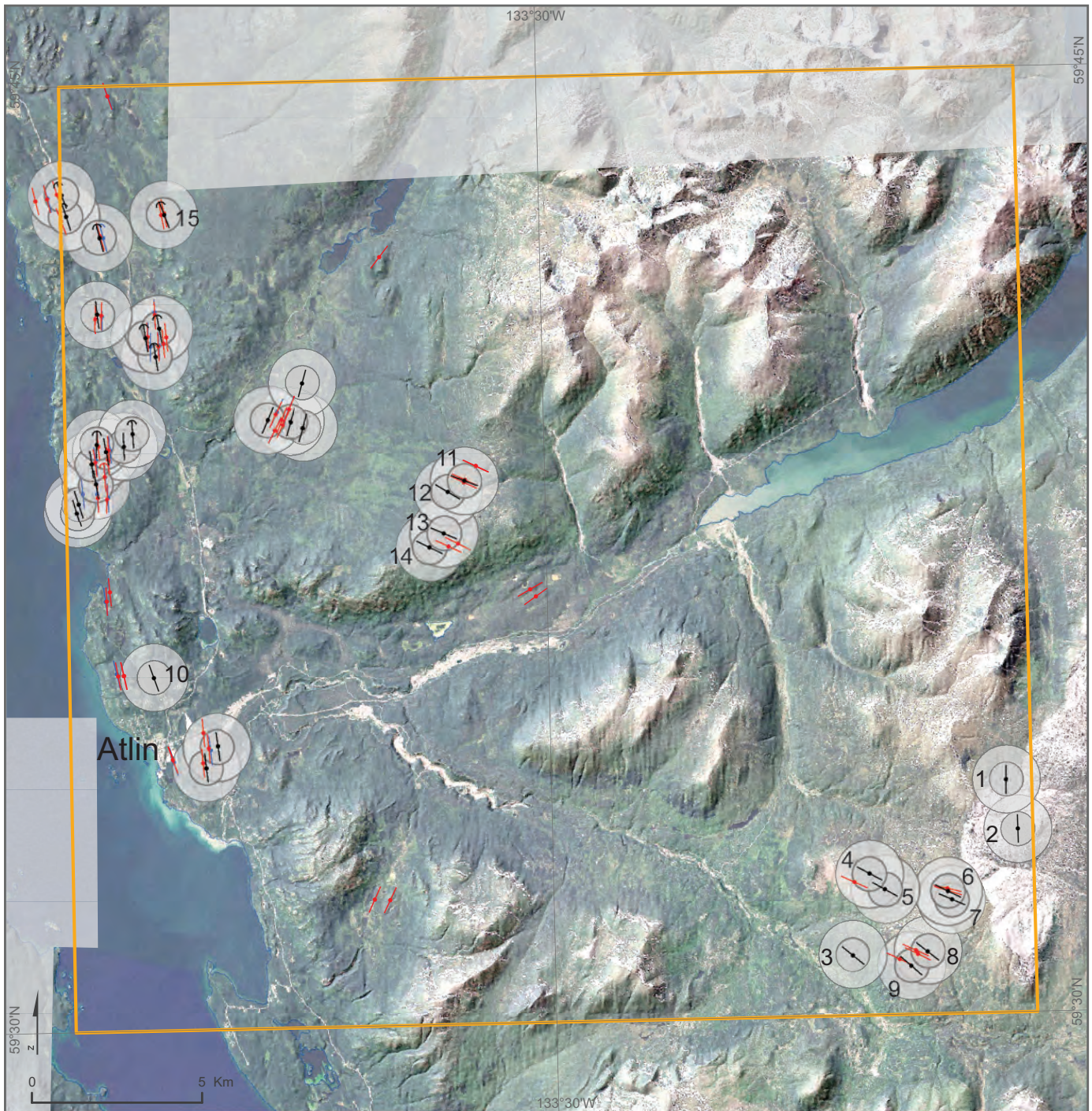


**Fig. 7.** Comparison of ice-flow mapping (orange box) completed by Levson et al. (2003) to features identified in airphotos and SPOT imagery. Two buffers of 500 m and 1,000 m were used. Numbers 1-3 depict features mapped by Levson et al. (2003) that were not identified in the airphotos. Numbers 1-15 depict features mapped by Levson et al. (2003) that were not identified in the SPOT imagery.

within 500 m of the ice-flow symbols in Levson et al. (2003). The 17 features are adjacent to 15 (of the 36) ice-flow symbols. Of these adjacent features, 35% of the ice-flow features from the SPOT imagery have an azimuth within 5° of the mapped symbols, and 94% are within 10° (maximum discrepancy of 12°). A total of 18 ice-flow features identified using SPOT imagery are within 1,000 m of the symbols on Levson et al. (2003). The 18 SPOT features are adjacent to 21 of the 36 ice-flow symbols in Levson et al. (2003). Of the SPOT ice-flow features, 28% have an azimuth within 5° of the symbols on the map and 72% are within 10° (maximum difference of 15°; Table 3). Fifteen of the 36 features symbolized in Levson et al. (2003) lacked corresponding features in the SPOT imagery (Fig. 7, points 1-15). One unidirectional ice-flow feature was identified in the SPOT imagery that is within 500 m of a unidirectional feature identified by Levson et al. (2003).

**4.1.3. Airphotos and SPOT imagery**

In the area of overlapping airphoto and SPOT imagery (about 4,000 km<sup>2</sup>), 579 ice-flow features were detected using airphotos; 35 were identified as unidirectional (Table 2). Using the SPOT

imagery, 349 ice-flow features were identified, nine of which are unidirectional (Table 2). Comparing the airphoto and SPOT imagery datasets, 249 of the ice-flow features are coincident in both imagery types (Figs. 6, 8). Several longer ice-flow features identified in the SPOT imagery appear as two separate features in the airphotos. In some cases, parallel features in the airphotos appear as a single feature in the SPOT imagery. Variance in the ice-flow direction of the features identified in the two imagery types is low; 91% of coincident features have azimuths within 5° (Table 3) and the largest discrepancy is 11°. The median difference in the length of a feature mapped using both imagery types is 119 m. However, the features were not longer consistently in one imagery type. Only one feature was mapped as unidirectional in both the airphotos and SPOT imagery.

**4.2. Liard Plain area**

**4.2.1. Orthomosaic imagery and features mapped by Gabrielse (1963)**

The Gabrielse (1963) map overlaps with the western half of the Liard Plain area. Gabrielse (1963) mapped 19 ice-flow features

**Table 2.** Ice-flow features identified in imagery types.

Map area	Ice-flow feature mapping	Total number of features	Unidirectional features
Atlin	Airphoto	579	35
	SPOT	349	9
	Single feature identified in airphoto & SPOT	249	1
	Levson et al. (2003)	36	9
Liard Plain	Orthomosaics	741	41
	SPOT	275	10
	Single feature identified in orthomosaic & SPOT	154	0
	Gabrielse (1963)	19	19

**Table 3.** Variability of ice-flow direction in features identified in two imagery types and each imagery type to published maps.

Map area	Ice-flow feature mapping	Ice-flow direction variance			Median absolute difference in length (m)	
		Buffer	within 5°	within 10°		max
Atlin	Airphoto & SPOT		91%	99.60%	11	119
	Levson et al. (2003) & airphoto	500 m	47%	92%	17	
		1000 m	43%	83%	18	
	Levson et al. (2003) & SPOT	500 m	35%	94%	12	
1000 m		28%	72%	15		
Liard Plain	Orthomosaic & SPOT		92%	100%	8	117
	Gabrielse (1963) & orthomosaic	500 m	64%	91%	11	
		1000 m	60%	86%	17	
	Gabrielse (1963) & SPOT	500 m	100%	100%	2	
1000 m		87%	100%	7		

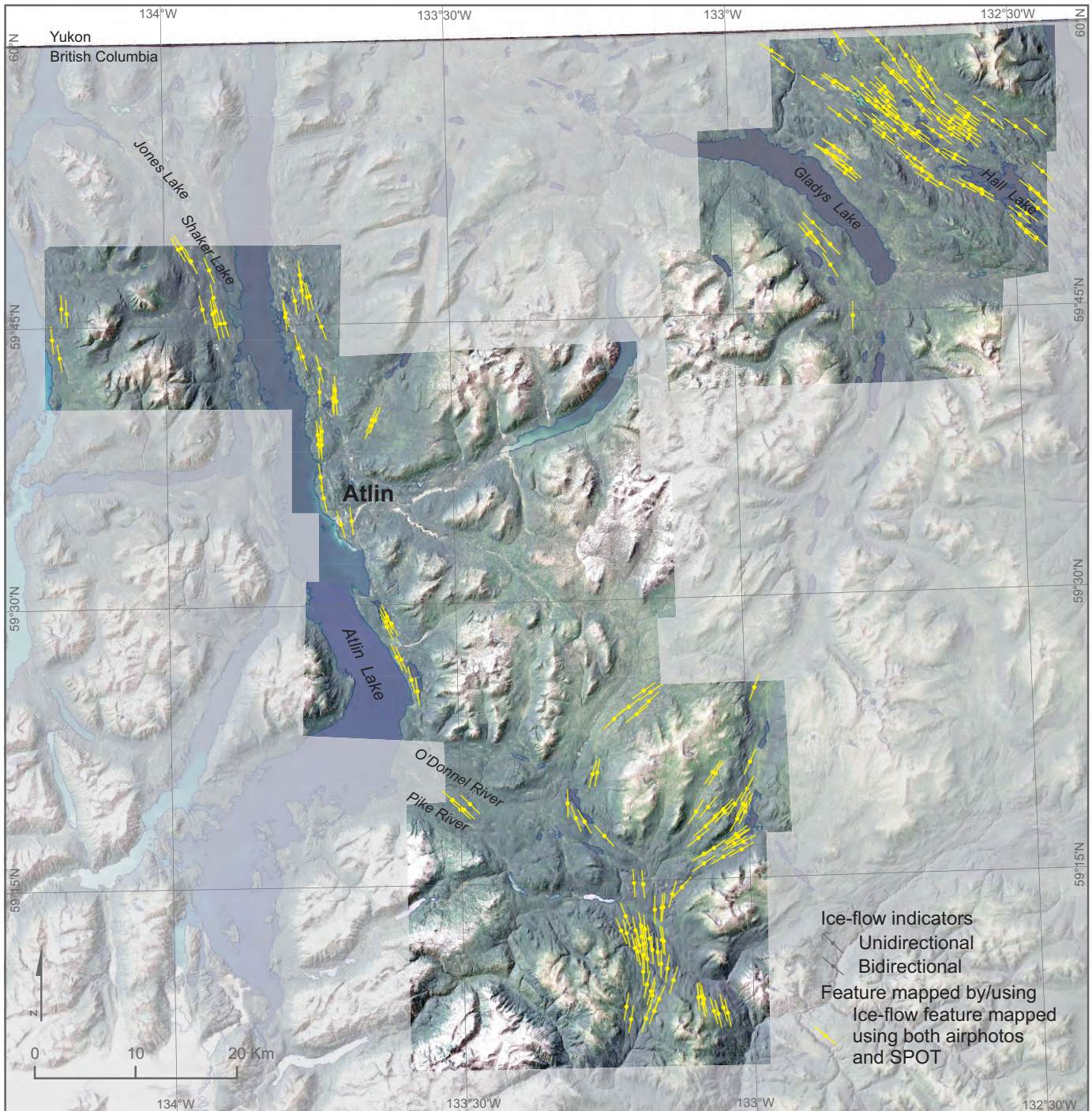


**Fig. 8.** Ice-flow features identified in both airphotos and SPOT imagery in the Atlin area.

in an area of about 2,020 km<sup>2</sup> (Fig. 9; Table 2). In the same area, 393 ice-flow features were identified in the orthomosaics. Eleven features identified using orthomosaics are within 500 m of eight of the 19 features in Gabrielse (1963). Eleven of the features symbolized on the Gabrielse (1963) map were not identified within 500 m in the orthomosaics. Of the Gabrielse (1963) symbols within 500 m, 64% of the orthomosaic features have an ice flow direction within 5°, and 91% are within 10°

(with maximum discrepancy of 11°). When comparing the ice-flow features identified in the orthomosaics to the symbols in the Gabrielse (1963) map using the 1,000 m buffer, 49 features identified using orthomosaics are within 1,000 m of 13 of the 19 ice-flow features symbolized by Gabrielse (1963). Of the adjacent features, 60% of the orthomosaic features have an azimuth within 5° of the symbolized features in Gabrielse (1963) and 86% are within 10° (maximum discrepancy of 17°;

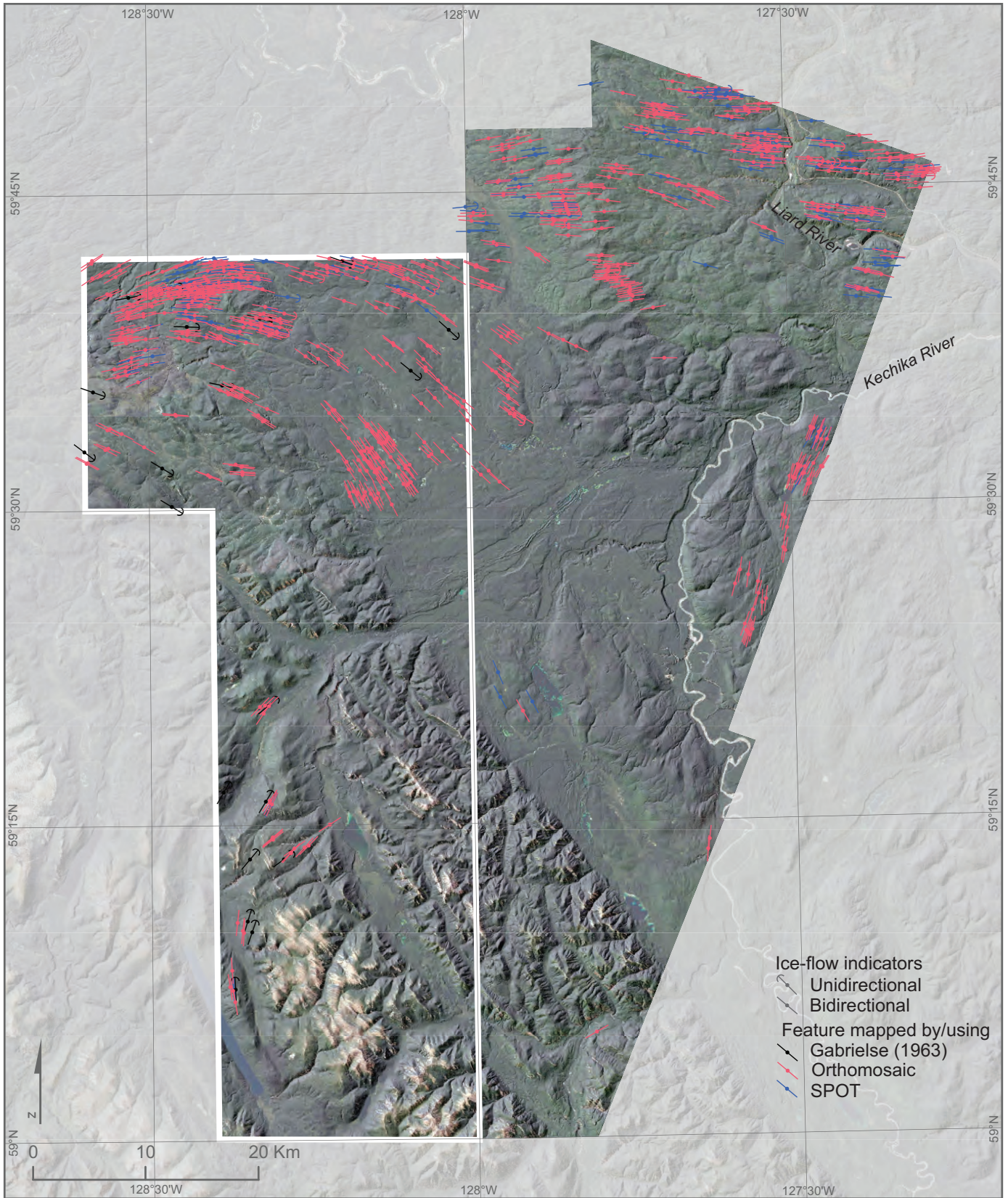


**Fig. 9.** Ice-flow features mapped in the Liard Plain area. Gabrielse (1963) map outlined in white.

Table 3). Six ice-flow features symbolized by Gabrielse (1963) were not identified in the orthomosaic (Fig. 10, points 1-6). All of the 19 features symbolized in Gabrielse (1963) indicate unidirectional flow. Of the 19 unidirectional features identified in the orthomosaics, only two are within 1,000 m of those symbolized by Gabrielse (1963).

#### 4.2.2. SPOT and features mapped by Gabrielse (1963)

Using the SPOT imagery, 94 ice-flow features were identified in the area mapped by Gabrielse (1963). Three features are immediately adjacent to two symbols on the Gabrielse (1963) map and have ice-flow directions within 5°. The SPOT imagery identified 15 ice-flow features within 1,000 m of six features symbolized by Gabrielse (1963). Of the adjacent SPOT ice-flow features, 87% have ice-flow directions within 5° of the symbolized features and all are within 10° (maximum discrepancy of 7°; Table 3). Thirteen symbols in the Gabrielse (1963) map were not identified using SPOT (Fig. 10, points 1-13). One unidirectional ice-flow feature was identified in the SPOT imagery, and it is within 1,000 m of a unidirectional symbol in Gabrielse (1963).

#### 4.2.3. Orthomosaic imagery and SPOT imagery

In the area with overlapping orthomosaic and SPOT imagery (approximately 4,450 km<sup>2</sup>), 741 ice-flow features were identified using orthomosaics, of which 41 are unidirectional. A total of 257 ice-flow features are identified using the SPOT imagery, of which 10 are unidirectional. In this overlap area, 154 ice-flow features coincide (Figs. 9, 11; Table 2). Several features identified as single features in the SPOT imagery appear as two separate features in the orthomosaics. In the orthomosaics, some appear as two shorter features with the same bearing, with the centreline of pairs coinciding with the feature mapped in the SPOT imagery. Variance in ice-flow directions of the coincident features identified in the two imagery types is low, as 92% of the features are within or below 5°, with a maximum discrepancy of 8° (Table 3). The median difference in length of a feature mapped using both imagery types is 117 m; 60% of coincident occurrences are longer in the orthomosaics. Three features were mapped as unidirectional in both imagery types.

### 5. Discussion

Consistencies between datasets indicate that derived-stereo imagery is useful for remotely generating macroscale ice-flow data for inclusion in regional compilations. Comparison of data from the Atlin area suggests that digital stereoscopic airphoto imagery, which has the highest spatial resolution, is the most effective. Although fewer ice-flow features are resolved in the SPOT data, major flow sets are discernible and the number of features mapped is adequate to determine a general ice flow history. Data comparison in the Liard Plain reveals that orthomosaics may be superior to SPOT, again reflecting better resolution of the imagery.

Airphotos are the traditional and proven method for mapping landforms (e.g., Mollard, 1976). Because ice flow-sets are often

depicted on maps as a symbol, direct comparison of ice-flow features identified in stereoscopic airphotos and those depicted by map symbols is limited. Two clusters of ice-flow features depicted on the Levson et al. (2003) map were not detected with the stereoscopic airphotos. These features may have been encountered during fieldwork (Fig. 7, points 1 and 2, and 3). Five clusters of ice-flow features depicted in the Levson et al. (2003) map were not detected in the SPOT data. Nevertheless, most of the major flow sets are clearly identified by the SPOT data (Fig. 7).

However, our evaluation suggests that most of the major flow sets identified in Levson et al. (2003) are recognizable by using the stereoscopic airphotos to map ice-flow features. Furthermore, there is limited variation in the flow azimuths between the stereoscopic airphotos datasets and the symbols depicted on the maps. In the Atlin area 40% fewer features were recognized in SPOT images (n=349) than in the airphotos (n=579). Some subtle features (e.g., points 4-9, 11-14, Fig. 7) were detected in the stereoscopic airphotos but not in the SPOT images.

The derived-stereo has a number of limitations. Whereas ice-flow direction is consistent in all the datasets, unidirectional features, mapping density, and spatial distribution differ. Each imagery type differs in imagery resolution, cloud cover, and light saturation/desaturation, which may lead to mapping inconsistencies. More ice-flow features were mapped and more unidirectional ice-flow features identified using higher resolution imagery. Cloud cover affected mapping using SPOT imagery, because one derived-stereo pair was completely obscured. Cloud cover was not a factor when using orthomosaics because the images selected are cloud free. Airphotos and SPOT images have areas of high and low tonal saturation, which reduces the ability to identify ice-flow features. This is not an issue with the orthomosaics because they have a consistent tonal range (white to black).

The derived-stereo pairs were produced with the same horizontal offset across imagery and terrain types. This produced variation in vertical exaggeration between derived-stereo pairs (Fig. 5). This may be a factor in the mapping distribution, density, and identification of unidirectional features. For example, SPOT images have a large spatial footprint compared to orthomosaics (Table 1). Due to the larger spatial footprint, difference in relief across a SPOT image is larger, creating a greater vertical exaggeration than in the overlapping multiple orthomosaics. This causes the same feature across imagery types to look different and, therefore, be mapped differently. Our evaluation indicates that most of the ice-flow sets symbolized in Gabrielse (1963) are recognizable using orthomosaics.

The cost of mapping using stereo derived imagery is a significantly less than traditional hardcopy airphoto mapping and digital stereo airphoto mapping (Table 1). Although there are cost savings through efficiencies gained through mapping in digitally, (e.g., Smith et al., 2011), digital stereo airphotos of large areas is still expensive. Orthomosaic derived imagery

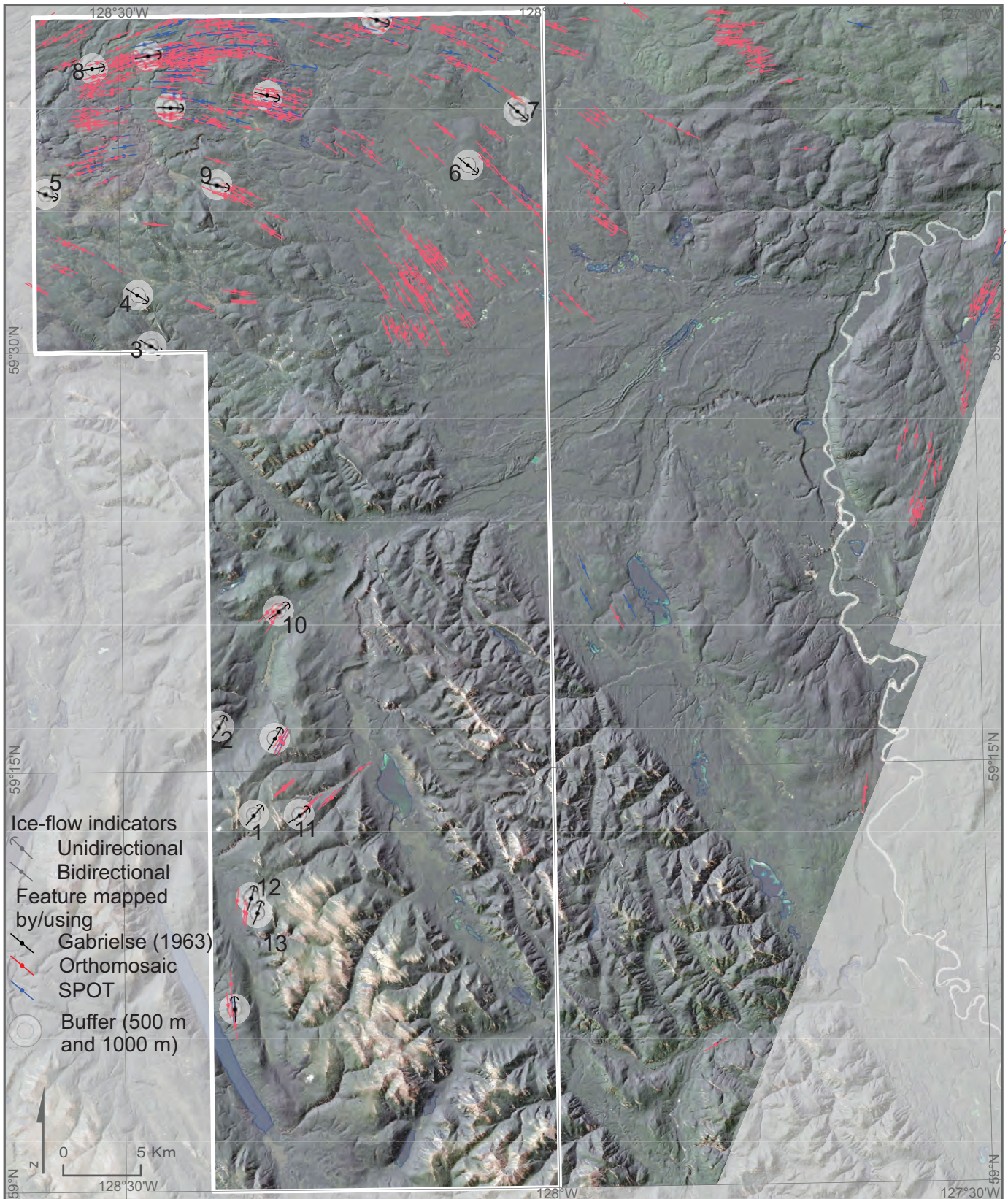


**Fig. 10.** Comparison of ice-flow mapping completed by Gabrielse (1963), outlined in white, to features identified in orthomosaics and SPOT imagery. Two buffers of 500 m and 1,000 m were used. Numbers 1-6 depict features mapped by Gabrielse (1963) that were not identified in the orthomosaics. Numbers 1-13 depict features mapped by Gabrielse (1963) that were not identified in the SPOT imagery.

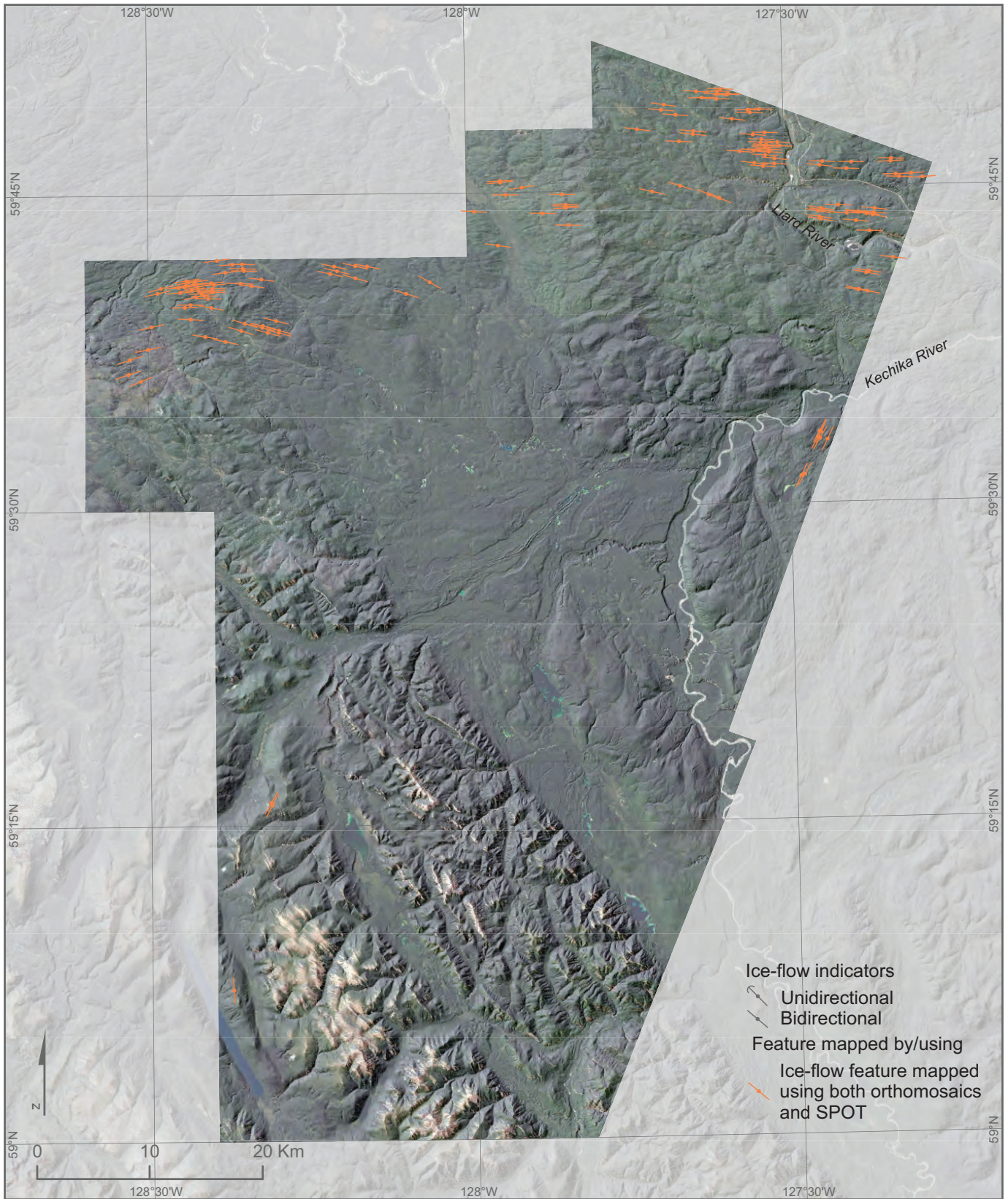


**Fig. 11.** Ice-flow features identified in both orthomosaics and SPOT imagery in the Liard Plain area.

costs 27% less than digital stereo airphoto derived imagery, with minimal loss in the accuracy and density of ice-flow features. The cost of SPOT derived-stereo imagery is less than 1% of the digital stereo airphoto and less than 3% of the orthomosaic derived-stereo imagery. Although the loss of fidelity is significant, the loss is at the regional scale and SPOT derived-stereo imagery highlight the most significant ice-flow sets. We conclude that, for mapping regional macroscale ice-flow features, the derived-stereo orthomosaic imagery balances accuracy with cost and provides the best value, but only for agencies within the British Columbia government. Outside of government, each orthomosaic frame has a maximum cost of about \$200, which equates to \$169/100 km<sup>2</sup>, making this dataset the most expensive.

## 6. Conclusions

Derived-stereo imagery provides the ability to incorporate single-frame imagery types into traditional stereo mapping methods at a significantly less cost than traditional hardcopy airphoto mapping and digital stereo airphoto mapping. Our evaluation indicates that derived-stereo orthomosaics provide the best value to remotely map ice-flow features, but only for government agencies that can access imagery at no cost. This evaluation was completed as part of the British Columbia Geological Survey's ice-flow indicator compilation for British Columbia and Yukon and might be useful to others. Ice-flow features mapped using derived-stereo SPOT imagery is inexpensive and has merit for regional ice-flow studies, but is inferior to digital stereo airphotos and derived-stereo orthomosaics.

## Acknowledgments

This project was partly funded by the Geological Survey of Canada Geo-mapping for Energy and Minerals phase 2 (GEM 2) program. We thank Ian Grady (iGi Consulting, Port Coquitlam, BC) for producing the derived-stereo imagery and appreciate the valuable input provided by Yao Cui (British Columbia Geological Survey). We also thank Daniel Kerr (Geological Survey of Canada) and the Geological Survey of Canada for their partnership and financial support.

## References cited

- Aber, J.S., Marzloff, I., and Ries, J.B., 2010. Small-format aerial photography: Principles, techniques and geoscience applications. Elsevier, The Netherlands, 265 p.
- Arnold, H., Ferbey, T., and Hickin, A.S., 2016. Ice-flow indicator compilation, British Columbia and Yukon. British Columbia Ministry of Energy and Mines, British Columbia Geological Survey Open File 2016-04; Geological Survey of Canada, Open File 8083, 1:1,750,000 scale.
- Aitken, J.D., 1959. Atlin area, British Columbia. Geological Survey of Canada Memoir 307, 89 p.
- Bednarski, J.M., 2008. Landform assemblage produced by the Laurentide Ice Sheet in northeast British Columbia and adjacent Northwest Territories – constraints on glacial lakes and patterns of ice retreat. *Canadian Journal of Earth Sciences* 45, 593-610.
- Benn, D.I., and Evans, D.J.A., 2010. *Glaciers and Glaciations*. Second Edition. Arnold, London, pp. 259-579.
- Boulton, G.S., 1987. A theory of drumlin formation by subglacial sediment deformation. In: Menzies, J., Rose, J. (Eds.), *Drumlin Symposium*. Balkema, Rotterdam, 25–80.
- Boulton G.S., Dongelmans, P., Punkari, M., and Broadgate, M., 2001. Palaeoglaciology of an ice sheet through a glacial cycle: the European ice sheet through the Weichselian. *Quaternary Science Reviews* 20, 591-625.
- Clague, J.J., 1989. Chapter 1: Quaternary geology of the Canadian Cordillera; in *Quaternary Geology of Canada and Greenland*. In: Fulton, R.J. (Ed.), *Geology of Canada Series No. 1.*, 17-96.
- Clague, J.J., and Ward, B., 2011. Pleistocene Glaciation of British Columbia. In: Ehlers, J., Gibbard, P.L., Huges, P.D., (Eds.), *Quaternary glaciations- extent and chronology, a closer look*. *Developments in Quaternary Science* 15, 563-573.
- Clark, C.D., 1993. Mega-scale lineations and cross-cutting ice-flow landforms. *Earth Surface Processes and Landforms* 18, 1–29.
- Clark C.D., Hughes, A.L.C., Greenwood, S.L., Jordan, C., and Sejrup, H.P., 2012. Pattern and timing of retreat of the last British-Irish ice sheet. *Quaternary Science Reviews* 44, 112-144.
- DATEM, 2012. Summit Evolution Operation Manual edition 6.4. DAT/EM Systems International, pp “4-11”.
- Evans, D.J.A., Rea, B.R., Hiemstra, J.F., and Ó Cofaigh, C., 2006. A critical assessment of subglacial mega-floods: A case study of glacial sediments and landforms in south-central Alberta, Canada. *Quaternary Science Reviews* 25 (13-14), 1638-1667.
- Ferbey, T., and Arnold, H., 2013. Compilation of micro- to macroscale ice-flow indicators for the Interior Plateau, central British Columbia. British Columbia Ministry of Energy, Mines and Natural Gas, British Columbia Geological Survey, Open File 2013-03, 1:900,000 scale.
- Ferbey, T., Arnold, H., and Hickin, A.S., 2013. Ice-flow indicator compilation, British Columbia. British Columbia Ministry of Energy, Mines and Natural Gas, British Columbia Geological Survey Open File 2013-06, 1:1 650,000 scale.
- Fulton, R.J., 1991. A conceptual model for growth and decay of the Cordilleran Ice Sheet. In: *Géographie physique et Quaternaire* 45, 281-286.
- Gabrielse, H., 1963. McDame map-area, Cassiar District, British Columbia. Geological Survey of Canada Memoir 319, 138 p.
- Holland, S.S., 1976. Landforms of British Columbia; a physiographic outline. British Columbia Ministry of Energy and Mines, British Columbia Geological Survey Bulletin 48, 138 p.
- Huntley, D.H., Hickin, A.S., and Lian, O.B., 2016. The pattern and style of deglaciation at the Late Wisconsinan Laurentide and Cordilleran ice sheet limits in northeastern British Columbia. *Canadian Journal of Earth Sciences*, doi:10.1139/cjes-2016-0066.
- Jackson, L.E., Jr., 1994. Terrain inventory and Quaternary history of the Pelly River area, Yukon Territory. Geological Survey of Canada Memoir 437, 41 p.
- Jackson L.E., Jr., and Clague, J.J. (Eds), 1991. The Cordilleran Ice Sheet. In: *Géographie physique et Quaternaire* 45, 261–377.
- Jackson, L.E., Jr. and Mackay, T.D., 1990. Glacial limits and ice flow directions for the last Cordilleran Ice Sheet in Yukon Territory between 60 and 63 degrees north. Geological Survey Open File 2329, 1 sheet, doi:10.4095/131319.
- Jackson, L.E., Jr., Ward, B., Duk-Rodkin, A., and Hughes, O.L., 1991. The last Cordilleran Ice Sheet in southern Yukon Territory. *Géographie Physique et Quaternaire*, 45, 341-354.
- Kennedy, K.E., and Bond, J.D., 2004. Evidence for a late-McConnell readvance of the Cassiar Lobe in Seagull Creek, Pelly Mountains, Central Yukon. In: Emond, D.S., and Lewis, L.L. (Eds), *Yukon exploration and geology 2003*, 121-128.
- King, E.C., Hindmarsh, R.C.A., and Stokes, C.R., 2009. Formation of mega-scale glacial lineations observed beneath a West Antarctic ice stream. *Nature Geoscience* 2, 585-588.
- Kleman, J., Hättestrand, C., Borgström, I., and Stroeven, A., 1997. Fennoscandian palaeoglaciology using a glacial geological

- inversion model, *Journal of Glaciology* 43, 283-299.
- Landgrebe, D.A., 2003. *Signal theory methods in multispectral remote sensing*. Wiley and Sons Inc., New Jersey, 508p.
- Levson, V.M., 1992. Quaternary geology of the Atlin area (104N/11W, 12 E). In: *Geological Fieldwork 1991*. British Columbia Ministry of Energy, Mines and Petroleum Resources, British Columbia Geological Survey Paper 1992-1, pp. 375-390.
- Levson, V.M., and Kerr, D.E., 1992. Surficial geology and placer gold setting of the Atlin – Surprise Lake area, NTS 104/11, 12. British Columbia Ministry of Energy, Mines and Petroleum Resources, British Columbia Geological Survey Open File 1992-7, 1:50,000 scale.
- Levson, V.M., Kerr, D.E., Lowe, C., and Blyth, H., 2003. Quaternary geology of the Atlin area, British Columbia. British Columbia Ministry of Energy and Mines, British Columbia Geological Survey Geoscience Map 2003-1; Geological Survey of Canada Open File 1562, 1:50,000 scale.
- Margold, M., Jansson, K.N., Kleman, J., and Stroven, A.P., 2013. Lateglacial ice dynamics of the Cordilleran Ice Sheet in northern British Columbia and southern Yukon Territory: retreat pattern of the Liard Lobe reconstructed from the glacial landform record. *Journal of Quaternary Science* 28 (2), 180-188.
- Menzies, J., 1979. A review of the literature on the formation and location of drumlins. *Earth Science Reviews* 14, 315-359.
- Mollard, J.D., 1976. *Landforms and surface materials of Canada – A Stereoscopic airphoto atlas and glossary*. Eighth edition. Regina, Saskatchewan, 171p.
- NRCAN, 2016. *Concepts of Aerial Photography*. Downloaded from <http://www.nrcan.gc.ca/earth-sciences/geomatics/satellite-imagery-air-photos/air-photos/about-aerial-photography/9687> [accessed October, 2016].
- Paine, D.P., and Kiser, J.D., 2012. *Aerial photography and image interpretation*. Third edition. Wiley, Hoboken, New Jersey, USA, 56.
- Ryder, J.M., and Maynard, D., 1991. The Cordilleran Ice Sheet in northern British Columbia. *Géographie Physique et Quaternaire* 45, 355-363.
- Sabins, F.F., 1997. *Remote sensing: principles and applications*. Third edition. Waveland Press Inc., Long Grove, Illinois, USA, 45.
- Seguinot, J., Rogozhina, I., Stroeven, A.P., Margold, M., and Kleman, J., 2016. Numerical simulations of the Cordilleran ice sheet through the last glacial cycle. *Cryosphere* 10, 639-664.
- Smith, M.J., Paron, P., Griffiths, J.S. (eds), 2011. *Geomorphological mapping, methods and applications*. Elsevier, 611p.
- Spagnolo, M., Clark, C.D., Ely, J.C., Stokes, C.R., Anderson, J.B., Andreassen, K., Graham, A.G.C., and King, E.C., 2014. Size, shape and spatial arrangement of mega-scale glacial lineations from a large and diverse dataset. *Earth Surface Processes and Landforms* 39, 1432-1448.
- SPOT (SPOT 4 and SPOT 5 satellite imagery), 2010. Downloaded from <http://www.geobase.ca> (November 2014).
- SRTM (Shuttle Radar Topography Mission 1 Arc-second Global). 2014. Downloaded from <https://lta.cru.usgs.gov/SRTM1Arc> [November 2014].
- Stokes, C.R., Tarasov, L., Blomdin, R., Cronin, T.M., Fischer, T.G., Gyllencreutz, R., Hättstrand, C., Heyman, J., Hindmarsh, R.C.A., Hughes, A.L.C., Jakobsson, M., Kirchner, N., Livingstone, S.J., Margold, M., Murton, J.B., Noormets, R., Peltier, W.R., Peteet, D.M., Piper, D.J.W., Preusser, F., Renssen, H., Roberts, D.H., Roche, D.M., Saint-Ange, R., Stroven, A.P., and Teller, J.T., 2015. On the reconstructions of paleo-ice sheets: Recent advances and future challenges. *Quaternary Science Reviews* 125, 15-49.
- Stumpf, A.J., Broster, B.E., and Levson, V.M., 2000. Multiphase flow of the late Wisconsinan Cordilleran ice sheet in western Canada. *Geological Society of America Bulletin* 112, 1850-1863.



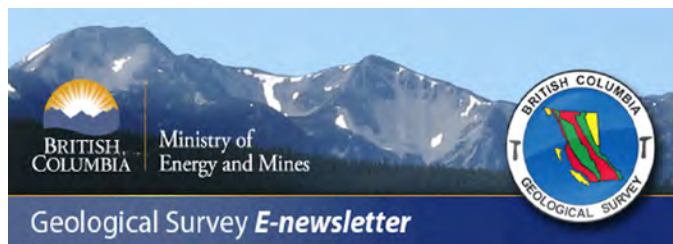
# Appendix: British Columbia Geological Survey publications and peer-reviewed journal papers authored by BCGS staff and released in 2016

All BCGS publications are available for download, free of charge, from:

[www.empr.gov.bc.ca/Mining/Geoscience/PublicationsCatalogue/Pages/default.aspx](http://www.empr.gov.bc.ca/Mining/Geoscience/PublicationsCatalogue/Pages/default.aspx)

To receive notification of our latest releases email:

[Geological.Survey@gov.bc.ca](mailto:Geological.Survey@gov.bc.ca)



---

## Papers

Paper 2016-1

Geological fieldwork 2015, a summary of field activities and current research, 211p.

Hickin, A.S., Jones, L.D., and Clarke, G., 2016. British Columbia Geological Survey annual program review 2015-2016. In: Geological Fieldwork 2015, British Columbia Ministry of Energy and Mines, British Columbia Geological Survey Paper 2016-1, pp. 1-11.

Mao, M., Simandl, G.J., Spence, J., Neetz, M., and Marshall, D., 2016. Trace element composition of fluorite and its potential use as an indicator in mineral exploration. In: Geological Fieldwork, 2015, British Columbia Ministry of Energy and Mines, British Columbia Geological Survey Paper 2016-1, pp. 181-206.

Martin, K., Zagorevski, A., Mihalyuk, M.G., and Creaser, R., 2016. Circa 180 Ma Ag-Bi-Pb-Mo-Cu-bearing quartz veins in a post-thrust calc-alkaline intrusion near Surprise Mountain, Iskut River area, northwestern British Columbia. In: Geological Fieldwork 2015, British Columbia Geological Survey Paper 2016-1, pp. 77-94.

Mihalyuk, M.G., Diakow, L.J., Friedman, R.M., and Logan, J.M., 2016. Chronology of southern Nicola arc stratigraphy and deformation. In: Geological Fieldwork 2015, British Columbia Ministry of Energy and Mines, British Columbia Geological Survey Paper 2016-1, pp. 31-63.

Mihalyuk, M.G., Zagorevski, A., Joyce, N.L., and Creaser, R.A., 2016. Age of magmatism and mineralization at the Star (Sheslay, Copper Creek) copper porphyry prospect: Inception of the Late Triassic mineralized arc. In: Geological Fieldwork 2015, British Columbia Ministry of Energy and Mines, British Columbia Geological Survey Paper 2016-1, pp. 65-75.

Milidragovic, D., Joyce, N.L., Zagorevski, A., and Chapman, J.B., 2016. Petrology of explosive Middle-Upper Triassic ultramafic rocks in the Mess Creek area, northern Stikine terrane. In: Geological Fieldwork 2015, British Columbia Ministry of Energy and Mines, British Columbia Geological Survey Paper 2016-1, pp. 95-111.

Rukhlov, A.S., Plouffe, A., Ferbey, T., Mao, M., and Spence, J., 2016. Application of trace-element compositions of detrital apatite to explore for porphyry deposits in central British Columbia. In: Geological Fieldwork 2015, British Columbia Ministry of Energy and Mines, British Columbia Geological Survey Paper 2016-1, pp. 145-179.

Schiarizza, P., 2016. Toward a regional stratigraphic framework for the Nicola Group: Preliminary results from the Bridge Lake – Quesnel River area. In: Geological Fieldwork 2015, British Columbia Ministry of Energy and Mines, British Columbia Geological Survey Paper 2016-1, pp. 13-30.

van Straaten, B.I., and Nelson, J., 2016. Syncollisional late Early to early Late Jurassic volcanism, plutonism, and porphyry-style alteration on the northeastern margin of Stikinia. In: Geological Fieldwork 2015, British Columbia Ministry of Energy and Mines, British Columbia Geological Survey Paper 2016-1, pp. 113-143.

## **Geoscience Maps**

GM 2016-1

Ferbey, T., Levson, V.M., and Plouffe, A., 2016. Surficial geology, Moffat Creek area, British Columbia, parts of NTS 93-A/3, NTS 93-A/4, NTS 93-A/5, and NTS 93-A/6. Geological Survey of Canada, Canadian Geoscience Map 252 (preliminary); British Columbia Geological Survey, Geoscience Map 2016-1, scale 1:50,000.

## **Open Files**

OF 2016-1

Clarke, G., Britton, J., Jago, P., Katay, F., Kyba, J., and Northcote, B., 2016. Selected exploration projects and operating mines in British Columbia, 2015.

OF 2016-2

Bustard, A.L., and Ferbey, T., 2016. An index of base and precious metal regional- to property-scale subglacial till geochemical and mineralogical surveys in British Columbia.

OF 2016-3

Arnold, H., and Ferbey, T., 2016. British Columbia surficial geology map index.

OF 2016-4

Arnold, H., Ferbey, T., and Hickin, A.S., 2016. Ice-flow indicator compilation, British Columbia and Yukon.

OF 2016-5

Hickin, A.S., Best, M.E., and Pugin, A., 2016. Geometry and valley-fill stratigraphic framework for aquifers in the Groundbirch paleovalley assessed through shallow seismic and ground-based electromagnetic surveys.

## **GeoFiles**

GF 2016-1

Rukhlov, A.S., Plouffe, A., Ferbey, T., Mao, M., and Spence, J., 2016. Supplementary data for application of trace-element compositions of detrital apatite to explore for porphyry deposits in central British Columbia.

GF 2016-2

Mihalynuk, M.G., and Zagorevski, A., 2016. Geochemical results from GEM2 Reconnaissance surveys between the Stikine River and Atlin, British Columbia.

GF 2016-3

Friedman, R.M., Mihalynuk, M.G., Diakow, L.J., and Gabites, J.E., 2016. Southern Nicola Arc Project 2015: Geochronologic data constraining Nicola Arc history along a transect near 50°N.

GF 2016-4

Han, T., Rukhlov, A.S., Naziri, M., and Moy, A., 2016. New British Columbia litho-geochemical database: Development and preliminary data release.

GF 2016-5

Arnold, H., and Ferbey, T., 2016. Ice-flow indicator compilation for the Cordilleran ice sheet. (Poster)

GF 2016-6

Simandl, G.J., Paradis, S., Neetz, M., and Akam, C., 2016. Graphite deposits: Origin and economic significance. (Poster)

GF 2016-7

Kyba, J.W., 2016. 2015 Skeena Region project highlights. (Poster)

GF 2016-8

Jago, C.P., 2016. Mining, exploration, and discovery in the Omineca and Northeast regions, 2015. (Poster)

GF 2016-9

Katay, F., 2016. Exploration and mining in the Kootenay-Boundary Region, 2015. (Poster)

GF 2016-10

Plouffe, A., and Ferbey, T., 2016. Till geochemistry, mineralogy and textural data near four Cu porphyry deposits in British Columbia. (Also released as Geological Survey of Canada Open File 8028).

GF 2016-11

Ferbey, T., Plouffe, A., and Bustard, A.L., 2016. Geochemical, mineralogical, and textural data from tills in the Highland Valley Copper mine area, south-central British Columbia. (Also released as Geological Survey of Canada Open File 8119).

## **Information Circulars**

IC 2016-1

Clarke, G., Britton, J., Jago, P., Katay, F., Kyba, J., and Northcote, B., 2016. Provincial overview of exploration and mining in British Columbia, 2015, 140p.

IC 2016-2

British Columbia coal industry overview, 2015, 14p.

IC 2016-3

British Columbia Mineral Development Office. (Brochure)

IC 2016-4

Rare metals in British Columbia. (Pamphlet)

IC 2016-5

The Groundhog coal field. (Poster)

IC 2016-6

British Columbia Geological Survey. (Brochure)

IC 2016-7

Online databases at the British Columbia Geological Survey. (Brochure)

## **Peer-reviewed journal publications**

Berger, A., Cousens, B.C., Ootes, L., and Jackson, V., 2016. Geochemistry of Late Archean volcanic rocks from the Slave craton, Northwest Territories. Northwest Territories Geological Survey, NWT Open Report 2015-029, 41 pp.

Du, X., Zhou, K., Cui, Y., Wang, J., Zhang, N., and Sun, W., 2016. Application of fuzzy analytical hierarchy process (AHP) and prediction-area (P-A) plot for mineral prospectivity mapping: a case study from the Dananhu metallogenic belt, Xinjiang, NW China. *Arabian Journal of Geosciences*, 9, DOI: 10.1007/s12517-016-2316-y.

Haugaard, R., Ootes, L., Creaser, R.A., and Konhauser, K., 2016. The nature of Mesoarchean seawater and continental weathering in 2.85 Ga banded iron formation, Slave craton, NW Canada. *Geochimica et Cosmochimica Acta*, 194, 34-56. DOI:10.1016/j.gca.2016.08.020.

Haugaard, R., Ootes, L., Heaman, L.M., Hamilton, M.A., Shaulis, B., and Konhauser, K., 2016. Depositional timing of Neoproterozoic turbidites of the Slave craton – recommended nomenclature and type localities. *Canadian Journal of Earth Sciences*. DOI:10.1139/cjes-2016-0098.

Hickin, A.S., Lian, O.B., and Levson, V.M., 2016. Coalescence of late Wisconsinan Cordilleran and Laurentide ice sheets east of the Rocky Mountain Foothills in the Dawson Creek region, Northeast British Columbia, Canada. *Quaternary Research* 85, 409-429.

Jackson, V.A., and Ootes, L., 2016. Petrographic summary of samples from the Snare River volcanic belt, Northwest Territories (NTS 85 O/13). Northwest Territories Geological Survey, NWT Open Report 2015-027.

Jackson, V.A., and Ootes, L., 2016. Petrographic summary of samples from the Sharrie Lake area, southern Beaulieu River volcanic belt, Northwest Territories (Part of NTS 85 I/10 and 11). Northwest Territories Geological Survey, NWT Open Report 2015-026.

Mackay, D.A.R., Simandl, G.J., Ma, W., Redfearn, M., and Gravel, J., 2016. Indicator mineral-based exploration for carbonatites and related specialty metal deposits— A QEMSCAN® orientation survey, British Columbia, Canada. *Journal of Geochemical Exploration*, 165, 159-173.

- Mao, M., Rukhlov, A.S., Rowins, S.M., Spence, J., and Coogan, L.A., 2016. Apatite trace-element compositions: A robust new tool for mineral exploration. *Economic Geology*, 111, 1187-1222.
- Manor, M.J., Scoates, J.S., Nixon, G.T., and Ames, D.E., 2016. The Giant Mascot Ni-Cu-PGE deposit, southwestern British Columbia: mineralized conduits and sulphide saturation mechanisms in a convergent margin tectonic setting. *Economic Geology*, 111, 57-87.
- Ootes, L., Jackson, V.A., Davis, W.J., Bennett, V.C., Smar, L., and Cousens, B.C., 2016. Parentage of Archean basement within a Paleoproterozoic orogen and implications for on-craton diamond preservation: Slave craton and Wopmay orogen, NW Canada; *Canadian Journal of Earth Sciences*, 10.1139/cjes-2016-0059.
- Paradis, S., Simandl, G.J., Keevil, H., and Raudsepp, M., 2016. Carbonate-Hosted Nonsulfide Pb-Zn Deposits of the Quesnel Lake District, British Columbia, Canada. *Economic Geology*, 111, 179-198.
- Plouffe, A., Ferbey, T., Hashmi, S., and Ward, B.C., 2016. Till geochemistry and mineralogy: vectoring towards Cu porphyry deposits in British Columbia, Canada. *Geochemistry: Exploration, Environment, Analysis*, <http://doi.org/10.1144/geochem2015-398>.
- Trofanenko, J., Williams-Jones, A.E., Simandl, G.J., and Migdisov, A.A., 2016. The nature and origin of the REE mineralization in the Wicheeda carbonatite, British Columbia, Canada. *Economic Geology*, 111, 199-223.
- Williamson, N., Ootes, L., Rainbird, R., Bédard, J., and Cousens, B., 2016. Initiation and early evolution of a continental flood basalt province preserved in the 720 Ma Natkusiak Formation, Victoria Island, Canadian Arctic. *Bulletin of Volcanology*, 78, 1-19.

### **Contributions to partner publications**

- Levson, V.M., Ferbey, T., and Kerr, D.E., 2016. Reconnaissance surficial geology, Hill Island Lake, Northwest Territories, NTS 75-C. Geological Survey of Canada, Canadian Geoscience Map 263, (ed. prelim.), 1:125,000, doi:10.4095/298836.
- Zagorevski, A., Mihalynuk, M.G., McGoldrick, S., Bedard, J.H., Golding, M., Joyce, N., Lawley, C., Canil, D., Corriveau, A.-S., Bogatu, A., and Tremblay, A., 2016. Geological framework of ancient oceanic crust in northwestern British Columbia and southwestern Yukon. Geological Survey of Canada, Open File 8140, 15p.
- Zagorevski, A., Mihalynuk, M., Milidragovic, D., Joyce, N., Kovacs, N., Allan, M., Friedman, R., and Kellett, D., 2016. Characterization of volcanic and intrusive rocks across the British Columbia - Yukon border. Geological Survey of Canada, Open File 8141, 15p.